

Evolution of the Graciosa, S. Miguel and Santa Maria volcanic islands : implications for the Nubia-Eurasia plate boundary in the Azores

Aurore Sibrant

▶ **To cite this version:**

Aurore Sibrant. Evolution of the Graciosa, S. Miguel and Santa Maria volcanic islands : implications for the Nubia-Eurasia plate boundary in the Azores. Volcanology. Université Paris Sud - Paris XI, 2014. English. ⟨NNT : 2014PA112303⟩. ⟨tel-01142723⟩

HAL Id: tel-01142723

https://theses.hal.science/tel-01142723v1

Submitted on 15 Apr 2015

HAL is a multi-disciplinary open access archive for the deposit and dissemination of scientific research documents, whether they are published or not. The documents may come from teaching and research institutions in France or abroad, or from public or private research centers.

L'archive ouverte pluridisciplinaire **HAL**, est destinée au dépôt et à la diffusion de documents scientifiques de niveau recherche, publiés ou non, émanant des établissements d'enseignement et de recherche français ou étrangers, des laboratoires publics ou privés.



HAL Authorization

UNIVERSITÉ PARIS-SUD

ÉCOLE DOCTORALE 534 :
MODÉLISATION ET INSTRUMENTATION EN PHYSIQUE, ÉNERGIES, GÉOSCIENCES ET ENVIRONNEMENT

Laboratoire : *GEOPS*

THÈSE DE DOCTORAT

SCIENCES DE L'UNIVERS

par

Aurore L. R. SIBRANT

Evolution of the Graciosa, S. Miguel and Santa Maria volcanic islands : Implications for the Nubia/Eurasia plate boundary in the Azores

Date de soutenance : 03/11/2014

Composition du jury :

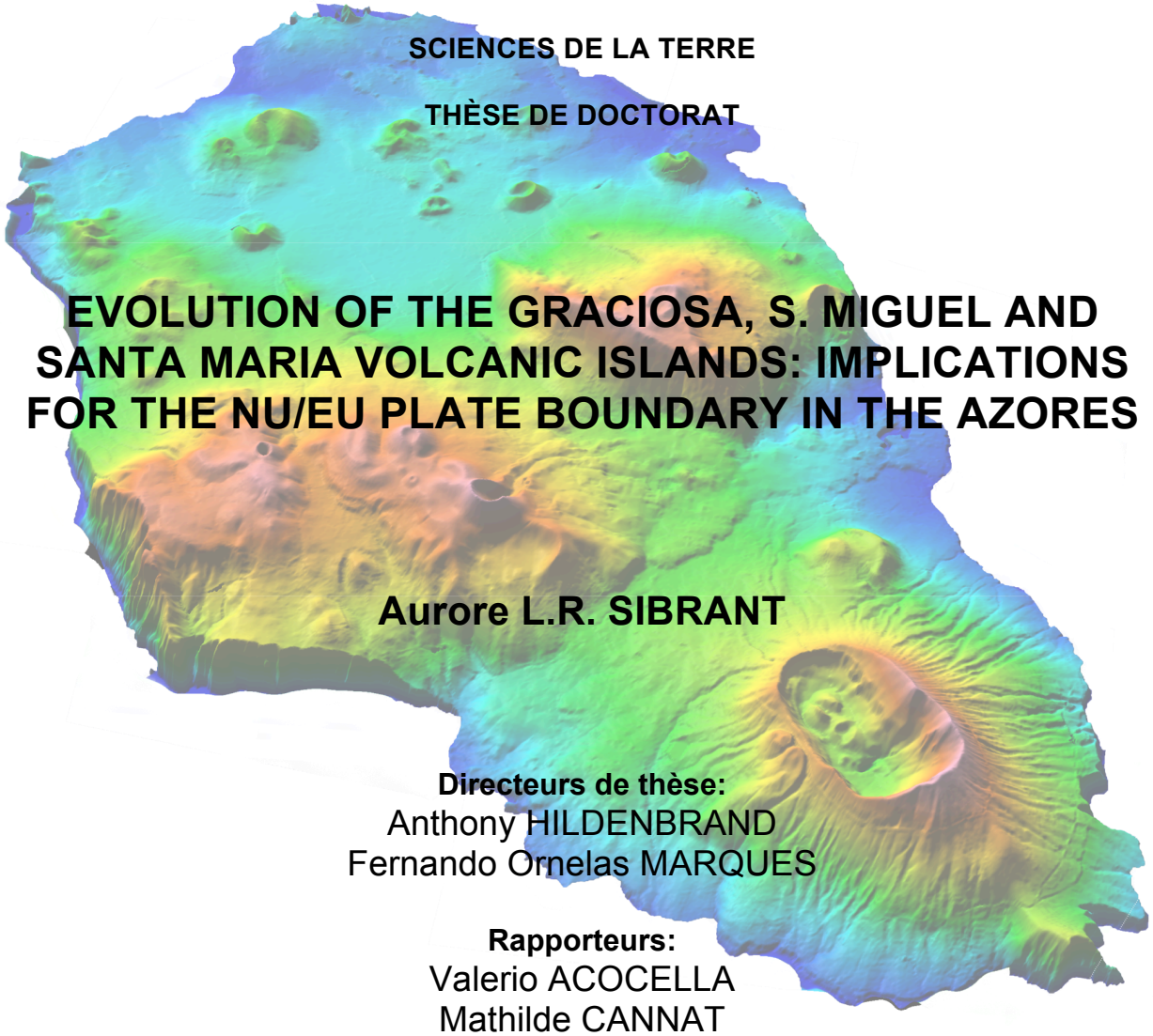
Directeur de thèse :	Anthony HILDENBRAND	Chargé de recherche CNRS (Université Paris-Sud)
Co-directeur de thèse :	Fernando MARQUES	Assistant Professor (Universidade de Lisboa)
Rapporteurs :	Valério ACOCELLA	Permanent Researcher (Universita Roma Tre)
	Mathilde CANNAT	Directrice de recherche CNRS (IPG Paris)
Examinateurs :	Andrew CALVERT	Assistant Professor (USGS Menlo Park, CA)
	Hermann ZEYEN	Professeur (Université Paris-Sud)
Membres invités :	Anne DAVAILLE	Directrice de recherche CNRS (Paris-Sud)
	Pierre-Yves GILLOT	Professeur (Université Paris-Sud)

UNIVERSITÉ PARIS-SUD

ÉCOLE DOCTORALE 534 MIPEGE
Laboratoire GEOPS

SCIENCES DE LA TERRE

THÈSE DE DOCTORAT



EVOLUTION OF THE GRACIOSA, S. MIGUEL AND SANTA MARIA VOLCANIC ISLANDS: IMPLICATIONS FOR THE NU/EU PLATE BOUNDARY IN THE AZORES

Aurore L.R. SIBRANT

Directeurs de thèse:
Anthony HILDENBRAND
Fernando Ornelas MARQUES

Rapporteurs:
Valerio ACOCELLA
Mathilde CANNAT

Examinateurs:
Andrew CALVERT
Hermann ZEYEN

Invités:
Anne DAVAILLE
Pierre-Yves GILLOT

2014

Evolution of the Graciosa, S. Miguel and Santa Maria volcanic islands: Implications for the Nubia/Eurasia plate boundary in the Azores

The Azores archipelago in the Atlantic comprises nine volcanic islands which developed on a thick oceanic plateau close to the Triple Junction between the North American (Na), the Nubian (Nu), and the Eurasian (Eu) lithospheric plates. The formation of the plateau and the origin of the volcanism remain controversial, but have been generally attributed to a plume-like mantle instability. However, the distribution of the volcanic edifices east of the Mid-Atlantic Ridge (MAR) appears greatly influenced by regional deformation associated with the northward migration of the Eu/Nu plate boundary from an extinct old transform fault, the East Azores Fracture Zone (EAFZ), up to the presently active ultra-slow Terceira Rift (TR).

In this thesis, we use the volcanism as a marker for regional deformation. We especially focus on S. Miguel and Graciosa, which are located within the TR, and on S. Maria, an old volcanically extinct island located between the EAFZ and the TR. These three islands thus constitute particularly suitable targets to track the architecture and the evolution of the Eu/Nu plate boundary during the last few Myr. From new geomorphological, stratigraphic, geochronologic, structural/tectonic data, and existing bathymetric and geophysical data, we reconstruct the successive stages of growth and destruction of the islands, and discuss their geodynamic meaning. These data are then complemented by fluid dynamic modelling using laboratory experiments to examine the possible links between mantle instability, plate boundary migration and the development of the volcanism on various spatial and temporal scales.

The new results on the islands show that the edifices located within the TR grew through short (<100 kyr) and partly synchronous volcanic pulses, separated by major mass-wasting episodes in the form of catastrophic sector collapses. We propose that such evolution reflects brief and intense episodes of regional deformation along the still active Eu/Nu plate boundary. The distribution of tectonic markers (dykes and faults) and the recognition of N110 and N150 tectonic structures in eastern S. Miguel leads us to propose that oblique extension in the TR is mainly accommodated by the master faults of the rift, and that the TR is presently not the locus of appreciable sea-floor spreading. Furthermore, we identify a new N050 trend, which may represent transform faults accommodating the variation in obliquity of the TR. The activity of S. Maria is here dated between 5.7 and 2.8 Ma. Like the recent islands, S. Maria experienced catastrophic flank collapses, most probably triggered by regional tectonics. We identify a new graben structure linking Santa Maria to the island of S. Jorge further NW. The shape of this graben is similar to the TR and it is located between the EAFZ and the current plate boundary. We interpret this graben as a former transient rift, and therefore an old Eu/Nu plate boundary. From the new data, we propose that the eastern part of the transient rift migrated to the eastern part of the TR between 2.8 Ma and 1.7 Ma.

The overall migration of the Eu/Nu plate boundary to the north and the creation of the Azores plateau has been interpreted by Vogt and Jung (2004) as resulting from successive NE jumps of the rift axis to maintain its position over a fixed 'hotspot'. Our fluid mechanics experiments suggest that the Azores, as Canary, Cape Verde, Madeira Islands and Great Meteor seamounts might be the surface signature of a cluster of mantle instabilities rising from the top of a large thermochemical dome located in the lower mantle. However, such secondary plumes present a strong time-dependence 5-40 Myr time scale. Moreover, they could be sufficiently weak to adapt their motions to the pre-existing force balances and morphology of the lithosphere. We therefore present a scenario of the Azores area evolution combining a triple junction and decompression melting buoyant material (i.e. such in volatiles and/or temperature) under a thickening lithosphere.

Evolution des îles volcaniques de Graciosa, S. Miguel et Santa Maria: implications pour la limite de plaque Nubie/Eurasie dans les Açores

L'archipel des Açores dans l'océan Atlantique est constitué de neuf îles volcaniques édifiées sur un épais plateau océanique, à proximité de la jonction triple entre les plaques Nord-américaine (Na), Nubienne (Nu) et Eurasienne (Eu). La formation du plateau et l'origine du volcanisme restent fortement débattus et ont été le plus souvent attribués à la présence d'une instabilité mantellique de type panache. Cependant, la répartition et la morphologie des édifices volcaniques situés du côté est de la dorsale Atlantique (MAR) semblent avoir été grandement influencés par la déformation régionale liée à la migration de la frontière de plaque (Eu/Nu) vers le NE. En effet, la frontière serait passée d'une faille transformante aujourd'hui inactive, la zone de fracture est des Açores (EAFZ), à un rift ultra lent actif appelé le Rift de Terceira (TR).

Lors de ce travail, nous utilisons le volcanisme comme marqueur de la déformation régionale. Nous nous intéressons particulièrement aux îles de S. Miguel et Graciosa, qui sont localisées à l'intérieur du TR, et à Santa Maria, une île volcanique éteinte qui se situe entre la EAFZ et le TR. De par leur position, ces trois îles constituent donc des cibles particulièrement appropriées afin d'étudier l'architecture et l'évolution de la frontière de plaque Eu/Nu durant les dernier Millions d'années. A partir de nouvelles données géomorphologiques, stratigraphiques, géochronologiques et tectoniques, couplées aux données bathymétriques et géophysiques disponibles, nous reconstruisons les étapes successives de construction et de démantèlement de ces îles puis discutons de leur signification géodynamique. Ces données sont ensuite complétées par des expériences de mécanique des fluides afin d'investiguer les liens possibles entre un panache mantellique, la migration de la frontière de plaque et le développement du volcanisme sur plusieurs échelles d'espace et de temps.

Les résultats montrent que les édifices localisés dans le TR se construisent via des pulses volcaniques courts (<100 kyr) et relativement synchrones, séparés par des épisodes d'effondrements sectoriels volumineux et catastrophiques. Nous proposons qu'une telle évolution reflète des épisodes brefs et intenses de déformation régionale le long de la frontière de plaque active. La distribution des marqueurs tectoniques (dykes et failles) ainsi que la reconnaissance de structures tectoniques orientées N110 et N150 dans la partie Est de S. Miguel, nous conduit à proposer que l'extension oblique du TR est principalement accommodée par les failles bordières majeures du rift sans expansion (formation de nouvelle croute océanique) associée. En outre, nous identifions une nouvelle tendance tectonique orientée N50° qui pourrait représenter des failles transformantes accommodant les variations d'obliquité du TR. L'activité de île de Santa Maria est ici datée entre 5.7 et 2.8 Ma. Comme les îles récentes, S. Maria a été façonnée par plusieurs effondrements sectoriels catastrophiques, le plus probablement déclenchés par les mouvements tectoniques régionaux. Nous identifions également une nouvelle structure de type graben reliant les îles de S. Maria et S. Jorge plus loin au NW. La forme de ce graben est semblable au TR et est située entre l'ancienne EAFZ et la frontière Eu/Nu actuelle. Nous interprétons ce graben comme un ancien rift transitionnel et donc comme une ancienne frontière de plaque Eu/Nu. A partir de nos données géochronologiques, nous proposons que la partie Est de ce rift transitionnel aurait migré vers la partie Est du TR entre 2.8 et 1.7 Ma.

La migration générale de la frontière Eu/Nu et la formation du plateau des Azores ont été interprétées par Vogt and Jung (2004) comme résultant de sauts successifs vers le NE de l'axe du Rift afin de maintenir sa position au dessus d'un point chaud fixe. Nos expériences de mécanique des fluides suggèrent que l'archipel des Açores, comme celui des Canaries, du Cap Vert, de Madère ainsi que les volcans sous marins de Great Meteor sont la signature en surface d'un groupe d'instabilités mantellique prenant naissance et remontant à partir du sommet d'un dôme thermochimique situé dans le manteau inférieur. Cependant, de telles plumes secondaires présentent une forte dépendance en temps d'environ 5-40 Myr. De plus, Ces panaches secondaires pourraient être suffisamment faibles pour adapter leurs mouvements aux équilibres de forces pré-existants, notamment la structure et la morphologie de la lithosphère.

Remerciements

A l'issue de la rédaction de cette thèse, je suis convaincue que la recherche est loin d'être un travail solitaire. En effet, je n'aurais jamais pu réaliser ce travail doctoral sans le soutien d'un grand nombre de personnes dont la générosité, la bonne humeur et l'intérêt manifestés à l'égard de ma recherche m'ont permis de progresser dans cette phase délicate de l'apprenti-chercheuse.

En premier lieu, je tiens à remercier mes directeurs de thèse, monsieur ANTHONY HILDENBRAND et monsieur FERNANDO ORNELAS MARQUES, pour la confiance qu'ils m'ont accordé en acceptant ma candidature à ce travail doctoral, pour leurs multiples conseils et pour toutes les heures qu'ils ont consacrées à édifier, consolider et corriger cette recherche. J'ai apprécié votre complémentarité, votre disponibilité sans faille et j'ai été extrêmement sensible à vos qualités humaines, d'écoute et de compréhension tout au long de cette thèse.

Je souhaite exprimer ma gratitude à madame ANNE DAVAILLE pour m'avoir proposé et m'avoir permis de réaliser une approche multidisciplinaire et multi-échelle inédite à ma connaissance grâce à la mécanique des fluides. Je vous remercie également pour votre accueil chaleureux ainsi que pour vos multiples encouragements, notamment durant ces dernières semaines.

Mes remerciements vont également à monsieur PIERRE-YVES GILLOT pour m'avoir donné envie de réaliser une thèse au travers de ses cours passionnant de master. Je vous remercie pour votre accueil chaleureux au sein de l'équipe Géochronologie et d'avoir accepté d'encadrer mon sujet de recherche de Master 1. Merci pour ce travail de terrain sur Ustica et pour avoir accepté de participer à ce jury de thèse.

Je suis grée à madame MATHILDE CANNAT et à monsieur VALERIO ACOCELLA de s'être rendu disponibles pour la soutenance ; de m'avoir prodigué maintes conseils et enfin d'avoir accepté la fonction de rapporteur. Merci de votre intérêt manifesté à l'égard de ce travail de doctorat.

Je souhaiterais aussi adresser ma gratitude à messieurs ANDREW CALVERT et HERMANN ZEYEN d'avoir accepté d'être examinateur de cette thèse. Vos spécialités respectives m'auront permis d'enrichir ce travail.

Mon travail de recherche sur le terrain a été particulièrement facilité par la fondation de la Faculté des Sciences de l'Université de Lisbonne (FCUL) et par le projet MEGAHazards.

Ces remerciements seraient incomplets si je n'en adressais pas à l'ensemble des MEMBRES de GEOPS et du FAST pour leur soutien moral ainsi que pour la très bonne ambiance que j'ai toujours trouvé au sein de l'équipe Géochronologie et du laboratoire FAST. Je remercie plus particulièrement XAVIER QUIDELLEUR, PIERRE LAHITTE, CLAIRE BOUKARI, CARLOS PALLARES, KIM-HO, LUDOVIC PAUCHARD, YANN BERTHO, VERONIQUE LAZARUS, GORGES GAUTHIER, NEIL RIBE, RAFAEL PIDOUX, ALBAN AUBERTIN pour leurs nombreux conseils, discussions et boutades sympathiques.

J'exprime ma gratitude à tous les amis chercheurs ou non initiés qui m'ont soutenue ces trois années, je pense particulièrement à JULIA RICCI, AMER AL KWATLI, CLAUDE LANOE, JEAN-CLAUDE LEFEVRE, SARAH BADR, ANTOINE CAMPAGNE, THIBAULT CHEVALIER, ANA COSTA, THOMAS BOULESTEIX, FANELIE RABAN, GREGORY PORET, MATHIAS LELOUTRE, TELEMACO TESEI, ANNA MASSMEYER et aux nombreux autres amis de longue haleine qu'il serait trop long de lister.

Un grand merci à ANTOINE CUVILLIEZ, ANNE DUPERRET et BERNARD HOYEZ pour être venu observer avec un œil bienveillant la soutenance de thèse.

Table of contents

Chapter I: Introduction……3

I. 1. Main motivation……**5**

I. 2. The Azores Volcanic Province. ……**6**

Chapter II: Previous studies on the Azores Area……13

II. 1. The main structures of the Azores. ……**15**

II. 2. The different kinematic models for the Azores Triple Junction. ……**17**

II. 2. 1. Triple junctions in the central Atlantic prior to 20 Ma: from King's Trough to Gloria Fault. ……**18**
II. 2. 2. The Azores Triple Junction prior to 20 Ma: Gloria Fault to Terceira Rift or to EAFZ?. ……**20**
II. 2. 3. The Azores Triple Junction in the last 20 Myr. ……**23**

II. 3. The Azores volcanism and its mantle source. ……**26**

II. 3. 1. Thickness of the Azores platform. ……**27**
II. 3. 2. Nature of the Azores melting anomaly: a weak and wet hotspot?.....**27**
II. 3. 3. The deep mantle underneath the Azores. ……**30**
II. 3. 4. Position of the Azores mantle instability center. ……**35**

II. 4. Interaction between the Azores hotspot and the Azores Triple Junction. ……**36**

Chapter III: Construction and destruction of a volcanic island developed inside an oceanic rift: Graciosa Island, Terceira Rift, Azores (Accepted by JVGR**)…….41**

III. 1. Introduction. ……**43**

III. 2. Geological setting. ……**44**

III. 3. Bathymetry, gravity, DEM analysis, fieldwork data and sampling strategy……**44**

III. 3. 1. Bathymetry and gravity. ……**44**
III. 3. 2. Inland DEM analysis. ……**46**
III. 3. 3. Field data and sampling strategy. ……**46**

III. 4. New K-Ar dating. ……**48**

III. 5. Discussion. ……**50**

III. 5. 1. Proposal of a new stratigraphy for the Graciosa Island. ……**50**
III. 5. 2. Repeated destruction of Graciosa: tectonic faulting or gravitional collapse?.**51**

III. 6. Conclusions. ……**54**

Chapter IV: São Miguel Island…..57

IV. 1. Morpho-structural evolution of a volcanic island developed inside an active oceanic rift: S. Miguel Island (Terceira Rift, Azores), (In prep, JVGR). ……..**59**

IV. 1. 1. Introduction. ……**61**
IV. 1. 2. Geological background. ……**62**
IV. 1. 3. Methods and Results. ……**65**
IV. 1. 4. Discussion. ……..**85**

IV. 2. Deformation in hyper-slow oceanic rifts: insights from the tectonics of the S. Miguel Island (Terceira Rift, Azores), (in prep, Tectonics). ……**103**

IV. 2. 1. Introduction. ……**105**
IV. 2. 2. Geological Background. ……**108**
IV. 2. 3. Methods. ……**110**
IV. 2. 4. Results. ……..**114**
IV. 2. 5. Discussion. ……**120**
IV. 2. 6. Conclusion. ……**126**

Chapter V: Volcano-tectonic evolution of the Santa Maria Island (Azores): implications for palaeostress evolution at the western Eurasia-Nubia plate boundary (submitted to JVGR**)……...149**

V. 1. Introduction. ……**153**

V. 2. Previous data on the Santa Maria island. ……...**155**

V. 3. Geomorphological analysis, fieldwork and sampling. ……..…**157**

V. 4. Structural analysis. ……..…**160**

V. 5. K-Ar dating on separated groundmass. ……..**161**

V. 6. Discussion. ……..…**163**

V. 6. 1. Volcano-tectonic evolution of Santa Maria. ……...**164**
V. 6. 2. Lithospheric control of volcanism. ……..**168**

V. 7. Conclusion. ……..**169**

Chapter VI: Geological synthesis: implications for the Eu/Nu boundary in the Azores……..179

VI. 1. The Eu/Nu plate boundary during the last Myr. ……**181**

VI. 1. 1. Spatial distribution of the volcanism and tectonic structures……**181**
VI. 1. 2. Temporal evolution of the volcanism. ……**183**
VI. 1. 3. Age and meaning of the destruction processes. ……..…**191**

VI. 2. The Nu/Eu plate boundary before the TR. ……**196**

VI. 2. 1. Introduction. ……..**196**
VI. 2. 2. Summary of the geology of Santa Maria Island……**197**
VI. 2. 3. Identification of a transient graben through SMa and parallel to the TR…..**198**
VI. 2. 4. From the EAFZ to the TR. ……..**203**
VI. 2. 5. Conclusions. ……..**206**

Chapter VII: Influence of the Central Atlantic geodynamics on the evolution of the Azores……..…….207

VII. 1. Introduction…….**209**

VII. 2. Laboratory experiments. ……..**212**

VII. 2. 1. Experimental set up. ……...…**212**
VII. 2. 2. Experimental parameters. ……...…**214**

VII. 3. Characteristics of mantle "secondary" plumes: results from the laboratory experiments. ……..…**216**

VII. 3. 1. Plume development. ……...…**216**
VII. 3. 2. Spacing between plumes. ……...…**218**
VII. 3. 3. Interactions between plumes. ……**220**
VII. 3. 4. Time recurrence. …… ……..…**221**

VII. 4. The Atlantic hotspots cluster. ……**222**

VII. 4. 1. Existence and spacing of the secondary plumes. ……...…**223**
VII. 4. 2. Evolution from King's Trough to Azores. ……**225**

VII. 5. Evolution of the Azores in the last 10 Myr. ……...…**225**

VII. 5. 1. Plume-root interaction. ……**226**
VII. 5. 2. Rifting and the northward growth of the Azores plateau. ……..…**228**

VII. 6. Conclusions. ……..…**232**

Chapter VIII: Conclusions……...233

Chapter IX : References……..239

Appendix I : Reconstructing the architectural evolution of volcanic islands from combined K/Ar, morphologic, tectonic, and magnetic data : The Faial Island example (Azores)……..269

Appendix II : Reply on: Reconstructing the architectural evolution of volcanic islands from combined K/Ar, morphologic, tectonic, and magnetic data : The Faial Island example (Azores)……281

Appendix III : Large-scale catastrophic flank collapses in a steep volcanic ridge: The Pico-Faial Ridge, Azores Triple Junction……..287

List of Figures

Chapter I: Introduction

Figure I. 1. Bathymetry of the Azores Plateau with the main morphological features discussed in the text (GeoMap database)……**6**

Figure I. 2. Bathymetry of the Azores Archipelago from Lourenço et al., (1998)……..**7**

Figure I. 3. 3D bathymetry (Lourenço et al., 1998) near the present diffuse triple junction…..**9**

Chapter II: Previous studies on the Azores Area

Figure II. 1. The Azores plateau. ……**16**

Figure II. 2. Evolution of the Iberian plate since anomaly M0 (~118 Ma) to anomaly C6 (~23 Ma) modified after Srivastava et al. (1990). ……..……**19**

Figure II. 3. Evolution of the Azores Triple Junction proposed by Krause and Watkins (1970). ……**20**

Figure II. 4. Evolution of the Azores Triple Junction according to Searle (1980). …...……**21**

Figure II. 5. Simplified sketch of successive stages of development of East Azores fracture zone and Azores Triple Junction from Searle (1980). ……..……**23**

Figure II. 6. Reconstruction's of the Eurasia and Nubia plate motions considering a fixe North America plate, after Gente et al. (2003). ……**24**

Figure II. 7. Evolution of the Azores Triple Junction after Luis et al. (1994). The thick black lines indicate the MAR axis. ……**25**

Figure II. 8. Distribution of 3He/4He ratios in Azores volcanic fluids and rocks. ……..**29**

Figure II. 9. Cross section of velocity anomaly at latitude 38° and longitude 27°W from the SMEAN tomographic model (Becker and Boschi, 2002). ……**31**

Figure II. 10. Cross-section of S-wave velocity along the MAR passing through the Azores. ……**33**

Figure II. 11. P-wave velocity model from Yang et al. (2006) obtained from finite-frequency tomography using 3-D travel-time sensitivity. ……**34**

Figure II. 12. Travel times computing from Silveira et al. (2010). ……..**35**

Figure II. 13. Magnetic anomaly map of Luis et al. (2008). ……**36**

Figure II. 14. Schematic reconstructions of the relative movement between the MAR and a hotspot located under the Azores and centred under Terceira Island (Gente et al., 2003)…**37**

Chapter III: Construction and destruction of a volcanic island developed inside an oceanic rift: Graciosa Island, Terceira Rift, Azores

Figure III. 1. Bathymetric map of the Azores region, after Lourenço et al. (1998)……...**44**

Figure III. 2. Geological map from Gaspar and Queiroz (2005), an previous ages in ka from Féraud et al. (1980) and Larrea et al. (2014) on Graciosa island. ……..……**45**

Figure III. 3. 3D bathymetric map viewed from the west and from the east. ……**45**

Figure III. 4. Gravity around Graciosa showing a flat platform in the south and cross section across the platform. ……**46**

Figure III. 5. Direction slope map of Graciosa island, cross section across the island and slope map of Graciosa in degrees. ……..……**47**

Figure III. 6. NW-SE sea cliff on the NE coast of the island, below the Quitadouro cone, with interpreted volcanic stratigraphy. ……..……**48**

Figure III. 7. E-W sea cliff at Baia do Filipe, with interpreted volcanic stratigraphy……**48**

Figure III. 8. NW-SE sea cliff of Serra Dormida, with interpreted volcanic stratigraphy..……**49**

Figure III. 9. Main stratigraphic units distinguished in this work, with the location of ours samples. ……..…**51**

Figure III. 10. Proposed evolution of the Baia do Filipe and Serra Dormida complexes along the E-W sea cliff at Baia do Filipe. ……..**53**

Figure III. 11. New schematic morphostructural evolution of the Graciosa Island. ……..…**54**

Chapter IV: São Miguel Island

Figure IV. 1. Bathymetric map of the Azores region from Lourenço et al. (1998).. ……**61**

Figure IV. 2. Elevation map of S. Miguel built from a Digital Elevation Model (DEM) with a 10 m spatial resolution. Ages measured with various methods and techniques in previous works are shown. ……..……**63**

Figure IV. 3. Maps of S. Miguel generated from the high-resolution DEM. ……..……**66**

Figure IV. 4. Topography of eastern S. Miguel with the location of our new samples. Cross sections show the main volcano-stratigraphic relationships and the schematic position of our samples. ……..……**67**

Figure IV. A1. W-E costal cliff on both sides of Faial da Terra. See Fig. IV. 2. for the precise location of the general picture. ……**69**

Figure IV. A2. Southern costal cliff of Furnas volcano composed of alternating surge, pumice and cinder. ……..**70**

Figure IV. 5. 3D view of Fogo seen from the south. The cross-sections highlight the irregular topography of the area. ……**72**

Figure IV. A3. Outcrop comprising boulders of different nature (from basalt to trachyte) in a cinder matrix. The debris sit on a thin cinder layer without boulders. ……**73**

Figure IV. 6. 3D view on the eastern part of S. Miguel, obtained by superimposing the satellite image over the high resolution DEM. The new K-Ar ages are shown. ……..…**77**

Figure IV. 7. High-resolution bathymetry of the southeastern part of S. Miguel. ……**79**

Figure IV. 8. N-S seismic profile offshore Povoação showing the stratigraphy of mass-wasting deposits sourced in Nordeste. The rugged seafloor is here interpreted as a flank collapse deposit. Notice the presence of kilometre size blocks. ……**81**

Figure IV. 9. E-W distal seismic profile offshore south of Nordeste. Notice the length of the lateral deposit and the absence of reflections at the bottom of the lenticular flank collapse deposit. ……**82**

Figure IV. 10. E-W seismic profile further south. ……..…**83**

Figure IV. 11. N-S seismic profile south of Faial da Terra canyon, showing the stratigraphy of mass-wasting deposits offshore Nordeste. Note the presence of volcanic cones……...**84**

Figure IV. 12. Aeromagnetic map of S. Miguel from Miranda et al. (2013). ……**87**

Figure IV. 13. Proposed schematic morphostructural evolution of S. Miguel. ……..**89**

Figure IV. 14. Shaded relief map of the western part of S. Miguel. ……..…**92**

Figure IV. 15. (A) Bathymetric map of the Azores. (B) Free–air gravity field map of the Azores Archipelago (Catalão, 2006; Catalão and Bos, 2008). ……**107**

Figure IV. 16. Shaded relief map of S. Miguel generated from a high-resolution DEM (10 m) showing the main volcanic edifices and tectonic structures as defined by Moore (1990)….**109**

Figure IV. 17. Slope map of S. Miguel generated from the high-resolution Digital Elevation Model (DEM) with dip of lava flows measured during our fieldwork. ……..…**111**

Figure IV. 18. (A) Map of the newly measured faults and dikes for the eastern part of S. Miguel displayed over a high resolution shaded relief map. B) Computation of great circles and pole to planes (Wülff net, equal angle lower hemisphere projection) of the faults, dikes and stress tensor for zones 1, 2, 3 and 4. N is the numbers of measurements in each zone. ……..…**112**

Figure IV. 19. Set of N-dipping normal faults along the eastern end of the island. Location of the outcrop is shown in Fig. IV.16. ……**115**

Figure IV. 20. Example of fault surface materialising the southern wall of the graben newly recognized in Água Retorta. It has a N115 strike and dip from 60 to 65º NE, and sub-vertical striations (black dashed lines). ……..**117**

Figure IV. 21. W-E sea cliff to the west of the village of Povoação (see Fig. 2 for location). The black lines indicate the dip of the Lava flows (LF). ……**118**

Supplementary material Fig. IV. A5. W-E sea cliff to the east of the village of Povoação. ……**119**

Figure IV. 22. Location of the main recognized structures on S. Miguel. ……..**121**

Figure IV. 23. (A) Zoom on the 3D bathymetry near S. Miguel (bathymetry from Lourenço et al., 1998). (B) is a NE-SW cross section through the basin west of S. Miguel; (C) is a N-S cross section of the basin east of S. Miguel. ……..……**123**

Figure IV. 24. (A) Schematic scenario for the pre-rifting stage of the TR, and for the opening of the Terceira Rift without spreading (B) and with spreading (C), respectively. ...……**124**

Supplementary Material. Figure A4. Clean version of the shaded relief map of S. Miguel generated from a high-resolution DEM (10 m). ……..……**137**

Supplementary material Fig. IV. A6. W-E sea cliff to the east of the village of Povoação. See Fig. IV. 16. for location. The faults have been measured with a ca. N150 strike and a dip of 80° to the SW. ……..……**138**

Chapter V: Volcano-tectonic evolution of the Santa Maria Island (Azores): implications for palaeostress evolution at the western Eurasia-Nubia plate boundary

Figure V. 1. Bathymetric map of the Azores (data from Lourenço et al., 1998)……**154**

Figure V. 2. Geological map of Santa Maria adapted from Serralheiro et al. (1987)……...**155**

Figure V. 3. (A) Preferred geological map of Santa Maria, simplified after Zbyszewski and Ferreira (1960) and Serralheiro et al. (1987). (B) Shaded relief map of Santa Maria Island generated from a high-resolution DEM (10 m). ……..…**156**

Figure V. 4. Base of the sea cliff along the SE part of Santa Maria (see Fig. V.3 for location). ……..**159**

Figure V. 5. Sea cliff along the SW tip of Santa Maria, close to Vila do Porto. ……..**160**

Figure V. 6. Stratigraphic relationships between the three main units of Santa Maria and the Facho complex. ……**163**

Figure V. 7. E-W cross-section summarizing our field observations and interpretation. Vertical exaggeration = 20. ……**164**

Figure V.8. Cartoon illustrating the evolution of Santa Maria. ……**165**

Figure V.9. Normal fault dipping to the east (right) cutting the eastern volcanic succession, which we dated in this study between 4.32 Ma and 3.94 Ma. ……..……**167**

Chapter VI: Geological synthesis: implications for the Eu/Nu boundary in the Azores

Figure VI. 1. Current volcano-tectonic model of the Azores Triple Junction and the Eu/Nu plate boundary in Yellow area (after Marques et al., 2013a; 2014a). ……..……**182**

Figure VI. 2. Timelines summarizing the construction stages of the islands to the east of the MAR and active during the last 1.3 Myr. ……..……**185**

Figure VI. 3. Cartoon illustrating the synchronous phases of volcanic construction of the Azores islands localized east of the Mid Atlantic Ridge (MAR) axis. ……..……**190**

Figure VI. 4. Timelines summarizing the known destruction stages on the islands of Faial, Pico, Graciosa, Terceira and S. Miguel during the last 800 kyr. ……..……**191**

Figure VI. 5. Bathymetric map of the Azores and geochronological data on volcanic rocks from the eastern and central islands (Féraud et al., 1980; Costa et al., in prep; Johnson et al., 1998; Calvert et al., 2006; Hildenbrand et al., 2008; 2012b; this study). ……**197**

Figure VI. 6. Upper panel: Simplified map of the Azores archipelago. A, B, C and D show the location of the cross sections shown in the lower panel. (AB) is a cross section along the TR and (CD) is a cross section along the S. Jorge-SMa Graben. ……..……**199**

Figure VI. 7. (A) Free-air gravity anomaly map (contour interval of 20 mGal) from Sandwell and Smith (2009). (B) Bathymetric map of the Azores. ……..……**200**

Figure VI. 8. 3D bathymetry (Lourenço et al., 1998) near the present diffuse triple junction. ……..……**202**

Figure VI. 9. Azores Triple Junction migration model. (A) Vogt and Jung model (2004) based on the plate boundary successive jumps over the Azores hotspot (B) Our new Azores Triple junction migration from subaerial volcanic evidences. ……..……**204**

Chapter VII: Influence of the Central Atlantic geodynamics on the evolution of the Azores

Figure VII. 1. The large dome of low S-wave velocity under the central Atlantic ocean (zoom of Fig. II. 9. in chap.II)……..…**210**

Figure VII. 2. Laboratory experiment from Kumagai et al (2007). ……..…**211**

Figure VII. 3. A) Map of the Azores area. B) Tomographic model of Yang et al (2006) at 112 km (cf Fig. II. 11. of chapter 2). ……..……**212**

Figure VII. 4. Experimental set-up. ……..……**213**

Figure VII. 5. Development of the first plume localized on the copper disk. ……**217**

Figure VII. 6. Evolution trough of the instabilities impacts at the surface. ……**217**

Figure VII. 7. Time evolution of the thermal structures close to the surface of the fluid (Top) and just above the TBL (Bottom). ……**219**

Figure VII. 8. Distance between two instabilities (normalized by the fluid thickness) as a function of the Rayleigh number Ra(H,v(Tm)). ……**220**

Figure VII. 9. Time evolution of the thermal structures of the TBL from the bottom to the surface of the fluid. ……..…**222**

Figure VII. 10. Map of the central Atlantic (from Silveira et al., 2006). ……..…**223**

Figure VII. 11. Plumes spacing (Top) and recurrence time (Bottom) as a function of temperature difference and mantle viscosity. ……..…**224**

Figure VII. 12. Top: Schematic view of the lithosphere thickness in the Azores area as a function of the distance along the MAR and the age of the lithosphere. Bottom: Top view of the area, showing the present-day active zones of volcanism. ……**226**

Figure VII. 13. Morphology and evolution of the impact of a plume on a thickened lithosphere. ……..…**227**

Figure VII. 14. Evolution of the Azores plateau and volcanism during the last 10 Ma……..**228**

Chapter VIII: Conclusions

Figure VIII. 1. Bathymetry of the northern part of the Galapagos islands collected during the FLAMINGO cruise (Modify after Mittelstaedt et al., 2012)……..**238**

List of Tables

Chapter III: Construction and destruction of a volcanic island developed inside an oceanic rift: Graciosa Island, Terceira Rift, Azores

Table III. 1. New K-Ar ages obtained with the unspiked Cassignol-Gillot technique on fresh separated groundmass and alkali feldspars……**50**

Chapter IV: São Miguel Island

Table IV. 1. New K-Ar ages obtained with the unspiked Cassignol-Gillot technique on fresh separated groundmass (Gdm) and alkali feldspars (feld). ……..**74**

Table IV. 2. Results of the P-T method, NDA and inverse method……..**114**

Table IV. S1. Fault and dykes new measurements realized in the present study. Fault kinematics ranges from purely normal (pitch 90°) to normal with strike-slip component…..**139**

Chapter V: Volcano-tectonic evolution of the Santa Maria Island (Azores): implications for palaeostress evolution at the western Eurasia-Nubia plate boundary

Table V. 1. New K/Ar determinations obtained with the unspiked Cassignol-Gillot technique on fresh-separated groundmass. For each sample, the mean age is obtained by weighing by the amount of radiogenic argon. Uncertainties quoted at the 1σ level. ……...**162**

Chapter VII:

Table VII. 1. Physical properties of the sugar syrup and of the mantle……**214**

Table VII. 2. Characteristics of the experiments. ……**215**

CHAPTER I
Introduction

I. Introduction

I. 1. Main motivation

A fundamental tenet of the theory of plate tectonics is that the lithosphere is essentially rigid except at plate boundaries (DeMets et al., 1994; DeMets et al., 2010; Kreemer et al., 2003; LePichon, 1968; Wilson, 1965). Plate boundaries form a global interconnected network. Occasionally, three plate boundaries meet, forming a triple junction (McKenzie and Morgan, 1969; McKenzie and Parker, 1967). The type of motion present on each of the three boundaries and the azimuth of each boundary control the kinematic stability of a triple junction, which is defined by its ability to retain its geometry over time (McKenzie and Morgan, 1969; Patriat and Courtillot, 1984). Of the sixteen configurations discussed by McKenzie and Morgan (1969), combining ridges, transform faults and trenches, only six are presently identified on Earth, and ridge-ridge-ridge (RRR) triple junctions are the most stable. However, several RRR triple junctions display a more complex geologic history than their long-term kinematic stability might suggest (e.g. Bird et al., 1999; Ligi et al., 1999; Mitchell, 1991; Schouten et al., 2008; Searle, 1980; Viso et al., 2005). Diffuse deformation is observed in a number of triple junctions and plate boundaries such as in the equatorial Indian Ocean (Wiens et al., 1985; Gordon et al., 1998), the Sinai Triple Junction (Courtillot et al., 1987), the Juan de Fuca plate (Wilson, 2012); the Chile Triple Junction (Lagabrielle et al., 2000), the India-Capricorn-Somalia Triple Junction (Drolia and DeMets, 2005), or the Azores Triple Junction, a RRR triple junction in the north Atlantic Ocean. The Azores Triple Junction also shows a significant excess in magmatism and an abnormally thick plateau, which cannot be explained only by the geometry and configuration of this Triple Junction between the American, Eurasian and Nubian plates. Moreover, recent GPS data show that the major plate-bounding rifts in the region are not directly connected (Marques et al., 2013a, 2014a). It has also been proposed that the Eurasia-Nubia plate boundary has moved northward by a succession of short-lived rifts (e.g. Vogt and Jung, 2004). Interaction with a hot mantle plume below the Azores was proposed as an explanation for the excess of volcanism in the region (e.g. Vogt, 1976; Schilling, 1985; Gente, 1987; Thibauld et al., 1998; Gente et al., 2003) and for the position of the Eurasia-Nubia rifting (Vogt and Jung, 2004). However, the sequence of rifting events, and the number of successive rifts is still unclear. In this PhD thesis, we investigate how the Eurasia/Nubia plate boundary evolved in space and time in the Azores Triple Junction. We especially use the Azores volcanism as a marker of the main stages of regional deformation. From new geomorphological, stratigraphic, geochronologic, structural/tectonic data, and existing bathymetric and geophysical data, we reconstruct the

successive stages of growth and destruction of selected islands, and discuss their significance regarding the architecture and the evolution Eu/Nu plate boundary. These data are then complemented by fluid dynamic modelling using laboratory experiments to examine the possible links between mantle instability, plate boundary migration and the development of the volcanism on various spatial and temporal scales.

I. 2. The Azores Volcanic Province

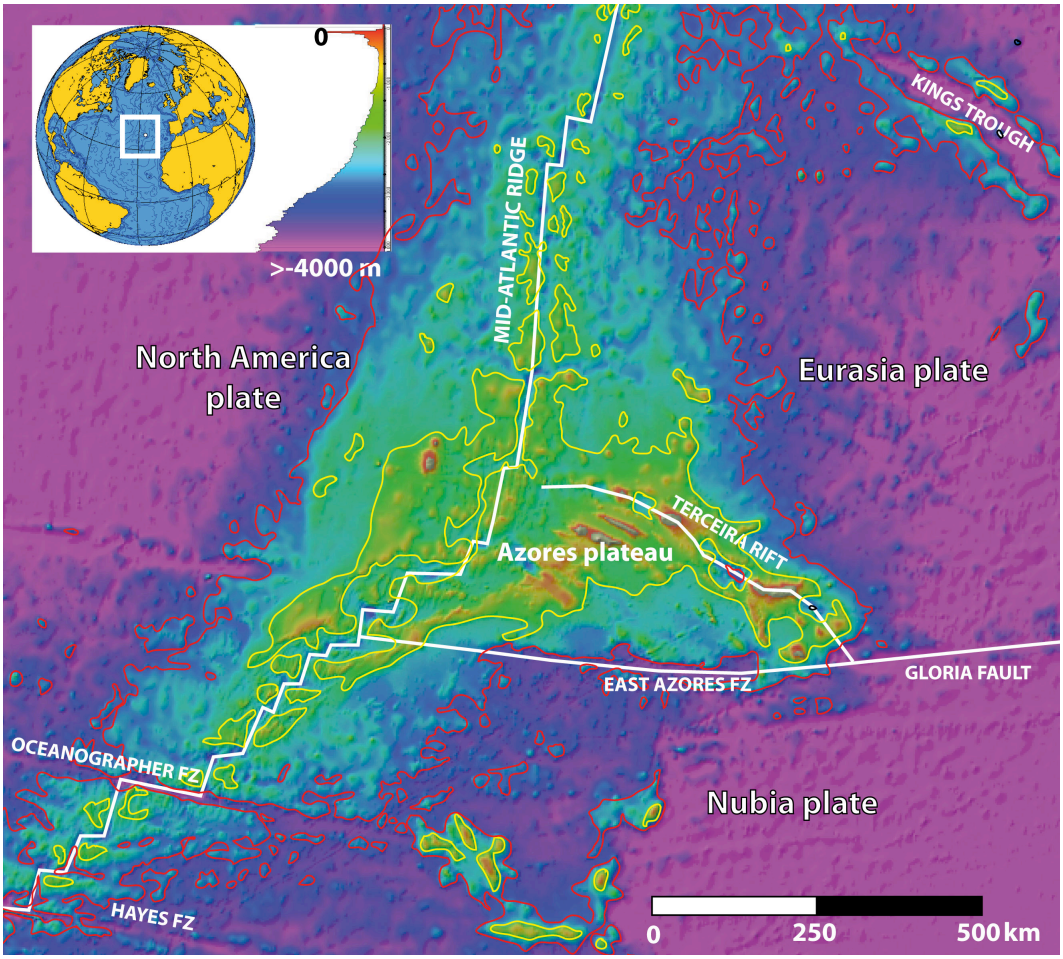


Figure I. 1. Bathymetry of the Azores Plateau with the main morphological features discussed in the text (GeoMap database). The top inset on the left indicates the location of the Azores region. The yellow and the red lines indicate the -2000m and -3000 m isobaths, respectively.

The Azores Archipelago consists of nine volcanic islands, distributed as three groups. The Western group (Corvo and Flores islands) is located on the stable North America plate (NA). The Central (Graciosa, Terceira, S. Jorge, Faial and Pico islands) and the Eastern (S. Miguel and Santa Maria islands) groups lie in the Eurasian (EU) / Nubian (NU) plate boundary area. The Azores islands represent the emerged area of an elevated portion of the seafloor usually referred to as the Azores plateau. This platform is classically defined by the

2000m isobath (Lourenço et al., 1998) and is related to an excess of volcanism/magmatism (Fig. I.2). The Azores region is also characterized by a strong and asymmetric geoid anomaly, which encompasses a larger area than the 2000m isobaths, extending further south-westward along the ridge than it does north of the Azores plateau (e.g. Goslin et al., 1998). A similar asymmetry is also evidenced from the geochemical data collected along the Mid-Atlantic ridge (e.g. Dosso et al., 1999). Thus the Azores region presents a triangular shape, whose western side is located west of the Mid-Atlantic Ridge (MAR). It is limited to the south by the East Azores Fracture Zone (EAFZ), and to the northwest by the Terceira Rift (TR) (Machado, 1957).

Within the Azores plateau the volcanism is localized along two general trends. The first one, closely follows the Terceira Rift and ranges in orientation between N110 and N150. The second trend is closer to NE-SW i.e., parallel to the MAR (Fig. I.1), and reveals an episode of enhanced magmatism along the MAR. Such excess magma production likely reflects the interaction between a buoyant mantle instability (either due to temperature or to a high volatile content, or to both), designated as the Azores "hotspot"-, and the MAR (Cannat et al., 1999; Escatin et al., 2001, Gente et al., 2003).

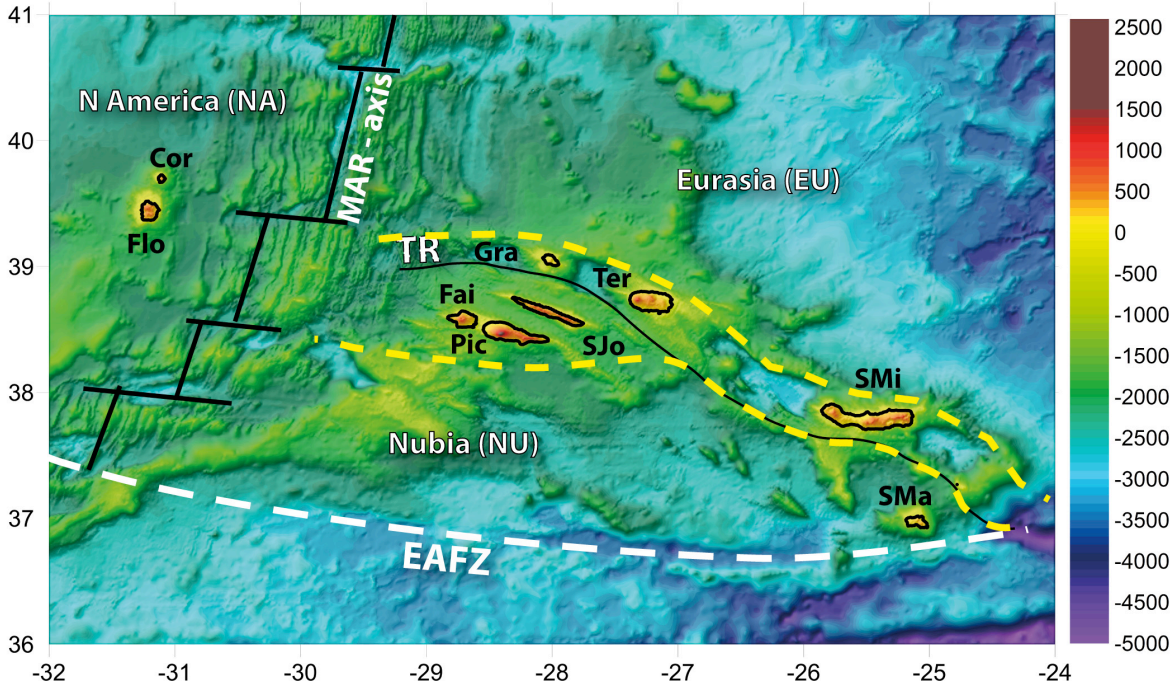


Figure I. 2. Bathymetry of the Azores Archipelago from Lourenço et al. (1998). The thick black lines indicate the location of the Mid-Atlantic Ridge (MAR) axis. The white dashed lines mark the East Azores Fracture Zone (EAFZ). The yellow dashed lines mark the current Eurasia/Nubia plate boundary (after Marques et al., 2013a, 2014a). The thin black lines indicate the southern wall of the Terceira Rift. The -2000 m isobathymetric is defined by the deep green color. Cor: Corvo; Flo: Flores; Fai: Faial; Pic: Pico; Gra: Graciosa; Ter: Terceira; SJo: S. Jorge; SMi: S. Miguel; SMa: Santa Maria.

The precise location of the MAR (Fig. I.2), which forms the boundary between the North American and Eurasian/Nubian plates, is reasonably well known, particularly after the efforts developed to map the ridge system in the Azores area. In contrast, the nature of the boundary between the Eurasian and Nubian plates, its location and segmentation pattern, the evolution of this triple junction and the way in which tectonic and volcanic processes interact within the plate boundary zone, remain unclear.

The westernmost part of the plate boundary between Eurasia and Africa is presently characterized by oblique extension within the ultra-slow oceanic Terceira Rift, which links the MAR to the Gloria Fault (GF). The spreading rate across the TR, amounts to 4 mm/yr in average along a N75E direction (Euler rotation pole located at 19.5°N, 23.7°W, (DeMets et al., 1994; DeMets et al., 2010). However, the direction of motion predicted by the global kinematic model does not account for the orientation of all the structures and their variations from south to north (Lourenço et al., 1998). A combined study of GPS, seismic and tectonic data (Marques et al., 2013a; 2014a) showed that the EU/NU boundary coincides with the TR in the east but is diffuse in the west, where deformation is distributed along several horsts and grabens comprising the TR, the S. Jorge, and the Pico-Faial grabens (Fig. I.3).

The internal structure of the plateau (Figs. I.2 and I.3) displays a coherent structure of linear volcanic ridges developed along fissure systems roughly aligned sub-parallel to the TR (Lourenço et al., 1998). The TR axis presents a marked clockwise rotation from N110-120° near its intersection with the MAR to directions closer to N140-150° at its intersection with the GF. These directions appear to characterize also the geometry and the tectonic patterns on the Islands and in the extensional basins between them, as well as some elongated volcanic ridges (e.g., Hildenbrand et al., 2008). Guest et al. (1999) suggested that the conical volcanic edifices are emplaced at the intersection of tectonic structures with both directions. In particular, the Furnas volcano on S. Miguel Island, developed in such a tectonic setting.

During the Quaternary, extended volcanic activity has been distributed over most of the Azores Islands. The Central and Eastern Azores Islands, especially, have recorded significant historical activity, except Santa Maria. The most recent volcanic activity occurred on the Serreta ridge (Luis et al., 1999), northwest of Terceira Island.

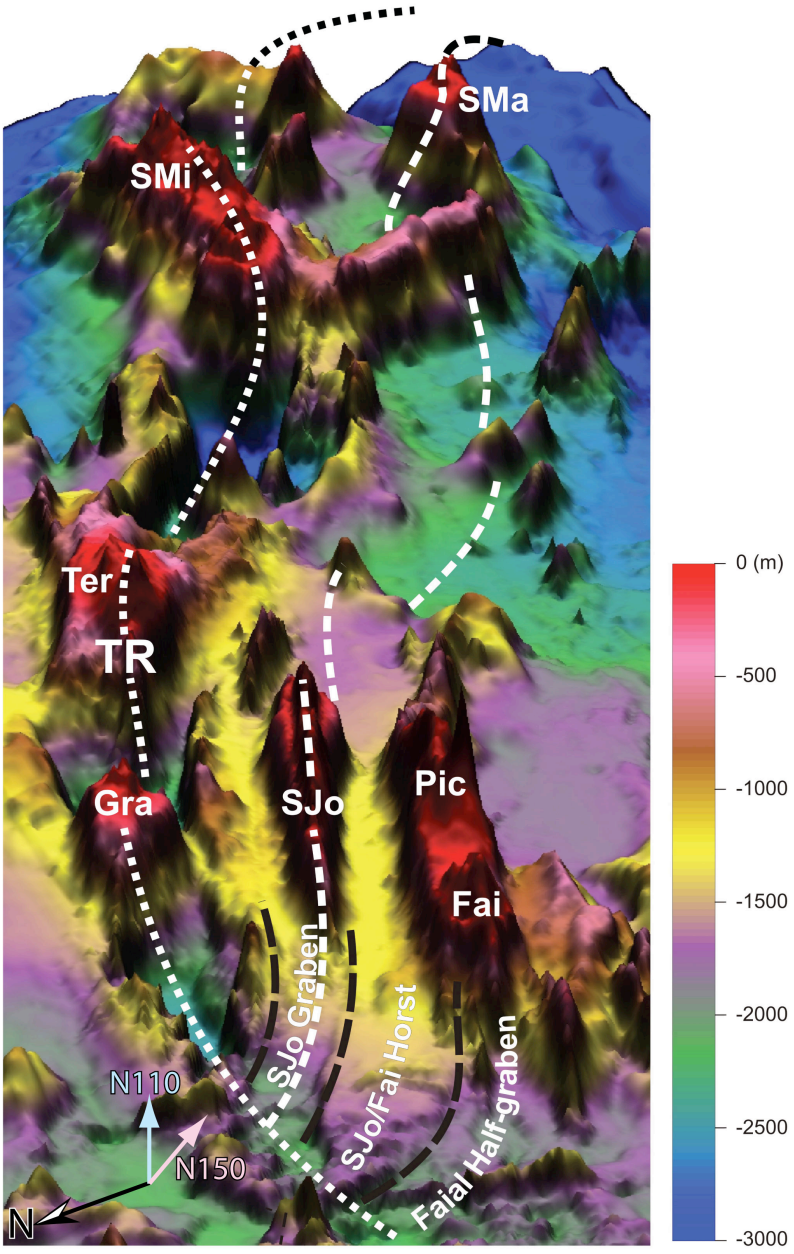


Figure I. 3. 3D bathymetry (Lourenço et al., 1998) near the present diffuse triple junction. The dashed lines define graben boundaries.

However, the age of the Azores Plateau, the timing of initiation of the TR, and the age of most linear volcanic ridge within the plateau are still largely unknown. Little insight is provided by magnetic anomalies in what concerns island evolution. Available isotopic age determinations show some contradictions, and only provide an upper bound for the age of these structures. Little is also known about the thermal structure (or lithospheric structure) of the TR and the style, the dynamics and the partition between magmatic and tectonic processes, which have shaped the plate boundary and the Azores plateau.

An analysis based on an aeromagnetic survey and the compilation of ship-borne magnetic data of the plateau showed that only the Brunhes and possibly Matuyama magnetic

epochs can be identified in the rift area, even though the magnetic anomalies generated along the MAR are disrupted on the plateau (Miranda et al., 1991; Luis et al., 1994). The lack of older magnetic lineations on either side of the TR suggests that the relative motion between Africa and Eurasia in the westernmost part of the plate boundary was accommodated by extension distributed across the plateau rather than by accretion focused along the Rift or that the rift is too young to create significant new oceanic crust. Several major questions on the kinematics and the dynamics of the area are therefore still unresolved:

Has the kinematic setting of the plateau boundary and of the triple junction changed with time, and how? How do ultra-slow extensive rifts (TR) and the EU/NU plate boundary evolve in space and time?

Is the NA-EU-NU Triple junction clearly a ridge-ridge-ridge junction? In other terms, is there significant seafloor spreading along the three branches of the TJ, especially along the TR? If so, when did it possibly start?

How has the relative motion between Nubia and Eurasia been accommodated in the westernmost part of the plate boundary? Was the EU/NU plate boundary diffuse in the recent past?

What is the architecture of the TR in the eastern boundary? How do lithospheric and asthenospheric processes control the development of the volcanism and plateau near such plate boundary and triple junction?

How do the local and regional stresses affect the morphology and the evolution of the islands? How do the construction and the destruction of volcanic island evolve in an active oceanic rift? And in a diffuse plate boundary?

The Azores is a particularly suitable area to study tectono-magmatic interactions in space and time and at different scales. It comprises the existence of significant upper mantle anomaly: the Azores hotspot which is considered the main intervening factor for the formation of the Azores volcanic plateau. The internal structure of this plateau can be explained by the interaction through time of the Azores hotspot with both the MAR and the Azores Triple junction. Significant consequences of this interaction are the position, kinematic and related tectonic response of the Azores Triple Junction, the distribution of magmatic contribution for lithospheric structure and thermal structure of the Azores plateau.

More precisely, we will take advantage of the close interactions of tectonics and volcanism to track the main regional deformation through the evolution of three key volcanic islands. Graciosa Island is localized both in the diffuse plate boundary and in the TR and can provide us information on the interaction between these two close structures. S. Miguel Island is localized in the TR. The eastern part of the island has grown on the northern

shoulder of the TR and the central and western parts have grown inside the TR. This unique position allows to study through tectonic markers (faults and dikes) the style and distribution of the deformation taking place across an active rift and across the EU/NU plate boundary. Finally, Santa Maria Island is the oldest of the Azores islands and seems to have developed independently of the current EU/NU plate boundary. Furthermore, it sits close to the junction between the older EAFZ and the current TR plate boundary. In addition, the island has been active for several Myr and thus recorded a story that no other island in the Azores can tell.

Based on Geomorphological analyses, fieldworks investigations (close to 3 months, on three islands), stratigraphic and structural analyses, measurement of faults and dikes, high resolution K-Ar dating and fluid dynamics approach, we will:

(1) propose a new evolution of the construction and destruction of Graciosa, S. Miguel and Santa Maria islands,
(2) integrate all the informations from these islands to propose a scenario of the evolution of the current EU/NU plate boundary and the TR,
(3) propose a new geodynamic scenario of the EU/NU plate boundary migration during the last 20 Myr,
(4) and explore the link between Azores volcanism and instabilities in the lower and upper mantle underneath.

Chapter 2 describes previous works on the geodynamics of the Azores volcanic region. The excess of volcanism, the construction, the shape and the evolution of the Azores Plateau and islands are probably due to the interaction between two key processes, the Azores Triple Junction resulting from plate tectonics kinematics and the Azores Hotspot resulting from melting of a buoyant mantle instability (often referred to as a mantle plume). After a description of the main regional geodynamic features and their locations, we therefore present the different plate tectonic kinematic models already proposed for the EU/NU plate boundary in the literature. Then, we shall review the models focussing on the interaction of a mantle plume and the Azores Triple Junction.

In **Chapter 3,** we investigate the successive stages of construction and destruction of Graciosa Island. From DEM analysis, fieldwork and recognition of the volcanic stratigraphy, K-Ar dating and Bathymetry and gravity data, we discuss the nature of the destruction events occurring in Graciosa, and we identify a new N50 trend newly recognized and discussed in the Azores.

Chapter 4 is focussed on the S. Miguel Island and it is separated into two parts. The first one depicts the morpho-structural evolution of the island, based on high-resolution DEM data, fieldwork and structural investigations, and high-precision K-Ar dating on separated

mineral phases. We discuss the architecture of S. Miguel and propose a morpho-structural evolution of the island. Through the nature of the volcanism and the elongation of S. Miguel, we will also discuss about the tectonic control on the island. In the second part, from structural analysis and new measurements of 350 faults and dikes, we investigate the architecture of the Terceira Rift through the tectonic marker measured on S. Miguel and their concentrations along the S. Miguel Island. We estimate also the TR initiation time from simple geometry calculation.

Chapter 5 introduces the key role of Santa Maria Island in the reconstruction of the position of the old EU/NU plate boundary. We will propose a new evolution model of the island.

Chapter 6 is a geological synthesis taking into account the previous and current work conducted on the other islands. We discuss the implication of the volcanism along the TR and the EU/NU during the last Myr and identify a probable former plate boundary between the EAFZ and the TR.

Chapter 7 presents a new geodynamics evolution of the Azores Triple Junction in the broader context of the plume cluster region of the central Atlantic. Using fluid mechanic laboratory experiments, we investigate the spacing and time-dependence of a cluster of secondary plumes developing above a lower mantle instability, the surface interactions between secondary plumes, and the interaction between an upwelling plume and the thickened crust/lithosphere of the Azores. We propose a new evolution of the Azores area.

A summary of the main conclusions is the subject of the last part of the PhD thesis. Recommendations and guidelines for further work is also present in this last part.

CHAPTER II
Previous studies on the Azores Area

II. Previous studies on the Azores Area

This chapter describes the previous works on the geodynamics of the Azores volcanic region. The excess of volcanism, the construction, the shape and the evolution of the Azores Plateau and the Azores archipelago are most likely due to the interaction between two key processes, the Azores Triple Junction resulting from plate tectonic kinematics and the Azores Hotspot resulting from melting of a buoyant mantle instability (often referred to as a mantle plume). After a description of the main regional features and their location, we therefore present the different models proposed for the EU/NU plate boundary in the literature. Then, we review the models focusing on the interaction of a mantle plume and the Azores Triple Junction.

II. 1. The main structures of the Azores

The Azores archipelago is located in the Atlantic Ocean. It stands between North America and Europe, roughly between from 37°N to 40°N latitude and between 25°W and 31°W longitude, about 1500 km from Portugal (Fig. II.1). It is constituted of 9 volcanic islands, 7 of which are considered as currently still active. The Central Azores is the present-day location of the Triple Junction between the North America (NA), Eurasia (EU) and Nubia (NU) tectonic plates (Laughton et al., 1972). Flores and Corvo islands are anchored in the NA plate, whereas Graciosa, S. Jorge, Faial, Pico, Terceira, S. Miguel and Santa Maria are placed close to the boundary between NU and EU plates.

The Azores islands have developed on top of a thick plateau with a general anomalously shallow triangular-shaped topography, corresponding to an area of about 400-000 km^2 of shallow oceanic seafloor (Fig. II.1). The plateau is limited by Flores and Corvo islands west of the MAR axis, and by the East Azores Fracture Zone (EAFZ) in the south. The northern limit of the plateau roughly follows the strike of the Terceira Rift. It has a WNW-ESE trend close to the MAR, then passes north of the Graciosa, Terceira and S. Miguel islands, and connects to the western limit of Gloria Fault (GF – Laughton et al., 1972; Argus et al., 1989). Between latitudes 37°N and 41°N, the topography of the MAR flanks shows an attenuated roughness when compared to a normal ridge segment: the ridge axis, itself, is shallower or subded, and the crust is believed to be twice as thick as in the surrounding oceanic area (Luis et al., 1994). This plateau was formed in the last 20 Myr and has been attributed to the interaction between a mantle plume (hot spot) and the Mid-Atlantic Ridge (MAR) (e.g. Cannat et al., 1999; Gente et al., 2003).

Based on an aeromagnetic study of the MAR, Luis et al. (1994) showed that the central positive anomaly defining the axis of the MAR is offset by several discontinuities. The major ones correspond to N110 Fracture Zones often referred to as MAR transform faults (Fig. II.1). Forjaz, (1988), and later Miranda et al. (1991) and Luis et al. (1994) proposed the existence of a separate Azores microplate at least from 10 Ma to 3.85 Ma, with motion of this microplate as part of the Eurasian plate during the last 2.45 Myr. According to these authors the Azores plateau is currently part of the Eurasia plate.

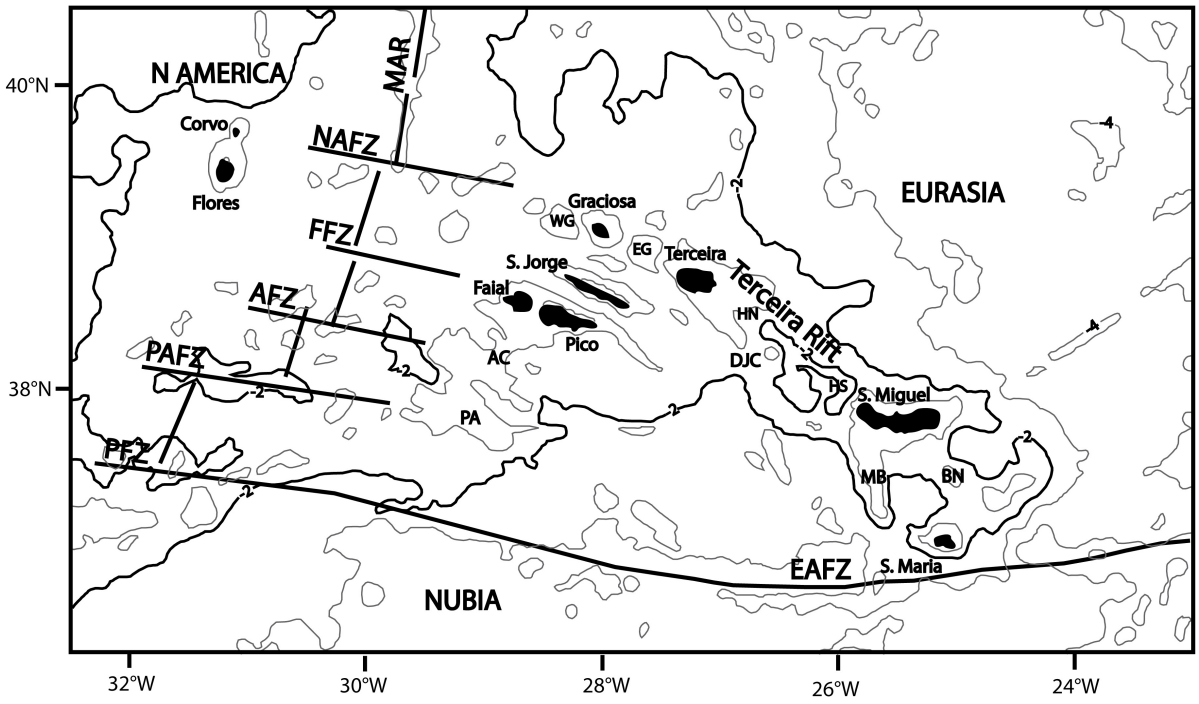


Figure II. 1. The Azores plateau. Bathymetric data from Lourenço et al. (1998) contours each 1 km. The dark contour indicates the – 2 km isobath. EAFZ : East Azores fracture Zone; MAR : Mid Atlantic Ridge ; PFZ : Pico Fracture zone ; PAFZ : Princess Alice Fracture Zone ; AFZ : Azor Fracture Zone ; FFZ : Faial Fracture Zone ; NAFZ : North Azores Fracture Zone; PA: Princesa Alice Bank; AC: Açor Bank; WG: west Graciosa basin; EG: east Graciosa basin; HN: Hirondelle north basin; DJC: João de Castro seamount; HS: Hirondelle south basin; MB: Monaco Bank; BN: Big North.

After almost half a century of intense data collection (bathymetry, magnetism, gravity, seismicity, volcanism, geochemistry, geodesy, and tectonics), several structures were identified in the Azores region. Most of them were recognized from a morphological analysis of the seafloor in the region (Krause and Watkins, 1970; Searle, 1980; Lourenço et al., 1998; Gente et al., 2003; Luis and Neves, 2006). By compiling different bathymetric data available for the Azores region, Lourenço et al. (1998) published a map with the morpho-structural pattern of the Azores area, combined with other results from seismology and neotectonics (Fig. II.1). Several structures were thus identified:

- The Mid Atlantic Ridge materializes the present boundary between the NA plate on the west side and the EU and NU plates on the east side. This divergent and accreting structure, with an axial rift valley, shows an orientation close to N10 north of the Azores and an average orientation NE-SW south of the Azores. Such a change in strike is believed to be the result of a clockwise rotation along MAR transform faults of small pieces of the rift striking in the range N10-N10W.

- The Terceira Rift comprises an alignment of deep basins, islands, and seamounts. It has a orientation ranging between N110 to N130. The rift includes the west Graciosa basin, Graciosa island, the east Graciosa basin, Terceira island, the Hirondelle north basin, the D. João de Castro seamount, the south Hirondelle basin and S. Miguel Island.

- The Gloria Fault is a major submarine lineament and is presently characterized by recurrent large earthquakes. This structure globally behaves as a transform fault with right lateral strike slip.

- The East Azores Fracture Zone corresponds to the segment of the Azores-Gibraltar Fault between the MAR and the meridian 24°30'W, i.e. west of the active Gloria fault. The EAFZ does not show seismicity anymore (Laughton et al., 1972) and is thus considered to be inactive. It materializes a relic of the NU/EU plate boundary.

Despite several on-land and offshore studies, the understanding of the past and recent evolution of the stress regime and kinematics of the EU/NU boundary remains a matter of debate and controversy. Most of the complexity of the Azores region is intrinsically associated with the ongoing kinematics of the TR. Part of the controversy comes from the orientation and magnitude of the stress/strain field regime in that region and where to place the actual boundary between EU and NU.

II. 2. The different kinematic models for the Azores Triple Junction

Two main types of interpretative models can be found in the literature: those which are based on constraints given by global kinematics thus providing plate tectonic reconstructions of the previous geometry of the triple junction (Krause and Watkins, 1970; McKenzie, 1972; Searle, 1980; Luis et al., 1994), and those that address particular aspects of the Azores tectonics, based on morpho-tectonic analysis (Madeira and Ribeiro, 1990; Lourenço et al., 1998; Vogt and Jung, 2004), isotopic dating (e.g. Abdel-Monem et al., 1975; Féraud et al., 1980; Hildenbrand et al., 2008), focal mechanisms and earthquake epicentre distributions (Miranda et al., 1998; Borges et al., 2007) and GPS observations (e.g. Fernandes et al., 2004, 2006; Marques et al., 2013a, 2014a).

II. 2. 1. Triple junctions in the central Atlantic prior to 20 Ma: from King's Trough to Gloria Fault

In regional studies comprising the kinematic evolution of the Atlantic basin and the evolution of the Gloria fault, the complex behaviour of the Iberian microplate is generally problematic. Some models consider that Iberia has moved independently from the two larger plates (Galdeano et al., 1989; Srivastava et al., 1990; and Roest and Srivastava, 1991). However, the analysis of the kinematic behaviour of the Iberian micro-plate is limited by the lack of prevalent magnetic lineations, and difficulties in following the trace of Fracture Zone between the North American Plate (Na) and Iberia (Campam, 1995).

About 400 km NNE of the Azores (Fig. I.1), King's Trough forms a submarine relief of more than 3500 m. It consists in a series of parallel or sub-parallel troughs linked en echelon by cols and flanked by ridges. This structure has been interpreted as marking the older Eurasia-Nubia plate boundary and/or Eurasia/Iberia plate boundary, and therefore it would correspond to one of the arms of the Na/Nu/Eu triple junction (Srivastava et al., 1990; Roest and Srivastava, 1991; Srivastava and Roest, 1992). According to previous studies, King's Trough complex was first initiated as a fault, without spreading (between 80 and 68 Ma or between 62-58 Ma for Srivastava et al., 1990 and Kidd and Ramsay, 1987, respectively). This fault was later reactivated as a propagating rift, created by extensional motion across the plate boundary from 37 Ma (Srivastava et al., 1990) or from 17 Ma to 9 Ma (Srivastava and Roest, 1992).

From magnetic anomalies of the seafloor and tectonic considerations, Srivastava et al. (1990) proposed the following evolution for Iberia motion from mid-Cretaceous to the present. The active seafloor spreading along the MAR started at the end of the mid-Cretaceous (since anomaly M0, 118 Ma, Fig. II.2), and in the Bay of Biscay the north Iberian margin formed a triple junction. The E-W plate boundary in the Bay of Biscay between Eurasia and Iberia became the main plate boundary north of King's Trough. The plate boundary was extensional between anomalies 33 (~80 Ma) and 31 (~68Ma) and then became the locus of strike slip until anomaly 21 (~46 Ma – Fig. II.2). After anomaly 19 (41.4 Ma) Iberia detached progressively from the African plate, with the development of a southern Iberian plate boundary defined by the Gloria fault. The unstable configuration of the triple junction led to its southward migration and the opening of the King's Trough at the time of anomaly 17 (ca. 37 Ma). Then, compression between Iberia and Eurasia in the Pyrenean domain and the change in motion of Iberia yielded the individualization of two new plate boundaries (anomaly 13 at 33 Ma, Fig. II.2): one linking King's Trough and the Azores-Biscay Rise to the North Spanish Trough and the Pyrenees, and the other to the south located along the present

Azores-Gibraltar Fracture Zone. The northern boundary was gradually abandoned and differential motion between Eurasia and Iberia plate nearly ceased at anomaly 10 (~28 Ma). At anomaly 6c (23.4 Ma – Fig. II.2), activity in the King's Trough ceased completely and Iberia became attached to the Eurasian plate. Only one triple junction remained active at the Azores latitude and the NU/EU plate boundary was then constrained along the Gloria fault. This model has been disputed as it presents several inconsistencies with inland geology, namely with respect to the Pyrenees tectonic history, where major key events are documented prior to 37.5 Ma.

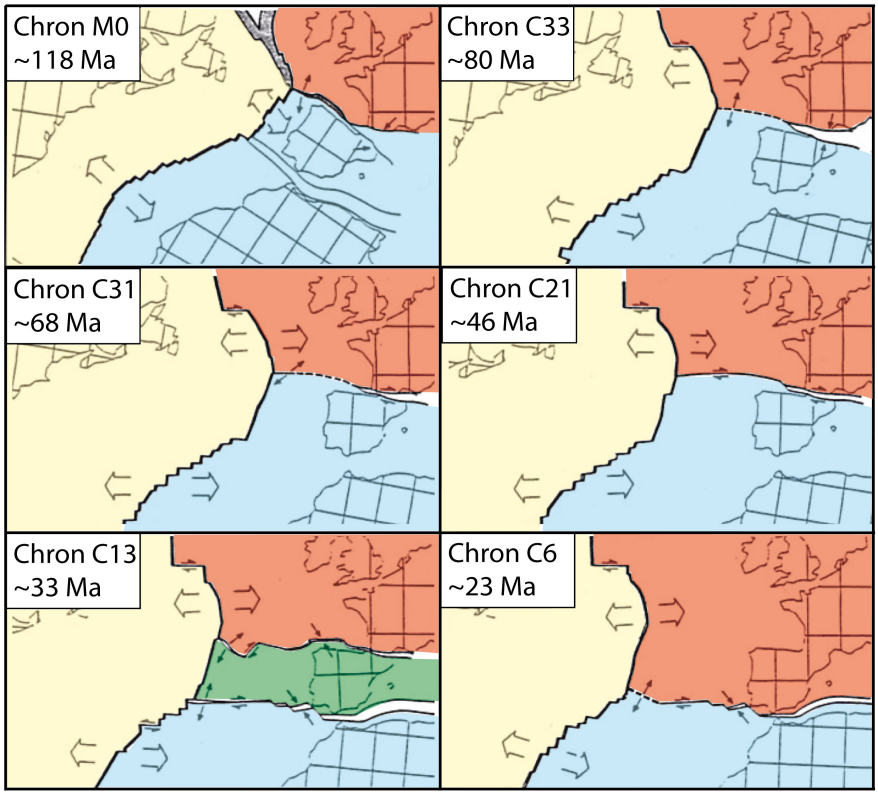


Figure II. 2. Evolution of the Iberian plate since anomaly M0 (~118 Ma) to anomaly C6 (~23 Ma) modified after Srivastava et al. (1990). The yellow, red, blue and green areas indicate the North America, Eurasia, Nubia and ephemera Iberia plates, respectively.

The transition between the strike slip fault and the rifting has been attributed to an extended period of igneous activity between 32 Ma and 20-16 Ma (Kidd, 1982; Kidd and Ramsay, 1987), which has been related to the activity of a mantle plume. However, the age of the plume-related volcanism varies greatly depending on the authors: around 26 Ma (Vogt and Avery, 1972), between 56 Ma and 28 Ma (Searle and Whitmarsh, 1978; from bathymetric seismic ad gravity studies), or between 59 and 26 Ma (Mello, 1999).

The Azores plateau presents the same degree of uncertainty in terms of age and

kinematics. Its evolution seems to have been marked by a transfer from the African to Eurasian megaplates, behaving sometimes as an independent block. Understanding the behaviour of the northern (Terceira Rift) and southern (EAFZ) limits of the Azores plateau is therefore crucial for tracing its evolution. Below, we review the attempts performed by different authors to constrain these aspects.

II. 2. 2. The Azores Triple Junction prior to 20 Ma: Gloria Fault to Terceira Rift or to EAFZ?

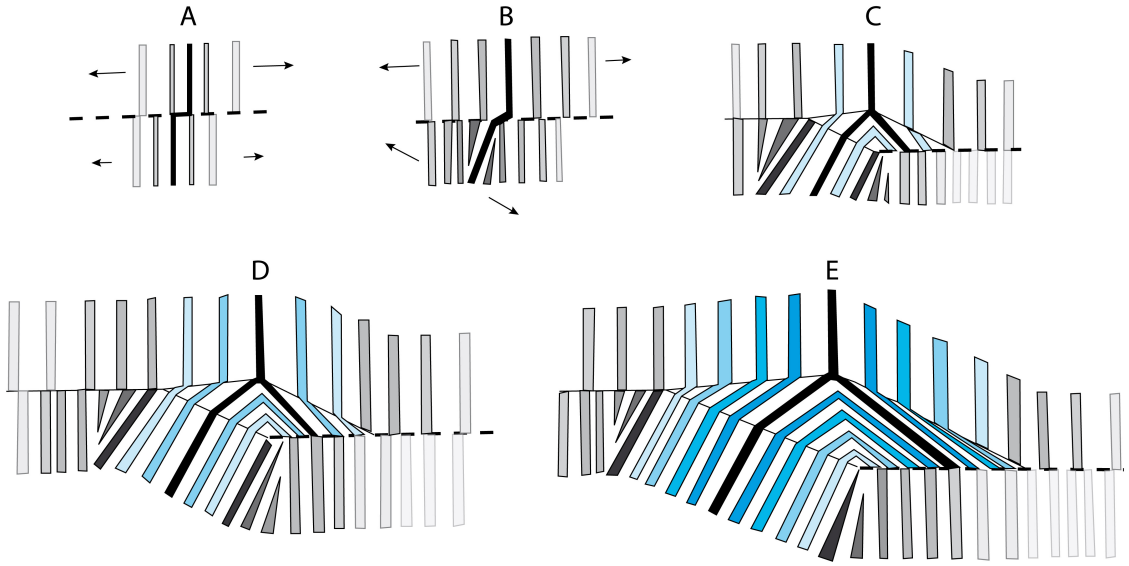


Figure II. 3. Evolution of the Azores Triple Junction proposed by Krause and Watkins (1970). (A) Initial conditions; (B) change in direction of crustal spreading south of the transverse fracture; (C) initiation of the Azores tectonic triangular structure with the initiation of offset of the western fracture system; (D) and (E) show the growth of the leaky transform and the triple junction, and the increasing northern offset of the western quiescent fracture.

Early studies, centred on the characterization of the Azores Triple Junction and the EU/NU plate boundary, were based on sparse ship-borne bathymetric and magnetic data. A first attempt was made by Krause and Watkins (1970) based on the first surface magnetic compilation. They considered a RRR (Ridge-Ridge-Ridge) triple junction type, with oblique spreading on the Eurasia-Nubia plate boundary. According to these authors, such a configuration would have evolved from a RFF (Ridge-Fault-Fault) triple junction with migration of the MAR westwards, south of the EAFZ and change in the spreading direction from E-W to ESE-WNW. This re-orientation of the spreading direction would additionally result in the creation of a Leaky transform in the Azores Triple Junction third arm, which

would ultimately facilitate the formation of the Terceira Rift as a secondary spreading center. These authors make no particular assumptions regarding the stability of the proposed configuration but attribute an age of at least 45 Ma for the beginning of the Terceira Rift leaky transform (Fig. II.3).

McKenzie (1972) reviewed critically this first model and discussed for the first time the stability of the Azores Triple Junction. His model is nevertheless very similar to that of Krause and Watkins, (1970) as it considers an evolution of the Azores Triple Junction from an initial RFF configuration originating at the junction between the MAR and the EAFZ. Northward migration along the MAR of this triple junction would result in the formation of two oblique spreading centers and a RRR type triple junction (Fig. II.4). McKenzie (1972) considered that the Triple Junction is stable through time provided that all three branches would spread obliquely. Contrary to the previous works, this model precludes any change in the spreading direction but as noted by McKenzie (1972), it would imply a tendency for the Azores Triple Junction to migrate northward.

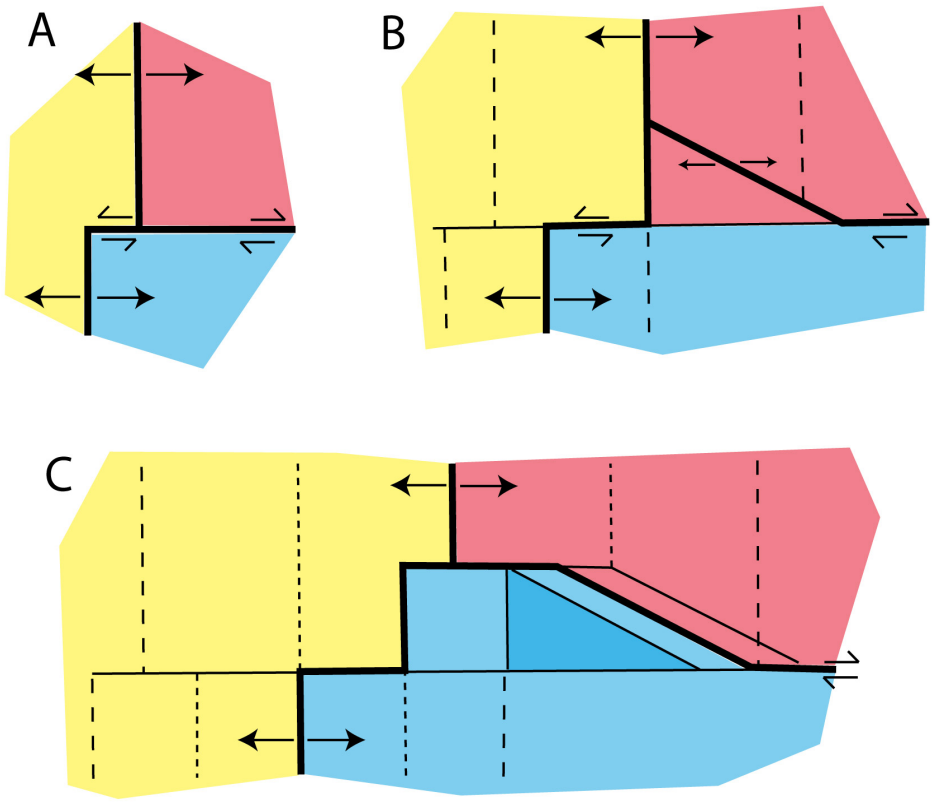


Figure II. 4. Evolution of the Azores Triple Junction according to Searle (1980). The NA, EU and NU are indicated in yellow, red and blue, respectively. (A) Initiation of the Azores Triple Junction as a RRF type; (B) The Triple Junction jumps from the MAR/EAFZ towards the north; (C) The oblique Azores spreading centre cuts the Azores plateau off the EU plate and adds it to the Nu plate.

The first strongly documented kinematic work on the Azores was presented by Searle (1980), using ship-borne magnetic and sonar mosaics along the Gloria. Searle re-evaluated the previous interpretations and defined a first overall segmentation pattern in the Terceira rift. According to this interpretation (Fig. II.5), the Azores Triple Junction evolved, again from the EAFZ intersection with the MAR, as a RFF (Ridge-Fault-Fault) configuration, to a position defined at the intersection between the Terceira Rift and the MAR at the North Azores Fracture Zone, due to a sudden northward jump of the triple junction. A triangular section of the lithosphere generated on the Eurasia side would thus be cut by the opening of Terceira Rift, and transferred to the African plate. Searle (1980) was reticent in assuming that the present ATJ position was on the NAFZ, because of the orientation of this Fracture zone with respect to predicted directions of opening between Eurasian and African plates (closer to ca. N58°E). Given the tectonic fabric interpreted from the sonar images and the recent volcanic activity, Searle (1980) did not exclude that the Triple Junction could be located further south around 38° 40' N in the region west of Faial. This author further considered the Terceira Rift as a spreading center. However, given the numerous linear ridges running sub-parallel to the Terceira Rift, Searle (1980) did not exclude the possibility that true sea-floor spreading generating Azores crust could be limited. And so the Azores would represent a rift zone with a complex architecture resulting probably from a mixture between crust generated previously at the MAR and newly created oceanic crust along pre-existing tectonic structures. Finally, Searle (1980) provided an estimate of the age of the Triple Junction migration and of the opening of the Terceira Rift: assuming that the TR spreading has remained constant, equal to 3 mm/yr, over the whole TR history, the present-day width of the spreading center (along the spreading direction) therefore gives an age of 55 Myr as an upper bound. However, Searle proposed that 36 Myr is a more realistic age for the generation of the Terceira Rift, as it would coincide with changes between the African and Eurasian plates relative motion (Fig. II.5).

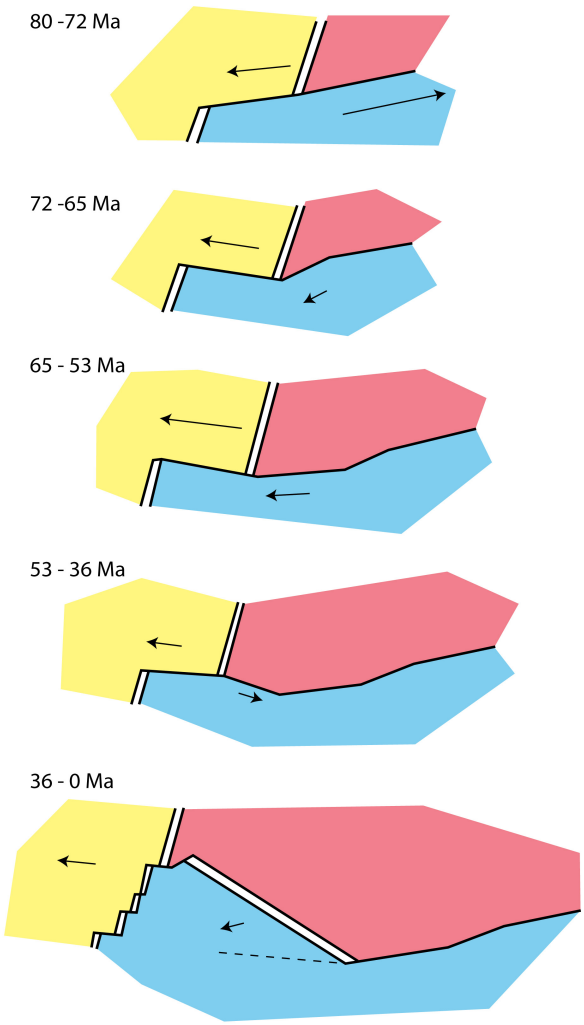


Figure II. 5. Simplified sketch of successive stages of development of East Azores fracture zone and Azores Triple Junction from Searle (1980). The NA, EU and NU plates are shown in yellow, red and blue, respectively.

II. 2. 3. The Azores Triple Junction in the last 20 Myr

Based on residual topography and magnetic chrons, Gente et al. (2003) reconstructed plate motion of the Eurasia and Nubia plate by closing the successive magnetic strips generated by seafloor spreading at the MAR-axis (Fig. II.6). This reconstruction indicates that the oceanic floor under Santa Maria is older than 35 Myr. However, the topographic anomaly is asymmetric, as the plateau extends much further to the east than to the west. If created by excess volcanism at the MAR axis, the plateau should not stop abruptly at one plate boundary and should not be concentrated along one arm of the TJ. Therefore, part of the plateau under Santa Maria may have been emplaced after 35 Ma. From the data of Gente et al. (2003), it seems also that most of oceanic crust under the Azores archipelago was generated between 20 and 10 Ma on both sides of the MAR-axis. In their reconstruction (Fig. II.6), this period also coincides with the northward jump of the ATJ from the EAFZ to the TR.

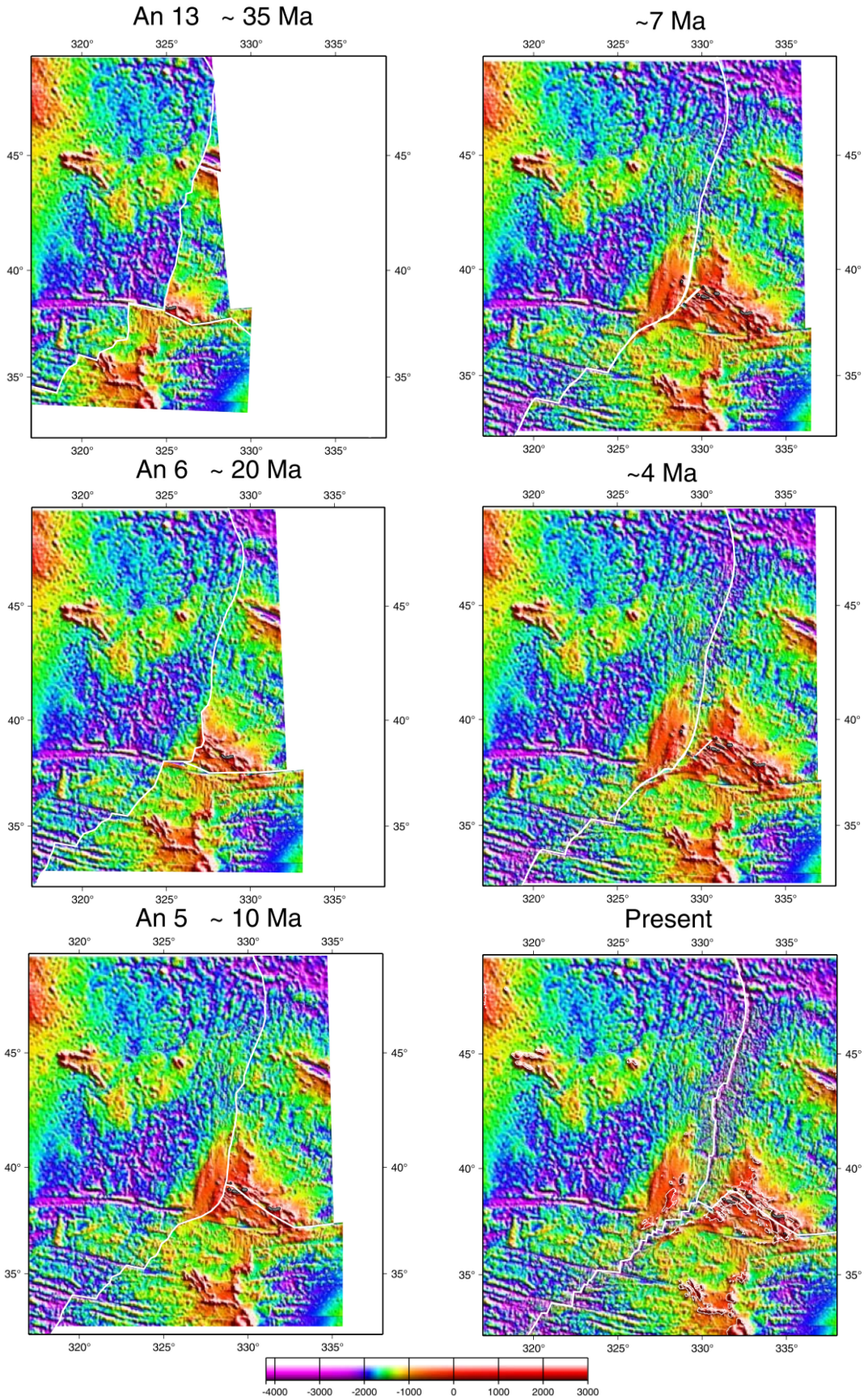


Figure II. 6. Reconstruction's of the Eurasia and Nubia plate motions considering a fixed North America plate, after Gente et al. (2003).

From a high-resolution aeromagnetic chart of the Azores Plateau (Fig. II.7), Miranda et al. (1991) and Luís et al. (1994) performed a highly detailed kinematic analysis of the Azores Triple Junction confined to the last 10 Myr. It revealed the recent evolution of the segmentation pattern of the MAR and in particular several northward migrations of the Eurasia-Nubia-North America triple junction, from a past location near 37° N up to its present location west of the Pico-Faial alignment. Their proposed evolution comprises the existence of an independently moving Azores block detached from both Eurasian and Nubia plate from Chron 5 to Chron 3 (~10 to 3.85 Ma). During this time span, two triple junctions were active at the northern and southern boundaries of the block. They could only constrain the position of the southern one initially at 38°00'N, 38°50'W and gradually jumping north to 38°20'N, 30°15' W between C4 (8 Ma) and C3A (6 Ma). At C2A (2.45 Ma), the ATJ reaches its current position at 38°55'N, 30°00'W (Luís et al., 1994). From that time on, they consider that the Azores block has been moving attached to the Eurasian plate.

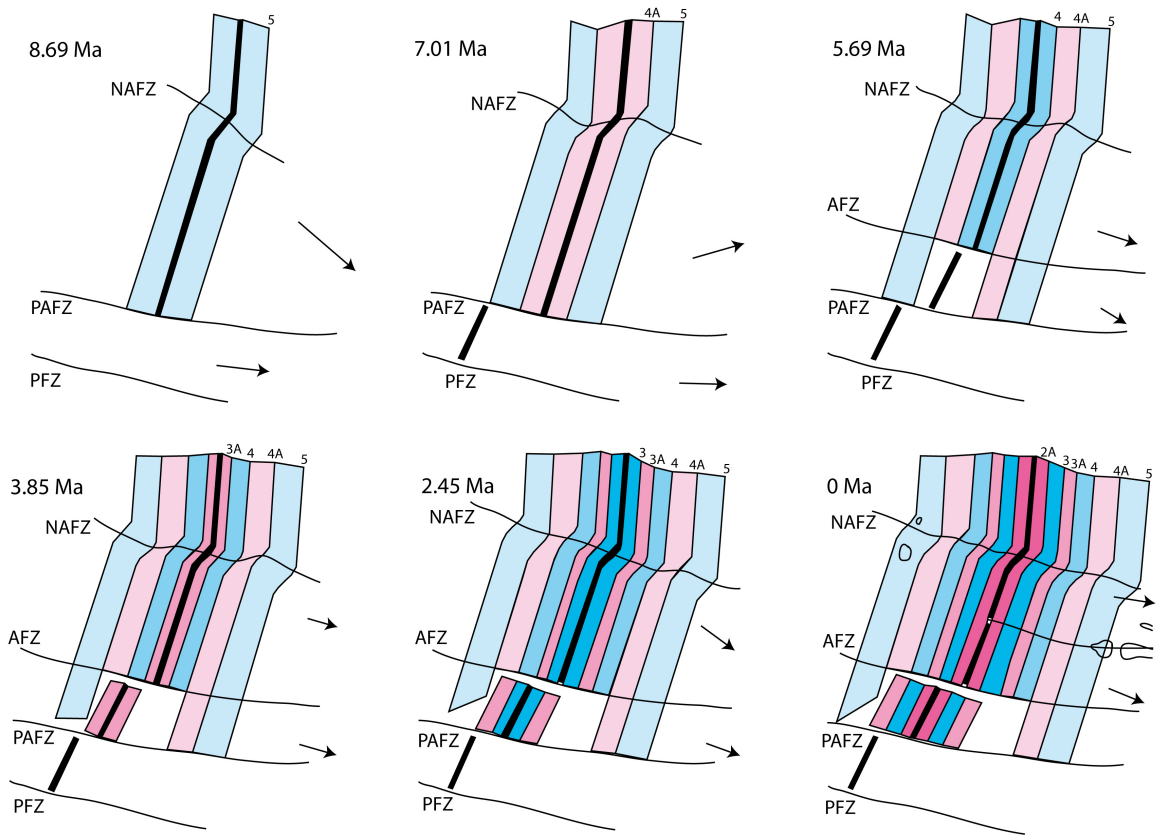


Figure II. 7. Evolution of the Azores Triple Junction after Luis et al. (1994). The thick black lines indicate the MAR axis. The arrows represent the velocity of the Azores and NU relative to the NA. NAFZ: North Azores Fracture Zone; PAFZ: Princess Alice Fracture Zone; PFZ: Pico Fracture Zone; AFZ: Azores Fracture Zone.

This analysis was however based on plate tectonic reconstructions with respect to the MAR, and little can be inferred about the tectonic implications of their proposed Azores Triple Junction evolution within the plateau. For example, the northward migration of the southern Azores Triple Junction implies that some amount of internal deformation should exist within the Azores block, and also that sections of the lithosphere in the Azores block have possibly been transferred to the African plate, as also suggested by Searle (1980). Lack of constraints on the kinematic behavior and position of the northern Azores Triple Junction from the past until anomaly 2A, limits the ability to understand the evolution of the ATJ during that period. Similarly, the locus and the behaviour of the ATJ during the last 2.85 Myr remain poorly constrained.

From recent GPS and tectonic data, Marques et al. (2013a; 2014a) have shown that the present ATJ is diffuse. They especially show that the present deformation along the western end of the EU/NU plate boundary is distributed along a series of horsts and grabens, extending 150 km SW of the TR. In such conditions, the study of the recent volcanism developed over the plateau (Eastern of the MAR) constitutes a key opportunity to track the recent evolution of the ATJ, and examine the links between mantle dynamics and lithospheric processes.

II. 3. The Azores volcanism and its mantle source

In the previous section, we considered the behavior of the Azores Triple Junction as a function of time. However, the ATJ also coincides with the Azores plateau. The latter was most likely formed by intense magmatism, which has been interpreted by several authors (e.g. Vogt, 1976; Schilling, 1985; Gente, 1987; Thibauld et al., 1998; Cannat et al., 1999; Gente et al., 2003) as a result of the interaction of a mantle plume ("hotspot") with the MAR. Absolute plate motion supports the creation of the Azores plateau by successive NE jumps of the TR to maintain its position over a fixed "hotspot" (e.g. Gripp and Gordon, 2002; Vogt and Jung, 2004). Although these authors suggest a ridge-hotspot interaction, the size, depth and precise location of the mantle anomaly at the origin of the volcanism is still greatly debated. We will thus now consider the different models describing the Azores "hotspot". The nature and dynamics of this mantle instability and the variations of the magma flux to the plateau are of key importance to understand the Azores geodynamic evolution and to resolve issues such as:

1) the existence and style of hot spot track paths across the plateau;

2) the present-day position and extent of the Azores hotspot;

3) the spatio-temporal distribution of magma generation and the constraints on the age of the plateau, its inner structures and their relation with the Azores Archipelago Islands;

4) the degree of interaction with the Azores Triple Junction evolution through time, and therefore

5) the relation with past and present plate boundary configuration between Eurasian and Nubian plates, the current location and the tectonic style of the Azores Triple Junction. Many of these points remain controversial or unanswered, even between those who agree on the existence of the Azores mantle plume.

II. 3. 1. Thickness of the Azores platform

One point which remains nevertheless undisputed is that the Azores volcanic platform results from excess in volcanism/magmatism. Accordingly, the crustal structure of the Azores is anomalous. Several published estimates of crustal thickness are available for the Azores Plateau, all indicating a thicker than average crust. Searle (1976) found a thickness of ~8 km for the central plateau using surface-wave dispersion measurements. Using gravity and bathymetry data, Detrick et al. (1995) suggest thickness of <8-9 km, although these calculations attribute the gravity anomaly entirely to crustal thickness variations and hence are likely a maximum estimate. With similar assumptions about the source of gravity anomalies, Gente et al. (2003) found that crustal thickness along the TR exceeds that along the nearby MAR by an upper bound of ~5-10 km, with locally higher values in the vicinity of the volcanic islands. Elastic plate model from Mantle Bouguer anomaly give a crust thicknesses of 9-12 km (Luis et al., 1998). From P and S receiver function Silveira et al. (2010) obtained a crust thickness up to 20-30 km below the islands.

II. 3. 2. Nature of the Azores melting anomaly: a weak and wet hotspot?

The sub-lithospheric causes of the magmatism, which produced the Azores platform and the volcanic islands still remain controversial. An excess in volcanism is often considered to be generated by the presence of hotter mantle underneath, i.e. a “hotspot”. And since hot material is also more buoyant, hotspots are thought to be produced by mantle plumes originating deep in the mantle. In the literature, the word “hotspot” is used for “hot thermal plume”, and vice-versa. Several observations are classically considered as evidence for such interaction between a hot spot and a Mid-ocean ridge: (i) a thermal interaction, resulting in a thicker crust near hot spots, (e.g. White and Schilling 1976; Sleep and Norman, 1990; Goslin et al., 1998; Cannat et al., 1999) (ii) a geochemical interaction, implying a

mixture of depleted mantle sources feeding the mid-ocean ridge and enriched mantle sources feeding the hot spot (e.g. Bourdon et al., 1996; Furi et al., 2009; Goslin et al., 1998), and finally (iii) a dynamic interaction, responsible for the migration of second-order segments away from the hot spot, and of an asymmetry of the accretion processes (Müller, 1998; Hardarson et al., 1997, Small, 1995). Frequent observations of spreading asymmetry and ridge jumps in sections of mid-ocean ridges close to hot spots suggest that mantle flow from the hot spot may control the distribution of stresses in the lithosphere above it (Ito et al., 2003; Mittelstaedt and Ito, 2005). We shall now present the observations for the Azores case.

Geophysical and geochemical anomalies in the Azores platform led to the suggestion that a buoyant mantle plume influences the region. Campaigns of relatively dense sampling reveal geochemical anomalies along the MAR axis (e.g. Schilling, 1975, 1985; Dosso et al., 1993; Yu et al., 1997; Goslin et al., 1998; Goslin et al., 1999). The islands also have been subject of numerous geochemical studies (e.g. Schmincke and Weibel, 1972; Moore, 1990; Widom et al., 1997; Haase and Beier, 2003; Beier et al., 2008; 2010; 2012; Hildenbrand et al., 2014). The subaerial volcanoes typically eject alkaline basaltic lavas as well as more differentiated lavas, and are strongly enriched in incompatible elements. The melting below the Azores islands began at about 90 km depth (Bourdon et al., 2005). MORB from the MAR close to the Azores are enriched in incompatible elements and have relatively high Sr, Pb, and He isotope ratios compared to normal depleted MORB (Kurz, 1982; Schilling et al., 1983; Bourdon et al., 1996; Dosso et al., 1999). Values of the isotopic Helium ratios are comprised between 11.2 Ra and 13.5 Ra for Graciosa and Terceira islands respectively. These values are usually interpreted as being characteristic of OIB signatures (Fig. II.8). In contrast, values of 8.5 Ra, 8.0 Ra and 8.5 Ra are obtained on Faial, Flores and Pico, respectively. Those values are typical of MORBs. Finally lower values between 5.2 Ra and 6.1 Ra were measured for São Miguel (Jean-Baptiste and al., 2009). Thus, coupled with a value of 15.9 Ra between the islands of Terceira and Sao Jorge (Moreira et al., 2002), the center of the plume would be in the central part of the archipelago where the He ratio is highest. Highly radiogenic Sr isotopic composition indicates a possible recycling of both highly altered oceanic crust and sediment by old subduction processes (Beier et al., 2012) and a lower $^{206}Pb/^{204}Pb$ indicate an EM like component (Millet et al., 2009; Madureira et al., 2011; Hildenbrand et al., 2014). These indicate that the composition of the mantle source is heterogeneous. The low $^{231}Pa/^{235}U$ measured in S. Miguel is interpreted by Bourdon et al. (2005) as an interaction of the MAR with a mantle plume. In addition, the low $^{230}Th/^{238}U$ ratios indicate an OIB source depleted in ^{238}U. Therefore the geochemistry of major and isotopic elements supports the presence of enriched material in the mantle below the Azores (e.g.

White and Schilling 1976, Turner et al., 1997; Moreira and Allègre, 2002; Madureira et al., 2005; Bourdon et al., 2005, Jean-Baptiste et al., 2009; Beier et al., 2012).

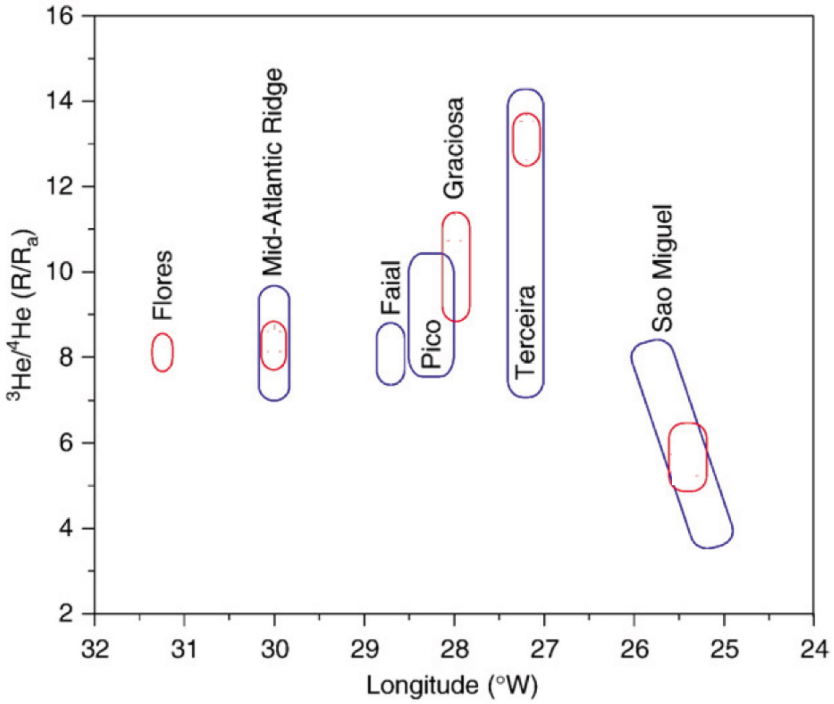


Figure II. 8. Distribution of $^3He/^4He$ ratios in Azores volcanic fluids and rocks. Rock data (Kurz, 1991; Moreira et al., 1999; Madureira et al., 2005) and Gas data (Jean Baptiste et al., 2009) are in blue and red, respectively. The data for the MAR are from Moreira and Allègre (2002).

Another important argument favouring the presence of a thermal plume beneath the Azores is the overall anomalously shallow MAR morphology, an effect which has been relatively well studied (Schilling, 1985; Detrick et al., 1995; Bourdon et al., 1996; Cannat et al., 1999; Escartin et al., 2001). V-Shaped bathymetric ridges extending south of the Azores Triple Junction are similar to features observed along the Reykjanes Ridges near Iceland (Vogt, 1971; Ito, 2001) and may reflect an along-axis melting anomaly pulse (Cannat et al., 1999; Escartin et al., 2001). The influence of a plume-related hotspot on ridge bathymetry and melt production is primarily a function of the plume flux (itself a function of temperature and size of the plume head), mantle viscosity, spreading rate and absolute motion of the ridge with respect to the plume (Ribe et al, 1995; Ribe, 1996; Escartin et al., 2001). Considering the Azores context, Ito and Lin, (1995) calculated values of approximately 70°C for temperature anomalies related with the Azores plume.

However, other evidences suggest that interpreting the anomalies in the Azores region using a classical deep-seated thermal plume hypothesis may be ambiguous. The Azores islands are young and do not form a clear age progression like Hawaii (Beier et al.,

2008). Nevertheless, an age progression is not a good criterion for the Azores because the islands are too young and the velocity of the plate motion is too slow (2 cm/yr, Gripp and Gordon, 2002) for a linear hotspot track to develop. Similarly, although seismic tomography studies generally reveal a shallow-mantle anomaly in the Azores region, the connection to the lower mantle is unclear (see chapter II.3.3, Zhang and Tanimoto, 1992; Courtillot et al., 2003; Montelli et al., 2004; Yang et al., 2006; Silveira et al., 2006).

An alternative explanation to a purely thermal plume invokes a compositional heterogeneity with enriched volatile contents (e.g. Bonatti, 1990; Asimow et al., 2004; Métrich et al., 2014). The enrichment in water of the Azores magmas was recognized by Schilling et al. (1980). This water anomaly was attributed to the recycling of old oceanic crust (Dixon et al., 2002; Beier et al., 2008). The analysis of peridotites sampled along the MAR suggests the presence of mantle domains enriched in H_2O and a lack of significant elevation in mantle temperatures (Bonatti, 1990). These aspects led Bonatti (1990) and Asimow et al. (2004) to propose an alternative model for the excess of magmatism. Bonatti (1990) considered that the volatile content should significantly lower the mantle solidus temperature therefore promoting high degrees of partial melting of a garnet source, without need for a significant mantle temperature anomaly (Asimow et al., 2004). A recent study from Métrich et al. (2014) on melt and fluid inclusions trapped in basaltic scoria in Pico island confirms the presence of a wet spot below the Azores. Gravimetric modelling of the plateau (Luis et al., 1998) and recent application of regional 3D admittance studies in the spectral domain (Luis and Neves, 2006) suggest that the plateau is regionally compensated and its shallow bathymetry is supported by regional lithospheric flexure only. These authors rule out the role of significant dynamic forces maintained by a current mantle upwelling as the cause for the bathymetric uplift.

To summarize, the generation of the Azores volcanism requires the existence of a heterogeneous mantle anomaly, either wetter and/or slightly hotter than normal upper mantle. Since both water and temperature increase the buoyancy of rocks, this mantle anomaly may result from the contribution of a mantle instability (or plume). However, the potential lack of dynamic support of the bathymetry points toward a presently rather weak plume. The question is now from where such a plume could have developed and risen.

II. 3. 3. The deep mantle underneath the Azores

Tomographic models show shallow structures beneath some debated hotspots (e.g. Ritsema and Allen, 2003) and have been used to try and constrain the position of the inferred

Azores plume. However, the description of the Azores plume varies depending on the different techniques and resolution. In the upper mantle, regional surface-wave tomography has a resolution of about 500-800 km (e.g. Silveira and Stutzmann, 2002), whereas body-wave tomography resolution can be better but at few hundreds of km (Foulger et al., 2001).

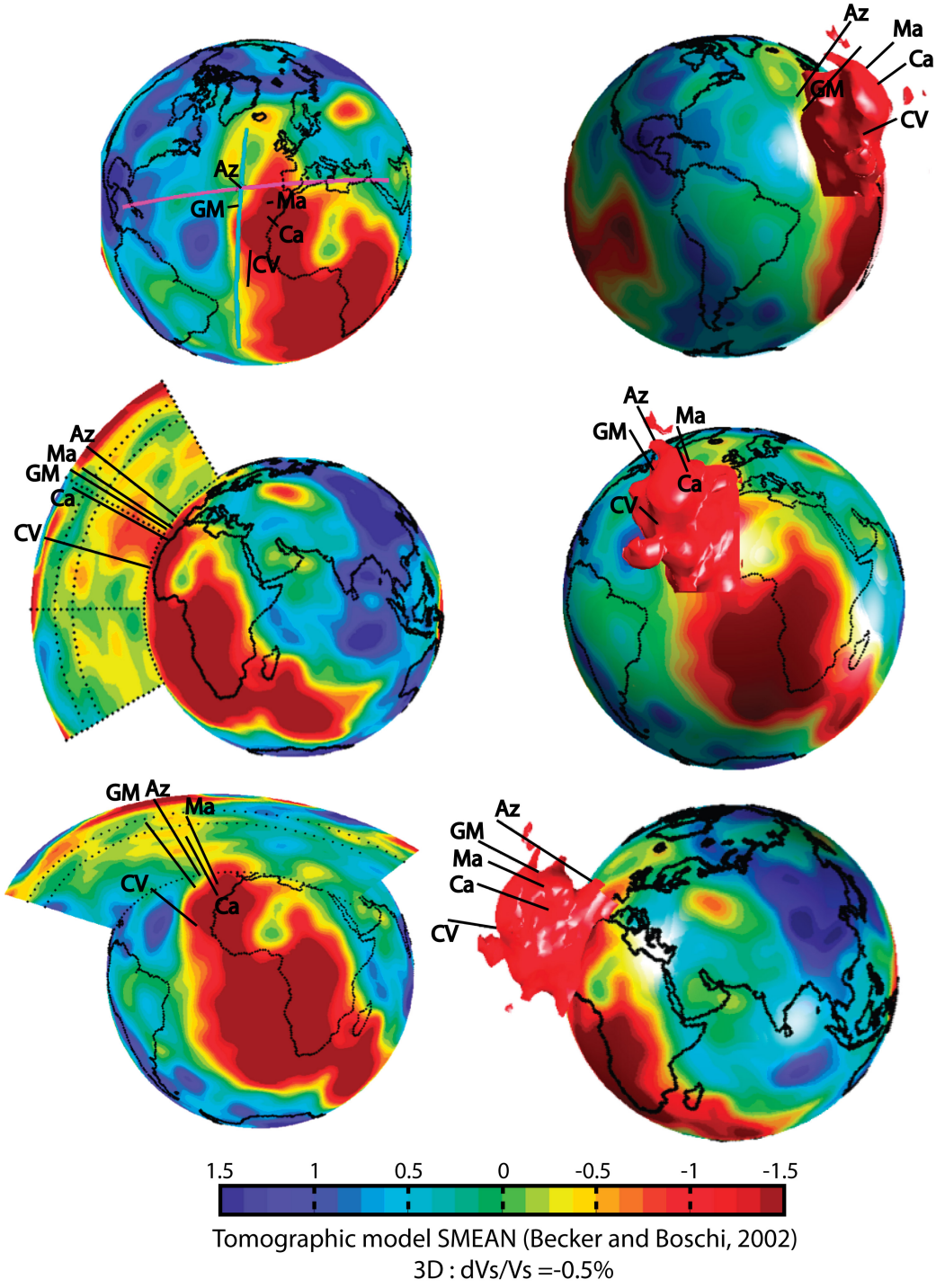


Figure II. 9. Cross section of velocity anomaly at latitude 38° and longitude 27°W from the SMEAN tomographic model (Becker and Boschi, 2002). The lower panel shows a 3D view of the mantle instability. The black lines indicate the position of the Azores (Az), Madeira (Ma), Canary (Ca), Cape Verde (CV) archipelago and Great Meteor (GM) seamounts.

In the Atlantic, the global tomography model by Zhang and Tanimoto (1992) reports anomalously low S-wave velocities marking the hot spot influence in a large area, slightly east of the MAR. S-wave speed tomographic model (Debayle et al., 2005), which uses regional waveforms to image the upper mantle at depths up to 400 km, also shows a negative velocity anomaly. On the SMEAN model constituted from S wave global data, a large anomaly in the lower mantle can be seen (Fig. II.9). Above this large instability, several lower anomalies can also be detected in the upper mantle. Indeed, a mantle anomaly below the Canary islands has been imaged by global tomography (Horn et al., 1995; Goes et al., 1999; Silveira and Stutzmann, 2002; Montelli et al., 2004), and another one below Cape Verde islands (Silveira and Stutzmann, 2002; Montelli et al., 2006; Forte et al., 2010; see Figs. II.9 and 10). Nevertheless, the velocity anomaly is lost in the upper mantle (depths < 200 km).

In other global tomographic models (lateral resolution of about ~1000 km), Montagner and Ritsema (2001) identified two anomalous zones under the axis of the Mid-Atlantic ridge. The first one is characterized by a shallow seismic signature (< 300 km). The second features a seismic signature at least down to the transition zone or even deeper. At the same large scale, P-wave tomographic model inversion suggests a plume propagation throughout the entire mantle (Montelli et al., 2006). These data also suggest the Azores and the Canary plumes merge at 1450 km depth. However, their resolution tests indicate a lack of resolution in the intermediate mantle under the Azores area.

The lack of information between 200 km and 400 km can be partly explained by the limit of detection. Indeed, the size of plume tails can be smaller than the capacity of detection of the global tomography, whereas plume heads are easier to detect. However, Davaille and Vatteville (2005) indicate that the lack of conduit in tomography models could also be the signature of a dying plume, i.e. the plume would not be connected any more with a tail at depth. These authors also indicate that the negative seismic velocity can be produced by either temperature, water content and partial melt or a combination of both, without necessarily the present of a “hot” material.

All the recent models revealed a low velocity zone in the first 200 km below the Azores region. Indeed, Silveira and Stutzmann, (2002) presented a first regional tomographic model with anisotropy retrieved from surface wave velocities. Their model reveals that the Azores-related SV velocity anomaly fades at a depth of 150 km and is not linked with any deeply rooted structure (Fig. II.10). In this model, the Azores plume is associated with velocity anomalies in the order of 4-5%. Silveira et al. (2006) conclude that there is a clearly visible anomaly at 100 km depth but which disappears below 250-300 km depth.

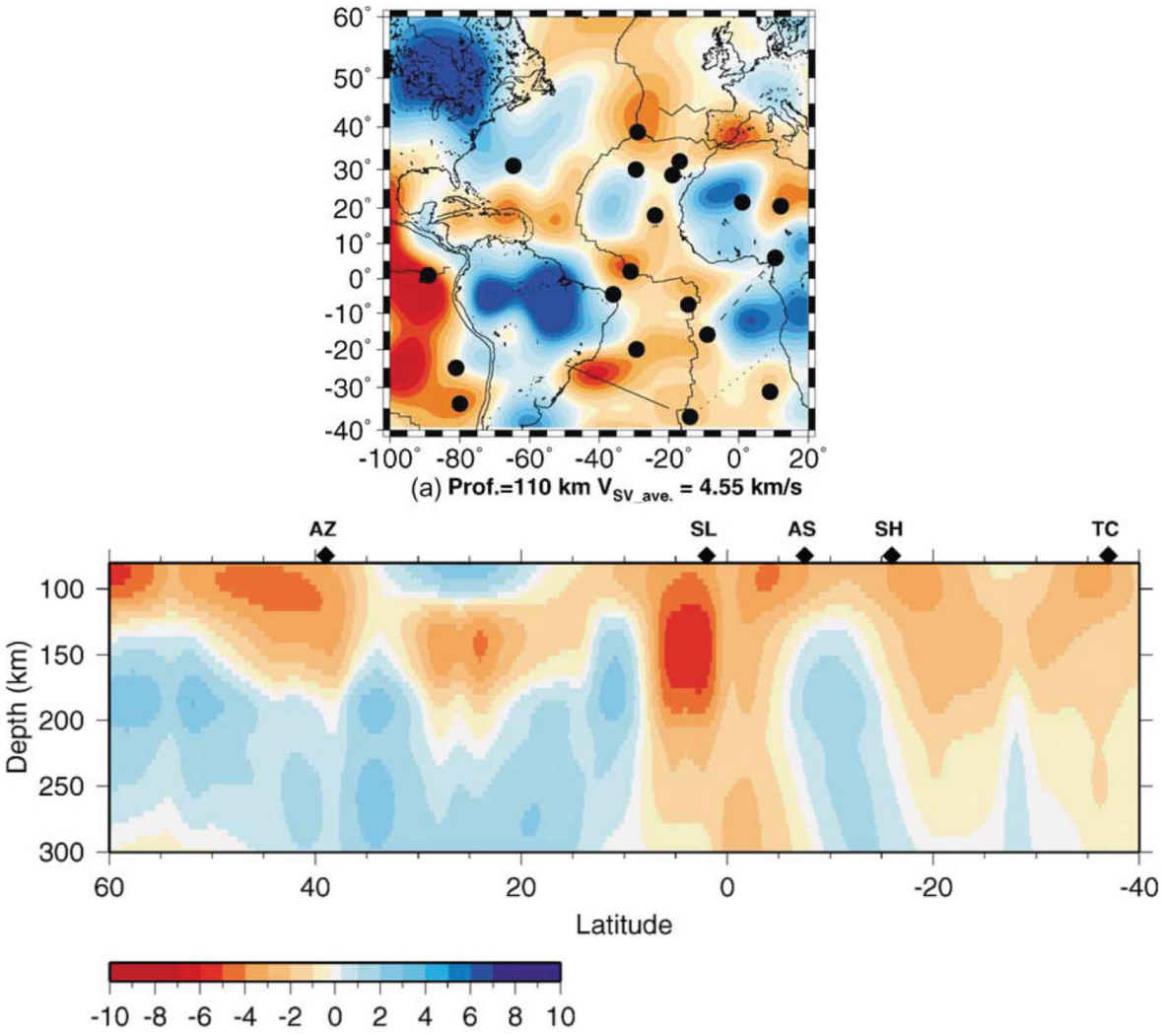


Figure II. 10. Cross-section of S-wave velocity along the MAR passing through the Azores (Az), Sierra Leone (SL), Ascension (AS), Santa Helena (SH) and Tristan da Cumba (TC). After Silveira and Stutzmann (2002), modified.

Using P wave tomography, Yang et al. (2006) also documented a generalized low-velocity anomaly at a depth of ~100 km underneath the Azores. This anomaly is in the order of 2%, and splits into two zones in the shallow mantle. At shallow depths (100- 200 km), this anomaly becomes elongated in NE-SW direction, and at depths from 250 km to 400 km a pipe-like structure NE of Terceira is imaged and interpreted as the present location of the Azores plume tail at depth. On Fig. II.11, we notice that the negative velocity anomaly at 112 km limits a zone with positive anomaly, the negative velocity can be interpreted as a thicker crust or lithosphere.

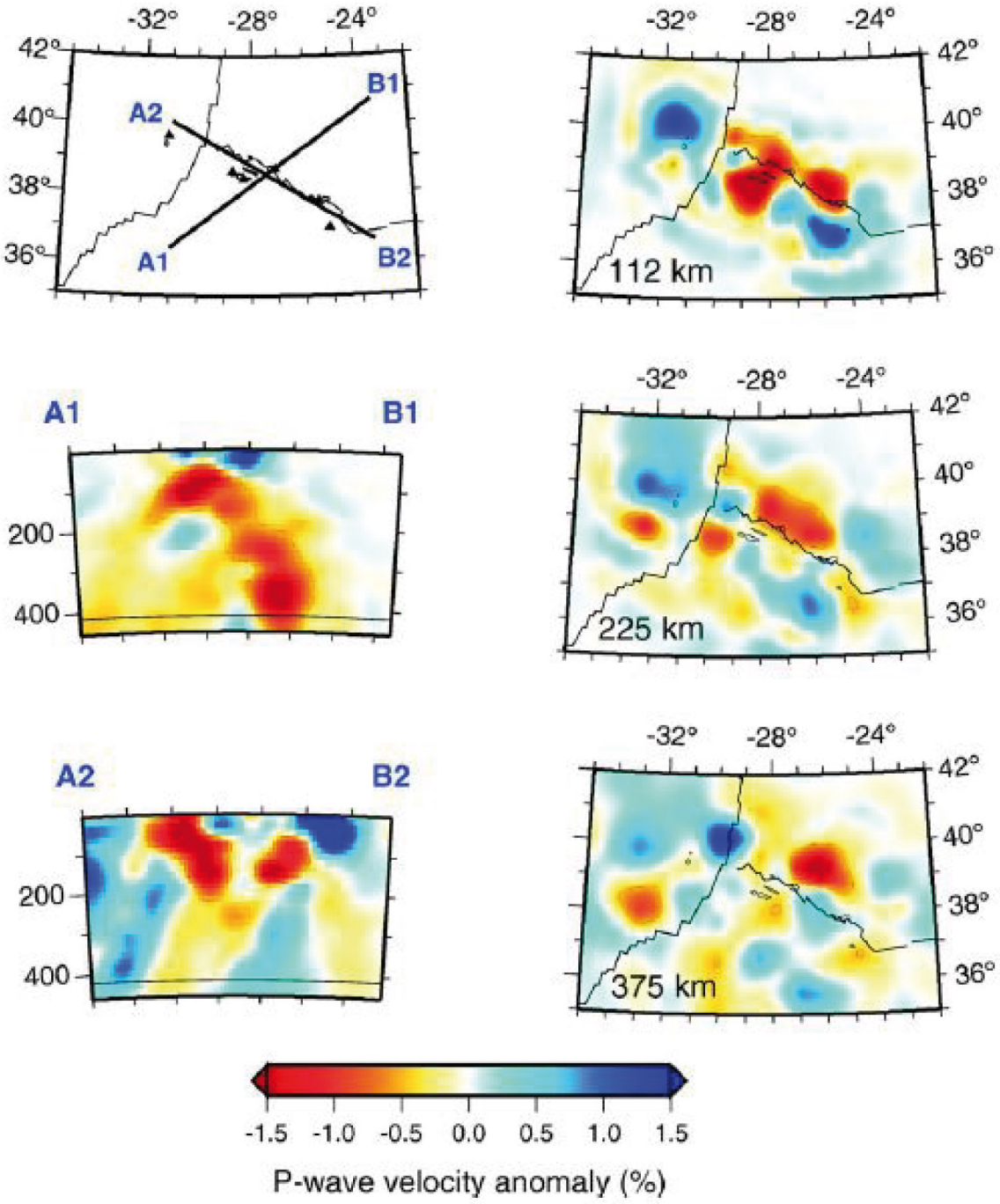


Figure II. 11. P-wave velocity model from Yang et al. (2006) obtained from finite-frequency tomography using 3-D travel-time sensitivity. Notice at depth of 112 km the negative velocity anomaly (red color) bordering a positive velocity anomaly (blue color).

More recently, Silveira et al. (2010) used teleseismic P and S travel time residuals, which give a higher radial and lateral resolution than surface waves and thus better image local/regional anisotropy in the upper mantle. From their velocity model, 4 different zones are distinguished as a function of increasing depth: (1) a low-velocity zone down to 20-30 km, which may represent the thickened crust; (2) a higher S-wave velocity between 30 km and

70-80 km, interpreted as an upper mantle lid (lithosphere?) depleted in fluids and basaltic components; (3) a lower velocity zone from 80 to 150-250 km; and (4) a zone where Vs increases gradually to get closer to a “normal upper mantle” value at a depth of ca. 250 km (Fig. II.12). Silveira et al. (2010) also distinguish a low Vs layer in the transition zone beneath the Azores, roughly between 450 and 500 km deep. They related it to the presence of a large, deep seated mantle plume. The small Vs anomaly in this layer is believed to indicate hydration of the mantle with a water content of ca ~1%.

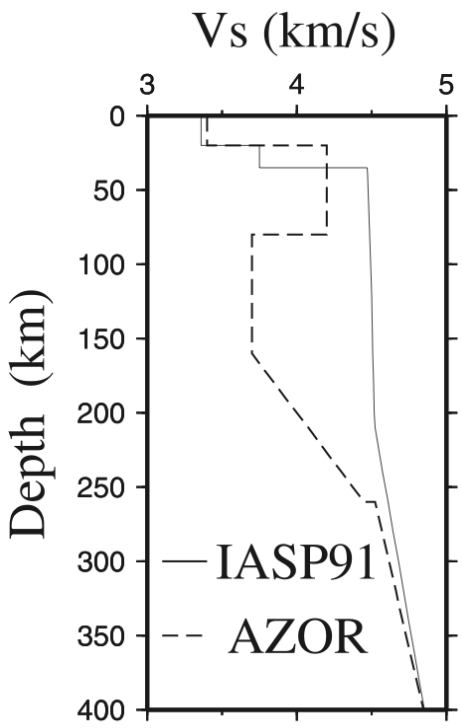


Figure II. 12. Travel times computed by Silveira et al. (2010). IASP91 is reference model parameterised the model of velocity. It has been constructed to be a summary of the travel time characteristics of the main seismic phases (Kennett, 1991).

II. 3. 4. Position of the Azores mantle instability center

Several authors have sought to constrain the position of the Azores plume at depth. Depending on the approaches used, it has been proposed that the plume would be centred either along the MAR (e.g. White et al., 1976), under the Island of Faial (Ito and Lin, 1995, Silver et al., 1998), nearby Terceira Island (Moreira et al., 1999; Madureira et al., 2005) or ca 100 km NE of Terceira (Yang et al., 2006). In turn, Escartin et al. (2001) places the Azores hotspot some 300 km east of the Princessa Alice in the vicinity of the S. Miguel Island, based on extrapolation of the model based on gravity and bathymetry data to periods older than 3.2 Ma. Given these disparities we conclude that the current position and the lateral extent of the Azores hotspot remain highly uncertain.

II. 4. Interaction between the Azores hotspot and the Azores Triple Junction

The formation of the Azores plateau and its inner structure are either attributed to the kinematic evolution of the Azores Triple Junction, or to the action of the Azores plume. It seems highly plausible that these two main processes may have significantly interacted in the past. However, the exact nature and the timing of such possible interactions remain unclear.

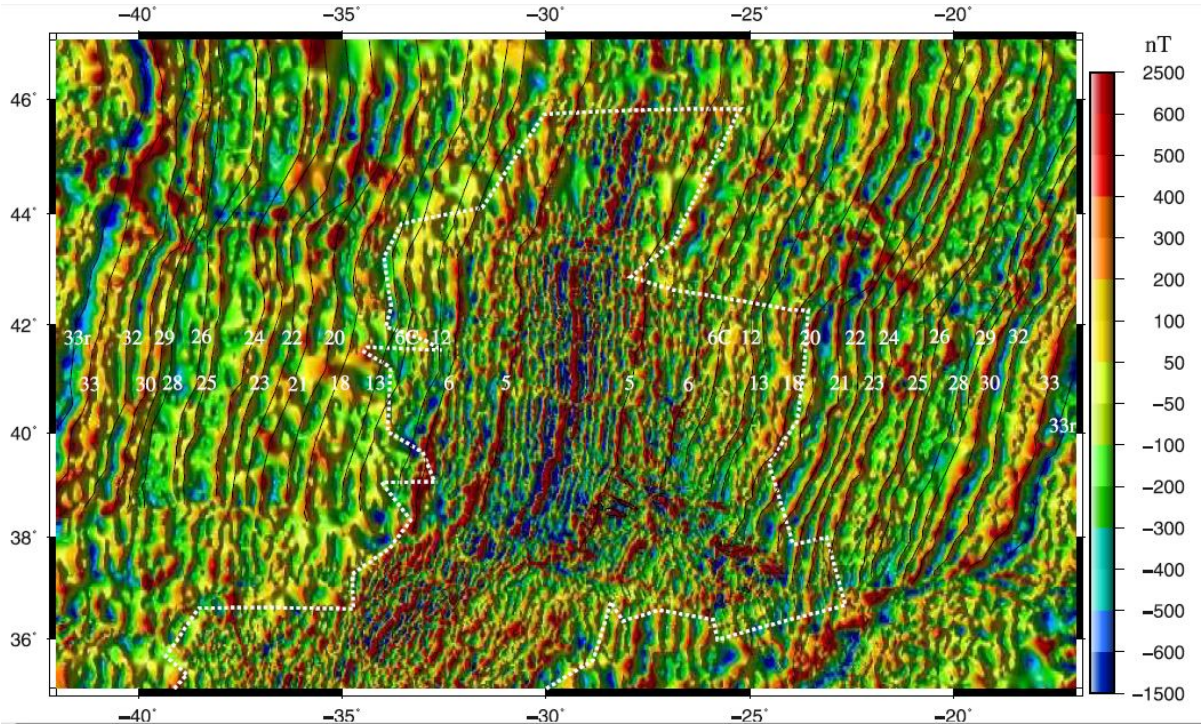


Figure II. 13. Magnetic anomaly map of Luis et al. (2008).

For instance, Luis et al. (1994) proposed that the dominant construction of the Azores plateau probably started before 20 Ma, from the position of anomaly C6 on the northern American plate (Fig. II.13). For Cannat et al. (1999), the formation of the pronounced plateau may have commenced ~36 Ma (Cannat et al., 1999), but significant part of it, especially in the Famous-Lucky strike area (close to the EAFZ) has been built by an episode of enhanced magmatism between 10 Ma and 4 Ma ago. Conversely, Gente et al. (2003) considered that the dominant interaction between the MAR and the Azores plume occurred between 20 Ma and 10 Ma (Figs. II.6 and II.14), and that most of the plateau was built ca. 7 Ma. Rifting of the plateau during the last 7 Myr is then attributed to a significant decrease in the plume activity. Gente et al. (2003) also consider that the current position of the hotspot is too much to the North to bear important interactions or consequences on the present Triple Junction.

Therefore, the evolution of the Azores plume and the ATJ would not be significantly linked during the recent period.

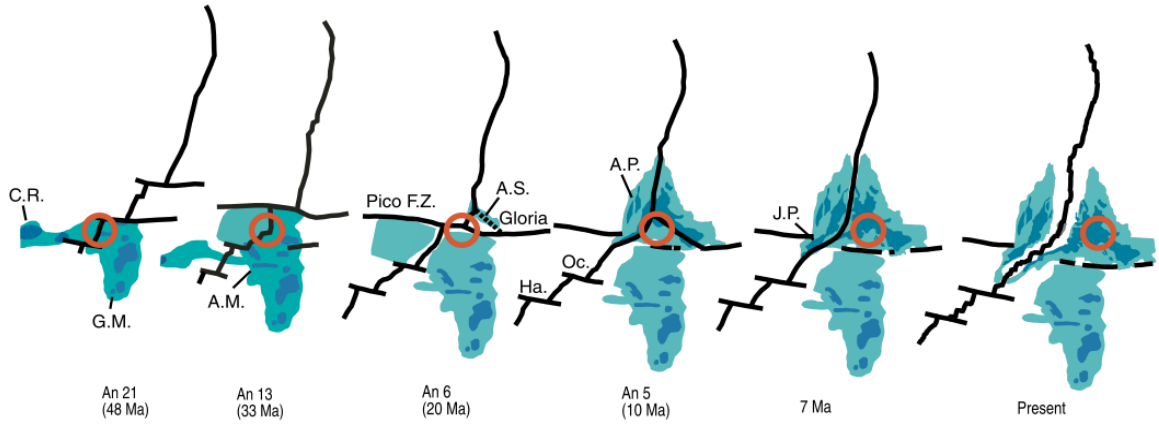


Figure II. 14. Schematic reconstructions of the relative movement between the MAR and a hotspot located under the Azores and centred under Terceira Island (Gente et al., 2003). CR: Corner Rise, GM: Great Meteor, AM: Atlantis mound, AS: Azores spreading Center, AP: Azores plateau, Oc: Oceanographer Fracture zone, HA: Hayes Fracture zones, JP: Jussieu Plateau.

If the Azores hotspot induced the formation of the plateau, the geometry of the plateau itself, its internal structure, and the northeastern and southeastern limits within the Eu/Nu plate boundary (i.e. Terceira Rift and EAFZ) are clearly influenced by tectonic features. This suggests that the surface expression of the excess in magmatism is tectonically controlled, at least during the last few Myr.

Vogt and Jung (2004) proposed that the TR is the world's slowest spreading axis plate boundary. They propose a mechanism to justify both the migration of the plate boundary (from EAFZ to TR) and the arcuate shape of the linear volcanic ridges formed by Faial-Pico, S. Jorge and the Azores bank (Figs. II.1, I.2 and I.3). They indicate that thickening of the crust could have caused a weakening zone near the edge of the spreading boundary, controlling its northward relocation. This mechanism remains valid at a broader scale, to explain the gradual northward migration of the Triple Junction. According to Vogt and Jung (2004), the Azores plateau would have been formed by successive NE jumps of the oblique spreading axis, the present Terceira Rift being the latest stage. These authors suggest that the Azores Triple junction is located in the prolongation of the Terceira Rift (ca. 39.4°N, 29.7°W). This model is the one that seems to better match with the presently available data in the Azores.

Other mechanisms of ridge-hotspot interaction include the possible influence of Triple Junction geometry on plateau formation (e.g. Sager, 2005). This possibility has been

investigated by Georgen and Sankar (2010). Using 3D finite element numerical models, these authors modelled the mantle structure to quantify the influence of the mantle dynamics on the surface observations. The model predicts a relatively little magmatic production along the TR except for regions closer to the TJ where the proximity of a spreading ridge like the MAR increases mantle temperature within the melting zone. These authors also tested the geometry of the triple junction, the role of a disconstinuity as the GF and a time-limited spreading and obliquity. Nevertheless, the results suggest a limited influence of these parameters on the thickness of the Azores plateau, Georgen and Sankar (2010) obtained a maximum of 2.5 km which is far from the crustal thickness measured (see before) and suggest the necessity of additional factors such as a mantle heterogeneity to explain the full scale of the observed magmatism.

Neves and Miranda (2013) use a 3D finite-element model of the brittle lithosphere and underlying ductile mantle, and assume that the deformation is driven only by plate boundary forces. They indicate that the plateau's internal structure and the linear volcanic ridges are the result of the vulnerability of the lithosphere (pre-existing damaged lithosphere) to magma penetration due to lithospheric stresses imposed by plate boundary forces. The factors controlling the fracturing pattern are the plate geometry and velocity boundary conditions, the shearing along the EAFZ and the interaction between the viscous mantle and the spatial variation of the brittle plate thickness. Nevertheless, they do not consider the interaction with the Azores hotspot. Adam et al. (2013) use the tomography model of Yang et al. (2006) to model the mantle convection occurring beneath the Azores region. They predict a dynamic topography fitting the anomalous elevation of the Azores plateau, and suggest two distinct narrow regions of present mantle upwelling. Adam et al. (2013) also postulate that such active mantle upwelling is presently responsible for the development of the Azores islands. Conversely, Hildenbrand et al. (2014) showed from combined geochronological and geochemical studies that a significant part of the Azores islands recorded short and partly synchronous episodes of melt production and extraction, leading to the successive development of N150 and N110 volcanic ridges during the last 1.3 Myr. These authors concluded that present deep mantle upwelling is not the main driving force responsible for the development of the recent volcanism. In turn, they proposed that magma generation results from decompression melting associated with recent deformation close to the ATJ. In this hypothesis, the enriched signatures recorded in the lavas reflect an earlier event of fertilization of the mantle, e.g., by a heterogenous plume responsible for the formation of the Azores plateau several Myr ago.

Summary

The most recent model of ATJ evolution proposed by Vogt and Jung (2004), which consists of the abandonment of the old Azores Triple Junction from the EAFZ and its progressive migration northward, seems to be the most satisfactory. Vogt and Jung (2004) attribute the generation of the linear volcanic islands, as a succession of failed rifts following this TJ migration, concomitant with the progressive hot spot track also to the north. Nevertheless, the lineaments of Faial-Pico and S. Jorge are comprised in the EU/NU current plate boundary, which is not taken into consideration in Vogt and Jung (2004) models. Thus timing the onset of this migration is of key importance for the age relationship of morphological features with the plateau and islands. Nevertheless, before examining the earlier possible location of the Eu/Nu plate boundary, we need to characterize the recent behaviour of the current plate boundary. We will first investigate the island of Graciosa because this island is localized both in the diffuse plate boundary zone and within the TR.

CHAPTER III
Construction and destruction of a volcanic island developed inside an oceanic rift: Graciosa Island, Terceira Rift, Azores

(Accepted by JVGR)

Journal of Volcanology and Geothermal Research 284 (2014) 32–45

Contents lists available at ScienceDirect

Journal of Volcanology and Geothermal Research

journal homepage: www.elsevier.com/locate/jvolgeores

Construction and destruction of a volcanic island developed inside an oceanic rift: Graciosa Island, Terceira Rift, Azores

A.L.R. Sibrant [a,b,*], F.O. Marques [c], A. Hildenbrand [a,b]

[a] Université de Paris-Sud, Laboratoire GEOPS, UMR8148, Orsay F-91405, France
[b] CNRS, Orsay F-91405, France
[c] Universidade de Lisboa, Lisboa, Portugal

ARTICLE INFO

Article history:
Received 26 April 2014
Accepted 21 July 2014
Available online 1 August 2014

Keywords:
Volcanic stratigraphy
Geochronology
Sector collapse
Graciosa Island
Terceira Rift
Azores Triple Junction

ABSTRACT

There is a great lack of knowledge regarding the evolution of islands inside active oceanic rifts, in particular the meaning of the different evolutionary steps. Therefore, we conducted an investigation in Graciosa Island, which lies at the northwestern end of the Terceira Rift in the Azores Triple Junction, with the objective of constraining the evolution of the island in terms of volcanic growth and mass wasting, in particular the meaning and age of the destruction events.

From digital elevation model (DEM) analysis, stratigraphic and tectonic observations, K/Ar dating on key samples, and available bathymetry and gravity data, we propose that Graciosa comprises five main volcanic complexes separated by major unconformities related to large scale mass wasting: (1) The older volcanic edifice (Serra das Fontes Complex) grew until ca. 700 ka, and was affected by a major flank collapse towards the southwest, which removed the whole SW flank, the summit and a part of the NE flank. (2) The Baía do Filipe Complex developed between at least 472 ka and 433 ka in two different ways: in the SW (presently offshore) as a main volcano, and in the NE unconformably over the sub-aerial remnants of the Serra das Fontes Complex, as secondary volcanic edifices. (3) The Baía do Filipe Complex was affected by a major flank collapse towards the SW, again removing most of the edifice. (4) The remnants of the Baía do Filipe Complex were covered in unconformity by the Serra Dormida Complex between ca. 330 and 300 ka, which in turn was unconformably covered by the younger Basaltic Cover Complex between ca. 300 ka and 214 ka. These two units were affected by a third major sector collapse that removed the whole western flank, the summit and part of the eastern flank of the Serra Dormida and Basaltic Cover complexes. (5) Despite the relatively young age of Graciosa, the collapse scars are not well preserved, and not active anymore. (6) A central-type volcano has been growing since at least 60 ka at the southeastern end of the island, inside the scar left by a fourth sector collapse towards the SE, which affected most previous complexes. Contemporaneously, parasitic strombolian cones formed all over the island. Despite the location of Graciosa inside the active Terceira Rift, the new data indicate that the evolution of the island has been driven by a competition between volcano growth and repeated destruction by catastrophic sector collapses, rather than by slow incremental faulting associated with the tectonics of the rift.

© 2014 Elsevier B.V. All rights reserved.

1. Introduction

The evolution of oceanic islands results from the interplay between volcanic construction and destruction by a variety of processes. Large-scale landslides, especially, are known to be one of the most efficient processes in the catastrophic destruction of oceanic volcanic islands. From onshore and offshore studies, lateral flank collapses have been recognized all over the world, either on large islands like Hawaii (e.g. Lipman et al., 1988; Moore et al., 1994), medium-size like the Canaries (e.g. Watts and Masson, 1995; Carracedo et al., 1999a,b; Hildenbrand et al., 2003; Boulesteix et al., 2012, 2013), Reunion Island (Lénat et al., 1989; Gillot et al., 1994) or French Polynesia (Clouard et al., 2001; Hildenbrand et al., 2004, 2006), and smaller islands like Pico Island in the Azores (Hildenbrand et al., 2012a, 2013; Costa et al., 2014).

In regions affected by active tectonics, in particular close to plate boundaries, large-scale gravitational instabilities occur typically associated with major faults. These instabilities can involve the development of slow and gradual rotational landslides along a deep detachment (usually termed slumps, e.g. Hildenbrand et al., 2012a, 2013), slides along major faults, or in turn may proceed as sudden catastrophic sector collapses of variable magnitude (e.g. Deplus et al., 2001; Le Friant et al., 2003; Samper et al., 2008). In seismically active areas, however, the contribution of slow-rate destruction by faulting and sudden lateral flank failure needs to be carefully assessed, since both gravitational and

* Corresponding author at: Université de Paris-Sud, Laboratoire GEOPS, UMR8148, Orsay F-91405, France. Tel.: +33 1 69 15 67 61.
E-mail address: aurore.sibrant@laposte.net (A.L.R. Sibrant).

http://dx.doi.org/10.1016/j.jvolgeores.2014.07.014
0377-0273/© 2014 Elsevier B.V. All rights reserved.

tectonic processes can produce scarps on the volcanic edifices, and thus can be confused.

The Graciosa Island in the central Azores (Atlantic) is a target of particular interest to address such problems. The island lies close to the present Triple Junction between North America (NA), Eurasia (EU) and Nubia (NU) lithospheric plates (Fig. 1), and has developed more specifically inside the western end of an active oceanic rift, known as the Terceira Rift (TR, Fig. 1), which presently materializes the northern limit of the Eurasia–Nubia plate boundary. Therefore, Graciosa offers a unique opportunity to study large-scale mass wasting in an environment of active tectonics. Here we examine the successive phases of volcanic construction and partial destruction of Graciosa. From stratigraphic relationships, the analysis of a high-resolution digital elevation model (DEM) (10 m), new K/Ar dating, and available gravity and bathymetry data, we reconstruct the multi-stage evolution of Graciosa and discuss the relative contribution of faulting processes and large-scale flank instabilities in the repeated destruction of the island over its lifetime.

2. Geological setting

The geology, stratigraphy, geochemistry and geochronology of Graciosa have been the subject of previous studies (e.g. Zbyszewski et al., 1972; Féraud et al., 1980; Gaspar and Queiroz, 1995; Gaspar, 1996; Hipólito, 2009; Hipólito et al., 2011; Larrea et al., 2014). According to Gaspar and Queiroz (1995), Graciosa comprises 3 main volcanic complexes (Fig. 2): (1) the older volcanic complex is partly preserved as a succession of hawaiitic lava flows. One of them was collected on a road-cut and dated at 620 ± 120 ka by K/Ar (Féraud et al., 1980), whilst a similar (same?) flow from this succession yielded a $^{40}Ar/^{39}Ar$ age of 1057 ± 28 ka on separated groundmass (Larrea et al., 2014, isochrone ages). (2) The intermediate volcanic complex is mostly composed of trachyte lava flows and pyroclastic deposits, with reported ages ranging between 350 ± 40 ka (Féraud et al., 1980) and 434 ± 13 ka (Larrea et al., 2014). (3) The younger volcanic complex comprises two subunits: a NW platform (basaltic cover) composed of many scattered small volcanic cones dated between 96 ± 32 ka and 46 ± 22 ka (Larrea et al., 2014), with associated basaltic lava flows blanketing most of the earlier volcanism; and the SE central-type volcano, composed of basaltic to trachytic lava flows, and pyroclastic deposits dated between 59 ± 19 ka and 4 ± 1 ka (Larrea et al., 2014).

According to Gaspar (1996) and Larrea et al. (2014), the evolution of Graciosa (Fig. 2) consists of a succession of volcanic edifices built one over the other, which have been affected and dismantled in a symmetric way by the active faulting of the Terceira Rift. This would mean that the current morphology of the edifice is tectonically induced, and due to the position of the island inside the rift. Many lineaments can be interpreted from the DEM, but their tectonic meaning has not been confirmed on the outcrop (e.g. Gaspar and Queiroz, 1995; Hipólito, 2009; Hipólito et al., 2011). Several of the lineaments are drawn using the alignment of young scoria cones, but the interpreted faults have not been observed inland or even on the coast. The measured fault directions are NW-SE and NNE-SSW, and the dip is to SW or NE, and WNW or ESE, respectively. These main fault orientations and the NW-SE elongated shape of the island have been interpreted as a consequence of the regional tectonics (Gaspar, 1996; Hipólito et al., 2011).

At present, no published work has, to our best knowledge, described or considered possible large-scale gravitational flank collapses in Graciosa.

3. Bathymetry, gravity, DEM analysis, fieldwork data and sampling strategy

3.1. Bathymetry and gravity

Despite the low resolution of the available bathymetry (Lourenço et al., 1998) and free-air gravity data (Catalão and Bos, 2008) near Graciosa, some relevant information can be extracted (Figs. 3 and 4). Graciosa has developed inside the TR, but not in the middle of the rift (Figs. 3 and 4); the northernmost part of the island sits on the TR's

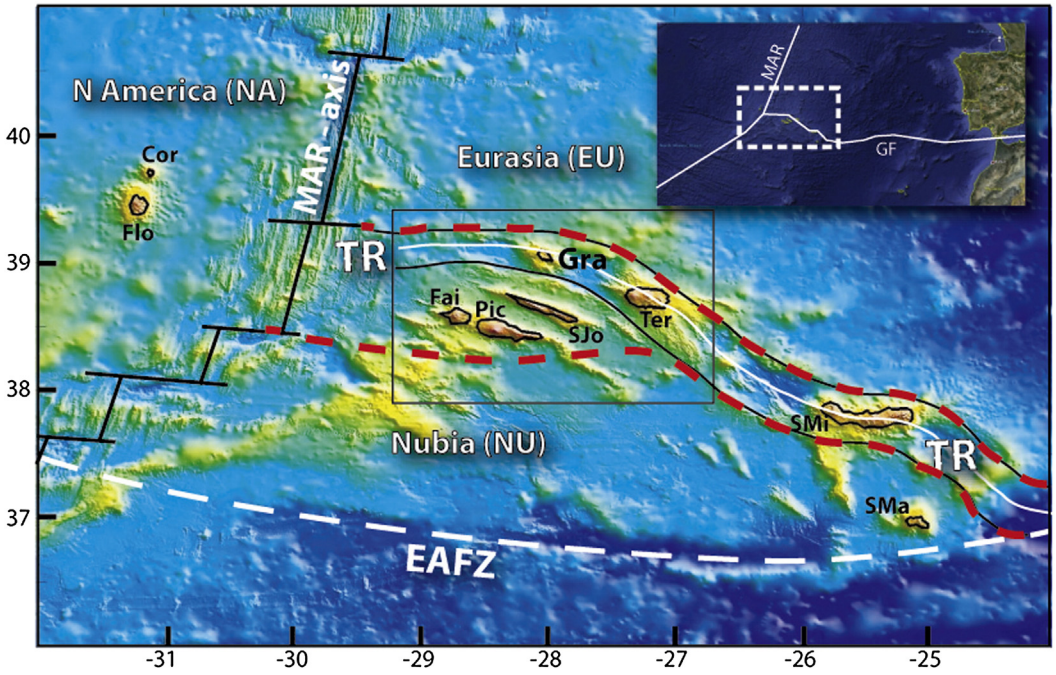


Fig. 1. Bathymetric map of the Azores region, after Lourenço et al. (1998). The black lines indicate the location of the Mid-Atlantic ridge (MAR) axis and associated fracture zones. The thin white and black lines indicate the wall and the centre of the Terceira Rift (TR), respectively. The white dashed line marks the East Azores fracture Zone (EAFZ). The black rectangle indicates the location of Fig. 3. The red dashed lines mark the diffuse boundary between the Eurasia and Nubia plates from Marques et al. (2013a, 2014a). The islands are referenced as Cor—Corvo; Flo—Flores; Fai—Faial; Pic—Pico; SJo—S. Jorge; Gra—Graciosa; Ter—Terceira; SMi—S. Miguel; SMa—Santa Maria. Inset on the right top for location. (For interpretation of the references to colour in this figure legend, the reader is referred to the web version of this article.)

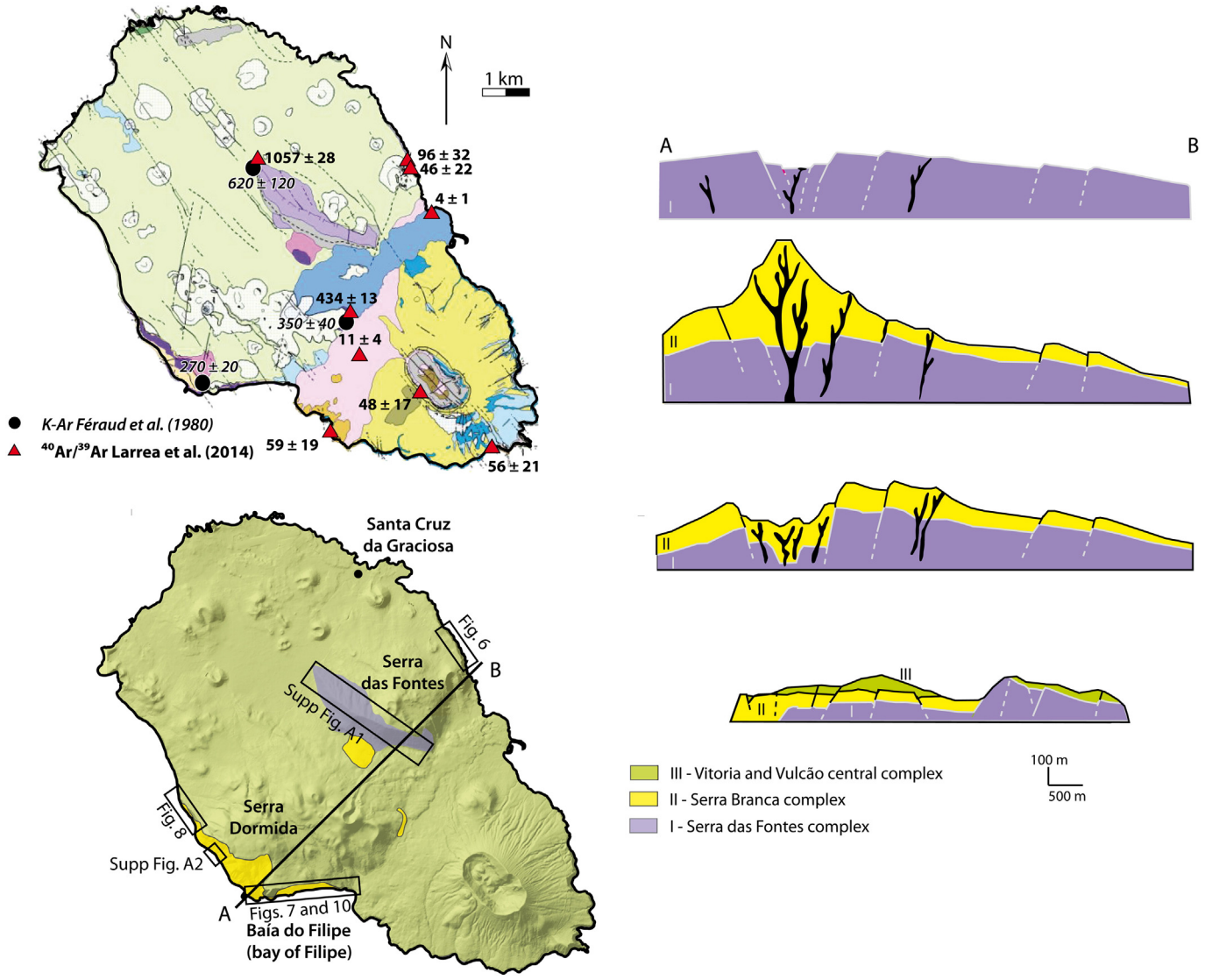


Fig. 2. (A) Geological map from Gaspar and Queiroz (1995), and previous ages in ka from Féraud et al. (1980) and Larrea et al. (2014). The light and dashed lines indicate the faults measured and presumed by Gaspar and Queiroz (1995), respectively. (B) Shaded relief map of Graciosa with the simplified geological map. The rectangles mark the location of Figs. 6, 7, 8 and 10, and Supplementary Figs. A1 and A2. (C) The panel on the right shows the evolution of the Graciosa Island after Gaspar (1996).

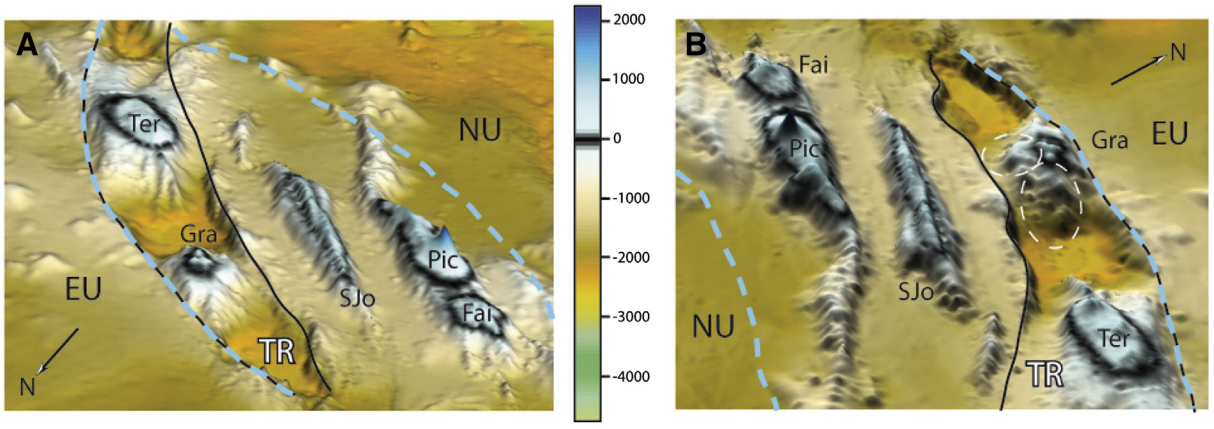


Fig. 3. 3D bathymetric map viewed from the west (left panel—A) and from the east (right panel—B). Depth in metres. The black lines indicate the northern and the southern walls of the Terceira Rift (TR), and the blue dashed lines indicate the diffuse plate boundary between the Eurasia (EU) and the Nubia (NU) plates. The white dashed circles indicate possible debris deposits. The islands are referenced as Ter—Terceira; Gra—Graciosa; SJo—S. Jorge; Pic—Pico; Fai—Faial. The raw figure without our interpretation is shown in the Supplementary Fig. A4. (For interpretation of the references to colour in this figure legend, the reader is referred to the web version of this article.)

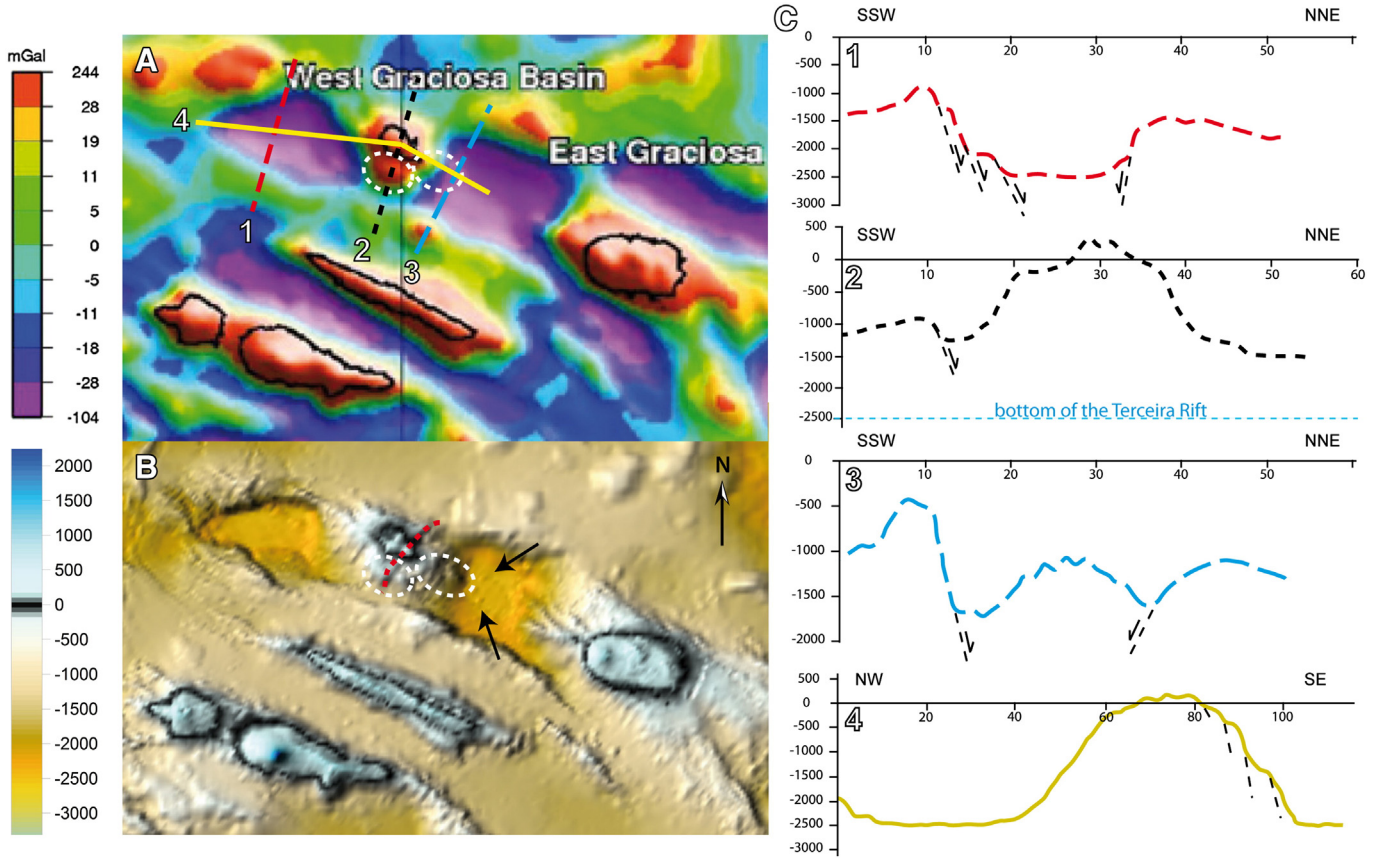


Fig. 4. (A) Gravity around Graciosa showing a flat platform in the south. Dotted circles highlight possible debris deposits that can be related to the landslides towards the SW and the SE. The coloured lines mark the location of the cross-sections shown in (C). (B) Bathymetry around Graciosa showing a flat morphology in the south. The white dashed circles show possible debris deposits. The arrows show possible few large debris blocks. The red line shows a possible collapse scar. The raw figure without interpretations is shown in the Supplementary Fig. A5. (For interpretation of the references to colour in this figure legend, the reader is referred to the web version of this article.)

northern wall (Fig. 4), thus concealing it, and leaving room between the submarine base of the edifice and the southern wall as seen on the topographic profile perpendicular to the rift and across the island (Fig. 4). Graciosa is flanked in the WNW and ESE by two deep basins (Western and Eastern Graciosa Basins, respectively). The Western Graciosa Basin shows a long flat bottom, whereas the bottom of the SE basin appears more irregular with a hummocky morphology suggesting the presence of large isolated blocks within a debris deposit. Graciosa's eastern flank is additionally characterized by a step-like topography, with a major NE-SW scarp at the top (Fig. 4b, c). On Graciosa's southwestern flank, there is a prominent flat platform bounded in the NE by a major curved scarp concave to the SW. Debris deposits and associated collapse scars can be interpreted from the bathymetry, as marked on Fig. 4.

Unfortunately, the resolution of the bathymetry available to us does not allow undisputable localization of the debris deposits resulting from the inferred large sector collapses discussed below. On the gravimetric map, Graciosa shows high gravity values (red and yellow, Fig. 4) like the other islands and seamounts in the central Azores (white and blue, Figs. 3 and 4). In contrast, the topographic lows, e.g. bottom of the adjacent basins (yellow and green, Fig. 3 and 4) correspond to low gravity (deep blue to purple, Fig. 4). However, it is important to notice that the gravity signature of the basins on both sides of Graciosa (deep blue to purple) is different than the signature of the rift bottom on the S part of Graciosa (light blue and green) and than the SW platform making up the southern submarine flank of the island (red colour).

3.2. Inland DEM analysis

Regarding topography, Graciosa is elongated NW-SE and may be divided into three main regions (Fig. 5), which are from NW to SE: (1) a low altitude and flat platform comprising the northwesternmost third of the island. It dips gently to the NW and is dotted by several well-preserved scoria cones (highlighted in yellow in the colour slope legend) attesting to their young age. (2) A central region dominated by two asymmetric topographic highs striking NW-SE, with a steep slope facing SW and a gentle slope facing NE (Fig. 5): (1) a prominent asymmetric topographic high, peaking at 375 m of altitude and named "Serra das Fontes" (Serra means hill in Portuguese), bounded by two steep scarps, with similar slope of ca. 45°, one facing SW and the other facing SE. The NE slope is gentle, in contrast to the steep SW and SE scarps. Along strike, the NW-SE scarp is curved and convex towards the SW. This prominent scarp is mostly made of the older volcanic complex. The scarps around Serra das Fontes comprise the older volcanic complex, and the NE facing gentle slope shows younger volcanic cones and lava flows lying unconformably over the lavas of the older volcanic complex. (2) A topographic high, known as "Serra Dormida", bounded by a prominent sea cliff peaking at 372 m of altitude in the SW, and by an E-W linear sea cliff in the South. Both Serra das Fontes and Serra Dormida die out to the NW and the SE. Serra Dormida is where the intermediate complex was recognized in the previous works (Gaspar and Queiroz, 1995; Gaspar, 1996). (3) A well-preserved central-type volcano peaks at 405 m and occupies the southeasternmost third of the island. The summit shows an elliptical collapse caldera elongated NW-SE. The volcano external slopes are gentle in all directions.

3.3. Field data and sampling strategy

Fieldwork was carried out to investigate the various volcano-stratigraphic units making up the island. As field criterion, we used major unconformities to establish a preliminary stratigraphy and

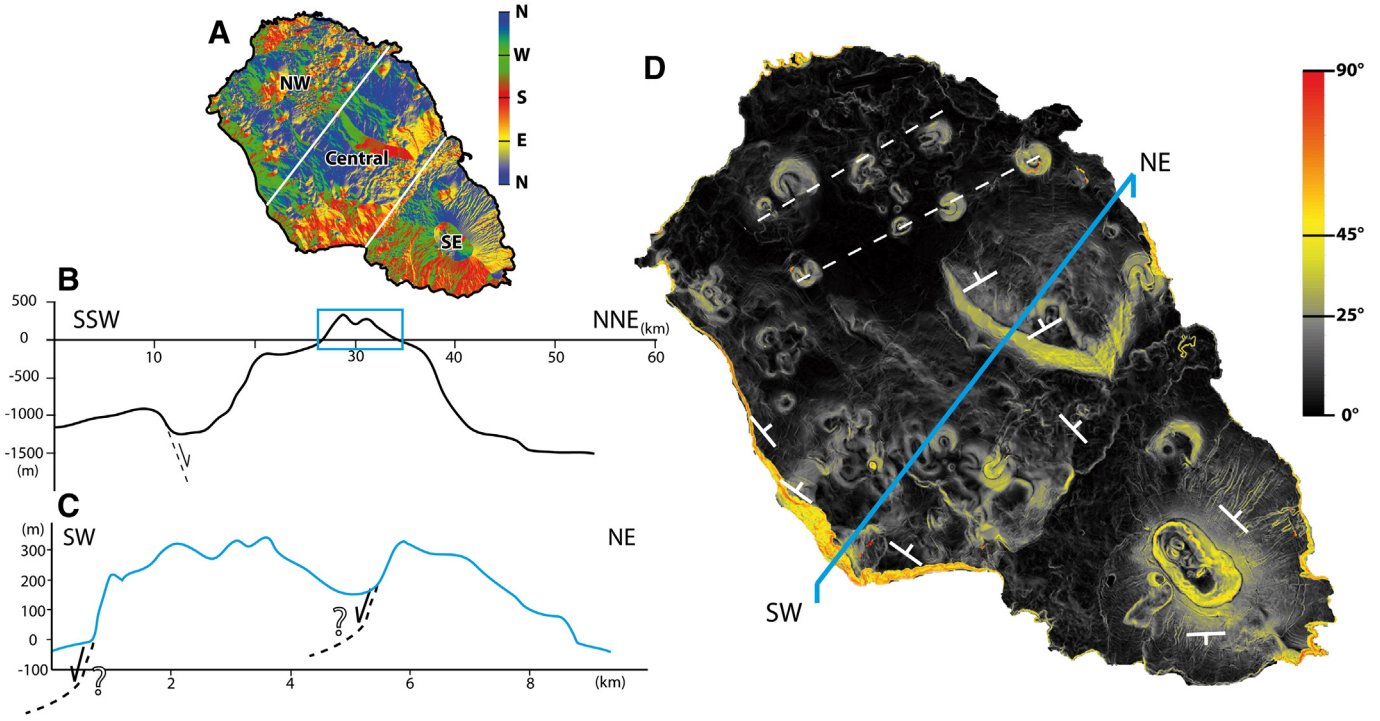


Fig. 5. (A) Direction slope map of Graciosa Island. (B) Cross-section perpendicular to the TR across the Graciosa Island. The blue rectangle indicates the cross-section zoom in (C). The location of the cross section is the blue line in (D). (D) Slope map of Graciosa in degrees. The white symbols indicate the attitude of lava flows. The white dashed lines indicate probable strombolian cones alignments. (For interpretation of the references to colour in this figure legend, the reader is referred to the web version of this article.)

guide us on sample collection for subsequent dating. The main outcrops occur mostly along the coast; therefore, we walked down the cliffs where possible, or took a boat to observe the cliffs from the sea and swim ashore to collect samples. Our sampling strategy was devised to constrain the main volcanic complexes of Graciosa, and ultimately the evolution of the island. We took advantage of the high coastal cliffs to observe the stratigraphic relationships between the different volcanic complexes and to sample the base and the top of the accessible units.

The top of Serra das Fontes is composed of basic lava flows dipping gently to the NNW (<10°). We did not observe lava flows dipping to the SW or the SE. Instead, there are two scarps steeply dipping to the SW and the SE, and bounding Serra das Fontes (Supplementary Fig. A1). This is where the older volcanic complex can be found (Fig. 2). On the ground, the SW scarp is made of rounded boulders of basalt comprising a slope deposit that covers the basement lavas, which we could thus not sample. This suggests that the SW facing scarp is the remnant of an earlier fault scarp associated with a fault dipping to the SW, which could be responsible for the displacement or removal of the missing volcanic edifice. Depending on the nature of the destructive event (tectonic normal fault or major flank collapse), a part of the older complex could be preserved at Serra Dormida, on the prominent southern SW sea cliff; therefore we paid special attention to the stratigraphy and sampling on this sea cliff. The SE termination of Serra das Fontes, striking NNE-SSW, is composed of lava flows pouring out of overlying young volcanic cones and cascading over a scarp on the older lavas. To constrain the age of Serra das Fontes, where the oldest part of the island has been defined, we sampled a lava flow at the top of Serra das Fontes (GR13G). We also sampled another lava flow further NW (GR13B), which corresponds to the sample previously collected and dated at 620 ± 120 ka by Féraud et al. (1980), and at 1057 ± 28 ka by Larrea et al. (2014). Due to the general NNW dip of the succession exposed in the Serra dos Fontes scarp (see Supplementary Fig. A1), our samples GR13G and GR13B correspond to very similar lava flows from the uppermost part of the volcanic pile.

A boat trip along the coastal cliff of the island revealed the presence of major unconformities. In the northern sector, the base of the coastal cliff close to Serra das Fontes comprises a reduced succession of thick basaltic lava flows, with an apparent dip towards the N (Fig. 6). We collected one of them (sample GR13Q). This succession appears to be overlain in unconformity by a suite of thinner lava flows inter-bedded with red strombolian deposits. The latter succession is itself intruded by a few dikes oriented mostly N70-N80E. The dykes apparently served as the feeders of very young strombolian cones (e.g. Quitadouro cone, Fig. 6), the products of which cascaded in unconformity over the older units.

On the geological map, differentiated lava flows (identified as the intermediate complex) can be found in a few places on the island. They crop out especially on the southern and western coastal sectors of Serra Dormida. The deep erosional surfaces cutting Serra Dormida comprise two steep and high sea cliffs, one E-W, in the south (Fig. 7), and another NW-SE, in the west (Fig. 8), which together allow a three dimensional view of the geometry and stratigraphy in the area. On the southern E-W sea cliff (Baía do Filipe, Figs. 2 and 7), we distinguished four main volcanic units (and one plug) separated by major unconformities:

1. The base of the cliff shows east dipping basaltic lava flows cut by faults and dykes. We collected samples from both sides of the main fault, GR13F in the SW and GR13O in the NE, in order to estimate possible fault displacement and determine whether the basaltic flows can be linked to the intermediate volcanic complex or come from an older volcanic complex. From the morphology, the dykes and the nature of the rocks, this unit looks similar to the one found at the base of the Quitadouro cliff on the NE coast (Fig. 6). The basal volcanic complex, here coined Baía do Filipe Complex, is capped by a prominent unconformity, on top of which lies thick and more differentiated rocks, mainly trachytic in character (sample GR13N). The Baía do Filipe Complex is interrupted to the west by a conspicuous and steep scarp, which can be due to a major tectonic fault or the lateral rim of a flank collapse. The lava succession cut by this major

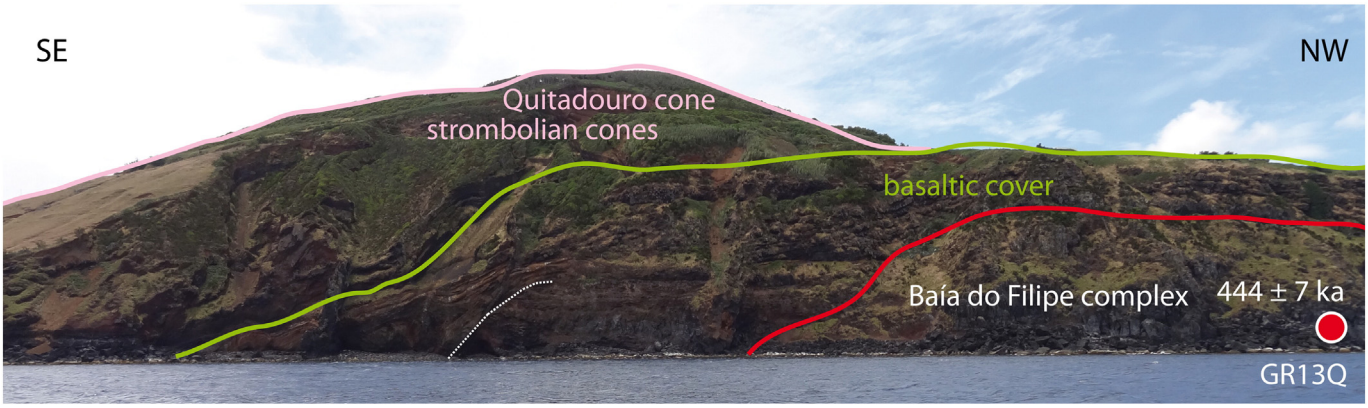


Fig. 6. NW-SE sea cliff on the NE coast of the island, below the Quitadouro cone, with interpreted volcanic stratigraphy. The number gives the age obtained by K/Ar dating in this study. The white dotted line indicates a scarp. The raw picture without our interpretations is shown in Supplementary Fig. A6.

discontinuity has a general dip towards the ENE. No similar lava flows are exposed further west over the whole cliff section, which indicates that most of the Baía do Filipe Complex is missing.

2. The volcanic succession lying unconformably on the Baía do Filipe Complex is mostly trachytic in nature. It includes pyroclastic deposits and thick lava flows, which dip to the ENE. This unit is here coined Serra Dormida Complex, which is also topped by a major unconformity. The Serra Dormida pyroclastic deposits hang steeply to, and cover, the scarp bounding the Baía do Filipe Complex in the west, which means that the steep palaeoscarp, and inferred fault (either tectonic or gravitational), predates the Serra Dormida Complex. This is relevant to the interpretation of the nature of the scarp, as discussed below. The Serra Dormida and the Baía do Filipe complexes are intruded by a few dikes trending N50-N70E.
3. The Serra Dormida Complex is unconformably overlain by basaltic lava flows dipping towards the NE (Figs. 7 and 8). We here coin this unit the Basaltic Cover Complex. The Serra Dormida Complex is intruded in the western half of the E-W cliff by a basaltic neck that seems to be one of the main feeders of the Basaltic Cover. We collected the most suitable and lowermost basaltic lava flows above the basal unconformity (samples GR13K—Fig. 8, and GR13M—Fig. 7).
4. The Basaltic Cover is unconformably overlain by the youngest basaltic lavas, related to the young cones developed over the island surface.

On the western sea cliff we could distinguish two units (Fig. 8): a lower unit composed of differentiated lava flows, which is unconformably covered by basaltic lava flows. Only the nature of the top of the differentiated rocks varies, passing upwards from trachytic lava flows and pyroclastic deposits into a massive ignimbrite flow (Fig. 8). Once we could not observe major faults displacing the lower unit between the southern and western sea cliffs, we infer that the differentiated rocks comprise the same unit, i.e. the Serra Dormida Complex. We collected one sample at the top of this unit (sample GR13E), and a sample at the base (sample GR13J). We also collected the base of the basaltic lava flows (sample GR13K) of the Basaltic Cover.

Relevant to the understanding of the evolution of Graciosa is the ca. 10° general northeastward dip of the lava flows of the Baía do Filipe and Serra Dormida complexes (Supplementary Fig. A2), and the remarkable absence of flows dipping to the SW over the whole width of the cliffs.

Finally, to better constrain the age of the SE central-type Volcano, we collected a lava flow within the caldera (sample GR13A), which probably corresponds to a lava lake stage, and a lava flow pouring out of the volcano (sample GR13P).

4. New K/Ar dating

Amongst the 17 samples collected, 12 were selected to constrain the key steps of evolution of Graciosa throughout its entire sub-aerial eruptive history (Table 1 and Fig. 9). Examination of thin sections (see photography in Supplementary Fig. A3) allowed ensuring the freshness of the samples, which is crucial to get meaningful geochronological data (see Hildenbrand et al., 2012b for a review). All the samples were prepared and dated at Lab. GEOPS in Orsay (France).

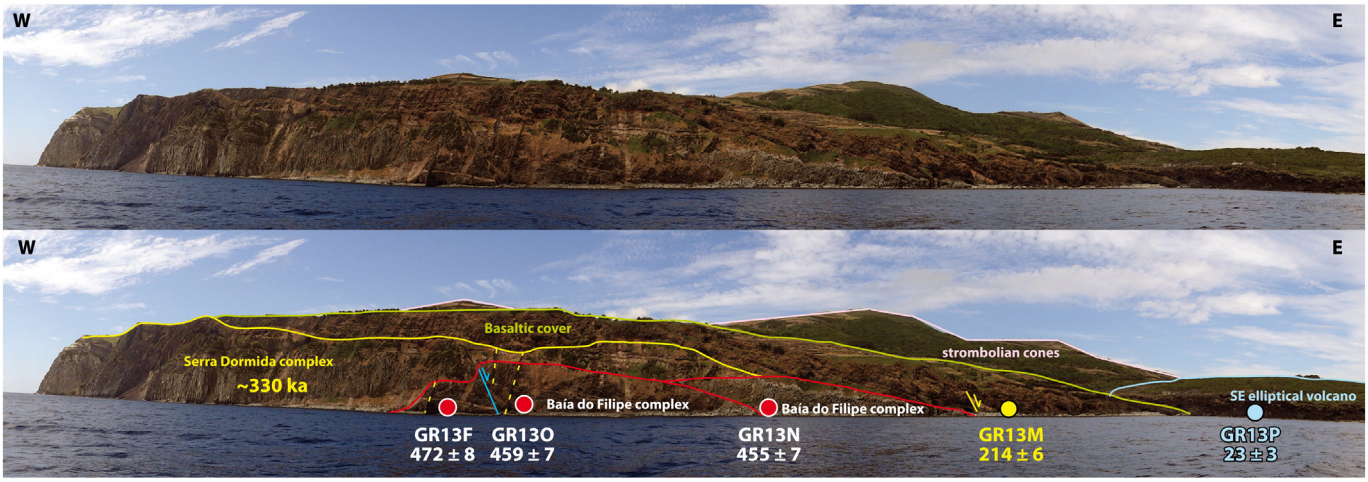


Fig. 7. E-W sea cliff at Baía do Filipe, with interpreted volcanic stratigraphy. The circles show the location of our samples and the new K/Ar ages (in ka).



Fig. 8. NW-SE sea cliff of Serra Dormida, with interpreted volcanic stratigraphy. The circles show the location of our samples and the new K/Ar ages (in ka).

The K/Ar Cassignol–Gillot technique used in the present study is particularly well adapted to date Pleistocene material (Gillot and Cornette, 1986; Gillot et al., 2006) and especially suitable to date low-K young volcanic rocks such as young basalts and andesites with an uncertainty of only a few ka (e.g. Hildenbrand et al., 2008, 2012b; Quidelleur et al., 2008; Samper et al., 2009; Boulesteix et al., 2012). Samples were crushed and sieved to the adequate size (typically 125–250 μm), deduced from thin-section examination. For most of our samples, especially basic rocks (basalts and hawaiites), the microlitic groundmass was extracted, whilst K-feldspar phenocrysts were separated for the differentiated lava GR13E. After a 10 mn ultrasonic cleaning in a 10% nitric acid solution followed by complete rinsing in distilled water and drying, heavy liquids were used to eliminate early crystallizing phenocrysts (olivine, pyroxene or plagioclase phenocrysts), and thus avoid any potential incorporation of inherited excess-argon. K was measured by flame emission spectroscopy, and compared with standards MDO-G and ISH-G (Gillot et al., 1992). Ar was measured with a mass spectrometer identical to the one described by Gillot and Cornette (1986). Owing to the stability of the analytical conditions, the mass spectrometer can perform highly reproducible ^{40}Ar measurements, thereby avoiding the need to deal only with ratios with the use a ^{38}Ar spike. For each analysis, the ^{40}Ar signal calibration is obtained from air-pipette measurements calibrated against the interlaboratory standard GL-O with the recommended value of 6.679×10^{14} at/g of ^{40}Ar* (Odin et al., 1982) and regularly checked with HD-B1 standard (see Germa et al., 2011 for a review). The correction of atmospheric contamination, also carried out after each sample analysis, is done by comparison of the ^{40}Ar/^{36}Ar ratio of the sample with an air-pipette measured in the same analytical conditions at strictly similar ^{40}Ar pressure. For a given ^{40}Ar signal, a reproducibility of better than 0.1% is observed for successive atmospheric ^{40}Ar/^{36}Ar measurements. Typical uncertainties of 1% are achieved for the ^{40}Ar signal calibration and for the K determination. The uncertainty on the ^{40}Ar* determination is a function of the radiogenic content of the sample, the detection limit of our system being presently of 0.1% of ^{40}Ar* (Quidelleur et al., 2001), corresponding to around 1 ka for a 1% K basaltic lava. Decay constants of Steiger and Jager (1977) were used. The K/Ar ages obtained in this study are reported in Table 1. Uncertainties are quoted at the 1σ confidence level.

The new ages range between 702 ± 10 ka and 23 ± 3 ka, with a K content between 1.063 and 4.128%, and a radiogenic argon content (^{40}Ar*) between 0.6 and 43.9%. These new ages are consistent but more precise than previous whole-rock K/Ar determinations (Féraud et al., 1980), and generally are comparable with the recent ^{40}Ar/^{39}Ar ages obtained by Larrea et al. (2014) on groundmass and mineral separates, except for one sample (see below). Our two samples on the west dipping upper lava flow of Serra dos Fontes yield strictly similar ages of 702 ± 10 ka (GR13G) and 700 ± 10 ka (GR13B). These are comparable with the age of 620 ± 120 ka obtained by Féraud et al. (1980) when uncertainties are accounted for, but significantly younger than the age of 1057 ± 28 ka obtained by Larrea et al. (2014) on the same succession.

Table 1
New K/Ar ages obtained with the unspiked Cassignol-Gillot technique on fresh separated groundmass and alkali feldspars (sample GR13E). For each sample, the mean age is obtained by weighing by the amount of radiogenic argon. The uncertainties are quoted at the 1σ level.

Sample material	UTM 26 E	UTM N	K%	40Ar* (%)	40Ar* (10^{11}at/g)	Age (ka)	Unc. (ka)
GR13G	412977	4323701	1.226	20.52%	8.951	699	10
Gdm				22.06%	9.040	706	10
						702	**10**
GR13B	411904	4324748	1.286	28.31%	9.311	693	10
Gdm				35.03%	9.477	705	10
						700	**10**
GR13F	411881	4319884	1.794	11.00%	8.918	476	8
Gdm				11.31%	8.765	468	8
						472	**8**
GR13N	412565	4320006	4.128	43.90%	19.654	456	7
Gdm				35.55%	19.555	454	7
						455	**7**
GR13O	412565	4320006	2.061	25.15%	9.829	457	7
Gdm				28.65%	9.926	461	7
						459	**7**
GR13Q	415117	4325069	1.063	14.82%	4.938	445	7
Gdm				16.76%	4.929	444	7
						444	**7**
GR13J	409146	4321678	1.776	10.75%	6.011	324	5
Gdm				4.05%	6.326	341	10
						329	**7**
GR13E	410339	4320458	3.603	40.11%	12.136	322	5
Feld				27.75%	12.160	323	5
						323	**5**
GR13K	409084	4321771	1.258	11.95%	3.884	296	5
Gdm				11.87%	3.982	303	5
						299	**5**
GR13M	412565	4320006	1.347	4.43%	3.023	215	6
Gdm				3.81%	3.002	213	6
						214	**6**
GR13A	416082	4320103	1.153	0.72%	0.492	41	6
Gdm				0.91%	0.569	47	5
						44	**5**
GR13P	412809	4319896	1.148	0.78%	0.273	23	3
Gdm				0.60%	0.277	23	4
						23	**3**

The bold data indicates the mean age for each sample.

The new ages measured on lava flows from the Baía do Filipe Complex range between 472 ± 8 ka and 455 ± 7 ka (samples GR13F and GR13N). The base of the Quitadouro cliff is dated at 444 ± 7 ka (sample GR13Q). These new results are comparable with the age of 434 ± 13 ka obtained by Larrea et al. (2014) on a lava collected between the two highest peaks of the island, in a small outcrop previously attributed to the intermediate complex (Fig. 2). The lavas from the Serra Dormida Complex are here dated between 329 ± 7 ka and 323 ± 5 ka. The samples collected at the base and top of the Basaltic Cover Complex are here dated between 299 ± 5 ka and 214 ± 6 ka (samples GR13K and GR13M, respectively), in agreement with an age of 270 ± 20 ka obtained by Féraud et al. (1980) on the same unit. Finally, the new ages measured on lava flows sampled at the SE elliptical volcano at the base of the caldera wall and the most recent lava flow range between 44 ± 5 ka and 23 ± 3 ka (samples GR13A and GR13P).

5. Discussion

5.1. Proposal of a new stratigraphy for the Graciosa Island

Based on the observed relationships between volcanic complexes and the new K/Ar data, we propose a new volcanic stratigraphy for the Graciosa Island (Fig. 9).

The late activity of the old volcanic stage is here constrained at around 700 ka from our two samples collected on the upper part of the succession exposed at Serra das Fontes. Therefore, we here coin it Serra das Fontes Complex. The older age obtained by Larrea et al. (2014) on their sample GRZF8 from the same succession may indicate that the earlier activity of this complex has not been sampled in the present study. However, the proximity between our sampling sites and the fact that no lava flow crops out in the lower parts of the SW Serra das Fontes scarp, renders this assumption improbable. In such circumstances, we cannot exclude that the age obtained by Larrea et al. (2014) on their sample GRZF8 is slightly over-estimated. On this sample, Larrea et al. (2014) obtained a very low K/Ca content of 0.0433, which is almost three times lower than for all their other samples (on groundmass). For such very low K/Ca, ^{36}Ar production from Ca during irradiation is significant, which renders the correction of atmospheric contamination delicate, and can bias the age.

The Serra das Fontes Complex is topographically truncated by two scarps oriented NNE-SSW and NW-SE, and no lavas dipping other than NNW were observed; therefore the original geometry of the older volcanic edifice is difficult to constrain. However, given the gentle slope of the still remaining lavas, we infer that it was a shield volcano.

Along the Baía do Filipe coastal cliff we observed three major unconformities that separate four complexes, instead of the two identified in the previous geological map (Gaspar and Queiroz, 1995):

1. At the base, we identified the new Baía do Filipe Complex. The age of the Baía do Filipe Complex is here bracketed between, at least 472 ± 8 ka and 434 ± 13 ka (this work and Larrea et al., 2014, respectively). Given that the lavas generally dip to the E, and Larrea et al.'s (2014) sample was collected to the E of our sample, it is stratigraphically logical that the age reported here is older. This temporal and spatial relationship between the two samples also means that no major faulting (tectonic or gravitational) occurred between the two outcrops since ca. 434 ka ± 13 ka. Therefore, it suggests that there is no major recent graben in the middle of the island, between Serra das Fontes and Serra Dormida, as proposed by Gaspar and Queiroz (1995) and Gaspar (1996). Our sample GR13Q collected at the base of the Quitadouro cliff and here dated at 444 ± 7 ka is topographically below the rock here dated at ca. 700 ka (Fig. 9). It is also located to the east of the NNW-dipping 700 ka flows, and therefore corresponds to lava flows unconformably overlying the Serra das Fontes Complex. The similar ages between GR13Q and the Baía do Filipe Complex allow linking one to the other. Considering together the location of the outcrops and the age obtained at Quitadouro sea cliff (ca. 444 ka), we infer that the Baía do Filipe Complex was built in two different ways: in the SW, as a main volcano (formerly offshore and currently destroyed), and in the NE unconformably over the subaerial eastern flank of the Serra das Fontes unit, as a secondary volcanic edifice. The eruptions were initially effusive and produced basaltic lava flows, and later more evolved trachytic lavas. The new ages here reported thus suggest that the differentiation in the magma chamber of the Baía do Filipe Complex, from basalt (GR13F) to trachyte rocks (GR13N), occurred over a maximal period of 30 kyr (between 472 ± 8 ka and 458 ± 7 ka), in the hypothesis of a single magma chamber.
2. The Serra Dormida Complex unconformably covers the Baía do Filipe Complex (Fig. 7), and is separated from the uppermost trachyte lava by ca. 100 ka. Indeed, we constrain the Serra Dormida Complex activity around 325 ka (329 ± 7 ka at the base and 323 ± 5 ka at the top). The ages are very similar, which indicates that either the edification of the Serra Dormida Complex was very fast, or there is a great deal of rocks missing. This complex comprises differentiated trachytic flows, pyroclasts and massive ignimbrites. The latter eruptions were thus mostly explosive, probably of sub-plinian type. This unit is the equivalent of the Serra Branca Complex of Gaspar and Queiroz (1995).
3. Previous studies proposed that the younger phases of volcanic activity in Graciosa could be separated into two distinct geographic areas, but they are stratigraphically not distinguished in the geological map: (1) a Basaltic Cover (Unidade de Vitória) constructed from

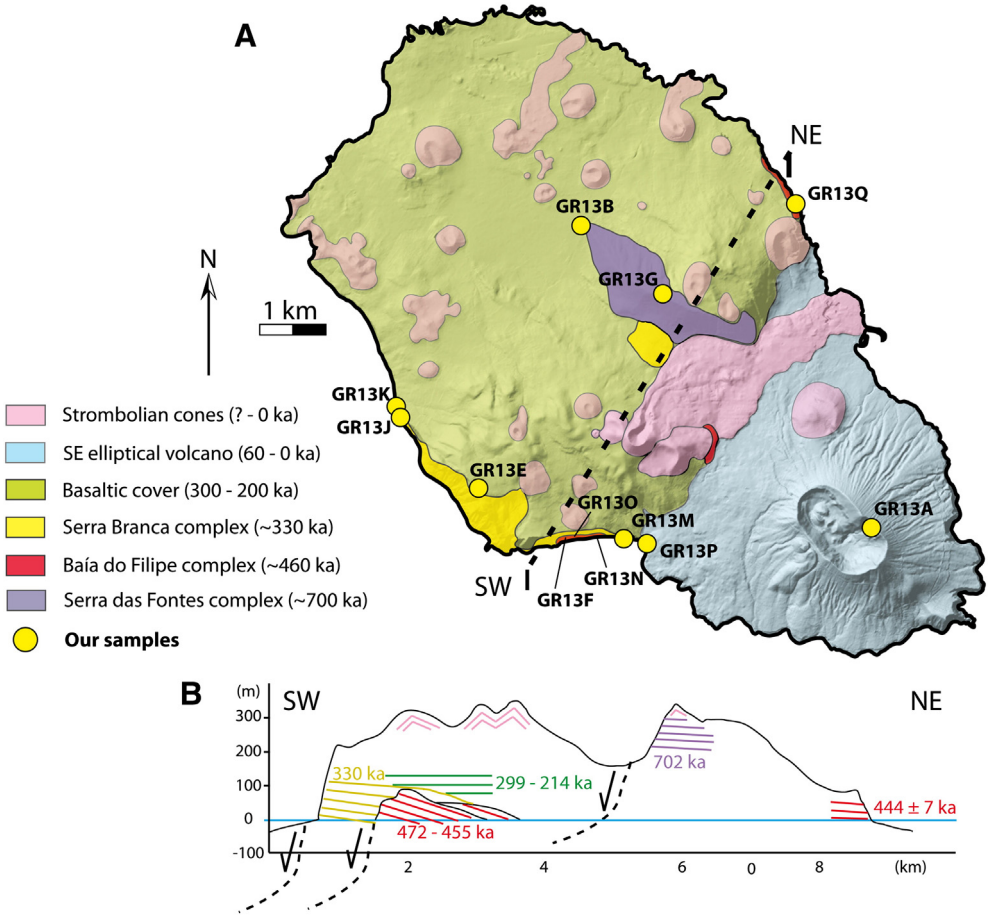


Fig. 9. (A) Main stratigraphic units distinguished in this work, with the location of our samples. Notice that we attributed the lenticular outcrop in the middle of the island as the Baía do Filipe complex, based on the ages of Larrea et al. (2014). (B) Schematic cross section summarizing our field observations and our new K/Ar ages.

monogenetic cones covering both Serra das Fontes and Serra Dormida, and making up the NW platform; and (2) a central-type volcano located in the SE end of the island. From our new dating, we propose that this separation is not only geographic but also chronologic. Here we constrain the Basaltic Cover on the southwestern part of the island between 299 ± 5 ka and 214 ± 6 ka (samples GR13K and GR13M, respectively). The new ages of 44 ± 5 ka and 23 ± 3 ka obtained on our samples GR13A and GR13P provide temporal constraints on the effusive volcanic activity of the SE central-type volcano. Further South, similar young flows are unconformably overlying the Basaltic cover at Baía do Filipe. Therefore, the activity of the SE central-type volcano cannot be related to the activity of the Basaltic Cover Complex (gap > 150 ka). Accordingly, we separated the former Vitória and Vulcão Central complexes into two distinct complexes, the Basaltic Cover and the SE Central-type Volcano complexes. Moreover, the younger eruptions from the young strombolian cones marked on our new stratigraphic map (Fig. 9) have yielded similar ages, or are even younger than the SE Central-type Volcano (Larrea et al., 2014). Therefore, we also separated them from the Basaltic Cover.

To conclude, based on major observed unconformities and new isotopic dating, we propose that the Graciosa Island comprises 6 well-individualized volcano-stratigraphic units (Fig. 9).

5.2. Repeated destruction of Graciosa: tectonic faulting or gravitational collapse?

The field observations and stratigraphic relationships are summarized in Fig. 9. They reveal that the remnants of the Serra das Fontes, Baía do Filipe and Serra Dormida are mostly composed of lava flows dipping to the NNW, E and NE, respectively. This means that the western flank, the summit and part of the eastern flank of these volcanic edifices are missing. The analysis of the DEM reveals that the lavas are truncated by a scarp and by a sea cliff in the SW, in Serra das Fontes and Serra Dormida, respectively, and a NNE-SSW scarp in Serra das Fontes. Moreover, field observation reveals that the Baía do Filipe Complex is truncated by a major scarp in the west, and topped by a major unconformity. We infer that these discontinuities comprise the scars of destruction affecting the Serra das Fontes Complex, the Baía do Filipe Complex, and then the Serra Dormida Complex and the Basaltic Cover. Therefore, the questions are: (1) what is the nature of dismantling? Is it tectonics via faults, or gravitational via major flank collapses? (2) What are the ages of the destruction processes?

5.2.1. The NNE-SSW scarp in Serra das Fontes

From the gentle NNW dip of the lava flows of the Serra das Fontes Complex, we infer that they are part of a shield volcano, whose summit and southern flank do not exist anymore. Instead of the SE dipping lava flows expected south of the scarp, the missing old volcano is presently occupied by the young SE central-type volcano. In between the two volcanoes, a clear NNE-SSW scarp is visible (Fig. 5). Although the difference in age between the lavas of the older and the younger volcanoes (ca. 640 kyr) is possibly enough for normal erosion (rain and wave erosion) to remove the large amounts of lava flows missing in the older complex, such a linear scarp is unlikely to result solely from protracted erosion. An alternative is that most of the older volcano has been removed by a large-scale catastrophic event, in the form of a giant sector collapse. Indeed, the NNE-SSW scar is also visible on the

available bathymetry (red dashed lines in Fig. 4), which indicates that this structure is bigger than the scale of the present island. Moreover, the irregular topography in steps on the SE submarine flank of Graciosa (white dashed circle in Figs. 3 and 4) and the abnormal high bottom of the basin further east (cross sections Fig. 4) can be interpreted as a large debris deposit.

The current NNE-SSW strike of the scarp is almost perpendicular to the main orientation of the TR; therefore, the flank collapse suggested here cannot be directly linked to the tectonic activity of the normal faults of the rift. It can, however, be linked to faults along the transform direction associated with the TR (Marques et al., 2014b), which is close to NE-SW in Graciosa (DeMets et al., 2010). The flank collapse created a scar that was later filled by the SE Central-type Volcano. From our K/Ar dating, previous ages, and our new field observations, the Quitadouro lavas cascade over the scarp. Some of them have been dated at 96 ± 32 ka (Larrea et al., 2014), which gives a minimum age to the flank collapse. Taking into consideration the location of the Baía do Filipe Complex outcrops on both the northern and southern coastal cliffs and inside the island (Fig. 9a), we infer that the eastern part of this complex was removed, which gives a maximum age of ca. 450 ka to the major SE-directed flank collapse here proposed.

5.2.2. The NW-SE scarp in Serra das Fontes

According to previous studies (Fig. 2), Graciosa comprises a central graben that affects all volcanic complexes (Gaspar and Queiroz, 1995; Gaspar, 1996). A topographic section across this proposed graben (Figs. 4, 5 and 9) shows two asymmetric topographic highs, with a steep slope facing SW and a gentle slope facing NE. This morphology is not consistent with what would be expected for a graben. Furthermore, the new ages and spatial distribution of the Baía do Filipe Complex indicate that there is no major graben developed in central Graciosa after ca. 434 ± 13 ka. We thus conclude that there is no graben, but we do not exclude, at this stage of the discussion, the existence of an older half-graben.

From the bathymetry and the topographic section across the rift, it is clear that Graciosa is asymmetrically located inside the TR, because the northwesternmost part of the island sits on top of the northern shoulder of the active TR. This means that: (1) possible flank collapses towards the SW (along NW-SE failures) may be arrested by the southern wall of the TR (Figs. 1, 3, 4 and 5); (2) the dismantling of the successive volcanoes towards the SW may have been triggered by normal fault displacement at the TR's northern wall.

Given that the TR is active, we need to determine if displacement along the faults inferred from scarps is compatible with the ages and known plate kinematics, in order to ascribe the scarps to a tectonic or gravitational origin. The major scarps show two main orientations, NE-SW and NW-SE, which we will discuss separately:

1. Regarding the NE-SW scarp, the tectonic vertical displacement is negligible because the transform faults with this direction are pure strike-slip (Marques et al., 2014b). Relevant to this discussion is the existence of conspicuous NE-SW alignments of strombolian cones in NW Graciosa (cf. Fig. 5), and the measured trend of dykes, which is also close to NE-SW on average. Therefore, if such a fault exists, it may have triggered a large-scale, earthquake-driven, landslide, but it cannot by itself be responsible for the displacement necessary to remove the summit and the SE flank of the Serra das Fontes volcano.
2. Regarding the NW-SE scarp, it could be a normal fault of tectonic or gravitational origin; therefore, we have to discuss displacement rates and ages. Graciosa sits in the western half of the TR, where the Nubia/Eurasia plate boundary is diffuse (Marques et al., 2013a, 2014a). Therefore, the ca. 4 mm/yr rifting is not all taken up by the TR, and Marques et al. (2013a, 2014a) estimated that the TR is most likely opening only ca. 2.4 mm/yr in the diffuse region. Once we are discussing the TR's northern wall only, the half opening is 1.2 mm/yr. However, at the longitude of Graciosa, the TR is ca. N110° in azimuth, i.e. it is significantly oblique to maximum extension (ca. N60°, DeMets et al., 2010), which implies that the orthogonal opening is $1.2\cos 30^\circ = 1$ mm/yr, using conservative values (not the actual 40°). If the whole half opening were taken up by only pure normal faulting (northern TR bounding fault), it would imply that the pure normal fault had an average vertical displacement ($1.0 \times \tan 60^\circ$) of ca. 1.7 mm/yr. If the 1.2 mm/yr half opening were taken up by two pure normal faults with similar displacement, then the average rate of vertical displacement on each pure normal fault would be ca. 0.85 mm/yr. However, the ca. N110° wall of the TR is significantly oblique to maximum extension, which means that the vertical component has to be shared with a horizontal component, and therefore the ca. 0.85 mm/yr is overestimated. Given such low tectonic rates of vertical displacement, it is most unlikely that the observed scarps and displacements of the main volcanic complexes can be due to tectonics alone. Finally, but most importantly, the possible normal faults we are discussing are located to the S of the actual TR's northern wall, actually closer to the centre of the TR. The topographic profile (Fig. 4c top panel) shows evidence of only one master fault bounding the TR in the north, and no evidence of major faults in the flat bottom. Therefore, it is not likely that the possible normal faults dismantling the three main volcanic edifices are directly related to the TR's northern wall.

The contact between the Serra das Fontes Complex and the younger Baía do Filipe Complex was not directly observed (Fig. 9). Nevertheless, most of the Baía do Filipe Complex grew to the SW of the Serra das Fontes Complex, and the new ages indicate an inverted stratigraphy, if no major erosion or displacement (tectonic or collapse) is considered: the Baía do Filipe rocks (~470 ka, close to sea level) are at much lower altitude than the Serra das Fontes rocks (~700 ka, 350 m altitude) (Fig. 9). Moreover, the lava flows of both complexes dip to the N, which, in the absence of faults or major erosion, puts the younger rocks in the SW below the older rocks in the NE. From the gentle NNW dip of the lava flows of the Serra das Fontes Complex, we infer that the Serra das Fontes main edifice could not exist, as a whole, when the Baía do Filipe Complex was active. If the vertical displacement were due to a normal fault, it would have to be significantly greater than 350 m, because we do not know the top of the older Serra das Fontes Complex, and the base of the younger Baía do Filipe Complex. A simple calculation (400 m divided by 200 000 years) gives an average 2 mm/yr of downward displacement, which is much greater than the tectonic vertical displacement estimated above.

Typically, fault scarps are straight along strike, and flank collapse scarps show a horseshoe shape (e.g. Ownby et al., 2007; Tibaldi et al., 2008; Karaoglu and Helvaci, 2012). Therefore we have to discuss the observed shapes. The current NW-SE scarp does not show a straight linear shape or a curved shape concave towards the SW. From field observation, it is clear that the scarp is almost exclusively composed of rounded debris blocks, which are covered by a dense forest where the trees show vertical trunks, i.e. there is no evidence for current movement rotating the trees. This indicates that the scarp is old, significantly retreated, and currently inactive; therefore if any active fault existed, it should crop out to the SW, where it has not been observed and is not expected from the new ages and volcanic unit spatial distribution. On the geological map of Gaspar and Queiroz (1995), some faults are inferred from the NW-SE alignment of a few strombolian cones. However, neither these cones nor their volcanic basement (even the oldest) show evidence for significant recent vertical movement, which would be expected if the present topography was the result of still active major normal faults. Instead, we propose that the NW-SE scarp making up Serra das Fontes is most probably an old scar of a main flank collapse that occurred between 700 and 472 ka (youngest age of the Serra das Fontes Complex, and oldest age of the Baía do Filipe Complex, respectively). The Baía do Filipe Complex filled the SW depression created by the flank collapse of the Serra das Fontes volcano, like in most flank

collapses in volcanic islands (Hildenbrand et al., 2006; Quidelleur et al., 2008; Samper et al., 2008; Boulesteix et al., 2012; Jicha et al., 2012).

5.2.3. The scarp bounding the Baía do Filipe Complex in the west

The lavas making up the Baía do Filipe Complex, here dated between 472 ± 8 ka and 455 ± 7 ka, dip to the ENE and are truncated in the west by a steep scarp. Therefore, most of the initial volcano is missing: the whole southwest flank, the summit, and part of the northeast flank (Figs. 7 and 10). The younger Serra Dormida Complex, here dated around 330 ka, sits unconformably on the Baía do Filipe Complex, which means that major dismantling of the Baía do Filipe Complex occurred after ca. 450 ka and prior to ca. 330 ka. Such major destruction may have occurred either by normal faulting or gravitational collapse, Given that the TR is active, we would expect to see a normal fault propagating upwards into the Serra Dormida Complex, if dismantling were due to vertical tectonic displacement associated with the activity of the TR. However, no major fault has been observed upward in the more recent units (cf. Figs. 7 and 10), which means that the fault (tectonic or gravitational) has been inactive during at least the last 330 kyr. The steep scarp at Baía do Filipe lies in the southwesternmost part of the island. This is close to the centre of the TR, where no tectonic faults are observed on the flat bottom, and already far from the TR's northern wall. In the context of an active rift like the TR, it is therefore difficult to attribute the missing part of the Baía do Filipe Complex to a tectonic normal fault. Instead we infer that the observed scarp is the result of an instantaneous event like a flank collapse. Therefore, the differentiated pyroclastic eruptions from the Serra Dormida Complex could have been triggered by the sector collapse through depressurization of an underlying differentiated magmatic chamber (e.g. Manconi et al., 2009; Boulesteix et al., 2012).

To conclude, we propose that the steep western scarp in Baía do Filipe Complex is an old scarp of a flank collapse, which occurred between ca. 450 ka and 330 ka, the youngest age of the Baía do Filipe Complex and the oldest age of the Serra Dormida Complex, respectively.

5.2.4. The NW-SE sea cliff of Serra Dormida

The Serra Dormida Complex and the Basaltic Cover Complexes are abruptly truncated by the coastal cliff, and both show lava flows generally dipping towards the NE (Figs. 8, 10 and A2). If we assume that the Serra Dormida volcano had a former typical conical shape, then the whole southwest flank, the summit and part of the northeast flank are missing. We note that both the Serra Dormida Complex and most of the Basaltic Cover developed in a previous flank collapse depression (dismantling of the Baía do Filipe and Serra das Fontes edifices). They thus settled in a weakened and probably unstable sector, which may have served as a main structure for subsequent gravitational destabilization. In such circumstances, the younger Serra Dormida and Basaltic Cover complexes may have also been affected by a lateral flank collapse towards the SW.

Bathymetric and geophysical data, even at low-resolution, are important to detect and better constrain the first-order characteristics of debris fields generated by large flank instabilities (e.g. Deplus et al., 2001; Masson et al., 2008; Costa et al., 2014). Directly southwest of Graciosa, the voluminous bathymetric platform (Figs. 3 and 4, and cross section Fig. 5) is associated with a positive gravity anomaly (Fig. 4). This could be interpreted as (1) a remnant volcanic basement of the island, apparently much more developed in the SW than in the NE, (2) a relief created by downward displacement of Graciosa's southern flank by normal faulting associated with the tectonics of the TR, or (3) the presence of material (either debris or recent volcanism) accumulated in the southwest in response to major sector collapses. In the first hypothesis, the flat submarine relief in the SW would represent an old volcanic edifice, which would have experienced significant subsidence and marine abrasion. However, the new age data do not support such a hypothesis, as the main volcanic complexes here dated are globally younger in the S and SW than in the N and NW. Hypothesis 2 would imply the existence of several faults successively developed towards the S. Each would affect/dismantle a given volcanic complex and then become inactive, whilst a new volcanic complex built to the south, and a new set of faults would appear southward and affect/dismantle it without affecting the previous volcanic complex(es). This seems improbable, because each fault would then have been active over a limited period of time, down to only a few tens of kyr, which appears rather short in the context of an active rift. Last but not least, successive jumps of faulting preferentially to the south are inconsistent with the overall morphology of the TR, which typically shows a flat bottom bounded by one or two master faults. Therefore, the hypothesis of several major flank collapses is the most likely in the light of the new data and the tectonic setting. The southern shoulder of the TR is close to the island, which may have reduced the dispersion of potential debris and led to buttressing of the deposits at the base of the TR's southern wall. The depth of the rift in this area is 300 m less than in the neighbouring SE basin. From this

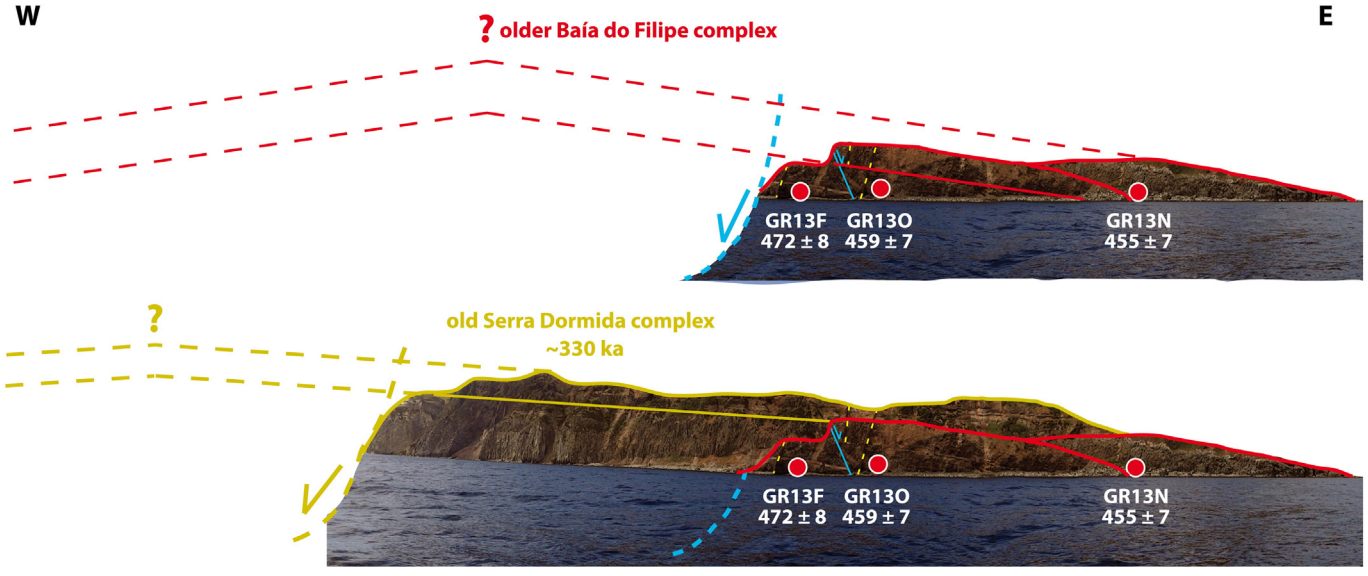


Fig. 10. Proposed evolution of the Baía do Filipe and Serra Dormida complexes along the E-W sea cliff at Baía do Filipe. The circles show the location of our samples and the new K/Ar ages (in ka). The location of the coastal cliff is show in Fig. 2.

observation, it seems reasonable to infer that the Serra Dormida Complex and a part of the Basaltic Cover have probably been affected by a flank collapse since 214 ± 6 ka, the youngest age of the Basaltic Cover in the Serra Dormida area.

The evidence presented here of major landsliding in Graciosa is consistent with previous work in the Azores by Hildenbrand et al. (2012a) and Costa et al. (2014), and work in progress (Marques et al., 2013b) and (Sibrant et al., 2013), who have found onshore and offshore evidence of major landslides in Pico, Santa Maria and S. Miguel islands.

6. Conclusions

Based on morphological analyses, stratigraphic and tectonic observations, and new geochronological data, we propose a new view of the geological evolution of the Graciosa Island. The island emerged and grew thanks to short and repeated volcanic construction punctuated by major flank collapses. The evidence encompasses the establishment of a volcanic stratigraphy (with special attention to the nature and geometry of the contacts between main volcanic complexes), the recognition of the geometry of the main volcanic successions, and the identification of landslide scars. Despite the position of the Graciosa Island partly along the northern shoulder of the TR, we conclude that the several destruction stages did not involve slow and gradual faulting linked to the tectonic activity of the rift, but in contrasts occurred through sudden and most probably catastrophic lateral flank collapses. However, we cannot exclude that such repeated destabilization episodes may have been triggered by major earthquakes.

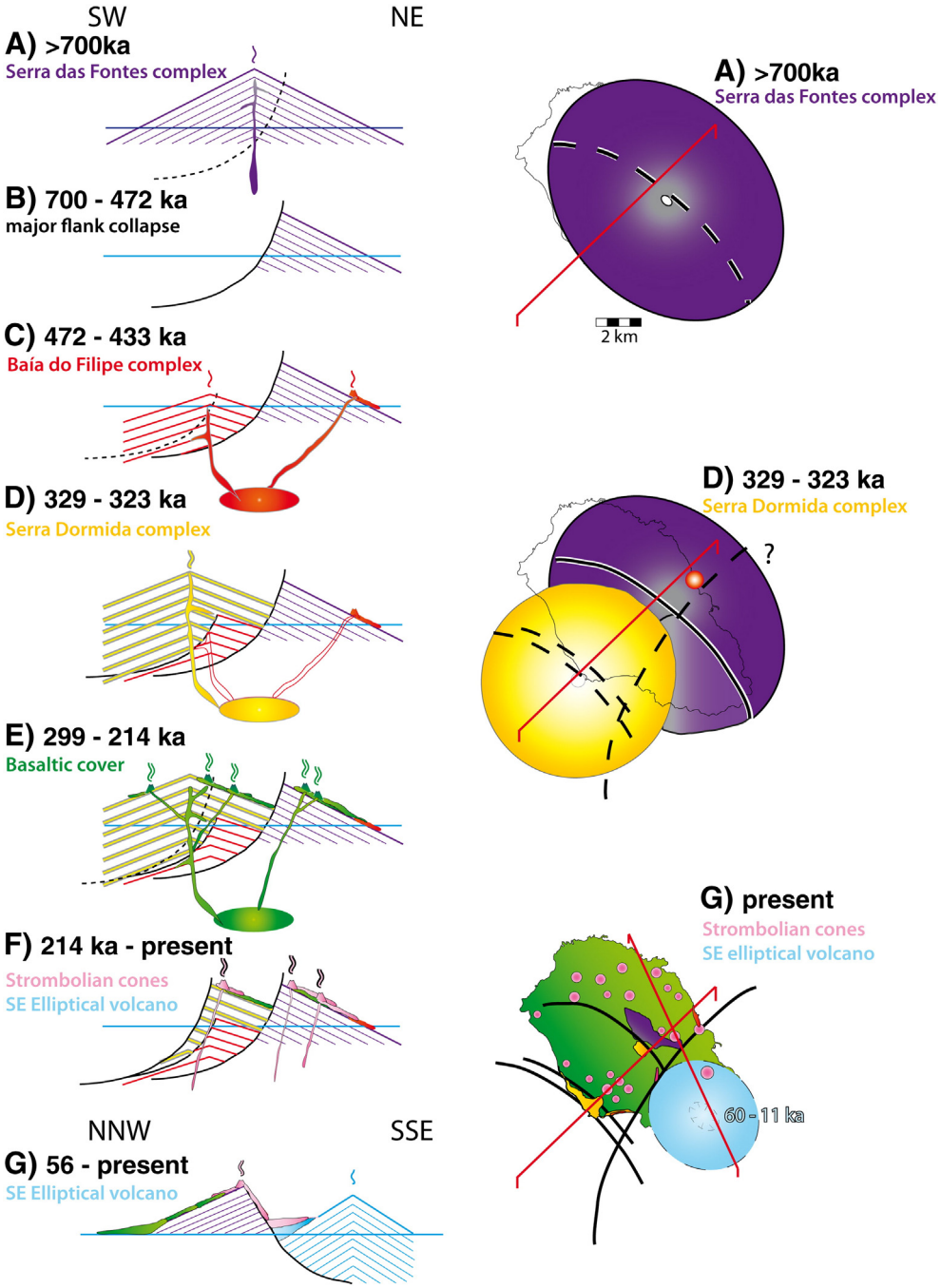


Fig. 11. New schematic morphostructural evolution of the Graciosa Island.

Before 700 ka, a volcano emerged to form the Graciosa Island (Fig. 11). A sudden catastrophic event towards the SW removed the SW flank, the summit and part of the NE flank of this older volcanic edifice (Serra das Fontes), between 700 ka and at least 472 ka. Then, a new basaltic edifice here called the Baía do Filipe Complex grew rapidly in the depression left by the flank collapse, until ca. 433 ka. This edifice was subsequently affected by a flank collapse towards the SW that only spared the eastern flank of the edifice. At ca. 330 ka, a new, differentiated, volcano (Serra Dormida Complex) was growing very rapidly in the depression left by the second flank collapse. The Serra Dormida Complex was then unconformably covered by the Basaltic Cover Complex between ca. 300 ka and 200 ka. Both were most probably affected by a flank collapse, which removed the western flank, the summit and part of the eastern flank of these complexes, and controlled the current shape of the island in the SW. More recently, the island was affected by a new flank collapse towards the SE, and the resulting depression was filled by the SE Central-type Volcano. The present day topography of Graciosa shows several very well preserved strombolian cones, recently built unconformably on top of the older volcanic units (probably during the last 30 ka).

Supplementary data to this article can be found online at http://dx.doi.org/10.1016/j.jvolgeores.2014.07.014.

Acknowledgements

This work was in great part supported by MEGAHazards (PTDC/CTE-GIX/108149/2008) research project funded by FCT (Portugal). We acknowledge X. Quidelleur and A. Davaille for fruitful discussions. We thank an anonymous reviewer and the Editor for their valuable comments, which helped to improve the manuscript.

References

Boulesteix, T., Hildenbrand, A., Gillot, P.Y., Soler, V., 2012. Eruptive response of oceanic islands to giant landslides: new insights from the geomorphologic evolution of the Teide-Pico Viejo volcanic complex (Tenerife, Canary). Geomorphology 138, 61–73.

Boulesteix, T., Hildenbrand, A., Soler, V., Quidelleur, X., Gillot, P.-Y., 2013. Coeval giant landslides in the Canary Islands: implications for global, regional and local triggers of giant flank collapses on oceanic volcanoes. J. Volcanol. Geotherm. Res. 257, 90–98.

Carracedo, J.C., Day, S.J., Guillou, H., 1999a. Quaternary collapse structures and the evolution of the western Canaries (Las Palmas and Hierro). J. Volcanol. Geotherm. Res. 94, 169–190.

Carracedo, J.C., Day, S.J., Guillou, H., Gravestock, P., 1999b. Later stages of volcanic evolution of Las Palma, Canary Islands: rift evolution, giant landslides, and the genesis of the Caldera Taburiente. Geol. Soc. Am. Bull. 111, 755–768.

Catalão, J., Bos, M.S., 2008. Sensitivity analysis of the gravity geoid estimation: a case study on the Azores plateau. Phys. Earth Planet. Inter. 168, 113–124.

Clouard, V., Bonneville, A., Gillot, P.Y., 2001. A giant landslide on the southern flank of Tahiti Island, Frenc Polynesia. Geophys. Res. Lett. 28, 2253–2256.

Costa, A.C.G., Marques, F.O., Hildenbrand, A., Sibrant, A.L.R., Catita, C.M.S., 2014. Large-scale flank collapses in a steep volcanic ridge: Pico-Faial Ridge, Azores Triple Junction. J. Volcanol. Geotherm. Res. 272, 111–125.

DeMets, C., Gordon, R., Argus, D.F., 2010. Geologically current plate motions. Geophys. J. Int. 181, 1–80.

Deplus, C., LeFriant, A., Boudon, G., Komorowski, J.C., Villemant, B., Harford, C., Ségoufin, J., Cheminée, J.L., 2001. Submarine evidence for large-scale debris avalanches in the Lesser Antilles Arc. Earth Planet. Sci. Lett. 192, 145–157. http://dx.doi.org/10.1016/S0012-821X(01)00444-7.

Féraud, G., Kaneoka, I., Allègre, C.J., 1980. K/Ar ages and stress pattern in the Azores: geodynamic implications. Earth Planet. Sci. Lett. 46, 275–286.

Gaspar, J.L., 1996. Ilha Graciosa (Açores): História Vulcanológica e Avaliação do Hazard. PhD thesis Universidade dos Açores (361 pp.).

Gaspar, J.L., Queiroz, G., 1995. Carta vulcanológica dos Açores, ilha Graciosa 1:10.000, folhas A e B. UAC, Centro de Vulcanologia UAC e Câmara Municipal de Santa Cruz da Graciosa.

Germa, A., Quidelleur, X., Lahitte, P., Labanieh, S., Chauvel, C., 2011. The K–Ar Cassignol–Gillot technique applied to western Martinique lavas: a record of the evolution of the recent Lesser Antilles island arc activity from 2 Ma to Mount Pelé volcanism. Quat. Geochronol. 6, 341–355.

Gillot, P.Y., Cornette, Y., 1986. The Cassignol technique for potassium-argon dating, precision and accuracy: examples from late Pleistocene to recent volcanism from southern Italy. Chem. Geol. 59, 205–222.

Gillot, P.Y., Cornette, Y., Max, N., Floris, B., 1992. Two reference materials, trachytes MDO-G and ISH-G, for argon dating K/Ar and $^{40}Ar/^{39}Ar$ dating of Pleistocene and Holocene rocks. Geostand. Geoanal. Res. 16, 55–60.

Gillot, P.Y., Lefevre, J.C., Nativel, P.E., 1994. Model for the structural evolution of the volcanoes of Reunion Island. Earth Planet. Sci. Lett. 122, 291–302.

Gillot, P.Y., Hildenbrand, A., Lefèvre, J.C., Albore-Livadie, C., 2006. The K/Ar dating method: principle, analytical techniques and application to Holocene volcanic eruptions in the southern Italy. Acta Vulcanol. 18, 55–66.

Hildenbrand, A., Gillot, P.Y., Soler, V., Lahitte, P., 2003. Evidence for a persistent uplifting of La Palma (Canary Islands), inferred from morphological and radiometric data. Earth Planet. Sci. Lett. 210, 277–289.

Hildenbrand, A., Gillot, P.Y., Le Roy, I., 2004. Volcano-tectonic and geochemical evolution of an oceanic intra-plate volcano: Tahiti-Nui (French Polynesia). Earth Planet. Sci. Lett. 217, 349–365.

Hildenbrand, A., Gillot, P.Y., Bonneville, A., 2006. Off-shore evidence for a huge landslide of the northern flank of Tahiti-Nui (French Polynesia). Geochem. Geophys. Geosyst. 7, 1–12.

Hildenbrand, A., Madureira, P., Marques, F.O., Cruz, I., Henry, B., Silva, P., 2008. Multi-stage evolution of a sub-aerial volcanic ridge over the last 1.3 Myr: S. Jorge Island, Azores Triple Junction. Earth Planet. Sci. Lett. 273, 289–298.

Hildenbrand, A., Marques, F.O., Catalão, J., Catita, C.M.S., Costa, A.C.G., 2012a. Large-scale active slump of the southeastern flank of Pico Island, Azores. Geology 40, 939–942.

Hildenbrand, A., Marques, F.O., Costa, A.C.G., Sibrant, A.L.R., Silva, P.M.F., Henry, B., Miranda, J.M., Madureira, P., 2012b. Reconstructing the architectural evolution of volcanic islands from combined K/Ar, morphologic, tectonic, and magnetic data: the Faial Island example (Azores). J. Volcanol. Geotherm. Res. 241–242, 39–48.

Hildenbrand, A., Marques, F.O., Catalão, J., Catita, C.M.S., Costa, A.C.G., 2013. Reply to the comment by Quartau and Mitchell on " Large-scale active slump of the southeastern flank of Pico Island, Azores. Geology 40, 939–942. http://dx.doi.org/10.1130/G33303.1 (by Hildenbrand et al., 2012) in Geology, 41).

Hipólito, A., 2009. Geologia estrutural da Ilha Graciosa: Enquadramento no âmbito da Junção Tripla dos Açores. MSc thesis Azores University, Ponta Delgada (257 pp.).

Hipólito, A., Madeira, J., Carmo, R., Gaspar, J.L., 2011. Neotectonics of Graciosa Island (Azores)—uncertainty in seismic hazard assessment in a volcanic area with variable slip-rates. 2nd INQUA-IGCP-567 International Workshop on Active Tectonics, Earthquake Geology, Archaeology and Engineering, Corinth, Greece.

Jicha, B.R., Coombs, M.L., Calvert, A.T., Singer, B.S., 2012. Geology and Ar-40/Ar-39 geochronology of the medium- to high-K Tanaga volcanic cluster, western Aleutians. Geol. Soc. Am. Bull. 124, 842–856.

Karaoglu, O., Helvaci, C., 2012. Growth, destruction and volcanic facies architecture of three volcanic centres in the Miocene Usak-Gure basin, western Turkey: subaqueous–subaerial volcanism in a lacustrine setting. J. Volcanol. Geotherm. Res. 245–246, 1–20.

Larrea, P., Wijbrans, P.R., Galé, C., Ubide, T., Lago, M., França, Z., Widom, E., 2014. 40Ar/39Ar constraints on the temporal evolution of Graciosa Island, Azores (Portugal). Bull. Volcanol. 76, 796. http://dx.doi.org/10.1007/s00445-014-0796-8.

Le Friant, A., Boudon, G., DePlus, C., Villemant, B., 2003. Large-scale flank collapse events during the activity of Montagne Pelee, Martinique, Lesser Antilles. J. Geophys. Res. Solid Earth 108 (B1). http://dx.doi.org/10.1029/2001JB001624.

Lénat, J.F., Vincencet, P., Bachelery, P., 1989. The offshore continuation of an active basaltic volcano: Piton de la Fournaise (Reunion Island Indian Ocean). J. Volcanol. Geotherm. Res. 36, 1–36.

Lipman, P.W., Normark, W.R., Moore, J.G., Wilson, J.B., Gutmacher, C.E., 1988. The giant submarine Alika debris slide, Mauna Loa, Hawaii. J. Geophys. Res. 93, 4279–4299.

Lourenço, N., Miranda, J.M., Luis, J.F., Ribeiro, A., Victor, L.A.M., Madeira, J., Needham, H.D., 1998. Morpho-tectonic analysis of the Azores Volcanic Plateau from a new bathymetric compilation of the area. Mar. Geophys. Res. 20, 141–156.

Manconi, A., Longpré, M.-A., Walter, T.R., Troll, V.R., Hansteen, T.H., 2009. The effects of flank collapses on volcano plumbing systems. Geology 37, 1099–1102.

Marques, F.O., Catalão, J.C., DeMets, C., Costa, A.C.G., Hildenbrand, A., 2013a. GPS and tectonic evidence for a diffuse plate boundary at the Azores Triple Junction. Earth Planet. Sci. Lett. 381, 177–187.

Marques, F.O., Sibrant, A.L.R., Hildenbrand, A., Costa, A.C.G., 2013b. Large-scale sector collapses in the evolution of Santa Maria Island, Azores. Abstract Meeting AGU, 2013.

Marques, F.O., Catalão, J.C., DeMets, C., Costa, A.C.G., Hildenbrand, A., 2014a. Corrigendum to "GPS and tectonic evidence for a diffuse plate boundary at the Azores Triple Junction" Earth Planet. Sci. Lett. 381 2013a. In Earth Planet. Sci. Lett. 387, 1–3.

Marques, F.O., Catalão, J., Hildenbrand, A., Costa, A.C.G., Dias, N.A., 2014b. The 1998 Faial earthquake, Azores: evidence for a transform fault associated with the Nubia–Eurasia plate boundary? Tectonophysics http://dx.doi.org/10.1016/j.tecto.2014.06.024.

Masson, D.G., Le Bas, T.P., Grevemeyer, I., Weinrebe, W., 2008. Flank collapse and large-scale landsliding in the Cape Verde Islands, off West Africa. Geochem. Geophys. Geosyst. 9, Q07015. http://dx.doi.org/10.1029/2008GC001983.

Moore, J.G., Normark, W.R., Holcomb, R.T., 1994. Giant Hawaiian landslides. Ann. Rev. Earth Planet. Sci. Lett. 22, 119–144.

Odin, G.S., et al., 1982. Interlaboratory standards for dating purposes. In: Odin, G.S. (Ed.), Numerical Dating in Stratigraphy. John Wiley and Sons, Chichester, pp. 123–150.

Ownby, S., Granados, H.G., Lange, R.A., Hall, C.M., 2007. Volcan Tancitaro, Michoacan, Mexico, $^{40}Ar/^{39}Ar$ constraints on its history of sector collapse. J. Volcanol. Geotherm. Res. 161, 1–14.

Quidelleur, X., Gillot, P.Y., Soler, V., Lefèvre, J.C., 2001. K/Ar dating extended into the last millennium: application to the youngest effusive episode of the Teide volcano (Spain). Geophys. Res. Lett. 28, 3067–3070.

Quidelleur, X., Hildenbrand, A., Samper, A., 2008. Causal link between Quaternary paleoclimatic changes and volcanic islands evolution. Geophys. Res. Lett. 35. http://dx.doi.org/10.1029/2007GL031849 (L02303).

Samper, A., Quidelleur, X., Boudon, G., Le Friant, A., Komorowski, J.C., 2008. Radiometric dating of three large volume flank collapses in the Lesser Antilles Arc. J. Volcanol. Geotherm. Res. 176, 485–492.

Samper, A., Quidelleur, X., Komorowski, J.C., Lahitte, P., Boudon, G., 2009. Effusive history of the Grande Decouverte Volcanic Complex, southern Basse-Terre (Guadeloupe, French West Indies) from new K–Ar Cassignol–Gillot ages. J. Volcanol. Geotherm. Res. 187, 117–130.

Sibrant, A.L.R., Hildenbrand, A., Marques, F.O., Boulesteix, T., Costa, A.C.G., 2013. Morpho-structural evolution of a volcanic island developed inside an active oceanic rift: S. Migeul Island (Terceira Rift, Azores). Abstract Meeting, IAG, 2013.

Steiger, R.H., Jager, E., 1977. Subcommission on geochronology: convention on the use of decay constants in geo and cosmochronology. Earth Planet. Sci. Lett. 36, 359–362.

Tibaldi, A., Pasquarè, F.A., Papanikolaou, D., Nomikou, P., 2008. Discovery of a huge sector collapse at the Nisyros volcano, Greece, by on-land and offshore geological–structural data. J. Volcanol. Geotherm. Res. 177, 485–499.

Watts, A.B., Masson, D.G., 1995. A giant landslide on the north flank of Tenerife, Canary Islands. J. Geophys. Res. 100, 24499–24507.

Zbyszewski, G., Medeiros, A., Ferreira, O., 1972. Carta Geológica de Portugal 1: 25.000, folha Ilha Graciosa (Açores). Ser. Geol. Portugal.

CHAPTER IV
São Miguel Island

IV. São Miguel Island

Chapter 4 is on the S. Miguel Island and it is separated in two parts. The first one depicts the morpho-structural evolution of the island, based on high-resolution DEM data, fieldwork and structural investigations, and high-precision K-Ar dating on separated mineral phases. We discuss the architecture of S. Miguel and propose a morpho-structural evolution of the island. Through the nature of the volcanism and the elongation of S. Miguel, we will also discuss the tectonic control on the island. In the second part, from structural analysis and new measurements of 350 faults and dikes, we investigate the architecture of the Terceira Rift through the tectonic markers measured on S. Miguel and their concentrations along the S. Miguel Island. We estimate also the TR initiation time from simple geometry calculation.

IV. 1. Morpho-structural evolution of a volcanic island developed inside an active oceanic rift: S. Miguel Island (Terceira Rift, Azores) (in prep, JVGR)

A.L.R. Sibrant [1*], A. Hildenbrand [1,2], F.O. Marques [3], B. Weiss[4], C. Hübscher[4]. T. Lüdmann[5], T. Boulesteix [6], A.C.G. Costa[1,7]

(1) Université Paris-Sud, Laboratoire GEOPS, UMR8148, Orsay, F-91405

(2) CNRS, Orsay, F-91405

(3) Universidade de Lisboa, Lisboa, Portugal

(4) University of Hamburg, Institute of Geophysics, Germany

(5) University of Hambourg, Institute for Geology

(6) GeoRessources, CNRS-CREGU, Université de Lorraine, France

(7) Universidade de Lisboa and IDL, Lisboa, Portugal

*Corresponding author. Tel.: +33 1 69 15 67 61

E-mail address: aurore.sibrant@u-psud.fr

Abstract

The evolution of volcanic islands is generally marked by fast construction phases alternating with destruction by a variety of mass-wasting processes, such as large-scale landslides, caldera collapse, or graben development. More specifically, volcanic islands located in areas of intense regional deformation can be particularly prone to gravitational destabilization. The island of S. Miguel (Azores) has developed during the last 1 Myr inside the active Terceira Rift (TR), a major tectonic structure defining the present boundary between the Eurasian and Nubian lithospheric plates. The new data show that the island is composed of 4 main volcanic complexes variably affected by collapse structures. In this work, we depict the evolution of the island, based on high-resolution DEM data, stratigraphic and structural analyses, high-precision K/Ar dating on separated mineral phases, and seismic (offshore) and aeromagnetic (onshore) data. The new results indicate that: (1) the oldest outcroping volcanic complex (Nordeste), composing the easternmost part of the island, was active between ca. 878 and 750 ka. From onshore topography and offshore bathymetric and seismic data, we infer a major southwards flank collapse. (2) The resulting depression was filled by basic volcanic activity here dated between 507 and 250 ka. (3) The Fogo volcano lies in the middle of S. Miguel and is here dated between 270 and 17 ka; it was affected by, at least, one southward flank collapse of unknown age. (4) The Furnas volcano developed between Nordeste and Fogo, and is here dated between ca. 138 and 23 ka; it was affected by caldera collapses here dated at 60 ka and, at least, 23 ka. (5) The Sete Cidades volcano is here dated between ca. 91 and 13 ka. From the predominance of the N150° and N75° trends, we infer that tectonics controlled the location of the volcanism, and to some extent the destruction events.

Keywords: Azores Triple Junction; S. Miguel Island; K-Ar dating; morpho-structural evolution; mass-wasting; submarine debris deposit

IV. 1. 1. Introduction

The growth of volcanic islands is generally punctuated by a variety of destructive episodes such as large-scale flank collapses, vertical caldera collapse, fault generation, meteoric and marine erosion (e.g. Oehler et al., 2005; Ramalho et al., 2013). Volcanic edifices developed in areas of active regional deformation, often experience a complex evolution, including effusive and explosive volcanic phases and repeated mass wasting at various scales (Hildenbrand et al., 2012a; Costa et al., 2014). As most of these processes represent a significant hazard, recognizing the several main construction and destruction phases is essential, especially in oceanic islands where populations and economic activities are concentrated.

S. Miguel is the largest and most densely populated of the Azores islands. It has developed inside the active Terceira Rift (TR), a major extensional structure making up the western end of the third arm of the Azores Triple Junction (Fig. IV.1). S. Miguel stretches most of the TR width, and is characterized by the location of volcanism along two main trends, the N75° and the N130°. The eastern part of S. Miguel has grown on the northern shoulder of the TR, and the central and western parts have developed inside the TR. This unique position allows investigating the impact of tectonics on the volcanic development and destruction of the island.

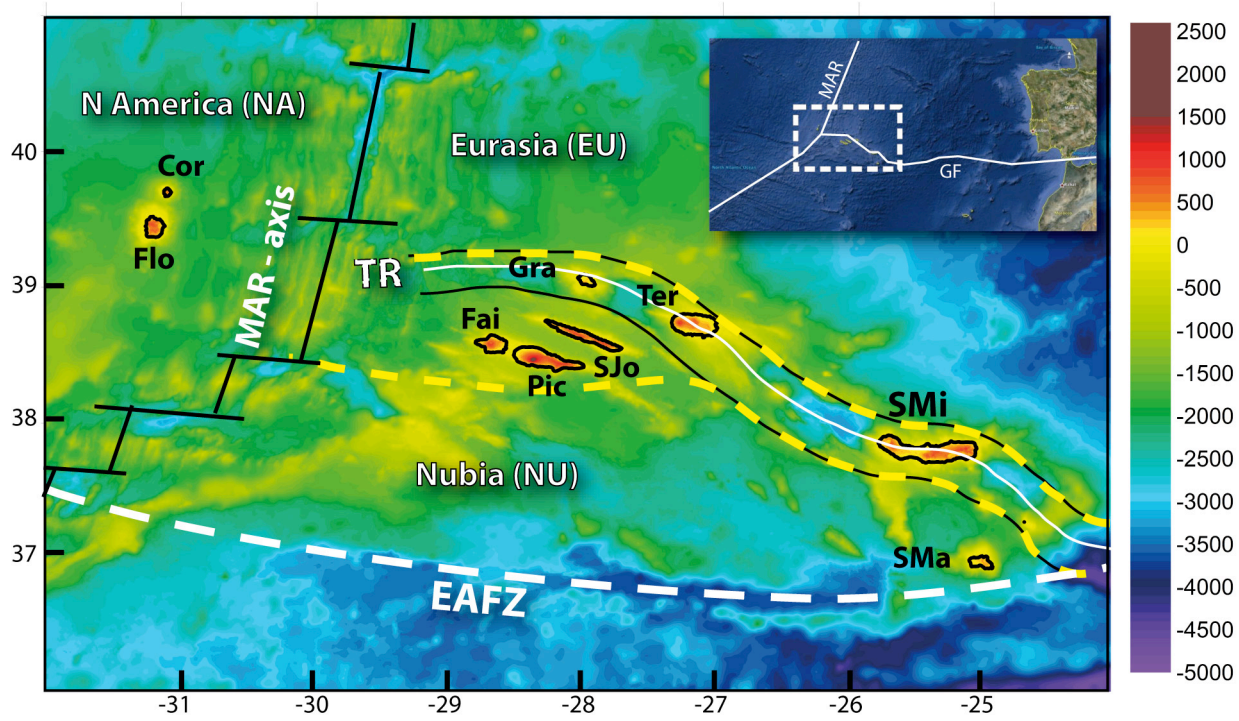


Figure IV. 1. Bathymetric map of the Azores region from Lourenço et al. (1998). The black lines indicate the location of the Mid-Atlantic ridge (MAR) axis, and associated transforms. The thin white and black lines indicate the centre and the wall of the Terceira Rift (TR), respectively. The white dashed line marks the East Azores Fracture Zone (EAFZ). The yellow dashed lines mark the diffuse boundary between the Eurasia and Nubia plates from Marques et al. (2013, 2014a). The colour scale is in meters. The islands are referenced as Cor - Corvo; Flo - Flores; Fai - Faial; Pic - Pico; SJo - S. Jorge; Gra - Graciosa; Ter - Terceira; SMi - S. Miguel; SMa - Santa Maria. Inset at the top right corner for location.

Using a high-resolution DEM, we first analysed and interpreted the morphological patterns of S. Miguel, including the main edifices and the various potential mass-wasting structures. We then focused our fieldwork strategy on the most relevant areas. The new high-precision K-Ar dating on separated mineral phases allowed us to constrain the chronology of the various stages of morpho-structural evolution of S. Miguel. We correlate the study of the available aeromagnetic data (onshore data) with the new seismic profiles to the south of eastern S. Miguel (offshore) to investigate our hypotheses of major flank collapses, to identify their potential location and extent, and then discuss the relationships between the volcanism of S. Miguel and the active tectonics of the TR.

IV. 1. 2. Geological background

S. Miguel is made up of several main polygenetic volcanoes and monogenetic strombolian cones, with eruptive style ranging from hawaiian - strombolian (Ferreira, 2000) to highly explosive Plinian events (e.g. in Fogo stratovolcano, Wallenstein, 1999). The existing geological maps of S. Miguel are somewhat different, depending on the authors. Zbyszewski et al. (1958, 1959) defined 8 volcanic zones (Fig. IV.2a), which are from east to west: (1) The Nordeste region; (2) the Northern plateau; (3) the Povoação volcano; (4) the Furnas volcano; (5) the eastern Waist Zone; (6) the Fogo volcano; (7) the western Waist Zone; and (8) the Sete Cidades volcano. More recently, other authors slightly modified this division (Queiroz, 1997; Wallenstein, 1999; Ferreira, 2000; Gomes et al., 2005). Moore (1990) simplified the previous map and grouped the eastern part of S. Miguel in one zone, and therefore proposed 6 zones in total (Fig. IV.2b). These are from east to west: (1) the Nordeste shield volcano, which comprises the Povoação caldera; (2) the trachytic stratovolcano of Furnas; (3) the eastern Waist Zone, a field of alkali basalt cinder cones and lava flows with minor trachyte and tristanite (K-benmoreites); (4) the trachytic stratovolcano of Fogo; (5) the western Waist Zone comprising a field of alkali-basalt cinder cones and lava flows with minor trachyte; (6) the trachytic stratovolcano of Sete Cidades.

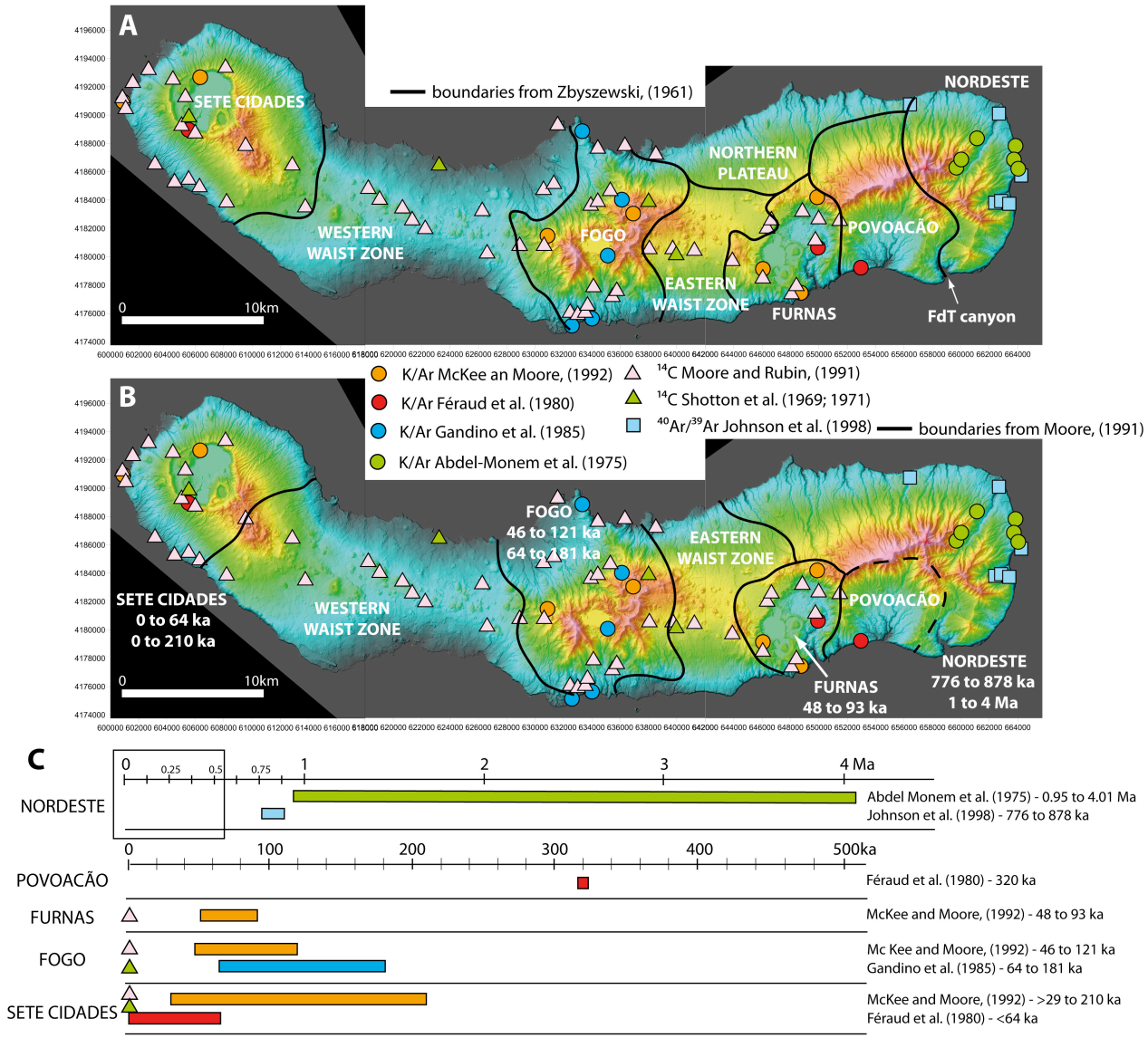


Figure IV. 2. Elevation map of S. Miguel built from a Digital Elevation Model (DEM) with a 10 m spatial resolution. Ages measured with various methods and techniques in previous works are shown. (A) Map with the volcanic zones defined by Zbyszewski (1961). (B) Map with the volcanic zones according to Moore (1991a). The zone of Povoãçao is in dashed lines because it is considered as a part of the Nordeste volcano by Moore (1991a). (C) Timeline summarizing the ages and methods as a function of the main volcanoes.

Although a significant amount of radio-isotopic dating has been carried out on the various volcanic units (Fig. IV.2), the geological evolution of S. Miguel remains poorly constrained in time. From early geochronological studies based on whole-rock K/Ar, the eruptive history of the island would span the last 4.0 Myr (Abdel-Monem et al., 1975). Alternatively, later works showed that the dominant part of the island was built during the last 1 Myr, with a generally accepted westward growing trend (Féraud et al., 1980; Gandino et al., 1985; McKee and Moore, 1992; Johnson et al., 1998).

According to stratigraphic and geochronological data, the Nordeste complex in easternmost S. Miguel comprises the oldest exposed rocks on the island. It is mostly composed of mafic rocks rich in olivine and pyroxene phenocrysts (Abdel-Monem et al., 1975; Fernandez, 1980). Based on

K-Ar dating of the upper (0.95 ± 0.07 Myr) and lower (4.01 ± 0.45 Myr) stratigraphic rocks of the Nordeste Volcano, Abdel-Monem et al. (1975) concluded that the time period for the main edification was about 2.16 Myr. Johnson et al. (1998) used $^{40}Ar/^{39}Ar$ dating on separate groundmass from the Nordeste Volcano and obtained ages in the interval 776 ± 12 ka to 878 ± 45 ka. Johnson et al. (1998) reported that these samples contain significant amounts of olivine and pyroxene phenocrysts, and thus likely contain excess argon, which can explain the large differences in ages between the study of Abdel-Monem et al. (1975) and Johnson et al. (1998). The main structural feature of the Nordeste complex is the Povoação depression, which affects the rocks of the Nordeste basaltic complex and is partly filled with volcanic deposits and ignimbrites produced by the Furnas volcano (Duncan et al., 1999). The interpretation of the volcanism in the Povoação depression differs according to the authors. It has been variably interpreted as (i) an autonomous volcano (Zbyszewski, 1961), (ii) a part of the Nordeste complex affected by a caldera collapse (Moore, 1990), or (iii) a graben (Sibrant et al., 2013). Yet, only one lava flow sample collected along the eastern costal cliff of Povoação was dated by Féraud et al. (1980), and gives an age of 320 ± 60 ka.

The Furnas Volcano is trachytic in nature, and most of its activity has involved explosive volcanism with voluminous eruptions of trachyte pumices. This edifice consists of a steep sided caldera complex, built on the outer flanks of the Nordeste complex and Povoação depression (Guest et al., 1999). Some relicts of the Furnas Volcano flank have been identified in the south, along the costal cliff, and in the west (Zbyszewski, 1961; Cole et al., 1999). According to Moore (1991b), the Furnas Volcano is the youngest of the three polygenetic active volcanoes of S. Miguel, with a subaerial activity starting at 93 ± 9 ka (McKee and Moore, 1992). The main caldera collapse would have occurred around 12 ka (Moore, 1990). The number of caldera collapse events is still under debate: one, two or three, according to Moore (1990), Duncan et al. (1999) and Montesinos et al. (1999), and Guest et al. (1999), respectively.

The eastern Waist Zone, between the Furnas and Fogo volcanoes, comprises a plateau mainly composed of lava flows and a ca. N110º alignment of basaltic cinder/spatter strombolian cones.

According to Wallenstein (1999), the Fogo Volcano is the most complex structure among the three stratovolcanoes (Furnas, Fogo, and Sete Cidades). It has a complex morphology with a summit caldera that appears to have formed as a result of numerous vertical caldeira collapse events. The oldest activity of the Fogo Volcano yields an imprecise age of 280 ± 140 ka on a submarine sample in the northern flank (Muecke et al., 1974), and an age of 181 ± 15 ka on a subaerial lava flow (Gandino et al., 1985). Two caldera events have been identified, one between 26.5 and 46 ka from K/Ar on whole rocks (McKee and Moore, 1992), and another at 15.2 ± 0.3 kyr from radiocarbon dating (Moore and Rubin, 1991).

The western Waist Zone, linking the Fogo and Sete Cidades stratovolcanoes, comprises mostly fissural volcanism (Ferreira, 2000). This low altitude area with rectangular shape in plan

view comprises several monogenetic scoria and spatter basaltic cones with minor trachytic domes, mostly installed along two trends, N75° and N130°.

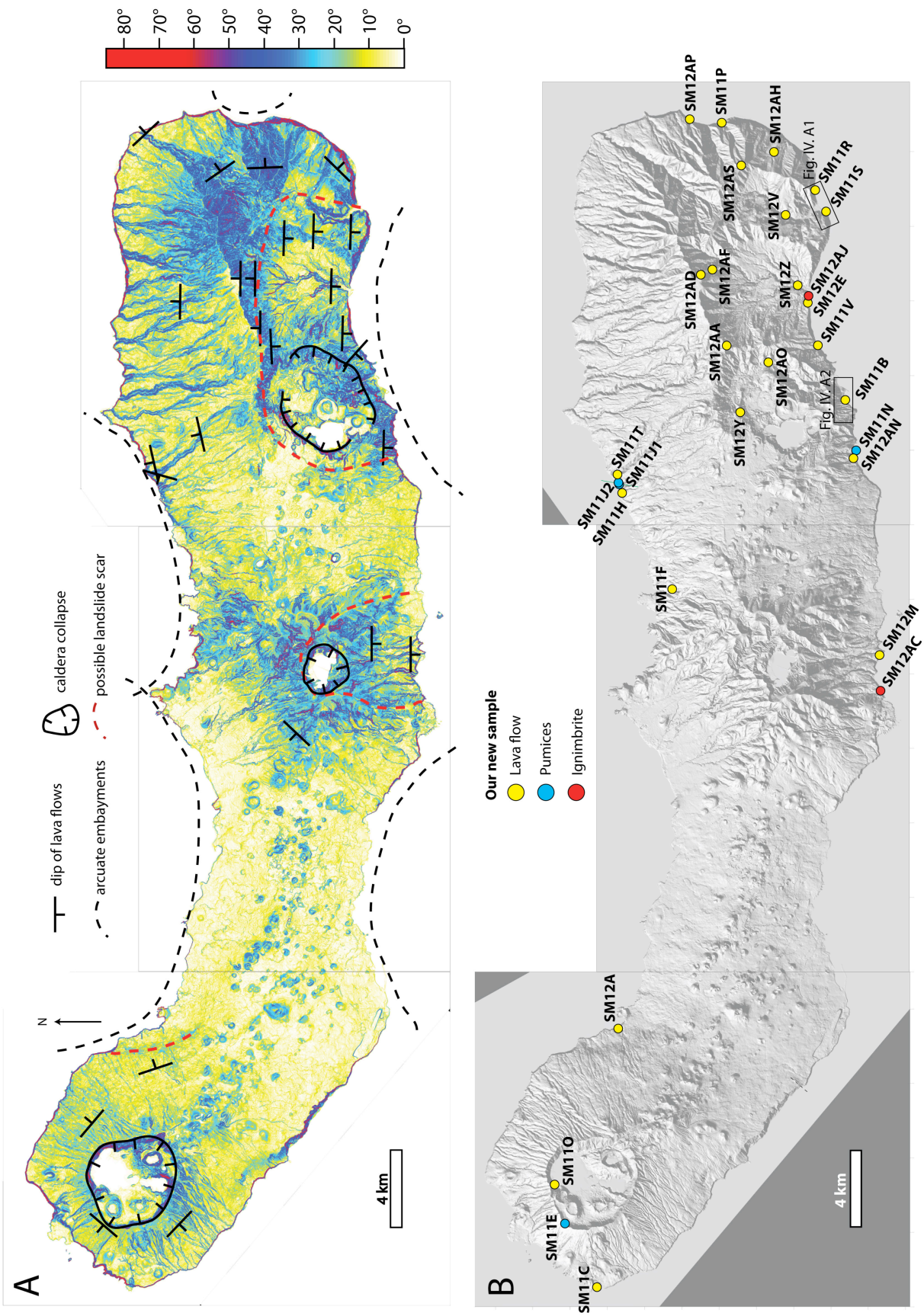
Sete Cidades is believed to be the most active stratovolcano in S. Miguel (Queiroz and Gaspar, 1998). This trachytic volcano is affected by a caldera where pumice cones, domes and maars can be observed, whereas domes and scoria/cinder cones are the dominant monogenetic structures outside the caldera. For McKee and Moore (1992), the Sete Cidades volcano had an initial sub-aerial phase at 210 ± 8 ka, and experienced a main unique caldera event at 22 ka. Queiroz et al. (2008) proposed that the current caldera structure results from three independent vertical collapse events at 36 ka, 29 ka and 16 ka, the last one involving the collapse of the N and NE caldera walls. Moore (1990) suggested a probable age around 22 ka for the last main collapse, which controlled the current caldera shape.

Two structural trends have been identified in S. Miguel, N110º and N150º, which seem to control the position and distribution of the volcanic edifices (Zbyszewski et al., 1959; Moore, 1991a). The surface expression of the faults is represented by fault scarps, which sometimes form large graben structures in Nordeste and Povoação, elongated N110º and N150º, respectively (Sibrant et al., 2013). Sibrant et al. (2013) also identified a new N50º trend that they interpreted as a transform trend similar to the trend recognized recently in Faial (Marques et al., 2014b) and in Graciosa (Sibrant et al., 2014).

IV. 1. 3. Methods and Results

IV. 1. 3. 1. Geomorphological analysis, fieldwork and sampling strategy

A geomorphological analysis of the island was performed from a digital elevation model (DEM) with a 10 m spatial resolution, in order to identify the main morpho-structural units and better define areas of particular importance for subsequent fieldwork (Fig. IV.3). We especially superimposed a mosaic of high-resolution satellite images (Orthophotomaps) over the high-resolution DEM to build 3D views and better examine the geometry of the various edifices and their mutual relationships, and put in evidence structures potentially created by destruction processes. The island comprises two main linear trends: a western third elongated N130º, and the eastern two thirds elongated N75º. The transition between these two main sectors comprises a narrow and flat zone with strombolian cones bounded in the north and in the south by conspicuous coastal embayments. Similar coastal embayments are also visible in the eastern half of the island (Fig. IV.3). The eastern sector of S. Miguel is additionally characterized by a significant morphological asymmetry. While the northern flank of the island shows rather regular and gentle external slopes (15° in average, fig. 3a), the southern flank features a large depression bounded by a prominent E-W scar. South of the scar, the topography appears irregular and rather complex. It comprises smaller structures, e.g., a sub-circular caldera, a series of canyons, and coastal cliffs of various heights.



189 **Figure IV. 3**. Maps of S. Miguel generated from the high-resolution DEM. (A) Slope map of S. Miguel with
190 our structural interpretation, main structural features, and dip of lava flows measured in the field. (B) Shaded
191 relief map of S. Miguel, with lighting from NW, and location of our samples and nature of the rocks collected
192 in the present study.

A significant part of the fieldwork was thus conducted in the eastern half of the island, which was complemented by focused investigations on the central and western parts. Our strategy was devised to constrain the age of the successive construction and potential destruction phases. Most of S. Miguel is covered by very young pyroclasts erupted from the trachytic Furnas, Fogo and Sete Cidades volcanoes, and by dense vegetation. Therefore, field investigations were conducted mostly along the coastal cliffs and in the deep canyons where accessible (Fig. IV.3).

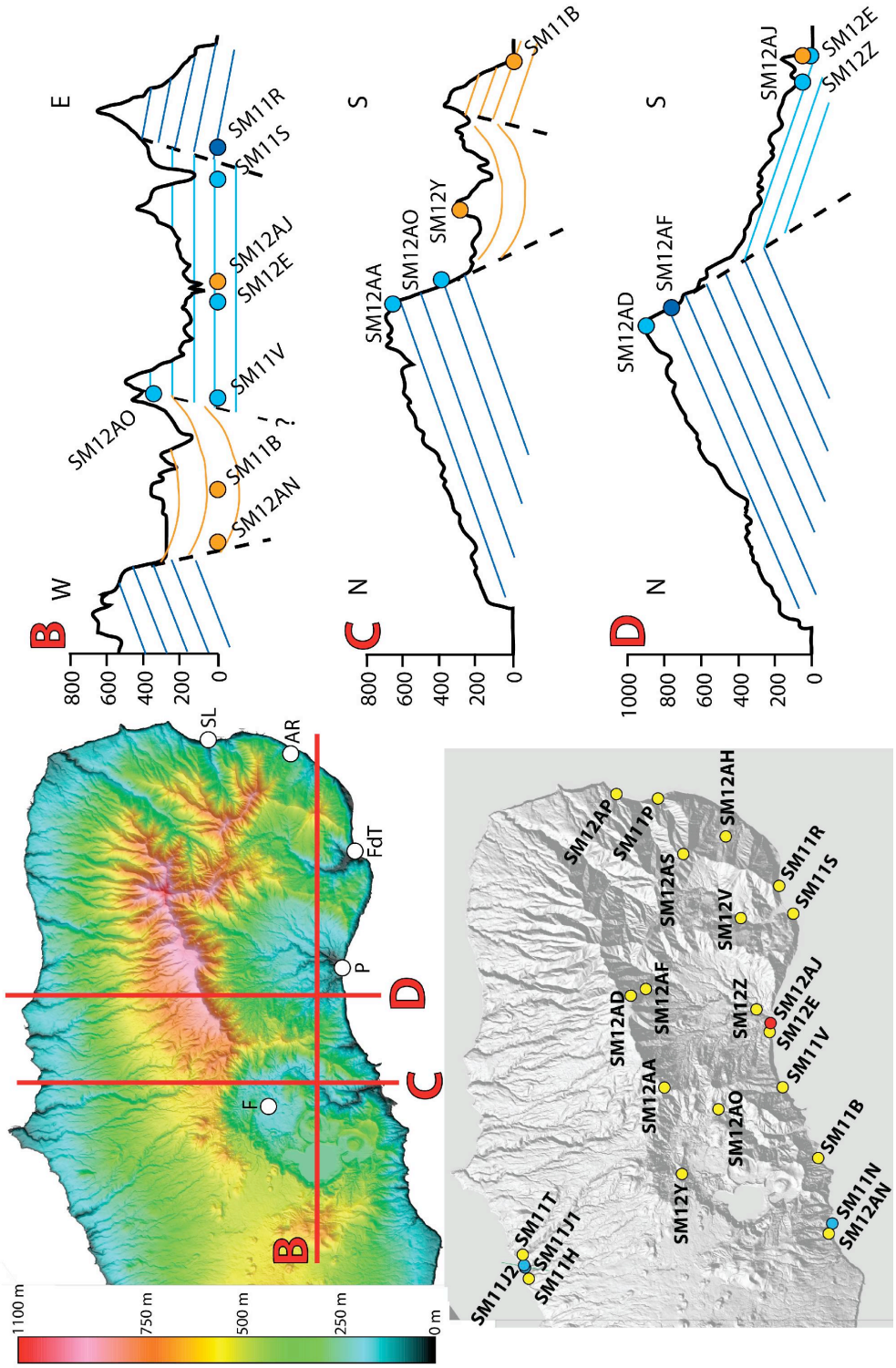


Figure IV. 4. Topography of eastern S. Miguel with the location of our new samples. Cross sections show the main volcano-stratigraphic relationships and the schematic position of our samples. The colour code stands for lava successions from the main volcanic complexes: dark blue for Nordeste, light blue for the Filling volcanism of Povoação, and orange for the Furnas volcano and associated ignimbritic deposits. F: Furnas; P: Povoação; FdT: Faial da Terra; AR: Água Retorta; SL: S. Lourenço.

In the easternmost part of the island, the Nordeste Complex comprises a succession of thick basaltic and ankaramitic lava flows dipping towards the east (Figs. IV.2, IV.3, IV.4). We collected two samples at the base of the eastern coastal cliff (SM12AP and SM11P), and a lava flow at the top of the succession (SM12AS). Similarly, we collected one of the uppermost lava flows (SM12AH) on a crest bounding a N110º depression interpreted recently as a graben (Sibrant et al., 2013). All the sampled lava flows show a dip of ca. 10° toward the ocean (Figs. IV.3, IV.4). Because of the dip, only the upper parts of the Nordeste are exposed in the coastal cliffs. To try and sample the lowermost part of the old succession, we took advantage of the main scar and canyons. Farther south, a major canyon cuts the same succession E of the Povoação depression (Faial da Terra, FdT, see Fig. IV.2 for the location), where we could observe different lava flows on each side of the canyon (supplementary material, Fig. A1). The lavas dipping to the S on the western slope are massive, thick, and with crystals of amphibole, whereas on the eastern slope the lava flows dip to the SE, are thin, numerous and basic, with basalt and ankaramite rocks (with olivine and pyroxene phenocrysts). The western differentiated lavas have been mapped by Moore (1991a) as coming from a differentiated dome. This difference in nature and geometry (dip of lavas) indicates that this canyon has incised a discontinuity that materializes the boundary between Povoação and Nordeste volcanic complexes (Fig. IV.4b). In order to constrain this discontinuity in time and then the nature of the discontinuity, lava flows were collected on both slopes of the main canyon (SM11S in the west, and SM11R in the east). Upstream in the canyon, we collected another massive and relatively acid lava flow (SM12V). Small canyons are disposed radially on the northern flank of Nordeste volcano, except the one most to the northwest, with a clear NW-SE direction (Fig. IV.3). In the field, this canyon materializes a clear discontinuity between massive and thick lava flows (summit of the cliff - SM11T) in the E, and pyroclasts and pumice deposits (SM11J1 and SM11J2) in the W. The pumices have been later covered by a recent lava flow, which we also sampled (SM11H). This discontinuity along the canyon probably materializes the boundary between an old structure (Nordeste Volcano or Povoação volcanism?) and the more recent volcanism from the Furnas Volcano.

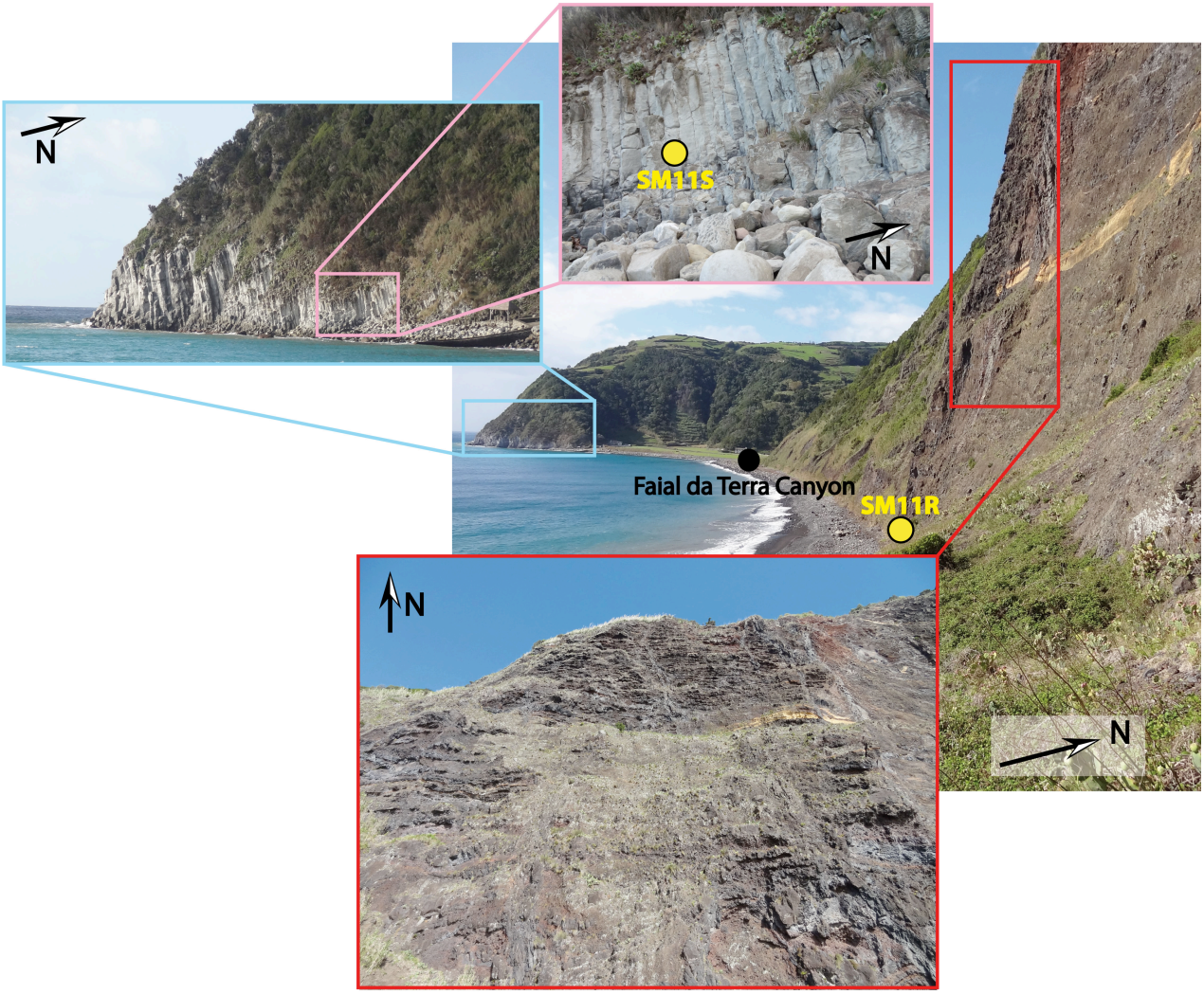


Figure IV. A1. W-E costal cliff on both sides of Faial da Terra. See Fig. IV.3 for the precise location of the general picture. Yellow circles indicate the position of samples SM11S and SM11R. Note the difference of nature of the rock to west and east of the canyon. Thick and differentiate in the west, and basic and thin lavas truncated by numerous dykes in the east.

234

235 The southern flank of the Nordeste Volcano comprises two depressions, Povoação in the E
236 and Furnas in the W. These two depressions share two common crests with E-W and N-S
237 directions (Figs. IV.3, IV.4). In the field, the E-W scar north of the Povoação depression is covered
238 by vegetation, which partially masks the volcanic units. Further down (ca. 650 m), the scarp
239 comprises several basaltic lava flows dipping towards the N, which means that the E-W crest
240 truncates the regular northern slope and lava flows of the Nordeste Volcano (or Povoação
241 Volcano?). No associated lava flows dipping to the S have been identified south of the E-W scar.
242 The most appropriate flow (SM12AF) was collected to know which complex is truncated by the
243 scar: is it the Nordeste Complex or Povoação volcano identified by Moore (1991a)? The nature of
244 the scar can be a caldera wall, a major fault or a flank collapse. The top of the scar comprises
245 several domes that are not cut by the scarp, and which sit on the north-dipping basaltic lava flows.
246 These domes are regularly found all along the E-W scarp close to Povoação. Two of them were

sampled (SM12AA and SM12AD, Figs. IV.3, IV.4). The western part of the scarp north of Furnas is more difficult to access, nevertheless some isolated outcrops indicate that the lava flows generally dip towards the NW (Figs. IV.3, IV.4). Unfortunately, these lavas were too altered to be sampled. The N-S crest making the boundary between the Furnas volcano and the Povoação depression is composed of several basaltic lava flows dipping towards the S (Fig. IV.4). We collected one of the uppermost at the top of the crest (SM12AO). We note that this lava flow is locally covered by ignimbrite deposits. The ignimbrite is continuous from Furnas to the SE shoreline (Povoação) as described by Duncan et al. (1999). It filled an existing depression and reached the sea near Povoação, where we collected a sample (SM12AJ). With a thickness of about ~10-15 m, the ignimbrite is mostly composed of welded glass (fiamme) and comprises centimetric alkali feldspar and few pyroxenes. In the south, the N-S crest splits towards the SW and the SSE (Fig. IV.4), and defines the rims of the two depressions. Along the coastal cliff, half way between the bifurcated crests, a canyon has developed at the discontinuity between two different units (Fig. IV.4b). The western coast is composed, at the base, of alternating pumice falls, pyroclastic flows and scoria with a westward dip. The eastern side comprises numerous basaltic lava flows dipping toward the S, where a sample was collected at the base of the cliff (SM11V). The nature of the discontinuity could not be identified, because the canyon has developed at the contact. However, the small width and the abrupt wall can be indicative of a major vertical contact between the Povoação volcanism and the Furnas volcano. Such contact may reflect either a caldera wall, a fault or the scar of a flank collapse.



Figure IV. A2. Southern costal cliff of Furnas volcano composed of alternating surge, pumice and cinder. See Fig. IV.3 for the location of the picture.

The depression of Povoação is much more regular than the Furnas calderas (Figs. IV.3, IV.4). It has a circular shape and a watershed configuration convergent towards the village of Povoação. This depression is floored by a lava flow (SM12Z) that is covered by a massive ignimbrite, which most probably originated at the Furnas Volcano (Duncan et al., 1999). In the field we can effectively follow with a relative precision the ignimbritic flow from the top of the caldera wall (along the N-S crest) down to Povoação watershed outlet, where we sampled it (SM12AJ). The southern part of the depression is composed of numerous lava flows dipping to the S. At the base of the cliff, we collected a lava flow (SM12E) immediately to the W of the main bounding fault of the N150º graben proposed by Sibrant et al. (2013).

On the DEM (Fig. IV.3), Furnas is composed of an elliptical discontinuous scarp, recognized as a caldera rim (Moore, 1990; Duncan et al., 1999; Guest et al., 1999; Montésinos et al., 1999). To constrain the maximum age of the caldera collapse, we collected a lava flow on the top of the northern scarp (SM12Y). The Furnas volcano is difficult to constrain geographically, because no classic conical shape can be followed. The southern flank of the volcano can be reasonably well discriminated, whereas the northern flank is elusive. The southwest part of the coastal cliff is composed of alternating pumice, cinder, surges and few scoria, which are truncated by several thick (up to 10 m) basaltic dykes. Towards the top, we collected one of the rare lava flows (SM12AN), and a pumice layer at the base of the cliff (SM11N). To the east, the coastal cliff is also composed of alternating surge, pumice and cinder, which cover basaltic lava flows (SM11B – supplementary material, Fig. A2). This part of the cliff seems younger than the SW part, because the canyons are less deep (on the DEM) and incise units of similar composition.

In the central part of the island, the Fogo volcano is cut by deep canyons, especially on the southern flank (Fig. IV.5). The summit depression, filled with a lake, has an irregular boundary and significantly departs from a typical caldera shape. The walls of the depression comprise several trachytic plugs and domes with chaotic debris intercalated with large blocks and pumices. Unfortunately, no sufficiently fresh lavas could be observed and sampled. On the northern flank of the edifice, the hydrological network shows a relatively radial pattern, whereas the southern flank is affected by linear, parallel and deep canyons oriented roughly N-S. In this sector, N-S and E-W topographic cross sections (Fig. IV.5) highlight three relevant features: (1) The N-S cross-section reveals that the southern flank is much steeper than the northern flank; (2) the northern flank shows two scarps, dipping to the south in the cross section (blue arrows) and curved in the 3D view, which could correspond to the headwall of major sector collapse(s); and (3) the E-W cross-section shows that the N-S canyons formed in an area of lower elevation, which is bounded by two high N-S crests. Between these two high crests (Fig. IV.5), the Fogo Volcano is composed of alternating pumice deposits, surges, pyroclastic flows and significant debris (supplementary material, Fig. A3). Only one thick lava flow could be observed and sampled (SM12M). Other lava flows were collected on the NE flank (SM11F), which seems to be the well-preserved flank of the volcano, and therefore probably the oldest rocks of Fogo. We also collected an ignimbrite rich in K

feldspar (SM12AC) and fiammes to constrain the most likely age of the inferred collapses.

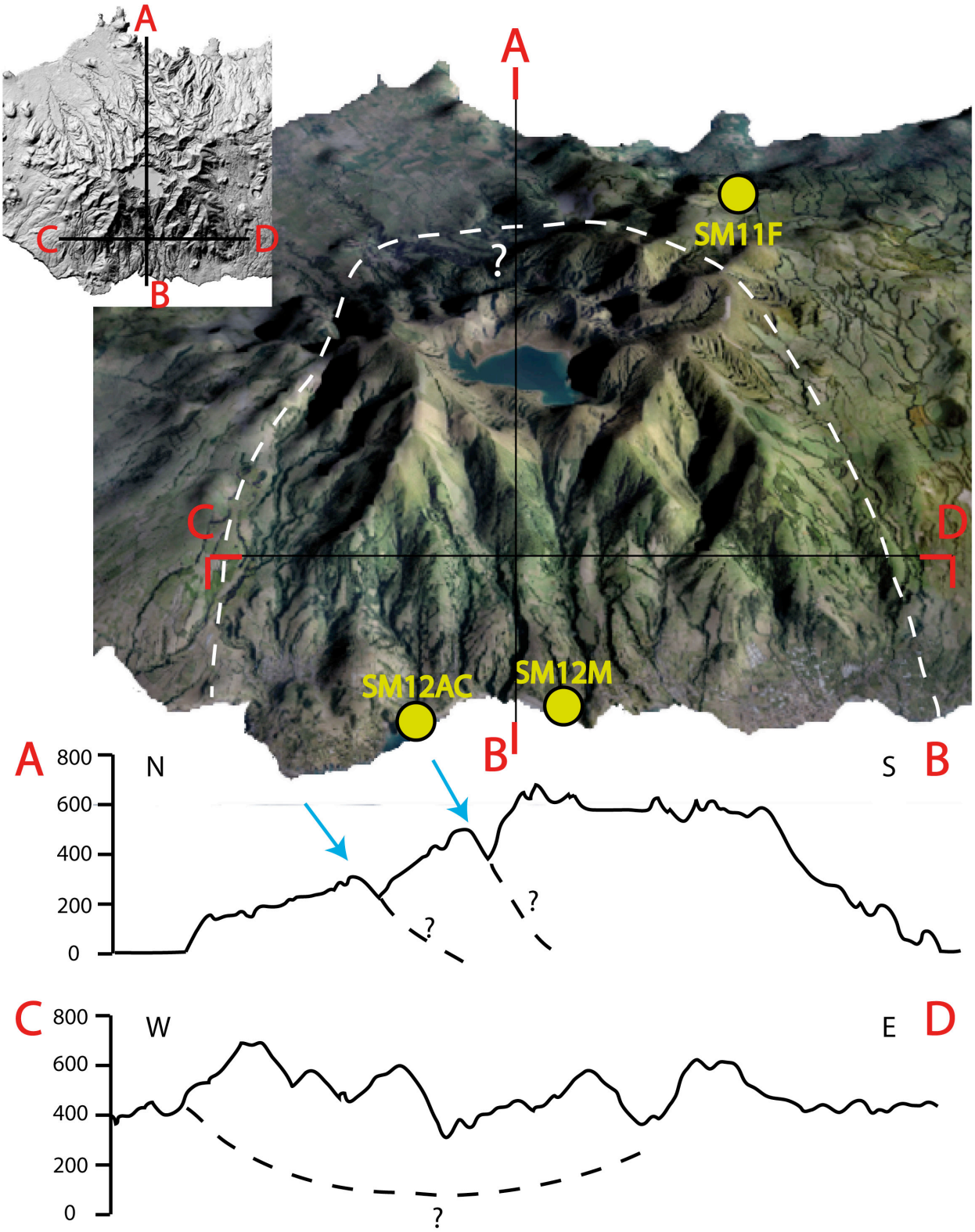


Figure IV. 5. 3D view of Fogo seen from the south. The cross-sections highlight the irregular topography of the area. The arrows indicate deep canyons, which can be associated with probable landslide(s). The dashed white line indicates the possible shape and location of the flank collapse(s).



Figure IV. A3. Outcrop comprising boulders of different nature (from basalt to trachyte) in a cinder matrix. The debris sit on a thin cinder layer without boulders.

In the western part of the island, the oldest accessible lava flows of the Sete Cidades Volcano were collected at the base of the caldera wall (SM11O) (Fig. IV.3), seemingly at the same place where McKee and Moore (1992) collected their samples (MF-81-75). The uppermost part of the volcano's activity is exposed at the top of the caldera rim and is made of pumice deposits (SM11E). Along the NW sea cliff, west of the Sete Cidades caldera, a major ignimbrite unit composed of fiammes and comprising numerous feldspar crystals is covered by lava flows; we collected one lava flow to constrain the minimum age of one of the caldera collapse events (SM11C). Along the NE sea cliff, east of the Sete Cidades caldera, where the shaded relief map (Fig. IV.3) indicates an arcuate scarp, we collected a lava flow comprising crystals of amphibole and pyroxene, which fills a paleotopography and seems cascading from the top of the cliff (SM12A). This sample will constrain the maximum age of the scarp.

IV. 1. 3. 2. New K-Ar dating

325

Sample	UTM 26 E	UTM N	phase	K%	40Ar* (%)	40Ar* (at/g) 1011	**Age (ka)**	Unc. (ka)
SM12AF	655306	4184790	Gmd	2.089	21.13%	17.834	817	12
					23.23%	17.784	815	12
							816	**12**
SM11P	663543	4183744	Gmd	1.836	20.3%	15.309	798	12
					25.51%	15.35	800	12
							799	**12**
SM12AP	650731	4181720	Gmd	1.96	20.84%	16.221	792	12
					23.92%	16.113	787	12
							789	**12**
SM11R	659859	4178832	Gmd	2.317	36.08%	18.778	776	11
					44.42%	19.186	793	11
							785	**11**
SM12AS	653287	4179068	Gmd	2.188	37.22%	17.43	763	11
					37.89%	17.519	766	11
							765	**11**
SM12AH	661756	4179342	Gmd	1.85	27.33%	14.44	747	11
					31.2%	14.539	752	11
							750	**11**
SM12AO	645433	4176650	Gmd	4.101	8.33%	21.601	504	9
					7.48%	21.865	510	10
							507	**10**
SM12V	658807	4180777	Gmd	2.213	22.29%	11.286	488	7
					32.22%	11.412	494	7
							491	**7**
SM12E	653847	4179187	Gmd	4.326	21.8%	19.697	436	6
					16.02%	19.447	430	7
							434	**7**
SM12AD	633109	4175281	Gmd	2.105	32.48%	9.025	410	6
					28.75%	9.045	411	6
							411	**6**
SM11V	651611	4178676	Gmd	1.641	14.43%	6.782	396	6
					16.36%	6.582	384	6
							389	**6**
SM12AA	651651	4183469	Gmd	5.424	35.27%	17.436	308	4
			feld	5.64	27.38%	17.897	304	4
							306	**4**
SM11S	658846	4178356	Gmd	5.428	48.03%	16.885	298	4
					52.62%	16.943	299	4
							298	**4**
SM11F	638812	4186603	Gmd	1.067	4.94%	2.95	265	7
					5.34%	3.065	275	6
							270	**6**

SM11T	644201	4189073	Gmd	3.419	17.62%	9.45	265	4
					26.74%	9.55	267	4
							266	**4**
SM12Z	654966	4179813	Gmd	3.02	11.07%	7.856	249	4
					12.25%	7.895	250	4
							250	**4**
SM11N	645890	4176602	feld	5.891	5.83%	8.519	138	3
					6.62%	8.524	139	3
							138	**3**
SM11J1	643818	4189256	feld	6.115	15.26%	7.582	119	2
					16.94%	7.404	116	2
							117	**2**
SM11O	606651	4192895	Gmd	2.654	4.24%	2.507	90	2
					3.59%	2.552	92	3
							91	**3**
SM11J2	643818	4189256	feld	6.253	6.33%	5.845	89	2
					18.23%	5.65	87	1
							87	**1**
SM12ACa	651616	4181517	feld	6.212	6.03%	5.434	84	2
					7.32%	5.572	86	2
							85	**2**
SM12A	614967	4189491	Gmd	3.226	4.4%	2.479	74	2
					3.47%	2.38	71	2
							72	**2**
SM11C	601041	4190599	Gmd	2.989	3.89%	1.994	64	2
					2.91%	2.031	65	2
							64	**2**
SM12AJ	661079	4180403	feld	6.52	5.55%	4.147	61	1
					5.25%	4.087	60	1
							60	**1**
SM12AN	650177	4177768	Gmd	2.949	1.54%	1.605	52	3
					2.03%	1.632	53	3
							53	**3**
SM11B	648699	4177214	Gmd	3.646	0.9%	1.943	51	6
					0.59%	1.764	46	8
							49	**7**
SM12Y	647940	4182848	Gmd	4.39	2.54%	1.107	24	1
					2.6%	1.011	22	1
							23	**1**
SM12M	635181	4175629	Gmd	3.905	0.42%	0.8763	21	5
					0.32%	0.6	15	5
							19	**5**
SM11H	643438	4189110	Gmd	1.862	0.16%	0.223	11	7
					0.35%	0.392	20	6
							17	**6**

SM11E	604544	4192374	feld	5.084	1.66%	0.673	13	1
					1.61%	0.753	14	1
							13	**1**

Table IV.1. New K-Ar ages obtained with the unspiked Cassignol-Gillot technique on fresh separated groundmass (Gdm) and alkali feldspars (feld). For each sample, the mean age is obtained by weighing by the amount of radiogenic argon. The uncertainties are quoted at the 1σ level.

In order to check the freshness state of the samples, thin sections were carefully observed under the microscope. The K-Ar Cassignol-Gillot technique used here is particularly well suited to date Quaternary volcanic material (Gillot and Cornette, 1986). Samples were crushed and sieved to the chosen fraction (typically 125-250 µm) depending on the mineral phase to be extracted (Table 1). For basic rocks (basalts and hawaite) and more acid rocks (mugearite to trachyte), the groundmass phase was concentrated, while sanidine were separated for pumices and ignimbrites. After ultrasonic cleaning in a 10% nitric acid followed by complete rinsing in distilled water and drying, heavy liquids were used in order to eliminate early crystallizing phases (e.g., plagioclase, pyroxene or olivine phenocrysts), to avoid any inherited excess ^{40}Ar. K was measured by flame emission spectrometry and compared with standards MDO-G (Gillot et al., 1992) and BCR-2 (USGS) dissolved and measured in the same conditions as the samples, and Ar was measured by mass sector spectrometry (Gillot and Cornette, 1986). Details about the analytical procedure can be found elsewhere (Gillot et al., 2006). ^{40}Ar and ^{36}Ar are measured simultaneously, avoiding any potential signal drift during peak switching. The atmospheric correction, also performed after each sample analysis, is achieved by comparison of the $^{40}Ar/^{36}Ar$ ratio of the rocks with a pipette measured in the same condition and level of signal. for a given ^{40}Ar signal, a reproducibility of better than 0.1% is observed for successive atmospheric $^{40}Ar/^{36}Ar$ measurements. Typical uncertainties of 1% are achieved for both the ^{40}Ar signal calibration and for the K determination. The uncertainty on the $^{40}Ar^*$ determination is a function of the radiogenic content of the sample, the detection limit is presently of 0.1% of $^{40}Ar^*$ (Quidelleur et al., 2001), corresponding to around 1 ka for a 1% K-basaltic lava. Decay constants and isotopic ratios of Steiger and Jäger (1977) have been used. K-Ar ages obtained in this study are reported in Table IV.1 and are quoted, together with all previous ages throughout this study, at the 1σ confidence level.

356

357

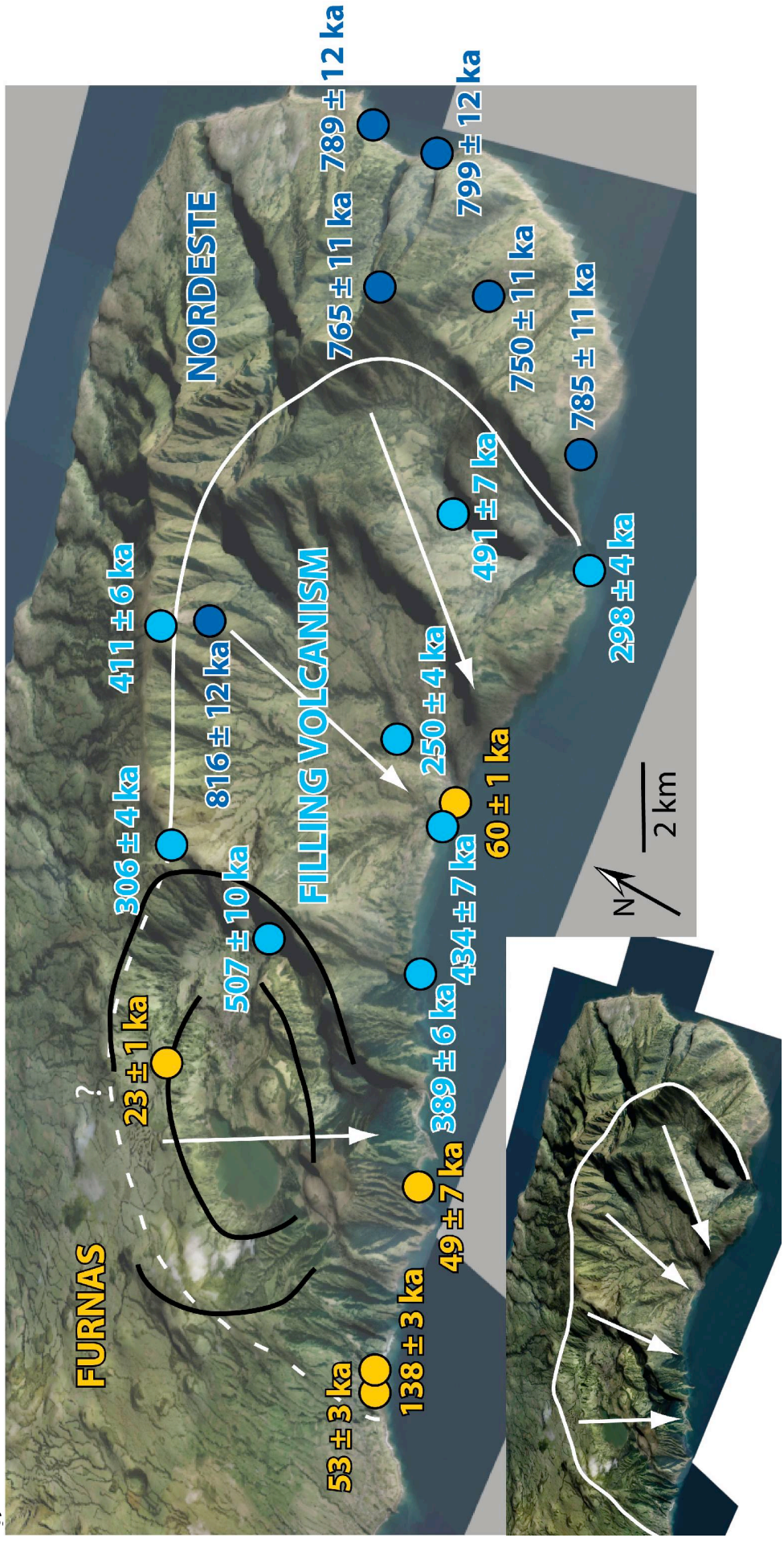

NORDESTE
FILLING VOLCANISM
FURNAS
789 ± 12 ka
799 ± 12 ka
765 ± 11 ka
750 ± 11 ka
785 ± 11 ka
491 ± 7 ka
298 ± 4 ka
411 ± 6 ka
816 ± 12 ka
250 ± 4 ka
60 ± 1 ka
306 ± 4 ka
507 ± 10 ka
434 ± 7 ka
389 ± 6 ka
23 ± 1 ka
49 ± 7 ka
138 ± 3 ka
53 ± 3 ka
?
N
2 km

Figure IV. 6. 3D view on the eastern part of S. Miguel, obtained by superimposing the satellite image over the high resolution DEM. The new K-Ar ages are shown. The colour code separates lava successions from main volcanic complexes: dark blue for Nordeste, light blue for the Filling Volcanism of Povoação, and orange for the Furnas volcano and associated ignimbritic deposits.

The ages measured on our samples from S. Miguel range between 816 ± 12 ka and 13 ± 1 ka (Table IV.1). The results obtained on the different lava flows from the Nordeste complex range between 816 ± 12 ka and 750 ± 11 ka. These results are significantly younger than previous K-Ar dating between 4 and 1 Ma (Abdel-Monem et al., 1975), and consistent with the $^{40}Ar/^{39}Ar$ ages of Johnson et al. (1998), which range between 878 ± 45 ka and 776 ± 12 ka. This range of activity shows that the Nordeste complex has experienced a rapid late stage of subaerial growth of about 100 kyr. The new ages measured on lava flows from the western slope of the eastern canyon of Povoação and in the Povoação depression range between 507 ± 10 ka and 250 ± 4 ka, which is significantly younger than Nordeste Volcano (Fig. IV.6). Our new results give an age of 60 ± 1 ka for the ignimbrite of Furnas collected in the Povoação depression. The lavas and pumices collected in Furnas volcano are dated here between 138 ± 3 ka and 23 ± 1 ka, which significantly expands the previous range between ca. 93 and 48 ka given by McKee and Moore, (1992). The lava truncated by the caldera is here dated at 23 ± 1 ka, which gives us a maximum age for second caldera collapse of Furnas. The new ages measured on lava flows and pumices on both sides of the northwestern canyon of Furnas range between 266 ± 4 ka and 17 ± 6 ka. The age obtained for our sample SM11F collected in Fogo volcano is here dated at 270 ± 6 ka, which overlaps with the age of sample SM11T (266 ± 4 ka). The age we obtained on an ignimbrite in southern Fogo is 85 ± 2 ka, and the age of an intercalated lava flow indicates a young activity of Fogo at 19 ± 5 ka. Finally, the new ages measured on Sete Cidades range between 91 ± 3 ka and 13 ± 1 ka, which is significantly less than the 210 ± 8 ka age reported by McKee and Moore (1992), using K-Ar on whole-rock of a sample seemingly collected at the same place.

IV. 1. 3. 3. High-resolution bathymetric data and seismic reflection profiles

The field observations (main scar and discontinuities), the stratigraphic relationships (geometry of the lavas), and the new K-Ar dating reveal that the Nordeste complex is preserved in the northern and eastern parts of the island. However, the lava succession is truncated by the E-W scar and the main canyon of Faial da Terra (Fig. IV.2). Therefore, the southern sub-aerial flank of the Nordeste complex is missing. We infer that the scar represents a destruction stage that affected most of the southern flank of the Nordeste complex. This destruction stage can be a fault displacing the southern flank, or a major flank collapse. In order to choose between these two hypotheses, we used new high-resolution bathymetry and several offshore seismic profiles acquired south of Nordeste to look for eventual debris deposits.

Multichannel seismic data sets were collected by the University of Hamburg on board of *RV METEOR* during cruise M79/2 in 2009 (Hübscher, 2013). Seismic signals were generated by an

array of two GI-Guns with a generator volume of 45 cui and an injector volume of 105 cui each. For data recording a 600 m long asymmetric digital streamer was used, containing 144 channels with an average increment of 4.2 m. Shots were released every 25 m at a speed of 5 kn. Data processing first encompassed trace editing and CMP sorting with a CMP increment of 5 m. Bandpass and spike & noise burst filters, FX-deconvolution and FK-filter were applied before NMO-correction and post stack time migration.

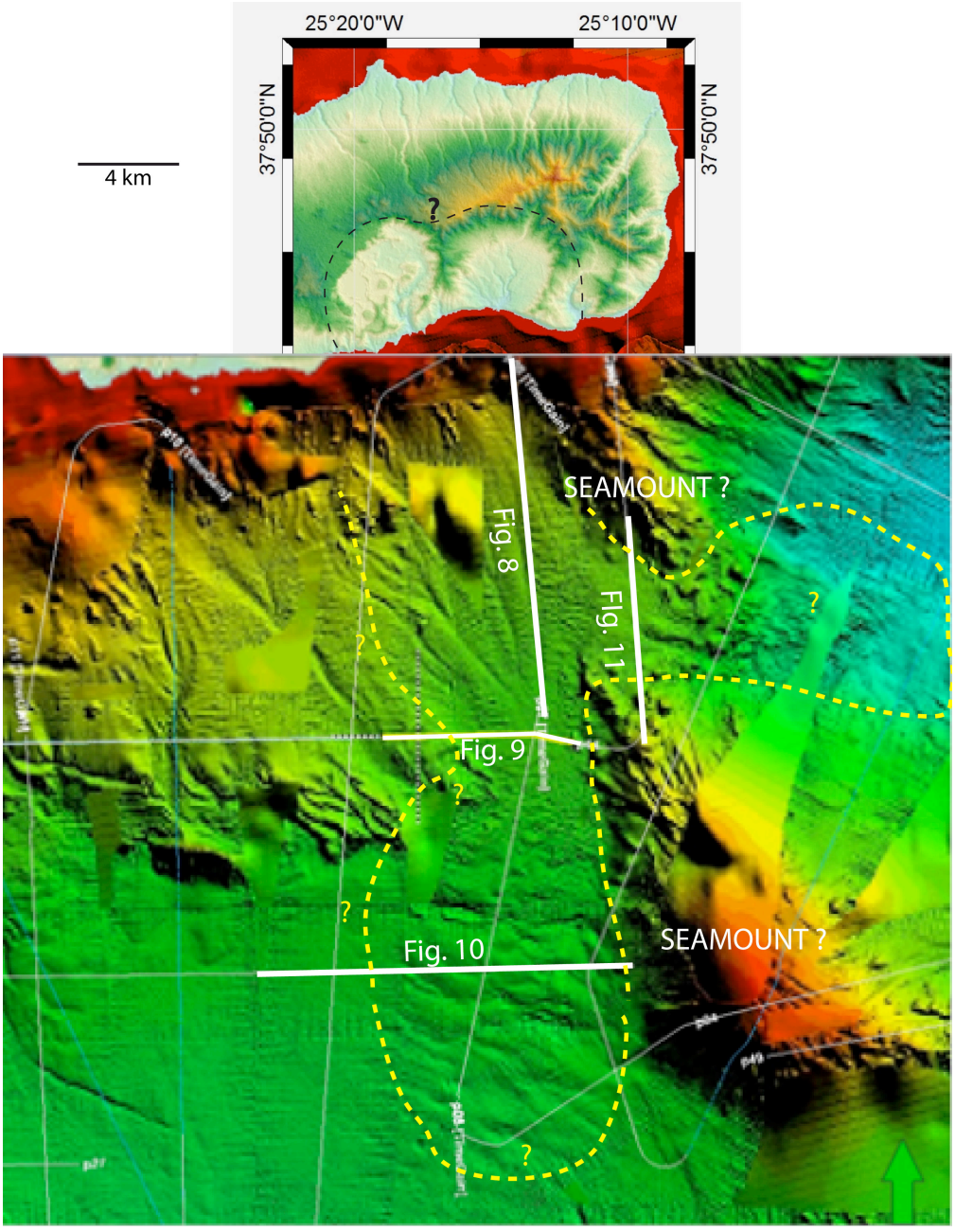


Figure IV. 7. High-resolution bathymetry of the southeastern part of S. Miguel. The yellow dashed line shows the inferred area potentially covered by landslide deposits. The white lines indicate the location of the seismic profiles shown in the Figs. IV.8, IV.9, IV.10, IV.11.

The high-resolution bathymetry south of Nordeste Volcano (Fig. IV.7) shows several relevant features: (1) a large prominent submarine relief located ca. 20 km SE of the island shore.

It is elongated roughly N150° and includes linear sub-parallel fractures. Therefore, it most probably constitutes a faulted seamount of volcanic origin. The northern flank of this large seamount is apparently covered by a few rounded blocks. (2) Another elongated relief is located in a more proximal position, and constitutes part of the island submarine flank. Its SE end comprises a very irregular morphology with a chaotic aspect. (3) Both seamounts are bounded in the west by a N-S elongated submarine lobe offshore the Povoação area. The distal part of the lobe shows an irregular and lenticular aspect, suggesting an accumulation of volcano-sedimentary deposits coming mostly from the island and/or the upper submarine flank where the shelf is interrupted by a steep arcuate embayment. (4) Finally, rounded blocks are not visible at the topography surface on front of Povoação, whereas some of them are visible around the large prominent submarine relief. The rounded blocks can be absent or Blanketing by recent explosive deposits from Furnas and Fogo and volcano- sedimentary deposits.

The location of the seismic lines is shown in Fig. IV.7, and the corresponding N-S and E-W seismic profiles are shown in Figs. IV.8, IV.9, IV.10, IV.11. On the seismic profiles, three seismic facies can be defined: (1) the material filling much of the sea floor topography is seismically imaged as laterally continuous beds with generally consistent amplitudes. We call this sediment facies, and interpret it as fine-grained sediments mostly coming from the island. (2) The lenticular and/or laterally discontinuous high-amplitude bedded reflections, which taper away from the island flanks, is here interpreted as pyroclastic facies. We suggest these units were deposited during periods of eruptive activity and represent stacked volcaniclastic flow deposits (e.g., from partial dome collapses or caldera events). According to LeFriant et al. (2010), this kind of deposit may accumulate rapidly like in the 1995 Montserrat eruption. (3) The acoustic basement shows convex-upwards rounded reflections of hundreds to thousands of meters in size, often with high amplitudes. This facies occurs nearby the island flanks and is associated with an irregular deposit surface. We interpret it as a deposit containing large blocks sourced from volcanic flank collapse, as recognized elsewhere (e.g. LeFriant et al., 2004; Lebas et al., 2011). This facies is also chaotic to transparent, with low amplitude bedded or deformed seafloor sediment. More transparent intervals may indicate greater sediment disaggregation or deposits of fine-grained volcaniclastic material. Here the landslide facies has an intermediate character, which we interpret as a mix of volcanic blocks with a relative proportion of sea floor and terrigenous sediments.

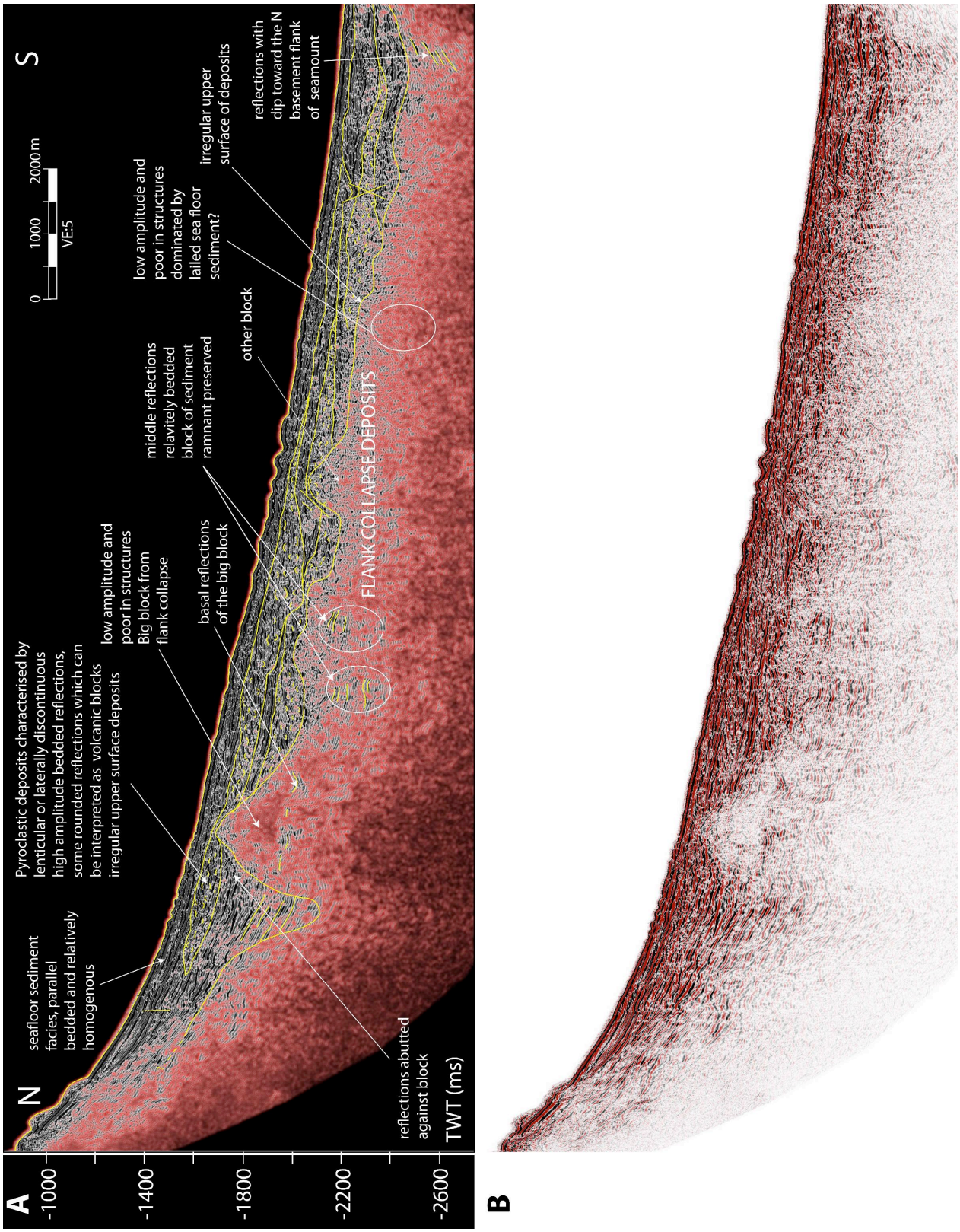


Figure IV. 8. N-S seismic profile offshore Povoação showing the stratigraphy of mass-wasting deposits sourced in Nordeste. The rugged seafloor is here interpreted as a flank collapse deposit. Notice the presence of kilometre size blocks. (A) Our interpretation; (B) profile without interpretation. VE is vertical exaggeration. Notice the presence of large blocks close to the island. Location of the seismic profile is reported in Fig. IV.7.

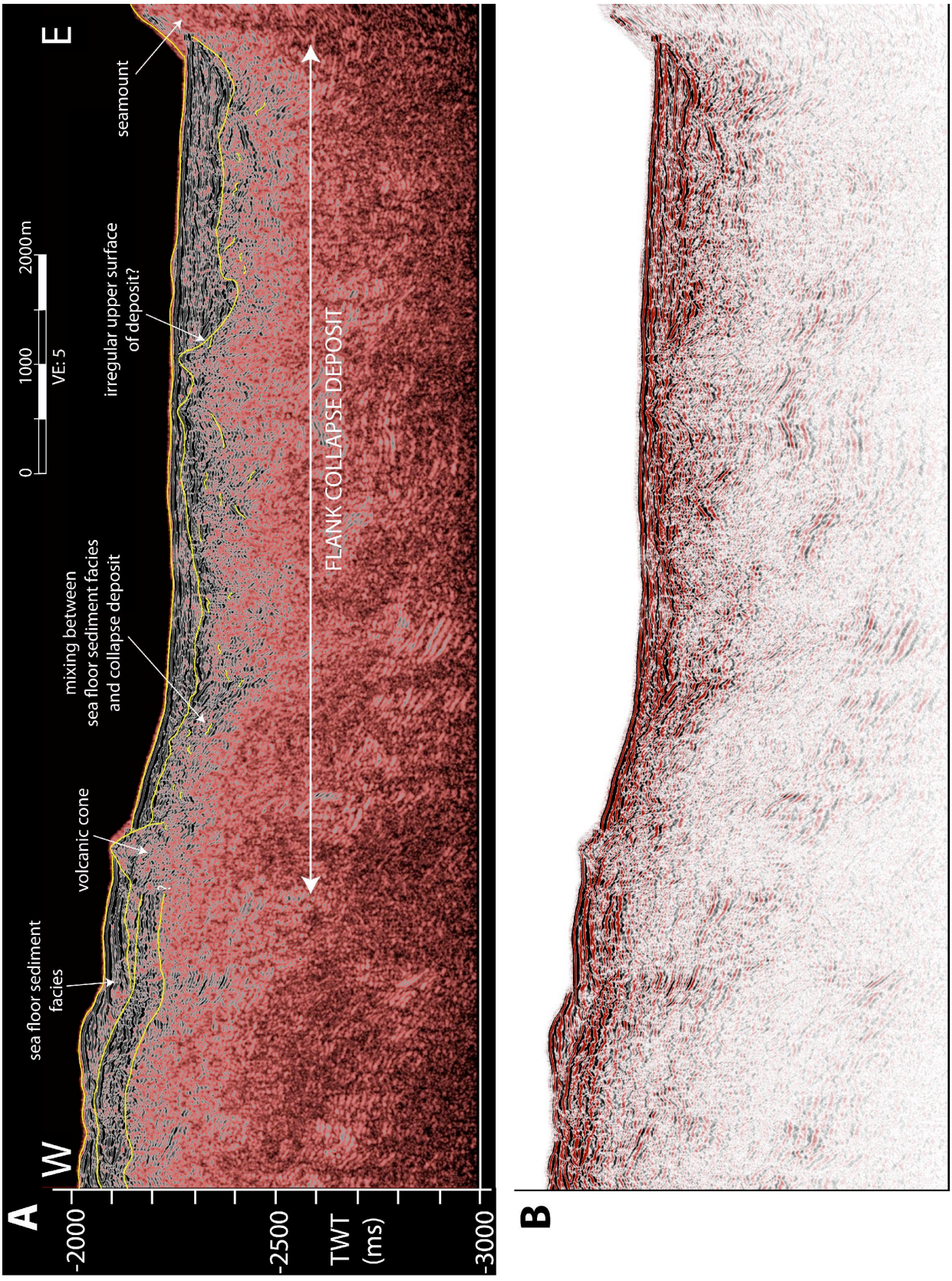


Figure IV. 9. E-W distal seismic profile offshore south of Nordeste. Notice the length of the lateral deposit and the absence of reflections at the bottom of the lenticular flank collapse deposit. (A) Our interpretation; (B) seismic profile without interpretation. VE is vertical exaggeration. Precise location of the seismic profile is reported in Fig. IV.7.

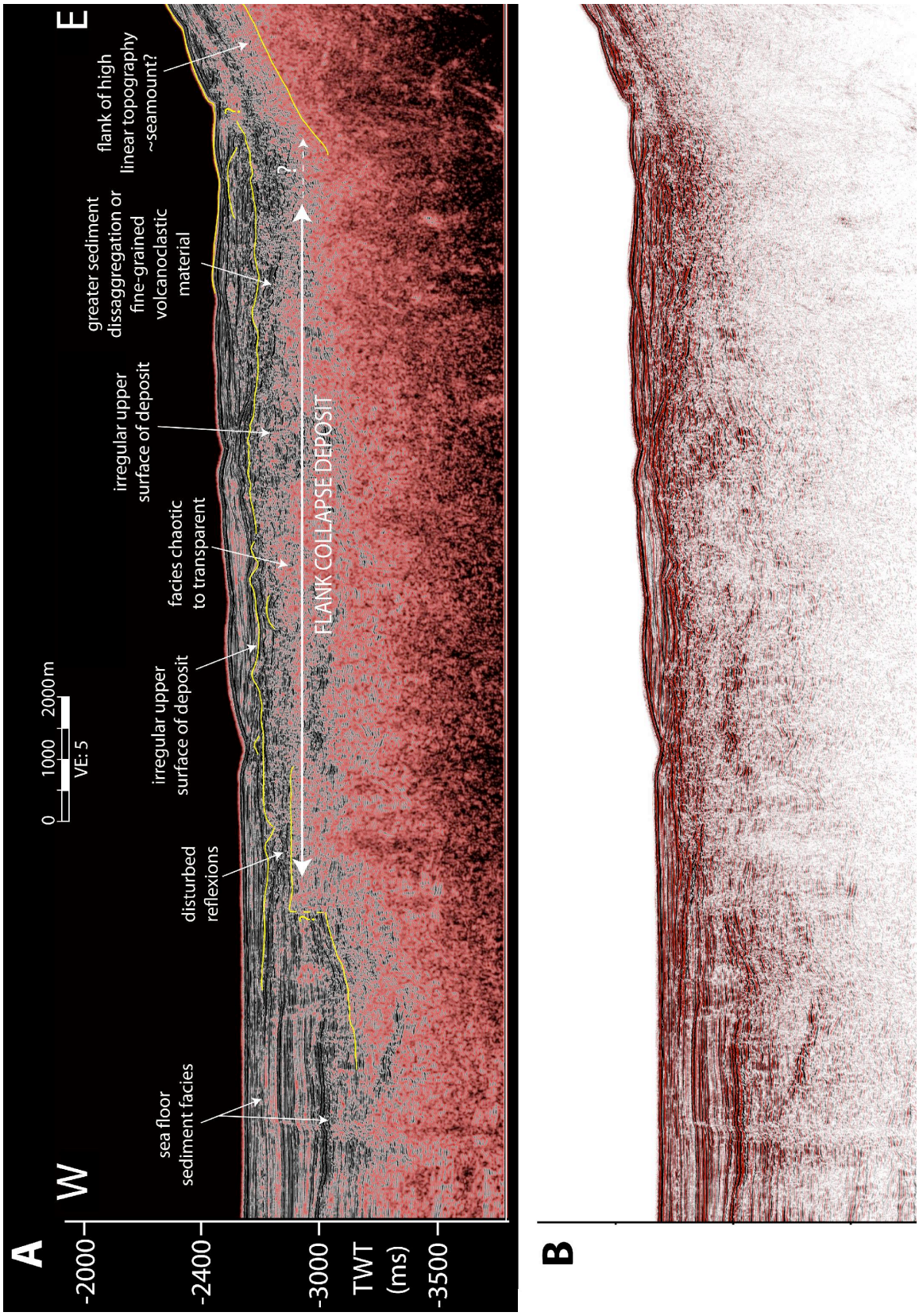


Figure IV. 10. E-W seismic profile further south. (A) Our interpretation; (B) seismic profile without interpretation. VE is vertical exaggeration. Notice the absence of large collapse blocks, the less irregular contact between the identified flank collapse deposit and the sediment, and the higher thickness of the sea-floor sediment facies in the W. Location of the seismic profile is shown in Fig. IV.7.

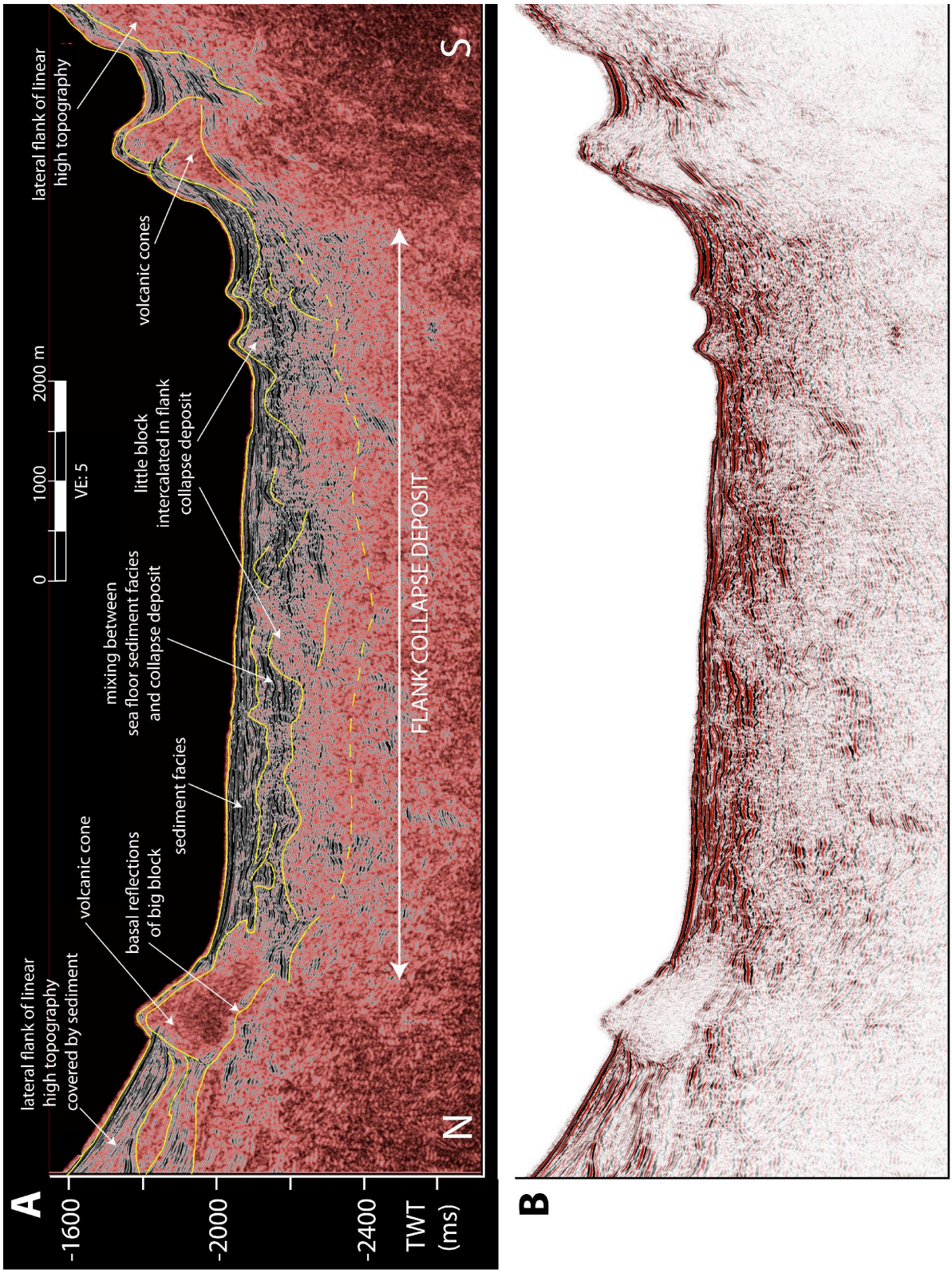


Figure IV. 11. N-S seismic profile south of Faial da Terra canyon, showing the stratigraphy of mass-wasting deposits offshore Nordeste. Note the presence of volcanic cones. Notice that the surface topography of the interpreted flank collapse is more irregular than the profiles in Fig. IV.10. This indicates that the profile is closer to the source of the flank collapse deposits. (A) Our interpretation; (B) seismic profile without interpretation. VE is vertical exaggeration. Location of the seismic profile is reported in Fig. IV.7.

In the four seismic profiles, we can distinguish flank collapse deposits. The morphology and content of what we identify as flank collapse debris depends on position and orientation of the seismic profiles. In the N-S seismic profile (south of Povoação – Fig. IV.8), several large blocks (up to 2000 m) can be distinguished. Their size decreases progressively towards the south, i.e. away from the source. In the two E-W seismic profiles (Figs. IV.9, IV.10), the inferred collapse deposit has a lenticular shape, which seems to decrease in thickness (from profile Figs. IV.8 to IV.10) and lateral extension towards the S. The debris dimensions decrease to the south (southernmost W-E seismic profile). It seems proportionally enriched in sedimentary and erosional content and less on pyroclastic deposit with distance from the island (Fig. IV.10). Unfortunately, the basement of the debris cannot be seen in the seismic profiles, which precludes the estimation of the landslide debris volume. The N-S seismic profile in front of the canyon of Faial da Terra is more difficult to interpret (Fig. IV.11). It shows two high submarine peaks (in the north and south), which can be interpreted as seamounts or large blocks kilometres in size (Fig. IV.11). High-resolution data is missing on the ridge like topographic relief offshore Povoação, nevertheless the size of this ridge is much greater than the size of the depression inherited from the major flank collapse which can be interpreted from our on land data, as the area of the submarine ridge is equivalent to the current area of the whole eastern part of the island (Fig. IV.7). Morphologically, it seems composed of linear fractures with a N150° trend, and the topography is irregular but mostly linear. In the light of this description we doubt that this topographic relief can be a collapsed block in the debris deposit. We interpret it as a linear seamount affected by N150° fractures which can be linked to the N150° graben identified in Povoação by Sibrant et al. (2013). Similarly, the topographic high closer to shore is linear and fractured in a N150° direction. It is probably the extension of the island, and not an individualised seamount.

IV. 1. 4. Discussion

IV. 1. 4. 1. The architecture of S. Miguel: new insights from our new data and available aeromagnetic map

Based on our new morphological analysis, fieldwork, K/Ar dating and offshore data, we propose that S. Miguel has been built by four main volcanoes, which have been affected by several destructive events. The oldest volcano, Nordeste, is here dated between 880 ± 12 ka and 750 ± 11 ka. This range of activity and the work done by Johnson et al. (1998) indicate that the volcano grew mainly during the last reversed magnetic polarity, prior to the Matuyama-Brunhes transition (dated at 789 ± 8 ka by Quidelleur et al., 2003). All the more recent volcanism in S. Miguel is younger than 750 ka, and thus has a positive magnetic anomaly. With this in mind, it is possible to investigate where the older volcanism is preserved under a thin cover of recent volcanism, or alternatively where it is missing, e.g. due to large-scale destruction by flank collapses. Therefore, we used available aeromagnetic map published recently (Miranda et al., 2013). For a better correlation

between rock ages, rock types and their magnetic signatures, we plotted the new ages on the aeromagnetic map of Miranda et al. (2013)(Fig. IV.12). The magnetic map (corrected for the topography) shows high amplitude positive magnetic anomalies corresponding to the young eruptive rocks covering the flanks of most of the volcanic systems. The NE part of Nordeste, the southern part of Fogo and the eastern part of Sete Cidades show negative magnetic anomalies (Fig. IV.12), therefore corresponding to rocks older than 789 ± 8 ka. Our new results on the Nordeste complex are consistent with the reversed polarity recorded in this area. However, we dated samples much younger than ca. 790 ka in Fogo and east of Sete Cidades, where the aeromagnetic data show a negative anomaly (Fig. IV.12). This apparent contradiction between isotopic and magnetic data shows that the aeromagnetic data should be used with precaution, because the observed magnetization is an average between various units with contrasting magnetic signatures. In this case, the apparent inconsistency could be due to: (1) a younger deposit not thick or dense enough to overcome the magnetic anomaly dominated by the underlying rocks older than ca. 790 ka; and (2) the more felsic nature of the younger rock. We conclude that the aeromagnetic data show an older basement, which might have evolved in two distinct ways: (1) it grew enough to form a proto-island that was subsequently destroyed, or (2) never produced an island, and the younger volcanoes grew on it.

We notice that on the southern coast of Nordeste, the signature is exclusively positive, therefore younger than ca. 790 ka as indicated by the new ages. This suggests that (1) the thickness of the positive lava is enough to overcome the negative signature of Nordeste, or (2) the Nordeste lava flows are much deeper in the Povoação depression. This second hypothesis is in agreement with the E-W scar, which truncated the lavas, the attitude of the lavas (dip), the younger lava that filled an arcuate depression, and the identification of a flank collapse deposit offshore.

The southern part of Fogo shows a negative polarity, whereas the northern flank shows a positive anomaly. The volcanic rocks in the south are pumice, surges, cinders and pyroclasts, i.e. more felsic and low density rocks. Northern Fogo is composed of several cones and recent lava flows. We thus infer that the asymmetrical polarity between north and south Fogo can be attributed to the nature and density of the rocks that constitute Fogo. Therefore, the question is why the rocks in Fogo are different in the north and south. The negative polarity seems to show a pattern close to a horseshoe shape, the morphology of the volcano, the irregular topography seen on the DEM and the lack of the lava flows in the southern part of Fogo can indicate a possible destructive event.

On Sete Cidades the lava flows younger than 789 ka covered the entire edifice except the NE part where the negative anomaly is detected. The shape of the negative polarity is arcuate toward the NE and open to the sea. This suggests that (1) a part of the thickness of the positive lavas is locally thinner; or (2) they have been removed by a flank collapse. In any case, we obtained an age of 72 ka for the lavas cascading on the scar partly visible on the DEM (Fig. IV.3a).

Here we argue that the negative magnetization of these three complexes is the result of the dominance of the magnetization acquired before ca. 790 ka. This means that the global elongated

shape of the island has been acquired before ca. 800 ka, and served as the basement for all subsequent volcanoes.

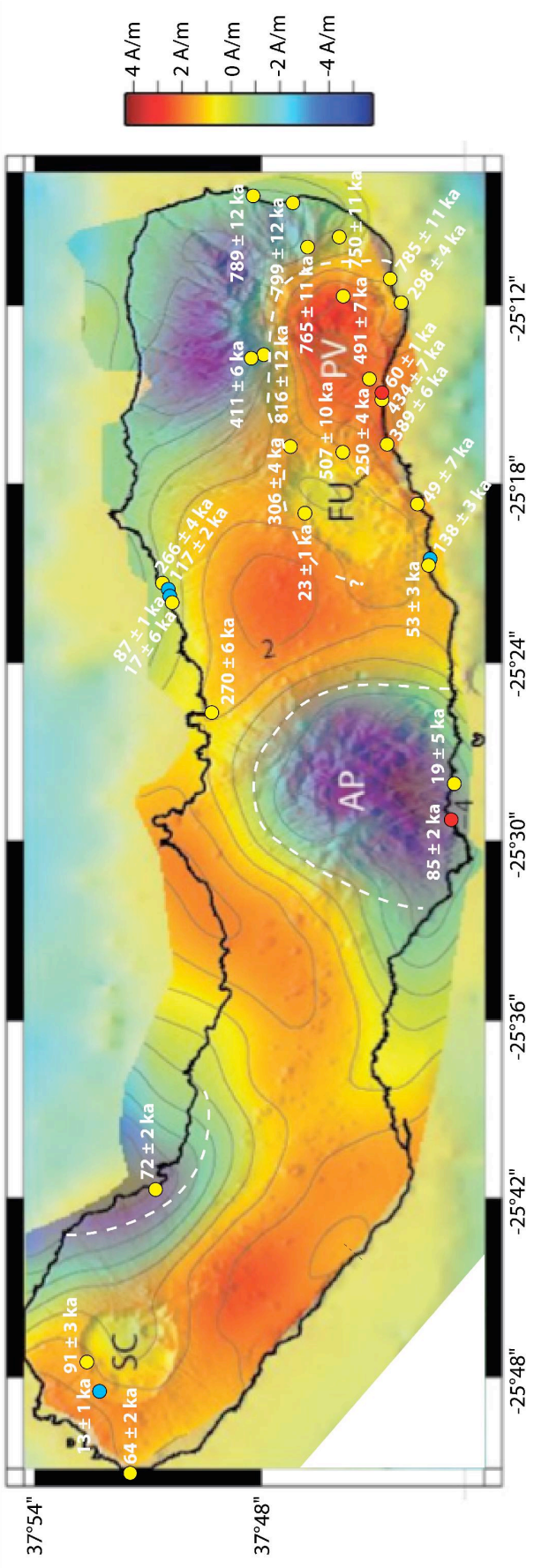


Figure IV. 12. Aeromagnetic map of S. Miguel from Miranda et al. (2013). The small coloured circles mark the location of the new K/Ar ages, and the colour of the circle indicates the nature of the rock: yellow for lava flows, blue for pumices, and red for ignimbrite flows. The dashed white lines indicate sharp variations in the magnetic signature east of Sete Cidades and on Fogo volcanoes.

IV. 1. 4. 2. Morpho-structural evolution of S. Miguel

Based on the morphological analysis, stratigraphic criteria, new K-Ar dating, marine data, and the correlation with aeromagnetic data, we can propose the following evolution for the S. Miguel Island (Fig. IV.13).

IV. 1. 4. 2. 1. The Nordeste Complex

The old volcanic succession cropping out in the eastern part of the island is dated here between 816 ± 12 ka and 750 ± 11 ka (Figs. IV.4, IV.12). These new results, coupled with previous $^{40}Ar/^{39}Ar$ ages of Johnson et al. (1998), indicate a phase of basic volcanic construction between 878 ± 45 ka and 750 ± 11 ka. The initial geometry of the Nordeste complex cannot be constrained precisely, because only the northern and eastern flanks of the original edifice are preserved. The contact between the young and the old rocks is well constrained and correlate well with the aeromagnetic data, the new ages and the morphology of S. Miguel. The filling volcanism of Povoação is here dated between 507 ± 10 ka and 250 ± 4 ka, which is significantly younger (ca. 250 ka) than the youngest dated Nordeste complex. Together with the recognition of an offshore flank collapse deposit (Figs. IV.8 to IV.11) in the southern part of the Nordeste complex, we infer that the Nordeste complex was affected by a major flank collapse toward the south. The flank collapse created a scar that was later filled by the volcanism of Povoação. From the new K-Ar dating and field observations, we infer that the flank collapse occurred between 750 ± 11 ka and 507 ± 10 ka. The contrast between the old and the filling volcanism makes the scar clearly visible in the 3D view shown in Fig. IV.6. The field observations indicate that the filling volcanism took place along a probable E-W rift zone, because all the new lava flows dip towards the south, and do not show a conical distribution. Part of this volcanism visibly occurred also through cones mostly located along the scar, the late lava flows which partly covered the preserved N and NW flanks of the Nordeste complex (Fig. IV.6).

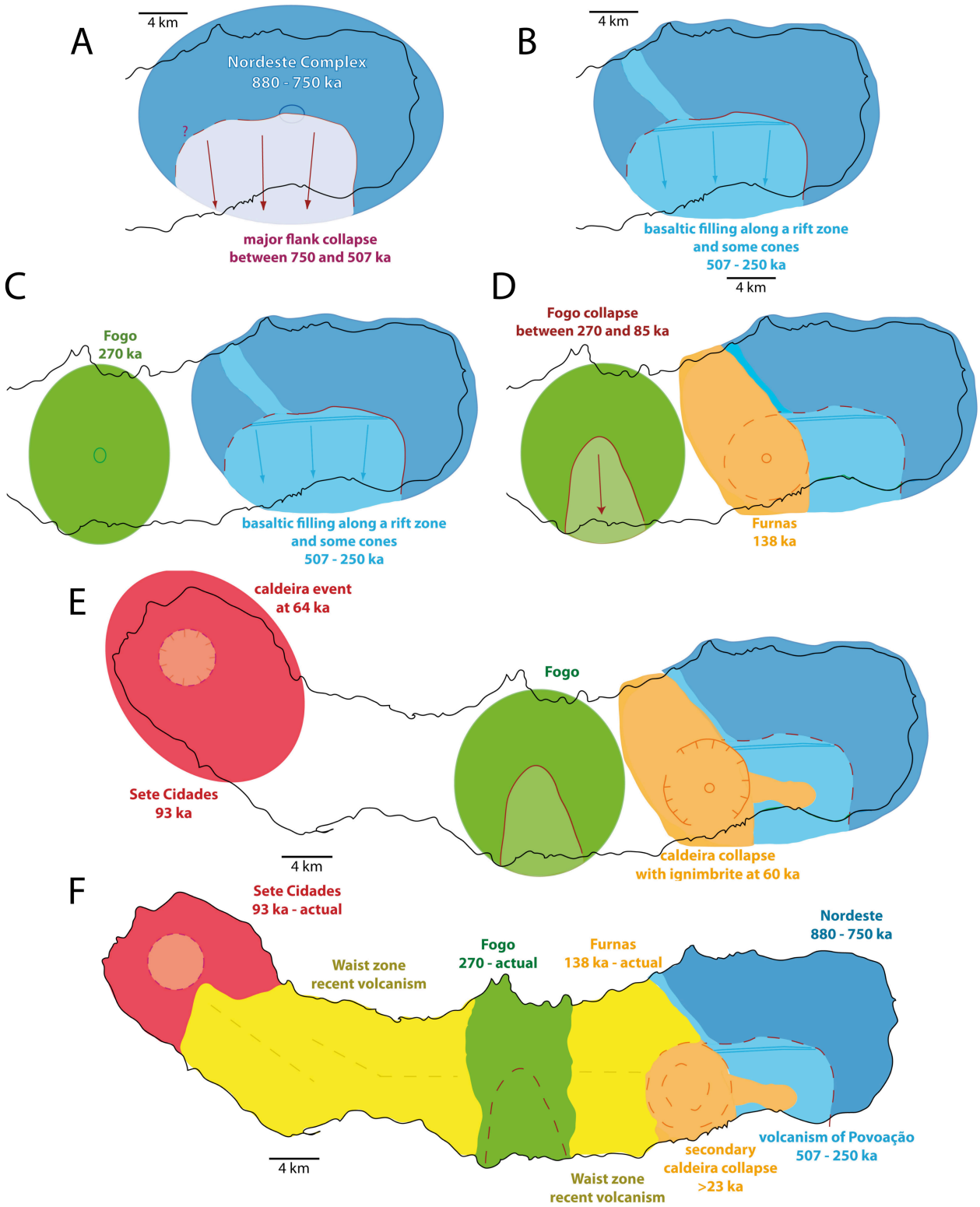


Figure IV. 13. Proposed schematic morphostructural evolution of S. Miguel.

571

572 *IV. 1. 4. 2. 2. Filling volcanism of Povoação*

573 The filling volcanism of Povoação was affected by a graben after 434 ka, the age of the
574 lavas truncated by the graben (sample SM12E). Sibrant et al. (2013) suggested that a caldera
575 collapse in Povoação is not necessary to explain the current morphology, and that the drainage
576 basin and erosion are enough. Especially, in an island where the erosion rate was estimated at

577 170-500 t/km^2/yr by Louvat and Allègre (1998), which is in the same order of magnitude of the
578 erosion rate calculated at 610 t/km^2/yr on Guadeloupe Island (Ricci et al., submitted).
579 The N-S crest that separates Furnas from Povoação is here attributed to the volcanism of
580 Povoação, based on the age of sample SM12AO (507 ± 10 ka). The crest seems modelled by
581 erosion in the east, whereas in the west it is steeper and in direct contact with the Furnas rocks
582 (Figs. IV.3, IV.4, IV.12). This crest has been previously interpreted as a caldera rim of the Furnas
583 Volcano (Cole et al., 1995; Montesinos et al., 1999). The youngest rock from Povoação is here
584 dated at ca. 250 ka (in the depression, SM12Z), and the oldest rock from Furnas is here dated at
585 ca. 138 ka (sample SM11N). This means that the Furnas volcano developed unconformably on the
586 volcanism of Povoação, as also attested by the age of the ignimbrite inside the Povoação Graben
587 (Figs. IV.4, IV.6). Moreover, the ca. N-S crest truncates the lavas identified as the filling volcanism
588 of Povoação (Figs. IV.4, IV.6). Therefore, the N-S crest can materialize (1) a scarp inherited from a
589 westwards flank collapse affecting the filling volcanism of Povoação, or (2) a normal fault, or (3) a
590 caldera rim. With the new K-Ar dating, we can estimate that the destruction event occurred
591 between ca. 250 ka and 138 ka. The hypothesis of a major flank collapse towards the west seems
592 improbable because during this time interval the edifice of Fogo was already partly built
593 immediately to the west. In the hypothesis of a normal fault, the scar should be linear instead of
594 arcuate as seen on the map, except if the scarp becomes elliptical due to regressive erosion. A
595 gap of ca. 110 ka does not seem enough to erode by regression ca. 2 km of basaltic lavas. The
596 third hypothesis seems the more likely explanation. As proposed by Cole et al. (1995) and later by
597 Montesinos et al. (1999), the scarp represents an old caldera rim (Fig. IV.13D). Unfortunately, our
598 sampling strategy cannot constrain this caldera event accurately. Our results only show that no
599 lavas younger than 250 ka have been found in the depression, which means that the caldera
600 collapse occurred after 250 ka.
601
602 *IV. 1. 4. 2. 3. The Fogo Volcano*
603 The oldest lava flow we dated in the Fogo volcano is 270 ± 6 ka (Fig. IV.13C), which is
604 consistent with the age obtained by Muecke et al. (1974). Despite Fogo being well within the
605 positive Matuyama Epoch, the aeromagnetic map (Fig. IV.12) shows both positive (northern flank)
606 and negative (central and southern areas) magnetic anomalies in the Fogo region. Together, the
607 positive and negative anomalies define a horseshoe shape. Moreover, the orientation of the
608 canyon and the nature of the rocks are different in the north and south. This contrast between
609 north and south flanks (and their morphology, see cross-section Fig. 5) indicates a story different
610 from simple construction of a homogenous and well-developed conical volcano. Inside the area
611 bounded by the two high crests, we collected an ignimbrite flow that we dated at 85 ± 2 ka on
612 feldspar crystals, therefore much younger than the lava flow dated at 270 ka in the northern flank
613 (Figs. IV.5, IV.12). These new data indicate that a great part of the southern flank of Fogo volcano
614 has been removed. Bearing in mind that Fogo shows acid volcanism of Plinian type, we propose

here that Fogo, similarly to the Mount St Helens's 1980 eruption (e.g., Bogoyavlenskaya et al., 1984), has been affected by a major sector collapse followed by a directed blast to the south. We can approximately determine the extension of the depression using the aeromagnetic map (boundary area between the positive and negative anomaly) and the 3D view (Figs. IV.5, IV.12). The Fogo volcano is still active as shown by the eruption in 1563 (Snyder et al., 2007). Although we did extensive fieldwork inside the Fogo's caldera, we could not collect suitable samples to constrain the potential caldera event, mainly because the internal part of the caldera is full of trachytic domes and blocks mixed with pumice. Also, we could not find evidence that these units are synchronous with the caldera collapse, because none of the plugs seemed truncated. We infer that these domes postdate the caldera collapse event, and are responsible for the irregular shape of the current summit of Fogo.

IV. 1. 4. 2. 4. The Furnas Volcano

According to the new ages, the activity of Furnas ranges between 138 ± 3 ka and present-day. Ten explosive eruptions have been recognized for the last 5000 years (Booth et al., 1978; Cole, 1995). The Furnas edifice was affected by a caldera collapse that produced the massive ignimbrite flow filling the depression of Povoação (Duncan et al., 1999). The old rims are currently barely visible, probably because Furnas has been affected by several caldera collapses that have removed the older walls (as on the top of Sete Cidades, where three caldera collapses have been recognized). We cannot exclude that the location of the old caldera scar has been partly inherited from the scar of the flank collapse that truncates Nordeste (previous section, Fig. IV.13B). We propose that this event occurred around 60 ka (Fig. IV.13E). The depression resulting from the caldera collapse at Furnas was filled by younger lava flows (here dated between 60 ± 1 ka and 23 ± 1 ka), some of which flowed over the caldera rims in the northwestern part (sample SM11H dated at 17 ± 6 ka). According to Duncan et al. (1999), a caldera collapse affected the Furnas Volcano, with a distinct scar oriented globally NW-SE (in part containing the lake of Furnas), which truncates the filling of the old caldera. We dated that caldera event up to 23 ± 1 ka (sample SM12Y), the age of the top of the rim (Fig. IV.13E). The formation of this caldera was followed by new filling volcanism. This multi-stage destruction of Furnas by caldera collapses is consistent with the gravity data reported in Montesinos et al. (1999), who concluded that the caldera complex results from several distinct collapses. These caldera collapses occurred after 250 ka, at ca. 60 ka, and after 23 ka.

IV. 1. 4. 2. 5. The Sete Cidades Volcano

According to the new ages, Sete Cidades is the youngest subaerial volcano of S. Miguel. Previous K/Ar dating on whole rock yielded an age of 210 ± 8 ka (McKee and Moore, 1992), in the same outcrop (at the base of the caldera rim) for which we obtained an age of 91 ± 3 ka. The most plausible explanation for such a large difference in ages is that the older age is significantly

contaminated by incorporation of phenocrysts, which most likely contain inherited Ar. Sete Cidades grew until 64 ± 2 ka, when a first caldera event truncated the summit of Sete Cidades and produced the ignimbrite of sample SM11C. The recognition of the number of caldera collapses of Sete Cidades was not a main objective of our work, therefore we just propose to add a new caldera collapse to the three previously proposed by Queiroz (1997, 2008), and estimated at 36, 29 and 16 ka.

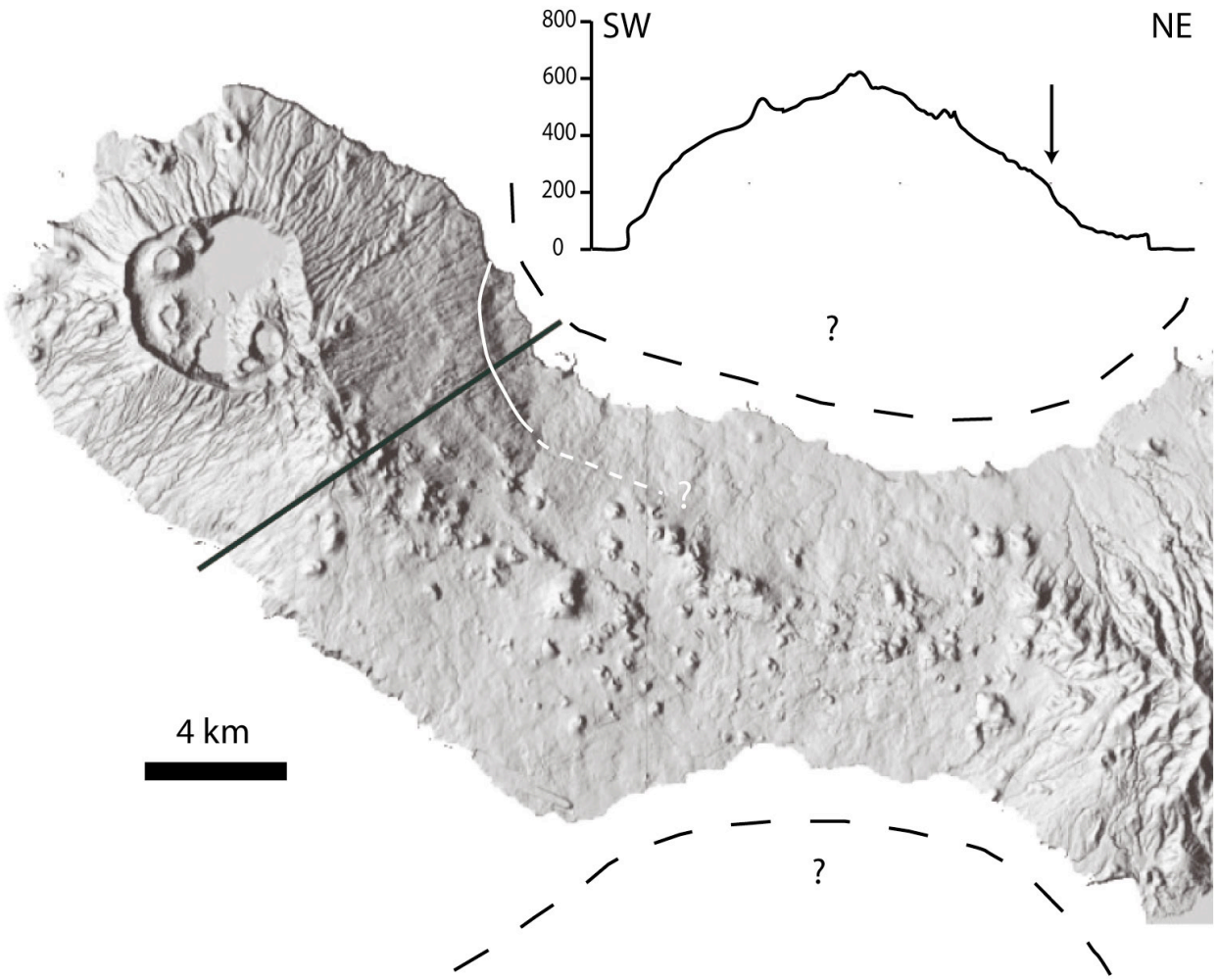


Figure IV. 14. Shaded relief map of the western part of S. Miguel. Notice the arcuate zone that we interpret as a possible landslide (in white). The dashed black lines highlight other possible destabilized zones following the coastline.

The magnetic data shows a global positive signature of Sete Cidades, and a negative polarity in the NE, with a curved shape concave to the sea. On the DEM and topographic cross-section (Fig. IV.14), this curved shape corresponds to a prominent scarp (indicated by white dashed line). Taking into account the magnetic, topographic and age data, we suggest that the eastern part of Sete Cidades has been affected by a flank collapse towards the NE. The collapse removed a part of the positive polarity lavas, which reveals the polarity of the negative rocks below what has been later covered by a thin sheet of volcanic products originated from the western Waist

Zone. The negative rocks and a part of the remaining positive lavas have been later covered by cascading lava flows at least at 72 ± 2 ka.

The youngest volcanism in S. Miguel occurs as strombolian cones in the waist zones, and on the caldera depression of Sete Cidades, Fogo and Furnas (Fig. IV.13F).

To summarize, the construction of S. Miguel Island has been affected by several caldera collapses, and at least 3 major flank collapses. For one of them we have been able to localize the debris deposit on the sea bottom thanks to the high-resolution bathymetry and seismic profiles. The particular shape of the island also indicates other possible zones of destabilization (Fig. IV.14).

IV. 1. 4. 3. Tectonic control of the nature of the volcanism in S. Miguel

Despite the ca. 100 kyr of sub-aerial volcanic activity, Nordeste is mainly composed of basic rocks (i.e. alkali basalt, trachy-basalt), and rare K-benmoreite locally called tristanite (Abdel-Monem et al., 1975; Fernandez, 1980; Moore, 1990). The volcanism of Povoação also shows basic rocks slightly more differentiated as basalt, trachy-basalt/hawaiite and trachy-andesite (Féraud et al., 1980; Moore, 1990; 1991b). In contrast, the Furnas volcano is essentially composed of trachytic units (Cole et al., 1995, 1999), and by some rare basalts from the recent secondary cones. Sete Cidades shows a complete alkali-series (e.g. Beier et al., 2006). The basic lavas occur at the base of the volcano and at younger secondary cones. The lavas in between indicate a more evolved magma due to differentiation in a magma reservoir (Beier et al., 2006). In the main construction stages of S. Miguel, the basic volcanism is located on the eastern part of the island, and the acid volcanism is located in the middle and western parts. This indicates that during the first activity of the central and western volcanoes, magma ascended directly to the surface, and later eruptions were differentiated, which implies the existence of magma chambers where differentiation occurred.

We suggest here that the difficulties of the magma ascent between the eastern part on the one hand, and the middle and the western part on the other hand are linked to dynamic activity of the Terceira Rift. Close to the wall of the rift, tectonics are active, the crust is fractured, which permits a fast rise of magma without significant storage in a magma chamber. In the middle of the Terceira Rift, the tectonic motions are more discrete, the fracturation of the crust is smaller than along the wall. The magma thus cannot go directly to the surface, and stops in the magma chamber.

However, S. Miguel is covered by young basaltic volcanism essentially coming from strombolian cones localized on the flanks of the main shield volcanoes, and between the main edifices along the two waist zones. We suggest that the island is mature and thick enough for that the local compressional stress in the crust caused by overthrust of the island in the middle of the rift, probably caused small volumes of magma to be expelled through few discontinuities of the oceanic crust and between the main volcanoes. This process of magma extraction accounts for the very low volumes erupted, and also explains repetitive character of this kind of monogenetic

706 volcanism and its unique very short duration.

707 Magma generation and ascent have been shown to be promoted in extensional tectonic
708 settings (Shaw, 1980; McKenzie and Bickle, 1988).

709 Here we suggest that the active stress-field of the area is a critical factor that has controlled
710 the ascent of magma through the crust and along main faults of the rift, and therefore has an
711 influence on eruption nature and probably intensity, controlling the rise of magma batches through
712 the crust, leading to their eruption.

713

714 ## CONCLUSIONS

715 This study shows the utility of using a combination of approaches to understand the
716 impacts of active regionally extensive tectonics on the growth and partial destruction of a volcanic
717 island, and the nature of the volcanism erupted. From combined morpho-tectonic analysis,
718 fieldwork investigation, high-precision K-Ar geochronology on separated groundmass, offshore
719 seismic profile, bathymetry data, and available magnetic data we conclude that:

720 (1) The evolution of S. Miguel is constituted by several stages of volcanic growth separated by
721 periods by repeated destruction in the form of flank collapses, caldera event and coastal and
722 stream erosion (Fig. IV.13).

723 (2) S. Miguel is affected by at least 3 flank collapses. Others are suspected from the shape of the
724 coastline, but a better identification would require additional high-resolution bathymetric data
725 and/or seismic lines all around the island.

726 (3) The nature of the volcanism appears intimately linked with the tectonics. Basic magma ascent
727 close to the northern wall of the TR and rise to the surface fast was probably controlled by the main
728 fault of the TR. In contrasts, the acid magmas are localize toward the middle of the TR, reflecting a
729 more difficult and discontinuous ascent, with storage in magma chamber which favoured the melt
730 differentiation.

731 The morphology, the evolution and the nature of volcanism of S. Miguel Island has been strongly
732 influenced by regional deformation along the Nubia and Eurasia plate boundary.

733

734 ## ACKNOWLEDGEMENTS

735 This is a contribution to Project MEGAHazards, funded by FCT (PTDC/CTE-
736 GIX/108149/2008), Portugal. ACG Costa benefitted from a PhD scholarship
737 (SFRH/BD/68983/2010), FCT, Portugal). Seimic data processing with supported by DFG grant
738 Hu698/19-1. The authors wish to thank V. Godard for preparing thin sections.

739

740 **REFERENCES**

741 Abdel Monem, A.A., Fernandez, L.A., Boone, G.M., 1975. K-Ar ages from the Eastern Azores
742 Group (Santa Maria, São Miguel, Formigas islands). Lithos, 8, 247-254.

743 Beier, C., Haase, K.M., Hansteen, T.H., 2006. Magma evoltuion of the Sete Cidades volcano, S.
744 Miguel, Azores. Journal Petrology 47, 1375-1411.

745 Bogoyavlenskaya, G.E., Braitseva, O.A., Melekestsev, I.V., Kiriyanov, V.Y., Miller, C.D., 1984.
746 Catastrophic eruptions of the directed-Blast type at mount st. Helens, Bezymianny and
747 Shiveluch volcanoes. Journal of Geodynamics 3, 189-218.

748 Booth, B., Croasdale, R., Walker, G.P.L., 1978. A quantitative study of five thousand years of
749 volcanism on S. Miguel, Azores. Phil. Trans. R. Soc. Lond., 228, 271-319.

750 Cole, P.D., Guest, J.E., Queiroz, G., Wallenstein, N., Pacheco, J.M., Gaspar, J.L., Ferreira, T.,
751 Duncan, A.M., 1999. Styles of volcanism and volcanic Hazards on Furnas Volcano, S.
752 Miguel, Azores. Journal of Volcanology and Geothermal Research 92, 39-54.

753 Cole, P.D., Queiroz, G., Wallenstein, N., Gaspar, J.L., Duncan, A.M., Guest, J.E., 1995. An historic
754 subplinian/phreatomagmatic eruption : the 1630 AD eruption of Furnas volcano, S. Miguel,
755 Azores. Jounral of volcanology and Geothermal Research 69, 117-135.

756 Costa, A.C.G., Marques, F.O., Hildenbrand, A. Sibrant, A.L.R., Catita, C.M.S., 2014. Large scale
757 flank collapse in steep volcanic ridge: Pico-Faial Ridge, Azores Triple Junction. Journal
758 Volcan. Geotherm. Res. 272, 111-125.

759 Duncan, A.M., Queiroz, G., Guest, J.E., Cole, P.D., Wallenstein, N., Pacheco, J.M., 1999. The
760 Povoação Ignimbrite, Furnas Volcano, São Miguel, Azores. J. Volcanol. Geotherm. Res. 92
761 (1-2), 55-65.

762 Féraud, G., Kaneoka, I., Allegre, C.J., 1980. K/Ar ages and stress pattern in the Azores:
763 geodynamic implications. Earth and Planetary science Letters 46, 275-286.

764 Fernandez, L.A., 1980. Geology and petrology of the Nordeste volcanic complex, S. Miguel,
765 Azores: summary. Geol. Soc. Am. Bull. 91, 675-680.

766 Ferreira, T., 2000. Caracterizacão da actividade vulcânica subaérea da ihla de S. Miguel (Açores):
767 vulcanismo basaltico recente e zonas de desgaseificação, Avaliação de riscos. Tese de
768 Doutoramento em Geologia, especialidade em Vulcanologia, Departemento de
769 Geociências, Universidade dos Açores, 248pp.

770 Gandino, A., Guidi, M., Merlo, C., Mete, L., Rossi, R., Zan, L., 1985. Preliminary model of the
771 Ribeira Grande Geothermal field (Azores islands). Geothermics 14, 91-105. 85

772 Gillot, P.Y., Cornette, Y., 1986. The Cassignol technique for potassium-argon dating, precision and
773 accuracy: examples from late Pleistocene to recent volcanics from southern Italy. Chemical
774 Geology 59, 205-222.

775 Gillot, P.Y., Hildenbrand, A., Lefèvre, J.C., Albore-Livadie, C., 2006. The K/Ar dating method:
776 Principle, Analytical Techniques and Application to Holocene Volcanic Eruptions in the southern
777 Italy. Acta Vulcanologica 18, 55-66.

778 Gillot, P.Y., Cornette, Y., Max, N., Floris, B., 1992. Two reference materials, trachytes MDO-G and
779 ISH-G, for argon dating K/Ar and 40Ar/39Ar datnig of Pleistocene and Holocene rocks.
780 Geostandards and Geoanalytical Research, 16, 55-60.
781 Gomes, A., Gaspar, J.L., Queiroz, G., 2006. Seismic vulnerability of dwellings at Sete Cidades
782 Volcano (S. Miguel, Azores). Natureal Hazards and Earth System Sciences 6, 41-48.
783 Guest, J.E., Gaspar, J.L., Cole, P.D., Queiroz, G., Duncan, A.M., Wallenstein, N., Ferreira, T.,
784 Pacheco, J.M., 1999. Volcanic geology of Furnas volcano, S. Migeul, Azores. Journal of
785 volcanology and geothermal Research 92, 1-29.
786 Hildenbrand, A., Marques, F.O., Catalão, J., Catita C.M.S., Costa, A.C.G., 2012a. Large-scale
787 active slump of the southeastern flank of Pico Island, Azores. Geology, 40, 939-942,
788 doi:10.1130/G33303.1.
789 Hildenbrand, A., Marques, F.O., Costa, A.C.G., Sibrant, A.L.R., Silva, P.F., Henry, B., Miranda,
790 J.M., Madureira, P., 2012b. Reconstructing the architectural evolution of volcanic islands
791 from combined K/Ar, morphologic, tectonic, and magnetic data: The Faial Island example
792 (Azores). Journal of Volcanology and Geothermal Research 241-242, 39-48.
793 Hübscher, C., 2013. Tragica - Cruise No. M79/2 - August 26 – September 21, 2009. Ponta
794 Delgada (Azores / Portugal) – Las Palmas (Canary Islands / Spain). *METEOR-Berichte,*
795 *M79/2, 37 pp.*, DFG-Senatskommission für Ozeanographie.
796 https://getinfo.de/app/details?id=awi:doi~10.2312%252Fcr_m79_2
797 Johnson, C.L., Wijbrans, J.R., Cosntable, C.G., Gee, J., Staudigel, H., Tauxe, L., Forjaz, V.H.,
798 Salgueiro, M., 1998. 40Ar/39Ar ages and paleomagnetism of São Miguel Lavas, Azores.
799 Earth Planet. Sci. Lett. 160 (3-4), 637 - 649.
800 Le Friant, A., Deplus, C., Boudon, G., Feuillet, N., Trofimovs, J., Komorowski, J.C., Sparks, R.S.J.,
801 Talling, P., Palmer, M., Ryan, G., 2010. Eruption of Soufrière Hills (1995-2009) from an
802 offshore perspective: insights from repeated swath bathymetry surveys. Geophysical
803 Research Letters 37 (L11307). Doi:10.1029/2010GL043580.
804 Le Friant, A., Harford, C.L., DePlus, C., Boudon, G., Sparks, R.S.J., Herd, R.A., Komorowski, J.C.,
805 2004. Geomorphological evolution of Montserrat (West Indies): importance of flank collapse
806 and erosional processes. Journal of the Geological Society 161, 147-160.
807 Lebas, E., Le Friant, A., Boudon, G., Watt, S., Talling, S., Feuillet, N., Deplus, C., Berndt, C.,
808 Vardy, M., 2011. Multiple widespread landslides during the long-term evolution of a volcanic
809 island: insights from high-resolution seismic data, Montserrat, Lesser Antilles.
810 Geochemistry, Geophysics, Geosystems 12 (5), Q05006. Doi:10.1029/2010GC003451.
811 Lourenço, N., Luis, J.F., Miranda, J.M., Ribeiro, A., Victor, L.A.M., 1998. Morpho-tectonic analysis
812 of the Azores volcanic plateau from new bathymetric compilation of the area. Marine
813 Geophysical Researches 20, 141–156.
814 Louvat, P., Allègre, C.J., 1998. Riverine erosion rates on s. Migeul volcanic island, Azores
815 archipelago. Chemical Geology 148 (3-4), 177-200.

816 Marques, F.O., Catalão, J.C., DeMets, C., Costa, A.C.G., Hildenbrand, A., 2014a. corrigendum to:
817 GPS and tectonic evidence for a diffuse plate boundary at the Azores triple junction, (Earth
818 Planet. Sci. Lett., 381, 177-187) Earth Planet. Sci. Lett., 387, 1-3.
819 Marques, F.O., Catalão, J., Hildenbrand, A., Costa, A.C.G., Dias, N.A., 2014b. The 1998 Faial
820 earthquake, Azores: Evidence for a transform fault associated with the Nubia-Eurasia plate
821 boundary? Tectonophysics, DOI: 10.1016/j.tecto.2014.06.024.
822 Marques, F.O., Catalão, J.C., DeMets, C., Costa, A.C.G., Hildenbrand, A., 2013. GPS and
823 tectonic evidence for a diffuse plate boundary at the Azores Triple Junction. Earth and
824 Planetary Science Letters, 381, 177-187.
825 McKenzie, D., Bickle, M.J., 1988. The volume and composition of melt generated by extension of
826 the Lithosphere. Jounral of Petrology 29 (3), 625-679, doi:10.1093/petrology/29.3.625.
827 McKee, E.H.. Moore R.B, 1992. Potassium–argon dates for trachytic rocks on Sa˜o Miguel,
828 Azores, Isochron West 58, 9–11.
829 Miranda, J.M., Luis, J.F., Lourenço, N., Fernandes, R.M.S., 2013. The structure of the Azores triple
830 junction : implications for S. Miguel Island. GSL (in press).
831 Montesinos, F.G., Camacho, A.G., Vierra, R., 1999. Analysis of gravimetric anomalies in Furnas
832 caldera (São Miguel, Azores). J. Volcanol. Geotherm. Res. 92 (1-2), 67 - 81.
833 Moore, R., 1991a. Geologic map of São Miguel, Azores (Scale 1: 50.000). U.S.G.S. MISC INV.
834 map I-2007.
835 Moore, R., 1991b. Geology of three late Quaternary stratovolcanoes on São Miguel, Azores.
836 U.S.G.S. Bull. 1900, 1–26.
837 Moore, R., and Rubin, M., 1991. Radiocarbon dates for lava flows and pyroclastic deposits on São
838 Miguel, Azores. Radiocarbon, 33 (1), 151-164.
839 Moore, R., 1990. Volcanic geology and eruption frequency, S. Miguel, Azores. Bull. Volcanol. 52,
840 602–614.
841 Muecke, G.K., Ade-Hall, J.M., Aumento, F., McDonald, A., Reynolds, P.H., Hyndman, R.D.,
842 Quintino, J., Opdyke, N., Lowrie, W., 1974. Deep drilling in an active geothermal area in the
843 Azores. Nature 252 (5481), 281–285.
844 Oehler, J.F., Wyk de Vries, B., Labazuy, P., 2005. Landslides and spreading of oceanic hot-spot
845 and arc shield volcanoes on Low Strength Layers (LSLs) : an analogue modeling approach.
846 Jounral Volcan. Geotherm. Res., 144 (1-4), 169-189.
847 Queiroz, G., Pacheco, J.M., Gaspar, J.L., Aspinall, W.P., Guest, J.E., Ferreira, T., 2008. The last
848 5000 years of activity at sete Cidades volcano (São Miguel island, Azores) implication for
849 hazard assessment. J. Volcanol. Geotherm. Res. 178 (3), 562 - 573.
850 Queiroz, G., 1997. Vulcão das Sete Cidades (S. Miguel, Açores) História Eruptiva e Avaliação do
851 Hazard. Unpublished PhD Thesis. Universidade do Açores, 226p.

852 Quidelleur, X., Carlut, J., Soler, V., Valet, J.P., Gillot, P.Y., 2003. The age and duration of the
853 Matuyama-Brunhes transition from new K-Ar data from La Palma (Canary Islands) and
854 revisited Ar-40/Ar-19 ages. Earth and Planetary Science Letters 208, 149-163.
855 Quidelleur, X., Gillot, P.Y., Soler, V., Lefèvre, J.C., 2001. K/Ar dating extended into the last
856 millennium : application to the youngest effusive episode of the Teide volcano (Spain).
857 Geophysical Research Letters 28, 3067-3070.
858 Ramalho, R., Quartau, R., Trenhaile, A.S., Mitchell, N.C., Woodroffe, C.D., Avila, S.P., 2013.
859 Coastal evolution on volcanic oceanic islands: a complex interplay between volcanism,
860 erosion, sedimentation, sea-level change and biogenic production. Earth Science Reviews,
861 127, 140-170.
862 Ricci, J., Lahitte, P., Quidelleur, X., submitted. Construction and destruction rates of volcanoes
863 within tropical environment: examples from the Basse-Terre Island (Guadeloupe, Lesser
864 Antilles). Accepted in Geomorphology.
865 Shaw, H.R., 1980. Fracture mechanisms of magma transport from the mantle to the surface. In
866 Physics of magmatic Processes, R.B., Hargraves, ed. Princeton U. Press, Princeton, N.J.,
867 pp 201-264.
868 Shotton, F.W., Blundell, D.J., Williams, R.E.G., 1971. Birmingham university radiocarbon dates III.
869 Radiocarbon 13 (2), 141-156.
870 Shotton, F.W., Blundell, D.J., Williams, R.E.G., 1969. Birmingham university radiocarbon dates III.
871 Radiocarbon 11 (2), 263-270.
872 Synder, D.C., Widom, E., Pietruszka, A.J., Carlson, R.W., Schmincke, H.U., 2007. Time scales of
873 formation of zones magma chambers: u-series disequilibria in the Fogo A and 1563 A.D.
874 trachyte deposits, S. Miguel, Azores. Chemical Geology 239, 138-155.
875 Sibrant 2014, A.L.R., Marques, F.O., Hildenbrand, A., 2014. Construction and destruction of a
876 volcanic island developed inside an oceanic rift: Graciosa Island, Terceira Rift, Azores.
877 Journal of Volcanology and Geothermal Research 284, 32-45.
878 Sibrant, A.L.R., Hildenbrand, A., Marques, F.O., Boulesteix, T., Costa, A.C.G., 2013. Morpho-
879 structural evolution of a volcanic island developed inside an active oceanic rift: S. Migeul Island
880 (Terceira Rift, Azores). Abstract Meeting, IAG, 2013.
881 Steiger, R.H., Jager, E., 1977. Subcommission on geochronology : convention on the use of decay
882 constants in geo and cosmochronology. Earth and Planetary Science Letters 36, 359-362.
883 Wallenstein, N., 1999. Estudo da historia recente e do comportamento eruptivo do Vulcão do Fogo
884 (S. Miguel, Açores). Avaliacão preliminar do hazard. Tese de doutoramento no ramo de
885 Geologia, especialidade de Vulcanologia, Departamento de Geocências, Universidade dos
886 Açores, 266pp.
887 Zbyszewski, G., 1961. Etude geologique de l'ile de S. Miguel (Açores). Comunicações dos
888 Serviços Geologicos de Portugal 45, 5-79.

889 Zbyszewski G, Ferreira, O.V., Torre de assuncao, C (1959) - Carta Geológica de Portugal na
890 escala de 1:50 000. Notícia explicativa da Folha A, S.Miguel (Açores). Publ. Serv. Geol. de
891 Portugal, 22p. Lisboa.
892 Zbyszewski G, D'Almeida FM, da Veiga Ferreira O (1958) Carta geologica de Portugal na escala
893 de 1:50000 (São Miguel). Serv Geol de Port, Lisboa
894

FIGURE CAPTIONS

Figure IV.1. Bathymetric map of the Azores region from Lourenço et al. (1998). The black lines indicate the location of the Mid-Atlantic ridge (MAR) axis, and associated transforms. The thin white and black lines indicate the centre and the wall of the Terceira Rift (TR), respectively. The white dashed line marks the East Azores Fracture Zone (EAFZ). The yellow dashed lines mark the diffuse boundary between the Eurasia and Nubia plates from Marques et al. (2013, 2014a). The colour scale is in meters. The islands are referenced as Cor - Corvo; Flo - Flores; Fai - Faial; Pic - Pico; SJo - S. Jorge; Gra - Graciosa; Ter - Terceira; SMi - S. Miguel; SMa - Santa Maria. Inset at the top right corner for location.

Figure IV.2. Elevation map of S. Miguel built from a Digital Elevation Model (DEM) with a 10 m spatial resolution. Ages measured with various methods and techniques in previous works are shown. (A) Map with the volcanic zones defined by Zbyszewski (1961). (B) Map with the volcanic zones according to Moore (1991a). (C) Timeline summarizing the ages and methods as a function of the main volcanoes.

Figure IV.3. Maps of S. Miguel generated from the high-resolution DEM. (A) Slope map of S. Miguel with our structural interpretation, main structural features, and dip of lava flows measured in the field. (B) Shaded relief map of S. Miguel, with lighting from NW, and location of our samples and nature of the rocks collected in the present study.

Figure IV.4. Topography of eastern S. Miguel with the location of our new samples. Cross sections show the main volcano-stratigraphic relationships and the schematic position of our samples. The colour code stands for lava successions from the main volcanic complexes: dark blue for Nordeste, light blue for the Filling volcanism of Povoação, and orange for the Furnas volcano and associated ignimbritic deposits. F: Furnas; P: Povoação; FdT: Faial da Terra; AR: Água Retorta; SL: S. Lourenço.

Figure IV.5. 3D view of Fogo seen from the south. The cross-sections highlight the irregular topography of the area. The arrows indicate deep canyons, which can be associated with probable landslide(s). The dashed white line indicates the possible shape and location of the flank collapse(s).

Figure IV.6. 3D view on the eastern part of S. Miguel, obtained by superimposing the satellite image over the high resolution DEM. The new K-Ar ages are shown. The colour code separates lava successions from main volcanic complexes: dark blue for Nordeste, light blue for the Filling Volcanism of Povoação, and orange for the Furnas volcano and associated ignimbritic deposits.

Figure IV.7. High-resolution bathymetry of the southeastern part of S. Miguel. The yellow dashed line shows the inferred area potentially covered by landslide deposits. The white lines indicate the location of the seismic profiles shown in the Figs. IV.8, IV.9, IV.10, IV.11.

Figure IV.8. N-S seismic profile offshore Povoação showing the stratigraphy of mass-wasting deposits sourced in Nordeste. The rugged seafloor is here interpreted as a flank collapse deposit. Notice the presence of kilometre size blocks. (A) Our interpretation; (B) profile without interpretation. VE is vertical exaggeration. Notice the presence of large blocks close to the island. Location of the seismic profile is reported in Fig. IV.7.

Figure IV.9. E-W distal seismic profile offshore south of Nordeste. Notice the presence of disaggregated blocks with smaller size than the ones observed in the proximal area shown in Fig. 8. Notice the length of the lateral deposit and the absence of reflections at the bottom of the lenticular flank collapse deposit. (A) Our interpretation; (B) seismic profile without interpretation. VE is vertical exaggeration. Precise location of the seismic profile is reported in Fig. IV.7.

Figure IV.10. E-W seismic profile further south. (A) Our interpretation; (B) seismic profile without interpretation. VE is vertical exaggeration. Notice the absence of large collapse blocks, the less irregular contact between the identified flank collapse deposit and the sediment, and the higher thickness of the sea-floor sediment facies in the W. Location of the seismic profile is shown in Fig. IV.7.

Figure IV.11. N-S seismic profile south of Faial da Terra canyon, showing the stratigraphy of mass-wasting deposits offshore Nordeste. Note the presence of large blocks that can have originated on the flank of the lateral seamount or be landslide blocks lying on the slope of the seamount. Notice that the surface topography of the interpreted flank collapse is more irregular than the profiles in Fig. IV.10. This indicates that the profile is closer to the source of the flank collapse deposits. (A) Our interpretation; (B) seismic profile without interpretation. VE is vertical exaggeration. Location of the seismic profile is reported in Fig. IV.7.

Figure IV.12. Aeromagnetic map of S. Miguel from Miranda et al. (2013). The small coloured circles mark the location of the new K/Ar ages, and the colour of the circle indicates the nature of the rock: yellow for lava flows, blue for pumices, and red for ignimbrite flows. The dashed white lines indicate sharp variations in the magnetic signature east of Sete Cidades and on Fogo volcanoes.

Figure IV.13. Proposed schematic morphostructural evolution of S. Miguel.

971 Figure IV.14. Shaded relief map of the western part of S. Miguel. Notice the arcuate zone that we
972 interpret as a possible landslide (in white). The dashed black lines highlight other possible
973 destabilized zones following the coastline.
974
975 Figure IV.A1. W-E costal cliff on both sides of Faial da Terra. See Fig. 4 for the precise location of
976 the general picture. Yellow circles indicate the position of samples SM11S and SM11R. Note the
977 difference of nature of the rock to west and east of the canyon. Thick and differentiate in the west,
978 and basic and thin lavas truncated by numerous dykes in the east.
979
980 Figure IV.A2. Southern costal cliff of Furnas volcano composed of alternating surge, pumice and
981 cinder. See Fig. 4 for the location of the picture.
982
983 Figure IV.A3. Outcrop comprising boulders of different nature (from basalt to trachyte) in a cinder
984 matrix. The debris sit on a thin cinder layer without boulders.
985
986 Table IV.1. New K-Ar ages obtained with the unspiked Cassignol-Gillot technique on fresh
987 separated groundmass (Gdm) and alkali feldspars (feld). For each sample, the mean age is
988 obtained by weighing by the amount of radiogenic argon. The uncertainties are quoted at the 1σ
989 level.

IV. 2. Deformation in hyper-slow oceanic rifts: insights from the tectonics of the S. Miguel Island (Terceira Rift, Azores) (in prep, Tectonics)

A.L.R. Sibrant [1*], F.O. Marques [2], A. Hildenbrand [1,3], T. Boulesteix [1,4], A.C.G. Costa[1,5]

(1) Univ. Paris-Sud, Laboratoire IDES, UMR8148, Orsay, F-91405
(2) Universidade de Lisboa, Lisboa, Portugal
(3) CNRS, Orsay, F-91405
(4) GeoRessources, CNRS-CREGU, Université de Lorraine, France
(5) University of Lisbon and IDL, Lisbon, Portugal

*Corresponding author. Tel.: +33 1 69 15 67 61
E-mail address: aurore.sibrant@u-psud.fr

ABSTRACT

In the Azores Triple Junction, two contrasting oceanic rifts coexist: the Mid-Atlantic rift (MAR) and the Terceira Rift (TR). The evolution of mature rifts like the MAR is currently reasonably well understood, which is not the case for young, ultra-slow oceanic rifts like the TR. Here we examine the distribution of strain and magmatism in the portion of the TR making up the Nubia-Eurasia plate boundary. Two persisting questions regarding the TR are its age and mode of rifting, i.e. with or without creation of new crust (spreading). We use an elongated volcanic island that stretches most of the TR width, the S. Miguel Island, which allows investigating the TR's architecture. From DEM and structural analysis, and new measurements of 350 faults and dikes, we show that: (1) S. Miguel comprises two main volcano-tectonic directions, N150 and N110, which are mostly concentrated in the eastern part of the island; (2) A N50 fault system is identified for the first time in S. Miguel. It is interpreted as a transform trend, which accommodates the variation in strike of the TR; (3) Faults and dikes geometry indicates that eastern S. Miguel materializes the TR's northern boundary, and lack of major faults in central and western S. Miguel indicates that rifting is mostly concentrated at the main faults bounding the TR. Based on the TR's geometry, structural criteria and plate kinematics, we estimate that the TR has initiated between 1 and 1.7 Ma ago, and that there is no appreciable sea floor spreading associated with rifting.

***Keywords*:** Terceira Rift; tectonic marker; S. Miguel Island; faults and dykes; Azores Triple Junction; transform fault

IV. 2. 1. INTRODUCTION

Tectonic processes largely control the deformation in young, slow rifts, whereas asthenospheric processes greatly influence the evolution of mature mid-ocean ridges [e.g., Magde et al., 1997; Tucholke et al., 1997]. Most of our knowledge on the accommodation of the deformation during continental breakup comes from active continental rifts and passive margins [e.g., Corti, 2009; Soares et al., 2012; Bache et al., 2013], which show a zone of thinned crust, with or without formation of new oceanic crust [Driscoll and Karner, 1998; Snow and Edmonds, 2007]. The extensional plate boundaries have been classified based on their structural, morphological, and volcanologic characteristics into two major types, mostly based on their spreading rate: "fast" (> 60 mm/yr full rate) and "slow" (< 60 mm/yr full rate). An intermediate type is often placed between them [e.g., MacDonald, 1982; Franchteau and Ballard, 1983; Malinverno and Pockalny, 1990].

The recognition of ultra-slow rifts (< 10 mm/yr full rate, [Michael et al., 2003; Cannat et al., 2003]) is recent and is characterized by a succession of magmatic and amagmatic rifts that expose mantle peridotite directly on the seafloor [Dick et al., 2003]. The mechanisms of deformation along the segments of ultra-slow rifts are poorly understood when compared to the opening and deformation occurring along mature mid oceanic ridges and continental rifts. This is mainly because of (1) the ultra-slow opening rates, which prevent the use of a classification based on their structural, morphological and volcanologic characteristics, as used for the oceanic ridges; and (2) because the morphology of ultra-slow is more dominated by tectonics than by volcanism, which limits the use of gravity and magnetic anomalies [Whittaker et al., 2008]. The knowledge of how deformation occurs along ultra-slow rifts has only been deduced from seismic data [e.g., Mutter and Karson, 1992], and numerical modelling [e.g., Van Wijk and Blackman, 2005; Henk, 2006]. Several ultra-slow ridges have been identified as the Arctic Gakkel ridge [e.g., Coakley and Cochran, 1998], the Southwest Indian Ridge [e.g., Dick et al., 2003] or the Reykjanes ridges [e.g., Appelgate and Shor, 1994].

Here we focus on the early stages of rifting and on the deformation along an oceanic hyper-slow rift: the Terceira Rift (TR), along which the extension rate is close to 4.5 mm/yr full rate [DeMets et al., 2010] so twice slower than at ultra-slow rifts [Vogt and Jung, 2004]. Since most of the TR lies below sea level, and the available geophysical data is scarce, we study the tectonic pattern of an island (S. Miguel) that spans most of the TR to investigate the TR's evolution (Fig. IV.15). The seismically and volcanically active TR is seemingly a young rift, and one of the few places in the world where the early stages of oceanic rifting can be investigated. The main problems we address in this work are related to the TR's tectonics, volcanism and age. The TR in part comprises the boundary between the Eurasia and Nubia plates in the Azores region (Fig. IV.15), therefore the knowledge of its evolution is critical to the understanding of the evolution of the Azores Triple Junction (ATJ). In the TR's western half, the plate boundary is diffuse and thus

only in part accommodated by the TR [Marques et al., 2013, 2014], but in its eastern half, the TR takes up most of the deformation imposed by the relative motions between Nubia and Eurasia. The ATJ is diffuse, unstable over time and has changed in configuration. Indeed, the old Eurasia/Nubia plate boundary is believed to be the East Azores Fracture Zone [e.g., Laughton et al., 1972], and the migration from the EAFZ (dextral transform fault) to the TR (oceanic rift) is believed to have occurred by successive jumps of short-lived rifts towards the NE [Vogt and Jung, 2004; Sibrant et al., 2013b]. Searle [1980] proposed that the ATJ migration occurred during the rearrangement of plate poles, which induced the transfer of a wedge of European plate to the Nubian plate.

The Azores region also shows a significant excess in magmatism and an abnormal thick plateau, the so-called Azores Plateau [Searle, 1976; Detrick et al., 1995; Gente et al., 2003; Luis et al., 1998; Silveira et al., 2010], which cannot be explained only by the geometry and configuration of the ATJ [Georgen and Sankar, 2010]. The interaction with a mantle plume (hot or wet) below the Azores was proposed as an explanation for the excess of volcanism in the region [e.g., Vogt, 1976; Schilling, 1985; Thibauld et al., 1998; Gente et al., 2003, Métrich et al., 2014] and for the position of the Eurasia-Nubia rifting [Vogt and Jung, 2004]. Indeed, according to some authors [e.g. Cannat et al., 1999; Gente et al., 2003] the plateau formed by the eruption of underwater traps during the impact head of a plume of deep origin, around ~36 Ma and between 20 and 10 Ma, respectively. Tomogprahic data evidence shallow anomalies at the regional scale, especially at the axis of the MAR [Yang et al., 2006]. The geographic extension and the dynamics of the inferred mantle instability remain controversial. For several authors, the volcanism is not due to an active hot-spot, but rather reflects the existence of volatile-enriched upper mantle domains [Schilling et al., 1975; Bonatti, 1990] or a wet-spot [Métrich et al., 2014]. Available geochronological data on the islands do not support a clear age progression along a well-individualized alignment, like in Hawaii or in Polynesia [Morgan, 1971; Duncan and McDougall, 1976; Hildenbrand et al., 2004; Ozawa et al., 2005]. Instead, they show synchronous volcanism during the last 1 Myr in the central and eastern Azores [e.g., Hildenbrand et al., 2014; Costa et al., in prep; Sibrant et al., in prep, see chapter VI], except on Santa Maria, which emerged during the last 5.7 Myr [Sibrant et al., 2013b; submitted, see Chapter V]. Furthermore, recent volcanic construction has resulted in the development of linear volcanic ridges elongated along two main directions: N150 and N110 [Lourenço et al., 1998; Hildenbrand et al., 2008]. Such characteristics have been attributed to a significant control of volcanic outputs by regional lithospheric deformation [e.g., Haase and Beier, 2003; Hildenbrand et al., 2008; Marques et al., 2013a; 2014a], which is not in contradiction with a mantle plume.

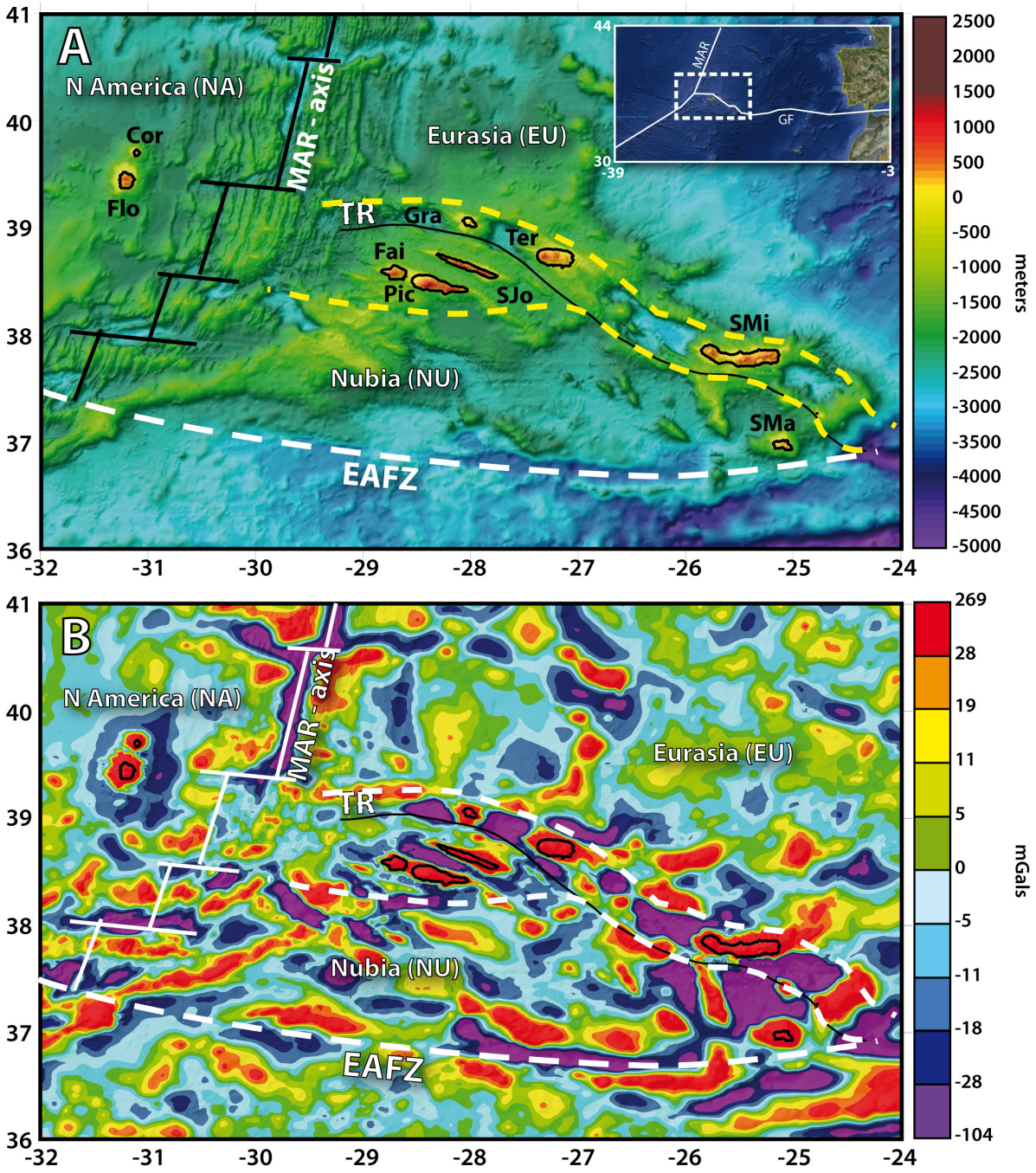


Figure IV. 15. (A) Bathymetric map of the Azores. The black lines indicate the location of the Mid Atlantic Rift (MAR) and associated Fracture Zones. The white dashed line indicates the East Azores Fracture Zone (EAFZ). The thin black line indicates the location of the southern shoulder of the Terceira Rift (TR), and the yellow dashed lines indicate the current Eurasia (Eu) – Nubia (Nu) plate boundary proposed by Marques et al. [2013, 2014]. Inset shows the location of the Azores archipelago in the Atlantic Ocean. Bathymetry from Lourenço et al. [1998]. (B) Free–air gravity field map of the Azores Archipelago [Catalão, 2006; Catalão and Bos, 2008]. The black thin lines represent the boundary of each island (sea level). The white lines indicate the location of the Mid Atlantic Rift (MAR) and associated transforms. The thicker black dashed lines show the current Eurasia/Nubia plate boundary from Marques et al. [2013, 2014]. The white dashed lines indicates the East Azores Fracture Zone (EAFZ). GF: Gloria Fault; Cor: Corvo; Flo: Flores; Fai: Faial; Pic: Pico; SJo: São Jorge; Gra: Graciosa; Ter: Terceira; SMi: São Miguel; SMa Santa Maria. Gravity image supplied by J. Catalão.

Thus, the formation of the TR can be due to plate tectonics and/or the existence of a mantle plume. The TR stretches from the Mid-Atlantic Ridge (MAR) axis to the intersection with the East Azores Fracture Zone, as a ca. 620 km-long sigmoidal graben marked at regular spaces (ca. 80 km) by large-volume central volcanism building up islands and seamounts (Fig. IV.15). Earlier studies have suggested that rifting in the TR started ca. 45 Myr ago [Krause and Watkins, 1970], ca. 36 Myr ago [Searle, 1980], less than 5 Myr ago [Luís et al., 1998], less than 1 Myr ago [Vogt and Jung, 2004], or during the last 25 Myr [Luís and Miranda, 2008]. Considering the oldest TR age and an average opening rate of ca. 4.5 mm/yr reported for the Nubia/Eurasia plate boundary in the Azores [DeMets et al., 2010; Marques et al., 2013], then the TR would have already opened ca. 203 km (45 Ma x 4.5 mm/yr), which is clearly not the case. The creation of new oceanic crust in the TR has never been unambiguously shown, likely because ultra-slow rifting makes the recognition of magnetic anomalies difficult [e.g., Krause and Watkins, 1970; Searle, 1980]. This supports a more recent initiation of the TR, in agreement with recent studies [e.g., Vogt and Jung, 2004; Sibrant et al., 2014]. In this work we estimate the age of the TR, and analyse if there has been spreading (creation of new oceanic crust) or not in the TR.

We focussed our attention on the tectonics of S. Miguel Island, because the eastern part of S. Miguel has grown on the northern shoulder of the TR, and the central and western parts have grown inside the TR. This unique position therefore allows the observation and measurement of tectonic and volcanic elements, which can be linked to the architecture and evolution of the TR. From onshore and offshore altimetric and morphologic data, combined with stratigraphic and structural analyses, including the measurement of more than 350 faults and dikes, we discuss the relationship between tectonics, volcanism and the TR's age.

IV. 2. 2. GEOLOGICAL BACKGROUND

S. Miguel is the largest island of the Azores Archipelago (Fig. IV.15), and has developed in the SE part of the TR. On the most recent available geological map [Moore, 1990 and 1991], six volcanic complexes (VC) have been distinguished (Fig. IV.16), from west to east: (1) the Sete Cidades VC, (2) a western fissural VC mostly made of clustered strombolian cones, (3) the Fogo VC, (4) a central fissural VC, (5) the Furnas VC, and (6) the Nordeste VC. Recent geochronological data acquired on the various VCs show that the sub-aerial volcanic construction of S. Miguel occurred during the last 1 Myr [Moore, 1990; Moore and Rubin, 1991; Johnson et al., 1998].

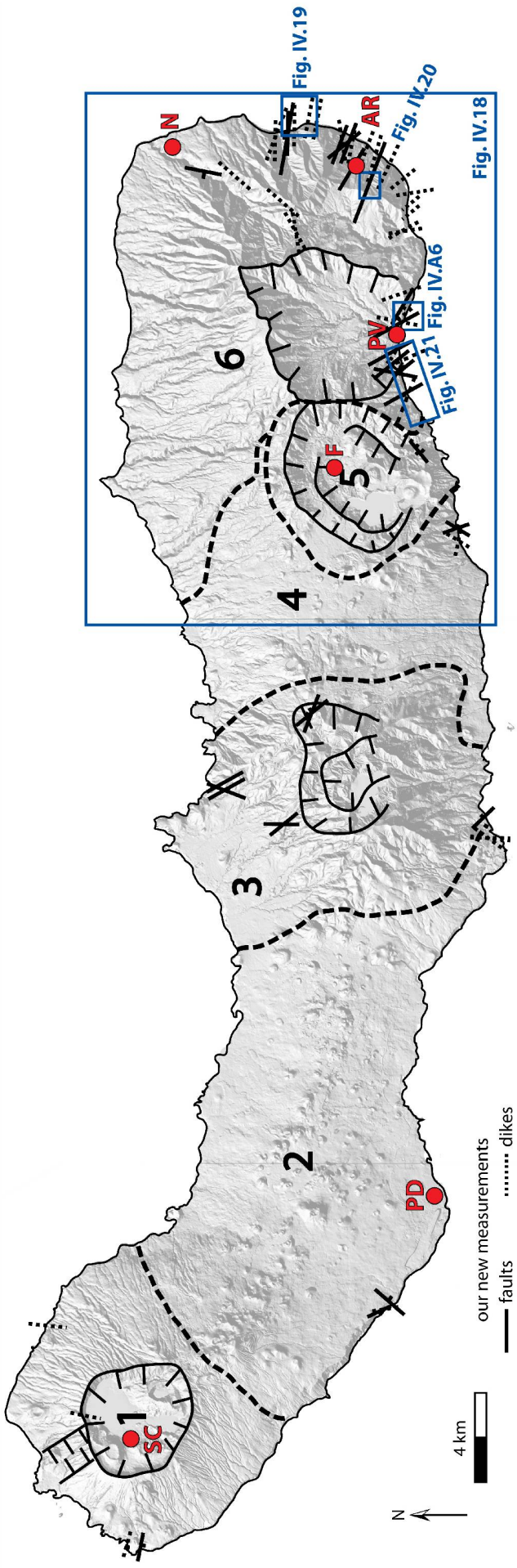

Fig. IV.19
Fig. IV.20
Fig. IV.18
Fig. IV.A6
Fig. IV.21
N
AR
PV
F
SC
PD
1
2
3
4
5
6
our new measurements
faults
dikes
4 km
N

Figure IV. 16. Shaded relief map of S. Miguel generated from a high-resolution DEM (10 m) showing the main volcanic edifices and tectonic structures as defined by Moore [1990]. (1) Sete Cidades volcano; (2) Fissural system; (3) Fogo volcano; (4) Fissural system; (5) Furnas volcano; (6) Nordeste complex. The solid and dashed black lines localize and summarize our measurements of faults and dikes, respectively. The red circle indicates the location of the City of Sete Cidades (SC), Ponta Delgada (PD), Furnas (F), Povoção (PV), Água Retorta (AR) and Nordeste (N). The blue squares mark the location of Figs. IV.18 to IV.21 and IV.A6. A clean version of the DEM (without the various structures) is given in the Supplementary materiel as Fig. IV.A4.

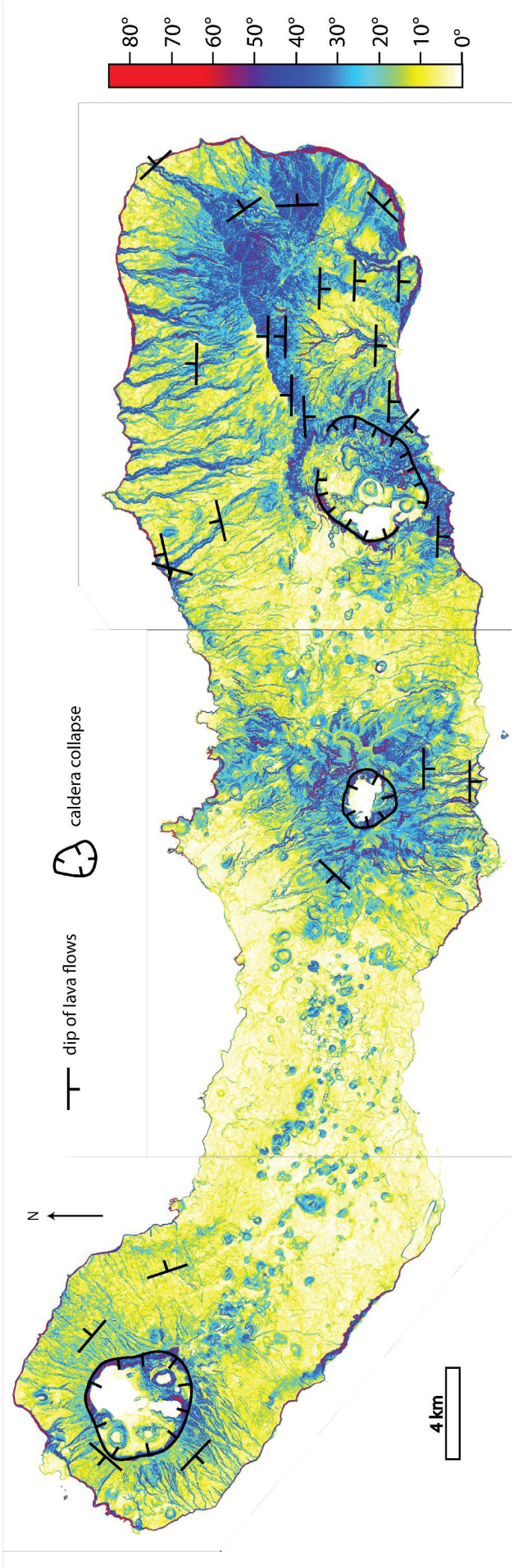
The major central volcanic edifices of S. Miguel have been affected by one or more caldera collapse events (Fig. IV.16). Zbyszewski et al. [1959] concluded that the Sete Cidades volcano (Fig. IV.16) has been affected by one caldera collapse, while for Queiroz et al. [2008] the collapse occurred in three stages. The Sete Cidades volcano comprises a graben in its northwestern flank [Machado, 1959]. The central volcano of Fogo (Fig. IV.16) has been affected by 1 or 2 caldera collapses [Zbyszewski et al., 1959; Moore, 1990], and presents active volcanic structures with a N150 trend, which could possibly pertain to a graben hosting hydrothermal systems [Carvalho et al., 2006]. The Furnas volcano (Fig. IV.16) is affected by at least one caldera collapse event [e.g., Moore, 1990; Duncan et al., 1999]. The Nordeste VC (Fig. IV.16) exhibits a circular depression, opened towards the south, known as the Povoação caldera [Moore, 1990].

Two main structural trends have been identified in S. Miguel, the N110 and N150, which have apparently controlled the position and distribution of the volcanic edifices [Zbyszewski et al., 1959; Moore, 1990]. The geological map of Moore [1990] indicates several normal faults, but it does not show the main dike swarms. Some dyke trends were earlier reported in the map of Zbyszewski et al. (1959), but their significance regarding deformation in the TR has not yet been addressed and discussed.

IV. 2. 3. METHODS

IV. 2. 3. 1. Morpho-structural analysis and fieldwork

The overall morphology of S. Miguel is dominated by two main trends: a N80 trend characterizing the eastern 2/3 of the island, and a N130 trend developed in the western 1/3 of the island. Both trends follow the main orientation of the TR and are separated by a narrow and flat zone with strombolian cones. In order to localise the main topographic lineaments within the island, and identify zones of potential major interest for fieldwork and structural analysis, we combined the information from the map of Zbyszewski et al. [1959], a digital elevation model (DEM) of the island at a spatial resolution of 10 m, and a slope map built from the DEM (Figs. IV.17, IV.18 and IV.A4). By varying the illumination angles, we could detect the main directions previously recognized (N150, N110). The slope map was used to detect the abrupt and irregular topographic surface without the bias of the illumination. Then we used cross-section to recognize and characterize areas potentially affected by major tectonic structures such as grabens and collapse scarps.


80°
70°
60°
50°
40°
30°
20°
10°
0°
caldera collapse
dip of lava flows
N
4 km

189

Figure IV. 17. Slope map of S. Miguel generated from the high-resolution Digital Elevation Model (DEM) with dip of lava flows measured during our fieldwork.

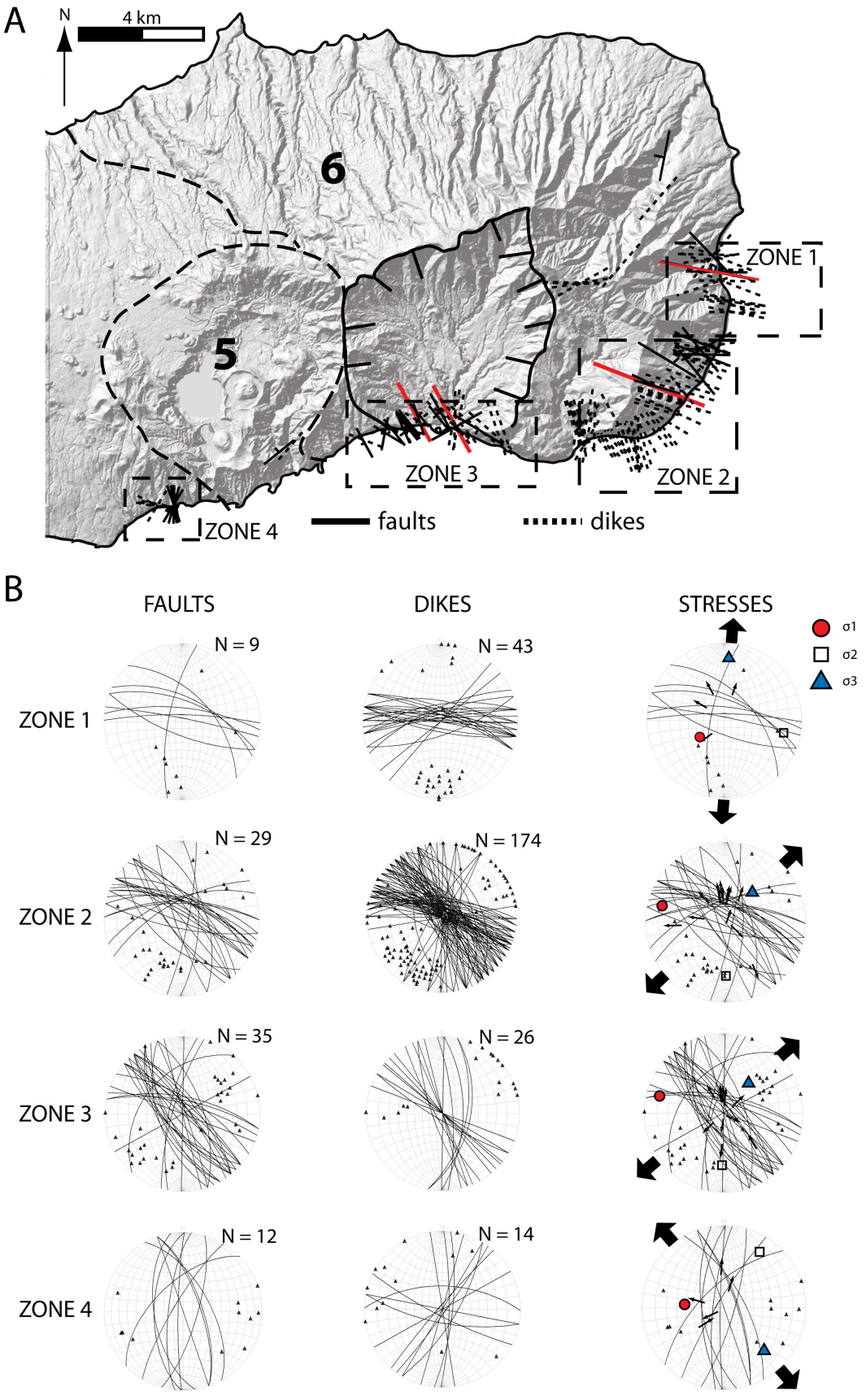


Figure IV. 18. (A) Map of the newly measured faults and dikes for the eastern part of S. Miguel displayed over a high resolution shaded relief map. The dashed squares indicate the 4 zones distinguished from our new morphological analysis, fieldwork observation and tectonic markers. Faults and dikes locations are simplified for better visualization. The red lines indicate the main structures recognized in this study. (B) Computation of great circles and pole to planes (Wulff net, equal angle lower hemisphere projection) of the faults, dikes and stress tensor for zones 1, 2, 3 and 4. N is the numbers of measurements in each zone. Red circle: σ_1; square: σ_2; triangle: σ_3.

Fieldwork was then focussed on the recognized lineaments to characterize and measure fault elements and dikes throughout the island. The outcrops are mainly localised along the coastal cliffs and canyons of the island, which constitute natural sections and represent by far the great majority of the outcrops on the island. We systematically measured the geometry (strike and dip) of dikes and faults, and defined their stresses from available markers (striations, shear criteria, and offset). A total of 104 faults and 276 dikes were measured on the whole island (Fig. IV.18).

IV. 2. 3. 2. Data processing

All the measured strikes were corrected for the present magnetic declination (www.rncan.gc.ca), assuming all four family is coeval. Faults and dikes data were processed using the tectonics software FP v1.7.5 [Ortner et al., 2002] for the determination of the orientations of the principal stress axes. Only fault data with observed striations were used to calculate the orientations of the principal stress axes.

Principal strain axes were calculated using the P-T method [Turner, 1953], the direct inversion method [Angelier, 1984; Angelier, 1994], and the numerical dynamic analysis [Spang, 1972]. The P-T method calculates the P-axis (pressure axis), B-axis (intermediate principal strain axis) and T-axis (tension axis) for each fault plane, and generates mean axes for a given fault set. The direct inversion method is based on the assumption that the direction and sense of slip on a single fault plane are those of the shear stress called maximum. The resolved shear stress is applied on this plane by the stress tensor [Wallace, 1951]. The commonly used stress inversion technique results in the orientation (azimuth and plunge) of the principal stress axes of a stress tensor: the stress ratio $R = (\sigma_1 - \sigma_2)/(\sigma_1 - \sigma_3)$ describes the relative stress magnitudes. The principal stress axes σ_1, σ_2 and σ_3 are the maximum, intermediate and minimum compressional stress axes, respectively. The inversion method aims at determining the stress tensor that best accounts for the strikes and sense of fault plane dip in massive rock indicated by a lineation. It fails in the analysis of strongly asymmetric fault sets, e.g. when one set of conjugate faults dominates over the other [Sperner et al., 1993]. The numerical dynamic analysis (NDA) allows giving the reciprocal strain tensor ($\lambda_1 \geq \lambda_2 \geq \lambda_3$) and strain ratio, $R_{strain} = (\lambda_2 - \lambda_3)/(\lambda_1 - \lambda_3)$. For all analyses, the angle (θ) between λ_1 and λ_2 was assumed to be 30º, which is a reasonable value for the angle of internal friction of newly formed faults [Byerlee, 1967], and is an average angle for fault sets consisting of pre-existing faults [Sperner and Zweigel, 2010].

To determine the different populations of faults in the various sectors of the island (zones), we used the P-T axis method. The method chosen for a given fault population was based on the best fit of principal axes orientations with respect to fault strike and dip. Our results suggest that the principal axes of most of the brittle fault sets are best represented by the inverse method (Table IV.2), and the resulting stress tensors are shown in Fig. IV.18.

Site		PBT			NDA			strain	Inverse			stress	Method
	N	P	B	T	λ1	λ2	λ3	ratio	σ1	σ2	σ3	ratio	used
Zone 1	4	270/79	83/28	211/06	294/84	113/06	203/00	0,2875	237/59	102/23	3/20	0,132	INV
Zone 2	13	257/79	105/24	01/02	262/78	102/12	11/04	0,3784	285/21	180/34	40/48	0,679	INV
Zone 3	10	138/87	309/04	36/02	239/88	124/01	33/02	0,5544	249/72	125/10	32/14	0,901	INV
Zone 4	5	284/73	180/02	89/07	300/76	171/09	79/11	0,224	274/51	33/21	137/31	0,131	INV

Table IV. 2. Results of the P-T method, NDA and inverse method.

IV. 2. 4. RESULTS

IV. 2. 4. 1. Morphology

The slope map reveals that Sete Cidades is a well preserved volcano with irregular coastlines, radial canyons and external slopes comprised between 5 and 20° (Fig. IV.17). The summit of the volcano is truncated by a large elliptical caldera. The NW part of Sete Cidades also seems to be affected by a graben structure with a N130 trend, compatible with the elongated western part of the island. On the southeast of Sete Cidades the slope decreases from ca 10° (deep yellow color, Fig. IV.17) to ca 5° (light yellow to white colors). The latter indicates a flatter portion, which may not correspond anymore to the external slopes of the Sete Cidades volcano. The eastern flank of Sete Cidades is additionally covered by a well-preserved N130 alignment of numerous scoriae cones (Figs. IV.17 and IV18). The tectonic and volcanic alignments are parallel to the local elongation of the island and to the trend of the TR in this sector. In contrast with the central edifice of Sete Cidades, they do not show a radial pattern. This suggests that the tectonic and volcanic trends are likely primarily controlled by a regional stress field, rather than an isotropic stress field due to the hydrostatic effects of the central magma chamber [e.g., Nakamura et al., 1977]. East of the strombolian cones (Fig. IV. 15, domain 2), the general trend of the island changes from ca. N130 to ca. N80, and comprises, from W to E, the volcanoes of Fogo, Furnas and Nordeste.

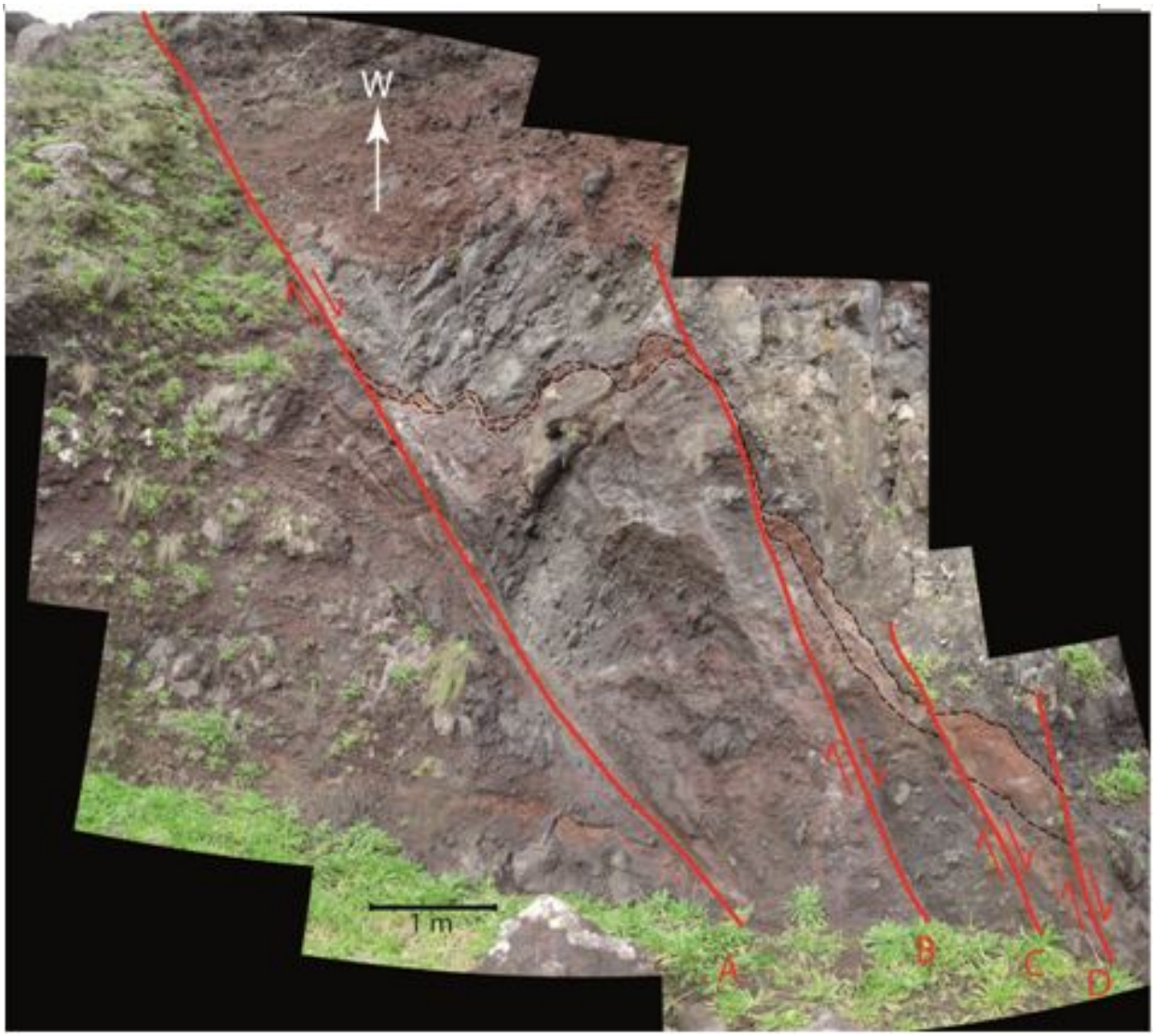


Figure IV. 19. Set of N-dipping normal faults along the eastern end of the island. Location of the outcrop is shown in Fig. IV.16.

262

263 The analysis of the DEM and slope map also reveals an asymmetric morphology of the
264 eastern part of the island (Fig. IV.16, domains 3, 4, 5, and 6): the northern flank of the island is
265 quite regular and characterized by gentle external slopes (< 25°, excluding locally higher slopes
266 inside canyons), while the southern side is much more irregular (Fig. IV.17). It comprises several
267 structures, e.g., a sub-circular caldera, a series of canyons, and coastal cliffs of various heights.
268 The calderas have developed at the southern foot of a prominent N80 scarp, the origin of which
269 has been attributed to large-scale sector collapse by Sibrant et al., [2013a]. The transition between
270 the domain 2 (Fig. IV 16) and the Fogo volcano to the east is marked by a significant increase in
271 average morphological slopes, from ca 5° to more than 20°. This abrupt change corresponds to a
272 variation in the nature of the volcanism (small strombolian cones versus central volcano).
273 Numerous steep-sided linear canyons truncate the slopes of the Fogo volcano (domain 3). They
274 are dominantly oriented N150-N160 in the North, and N-S on the southern slope of the volcano
275 (Figs. IV.16 and IV.17), where a S-directed sector collapse is believed to have occurred recently

[Sibrant et al., 2013a and Chapter IV.1]. East of Fogo, the domain 4 composes a flat morphological portion with gentle slopes and no significant canyons. Like the domain 2, this portion comprises several scoria cones. The cones are aligned along a N80 trend, so perpendicular to the local elongation of the island. The domains 5 and 6 in the easternmost part of the island show an irregular topography, with abrupt slope variations. This sector also bears much sharper canyons than the other parts of the island. The most obvious canyon is linear and roughly oriented ~N50. The northern slope of the Nordeste VC shows a relatively regular slope with deep canyons. If we consider an elliptical N80 shape for the original edifice, the canyons mimick a relative radial shape. The southern part shows two elliptical structures, which have been identified as the caldera of Furnas and Povoação, respectively [Sibrant et al., 2013]. On the southeastern end of the island, we identify two N110-120 walls bounding a depression, which looks like a graben structure. Due to these particular characteristics, the eastern sector of the island seems particularly affected by erosion and linear structures with a potential tectonic origin.

IV. 2. 4. 2. Tectonics

From our new measurements, the eastern end of S. Miguel is cut by faults and dikes almost exclusively striking N110. We call Zone 1 this sector of the island (Fig. IV.18). The stress tensor in Zone 1 indicates an approximate N-S trending σ_3 axis and a sub-vertical σ_1, which is consistent with the mean E-W strike of dikes measured in the eastern part of the Nordeste VC. The age of the rocks affected by the faults and dykes has been constrained between 880 and 780 ka by Johnson et al. [1998], and so provide us a maximum age of ca 780 ka deformation in this area. This stress state is recorded only in the easternmost part of the Nordeste VC. In Zones 1 and 3, several N110 faults with a dip to the NNE show a higher apparent normal offset, up to 20 m. The outcrop in Fig. IV.19 comprises normal faults with N105, N110, N100 and N100 strike (A, B, C and D, respectively), and shows a minimum cumulative displacement of 25 m.

Immediately to the south of Zone 1, in what we call Zone 2, two linear scarps oriented N110 can be identified on both sides of Água Retorta (Fig. IV.16). They bound a broad and linear topographic depression, which reaches a length of about 4 km and a width of 2.5 km (Figs. IV.17, IV.18 and IV.A4). There, faults and dikes strike either N110 or N150 (Fig. IV.18). Zone 2 also comprises a set of major faults oriented N115, dipping from 60 to 65º towards the NE (Fig. IV.20). The most significant shows a minimum offset of 25 m. The fault plane presents striations with a sub-vertical pitch. These faults correspond to the southern scarp bounding the N110 depression. Although a northern scarp is visible on the DEM (Figs. IV.20 and IV.A4), no faults or dikes could be observed in the field due to dense vegetation. Topographic evidence, orientation, dip and stresses of the faults (Figs. IV.20 and IV.22), suggest that the depression consists of a half graben close to the village of Água Retorta, but we do not exclude a possible graben made up of several faults striking N110 and dipping to NE and SW. The southern scarp shows a minimum vertical height of

nearly 250 m. The half graben is asymmetric and contains at least two volcanic cones (Fig. IV.22).



Figure IV. 20. Example of fault surface materialising the southern wall of the graben newly recognized in Água Retorta. It has a N115 strike and dip from 60 to 65º NE, and sub-vertical striations (black dashed lines). See Fig. IV. 16 for location.

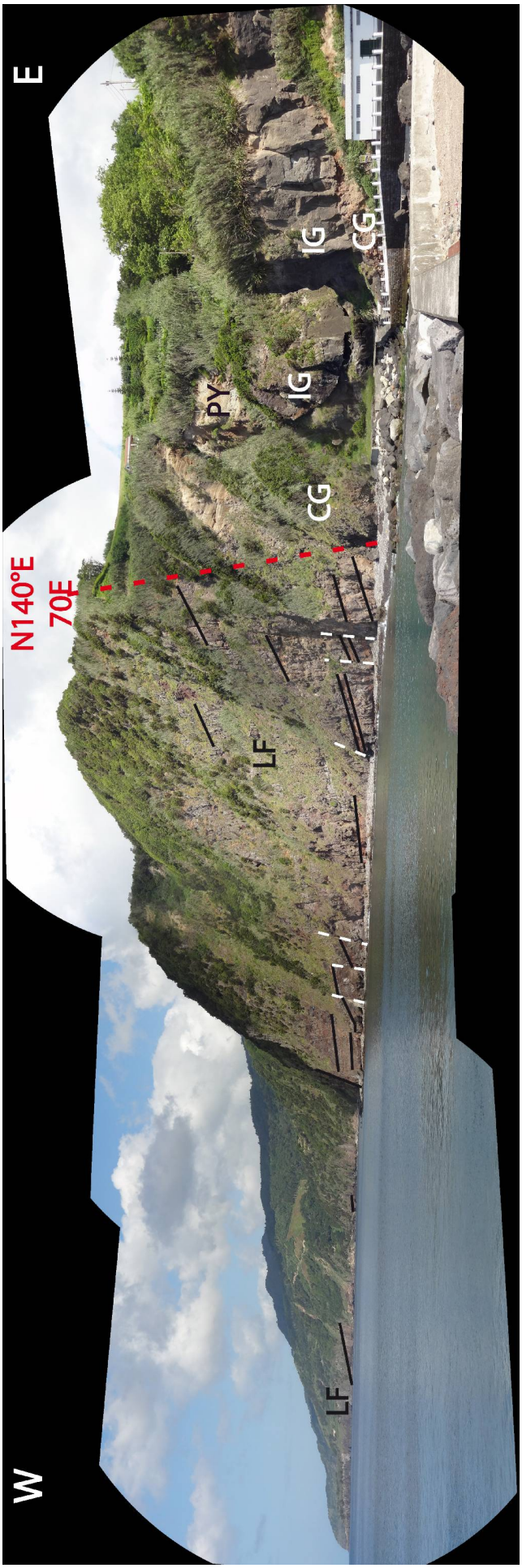
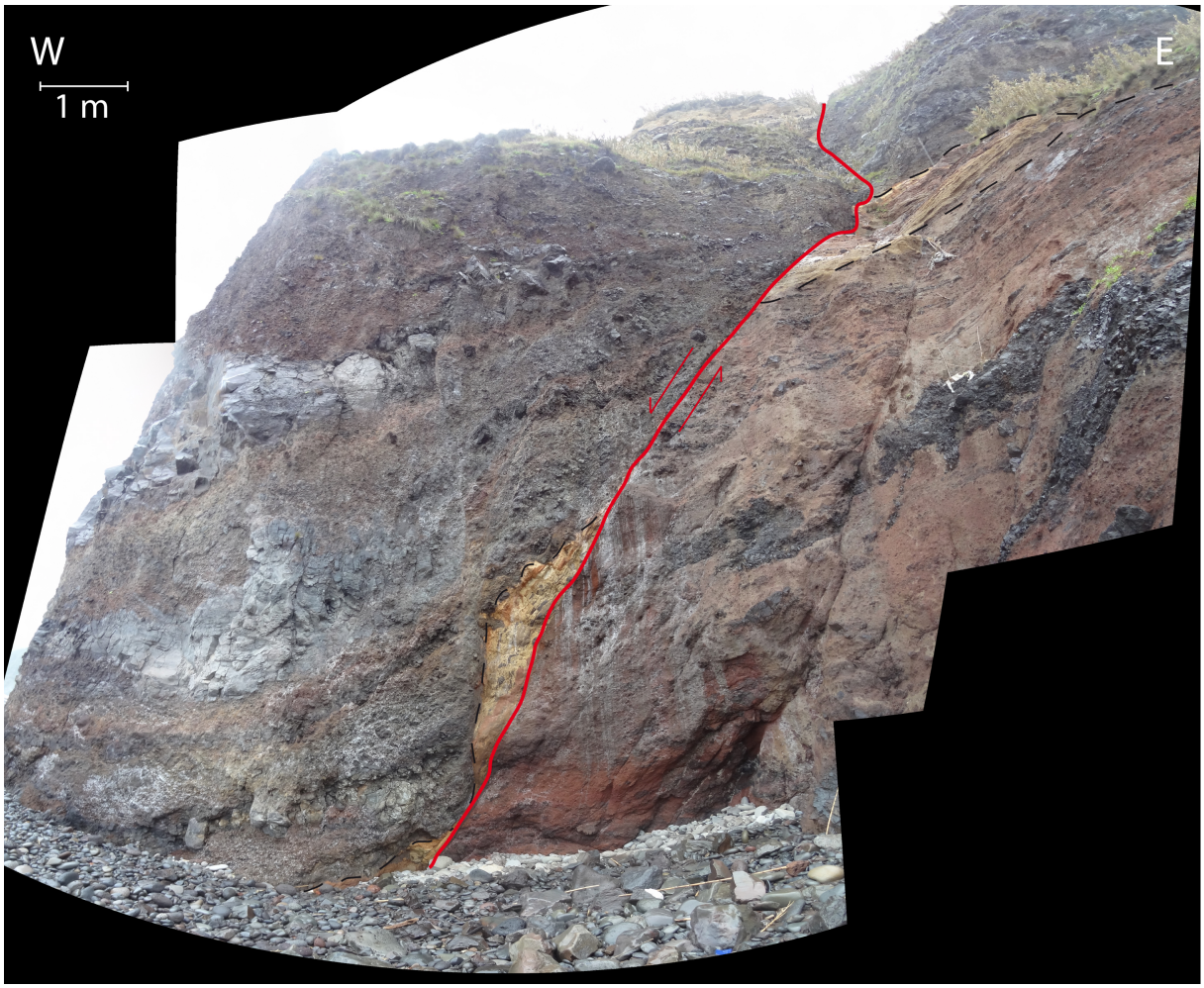

E
W
N140°E
70E
PY
IG
CG
IG
CG
LF
LF

Figure IV. 21. W-E sea cliff to the west of the village of Povoação (see Fig. 2 for location). The black lines indicate the dip of the Lava flows (LF). The dashed white and red lines indicate faults and the western wall of the graben identified in Povoação. CG: conglomerates; PY: Mixed pyroclasts and cinders; IG: Ignimbrite flow with fiamme.



Supplementary material Fig. IV. A6. W-E sea cliff to the east of the village of Povoação. See Fig. IV.16 for location. The faults have been measured with a ca. N150 strike and a dip of 80° to the SW.

Immediately to the west of Zone 2, Zone 3 coincides with the southern part of the Povoação depression (Nordeste VC, Fig. IV.16). This sector is characterized by faults and dikes mostly striking N150. The stress tensors for Zones 2 and 3 indicate approximate NE-SW extension. This extension direction is observed in two of the four zones defined in the present work. These zones are both located in the Nordeste VC (Figs. IV.16 and IV.18). To the west of the city of Povoação (Zone 3, Fig. IV.16), the coastal cliff shows a major discontinuity (Figs. IV.21 and IV.A5), which separates a succession of numerous lavas flows dipping gently to the SW in the west, from a succession of conglomerates, ignimbrite flow comprising fiamme at the base and mixed pyroclasts and cinder, in the east. These two successions are separated by a major fault striking N140 and dipping 70° to the E (Figs. IV.21 and IV.A5). To the east of Povoação, we also identified normal faults striking N150 and dipping between 70° and 80° to the WSW and ENE, respectively

(Supplementary material, Fig. IV.A6). The faults bound a depressed block ca. 1 km long, which has been apparently downthrown by a minimum of 125 m. The stress tensor estimation for the zone 3 (Fig. IV.18), and stereoplots also indicate the presence of a graben, here coined the "Povoação Graben" (Fig. IV.22).

Finally, Zone 4 is located to the SW of the Furnas volcano. There, faults and dikes strike N-S and N20-N50. The stress tensor in Zone 4 indicates σ_3 with a NW-SE direction, and subvertical σ_1. This stress regime is recorded throughout the Furnas Complex, and is different from the stress tensor obtained for the other three zones. This stress state is only recorded in rocks younger than 93 ± 9 ka [McKee and Moore, 1992].

Most of the measured faults exhibit a dominant normal component, with individual offset generally less than 1 m. In total, more than 94% of the recognized structures are located in the eastern part of the island. In the NW part of Sete Cidades we measured the southern wall of the graben (N160) identified by Moore [1990]. Another major fault shows a N110-65º SSW attitude (in the NW), and two other faults show N50-80SE attitude (in the SE). At the base of the Fogo volcano (Fig. 2), we measured faults and dikes striking N150 and N50.

IV. 2. 5. DISCUSSION

IV. 2. 5. 1. The tectonics of S. Miguel

Our new data delineates two newly recognized tectonic structures: the Água Retorta half-graben or graben, and the Povoação graben (Figs. IV.20, IV.21, IV.A6 and IV.22). However, while there is a clear relationship between the topography and the structure trend for the former, the graben of Povoação is not so obvious. The Nordeste complex shows an elliptical N80 shape, the northern lava flows dip indicates an elliptical shape too, whereas the southern part is composed of lava flows dipping to the south. The asymmetry between the northern and southern slopes is separated by a main E-W scarp (Figs. IV.17 and IV.18), and the lava on the south shows a clear exclusive south dip except close to the Furnas volcano. According to Sibrant et al. [2013a], it seems that the oldest Nordeste complex may have been affected by a catastrophic large-scale collapse towards the south. The scar was later filled by lava flows, which form the Povoação depression in the E and the Furnas volcano in the W. The depression in Povoação was previously interpreted as a caldera associated with the eruption of pyroclastic flows and ignimbrites [Moore, 1990]. However, our new structural work in the depression of Povoação shows the presence of major faults striking N150 and dipping to ENE and WSW on each side of the village of Povoação. The depression bounded by these two opposite-dipping fault sets is filled with conglomerates and thick ignimbrite flows.

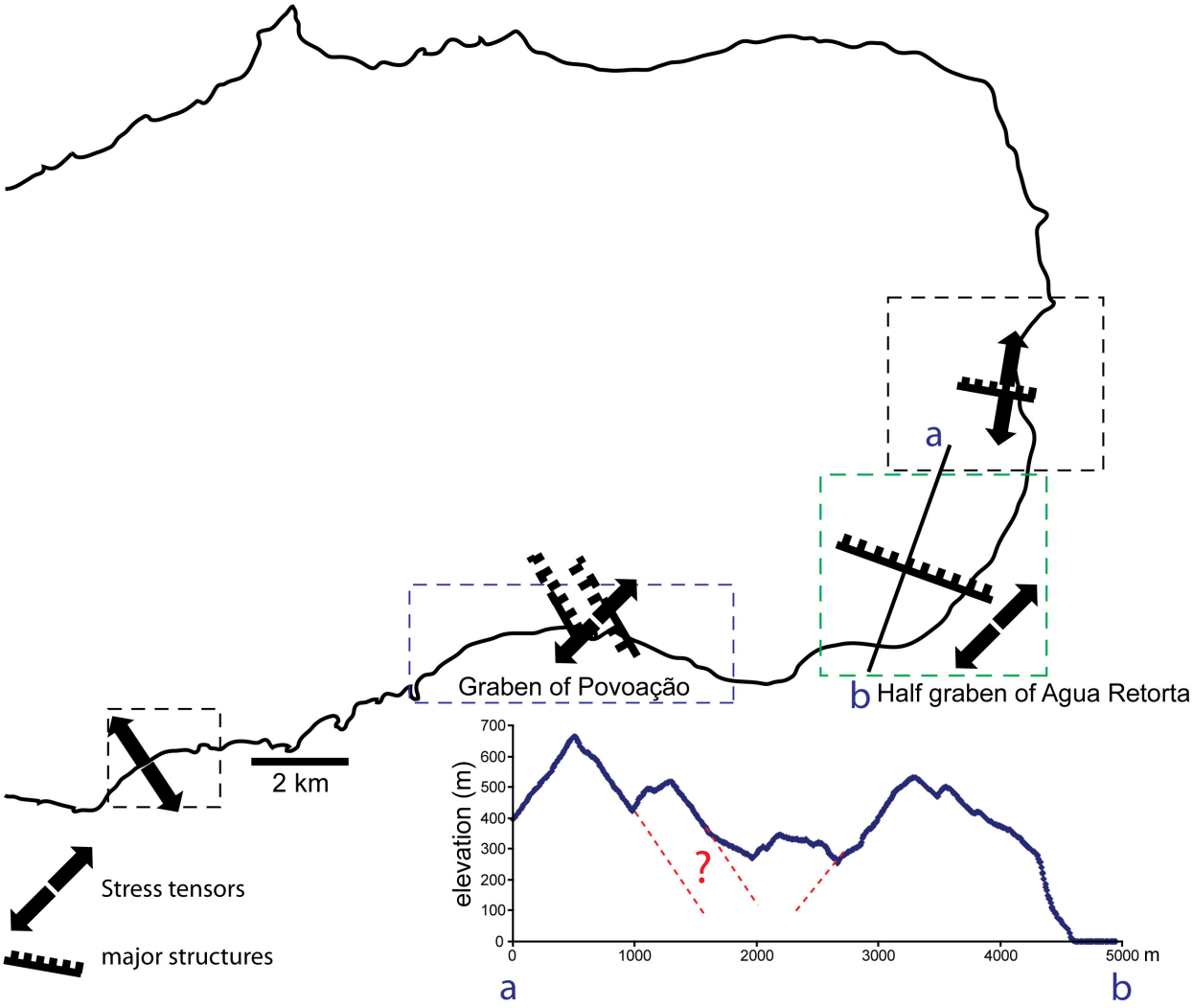


Figure IV. 22. Location of the main recognized structures on S. Miguel. The dashed squares show the location of the 4 zones here distinguished. The black arrows indicate the stress tensors of the 4 zones, deduced from the orientations of the principal stress axes shown in Fig. IV.18. Line a b marks the location of the NE-SW topographic profile of the half graben of Água Retorta shown on the inset. The dashed lines represent the inferred main associated faults.

372

373 Duncan et al. [1999] argued that the ignimbrites, which they called the Povoação ignimbrite
374 formation (PIF), are the product of the largest explosive eruption of the neighbouring Furnas
375 volcano and not by a "Povoação volcano". This means that the main deposit associated with the
376 concentric destruction, and thus the evidence for a caldera event, are debatable. Moreover, a
377 caldera collapse generally produces concentric fault patterns [e.g., Walker, 1984; Walter and Troll,
378 2001; Kinvig et al., 2009], even in areas dominated by regional tectonics [e.g., Francis et al., 1978;
379 Acocella et al., 2004]. None of our observations indicate the presence of concentric faults, and no
380 pyroclastic deposit other than the PIF was observed within the structure. Considering all the
381 evidence, we suggest that the depression of Povoação is not a caldera. Instead, we suggest,
382 based on the new proposed evolution of the Nordeste VC (Sibrant et al., 2013a; chapter IV.1) that
383 the filling volcanism has been affected by a graben oriented N150, which was subsequently filled

384 by at least 25 m of ignimbrite (PIF) from a Furnas volcano event, which smoothed the topography.
385 The current circular depression results from focused erosion processes and watershed
386 configuration of the ignimbrite flow. Such structural control on erosion processes and watershed
387 reconfiguration has been observed and described in other oceanic islands [e.g., Gillot et al., 1994;
388 Hildenbrand et al., 2008a].
389
390 Our new tectonic data do not solely show that S. Miguel is affected by the N110 and N150
391 main directions, but also by an additional N20-N50 direction. The meaning of the N50 fault system
392 will be discussed below. Our measurements indicate a progressive variation in the orientation of
393 the major structures and faults and dikes, within 20 km only, from N110-dominated in the east to
394 N150-dominated in the west. Moreover, the density of faults and dikes considerably decreases
395 from east to west in the whole island.
396 The structural trends measured within the island do not coincide with the main trends of the
397 island. The N110 and N150 trends (small scale, within island) are not coincident with N80 and
398 N130 (large scale, whole island and TR). Therefore, there is a clockwise rotation of 20-30º from the
399 large-scale structures to the small-scale structures. This rotation of structural trends could be the
400 result of the stresses inherent to the topography of the island. Due to its topography above the
401 seafloor, the island has its own stress field, and imposes its load and stresses in the underlying
402 oceanic crust. Therefore, the stresses deduced from fault kinematics and dikes in the island also
403 differ from the kinematics reported by DeMets et al. [2010], for the eastern TR: ENE-WSW
404 extension from plate kinematics versus NE-SW here deduced from faults and dikes.
405 S. Miguel is not only located in the TR, and partly on its northern shoulder, but also at the
406 inflection between two N130 rift segments, connected by an E-W segment. These orientations
407 coincide with the orientations of S. Miguel: approximately E-W in the eastern two thirds of the
408 island, and N130º in the westernmost third, where the TR inflects from E-W to SE-NW. We
409 propose that the variations in island shape and orientation of tectonic markers across the island
410 reflect the local sigmoidal shape of the TR and the particular position of S. Miguel inside the TR.
411 The tectonic structures are much more frequent near the TR wall than in the centre of the
412 island. However, the younger fissural systems in the central and western S. Miguel are elongated
413 along the N110 and N130 directions, which means that even if the structural markers such as
414 faults or dikes lack, the tectonic control is still present. Here, we propose that the tectonics induced
415 by Nubia and Eurasia plate motions along the TR is mainly accommodated by the wall of the TR
416 and not by the central axis. Such different tectonic expression between outer and inner parts of the
417 TR also favours the development of graben normal faults and numerous dikes preferentially in the
418 east. Moreover, the volcanoes localized in the middle of the rift are younger than volcanoes
419 localized along the shoulder of the rift. Nordeste volcano represents the first stage of the rift
420 opening, where the volcanism is located along the shoulder and the Sete Cidades indicates that
421 the opening is advanced enough to localize volcanism in the middle of the Rift.

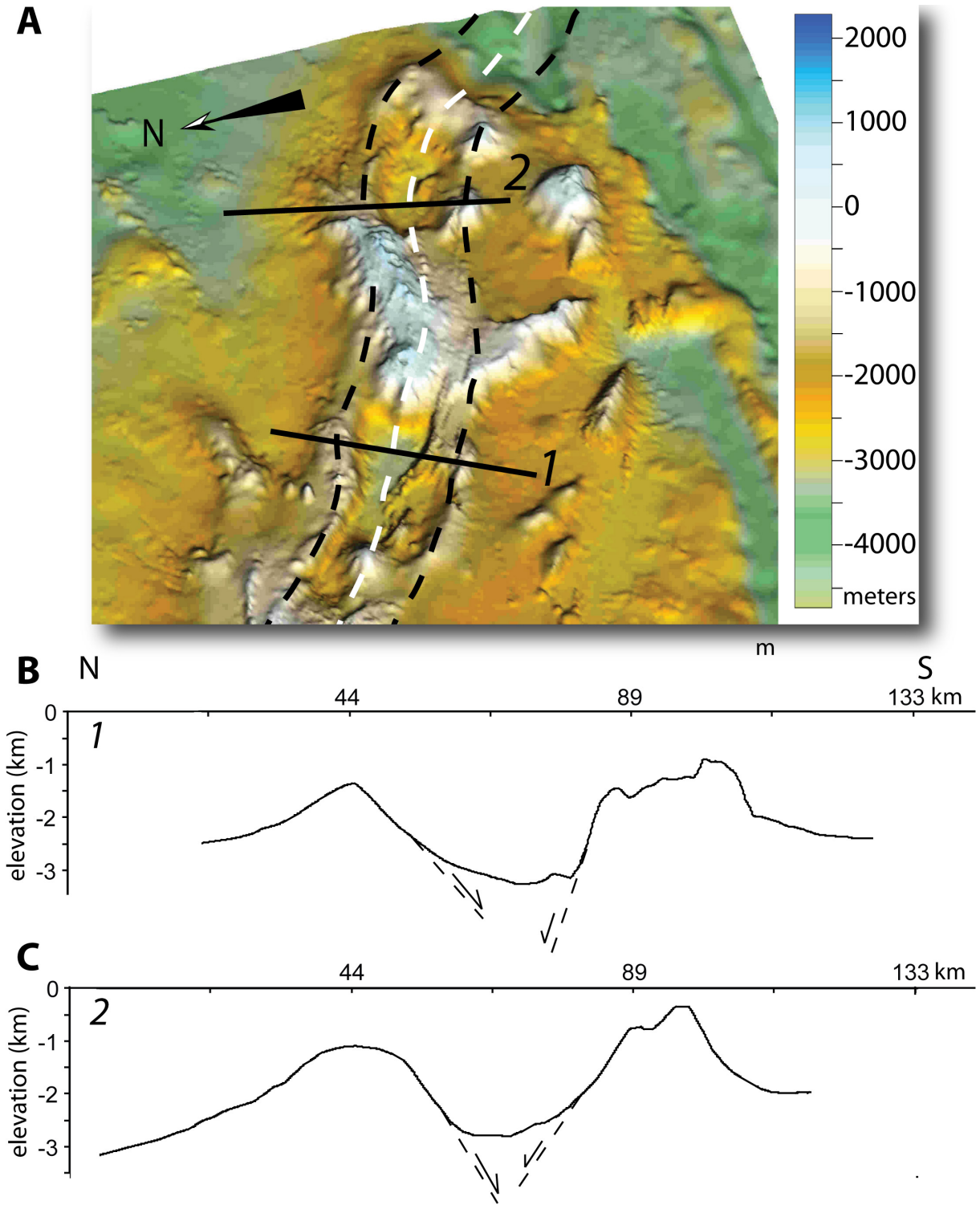


Figure IV. 23. (A) Zoom on the 3D bathymetry near S. Miguel [bathymetry from Lourenço et al., 1998]. The white and black dashed lines indicate the location of the main axial valley and the borders of the rift, respectively. The numbers 1 and 2 refer to the cross sections shown in the I(B) and (C) panel. (B) is a NE-SW cross section through the basin west of S. Miguel; (C) is a N-S cross section of the basin east of S. Miguel. The dashed lines indicate possible normal fault of the Rift (see text for details).

IV. 2. 5. 2. The architecture of the Terceira Rift

A large-scale study on the available low-resolution bathymetric data (1 km) in the study

area allows a first-order analysis of the morphology of the TR (Fig. IV.23). Cross-sections 1 and 2 (Fig. IV.23), west and east of S. Miguel, respectively, display a graben morphology for the ca. 40 km wide rift valley. They additionally show that the TR is bounded by two master normal faults dipping to the NE in the SW shoulder and to the SW in the NE shoulder. The northern part of the profil 1 indicates a slope close to 40° whereas the other border of the rift shows a dip of 60° of a classic normal fault. The northern part of profil 1 cuts the TR where we can see a little inflexion in the orientation of the TR. Thus, profil 1 does not cut exactly perpendicularly the TR, and so the degree of slope is underestimated. The low angle can be also due to sliding along the fault.

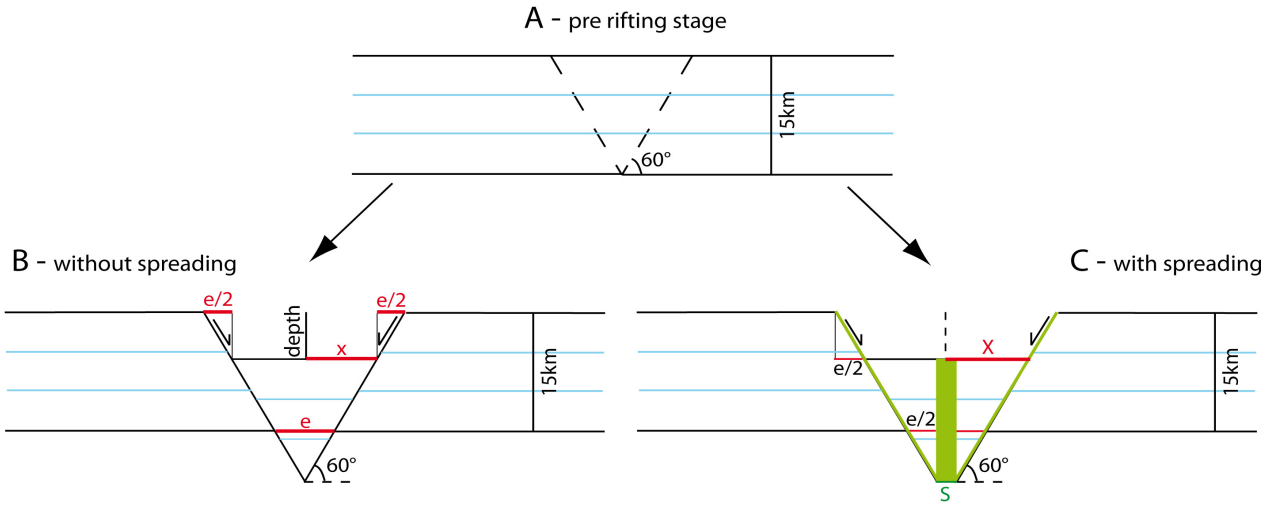


Figure IV. 24. (A) Schematic scenario for the pre-rifting stage of the TR, and for the opening of the Terceira Rift without spreading (B) and with spreading (C), respectively.

The width of the flat bottom of the basin in the TR southeast of Terceira Island is between 18 and 22 km (Fig. IV.23 and Vogt and Jung, [2004]). Given that the gravity data and magnetic anomalies do not indicate that the TR has progressed to sea floor spreading (creation of new oceanic crust), here we use the structure of the current TR to estimate (1) if sea floor spreading has or has not taken place along the TR, and (2) when the TR has likely initiated.

(1) First, we consider that the TR is opening without spreading, as faulted rigid blocks. This implies that the topography of the TR is due to opening by vertical offset of the lithosphere along two master normal faults (Fig. IV.24). The topographic section (Fig. IV.23) suggests that the rift is developed along only a pair of master conjugate normal faults dipping between 60º to NE and SW. Two published focal depths of 12 ± 5 and 15 ± 5 km [Grimison and Chen, 1986; Dias et al., 2007] for earthquakes in this part of the TR give a fairly good estimation of the thickness of the brittle seismogenic lithosphere. With a thickness of the brittle crust of 15 km, we can calculate the width at the bottom of the basins using simple trigonometry. The result indicates a width at the bottom comprised between 17 and 25 km, with fault dip of 60 or 50°, respectively. This theoretical estimation of the width at the bottom of the TR is similar to the current topographic width obtained from the bathymetry. Therefore, our calculations suggest that rifting at the TR has been

accommodated solely by normal faulting, without any, or only minor, sea floor spreading. Significant spreading would make the TR much wider than estimated and observed.

(2) Because the TR is seemingly opening without spreading (calculations with spreading are therefore not necessary), the horizontal extension can be determined from the current depth and from the dip of the main bounding faults (Fig. IV.24). The depth of the TR on both sides of S. Miguel is close to 2 km; however, our cross sections (Fig. IV.23) do no cross the deeper zone of the basins, which can reach 2.5 to 3 km [Vogt and Jung, 2004; Sibrant et al., 2013b]. According to Searle [1980], the sedimentary cover can reach 500 m in the oldest and deepest regions of the Azores plateau, which means that the depth of the TR in the regions of interest can reasonably be close to 3-3.5 km. Again, using simple trigonometry and the above parameters, the total horizontal extension (e) is estimated between 3.5 and 6 km. The present extension rate orthogonal to the TR is of ca. 3.5 mm/yr [DeMets et al., 2010; Marques et al., 2013], which indicates that the TR has initiated between 1.0 Ma and 1.7 Ma ago, in fairly good agreement with the recent estimates obtained independently by Vogt and Jung [2004] and Sibrant et al. [2013b, submitted].

The axial morphology of hyper-slow rifts like the TR is a function of two main competing processes that vary in time and space: the volcanic activity, which results in the construction of relatively smooth features, and faulting/rifting, which results in the creation of rough, linear features at many scales. The width of a rift, its structure, and the style of volcanism within it change considerably with opening rate.

Morphological studies on mature slow ridges, like the MAR, have shown that there are interactions between the morphology of rift valleys, mantle upwelling and rifting processes [Perfit and Chadwick, 1998]. A rift valley with a shallow graben morphology can be interpreted as non-volcanic, or sparsely magmatic (island), with dominant tectonic extension [Perfit and Chadwick, 1998]. Even if the existence of a plume below the Azores is still debated [e.g., Bonatti, 1990; Silveira and Stutzmann, 2002, Métrich et al., 2014], the emplacement and the evolution of the Azores volcanism is largely controlled by competing tectonic and volcanic processes, and mostly by the regional deformation due to plate kinematics [e.g., Lourenço et al., 1998; Hildenbrand et al., 2008b; 2012]. Montési and Behn, [2007] showed that the rate of expansion along an oceanic ridge has a direct influence on the thickness of the crust and the thermal structure of the ridge. If the extension rate is less than 6.5 mm/yr, the volcanism along the axis cannot be continuous. As the TR shows an extension rate between 4 mm/yr [DeMets et al., 2010] and 3 mm/yr [Marques et al., 2013], it is thus not surprising to have a discontinuous volcanism. For example, along the Ethiopian rift, the volcanism in the magmatic segments started ca. 1.6 Ma, and most flows emanated firstly as main shield volcanoes, which were later followed by fissures and small cinder cones with some differentiation [Boccaletti et al., 1999]. In oceanic rifts, the along-axis segmentation is defined by dike injection and faulting with an axial valley and flank morphology [e.g., Batiza, 1996]. Ultra-slow spreading ridges such as the South West Indian Ridge show a more extreme focusing of melt, with

the construction of large central volcanoes at the centre of some segments, while others are relatively magmatically starved [Cannat et al., 1999; Dick et al., 2003]. The TR and other slow opening oceanic ridges (as the SWIR or the Gakkel ridge) show some similarities in the position of the volcanism. Our estimation indicates that no significant spreading has occurred along the current TR, however, the TR is a very young rift, so asthenospheric processes may become more important in the future, if a reorganisation of plate motion and plate boundary migration does not occur before.

Finally, the N50 fault system newly evidenced in S. Miguel is not a common direction described in the Azores. The absence of N50 fault planes favourable for measurement of striations limited the determination of fault kinematics. However, the focal mechanisms of earthquakes between Graciosa and Terceira islands (NE of S. Jorge Island), and between the islands of S. Miguel and Sta. Maria show two sub-vertical nodal planes, one of which is oriented N50-N55 [Borges et al., 2007]. Similar trends have been recently recognized in Graciosa [Sibrant et al., 2014], S. Jorge [Silva et al., 2012], and in the 1998 Faial earthquake [Marques et al., 2014]. Thus, although not conspicuous within the islands, the N50 trend seems to be important for the recent tectonics of the Nubia-Eurasia plate boundary, because it seems to cut the very recent volcanic units, and the TR in particular. The N50 strike slip fault system is located between islands or where the direction of the TR changes. This is the case of the S. Miguel region, where the TR trend changes from N130 in the NW, to N80 in S. Miguel, and again to N130 further SE. This trend is measured through the faults and dykes, but is also shown in the main direction of canyons in the eastern part of the island. DeMets et al. [2010] in the model of the plate velocity configuration predicted the presence of such a ~N70-N50 fault system. Moreover, Marques et al. [2014] based on tectonic data, measured ground motion and modelling shows that the ENE-WSW fault plane solution of the 1998 earthquakes is associated with the Nubia-Eurasia diffuse plate boundary and can be a transform fault. Therefore, the N50 faults, dykes and canyons may reflect a transform trend consistent with the rotation of the Nu relative to Eu and the elongation of the eastern 2/3 of S. Miguel.

IV. 2. 6. CONCLUSION

Given that the TR is an active hyper-slow rift, which materializes in part the current Eurasia - Nubia plate boundary, and that the S. Miguel Island spreads across the entire width of the TR, the study of S. Miguel is crucial because it allows characterizing the way deformation has been accommodated across the TR.

From DEM and structural analyses, including new measurements of 350 faults and dikes, we conclude that:

(1) There is a clockwise rotation between the elongation of the island and the trend of the measured tectonic markers in the island.

(2) Tectonic markers are much more numerous in the eastern part of the island, which materializes the northern boundary of the TR, compared to the central and western parts.

(3) The orientation and distribution of faults and dikes indicate that eastern S. Miguel materializes the TR's northern boundary, and the lack of major faults in central and western S. Miguel indicates that rifting is mostly concentrated at the master faults bounding the TR.

(4) Ultra-slow rifts are typically very poor in magmatism, and rifting is preferentially concentrated along bounding master faults. This seems to be the case of the TR, in the middle of which tectonics seems to be much attenuated, and volcanism is concentrated in a few large volcanic edifices regularly spaced along the rift.

(5) The initiation of the eastern part of the TR began probably between 1 and 1.7 Ma and the rifting process has not included significant sea floor spreading.

(6) The N50 strike slip system recognized by Marques et al. [2014b] as a transform trend, is also recognized in S. Miguel and accommodates the variations in strike of the TR.

ACKNOWLEDGMENTS

Data supporting Figure IV.18 are available in supporting information Table IV.S1. This is a contribution to Project MEGAHazards, funded by FCT (PTDC/CTE-GIX/108149/2008), Portugal. ACG Costa benefitted from a PhD scholarship (SFRH/BD/68983/2010, FCT, Portugal). FO Marques benefits from a Sabbatical fellowship awarded by FCT Portugal.

547 **REFERENCES**

548 Acocella, V., R., Funiciello, E., Marotta, G., Orsi, and S., DeVita, (2004), The role of extensional
549 structures on expirimental calderas and resurgence, J. Volcanol. Geotherm. Res., 129, 199-
550 217, doi: 10.1016/S0377-0273(03)00240-3.

551 Angelier, J., (1984), Tectonic analysis of fault slip data sets, J. Geophys. Res., 89 (B7), 5835–
552 5848.

553 Angelier, J., (1994), Fault slip analysis and palaeostress reconstruction, In: Hancock, P.L. (Ed.),
554 Continental Deformation. Pergamon Press, Oxford, pp. 53–100.

555 Appelgate, B., and A.N., Shor, (1994), The northern Mid-Atlantic and Reykjanes Ridges: Spreading
556 center morphology between 55°50'N and 63°00'N, J. Geophys. Res., 99 (B9), 17935-
557 17956.

558 Bache, F., N., Mortimer, R., Sutherland, J., Collot, P., Rouillard, V., Stagpoole, and A., Nicol,
559 (2013), Seismic stratigraphic record of transition from Mesozoic subduction to continental
560 breakup in the Zealandia sector of eastern Gondwana, Gondwana Research, in press,
561 Corrected Proof.

562 Batiza, R., (1996), Magmatic segmentation at mid-ocean ridges, A review, in MacLeod, C., et al.,
563 eds., Tectonic, magmatic, hydrothermal, and biological segmentation of mid ocean ridges.
564 Geological Society of London, Special Publication, 118, 39-49.

565 Boccaletti, M., R., Mazzuoli, M., Bonini, T., Trua, and B., Abebe, (1999), Plio-Quaternary
566 volcanotectonic activity in the northern sector of the Main Ethiopian rift: Relationships with
567 oblique rifting, Journal of African Earth Sciences, V.29, 679-698.

568 Bonatti, E., (1990), Not so hot "hot spots" in the oceanic mantle, Science, 250, 107–111, doi:
569 10.1126/science.250.4977.107.

570 Borges, J.F., M., Bezzeghoud, E., Buforn, C., Pro, and A., Fitas, (2007), The 1980, 1997 and 1998
571 Azores earthquakes and some seismo-tectonic implications, Tectonophysics, 435, 37-54,
572 doi: 10.1016/j.tecto.2007.01.008.

573 Borgia, A., (1994), Dynamic basis of volcanic spreading, J. Geophys. Res., Solid Earth, 99 (B9),
574 17791-17804.

575 Byerlee, J.D., (1967), Frictional characteristics of granite under high confining pressure, J.
576 Geophys. Res., 72, 3639–3648.

577 Cannat, M., C., Rommevaux-Jestin, D., Sauter, C., Deplus, and V., Mendel, (1999), Formation of
578 the axial relief at the very slow spreading Southwest Indian Ridge (49° to 69°E), Journal of
579 Geophysical Research, 104, B10, 22,825-22,843.

580 Cannat, M., C., Rommevaux-Jestin, and H., Fujimoto, (2003), Melt supply variations to a magma-
581 poor ultra-slow spreading ridge (Southwest Indian Ridge 61° to 69°E, Geochem. Geophys.
582 Geosyst. 4, 9104, doi:10.1029/2002GC000480.

583 Catalão, J., (2006), Iberia-Azores Gravity Model (IAGRM) using multi-source gravity data, Earth
584 Planets and Space, 58, 277–286, 2006.

585 Catalão, J., and M.S., Bos, (2008), Sensitivity analysis of the gravity geoid estimation: A case
586 study on the Azores plateau, Physics of the Earth and Planetary Interiors 168, 113-124,
587 DOI: 10.1016/j.pepi.2008.05.010.
588 Carvalho, M.R., V.H., Forjaz, and C., Almeida, (2006), Chemical composition of deep hydrothermal
589 fluids in the Ribeira Grande geothermal field (São Miguel), J. Volcanol. Geotherm. Res., 156
590 (1-2), 116 – 134, doi: 10.1016/j.jvolgeores.2006.03.015.
591 Coalkey, B., and J., Cochran, (1998), Gravity evidence of very thin crust at the Gakkel Ridge (Artic
592 Ocean), Earth Planet. Sc. Lett., 162, 81-95.
593 Corti, G., (2009), Continental rift evolution: From rift initiation to incipient break-up in the Main
594 Ethiopian Rift, East Africa, Earth-Science Reviews, 96 (1-2), 1-53.
595 Costa, A.C.G., A., Hildenbrand, F.O., Marques, A.L.R., Sibrant, and A. Santos de Campos, (in
596 prep), Incremental growth and collapse of Pico Island during the last 200 kyrs (Pico-Faial
597 ridge, Azores Triple Junction).
598 DeMets, C., R.G., Gordon, and D.F., Argus, (2010), Geologically current plate motions, Geophys.
599 J. Int., 181, 1-80, doi: 10.1111/j.1365-246X.2009.04491.x.
600 Detrick, B., H.D., and V., Renard, (1995), Gravity anomalies and crustal thickness variations along
601 the Mid-Atlantic Ridge between 10°N and 40°N, J. Geophys. Res., 100, 3767-3778.
602 Dias N.A., L. Matias, N. Lourenço, J. Madeira, F. Carrilho and J.L. Gaspar, (2007), Crustal seismic
603 velocity structure near Faial and Pico Islands (Azores), from local earthquake tomography,
604 *Tectonophysics,* 445 (3-4): 301-317.
605 Dick, H.J.B., J., Lin, and H., Schouten, (2003), Ultra slow spreading – a new class of ocean ridge,
606 Nature, 426, 405-412.
607 Dieterich, J.H., (1988), Growth and persistence of Hawaiian volcanic rift zones J. Geophys. Res.,
608 93, 4258-4270.
609 Driscoll, N., and G., Karner, (1998), Lower crustal extension across the Northern Carnarvon basin,
610 Australia: Evidence for an eastward dipping detachment, Journal of Geophysical Research,
611 103, 4975-4991.
612 Duncan, R.A., and I., McDougall, (1976), Geologically current plate motions. Geophys. J. Int., 181,
613 1-80.
614 Duncan, A.M., G., Queiroz, J.E., Guest, P.D., Cole, N., Wallenstein, and J.M., Pacheco, (1999),
615 The Povoação Ignimbrite, Furnas Volcano, São Miguel, Azores, J. Volcanol. Geotherm. Res.,
616 92 (1-2), 55-65, doi: 10.1016/S0377-0273(99)00067-0.
617 Franchteau, J., and R.D., Ballard, (1983), The East Pacific Rise near 21°N, 13", and 20°S:
618 inferences from along-strike variability of axial processes of the mid-ocean ridges, Earth
619 Planet. Sci. Lett., 64, 93-116.
620 Francis, P.W., M., Hammill, G., Kretzschmar, and R.S., Thorpe, (1978), The Cerro Galan Caldera,
621 North west Argentina and its tectonic setting, Nature, 274, 749-751.

622 Gente, P., J., Dyment, M., Maia, and J., Goslin, (2003), Interaction between the Mid Atlantic ridge
623 and the Azores hotspot during the last 85 Myr: Emplacement and rifting of the hotspot
624 derived plateaus, Geochem. Geophys. Geosyst., 8, Q03013, doi:10.1029/2006GC001318.
625 Georgen, J.E., and R.D., Sankar, (2010), Effects of ridge geometry on mantle dynamics in an
626 oceanic triple junction region: Implications for the Azores Plateau, Earth Planet. Sci. Lett.,
627 298, 23-34.
628 Gillot, P.Y., J.C., Lefevre, and P.E., Nativel, (1994), Model for the structural evolution of the
629 volcanoes of Reunion island, Earth Planet. Sci. Lett., 122, 291-302, doi: 10.1016/0012-
630 821X(94)90003-5.
631 Grimison, N.L., and W.P., Chen, (1986), The Azores-Gilbraltar plate boundary: Focal mechanisms,
632 depths of earthquakes, and their tectonic implications, Journal of Geophysical Research,
633 91, B2, 2029-2047.
634 Haase, K.M., and C., Beier, (2003), Tectonic control of ocean island basalt source on São Migeul,
635 Azores? Geophys. Res. Lett., 30, doi:10.1029/2003GL017500.
636 Henk, A., (2006), Stress and strain during fault-controlled lithospheric extension-insights from
637 numerical experiments, Tectonophysics, 415, 39-55.
638 Hildenbrand, A., P.Y., Gillot, and I., LeRoy, (2004), Volcano-tectonic and geochemical evolution of
639 an oceanic intra-plate volcano: Tahiti-Nui (French Polynesia), Earth Planet. Sci. Lett., 217
640 (3), 349-365.
641 Hildenbrand, A., P.Y., Gillot, and C., Marlin, (2008a), Geomorphological study of long term erosion
642 on a tropical volcanic ocean island: Tahiti-Nui (French Polynesia), Geomorphology 93, 460-
643 481, doi: 10.1016/j.geomorph.2007.03.012.
644 Hildenbrand, A., P., Madureira, F.O., Marques, I., Cruz, B., Henry, and P., Silva, (2008b), Multi-
645 stage evolution of a sub-aerial volcanic ridge over the last 1.3 Myr: S. Jorge Island, Azores
646 Triple Junction, Earth and Planet. Sci. Lett., 273, 289-298.
647 Hildenbrand, A., F.O., Marques, A.C.G., Costa, A.L.R., Sibrant, P.F., Silva, B., Henry, J.M.,
648 Miranda, and P., Madureira, (2012), Reconstructing the architectural evolution of volcanic
649 islands from combined K/Ar, morphologic, tectonic, and magnetic data: The Faial Island
650 example (Azores), J. Volcanol. Geotherm. Res., 241-242, 39-48,
651 doi:10.1016/j.jvolgeores.2012.06.019.
652 Hildenbrand, A., F.O., Marques, A.C.G., Costa, A.L.R., Sibrant, P.M.F., Silva, B., Henry, J.M.,
653 Miranda and P., Madureira (2013), Reply to the comment by Quartau and Mitchell on
654 Reconstructing the architectural evolution of volcanic islands from combined K/Ar,
655 morphologic, tectonic and magnetic data: the Faial Island example (Azores), J. Volcan.
656 Geotherm. Res., 241-242, 39-48, by Hildenbrand et al., (2012). J. Volcanol. Geotherm.
657 Res., 255, 127-130.

658 Hildenbrand, A., D., Weis, P., Madureira, and F.O., Marques, (2014), Recent plate re-organization
659 at the Azores Triple Junction: evidence from new geochemical and geochronological data
660 on Faial, S. Jorge and Terceira volcanic islands. Manuscript accepted with minor revision.
661 Johnson, C.L., J.R., Wijbrans, C.G., Constable, J., Gee, H., Staudigel, L., Tauxe, V.H., Forjaz, and
662 M., Salgueiro, (1998), 40Ar/39Ar ages and paleomagnetism of São Miguel Lavas, Azores,
663 Earth Planet. Sci. Lett., 160 (3-4), 637 – 649, doi: 10.1016/S0012-821X(98)00117-4.
664 Kinvig, H. S., A., Geyer, and J., Gottsmann, (2009), On the effect of crustal layering on ring-fault
665 initiation and the formation of collapse calderas, J. Volcanol. Geotherm. Res., 186, 293-
666 304, doi: 10.1016/j.jvolgeores.2009.07.007.
667 Klugel, A., T.R., Walter, S., Schwarz, and J., Gelmacher (2005), Gravitational spreading causes
668 en-echelon diking along a rift zone of Madeira Archipelago: an experimental approach and
669 implications for magma transport, Bull. Volcan., 68 (1), 37-46.
670 Krause, D.C., and N.D., Watkins, (1970), North Atlantic crustal genesis in the vicinity of the Azores,
671 Geophys. J. R. Astron. Soc., 19, 261–283.
672 Laughton, A.S., R.B., Whitmarsh, J.S.M., Rusby, M.L., Somers, J., Revie, B.S., McCartney, and
673 J.E., Nafe, (1972), A continuous East-West Fault on the Azores-Gibraltar Ridge, Nature, 237,
674 217- 220.
675 Lourenço, N., J.F., Luís, J.M., Miranda, A., Ribeiro, and L.A.M., Victor, (1998), Morpho-tectonic
676 analysis of the Azores volcanic plateau from new bathymetric compilation of the area,
677 Marine Geophysical Researches, 20, 141–156, doi: 10.1023/A:1004505401547.
678 Luís, J.F., J., Miranda, P., Patriat, A., Galdeano, J.C., Rossignol, and L., Mendes-Victor, (1994),
679 Açores Triple junction Evolution in the last 10Ma from a New AeromagneticSurvey, Earth
680 and Planet. Sci. Lett., 125, 439-459.
681 Luís, J.F., J., Miranda, A., Galdeano, and P., Patriat, (1998), Constraints on the structure of the
682 Azores spreading center from gravity data. Mar, Geophys. Res., 20, 157–170, doi:
683 10.1023/A:1004698526004.
684 Luís, J.F., and J.M., Miranda, (2008), Reevaluation of magnetic chrons in the North Atlantic
685 between 35°N and 47°N: Implications for the formation of the Azores Triple Junction and
686 associated plateau, J. Geophys. Res., 113, B10105, doi:10.1029/2007JB005573.
687 MacDonald, K.C., (1982), Mid-ocean ridges: Fine scale tectonic, volcanic and hydrothermal
688 processes within the plate boundary zone, Annu. Rev. Earth Planet. Sci. Lett., 10, 155-190.
689 Machado, F., (1959), Submarine pits of the Azores plateau, Bull. Volcanol., 109–116 Série II,
690 Tome XXI.
691 Magde, L., D., Sparks, and R., Detrick, (1997), The relationship betwween buoyant mantle flow,
692 melt migration, and gravity bull's eyes at the Mid-Atlantic Ridge between 33°N and 35°N,
693 Earth Planet. Sci. Lett., 148, 59-67.
694 Malinverno, A., and R.A., Pockalny, (1990), Abyssal Hill topography as an indicator of episodicity in
695 crustal accretion and deformation, Earth Planet. Sci. Lett., 99, 154-169.

696 Marques, F.O., J.C., Catalão, C., DeMets, A.C.G., Costa, and A., Hildenbrand, (2013), GPS and
697 tectonic evidence for a diffuse plate boundary at the Azores Triple Junction, Earth Planet.
698 Sci. Lett., 381, 177-187.
699 Marques, F.O., Catalão, J.C., DeMets, C., Costa, A.C.G., Hildenbrand, A., 2014a. Corrigendum to
700 "GPS and tectonic evidence for a diffuse plate boundary at the Azores Triple Junction"
701 [Earth Planet. Sci. Lett. 381 (2013) 177–187]. Earth and Planetary Science Letters 387, 1–
702 3.
703 Marques, F.O., Catalão, J., Hildenbrand, A., Costa, A.C.G., Dias, N.A., 2014b. The 1998 Faial
704 earthquake, Azores: Evidence for a transform fault associated with the Nubia-Eurasia plate
705 boundary? Tectonophysics, in press.
706 McKee, E.H., and R.B., Moore, (1992), Potassium–argon dates for trachytic rocks on São Miguel,
707 Azores, Isochron West, 58, 9–11.
708 Métrich, N., V., Zanon, L., Créon, A., Hildenbrand, M., Moreira, and F.O., Marques, (2014), Is the
709 "Azores hotspot" a wetspot? Insights from the geochemistry of fluid and melt inclusions in
710 olivine of Pico basalts, Journal of Petrology, 55, 377-393.
711 Michael, P.J., D.W., Langmuir, H.J.B., Dick, J.E., Snow, S.L., Goldstein, D.W., Graham, K.,
712 Lehnert, G., Kurras, W., Jokat, R., Muehe, and H.N., Edmonds, (2003), Magmatic and
713 amagmatic seafloor generation at the ultraslow-spreading Gakkel ridge, Arct, Ocean Nat.
714 423, 956-961.
715 Montési, L.G., and M.D., Behn, (2007), Mantle flow and melting underneath oblique and ultraslow
716 mid-ocean ridges, Geophys. Res. Lett., 34, L24307, doi:10.1029/2007GL031067.
717 Moore, R., (1990), Volcanic geology and eruption frequency, S. Miguel, Azores, Bull. Volcanol., 52,
718 602–614, doi: 10.1007/BF00301211.
719 Moore, R., (1991), Geologic map of São Miguel, Azores (Scale 1: 50.000). U.S.G.S. MISC INV.
720 map I-2007.
721 Moore, R., and M., Rubin, (1991), Radiocarbon dates for lava flows and pyroclastic deposits on
722 São Miguel, Azores, Radiocarbon, 33 (1), 151-164.
723 Morgan, W.J., (1971), Convection plumes in the lower mantle, Nature 230, 43-44.
724 Mutter, J.C., and J.A., Karson, (1992), Structural processes at slow-spreading ridges, Science, 257
725 (5070), 627-634.
726 Nakamura, K., K.H., Jacob, and J.N., Davies, (1977), Volcanoes as possible indicators of tectonic
727 stress orientation – Aleoutians and Alaska, Pure Appl. Geophys., 115, 87-112.
728 Ortner H., F., Reiter, and P., Acs, (2002), Easy handling of tectonic data the programs TectonicVB
729 for Mac and TectonicsFP for Windows, Computers and Geosciences, 28, 1193-1200, doi:
730 10.1016/S0098-3004(02)00038-9.
731 Ozawa, A., T., Tagami, and M.O., Garcia, (2005), Unspiked K-Ar dating of the honolulu
732 rejuvenated and Ko'olau shield volcanism on O'ahu, Hawaii. Earth Planet. Sci. Lett., 232, 1-
733 11.

734 Queiroz, G., J.M., Pacheco, J.L., Gaspar, W.P., Aspinall, J.E., Guest, and T., Ferreira, (2008), The
735 last 5000 years of activity at sete Cidades volcano (São Miguel island, Azores) implication for
736 hazard assessment, J. Volcanol. Geotherm. Res., 178 (3), 562–573, doi:
737 10.1016/j.jvolgeores.2008.03.001.
738 Perfit, M. R., and W.C., Chadwick, (1998), Magmatism at mid oceanic ridges: constraints from
739 volcanological and geochimical invesgitations in : faulting and magmatism at mid ocean
740 ridges, Buck, W. R., et al (eds), Am. Geophys. U. Geophys. Monograph., 106, 59-116.
741 Pinel, V., and C., Jaupart, (2004), Magma storage and horizontal dike injection beneath a volcanic
742 edifice, Earth Planet. Sci. Lett., 221, 245-262.
743 Sandwell, D.T., and W.H.F., Smith, (2009), Global marine gravity from retracked Geosat and ERS-
744 A altimetry: Ridge segmentation versus spreading rate, J. Geophys. Res., 114, B01411,
745 doi:10.1029/2008JB006008.
746 Schilling, J.G., (1975), Azores mantle blob: rare earth evidence. Earth Planet. Sci. Lett., 25, 103-
747 115.
748 Schilling, J.G., (1985), Upper mantle heterogeneities and dynamics, Nature 314, 62-67.
749 Searle, R.C., (1976), Lithospheric structure of the Azores Plateau from Rayleigh-wave dispersion,
750 Geophys. J. Roy. Astron. Soc., 44, 537-546. 186.
751 Searle, R., (1980), Tectonic pattern of the Azores spreading centre and triple junction, Earth
752 Planet. Sci. Lett., 51 (2), 415 - 434.
753 Sibrant, A.L.R., A., Hildenbrand, F.O., Marques, T., Boulesteix and A.C.G., Costa, (2013a).
754 Morpho-structural evolution of a volcanic island developed inside an active oceanic rift: S.
755 Miguel Island (Terceira Rift, Azores), Abstract Meeting, IAG, 2013, Paris, France.
756 Sibrant, A.L.R., A., Hildenbrand, F.O., Marques, and A.C.G., Costa, (2013b), Volcano-tectonic
757 evolution of Santa Maria Island: implications for the Nubia-Eurasia plate boundary in the
758 Azores, AGU Fall Meeting, Suppl. Abstract, T51F-2531.
759 Sibrant, A.L.R., F.O., Marques and A., Hildenbrand, (2014), Construction and destruction of a
760 volcanic island developed inside an oceanic rift: Graciosa Island, Terceira Rift, Azores, J.
761 Volc. Geotherm. Res., 284, 32-45.
762 Silveira, G., and E., Stutzmann, (2002), Anisotropic tomography of the Atlantic Ocean, Phys, Earth
763 Planet. Inter., 132, 237-248, doi: 10.1016/S0031-9201(02)00076-6.
764 Silveira, G., L., Vinnik, E., Stutzmann, V., Farra, S., Kiselev and I., Morais, (2010), Stratification of
765 the Earth beneath the Azores from P and S receiver functions, Earth Planet. Sci. Lett., 299,
766 91-103.
767 Snow, J.E., and H.N., Edmonds, (2007), Ultraslow-spreading ridges rapid paradigm changes,
768 Oceanography, 20, special issue 1, 90-101
769 Soares, D.M., T.M., Alves, and P., Terrinha, (2012), The breakup sequence and associated
770 lithospheric breakup surface: Their significance in the context of rifted continental margins
771 (West Iberia and Newfoundland margins, North Atlantic), Earth Planet. Sci. Lett., 355-356,

311-326.
Spang, J.H., (1972), Numerical method for dynamic analysis of calcite twin lamellae, Geological Society of America Bulletin, 83 (2), 467–472.
Sperner, B., L., Ratschbacher, and R., Ott, (1993), Fault-striae analysis: a Turbo Pascal program package for graphical presentation and reduced stress tensor calculation, Computers & Geosciences, 19 (9), 1361–1388.
Sperner, B., and P., Zweigel, (2010), A plea for more caution in fault–slip analysis, Tectonophysics, 482 (1–4), 29–41.
Thibauld, R., P., Gente, and M., Maia, (1998), A systematic analysis of the Mid-Atlantic Ridge morphology and gravity between 15°N and 40°N: constraints on the thermal structure, J. Geophys. Res., 103, 24223-24243.
Tucholke, B., J., Lin, M., Kleinrock, M., Tivey, T., Reed, J., Goff, and G., Jaroslow, (1997), Segmentation and crustal structure of the western Mid-Atlantic Ridge flank, 25°25'-27°10'N and 0-29 m.y, Journal of Geophysical Research, 102, 10,203-10,223.
Turner, F.J., (1953), Nature and dynamic interpretation of deformation lamellae in calcite of three marbles, American Journal of Science, 251 (4), 276–298.
Van Wijk, J.W., and D.K., Blackman, (2005), Deformation of oceanic lithosphere near slow-spreading ridge discontinuities, Tectonophysics, 407, 211-225.
Vogt, P.R., (1976), Plumes, sub-axial pipe flow, and topography along the Mid-oceanic ridge, Earth Planet. Sci. Lett., 29, 309-325.
Vogt, P.R., and W.Y., Jung, (2004), The Terceira Rift as hyper slow, hotspot dominated oblique spreading axis: A comparison with other slow spreading plate boundaries, Earth Planet. Sci. Lett., 218, 77-90.
Walker, G.P.L., (1984), Downsag calderas, ring faults, caldera sizes, and incremental caldera growth, J. Geophys. Res., 89(B10), 8407–8416, doi: 10.1029/JB089iB10p08407.
Wallace, R.E., (1951), Geometry of shearing stress and relation to faulting, Journal of Geology, 59, 118–130.
Walter, T. R., and V.R., Troll, (2001), Formation of caldera periphery faults: an experimental study, Bulletin of Volcanology, 63, 191-203.
Whittaker, J.M., R.D., Muller, W.R., Roest, P., Wessel, and W.H.F., Smith, (2008), How supercontinents and superoceans affect seafloor roughness, Nature, 456, 938-941, doi:10.1038/nature07573.
Yang, T., Y., Shen, S., Van Der Lee, and C., Solomon, (2006), Upper mantle structure beneath the Azores hotspot from finite frequency seismic topography. Earth Planet. Sci. Lett., 250 (1-2), 11-26.
Zbyszewski G, O.V., Ferreira, and C., Torre de assuncao, (1959), Carta Geológica de Portugal na escala de 1:50 000. Notícia explicativa da Folha A, S.Miguel (Açores), Publ. Serv. Geol. de Portugal, 22p. Lisboa.

FIGURE CAPTIONS

Figure IV. 15. (A) Bathymetric map of the Azores. The black lines indicate the location of the Mid Atlantic Rift (MAR) and associated transforms. The white dashed line indicates the East Azores Fracture Zone (EAFZ). The thin black line indicates the location of the southern shoulder of the Terceira Rift (TR), and the yellow dashed lines indicate the current Eurasia (Eu) – Nubia (Nu) plate boundary proposed by Marques et al. [2013, 2014]. Inset shows the location of the Azores archipelago in the Atlantic Ocean. Bathymetry from Lourenço et al. [1998]. (B) Free–air gravity field map of the Azores Archipelago [Catalão, 2006; Catalão and Bos, 2008]. The black thin lines represent the boundary of each island (sea level). The white lines indicate the location of the Mid Atlantic Rift (MAR) and associated transforms. The thicker black dashed lines is the Eurasia/Nubia plate boundary from Marques et al. [2013, 2014]. The white dashed lines indicates the East Azores Fracture Zone (EAFZ). GF: Gloria Fault; Cor: Corvo; Flo: Flores; Fai: Faial; Pic: Pico; SJo: São Jorge; Gra: Graciosa; Ter: Terceira; SMi: São Miguel; SMa Santa Maria. Gravity image supplied by J. Catalão.

Figure IV. 16. Shaded relief map of S. Miguel generated from a high-resolution DEM (10 m) showing the main volcanic edifices and tectonic structures as defined by Moore [1990]. (1) Sete Cidades volcano; (2) Fissural system; (3) Fogo volcano; (4) Fissural system; (5) Furnas volcano; (6) Nordeste complex. The solid and dashed black lines localize and summarize our measurements of faults and dikes, respectively. The red circle indicates the location of the City of Sete Cidades (SC), Ponta Delgada (PD), Furnas (F), Povoção (PV), Água Retorta (AR) and Nordeste (N). The blue squares mark the location of Figs. IV.18 to IV.21 and IV.A6. A clean version of the DEM is given in the Supplementary materiel as Fig. IV.A4.

Figure IV. 17. Slope map of S. Miguel generated from the high-resolution Digital Elevation Model (DEM) with dip of lava flows measured during our fieldwork.

Figure IV. 18. (A) Map of the newly measured faults and dikes for the eastern part of S. Miguel displayed over a high resolution shaded relief map. The dashed squares indicate the 4 zones distinguished from our new morphological analysis, fieldwork observation and tectonic markers. Faults and dikes locations are simplified for better visualization. The red lines indicate the main structures recognized in this study. (B) Computation of great circles and polse to planes (Wülff net, equal angle lower hemisphere projection) of the faults, dikes and stress tensor for zones 1, 2, 3 and 4. N is the numbers of measurements. Red circle: s_1; square: s_2; triangle: s_3.

Figure 5. Set of normal faults dipping to the N along the N-S eastern end of the island. Location of the outcrop is shown in Fig. IV.16.

Figure IV. 20. Example of the numerous fault surfaces materialising the southern wall of the graben newly recognized in Água Retorta. N115 trend and dip from 60 to 65º NE, and pitch of striations (black dashed lines) 85° toward the NE. See Fig. IV.16 for location.

Figure IV. 21. W-E sea cliff to the west of the village of Povoação (see Fig. IV.16 for location). The black lines indicate the dip of the Lava flows (LF). The dashed white and red lines indicate faults and the western wall of the graben identified in Povoação. CG: conglomerates; PY: Mixed pyroclasts and cinders; IG: Ignimbrite flow with fiamme.

Figure IV. 22. Location of the main recognized structures on S. Miguel. The dashed squares show the location of the 4 zones here distinguished. The black arrows indicate the stress tensors of the 4 zones, deduced from the orientations of the principal stress axes shown in Fig. IV.18. Line a b marks the location of the NE-SW topographic profile of the half graben of Água Retorta shown on the inset. The dashed lines represent the inferred main associated faults.

Figure IV. 23. (A) Zoom on the 3D bathymetry near S. Miguel [bathymetry from Lourenço et al., 1998]. The white and black dashed lines indicate the location of the main axial valley and the borders of the rift, respectively. The numbers 1 and 2 refer to the cross sections shown in the l(B) and (C) panel. (B) is a NE-SW cross section through the basin west of S. Miguel; (C) is a N-S cross section of the basin east of S. Miguel. The dashed lines indicate possible normal fault of the Rift (see text for details).

Figure IV. 24. (A) Schematic scenario for the pre-rifting stage of the TR, and for the opening of the Terceira Rift without spreading (B) and with spreading (C), respectively.

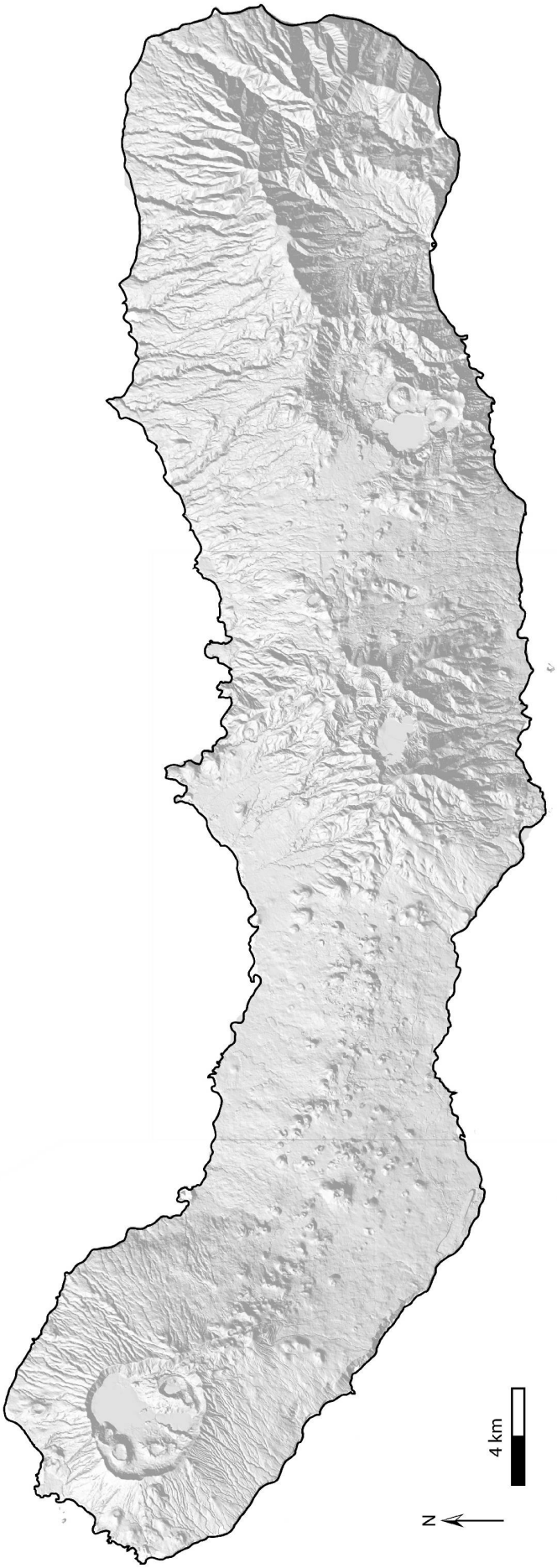
Supplementary Material. Figure A4. Clean version of the shaded relief map of S. Miguel generated from a high-resolution DEM (10 m).

Supplementary Material. Figure A5. Clean W-E sea cliff to the west of the village of Povoação.

Supplementary material Fig. IV. A6. W-E sea cliff to the east of the village of Povoação. See Fig. IV.16 for location. The faults have been measured with a ca. N150 strike and a dip of 80° to the SW.

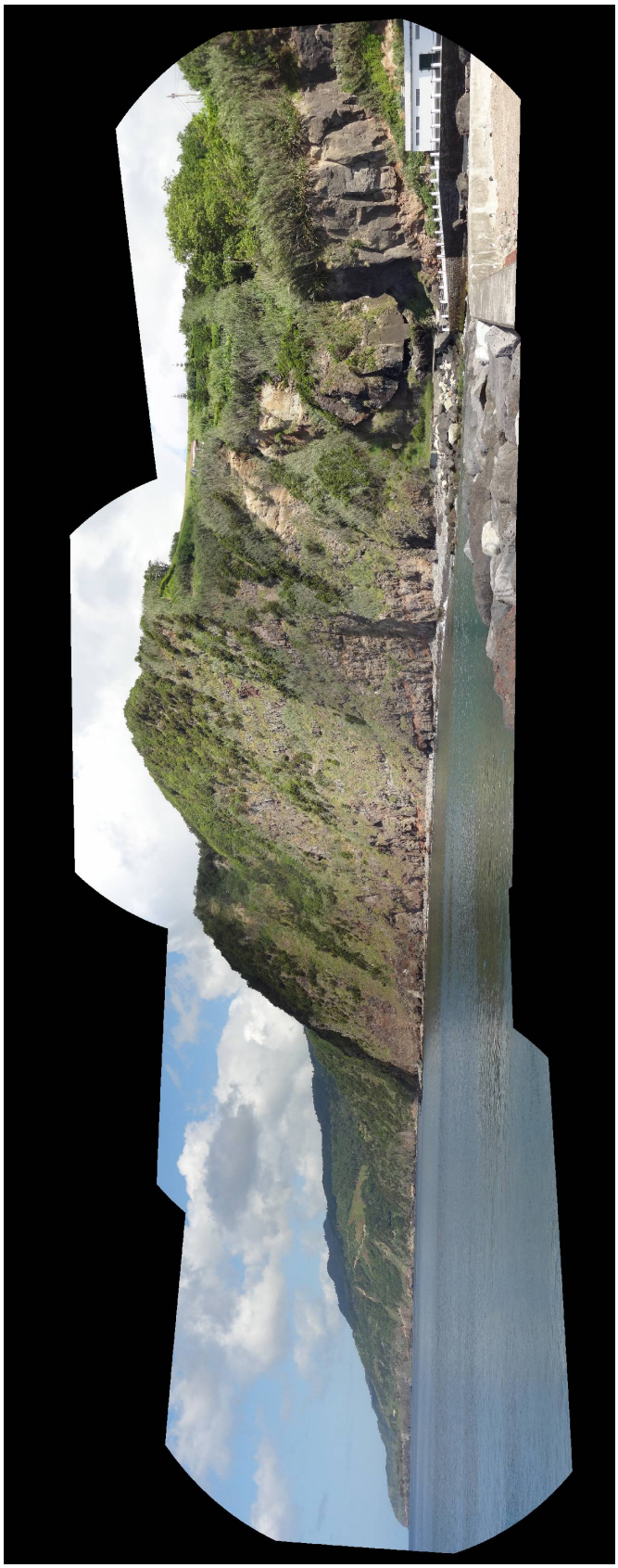
Table IV. 2. Results of the P-T method, NDA and inverse method.

Table IV. S1. Fault and dykes new measurements realized in the present study. Fault kinematics ranges from purely normal (pitch 90°) to normal with strike-slip component.



887 **Supplementary Material. Figure A4**. Clean version of the shaded relief map of S. Miguel

generated from a high-resolution DEM (10 m).



Supplementary material Fig. IV. A6. W-E sea cliff to the east of the village of Povoação. See Fig. IV.16 for location. The faults have been measured with a ca. N150 strike and a dip of 80° to the SW.

893 **FAULTS**

UTM 26E	UTM N	Strike (N)	dip (°)	Pitch (°)
635197	4187218	5	90	-
635232	4187221	10	65 E	-
635267	4187224	10	90	-
645704	4176615	10	60 W	-
645704	4176615	10	85 W	-
632128	4175166	15	75 W	80 S
645704	4176615	15	75 W	-
662239	4181366	20	80 E	55 N
661404	4187327	20	70 NW	70 NE
652999	4179052	20	70 W	-
645704	4176615	25	75 E	-
652124	4178916	25	75 W	-
634988	4187184	30	60 E	-
645704	4176615	40	80 NW	70 S
645734	4179105	50	35 W	-
611446	4180273	50	80 SE	-
649287	4178478	55	60 NW	75 NE
649287	4178478	70	90	-
663204	4181041	70	65 N	65 SE
663124	4180910	80	60 NE	40 SE
611446	4180273	85	90	-
663543	4183750	100	80 N	-
663543	4183751	100	80 N	-
663108	4180953	100	68 NE	90
663123	4180948	100	65 N	70 E
663543	4183744	105	70 N	65 E
601041	4190599	110	65 SW	-
663543	4183749	110	85 N	-
663578	4183752	110	75 W	-
662521	4180140	110	60 NE	-
653545	4179078	110	70 N	75 NE
653545	4179078	110	65 N	-
663104	4180888	110	60 NE	-
661673	4180306	115	65 NE	80 SE
652271	4178934	115	75 NE	-
663467	4184380	120	70 S	-
663305	4183529	120	60 N	-
653729	4179164	120	90	80 SE & 20 SE
661032	4180523	120	65 N	75 SE
661798	4180191	120	67 NE	77 SE
637565	4182768	120	65NE	-
663235	4181035	120	65 N	-
663112	4180950	120	85 SW	78 SE
661312	4180392	122	60 NE	75 SE
661175	4180457	125	65 NE	80 SE
663700	4182365	125	55 NE	65 S

661832	4181168	130	85 NE	-
662340	4179895	130	55 NE	-
662407	4180016	130	75 NE	-
653175	4179064	130	67 NE	-
663039	4180808	130	80 NE	-
654810	4179105	140	75 E	-
654810	4179105	140	80 E	-
635211	4187247	140	70 W	-
653300	4179067	140	65 SW	-
652124	4178916	140	90	-
663124	4180920	140	50 SW	35 SE
633263	4175351	145	70 NE	-
663362	4184539	145	50 E	75 WSW
662319	4179865	145	60 NE	70 SE
653607	4179109	145	65 SW	70 SE
652999	4179052	145	85 NE	-
659942	4181024	150	65 E	-
655105	4179028	150	40 SSE	-
635253	4187280	150	55 NE	-
653737	4179154	150	70 W	90 NW
653695	4179158	150	65 W	-
654289	4179105	150	80 NE	80 SE
653693	4179144	150	80 SW	80 SE & 20 SE
653693	4179144	150	70 W	25 SW
654076	4179212	150	80 NE	75 SE
662475	4180108	150	90	-
653287	4179068	150	70 NE	90
653287	4179068	150	65 NE	-
637553	4182956	150	-	-
637565	4182768	150	60 NE	-
663148	4180976	150	70 SW	-
663042	4180803	150	75 NE	-
653614	4179088	155	80 ENE	75 SE
663122	4180954	155	70 SW	-
632128	4175166	160	62 E	55 S
632128	4175166	160	70 W	-
632128	4175166	160	55 W	-
634970	4187179	160	75 W	-
635014	4187190	160	45 E	-
635038	4187194	160	90	-
635211	4187247	160	70 E	-
635317	4187230	160	85 NW	-
653153	4179064	160	55 SW	-
652124	4178916	160	60 W	-
655590	4178853	160	70 SW	-
610928	4180658	164	78 W	-
635009	4187189	165	85 E	-
653359	4179066	165	65 SW	-

632128	4175166	170	70 E	50 S
632128	4175166	170	90	-
632158	4179105	170	60 E	-
654015	4179208	170	85 E	-
645704	4176615	170	72 E	70 N
662475	4180108	170	80 SW	-
660210	4178836	170	55 E	-
652811	4179044	170	55 SW	-
652811	4179044	175	90	-
645704	4176615	180	60 W	-

894
895

896 **DIKES**

UTM 26E	UTM N	Strike (N)	Dip (°)	Thickness (m)
632128	4175166	0	90	1
659005	4179240	5	90	0.5
659005	4179240	5	75 E	0.3
660305	4178827	5	90	0.5
660252	4178831	5	90	0.7
660133	4178826	5	90	1
632128	4175166	10	80 E	1
659499	4178785	10	90	1
659052	4178994	10	80 E	0.5
659076	4179033	10	90	1
659229	4179256	10	80 E	0.5
659009	4179247	10	80 E	1
659009	4179247	10	90	1
659009	4179247	10	60 E	1
660078	4178808	10	90	1
632128	4175166	15	75 E	1
611037	4194710	15	90	0.5
606973	4193046	20	90	4
659059	4183784	20	60 W	0.5
659052	4178993	20	65 E	1
659059	4178998	20	80 E	1
659005	4179240	20	90	0.5
659335	4179743	20	90	3
654810	4179105	20	50 E	1
654810	4179105	20	55 E	3
655084	4179023	20	55 E	1
632128	4175166	25	90	1
632163	4175169	40	75 W	1
659047	4178992	40	80 E	1
645238	4176520	40	90	15
645037	4176358	40	70 SE	1.5
660071	4178791	40	90	1
632128	4175166	45	85 E	1
649653	4178487	50	85 NW	3
661183	4185941	50	65 SE	0.5
660032	4184481	50	65 NW	1
663239	4184494	50	90	1.5
613692	4192191	55	90	2
663442	4184587	60	90	2
663487	4183672	60	90	2
660414	4183737	60	70 NNW	1
632128	4175166	70	90	1
659046	4183746	70	90	0.5
663255	4183701	75	70 N	1
663494	4183704	80	75 N	2
663235	4183632	80	70 S	3

663546	4183763	90	85N	1
663278	4183661	90	65 N	1
663235	4183632	90	75 N	1.5
659047	4183742	90	75 N	1.5
663239	4184494	90	85 N	2
663695	4182213	90	80 N	1
663695	4182213	90	90	0.7
663547	4183868	95	85 N	2
663552	4183752	100	90	1
663549	4183796	100	75 N	3.5
663495	4184326	100	90	0.5
663495	4184331	100	90	1
663492	4183725	100	90 N	2
663366	4183662	100	88 E	4
663256	4183708	100	70 N	1
659040	4183734	100	65 N	3
659053	4183755	100	60 N	2
659059	4183784	100	80 N	0.15
658467	4180050	100	90	1
661055	4180489	100	90	2
661029	4180497	100	90	
645085	4176398	100	57 NNE	3
663695	4182213	100	90	2
663695	4182213	100	90	1
662218	4179658	100	85 ENE	0.7
662705	4180391	100	65 NNW	1
663530	4184007	105	80 N	2
663495	4184306	105	90	0.75
663366	4183662	105	90	4
663765	4182553	105	90	4
663765	4182553	105	65 ENE	1
663149	4180993	105	60 N	2
663113	4180954	105	70 NE	2
663546	4183867	110	85 N	3.5
663495	4184316	110	75 N	0.5
663443	4184440	110	60 N	1
663496	4183831	110	75 N	1
663461	4183768	110	80 N	1.5
663275	4183544	110	80 S	1
663275	4183544	110	80 S	1
663130	4183720	110	80 N	3
661032	4180523	110	70 N	2
661921	4179688	110	90	5
661878	4179466	110	80 NE	2
645443	4176578	110	70 S	12
645121	4176437	110	90	10
644933	4176271	110	90	>2
663766	4182717	110	75 SSW	2

663740	4182630	110	90	3
663721	4182453	110	90	1.5
663721	4182412	110	85 N	2
663720	4182295	110	70 N	1
663720	4182295	110	80 N	1
663695	4182213	110	80 N	1
660273	4183898	110	80 NNE	1.5
663191	4181042	110	80N	0.5
663164	4181013	110	90	0.7
663123	4180907	110	90	1.5
663103	4180866	110	70NNW	1.5
663081	4180855	110	90	0.15
663077	4180852	110	75N	2.5
663042	4180783	110	80E	1
663015	4180781	110	90	0.7
663019	4180756	110	70ENE	0.5
601026	4191124	115	90	1
661033	4180515	115	90	2
661096	4180445	115	75 N	1.5
661812	4179663	115	90	2
661878	4179466	115	80 NE	1.5
661878	4179466	115	76 ENE	1
661878	4179466	115	60 ENE	2
662336	4179903	115	80 NE	0.7
660774	4184396	115	90	1
661812	4179663	117	90	3
663584	4183693	120	75 N	1.5
663569	4183713	120	80 N	2
663524	4184084	120	75 N	1
663546	4183826	120	70 N	1
658354	4179766	120	90	1
661096	4180445	120	75 N	1
661752	4179385	120	90	1
661752	4179385	120	87 ENE	1
662377	4179974	120	70 NE	0.5
662375	4179980	120	70 NE	1
662526	4180197	120	70 SW	2
652231	4178936	120	90	0.5
663252	4181043	120	70 NE	1
663166	4181009	120	90	2
663125	4180923	120	80NE	1
663082	4180847	120	85NE	0.5
663031	4180779	120	80N	2
662732	4180392	120	90	1
661812	4179663	123	85 NE	6
661812	4179663	123	90	1
661096	4180445	125	80 N	2
661106	4180399	125	90	2

661927	4179692	125	80 NE	4
661854	4179687	125	90	1
661830	4179394	125	90	1
662919	4182193	125	90	1
662919	4182193	125	75 ENE	0.5
662153	4179583	125	75 ENE	3
662320	4179878	125	82 NE	1.5
662320	4179878	125	90	3
662397	4179996	125	90	1.5
662457	4180075	125	90	3
662458	4180083	125	75 NE	0.7
662524	4180129	125	80 NE	1.5
645270	4176541	126	80 S	15
654034	4179215	130	90	1.5
654034	4179215	130	90	1.5
661830	4179394	130	90	3
661400	4179031	130	90	10
662382	4179954	130	90	3
662389	4179990	130	80 NE	1
662514	4180122	130	80 NE	1
660639	4178813	130	90	1
653029	4179056	130	80 SW	1
663020	4180775	130	70ENE	2
662318	4179842	135	70 ENE	1
662348	4179943	135	85 NE	2
663132	4180913	135	55NE	1.5
663078	4180899	135	75NE	2
655603	4178845	138	90	1.5
655633	4179105	140	90	1
655663	4179105	140	90	1.5
662364	4179948	140	75 NE	2
662457	4180075	140	90	2
662615	4180248	140	80 NE	1
660620	4178808	140	90	0.7
660543	4178812	140	90	1.5
653582	4179083	140	90	2
653582	4179084	140	90	2
655634	4178828	140	90	0.5
663165	4181010	140	90	0.7
663105	4180904	140	65E	2
663078	4180899	140	70 NE	3
663010	4180694	140	90	2
653871	4179187	145	90	1
655492	4184703	145	90	2
655492	4184703	145	90	1
655492	4184703	145	65 ENE	1
655492	4184703	145	65 ENE	1
655492	4184703	145	90	1

655492	4184703	145	75 NE	4
662427	4180067	145	90	1.5
660534	4178816	145	90	2.5
660454	4178822	145	75 SW	0.7
660489	4178825	150	90	0.5
658997	4179232	150	70 E	2.5
655019	4179079	150	90	1
655051	4179041	150	90	2
655162	4179014	150	90	2
658375	4179672	150	77 SW	1.5
661087	4180413	150	80 N	5
662110	4179499	150	85 ENE	2
662110	4179499	150	62 ENE	3
662110	4179499	150	70 ENE	1
662110	4179499	150	64 ENE	1
662411	4180048	150	90	1.5
660492	4178810	150	80 NE	2
660279	4178832	150	90	1
652768	4179044	150	90	5
652803	4179047	155	75 W	0.5
652838	4179050	155	85 ENE	1.5
660620	4178810	155	80 E	4
660604	4178808	155	90	1
660482	4178815	155	80 NE	0.7
660428	4178817	155	70 SW	1
660345	4178822	155	90	0.5
660210	4178836	155	90	0.7
663087	4180894	155	75 E	3
660577	4178804	157	90	1.5
659059	4183784	160	65 NE	1
659094	4183787	160	90	3
659129	4183790	160	90	0.5
659164	4183793	160	35 E	0.5
659199	4183796	160	60 E	1
659129	4179249	160	90	0.3
659107	4179254	160	90	1
659918	4179685	160	60 E	0.5
653814	4179182	160	80 W	1.5
661087	4180413	160	90	10
661087	4180413	160	79 ENE	1
661087	4180413	160	90	0.7
661087	4180413	160	90	0.7
661087	4180413	160	90	1
660625	4178809	160	80 E	3
660551	4178810	160	90	1.5
660245	4178836	160	90	0.7
660061	4178800	160	90	10
659056	4179264	165	90	0.5

660153	4178830	165	90	1
653478	4179072	166	90	1
659391	4178751	170	90	1
659494	4178782	170	90	2
659520	4178800	170	90	4
659555	4178803	170	75 W	1
659590	4178806	170	90	0.5
659625	4178809	170	90	0.3
659062	4179001	170	80 E	1
659128	4179249	170	90	1
659098	4179246	170	75 E	2
659045	4179268	170	75 E	0.5
659002	4179229	170	60 E	5
659002	4179229	170	60 E	5
659002	4179229	170	60 E	5
659002	4179229	170	60 E	5
659032	4179105	170	75 W	1
658892	4181035	170	85 W	2
660384	4178820	170	90	0.7
660301	4178832	170	90	0.5
660210	4178836	170	82 W	0.5
660187	4178831	170	90	1
660160	41788834	170	45 E	0.7
660128	4178826	170	90	2
660120	4178830	170	90	2
656489	4178524	170	90	3
656530	4178504	170	90	1.5
654962	4179105	175	90	1
660556	4178805	176	90	2
659984	4178839	180	90	0.5
659107	4179254	180	90	0.5
659078	4179253	180	50 W	3
611001	4180565	180	90	2
659276	4183833	180	90	1
660330	4178825	180	70 E	0.7
660153	4178830	180	90	2
660109	4178824	180	90	3
660083	4178815	180	90	1

Table IV. S1. Fault and dykes new measurements realized in the present study. Fault kinematics ranges from purely normal (pitch 90°) to normal with strike-slip component.

CHAPTER V
Volcano-tectonic evolution of the Santa Maria Island (Azores): implications for palaeostress evolution at the western Eurasia-Nubia plate boundary

V. Volcano-tectonic evolution of the Santa Maria Island (Azores): implications for palaeostress evolution at the western Eurasia-Nubia plate boundary (Submitted to JVGR)

A.L.R. Sibrant[1,2*], A. Hildenbrand[1,2], F.O. Marques[3], A.C.G. Costa[1,4]

(1) Université Paris-Sud, Laboratoire GEOPS, UMR8148, Orsay, F-91405
(2) CNRS, Orsay, F-91405
(3) Universidade de Lisboa, Lisboa, Portugal
(4) Universidade de Lisboa and IDL, Lisboa, Portugal

*Corresponding author. Tel.: +33 1 69 15 67 61
E-mail address: aurore.sibrant@u-psud.fr

Abstract

It is now acceptal that the westernmost part of the Eurasia-Nubia plate boundary migrated northward, from the East Azores Fracture Zone (EAFZ) to an active oceanic rift, the Terceira Rift (TR). Santa Maria Island in the Azores sits close to the junction between the EAFZ and the TR. In contrast to the other Azores islands, which have all been active during the last 1.5 Myr, Santa Maria is an old extinct volcanic island, with an activity previously dated between ca. 9 Ma and 4.5 Ma. Therefore, Santa Maria records a story that no other island in the Azores can tell. From morphologic, stratigraphic, tectonic and new high-precision K-Ar data, we reconstruct the volcano-tectonic history of the island, and discuss its significance regarding the stress evolution and regional deformation. Our new data show that: (1) the western flat portion of the island is composed of the remnants of an Old Shield Volcano here dated between 5.70 ± 0.08 and 5.33 ± 0.08 Ma; (2) more than half of this early volcanic complex has been cut by an east-directed large flank collapse; (3) a second volcano (here coined Young Shield Volcano) grew rapidly into the collapse scar between at least 4.32 ± 0.06 and 3.94 ± 0.06 Ma; (4) the eastern flank of the new volcano has been deeply modified by a second large-scale sector collapse at around 3.6 Ma, which is the age of the here dated parasitic strombolian cones sitting unconformably on the Young Shield Volcano; (5) the latest parasitic volcanic activity is here dated at 2.84 ± 0.04 Ma, extending significantly the known eruptive history of Santa Maria. Morpho-structural data (shape of the island, faults, dikes, volcanic cones and canyon distribution) show a significant control of construction and destruction episodes along the N045º and N150º directions. The age of the lavas intruded by dikes suggests that the N45º and the N150º trends are ca. 5.3 Ma old and younger than ca. 4.3 Ma, respectively. Based on the new data, we conclude that a sudden change of the regional stress field occurred between 5.3 and 4.3 Ma, most likely associated with a sudden reconfiguration of the Eurasia/Nubia plate boundary.

Keywords: Santa Maria Island; volcanic evolution; K-Ar geochronology; dikes; flank collapse; Azores Triple Junction.

V. 1. Introduction

Santa Maria is the oldest volcanic island in the Azores. It is situated at the intersection between the Gloria Fault (GF), the East Azores Fractures Zone (EAFZ) and the Terceira Rift (TR). Santa Maria sits on the eastern edge of a region of abnormally elevated seafloor generally referred to as the "Azores plateau", which roughly coincides with the -2000 m isobath. The genesis of the plateau and the islands have been generally attributed to a hotspot on the basis of geomorphological (Searle, 1980; Cannat et al., 1999; Gente et al., 2003), geophysical (Vogt and Jung, 2004; Yang et al., 2006) and geochemical arguments (White et al., 1976; Moreira and Allègre, 2002). However, according to other authors, the volcanism is not due to an active hot-spot, but rather reflects the existence of volatile-enriched upper mantle domains (Schilling et al., 1975; Bonatti et al., 1990) or a wet-spot (Métrich et al., 2014). To the east of the Mid Atlantic Ridge (MAR) axis, the plateau shows a triangular shape and encompasses portions of the North American (NA), the Eurasian (EU), and the Nubian (NU) plates (Fig. V.1). The NA/EU and NA/NU plate boundaries coincide with the conspicuous MAR axis, whose morphology has been relatively stable over the last few Myrs (Laughton et al., 1972). In contrast, the morphology and the history of the EU/NU boundary in the Azores are more complex and still greatly debated. Immediately to the east of the Azores region, the EU/NU boundary presently comprises a dextral transcurrent fault called the Gloria Fault (GF). Some time in the past, the GF was connected to the MAR by an active fault called the East Azores Fracture Zone (EAFZ) (Laughton et al., 1972). However, the western portion of the EAFZ seems presently seismically inactive and thus not anymore part of the EU/NU boundary (e.g. Krause and Watkins, 1970; Searle, 1980). It is quite acceptal that this part of the EU-NU plate boundary has migrated to the North and is now following the hyper-slow oceanic Terceira Rift (TR) (e.g., Machado, 1959; Krause and Watkins, 1970; McKenzie, 1972; Searle, 1980; Vogt and Jung, 2004). However, a recent combined study of GPS, seismic and tectonic data (Marques et al., 2013a; 2014) indicates that the EU/NU boundary presently coincides with the TR in the east but is diffuse in the west (Fig. V.1).

Recent morpho-structural, geodetic, geochemical and geochronological studies have shown that the volcanic construction and destruction of Graciosa, Terceira, S. Jorge, Faial, Pico and S. Miguel has resulted in the development of linear volcanic ridges elongated along two main directions: N110° (mostly) and N130°. Such characteristics have been attributed to a significant control of volcanic outputs by regional lithospheric deformation of the current EU/NU plate boundary (e.g. Lourenço et al., 1998; Haase and Beier, 2003; Hildenbrand et al., 2008; 2012a,b; 2013a,b; Navarro et al., 2009; Quartau et al., 2012; Marques et al., 2013a; 2014; Costa et al., 2014). This suggests that the volcanism and the islands can be used to track the main regional tectonic deformation.

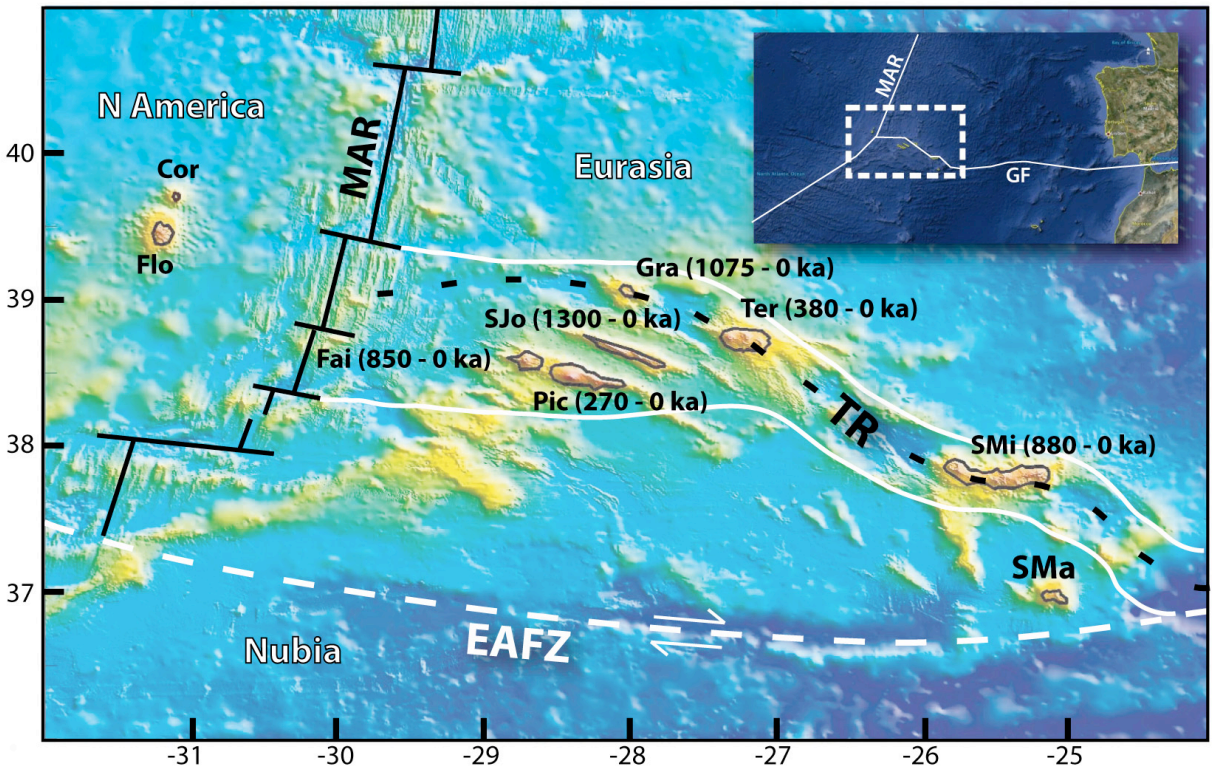


Figure V. 1. Bathymetric map of the Azores (data from Lourenço et al., 1998). The thick black lines indicate the location of the Mid-Atlantic Ridge (MAR) axis, which separate the North American and Eurasian plates, and the North American and Nubian plates. The white lines mark the current Eurasia/Nubia diffuse plate boundary (after Marques et al., 2013, 2014). The black dashed line indicates the location of the Terceira Rift (TR), and the white dashed line the East Azores Fracture Zone (EAFZ). Black numbers show previous geochronological data on volcanic rocks from the eastern and central islands (Féraud et al., 1980; Chovelon, 1982; Johnson et al., 1998; Calvert et al., 2006; Hildenbrand et al., 2008, 2012a; Larrea et al., 2014). The inset shows the location of the Azores archipelago in the Atlantic Ocean. Bathymetric GF: Gloria Fault (on the inset); Cor: Corvo; Flo: Flores; Fai: Faial; Pic: Pico; SJo: S. Jorge; Gra: Graciosa; Ter: Terceira; SMi: S. Miguel; SMa: Santa Maria.

The central and eastern Azores islands are dated at less than 1.35 Ma (e.g. Hildenbrand et al., 2008), with the exception of Santa Maria, which seems to have developed independently of the current EU/NU plate boundary. The early sub-aerial volcanic activity of Santa Maria was firstly dated at 8.02 ± 0.85 Ma (Abdel-Monem et al., 1975), and later re-evaluated at 5.5 ± 1.2 Ma (Féraud et al., 1981). Therefore, in the hypothesis that the TR is younger than 1 Ma (Vogt and Jung, 2004), Santa Maria is older than the TR opening, and has been active for several Myr thus recording a story that no other island in the Azores can tell.

Despite this key position and the importance of the age constraint, the geological evolution of the island remains poorly understood. From new morphological data, fieldwork, structural analysis, and K-Ar dating, we here constrain the volcano-tectonic evolution of Santa Maria and discuss its significance regarding regional tectonics associated with the evolution of the EU/NU plate boundary in the Azores.

V. 2. Previous data on the Santa Maria Island

The evolution of Santa Maria remains poorly constrained in time. From early stratigraphic studies, two main volcanic systems, separated by a volcano-sedimentary complex, have been first distinguished (Agostinho, 1937). Zbyszewski and Ferreira (1960) further assigned a Vindobonian age to the volcano-sedimentary complex, which would be therefore as old as ca. 11 Ma. Subsequent whole-rock K-Ar ages acquired on the two main volcanic units ranged between 8.12 ± 0.85 and 6.08 ± 0.51 Ma (Abdel Monem et al., 1975), and between 5.5 ± 1.2 Ma and 4.6 ± 0.1 Ma (Féraud et al., 1981). From $^{87}Sr/^{86}Sr$ ratios measured on bivalves collected in the volcano-sedimentary deposit, Kirby et al. (2007) estimated ages ranging from 10.03 to 2.24 Ma. However, based on the local magnetic field, Storetvedt et al. (1989) reported that the younger volcanic activity shows a Gauss normal polarity (3.4 - 2.5 Ma). All the available ages, however, have been acquired on a limited number of samples, and most of them are not precise enough to accurately constrain the volcano-tectonic evolution of Santa Maria. Furthermore, existing ages are sometimes even inconsistent as a given unit sometimes differs by almost 3 Ma depending on the authors.

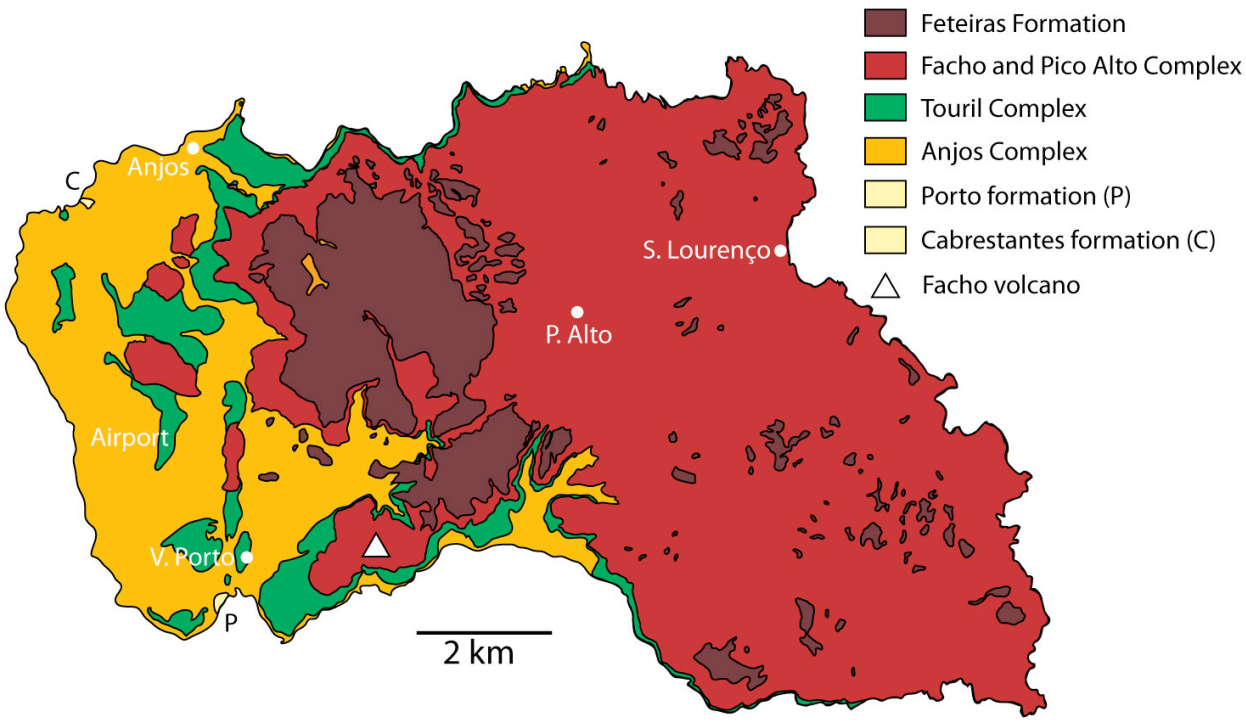


Figure V. 2. Geological map of Santa Maria adapted from Serralheiro et al. (1987).

Serralheiro et al. (1987) proposed a new volcanic stratigraphy, in which Santa Maria is divided into 6 units (Fig. V.2). Two of these, locally known as the Porto and Cabrestantes formations, have minor representation, and their relationship with the older volcanic complex is not

clear. The youngest formation (Feteiras) is not a volcanic unit *sensu stricto*, as it results from the alteration of older lavas. The remaining three units correspond to the previously proposed stratigraphy, with the exception of the (minor) Facho unit, which Zbyszewski and Ferreira (1960) considered to be the top of the younger volcanic complex, and Serralheiro et al. (1987) considered to be the base.

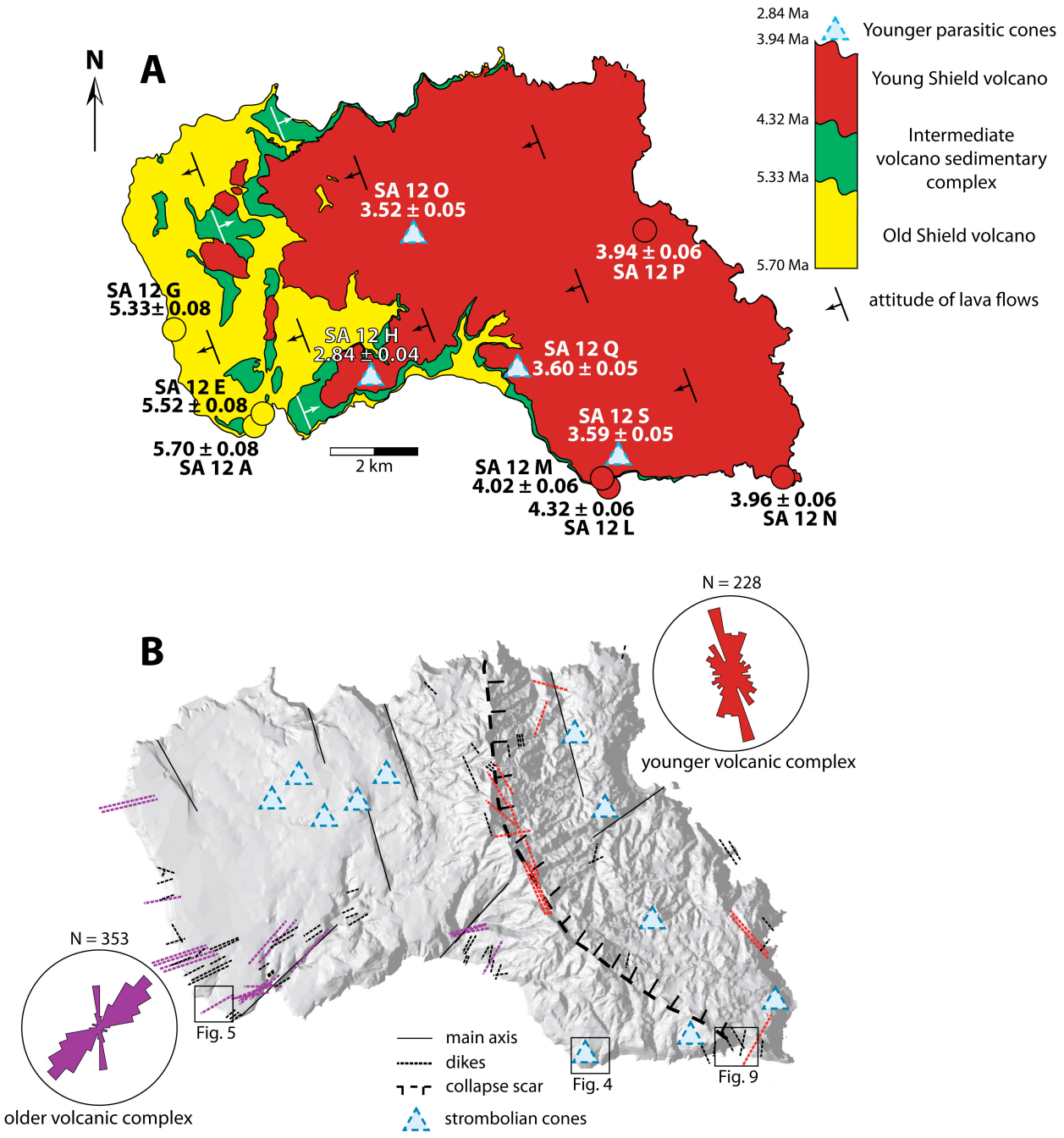


Figure V. 3. (A) Preferred geological map of Santa Maria, simplified after Zbyszewski and Ferreira (1960) and Serralheiro et al. (1987). Circles show the location of our samples and our new K/Ar ages. Note the distribution of volcanic and volcano-sedimentary units and their dip. (B) Shaded relief map of Santa Maria Island generated from a high-resolution DEM (10 m). Dikes measured in this study along with previous measurements by Zbyszewski and Ferreira (1960) are shown in purple and red for the western and eastern

parts of the island, respectively. Dashed black lines show interpreted scarps, and dashed triangles scoria cones. Stereoplots show orientation of dikes for the western and the eastern parts of the island, from our measurements and previous measurements (Madeira, 1986). Black squares indicate the location of Figs. V.4, V.5 and V.9.

In order to avoid local names, which can even differ according to different authors, we will use stratigraphy-related names, from older to younger (Figs. V.2, V.3): the Old Shield Volcano (locally known as the Anjos Complex), the Intermediate Volcano-sedimentary Complex (locally known as the Touril Complex), the Young Shield Volcano (locally known as the Pico Alto Complex), and the Later Parasitic Activity (locally known as the Feteiras Formation).

Structurally, two groups of dikes have been identified in Santa Maria. One trends ca. N045° and is mostly restricted to the Old Shield Volcano (below the Intermediate Volcano-sedimentary Complex), and the other strikes ca. N150° and is mostly found in the Young Shield Volcano (Zbyszewski and Ferreira, 1960; Madeira, 1986, and this study). However, the significance of these trends and their geodynamic implications regarding regional tectonics has been overlooked.

V. 3. Geomorphological analysis, fieldwork and sampling

Our strategy was devised to constrain, in time, the main complexes of Santa Maria and their interrelationships (Fig. V.3). First, a morphological analysis of the island was performed from a digital elevation model with a 10 m spatial resolution, in order to identify the main morpho-structural units and better define areas of particular importance for the subsequent fieldwork. Then, we went around the island by boat to get a full picture of the main volcanic sequences and their first-order relationships, mostly major unconformities and faults. Fieldwork was then carried out over the whole island, through available road cuts, quarries, and sea cliff exposures. We especially took advantage of the high coastal cliffs to investigate and sample the base and the top of the accessible volcanic successions. We systematically measured the attitude of the lava flows, the relationships between the various lava sequences, the position and the architecture of major unconformities, and structural elements (faults and dikes).

From the DEM and fieldwork, the island can be divided into two main sectors (Fig. V.3):

(1) The western sector is remarkably flat, with a regular slope gently dipping to the west. It constitutes the upper part of a ca. 200 m-thick succession of basaltic lava flows, with a general gentle dip to the WSW (< 10°). This succession has been identified previously as belonging to the Old Shield Volcano (e.g. Zbyszewski and Ferreira, 1960; Serralheiro et al., 1987). We note that lava flows dipping to the east have not been observed by us or by previous authors. Serralheiro et al. (1987) also noted the gentle dip to the WSW. We collected two lava flows from the base and the middle of the pile in the southern coastal cliff (samples SA12B and SA12E, respectively). A lava flow from the top of this succession constitutes the flat topography near the airport, and was

160 also collected (sample SA12G). The Facho unit was mapped by Serralheiro et al. (1987) below the
161 Young Shield Volcano, which constitutes most of the eastern part of the island. This seems
162 surprising, because the Young Shield Volcano is much more eroded than the Facho edifice. The
163 latter is very well preserved, except in the central part, where the feeding system (neck) is being
164 exploited in a large quarry. There, we sampled a lava flow (sample SA12H) associated with the
165 neck.
166 (2) The eastern sector comprises the Pico Alto chain (Young Shield Volcano), which is deeply
167 dissected by the modern hydrographical network. Several morphological characteristics can be
168 noted. First, Pico Alto is not straight, but a rather curved morphological feature. Furthermore, it is
169 topographically asymmetric. The slope is much steeper in the east than in the west, but both flanks
170 are incised by narrow canyons roughly perpendicular to the Pico Alto chain. The ravines cut
171 through a thick sequence of lava flows and conglomerates. The lava flows gently dip (< 10°) to the
172 WSW, similarly to the flows in the Old Shield Volcano. In the east, coastal cliffs cutting the Pico
173 Alto volcanic succession show a curved shape in plan view. Along the SE coast of the island, the
174 base of the sea cliff comprises alternating marine sediments and lava flows with well-preserved
175 internal pillow structures (Fig. V.4). The sediments and underlying lava flows, mapped as the
176 “Touril complex” in earlier works (Fig. V.2), correspond to what we call here the “Intermediate
177 Volcano-sedimentary Complex”. Just above the base of the sea cliff, a thick sedimentary layer
178 covers two lava flows in apparent local unconformity. Therefore, these flows may either represent
179 the remnants of the Old Shield Volcano, or lava flows within the Intermediate Volcanic Complex.
180 The sediments are unconformably covered by a suite of thick and massive sub-aerial lava flows,
181 which should belong to the Young Shield Volcano according to existing geological maps and our
182 field observations. Therefore, we collected the freshest and more aphyric lavas below (sample
183 SA12L) and above (sample SA12 M) the sediments. A flow belonging to the easternmost part of
184 the Young Shield Volcano was collected close to S. Lourenço (sample SA12P).
185 Several strombolian cones are present across the entire island and referred to as belonging
186 to the Feteiras formation (Serralheiro et al., 1987). Lava flows from several of the cones were
187 sampled in the western, central and southeastern parts of the island (SA12O, SA12Q and SA12S
188 respectively).
189

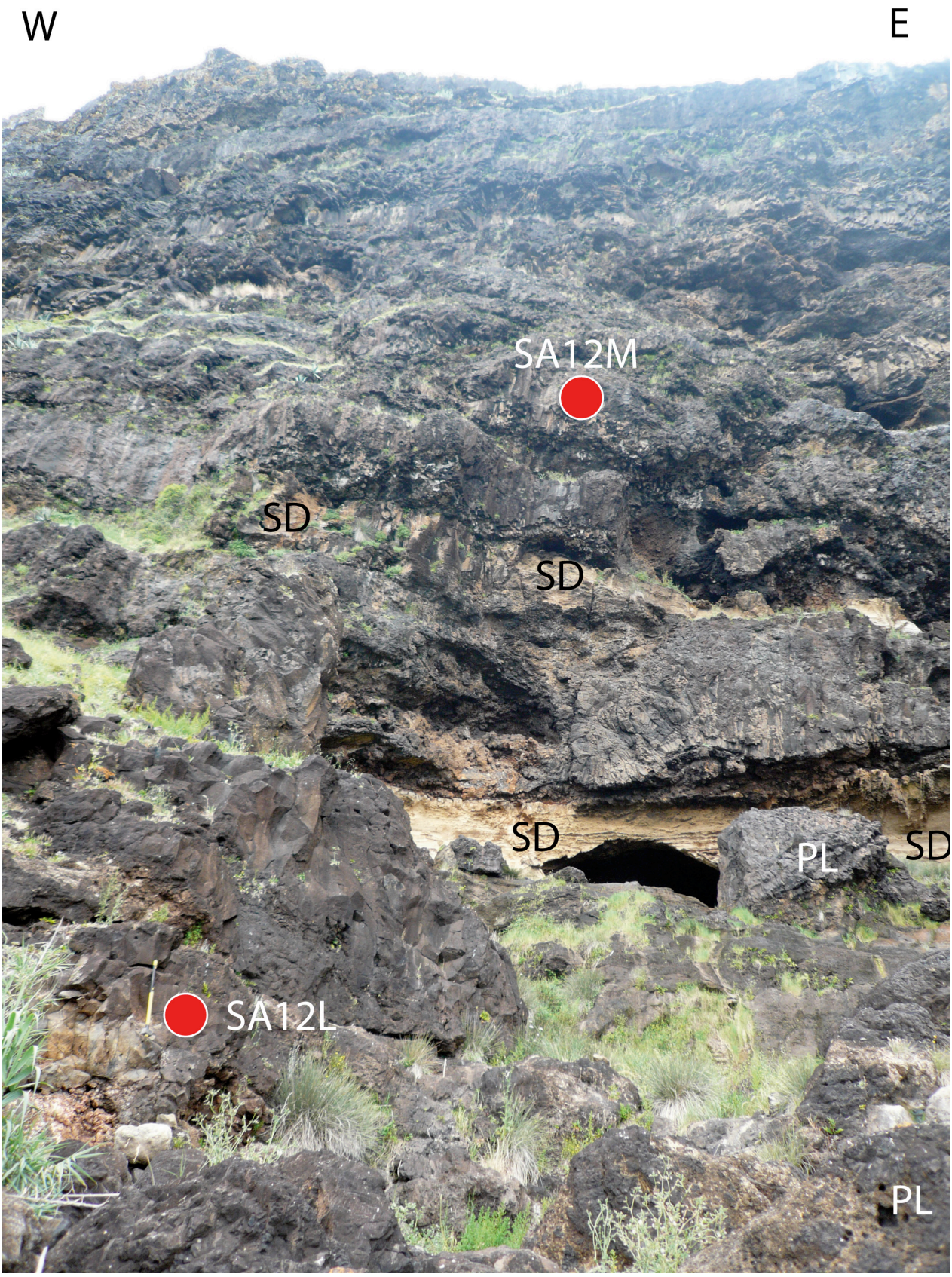


Figure V. 4. Base of the sea cliff along the SE part of Santa Maria (see Fig. V.3 for location). The picture shows alternating sedimentary deposits (SD) and lava flows, including pillow-lavas (PL). Red circles show the position of our samples SA12L and SA12M, from lava flows below and above sedimentary deposits, respectively.

V. 4. Structural analysis

A particular attention was paid to structural markers of deformation. Faults and dike swarms, especially, provide important information about the stress field at different times, which can be used to discuss the relationships between tectonics and volcanism at both local and regional scales, as successfully applied to other islands in the Azores (e.g. Lourenço et al., 1998; Hildenbrand et al., 2008, 2012a).

Several faults have been recognized along the coastal cliff near the airport and at the southeastern coast of the island. Our new data on dikes consist of about 30 new measurements, which complement the existing database of almost 600 dikes measured in total across the island (Madeira, 1986). We measured few faults oriented N045° on the western part of the island, with individual offsets from about one meter to tens of meters.

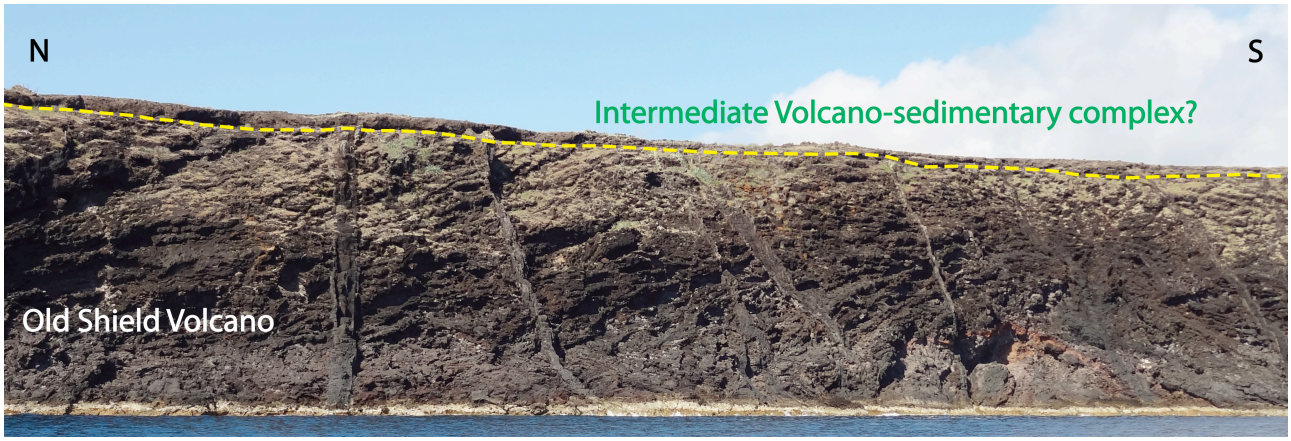


Figure V. 5. Sea cliff along the SW tip of Santa Maria, close to Vila do Porto (see Fig. V.3 for location). The picture shows lava flows of the Old Shield Volcano intruded by dykes. Note that the dykes are sealed at the top by younger lava flows.

Two major populations of dikes are recognized, as schematically represented on the simplified structural map shown in Fig. V.3:

- A ca. NE-SW (N045°) trend is localized mainly in the western part of Santa Maria, and much more on the southern than on the northern part of the island. The dikes are truncated by a regular erosional surface (Fig. V.5), and covered, in angular unconformity, by lava flows of the unit that has been mapped as the Intermediate Volcano-Sedimentary Complex (Fig. 3).
- A ca. NNW-SSE (N150°) trend is mainly measured along the Pico Alto axis, especially in the eastern sector. Despite the main N150° direction, the dikes in this sector show a slightly curved distribution in plan view (concave eastward), gradually changing from NNW-SSE in the south to NNE-SSW in the north. This curved trend is similar to the distribution of Later Parasitic Cones further to the east (Fig. V.3).

V. 5. K-Ar dating on separated groundmass

We systematically collected fresh lava flows with no visible traces of alteration. All the samples were carefully observed in thin-section to ensure the freshness of the rocks. Santa Maria rocks are primary basalts with phenocrysts of olivine, pyroxene and/or plagioclase in various proportions. Based on the micro-textural characteristics, the samples were crushed and sieved to a 125-250 micrometre size fraction and ultrasonically cleaned for 10 min in dilute nitric acid solution. To avoid weathered material as well as excess argon potentially carried by the phenocrysts, the freshest part of the groundmass was separated, within a narrow density interval, with heavy liquids and a magnetic separator. K and Ar were measured in Lab. GEOPS (Orsay, France) on the homogeneous preparation of the groundmass by flame spectrometry and mass spectrometry, respectively. K was released from the groundmass during an acid attack, and the sample solution was measured and compared with the one obtained on BCR-2 and MDO-G geostandards. K was determined with a 1% uncertainty (Gillot et al., 1992). Ar was measured with the unspiked K/Ar Cassignol-Gillot technique (Cassignol and Gillot, 1982), with a mass spectrometer similar to the one described in Gillot and Cornette (1986). The unspiked Cassignol-Gillot has been shown especially suitable to date precisely young volcanic rocks, even basic in composition (e.g. Gillot et al., 2006; Al Kwatli et al., 2012; Boulesteix et al., 2012; 2013). The standards GLO and HDB-1 were used for ^{40}Ar signal calibration. Typical uncertainties of 1% are achieved for the ^{40}Ar signal calibration. The uncertainty on the correction of atmospheric contamination is a function of the radiogenic content of the sample (^{40}Ar*). It rapidly vanishes and becomes rapidly negligible for ^{40}Ar* exceeding 10%. The detection limit for 40Ar* is presently 0.1% (Quidelleur et al., 2001; Gillot et al., 2006). Decay constants and isotopic ratios of Steiger and Jager (1977) were used. K and Ar measurements were duplicated for each sample. The age uncertainties are given at 1σ.

The new age results range between 5.70 ± 0.08 Ma and 2.84 ± 0.04 Ma (Fig. V.3 and Table V.1). They are fully consistent with the stratigraphic control of Zbyszewski and Ferreira (1960), and provide new important insight into the geological evolution of Santa Maria. The Old Shield Volcano succession exposed in the western cliffs of the island is here dated between 5.70 ± 0.08 and 5.33 ± 0.08 Ma. This is compatible with a previous age of 5.27 ± 0.15 Ma obtained by Féraud et al. (1981) on the same unit, but much younger than the value of 8.12 ± 0.85 Ma measured by Abdel Monem et al. (1975). The most plausible explanation for such a large difference is that the older age measured by Abdel-Monem et al. (1975) on whole rock is significantly biased by the unsuitable incorporation of phenocrysts and/or weathered phases. The lava flows sampled below and above the thick sedimentary layer at the base of the SE coastal cliff are here dated at 4.32 ± 0.06 Ma (SA12L) and 4.02 ± 0.06 Ma (SA12M), respectively. The thick lava flows collected in the middle and upper parts of the second shield volcanic succession (samples SA12N and SA12P) yield ages of 3.96 ± 0.06 and 3.94 ± 0.06 Ma. We note that these two ages are undistinguishable, within the range of uncertainties, from the age obtained on our sample SA12M. Lava flows from

strombolian cones sampled in the eastern part of the island (SA12Q and SA12S) yield undistinguishable ages of 3.60 ± 0.05 and 3.52 ± 0.05 Ma. Finally, the Facho volcanic unit is here dated at 2.84 ± 0.04 Ma. This is much younger than previously reported, thus extending the volcanic activity on Santa Maria down to a bit less than 3 Ma ago. The new age here obtained also confirms that the Facho volcanic cone overlies the second main volcanic complex (Young Shield Volcano), as deduced from our field observations (Fig. V.6), and thus supports the stratigraphic analysis of Zbyszewski and Ferreira (1960).

Sample	UTM 26 E	UTM N	K%	40Ar* (%)	40Ar* (10^{12}at/g)	**Age (Ma)**	Unc. (Ma)
SA12B	664691	4090402	0.971	26.8%	5.853	5.76	0.08
				33.0%	5.741	5.65	0.08
						5.70	**0.08**
SA12E	664691	4090402	1.382	49.5%	7.966	5.51	0.08
				43.9%	8.010	5.54	0.08
						5.52	**0.08**
SA12G	662605	4092350	0.729	36.8%	4.123	5.41	0.08
				57.8%	4.021	5.27	0.08
						5.33	**0.08**
SA12L	672509	4088860	1.025	40.5%	4.648	4.34	0.06
				40.7%	4.617	4.31	0.06
						4.32	**0.06**
SA12M	672509	4088860	1.067	24.3%	4.529	4.06	0.06
				28.5%	4.445	3.98	0.06
						4.02	**0.06**
SA12N	676542	4088923	1.110	8.9%	4.544	3.92	0.07
				18.4%	4.622	3.98	0.06
						3.96	**0.06**
SA12P	673336	4094610	0.756	16.1%	3.182	4.03	0.06
				38.8%	3.081	3.90	0.06
						3.94	**0.06**
SA12Q	670441	4091421	0.693	35.2%	2.609	3.60	0.05
				29.5%	2.615	3.61	0.05
						3.60	**0.05**
SA12S	672714	4089409	0.610	14.8%	2.308	3.62	0.06
				31.0%	2.279	3.57	0.05
						3.59	**0.05**
SA12O	668132	4094528	0.803	41.1%	2.950	3.51	0.05
				43.3%	2.960	3.52	0.05
						3.52	**0.05**
SA12H	667044	4091159	0.466	13.3%	1.376	2.82	0.05
				16.0%	1.392	2.86	0.04
						2.84	**0.04**

Table V.1. New K/Ar determinations obtained with the unspiked Cassignol-Gillot technique on fresh-separated groundmass. For each sample, the mean age is obtained by weighing by the amount of radiogenic argon. Uncertainties quoted at the 1s level.

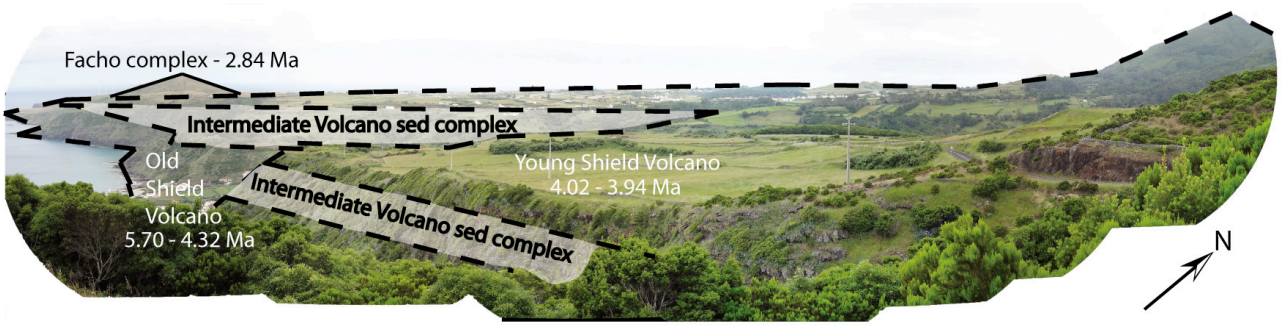


Figure V. 6. Stratigraphic relationships between the three main units of Santa Maria and the Facho complex.

V. 6. Discussion

The meaning of the ages obtained on our samples SA12L and SA12M collected below and above the thick marine sediments on the SE coast needs to be carefully discussed (Fig. V.4). The value of 4.32 ± 0.06 Ma obtained on SA12L is about 1 Myr younger than the age of 5.33 ± 0.08 Ma measured on the lava flow sampled at the top of the Old Volcano succession near the airport (our sample SA12G). The current topography on top of this western succession is gently sloping to the west, and therefore could be interpreted in two different ways: (1) a structural surface, i.e. following the dip of the youngest lava flows of the Old Shield Volcano; or (2) a gently dipping platform created by marine abrasion. Marine sediments are encountered up to several tens of meters high in SMa. Some of them lie on top of the old succession, or at the base of the Young Shield Volcano. By comparison, the Young Shield Volcano shows an irregular topography, deeply incised by numerous canyons, whereas the Old Shield Volcano is flat, despite being much older. With this in mind, we suggest that the western topographic surface is most likely due to more recent marine erosion, which removed the upper part of the former volcanic succession, and was responsible for the development of several marine terraces (e.g. Winkelmann et al., 2010; Meireles et al., 2013). Therefore, the ultimate activity of the first Shield Volcano must have ended after ca. 5.3 Ma ago. However, the original dip of the old lava flows is very gentle. So regular marine erosion may truncate only slightly the distal part of the former lava pile and thus may not have removed a great thickness of volcanic products above our sample SA12G. Consequently, it seems unlikely that the missing part would cover a period as long as 1 Myr.

In such hypothesis, the lava here dated at 4.32 ± 0.06 Ma does not belong to the Old Shield Volcano, i.e. it cannot represent an in-situ upper flank or even a block displaced, e.g. by normal

faulting. Alternatively, the lava flows under the sediments most likely represent one of the several submarine lava flows from the Intermediate Volcano-sedimentary Complex. The overall small difference in age between the two lava flows bracketing the thick sediments, and with subsequent lava flows up to the top of the Pico Alto Chain, supports a rather rapid construction of a volcano, first in a shallow submarine environment and then under sub-aerial conditions. In other terms, the part of the Intermediate Volcano-sedimentary Complex exposed in the SE sector most probably reflects the early emerging part of the Young Shield Volcano. This is consistent with what is observed along the eastern cliff of the island. Unlike the western sector, where the old succession is apparently composed of sub-aerial volcanic deposits (strombolian scoriae deposits, lava flows altered under oxidising conditions, presence of palaeosoils, and, mostly, absence of pillow lavas), the base of the eastern coastal cliffs is dominantly constituted by alternating marine sediments, pillow-lavas and/or hyaloclastites, exposed up to 20 m above current sea level.

V. 6. 1. Volcano-tectonic evolution of Santa Maria

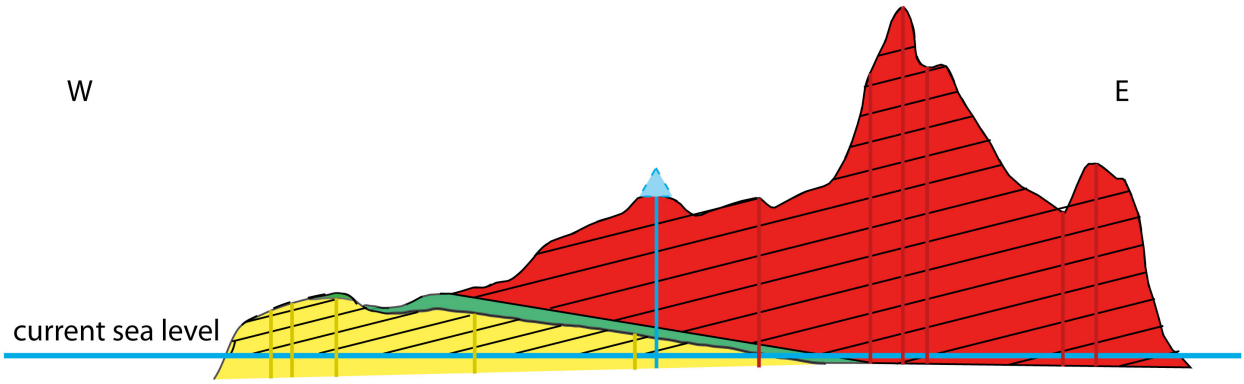


Figure V. 7. E-W cross-section summarizing our field observations and interpretation. Vertical exaggeration = 20.

According to our new data, the evolution of Santa Maria involved the construction and partial destruction of two main volcanoes, the Old and the Young Shield Volcanoes, which have been active from 5.7 Ma to 5.33 Ma, and between 4.32 and 3.94 Ma, respectively (Figs. V.3, V.6, V.7, V.8).

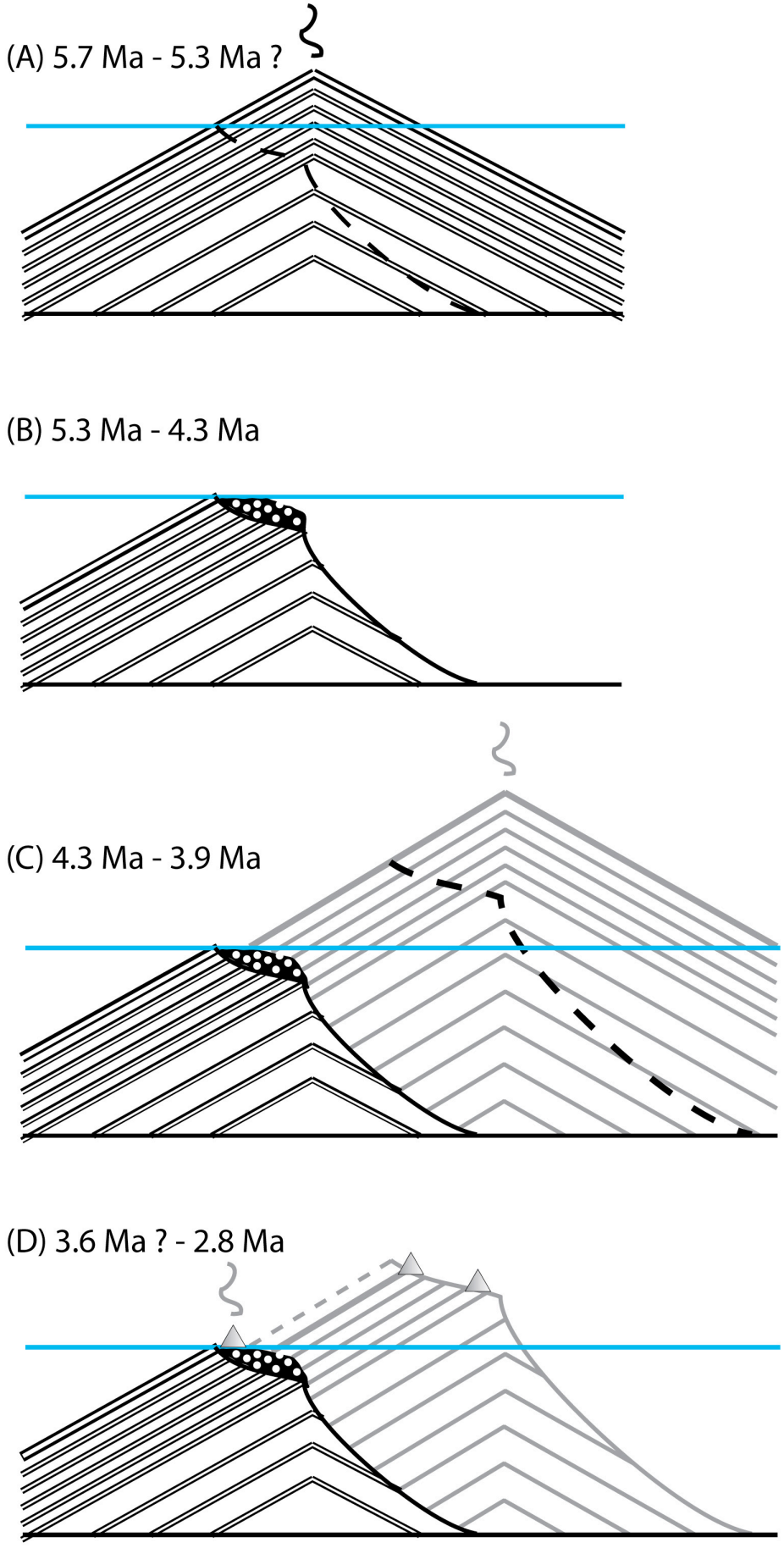


Figure V. 8. Cartoon illustrating the evolution of Santa Maria. The blue line represents sea level.

311

From the gentle westward dip of lava flows of both Old and Young Shield volcanoes, we infer that they were originally shield volcanoes, whose summits, eastern flanks, and part of the western flanks do not exist anymore. The distribution and geometry of the three main Santa Maria units show that only a part of them is presently preserved. The difference in age between the lavas of the Old and Young Shield Volcanoes (at most 1 Ma) appears not enough for stream and coastal erosion to remove completely the large amount of lava flows missing in the Old Shield Volcano (the whole eastern flank, the summit, and part of the western flank). Therefore the alternative is that they have been removed by a large-scale catastrophic event, in the form of a giant sector collapse as suggested by Marques et al. (2013b). This first sector collapse toward the east (Fig. V.8b) left a scar that comprises the east dipping unconformity on top of which the Intermediate Volcano-sedimentary Complex was deposited. Such sector collapse likely changed the stress field in the earlier volcanic edifice, and thus probably influenced the magma plumbing system of the island leading to the fast growth of the Young Shield Volcano in the landslide scar (Fig. V.8c). Such rapid eruptive response to giant landslides has been extensively recognized in other oceanic islands worldwide (e.g. Lipman et al., 1988; Watts and Masson, 2001; Gillot et al., 1994; Hildenbrand et al., 2004; 2006; Quidelleur et al., 2008; Boulesteix et al., 2012; 2013). Quidelleur et al. (2008) proposed that dating the base of the post-collapse volcanism provides the best constraint on the age of a given large sector collapse. Based on such considerations, the first flank collapse in Santa Maria would have happened soon before 4.3 Ma.

In Santa Maria, at least the eastern flank and the summit of the Young Shield Volcano are also missing. The current steep and curved topography in the east mimics a horseshoe shape depression, which could therefore represent the remnants of the scar of a second major flank collapse (Fig. V.8d). The inferred scar of the second sector collapse is greatly degraded, and most likely rooted in the nearby sea, but the distribution of later (ca. 3.56 Ma) parasitic cones and a part of the dikes along an arc concave to the east in the easternmost part of Santa Maria could have been triggered by the sector collapse through depressurization of the main feeding system (e.g. Manconi et al., 2009; Pinel and Albino, 2013). Therefore, at least two major faults should exist: one that affected the Old Shield Volcano and occurred before the construction of the Young Shield Volcano (i.e. between ca. 5.33 and 4.32 Ma, and probably soon before 4.3 Ma), and another that affected the Young Shield Volcano, and thus occurred after 3.94 Ma. The one most to the west could not be found yet, because the fault has been most likely covered by the Young Shield Volcano, and is below sea level. In contrast, a fault displacing the Young Shield Volcano succession can be observed most to the east on the sea cliff (Fig. V.9). It may represent one of the faults branching under the sea on the main fault of the second sector collapse. Unloading of the volcanic edifice and associated decompression of the magma feeding system was likely responsible for the emplacement of part of the dikes and volcanic cones along the arcuate scar, concave to the east, between 3.60 ± 0.05 and 3.52 ± 0.05 Ma, which suggests that the second flank collapse may have occurred about 3.6 Ma ago. From the new ages here reported, the

volcanic activity in Santa Maria lasted until at least 2.84 ± 0.04 Ma ago (Figs. V.3, V.8).

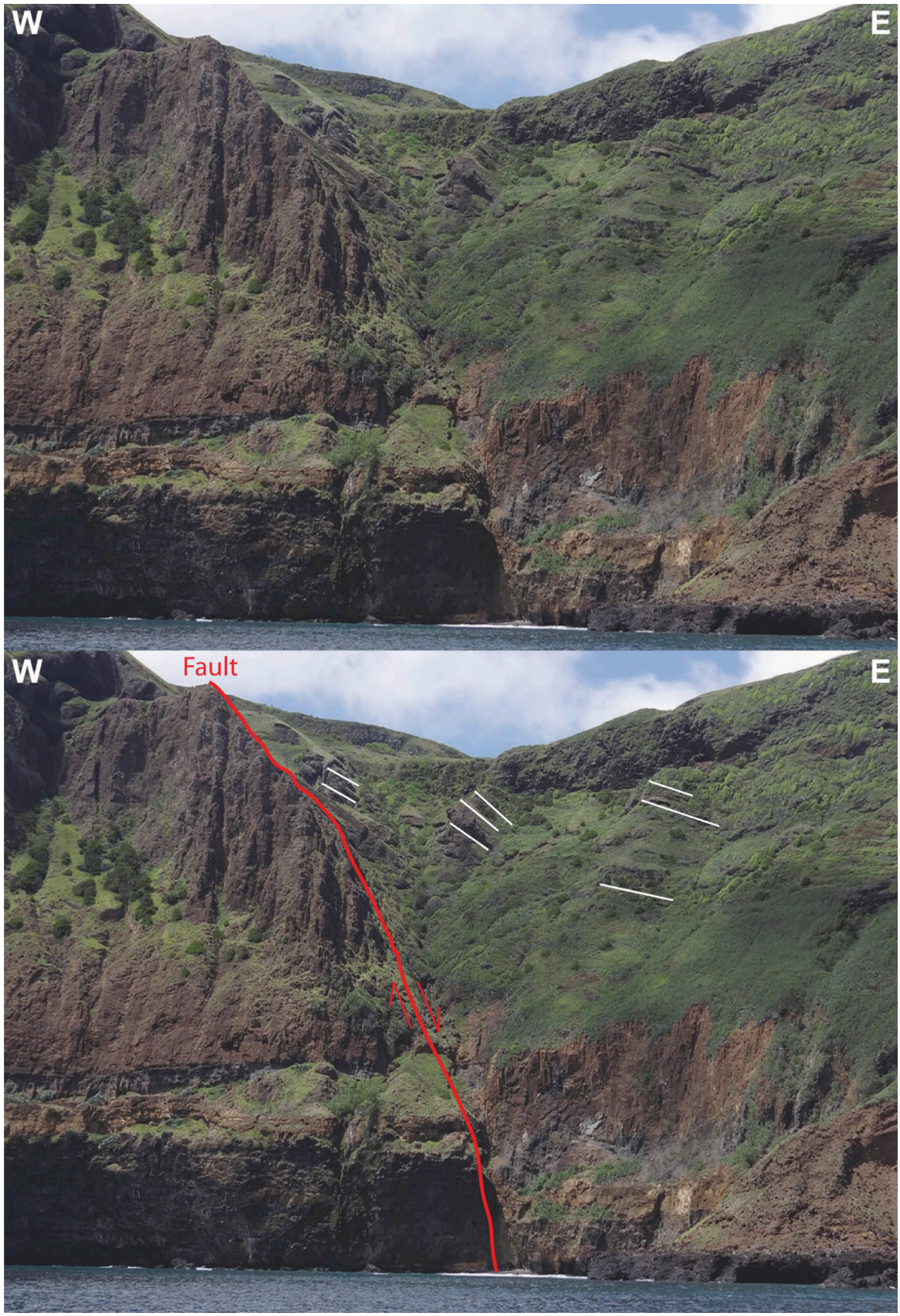


Figure V. 9. Normal fault dipping to the east (right) cutting the eastern volcanic succession, which we dated in this study between 4.32 Ma and 3.94 Ma.

V. 6. 2. Lithospheric control of volcanism

The construction of Santa Maria at the SE edge of the Azores plateau has been interpreted by some authors as reflecting the older activity of the "Azores plume" (e.g. Beier et al., 2013). However, our new ages indicate that the sub-aerial volcanic activity in Santa Maria occurred at the same location during a period of ca. 3 Myr. The half-spreading rate at the MAR is presently ca. 11 mm/yr (DeMets et al., 2010), so relative plate movement over an eventual stationary plume would have resulted in a drift of the volcanism by ca. 33 km toward the west, which is the opposite of what we measured in Santa Maria: older volcanics in the west (> ca. 5.3 Ma), and younger volcanics in the east (< ca. 4.3 Ma). On the other hand, the absolute motion of both Nubia and Eurasia plates towards the SW at a mean rate of 2 cm/yr (Gripp and Gordon, 2002), over a plume fixed in the absolute reference frame, would have resulted in a migration of volcanism of ca. 70 km towards the NE. However, this magnitude of displacement is not observed in Santa Maria. Moreover, both 33 km and 70 km migrations are smaller than the lithospheric thickness (Silveira et al., 2010), and might therefore be filtered by lithospheric processes. This suggests that the magma upwelling has been persistently focussed along main lithospheric fractures, and therefore that Santa Maria's evolution and dike emplacement has been greatly influenced by regional deformation.

The distribution of the two dike swarms in the Old and Young Shield Volcanoes of Santa Maria is not radial to the volcanic edifice. Therefore, their emplacement does not seem to be directly linked to local shallow stresses, e.g. due to inflation of the edifice over a magma chamber (Nakamura, 1977; Fiske and Jackson, 1972; Takada, 1999). Moreover, the overall basic composition of the lavas erupted on Santa Maria does not support the existence of a large magmatic chamber underneath the island (e.g., Beier et al., 2013). Linear dike concentrations in an individual volcano can be considered as a marker of tectonic stress and/or re-activation of inherited geological structures in the regional stress field (Nakamura, 1977; Tibaldi et al., 2014 and reference therein). The N150° trend has been mapped in other islands in the Azores (e.g., Féraud et al., 1980; Hildenbrand et al., 2008; Hipólito et al., 2011; Silva et al., 2012; Sibrant et al., submitted to Tectonics). Therefore, it seems reasonable to assume that the N150° dike swarm mapped in Santa Maria records, to a first approximation, the regional stress field (Fig. V.3). If one accepts that dikes result from magma intrusion in fractures roughly orthogonal to the least compressive stress, then the stress field changed when dike intrusion changed in orientation from N045° to N150°.

The N045° and N150° dike trends are found in the Old and Young Shield Volcanoes, respectively. As the N045° swarm does not intrude the Young Shield Volcano, we can reasonably infer that it fed the late activity of the Old Shield Volcano and thus was active between 5.3 Ma and 4.3 Ma. In turn, the younger N150° dikes intrude the base of the Young Shield Volcano and is therefore younger than 4.3 Ma. This suggests that the two main phases of volcanic growth on

Santa Maria record a major tectonic change, which occurred between 5.3 and 4.3 Ma. According to DeMets et al. (2010), the NU/EU relative motion trends approximately N060°, which means that the N150° faults are orthogonal to extension and thus prone for magma intrusion. Luís et al. (1994), based on the analysis of an aeromagnetic survey of the Azores, recognized a plate reconfiguration between anomalies 4 and 3A time (between 8.69 and 3.85 Ma), which is consistent with our new data and interpretation.

We note that a N150° trending dike swarm has also been found in the oldest part of S. Jorge Island (Hildenbrand et al., 2008). From a palaeomagnetic study, Silva et al. (2012) obtained a reversed polarity on the N150° dikes of SE S. Jorge, which, together with the ages measured by Hildenbrand et al. (2008), constrains dike emplacement in S. Jorge between ca. 1.32 and 0.79 Ma. Hildenbrand et al. (2008) also showed that the N150° dike system in S. Jorge was followed by a new dike system striking N110°, which is consistent with the direction of construction of the linear volcanic ridges in the Central Azores during the last 0.79 Myr. The N110° direction has not been found in Santa Maria. However, the N045° trend here evidenced is similar to the N050° structures recently recognized in the S. Miguel Island further north in the TR (Sibrant et al., submitted). These directions are similar to the transform direction due to the rotation of NU relative to EU (DeMets et al., 2010). According to Sibrant et al. (submitted), the N050° faults can accommodate the change in strike of the TR. By analogy, the two main dike swarms recognized in Santa Maria may reflect a change in palaeostress in the Azores between 5.33 and 4.32 Ma. Because some dikes seem to follow the direction of the Pico Alto chain, and because the direction of the landslides are coherent with the local extension deduced from dikes, we suggest that the major tectonic reorganization could have favoured the localization and the triggering of the major flank instabilities here proposed.

V. 7. Conclusion

From morphologic, stratigraphic, tectonic and new high-precision K-Ar data, we constrain the volcanic activity of Santa Maria between ca. 5.7 and 2.8 Ma. The history of Santa Maria is marked by two phases of fast volcanic growth (5.7 to 5.3 Ma, and 4.3 to 3.9 Ma), with the construction of two large shield volcanoes, separated by a large-scale flank collapse between 5.33 ± 0.08 Ma and 4.32 ± 0.06 Ma. A second sector collapse occurred around 3.60 Ma, which removed a great part of Santa Maria. The most recent volcanic activity in Santa Maria is represented by Parasitic strombolian Cones unconformably siting on top of the younger volcanic complex, up to at least 2.8 Ma ago.

From the strike of dikes and the age of the lavas intruded by the dikes, we identify an older N045° system (< ca. 5.3 Ma), and a younger N150° system (< ca. 4.3 Ma), from which we propose that the stress field dramatically changed ca. 5.3 - 4.3 Ma. The N045° trend, also recognized in the nearby S. Miguel Island, may materialize major lithospheric discontinuities associated with the

development of lithospheric structures after the end of the activity in the East Azores Fracture Zone. Therefore, the sudden jump in dike swarms direction here evidenced on S. Maria may reflect a major tectonic change accompanying the reconfiguration of the EU-NU boundary in the area between the EAFZ and the TR.

ACKNOWLEDGMENTS

This study has been mostly supported by research project MEGAHazards (PTDC/CTE-GIX/108149/2008) funded by FCT (Portugal). ACG Costa benefitted from a PhD scholarship (SFRH/BD/68983/2010), FCT (Portugal). The authors wish to thank V. Godard for preparing thin sections. We acknowledge A. Davaille for her critical reading of the manuscript.

REFERENCES CITED

Abdel Monem, A.A., Fernandez, L.A., Boone, G.M., 1975. K-Ar ages from the Eastern Azores Group (Santa Maria, São Miguel, Formigas islands). Lithos, 8, 247-254.

Agostinho, J., 1937. Sobre a tectónica da Ilha de Santa Maria. Açoreana, 1, 281-286.

Al Kwatli, M.A., Gillot, P.Y., Zeyen, H., Hildenbrand, A., Al Gharib, I., 2012. Volcano-tectonic evolution of the northern part of the Arabian plate in the light of the new K-Ar ages and remote sensing: Harrat Ash Shaam volcanic province (Syria). Tectonophysics, 580, 192-207.

Beier, C., Mta, J., Stöckhert, F., Mattielli, N., Brandl, P.A., Madureira, P., Genske, F.S., Martins, S., Madeira, J., Haase, K.M., 2013. Geochemical evidence for melting of carbonated peridotite on Santa Maria Island, Azores. Contrib. Mineral Petrol., 165, 823-841.

Bonatti, E., 1990. Not so hot "hot spots" in the oceanic mantle. Science, 250, 107–111.

Bouleisteix, T., Hildenbrand, A., Soler, V., Gillot, P.Y., 2012. Eruptive response of oceanic islands to giant landslides: new insights from the geomorphologic evolution of the Teide-Pico Viejo volcanic complex (Tenerife, Canary). Geomorphology, 138 (1), 61-73.

Bouleisteix, T., Hildenbrand, A., Soler, V., Quidelleur, X., Gillot, P-Y., 2013. Coeval giant landslides in the Canary Islands: Implications for global, regional and local triggers of giant flank collapses on oceanic volcanoes. Journal Volcan. Geotherm. Res., 257 (1), 90-98.

Calvert, A.T., Moore, R.B., McGeehin, J.P., Rodrigues da Silva, A.M., 2006. Volcanic history and 40Ar/39Ar and 14C geochronology of Terceira Island, Azores. Protugal, Journal Volcano. Geotherm. Res., 156, 103-115.

Cannat, M., Briais, A., Deplus, C., Escartin, J., Georgen, J., Lin, J., Mercouriev, S., Meyzen, C., Muller, M., Pouliquen, G., Rabain, A., Da Silva, P., 1999. Mid Atlantic rige Azores hotspot interactions: along axis migration of a hotspot derived event of enhanced magmatism 10 to 4 Ma ago. Earth Planet. Sci. Lett., 173 (3), 257-269.

Cassignol, C., Gillot, P.Y., 1982. Range and effectiveness of unspiked potassium-argon dating: Experimental groundwork and applications. John Wiley, New York, 159-179.

Chovelon, P., 1982. Evolution volcano-tectonique des îles de Faial et Pico. Thèse, faculté des sciences de la Terre, université Paris Sud 11, 242pp.

Costa, A.C.G., Marques, F.O., Hildenbrand, A. Sibrant, A.L.R., Catita, C.M.S., 2014. Large scale flank collapse in steep volcanic ridge: Pico-Faial Ridge, Azores Triple Junction. Journal Volcan. Geotherm. Res. 272, 111-125.

DeMets, C., Gordon, R., Argus, D.F., 2010. Geologically current plate motions. Geophys. J. Int., 181, 1-80.

Féraud, G., Kaneoka, S., Allègre, C., 1980. K/Ar ages and stress pattern in the Azores: Geodynamic implications. Earth Planet. Sci. Lett., 46, 275-286.

Féraud, G., Schmincke, H.U., Lietz, J., Gastaud, J., Pritchard, G., Bleil, U., 1981. New K-Ar Ages, Chemical Analyses and Magnetic Data of Rocks from the Islands of Santa Maria (Azores), Porto Santo and Madeira (Madeira Archipelago) and Gran Canaria (Canary Islands). Bulletin

of Volcanology, 44, 359-357.
Fiske, R.S., Jackson, E.D., 1972. Orientation and growth of Hawaiian rifts: The effect of regional structure and gravitational stresses. Proc. Roy. Soc. London, 329, 299-326.
Gente, P., Dyment, J., Maia, M., Goslin, J., 2003. Interaction between the Mid Atlantic ridge and the Azores hotspot during the last 85 Myr: Emplacement and rifting of the hotspot derived plateaus. Geochem. Geophys. Geosyst., 8, Q03013, doi:10.1029/2006GC001318.
Gillot, P.Y., Cornette, Y., 1986. The Cassignol technique for potassium-argon dating, precision and accuracy: examples from late Pleistocene to recent volcanics from southern Italy. Chemical Geology 59, 205-222.
Gillot, P.Y., Cornette, Y., Max, N., Floris, B., 1992. Two reference materials, trachytes MDO-G and ISH-G, for argon dating K/Ar and 40Ar/39Ar datnig of Pleistocene and Holocene rocks. Geostandards and Geoanalytical Research, 16, 55-60.
Gillot, P.Y., Lefèvre J.C., Nativel, P.E., 1994. Model for the structural evolution of the volcanoes of Reunion Island. Earth Planet. Sci. Lett., 122 (3-4), 291-302, doi:10.1016/0012-821X(94)90003-5.
Gillot, P.Y., Hildenbrand, A., Lefèvre, JC., Albore-Livadie, C., 2006. The K/Ar dating method: Principle, analytical techniques, and application to Holocene volcanic eruptions in the southern Italy. Acta Vulcanologica, 18, 55-66.
Gripp, A.E., Gordon, R.G., 2002. Young tracks of hotspots and current plate velocities. Geophys. J. Int., 150, 321-361.
Haase, K.M., Beier, C., 2003. Tectonic control of ocean island basalt sources on São Miguel, Azores? Geophys. Res. Lett., 30, doi:10.1029/2003GL017500.
Hildenbrand, A., Gillot, P.Y., Le Roy, I., 2004. Volcano-tectonic and geochemical evolution of an oceanic intra-plate volcano: Tahiti-Nui (French Polynesia). Earth Planet. Sci. Lett., 217 (3), 349-365.
Hildenbrand, A., Gillot, P.Y., Bonneville, A., 2006. Off-shore evidence for a huge landslide of the northern flank of Tahiti-Nui (French Polynesia). Geochem. Geophys. Geosyst. 7 (3), 1-12.
Hildenbrand, A., Madureira, P., Marques, F.O., Cruz, I., Henry, B., Silva, P., 2008. Multi-stage evolution of a sub-aerial volcanic ridge over the last 1.3 Myr: S. Jorge Island, Azores Triple Junction. Earth Planet. Sci. Lett., 273, 289-298.
Hildenbrand, A., Marques, F.O., Costa, A.C.G., Sibrant, A.L.R., Silva, P.F., Henry, B., Miranda, J.M., Madureira, P., 2012a. Reconstructiong the architectural evolution of volcanic island from combined K/Ar, morphologic, tectonic, and magnetic data: The Faial Island example (Azores). Journal Volcanol. Geotherm. Res., 241-242, 39-48.
Hildenbrand, A., Marques, F.O., Catalão, J., Catita C.M.S., Costa, A.C.G., 2012b. Large-scale active slump of the southeastern flank of Pico Island, Azores. Geology, 40, 939-942, doi:10.1130/G33303.1.

514 Hildenbrand, A., Marques, F.O., Costa, A.C.G., Sibrant, A.L.R., Silva, P.F., Henry, B., Miranda,
515 J.M., Madureira, P., 2013a. Reply to the comment by Quartau and Mitchell on
516 “Reconstructiong the architectural evolution of volcanic island from combined K/Ar,
517 morphologic, tectonic, and magnetic data: The Faial Island example (Azores),” Journal
518 Volcanol. Geotherm. Res., 241-242, 39-48, by Hildenbrand et al. (2012) in Journal Volcanol.
519 Geotherm. Res., 255, 127-130.
520 Hildenbrand, A., Marques, F.O., Catalão, J., Catita C.M.S., Costa, A.C.G., 2013b. Reply to the
521 comment by Quartau and Mitchell on “ Large-scale active slump of the southeastern flank of
522 Pico Island, Azores,” Geology, 40, 939-942, doi:10.1130/G33303.1, by Hildenbrand et al.,
523 2012) in Geology, 41, doi:10.1130/G34879Y.1.
524 Hipólito, A., Madeira, J., Carmo, R., Gaspar, J.L., 2011. Neotectonics of Graciosa Island (Azores) -
525 Uncertainty in seismic hazard assessment in a volcanic area with variable slip-rates. 2nd
526 INQUA-IGCP-567 International Workshop on Active Tectonics, Earthquake Geology,
527 Archaeology and Engineering, Corinth, Greece.
528 Johnson, C.L., Wijbrans, J.R., Constable, C.G., Gee, J., Staudigel, H., Tauxe, L., Forjaz, V.H.,
529 Salgueiro, M., 1998. 40Ar/39Ar ages and paleomagnetism of São Miguel Lavas, Azores. Earth
530 Planet. Sci. Lett., 160, 637-649.
531 Kirby, M.X., Jones, D.S., Avila, S.P., 2007. Neogene shallow-marine paleoenvironments and
532 preliminary strontium isotope chronostratigraphy of Santa Maria island, Azores. Açoreana, 5,
533 112-125.
534 Krause, D.C., Watkins, N.D., 1970. North Atlantic crustal genesis in the vicinity of the Azores.
535 Geophys. J. R. Astron. Soc., 19, 261-283.
536 Larrea, P., Wijbrans, P.R., Galé, C., Ubide, T., Lago, M., França, Z., Widom, E., 2014. 40Ar/39Ar
537 constraints on the temporal evolution of Graciosa Island, Azores (Protugal). Bull Volcanol.
538 76:796, doi:10.1007/s00445-014-0796-8.
539 Laughton, A.S., Whitmarsh, R.B., Rusby, J.S.M., Somers, M.L., Revie, J., McCartney, B.S., Nafe,
540 J.E., 1972. A continuous East-West Fault on the Azores-Gibraltar Ridge. Nature, 237, 217-
541 Lipman, P.W., Normark, W.R., Moore, J.G., Wilson J.B., Gutmacher, C.E., 1988. The giant
542 submarine Alika debris slide, Mauna Loa, Hawaii. J. Volcanol. Geortherm. Res., 93, 4279-
543 4299.
544 Lourenço, N., Luis, J.F., Miranda, J.M., Ribeiro, A., Victor, L.A.M., 1998. Morpho-tectonic analysis
545 of the Azores volcanic plateau from new bathymetric compilation of the area. Mar. Geophys.
546 Res., 20, 141–156.
547 Luís, J.F., Miranda, J., Patriat, P., Galdeano, A., Rossignol, J.C., Mendes-Victor, L., 1994. Açores
548 Triple junction Evolution in the last 10Ma from a New AeromagneticSurvey. Earth and
549 Planet. Sci. Lett., 125, 439-459.
550 Machado, F., 1959. Submarine pits of the Azores plateau. Bull. Volcanol., 21, 109-116.

551 Madeira, J., 1986. Geologia estructural e enquadramento geotectonico da ilha de Santa Maria
552 (Açores). M.Sc Thesis, Univ. Lisbon, 107pp.
553 Manconi, A., Longpré, M.-A., Walter, T.R., Troll, V.R., Hansteen, T.H., 2009. The effects of flank
554 collapses on volcano plumbing systems. Geology, 24, 321-234.
555 Marques, F.O., Catalão, J.C., DeMets, C., Costa, A.C.G., Hildenbrand, A., 2013a. GPS and
556 tectonic evidence for a diffuse plate boundary at the Azores triple junction. Earth Planet. Sci.
557 Lett., 381, 177-187.
558 Marques, F.O., Sibrant, A.L.R., Hildenbrand, A., Costa, A.C.G., 2013b. Large-scale sector
559 collapses in the evolution of Santa Maria Island, Azores. Abstract Meeting AGU, 2013.
560 Marques, F.O., Catalão, J.C., DeMets, C., Costa, A.C.G., Hildenbrand, A., 2014. corrigendum to:
561 GPS and tectonic evidence for a diffuse plate boundary at the Azores triple junction, (Earth
562 Planet. Sci. Lett., 381, 177-187) Earth Planet. Sci. Lett., 387, 1-3.
563 McKenzie, D., 1972. Active Tectonics of the Mediterranean region. Geophys. J. R. Astron. Soc.,
564 30, 109-185.
565 Meireles, R.P., Faranda, C., Gliozzi, E., Pimentel, A., Zanon, V., Avila, S.P., 2013. Late Miocene
566 marine ostracods from Santa Maria island, Azores (NE Atlantic): Systematics, palaeoecology
567 and palaeobiogeography. Revue de micropaleontology 55, 133-148.
568 Métrich, N., Zanon, V., Créon, L., Hildenbrand, A., Moreira, M., Marques, F.O., 2014. Is the
569 “Azores hotspot” a wetspot? Insights from geochemistry of fluid and melt inclusions in olivine
570 of Pico basalt. Journal of Petrology, 55, 377-393.
571 Moreira, M., Allegre, J.C., 2002. Rare gas systematics an Mid Atlantic ridge (37°-40°N). Earth
572 Planet. Sci. Lett., 198 (3-4), 401-416.
573 Nakamura, K., 1977. Volcanoes as possible indicators of tectonic stress orientation – principle and
574 proposal. J. Volcanol. Geotherm. Res. 2, 1-16.
575 Navarro, A., Lourenço, N., Chorowicz, J., Miranda, J.M., Catalao, J., 2009. Analysis of geometry of
576 volcanoes and faults in Terceira Island (Azores): Evidence for reactivation tectonics at the
577 EUR/AFR plate boundary in the Azores triple junction. Tectonophysics, 465 (1-4), 98-113.
578 Pinel, V., Albino, F., 2013. Consequences of volcano sector collapse on magmato storage zones:
579 Insights from numerical modeling. J. Volcanol. Geotherm. Res., 252, 29-37.
580 Quartau, R., Tempera, F., Mitchell, N.C., Pinheiro, L.M., Duarte, H., Brito, P.O., Bates C.R.,
581 Monteiro, J.H., 2012. Morphology of the Faial Island shelf (Azores): The interplay between
582 volcanic, erosional, depositional, tectonic and mass-wasting processes. Geochemistry,
583 Geophysics, Geosystems, 13 (4), doi:10.1029/2011GC003987.
584 Quidelleur, X., Gillot, P.Y., Soler, V., Lefevre, J.C., 2001. K/Ar dating extended into the last
585 millennium: Application to the youngest effusive episode of the Teide volcano (Canary islands,
586 Spain). Geophysical Res. Lett., 28, 3067-3070.

587 Quidelleur, X., Hildenbrand, A., Samper, A., 2008. Causal link between Quaternary paleoclimatic
588 changes and volcanic islands evolution. Geophys. Res. Lett., 35, L02303,
589 doi:10.1029/2007GL031849.
590 Schilling, J.G., 1975. Azores mantle blob: rare earth evidence. Earth Planet. Sci. Lett., 25, 103–
591 115.
592 Searle, R., 1980. Tectonic pattern of the Azores spreading centre and triple junction. Earth Planet.
593 Sci. Lett., 51, 415-434.
594 Serralheiro, A., Alves, C.A.M., Forjaz, V.H., Rodrigues, B., 1987. Carta vulcanológica dos Açores,
595 Ilha de Santa Maria. Escala 1:15000 (folhas 1 e 2): Serviço regional de Protecção Civil dos
596 Açores e Universidade dos Açores (Ed.). Ponta Delgada.
597 Sibrant, A.L.R., F.O., Marques, A., Hildenbrand, T., Boulesteix, and A.C.G., Costa, (submitted),
598 The architecture of the Terceira Rift as shown by the tectonics of S. Miguel Island, Azores,
599 Submitted to Tectonics.
600 Silva, P.F., Henry, B., Marques, F.O., Hildenbrand, A., Madureira, P., Mériaux A., Kratinova, Z.,
601 2012. Palaeomagnetic study of a subaerial volcanic ridge (Sao Jorge Island, Azores) for the
602 past 1.3 Myr: evidence for the Cobb Mountain Subchron, volcano flank instability and
603 tectonomagmatic implications. Geophysical Journal International, 188, 959-978.
604 Silveira, G., Vinnik, L., Stutzmann, E., Farra, V., Kiselev, S., Morais, I., 2010. Stratification of the
605 Earth beneath the Azores from P and S receiver functions. Earth Planet. Sci. Lett., 299 (1-2),
606 91-103.
607 Steiger, R.H., Jäger, E., 1977. Subcommission on geochronology: Convention on the use of decay
608 constants in geo- and cosmochronology. Earth Planet. Sci. Lett., 36, 359-362.
609 Storetvedt, K.M., Serralheiro, A., Moreira, M., Abranches, M.C., 1989. Magnetic structure and
610 evolution of the island of Santa Maria, Azores. Physics of the earth and planetary interiors, 58,
611 228-238.
612 Takada, A., 1999. Variations in magma supply and magma partitioning: the role of tectonic
613 settings. Journal Volcano. Geotherm. Res., 93, 93-110.
614 Tibaldi, A., Bonali, F.L., Corazzato, C., 2014. The diverging volcanic rift system. Tectonophysics,
615 611, 94-113.
616 Vogt, P.R., Jung, W.Y., 2004. The Terceira Rift as hyper slow, hotspot dominated oblique
617 spreading axis: A comparison with other slow spreading plate boundaries. Earth Planet. Sci.
618 Lett., 218, 77-90.
619 Watts, A.B., Masson, D.G., 2001. New sonar evidence for recent catastrophic collapses of the
620 north flank of Tenerife, Canary Islands. Bull. Volcanol., 63 (1), 8-19.
621 White, W.M., Schilling, J.-G., Hart, S.R., 1976. Evidence for the Azores mantle plume from
622 strontium isotope geochemistry of the Central North Atlantic. Nature, 263, 659-663.
623 Winkelmann, K., Buckeridge, J.S., Costa, A.C., Dionisio, M.A.M., Medeiros, A., Cachão, M., Avila,
624 S.P., 2010. Zullobalanus santamariaensis sp. Nov., a new late Miocene barnacle species of

625 the family Archaeobalanidae (Cirripedia: Thoracica), from the Azores. Zootaxa 2680, 33-44.
626 Yang, T., Shen, Y., Van Der Lee, S., Solomon, C., 2006. Upper mantle structure beneath the
627 Azores hotspot from finite frequency seismic topography. Earth Planet. Sci. Lett., 250 (1-2),
628 11-26.
629 Zbyszewski, G., Ferreira, O.V., 1960. Carta geológica de Portugal, Ilha de Santa Maria (Açores),
630 scale 1:50 000: Serviços Geológicos de Portugal.
631

FIGURE CAPTIONS

Figure V.1. Bathymetric map of the Azores (data from Lourenço et al., 1998). The thick black lines indicate the location of the Mid-Atlantic Ridge (MAR) axis, which separate the North American and Eurasian plates, and the North American and Nubian plates. The white lines mark the current Eurasia/Nubia diffuse plate boundary (after Marques et al., 2013, 2014). The black dashed line indicates the location of the Terceira Rift (TR), and the white dashed line the East Azores Fracture Zone (EAFZ). Black numbers show previous geochronological data on volcanic rocks from the eastern and central islands (Féraud et al., 1980; Chovelon, 1982; Johnson et al., 1998; Calvert et al., 2006; Hildenbrand et al., 2008, 2012a; Larrea et al., 2014). The inset shows the location of the Azores archipelago in the Atlantic Ocean. Bathymetric GF: Gloria Fault (on the inset); Cor: Corvo; Flo: Flores; Fai: Faial; Pic: Pico; SJo: S. Jorge; Gra: Graciosa; Ter: Terceira; SMi: S. Miguel; SMa: Santa Maria.

Figure V.2. Geological map of Santa Maria adapted from Serralheiro et al. (1987).

Figure V.3. (A) Preferred geological map of Santa Maria, simplified after Zbyszewski and Ferreira (1960) and Serralheiro et al. (1987). Circles show the location of our samples and our new K/Ar ages. Note the distribution of volcanic and volcano-sedimentary units and their dip. (B) Shaded relief map of Santa Maria Island generated from a high-resolution DEM (10 m). Dikes measured in this study along with previous measurements by Zbyszewski and Ferreira (1960) are shown in purple and red for the western and eastern parts of the island, respectively. Dashed black lines show interpreted scarps, and dashed triangles scoria cones. Stereoplots show orientation of dikes for the western and the eastern parts of the island, from our measurements and previous measurements (Madeira, 1986). Black squares indicate the location of Figs. V.4, V.5 and V.9.

Figure V.4. Base of the sea cliff along the SE part of Santa Maria (see Fig. V.3 for location). The picture shows alternating sedimentary deposits (SD) and lava flows, including pillow-lavas (PL). Red circles show the position of our samples SA12L and SA12M, from lava flows below and above sedimentary deposits, respectively.

Figure V.5. Sea cliff along the SW tip of Santa Maria, close to Vila do Porto (see Fig. V.3 for location). The picture shows lava flows of the Old Shield Volcano intruded by dykes. Note that the dykes are sealed at the top by younger lava flows.

Figure V.6. Stratigraphic relationships between the three main units of Santa Maria and the Facho complex.

Figure V.7. E-W cross-section summarizing our field observations and interpretation. Vertical

670 exaggeration = 20.
671
672 Figure V.8. Cartoon illustrating the evolution of Santa Maria. The blue line represents sea level.
673
674 Figure V.9. Normal fault dipping to the east (right) cutting the eastern volcanic succession, which
675 we dated in this study between 4.32 Ma and 3.94 Ma.
676
677 Table V.1. New K/Ar determinations obtained with the unspiked Cassignol-Gillot technique on
678 fresh-separated groundmass. For each sample, the mean age is obtained by weighing by the
679 amount of radiogenic argon. Uncertainties quoted at the 1s level.

CHAPTER VI
Geological synthesis: implications for the Eu/Nu boundary in the Azores

VI. Geological synthesis: implications for the Eu/Nu boundary in the Azores

In the previous chapters, we have presented separately the volcano-tectonic evolution of Graciosa, S. Miguel and Santa Maria islands. We will here synthetize our main results from these three islands and compare them with available data on other islands developed east of the MAR.

We will first focus on the recent, still active volcanic active islands (Graciosa, S. Miguel, Pico, Faial, S. Jorge, Terceira), which all developed along the present eastern branch of the ATJ, and thus may provide important information regarding the recent evolution of Eu/Nu plate boundary during the last 1 Myr.

In a second step, we will focus on the information provided by Santa Maria volcanism and will discuss its significance regarding the possible location and evolution of an older plate boundary.

VI. 1. The Eu/Nu plate boundary during the last Myr

VI. 1. 1. Spatial distribution of the volcanism and tectonic structures

As we saw in the previous chapters, the volcanism along the present limit of the Eu/Nu plate boundary has developed along preferential structural directions. The available bathymetry of the archipelago (Fig. VI.1) reveals the existence of several lineations, seamounts and elongated islands with trends ranging between N100° and N160°, as previously recognized by Lourenço et al. (1998) and Stretch et al. (2006). In this range, the two most frequent strikes are N110-N120°, in the west, and N140-150° in the east.

In this study, the two main regional directions have been measured on both Graciosa (Chapter III) and S. Miguel (Chapter IV.2). Indeed, the elongation of most edifices (except Nordeste) and the various faults and dyke swarms generally follow the N110-N120° and N140-150° strikes. However, we recognized for the first time the existence of N050 sub-vertical faults and dyke swarms in both islands. Marques et al. (2014b) have proposed that the 1998 large earthquake North of Faial has been linked to strike-slip movement on a ENE-WSW fault. This fault is interpreted as the WSW termination of a transform associated with the TR. Prolongation of the inferred fault towards the NE reaches Graciosa Island, in a sector fitting fairly well with the location of the N070 dykes measured on the cliff of Quitadouro, and

with the scarp affecting the Serra dos Fontes old volcanic edifice (Sibrant et al., 2014; Chapter III). On S. Miguel, we measured several N050 dykes and faults in the central part of the island, in a sector close to the junction between two segments of the TR. These faults and dykes also can be reasonably attributed to the presence of a transform fault associated with the TR. In eastern S. Miguel, the elongation of the Nordeste Complex, and the linear canyons incised within its NE slope, are closer to N070. This direction is significantly oblique with the N050, but appears closer to the strike of the Gloria Fault farther East (Fig. VI.1), and is close to the present vectors of displacement proposed by DeMets et al. (2010).

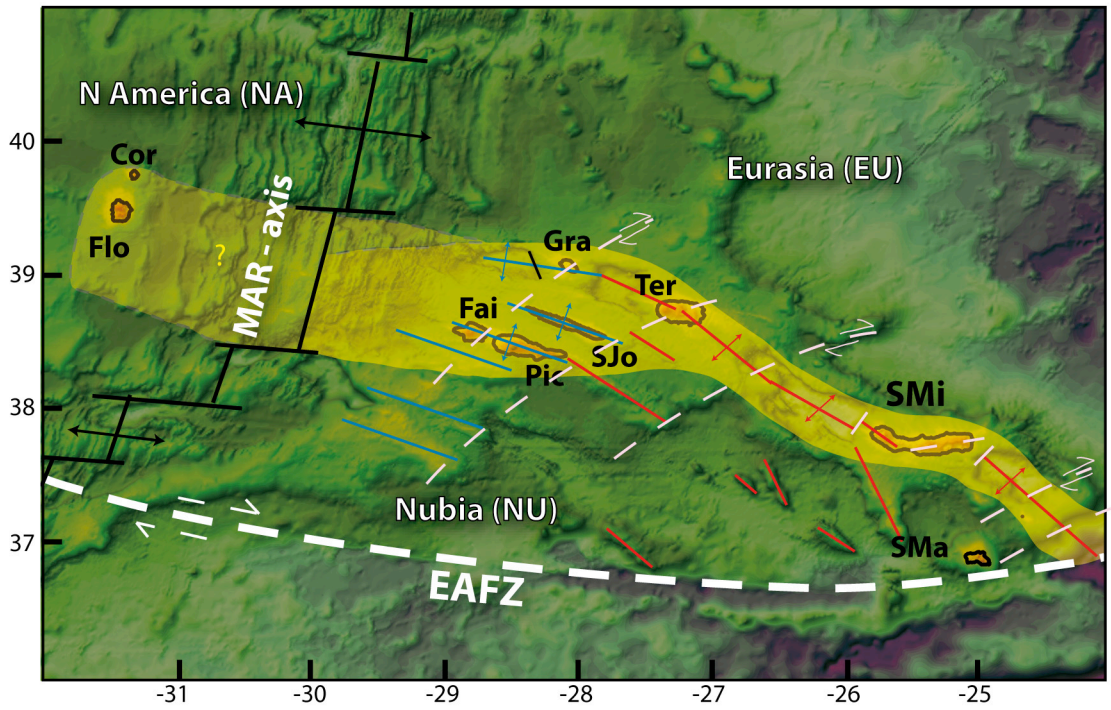


Figure VI. 1. Current volcano-tectonic model of the Azores Triple Junction and the Eu/Nu plate boundary in Yellow area (after Marques et al., 2013a; 2014a). The black dashed lines stand for the MAR axis and its spreading orientation. The white thick dashed line indicate the presently inactive EAFZ and its past kinematics. The blue and red lines indicate the N110-120° and the N150-N160° structural trends, respectively. The light pink dashed lines indicate the transform faults associated with the EU/NU relative plate motion. Cor: Corvo; Flo: Flores; Fai: Faial; Pic: Pico; SJo: São Jorge; Gra: Graciosa; Ter: Terceira; SMi: São Miguel; Sma: Santa Maria.

On each of the two islands here studied, major central volcanoes (Nordeste, Furnas and Fogo), have developed near the transform faults here inferred. In contrast, the edifices built inside linear portions of the TR mostly comprise alignments of basaltic strombolian cones (except Sete Cidades). In a similar fashion, Graciosa and Faial islands comprise large central volcanoes, which could well have developed at the intersection between the main direction of the TR (either N110 or N150) and the transforms associated with the TR.

At a larger scale, a similar pattern can be identified. The islands developed within sub-parallel linear segments of the EU-Nu plate boundary (especially in the diffuse area) are mostly narrow linear volcanic ridges, which closely follow the main strike of the EU/Nu boundary. In contrast, the volcanic islands developed close to the junction between several segments with contrasted orientation have more complex shape, as they are characterized by the existence of central type volcanoes. This is the case of Graciosa, Terceira, and S. Miguel.

The position of the islands with respect to these several lithospheric structures also shows a rather regular spacing (Fig. VI.1). The volcanic edifices built in the TR are separated by an average distance of ca 80-100 km. Similarly, the distance between the several parallel volcanic alignments in the central Azores appear to be regularly spaced, with the succession of the Princess Alice bank, Faial-Pico and S. Jorge linear volcanic ridges, and Graciosa Island. In fact, all the volcanism seems localized within extensional structures developed on the plateau, i.e. in zones where the structure of the thick plateau has been locally thinned by tectonic processes.

VI. 1. 2. Temporal evolution of the volcanism

In this thesis, we have reconstructed with a fairly good temporal resolution the volcano-structural evolution of two key islands located in the TR: Graciosa and S. Miguel. However, the several phases of volcanic construction and destruction of a given island may depend on a number of processes, including local melt production and extraction, intermittent storage in shallow magma reservoir, volcano deformation either by tectonic and/or gravitational processes, such as large landslides. As shown in the previous section, the location of each island seems intimately linked to the regional tectonic structures. Therefore, it is worth comparing the main episodes of construction of the islands at the regional scale, in order to examine if a first-order general pattern exists or not.

VI. 1. 2. 1. Description of the geochronological data

Previous geochronological studies on the islands developed east of the MAR axis have been carried out with various objectives. For instance, the work by Johnson et al. (1998) was focussed on a lava succession in S. Miguel to track the Brunhes-Matuyama palaeomagnetic inversion. This means that the following discussion is partly dependent on the sampling strategy. However, increasing effort has been paid over the last years to constrain in time the main phases of volcanic construction, especially in the central Azores, providing a robust first-order temporal framework for intra-archipelago comparisons.

Nevertheless, early K-Ar ages obtained on whole-rock samples (Abdel-Monem et al., 1975; Féraud et al., 1980; Féraud et al., 1981; Chovelon et al., 1982; Demande, 1982; Gandino et al., 1985; McKee and Moore, 1992) will not be considered here. Indeed, it has been shown recently that whole-rock analyses on porphyric basalts generally yield much older ages than K-Ar and $^{40}Ar/^{39}Ar$ on separated groundmass (Hildenbrand et al., 2012a; Sibrant et al., 2014; Chapter IV.1 and V). Such "too old ages" most likely result from the unsuitable incorporation of inherited excess ^{40}Ar trapped as fluid inclusions in mafic phenocrysts during crystallisation at a deep level in the magma chamber. Therefore, K-Ar ages on such whole-rock are in most cases significantly biased and are not representative of the eruption age at the surface. For this reason we used the 53 new K-Ar determinations on Graciosa, S. Miguel and Santa Maria presented in this work (Tables II.1, IV.1 and V.1), coupled with:

(1) 6 previous ages on Terceira (Hildenbrand et al., 2014), 11 on S. Jorge (Hildenbrand et al., 2008); 15 on Faial (Hildenbrand et al., 2012b, 2013a) and 31 on Pico Island (Costa et al., 2014; Costa et al., in prep) obtained with the same protocol of sample preparation, and the same analytical procedure (unspiked K-Ar, Cassignol-Gillot technique) at Lab. GEOPS (Orsay).

(2) 29 previous $^{40}Ar/^{39}Ar$ determinations; including 10 ages on Graciosa (Larrea et al., 2014); 7 ages on Terceira (Calvert et al., 2006); and 12 ages on S. Miguel (Johnson et al., 1998).

(3) 90 previous ^{14}C determinations; including 67 ages on S. Miguel (Shotton et al., 1969, 1971; Moore and Rubin, 1991) and 23 ages on Terceira (Calvert et al., 2006).

VI. 1. 2. 2. Evidence for coeval regional volcanic pulses

All these selected geochronological data are compiled in Figs. VI.2 and IV.4. They allow us to investigate the temporal recurrence of the main volcanic phases of construction on each island, and to examine how volcanic construction developed at the regional scale. The data are reported as a function of increasing distance to the MAR axis, in order to examine if age-progression eventually exists. We also indicate the dominant elongation of the main volcanic systems.

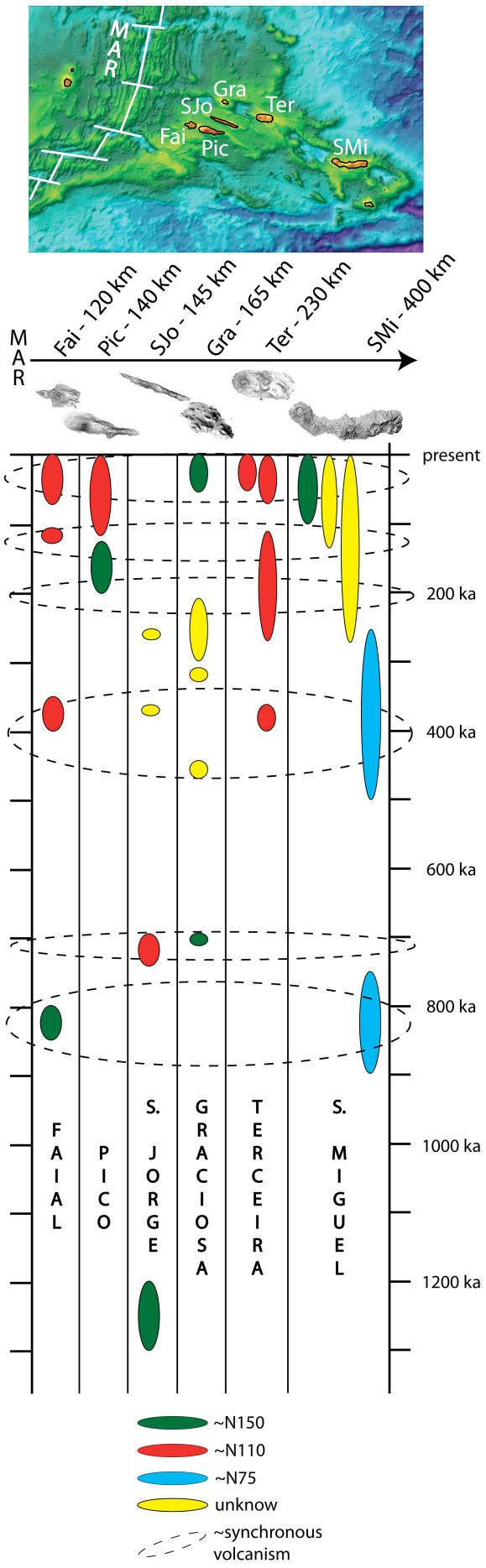


Figure VI. 2. Timelines summarizing the construction stages of the islands to the east of the MAR and active during the last 1.3 Myr (Johnson et al., 1998; Calvert et al., 2006; Hildenbrand et al., 2008; Hildenbrand et al., 2012b, 2013a; Costa et al., 2014; Larrea et al., 2014; Hildenbrand et al., 2014; Costa et al., in prep; this study). The position of the islands and the distances from the MAR-axis are indicate at the top of the timeline. Below is the legend for island orientation and synchronous volcanism.

From this graphic, several characteristics can be noticed:

(1) The majority of the construction stages occurred over rather short periods (less than 100 kyr), except on S. Miguel, where some episodes of volcanic construction lasted up to 200 kyr.

(2) There is no clear general age-progression of volcanic construction from the MAR-axis. In particular, an old stage of volcanism occurred in S. Jorge around 1.3-1.2 Ma, and volcanic episodes around 850 ka occurred in both Faial and S. Miguel.

(3) sub-aerial volcanism of comparable age occurred throughout the whole TR, and along the various structures of the present diffuse plate boundary.

(4) This generalized volcanic construction was not continuous in time, as long volcanic hiatuses (up to 300 kyr) can be noticed at the regional scale.

A closer examination reveals several synchronous stages of volcanic construction. These are shown with dashed ellipses in Fig. VI.2.

A first phase of sub-aerial volcanism can be identified between **850 and 800 ka** in both Faial and S. Miguel, i.e. along the southwestern border of the Eu/Nu plate boundary in the presently diffuse area, and along the easternmost wall of the TR, respectively (Figs. VI.1 and VI.2). These two islands are separated by ca. 300 km.

At about **700 ka** (Figs. VI.1 and VI.2)**,** a new stage of synchronous volcanism occured in the islands of S. Jorge (729 ± 11 to 690 ± 11 ka, from the base to the top of the southern central cliff, Hildenbrand et al., 2008) and Graciosa (702 ± 10 ka and 700 ± 10 ka, this study). S. Jorge and Graciosa are both localized in the western part of the diffuse plate boundary, outside and within the TR, respectively.

Between **400 and 350 ka (**Figs. VI.1 and VI.2), a relatively important sub-aerial phase of coeval volcanic construction occurred in S. Miguel, Faial, S. Jorge and Terceira islands. However, the oldest phases of volcanic construction of Pico Island have been constrained around 200 ka (Costa et al., 2013; Costa et al., in prep). Therefore, we cannot exclude submarine volcanic construction under Pico during the same period. The stage of extensive and intensive volcanism between 400 ka and 350 ka can be seen as a major pulse over the whole current diffuse plate boundary area. The volume erupted cannot be constrained accurately, but it has to be quite large, because volcanic construction represents

- a significant part of the filling volcanism in S. Miguel (this study),
- the whole eastern half of Faial (Hildenbrand et al., 2012b, 2013a),
- the northwestern part of S. Jorge (Hildenbrand et al., 2008) and;
- the whole eastern half of Terceira (Calvert et al., 2006; Hildenbrand et al., 2014).

We note that all this volcanism is basic in composition. This supports rapid melt production and extraction towards the surface, over lateral distances exceeding 300 km.

Around **200 ka (**Figs. VI.1 and VI.2), the volcanism was active in S. Miguel (range activity of Fogo volcano, this study), and in Graciosa island with the main phase of construction of the basaltic cover (Sibrant et al., 2014; see chapter II). This period also corresponds to the fast sub-aerial edification of the oldest part of Pico Island (Costa et al., in prep), and the construction of a trachytic dome on the northern flank of the Guilherme Moniz volcano in Terceira (Calvert et al., 2006). During this stage, the volcanism seemed more and more diffuse along the plate boundary, and expanded to Graciosa and Pico islands. At 200 ka, all the sub-aerial volcanic edifices had emerged.

Around **120 ka**, a new period of synchronous volcanism is indicated by our study, with the construction of Furnas, Sete Cidades and Fogo volcanoes (plinian activity) in S. Miguel. It also corresponds to the late activity of the Guilherme Moniz volcano in Terceira, with the eruption of thick trachytic lava flows (Calvert et al., 2006; Hildenbrand et al., 2014). In the Pico Island, this also coincides with the late activity of the older complex and take off of volcanic activity along the fissural system (Costa et al., in prep). At the same time, the large Caldera volcano developed fast in Faial (118 ± 3 ka, 118 ± 6 ka and 116 ± 3 ka, Hildenbrand et al., 2012b, 2013a). Therefore, once again, voluminous synchronous volcanism occurred over most of the present diffuse plate boundary. It is important to note that a significant part of the products erupted during this period are slightly evolved (trachytes), and involved both effusive and highly explosive activity. This suggests intermittent storage in shallow magma reservoirs under each island, possibly favoured by the load of the crust by the edifices developed earlier (e.g. 400 – 350 ka).

Finally, from ca **50 ka** to the **present day**, all the islands have been active, as indicated by the K-Ar and the $^{40}Ar/^{39}Ar$ ages and the numerous ^{14}C available ages, and the historic eruptions (Figs. VI.1 and VI.2). In S. Miguel this period includes major plinian eruptions in Furnas, associated with the production of ignimbrites in Sete Cidades (this study). In Graciosa, the SE central volcano is growing (this study), in Terceira it corresponds to the main construction of the Santa Bárbara volcano (Calvert et al., 2006, Hildenbrand et al., 2014). The two fissural systems in Pico also grew during this period (Costa et al., 2014; Costa et al., in prep). This period of time also corresponds to the eruption of basic products from several strombolian cones, and recent lava flows filling the graben of Faial and building the western end of the island (Hildenbrand et al., 2012b). Despite the very high precision of our new K/Ar ages, (relative uncertainty typically lower than 5% for most of the volcanic units here dated around 50 ka), radiocarbon data yield more precise ages for the Holocene period. Among the 26 historical eruptions reported in the Azores, 12 were subaerial and located in the islands of S. Miguel, Terceira, S. Jorge, Pico and Faial (França et al., 2003). The most

recent submarine eruptions were the Capelinhos in 1957-1958 to the west of Faial Island, and Serreta in 1998-2000, which occurred 8.5 km to the NW of Terceira Island (Gaspar et al., 2003). Therefore, from 120 ka to the present day, the volcanism has been partly synchronous in all the islands constituting the northern and the southern part of the Eu/Nu plate boundary, with extensive volcanism during the last 50 kyr.

VI. 1. 2. 3. Which process(es) trigger(s) the volcanism?

In oceanic intra-plate settings, linear chains of volcanic islands, like the Hawaii-Emperor chain (e.g. Wilson, 1963) or Cook-Austral volcanic chain (e.g. Duncan and McDougall, 1976; Bonneville et al., 2006) are classically attributed to the existence of stationary hot-spots associated with narrow (<100 km) mantle plumes. The linear character of these chains is generally attributed to the motion of the plate over a stationary hot-spot, yielding progressive increase in the age of volcanic construction, with increasing distance from the mantle anomaly.

Despite the aforementioned existence of a mantle anomaly under the Azores, the several pulses of coeval volcanic construction presented in the previous section do not support a clear age-progression over a narrow (<100 km) melting anomaly. However, it should be kept in mind that the absolute plate motion in the Azores is rather slow, close to 2 cm/yr towards the SSW (Gripp and Gordon, 2002), and that a shallow mantle anomaly evidenced from regional tomography is present under most of the Azores plateau.

Another hypothesis for the development of island chains in oceanic settings is the development of propagating fractures, due to stress transmitted from the plate margins (Smith, 2003, 2004; Natland and Winterer, 2005). For example, the en-echelon arrangement of volcanic ridges along the Pukapuka Seamount Chain (Winterer and Sandwell, 1987; Sandwell et al., 1995) support this tensional origin. The volcanic chain of the Line Islands also shows no progressive ages along its length, supporting a synchronous episode of volcanism (ca. 8 Ma) consistent with a mechanism of lithospheric extension (Davis et al., 2002). The development of such volcanic chains can also be caused by warps and cracks caused by uneven thermal contraction of the cooling lithosphere (Sandwell and Fiialko, 2004; Ballmer et al., 2007). Hieronymus and Bercovici (1999) showed that the measured spacing of volcanoes may also have some correlation with edifice volume, which induce bending of the lithosphere and control volcano spacing. In all these processes, the lithosphere elastic thickness and/or regional tectonics play a major role.

Based on compilation of GPS observations from sites in the Azores archipelago from STAMINA project (Navarro et al., 2003), SARAZORES project (Catalão et al., 2006), data in the public domain (EUREF, NGS, SOPAC, TRIGNET and UNAVCO), GPS campaigns on S. Jorge (Mendes et al. (2013), and seafloor morphology, Marques et al. (2013a, 2014a)

defined the volcanic and tectonic framework of the western end of the Eu/Nu plate boundary. They proposed that the Nubia-Eurasia plate motion in the Azores is accommodated by a wide zone of oblique extensional deformation limited by the MAR axis in the west, the northern shoulder of the TR in the north, and in the south, by a line that connects the MAR axis at 38.4°, 30.5°W (Fig. VI.1). However, they did not provide a time range for the initiation of the presently active diffuse plate boundary.

In the central and east Azores, the several regional volcanic pulses here evidenced at various epochs (between 850 and 800 ka, around 700 ka, between 400 and 350 ka, around 200 ka, 100 ka and during the last 50 kyr) indicate that the regional tectonics controlled, at least in part, melt production and magma ascent over an area exceeding 300 km in width. The volcanic pulses depend on the regional tectonics and lithospheric architecture, and, thus, the location of the volcanic eruptions may provide information on the evolution of the deformation along the Eu/Nu plate boundary.

It is important to note that the oldest volcanic phases in S. Jorge and Faial (between 1.3-1.2 Ma, and around ca 850 ka, respectively) led to the construction of N150 ridges and N150 dyke swarms, which do not follow the N110 pattern of recent volcanic construction in the central Azores. These old lavas also have distinctive geochemical signatures (Hildenbrand et al., 2008; 2014). Therefore, they most probably record a story of “oblique” deformation in the central Azores, prior to sudden re-localization of the volcanism along the present diffuse part of the Eu/Nu plate boundary (Fig. VI.3). This sudden reconfiguration also coincides in time with the development of the N075 elliptical Nordeste complex in eastern S. Miguel. If the latter follows a transform (see previous section), the sudden volcano-structural change evidenced in the central Azores may coincide in time with significant re-organization over the whole plate boundary in the Azores.

In fact, S. Miguel is active at each regional pulse of volcanism except around 750-700 ka, whereas volcanism in the central Azores (including Graciosa, this study) has greatly developed in the diffuse plate boundary (Central Azores) during the last 750kyr. This could reflect a rapid western propagation of lithospheric deformation. In such hypothesis, discrete rifting was first concentrated along the eastern part of the TR, and was followed rapidly by a westward generalization of the deformation in the form of diffuse rifting in the west.

The recurrence time of the synchronous volcanism appears to decrease over time, and shows a global time frequency multiplied by two at each synchronous pulse. This may result from an increasing effect of tectonic activity. Such increase could reflect the increasing maturity of the TR, once it has developed enough to accommodate along its entire length the differential motion between the Eurasia and the Nubia plates.

Because the deformation occurring along the Eu/Nu boundary plate is a first order indication of magma extraction, it should also influence the destruction events that have occurred in each island.

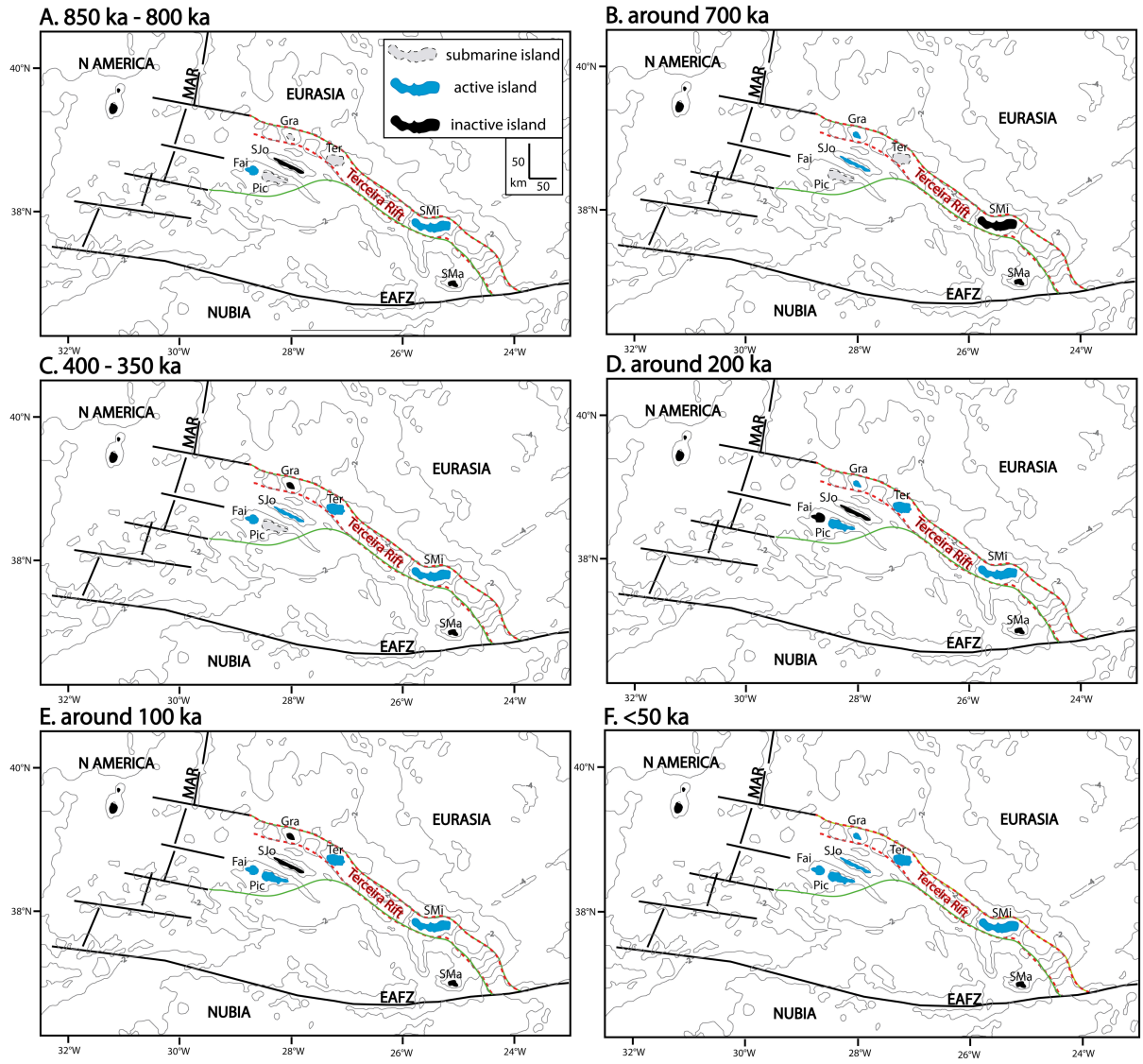


Figure VI. 3. Cartoon illustrating the synchronous phases of volcanic construction of the Azores islands localized east of the Mid Atlantic Ridge (MAR) axis. For each period, solid lines represent the MAR, and the East Azores Fracture zone (EAFZ). The red dashed lines indicate the location of the Terceira Rift, the green solid line the southern boundary of the diffuse plate boundary. The blue and black islands represent active and inactive volcanism, respectively.

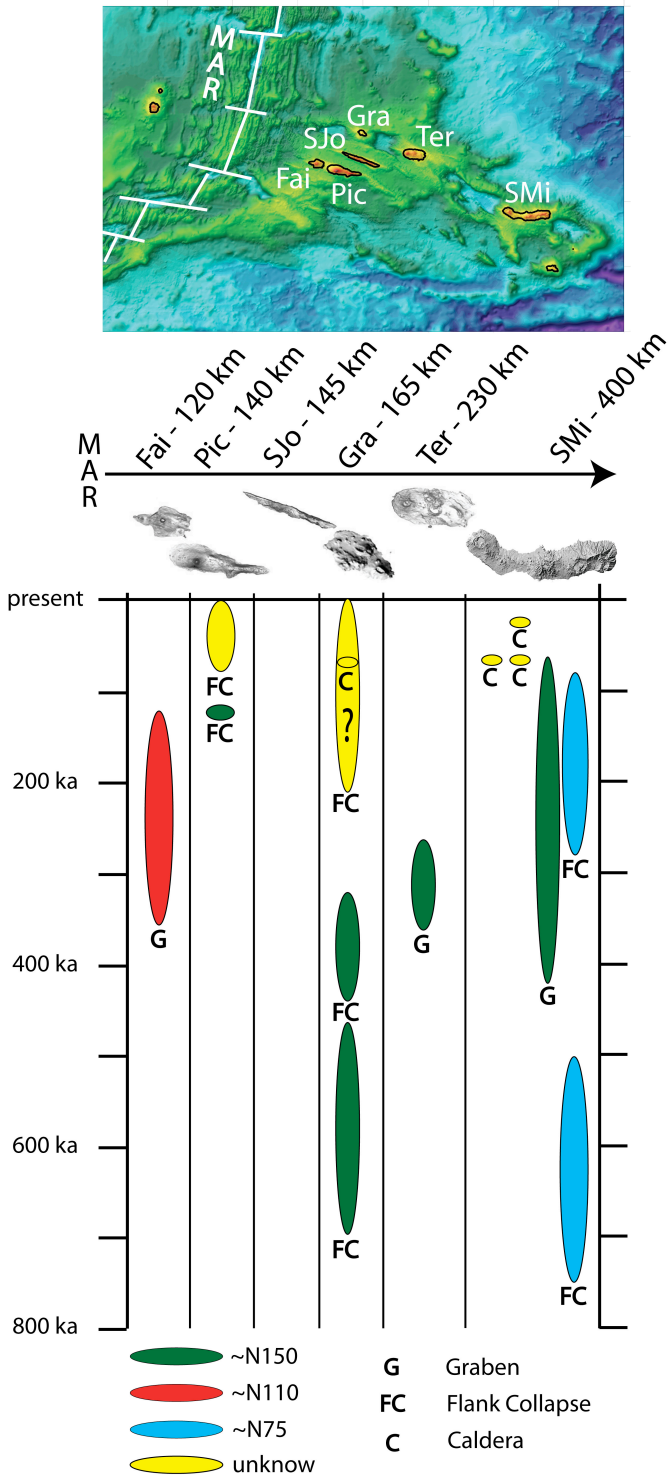


Figure VI. 4. Timelines summarizing the known destruction stages on the islands of Faial, Pico, Graciosa, Terceira and S. Miguel during the last 800 kyr. The time range of each destructive event is preceded by a letter indicating the nature of the destruction. (Johnson et al., 1998; Calvert et al., 2006; Hildenbrand et al., 2008; Hildenbrand et al., 2012b, 2013a; Costa et al., 2014; Larrea et al., 2014; Hildenbrand et al., 2014; Costa et al., in prep; this study).

VI. 1. 3. Age and meaning of the destruction processes

VI. 1. 3. 1. Gradual deformation: the graben structures

The existence of the TR, an active rift which partly accommodates the extension between the Eurasia and the Nubia plates should, at a smaller scale, induce the

development of graben structures in the islands localized in the TR, but also along the diffuse EU/NU plate boundary.

Two new graben structures have been identified on S. Miguel. They are oriented N110 and N150°, which is consistent with the orientation of the structural trend measured on faults and dykes in the island. The first graben we identified has developed close to the village of Água Retorta, and is elongated N110 (Chapter IV, Figs. IV.20 and IV.22). The faults bounding the graben affected lavas from the upper part of Nordeste, locally dated at 765 ± 11 ka and 750 ± 11 ka. This graben comprises a morphological crest oriented roughly N25°. This is more or less parallel to the scarp inherited from the main flank collapse, which indicates that the graben is probably younger than the flank collapse, itself dated between ca. 750 and 500 ka (Fig. VI.4).

The second graben on S. Miguel was identified in the area around the village of Povoação, on both sides of the main basin outlet (Chapter IV, Figs. IV.21 and IV.22). The graben has a dominant N150 direction, and cuts rocks here dated at 434 ± 7 ka (SM12E). It is additionally partially filled by a massive ignimbrite dated at 60 ± 1 ka (SM12AJ). As the ignimbrite does not show apparent signs of deformation along the graben wall, we can reasonably infer that the graben formed between ca. 434 and 60 ka, though more recent activity cannot be excluded. We note that the N150 trend on S. Miguel is similar to the TR trend (N130) in the south.

During a similar period of time, a conspicuous N110° graben formed in Faial (Hildenbrand et al., 2012b, 2013a). The top of the volcanic succession truncated by the northern fault of the graben has been dated at 389 ± 7 ka (FA10D), providing a maximal age for the initiation of the graben. The graben is partially filled by recent lavas and shows very recent activity, down to historical time (Hildenbrand et al., 2012b; Trippanera et al., 2013 Marques et al., 2014b). The N110 trend is consistent with the elongation of the LVRs in the diffuse plate boundary, and parallel to the TR further north.

Finally, in Terceira, a graben with a N140 trend affects the oldest volcanic succession exposed in the NE part of the island (Calvert et al., 2006; Navarro et al., 2009; Hildenbrand et al., 2014). The age determinations on the rocks at the top of the NE wall of the graben and affected by the graben constrain its initiation after 370 ± 6 ka (Fig. VI.4). The seismicity shows that the graben is still active. The N140 trend of the graben is parallel to the orientation of the TR on the southern part of Terceira and almost perpendicular to present extension.

From our new data, and available geochronological constraints, it appears that in the same period of time several grabens developed on 3 different islands. We are aware that such structures do not form instantaneously and grow over relative large temporal scales.

Nevertheless, several authors have proposed that such grabens are intimately linked to the fast volcanic construction, e.g., when emptying of a magma chamber triggers deflation of the edifice, triggering vertical collapse (e.g., MacDonald, 1982; Hildenbrand et al., 2012b; 2013a).

VI. 1. 3. 2. Large catastrophic flank collapses

The construction stages and the gradual development of tectonic structures during the last hundreds of kyr seem intimately associated with the activity of the Eu/Nu plate boundary, especially along the TR. What about the catastrophic events? Were they also influenced by the hyper-slow extension regime between the Eu/Nu plates, or are they only induced by purely gravitational destabilization?

During this PhD thesis, we newly identified 9 large-scale flank collapses: 2 on S. Maria, 3 on S. Miguel and 4 on Graciosa.

Most of them appear to have occurred in a catastrophic way. Their possible age is reported on Fig. VI.4. Two of these flank collapses have occurred in similar time intervals. Indeed, the sub-aerial part of the Nordeste volcano was affected by a flank collapse occurring between ca. 750 and 500 ka. In the same time interval, we have shown that the Serra das Fontes complex in Graciosa was affected by a destructive event toward the SW between ca. 700 ka and 470 ka. Each of the events is not so well constrained in time. The possible temporal window for their occurrence is fairly large (ca 250 kyr) and is equivalent, for sake of comparison, to the whole period of Pico sub-aerial evolution. Nevertheless, we cannot exclude that they could have been coeval. Synchronous catastrophic flank collapse events have been already described in other oceanic archipelagos, especially in the Canary Islands (Ancochea et al., 1990; Carracedo et al., 1999a; Boulesteix et al., 2013).

Numerous local factors can trigger flank instabilities on volcanic islands: the presence of weak layers in the volcano (e.g. Ancochea et al., 1994; Thompson et al., 2008), which induce spreading in the volcano (e.g. Walter and Troll, 2003), focus of magma ascent along rift zones (Carracedo, 1994; Masson et al., 2002; Hildenbrand et al., 2004) and dike intrusion (e.g. Elsworth and Voight, 1995). In the cases of Graciosa and S. Miguel, we note that both collapse episodes were triggered towards the South, and initiated close to the main northern wall of the TR. Therefore, it seems plausible that both were generated/triggered by major earthquakes along the master faults of the TR. The position of Graciosa and S. Miguel (especially Nordeste complex) closer to the northern wall of the Rift can explain why most flank collapses have occurred towards the S-SW, depending on the local trend of the TR.

On S. Miguel (Fig. VI.4), we have proposed that the southern flank of Fogo has been removed by a flank collapse towards the south, and along a close to W-E scarp, between 270 and 85 ka. Sete Cidades has been also affected by a flank collapse toward the NE between 91 and 72 ± 2 ka ages of the filling volcanism.

The orientation of these two collapses in a W-E and close to N150° are respectively the elongation of the S. Miguel and one of the two main structural trends recognized in the Azores. Therefore, we cannot exclude that the location and triggering of these two collapses have been influenced by ground motion associated with earthquakes generated along the faults of the TR. This is also consistent with the direction of the collapses occurring in Graciosa. Indeed, the Baía do Filipe Complex developed between at least 472 and 433 ka and was affected by a major flank collapse toward the SW, so along a close to N160° trend. The Serra Dormida Complex and the younger basaltic cover complex were then affected by a new sector collapse toward the SW. These last two flank collapses also apparently initiated along a close to N160° trend. We suggest that the flank collapses have been triggered by earthquakes along the faults of the TR.

The last flank collapse identified in Graciosa occurred before 60 ka ago. The SE dipping lava flows of the Serra das Fontes complex (700 ka) are missing and occupied by the young SE central-type volcano (60 ka). In between the two volcanoes, a clear N40° scarp is visible. We infer that this scarp is a flank collapse scar, which is also visible on the available bathymetry and so indicates a structure bigger than the island.

This N40° strike of the scarp is almost perpendicular to the main orientation of the TR and, before this study, this direction was not a common direction described in the Azores. Nevertheless, it does not seem isolated in the Azores. Indeed, several faults and dykes oriented N50 were measured in S. Miguel (Chapter IV.2), and also in Faial island (Marques et al., 2014). Moreover, the focal mechanisms of earthquakes near the island of Faial, between Graciosa and Terceira islands (NE of S. Jorge Island), and between the islands of S. Miguel and S. Maria show two sub-vertical nodal planes, one of them is oriented N50-N55°E (Borges et al., 2007). As mentioned in Chapter IV.2, and the previous sections, the N50 faults are localized between the islands or where the direction of the TR changes (Fig. VI.1). According to DeMets et al. (2010), the N50 is a transform trend, which accommodates the differential motion between the Nubia and the Eurasia plates.

VI. 1. 3. 3. Caldera collapses

Numerous caldera collapses affected various central volcanoes in the Azores, and have been generally associated with large differentiated pyroclastic eruptions. This is particularly true in S. Miguel and Graciosa. The formation of a caldera collapse is generally attributed to the sudden emptying of a magmatic chamber (e.g. Lipman, 1997). Such process may thus be due to the local structure and intrinsic evolution of each volcano. Nevertheless, as we saw, the main eruptive phases have been closely linked with the deformation occurring along the Eu/Nu plate boundary, and so the role of regional tectonics cannot be excluded. The age of the episodes of caldera development are also shown on Fig. VI.4.

Around **60 ka**, 2 caldera collapses occurred in S. Miguel and 1 in Graciosa. The Furnas volcano (S. Miguel) experienced a plinian eruption producing a massive ignimbritic flow, which has been associated by Duncan et al. (1999) to a caldera collapse. During this PhD we dated the ignimbrite at 60 ± 1 ka, which therefore constrains the age for the caldera collapse. Sete Cidades volcano (S. Miguel) also has been affected by several caldera events identified by Queiroz et al. (2008). These authors propose that the 3 massive paroxysmal eruptions have produced 3 independent events of caldera formation at 36 ka, 29 ka and 16 ka, based on associated deposits found in the wall of the current caldera. During our work, we newly identified a dense ignimbrite flow on the northern outer flank of the volcano. The rock covered by the ignimbrite flow has been dated at 64 ± 2 ka. This suggests that a previously unrecognized caldera event occurred between 64 and 36 ka.

The SE volcanic complex on Graciosa has been dated younger than 59 ± 19 ka (Larrea et al., 2014). Its NW-SE elliptical summit has been identified as a caldera structure by Gaspar (1996). The caldera was later filled by a lava lake. We collected a basaltic sample in the wall dated at 44 ± 5 ka. Thus according to these data, the caldera event in Graciosa occurred between 59 and 44 ka.

The several caldera collapses here discussed apparently occurred over the same period of time. They affected 3 volcanoes from 2 islands separated by 240 km, and both developed within the TR. Therefore, we propose that, at least part of the caldera collapses and plinian eruptions in the Azores have been triggered by short episodes of regional deformation linked to the recent accommodation of the Eurasia and Nubia plate motions.

Conclusions on the Eu/Nu plate boundary during the last Myr

The distribution of the volcanism, the episodes of magma ascent/melt extraction, and the various stages of destruction (either gradual or catastrophic) on Graciosa, S. Jorge, Faial, Pico, Terceira and S. Miguel have been largely controlled by regional tectonics associated with the evolution of the western portion of Eu/Nu plate boundary during the last 1 Myr. This also means that studying the architecture and volcano-tectonic history of such islands provides valuable insights into the evolution of deformation near the eastern branch of the ATJ. So the next question is: Where was the Eu/Nu plate boundary before 1 Ma? What about the volcanism of Santa Maria Island?

VI. 2. The Nu/Eu plate boundary before the TR

VI. 2. 1. Introduction

The history of the EU/NU boundary is still greatly debated (Fig. VI.5). Immediately to the east of the Azores region, the EU/NU boundary presently comprises a dextral transcurrent fault called the Gloria Fault (GF). Some time in the past, the GF was connected to the MAR by an active fault on the southern edge of the Azores plateau, and together were called the East Azores Fracture Zone (EAFZ) (Laughton et al., 1972). However, the western portion of the EAFZ, from the Gloria Fault to the MAR-axis, seems presently seismically inactive and thus not anymore part of the EU/NU boundary (e.g. Krause and Watkins, 1970; Searle, 1980). The current plate boundary is along a diffuse area in the west, and coincides with the TR in the east (Marques et al., 2013a, 2014a). It is now accepted that the westernmost part of the Eurasia-Nubia plate boundary migrated northward, from a transform fault, the EAFZ, to partly an active oceanic rift, the Terceira Rift (TR). The Santa Maria Island (SMa) in the Azores is a key target to examine how such transition may have occurred, because it sits close to the junction between the EAFZ and the TR.

Searle (1980) proposed that the triple junction migration to the north occurred suddenly during the rearrangement of plate poles, which induced the transfer of the Azores wedge from the European plate to the Nubian plate. But depending on the authors, rifting along the TR is proposed to have started ca. 45 Myr ago (Krause and Watkins, 1970), ca. 36 Myr ago (Searle, 1980), during the last 25 Myr (Luis and Miranda, 2008), less than 5 Myr ago (Luis et al., 1998), or even less than 1 Myr ago (Vogt and Jung, 2004). A long duration would imply that the TR was also active during the EAFZ activity, while a short TR activity would result in a quick migration from the EAFZ to the TR.

In this part of the study, we investigated (1) whether the TJ has migrated in one jump from EAFZ to TR, or in several gradual steps, and (2) when it has happened. For Vogt and Jung (2004), the migration from the EAFZ to the TR involved successive NE jumps of oblique spreading axes, due to the motion of the plate boundary over a (fixed) Azores hotspot. These authors identified several linear volcanic ridges visible on the bathymetric charts, and proposed that these structures constituted plausible candidates for fossil transient plate boundaries. One of these, in particular, passes through the island of S. Jorge and follows to the SE along volcanic ridges to the west of SMa (Fig. VI.5). As we have seen before, the volcanism and the islands can be used to track the main regional tectonic deformation. All

the eastern islands are dated at less than 1.3 Ma (Hildenbrand et al., 2008), with the exception of SMa, which seems to have developed independently of the current EU/NU plate boundary.

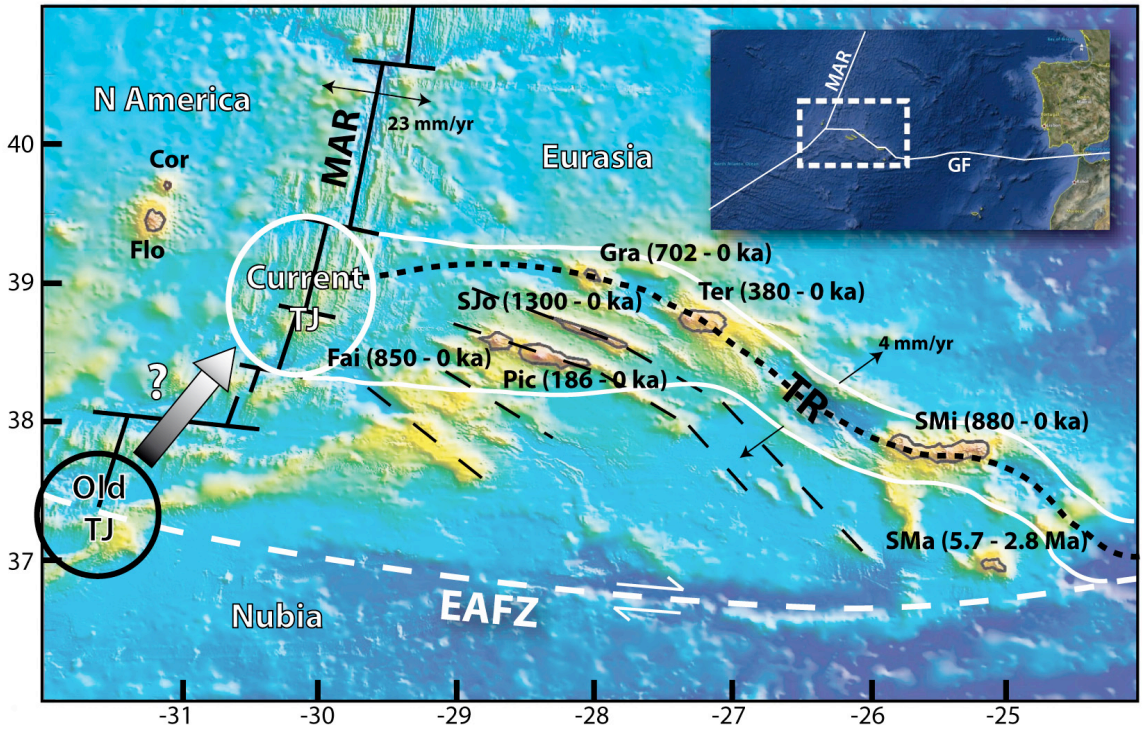


Figure VI. 5. Bathymetric map of the Azores and geochronological data on volcanic rocks from the eastern and central islands (Féraud et al., 1980; Costa et al., in prep; Johnson et al., 1998; Calvert et al., 2006; Hildenbrand et al., 2008; 2012b; this study). The thicker black lines indicate the location of the Mid-Atlantic Ridge (MAR) which separate the N America- Eurasia plate and the N America – Nubia plate. The white lines are the current Eurasia/Nubia diffuse plate boundary from Marques et al. (2013a, 2014a). The black dashed lines indicate the location of the Terceira Rift (TR), and the white dashed line indicates the East Azores Fracture Zone (EAFZ). The thin black dashed lines indicate the fossil plate boundaries after Vogt and Jung, (2004). Inset shows the location of the Azores archipelago in the Atlantic Ocean.GF: Gloria Fault; Cor: Corvo; Flo: Flores; Fai: Faial; Pic: Pico; SJo: São Jorge; Gra: Graciosa; Ter: Terceira; SMi: São Miguel; SMa Santa Maria.

VI. 2. 2. Summary of the Geology of Santa Maria Island

From morphologic, stratigraphic, tectonic and new high-precision K-Ar data, we constrain the volcanic activity of Santa Maria between ca. 5.7 and 2.8 Ma. The history of Santa Maria is marked by two phases of fast volcanic growth (5.7 to 5.3 Ma, and 4.3 to 3.9 Ma), with the construction of two large shield volcanoes, separated by a large-scale flank collapse between 5.33 ± 0.08 Ma and 4.32 ± 0.06 Ma. A second sector collapse occurred around 3.60 Ma, which removed a great part of Santa Maria. The most recent volcanic

activity in Santa Maria is represented by Parasitic strombolian Cones unconformably siting on top of the younger volcanic complex, up to at least 2.8 Ma ago (See Chapter V).

VI. 2. 3. Identification of a transient graben through SMa and parallel to the TR

In order to better evaluate the hypothesis of a transient graben going through SMa, we used the bathymetric chart of Lourenço et al. (1998) and the gridded global gravimetry database of Sandwell and Smith (2009) to examine the large-scale morphology of the TR, and discuss the probable fossil boundary between EU and NU passing through SMa. The TR presently does not have a straight shape, instead it has the shape of a sigmoid, which shows an orientation varying between N80° and N130°. A topographic profile along the TR (Fig. VI.6) shows a series of peaks corresponding to volcanic islands and major seamounts, which alternate with lows that correspond to deep basins. Gravimetrically (Fig. VI.7), the islands and seamounts show a positive anomaly (colour range from red to orange), while basins show a negative anomaly (colour range from dark blue to yellow-green). A detailed bathymetric analysis of the SW part of Graciosa has revealed a succession of horsts and grabens (Figs. VI.8, VI.7), which Marques et al. (2013a, 2014a) have coined the S. Jorge graben, the S. Jorge-Faial horst, and the Faial-Pico half-graben (Fig. VI.8). Besides this horst-graben structure, Marques et al. (2013a) recognized a series of aligned trapezoidal basins connecting the western part of the TR to the MAR. The topographic profile shows basin depths ranging from 2000 to 3200 m, with increasing depth toward the southeast. The profile also shows that the succession of islands and basins along the TR has a rather regular spacing of about 80 km, from the Graciosa Island to the junction of the TR with the EAFZ (Fig. VI.6).

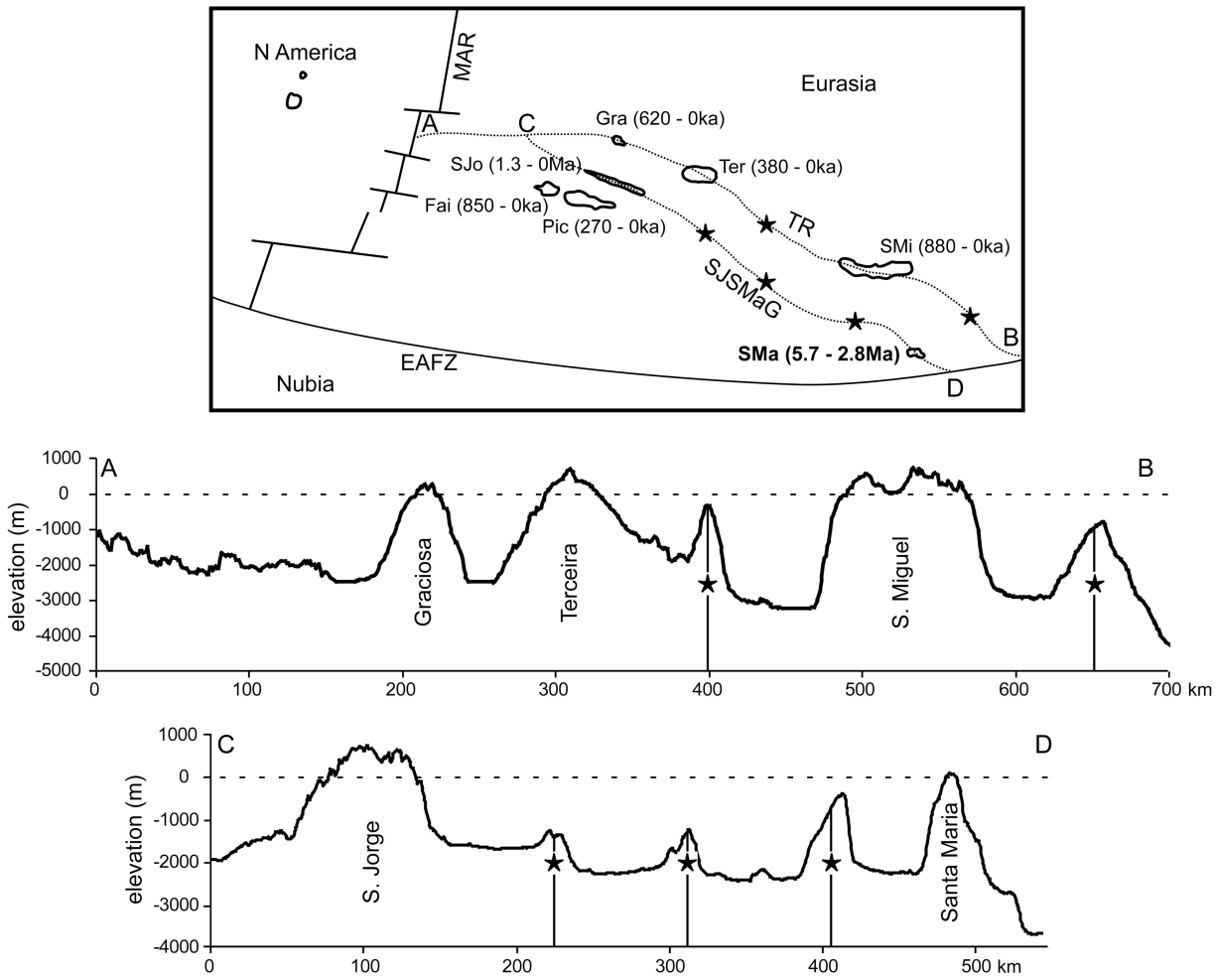


Figure VI. 6. Upper panel: Simplified map of the Azores archipelago. The black star indicates the position of seamounts. Black solid lines indicate the location of the MAR and the EAFZ. Dashed lines show the position of the TR, and the S. Jorge-SMa Graben (SJSMaG). A, B, C and D show the location of the cross sections shown in the lower panel. (AB) is a cross section along the TR and (CD) is a cross section along the S. Jorge-SMa Graben. Note the regular spacing between the islands and seamounts on both cross sections. Within each rift, available ages suggest a migration of the volcanic construction from southeast to northwest.

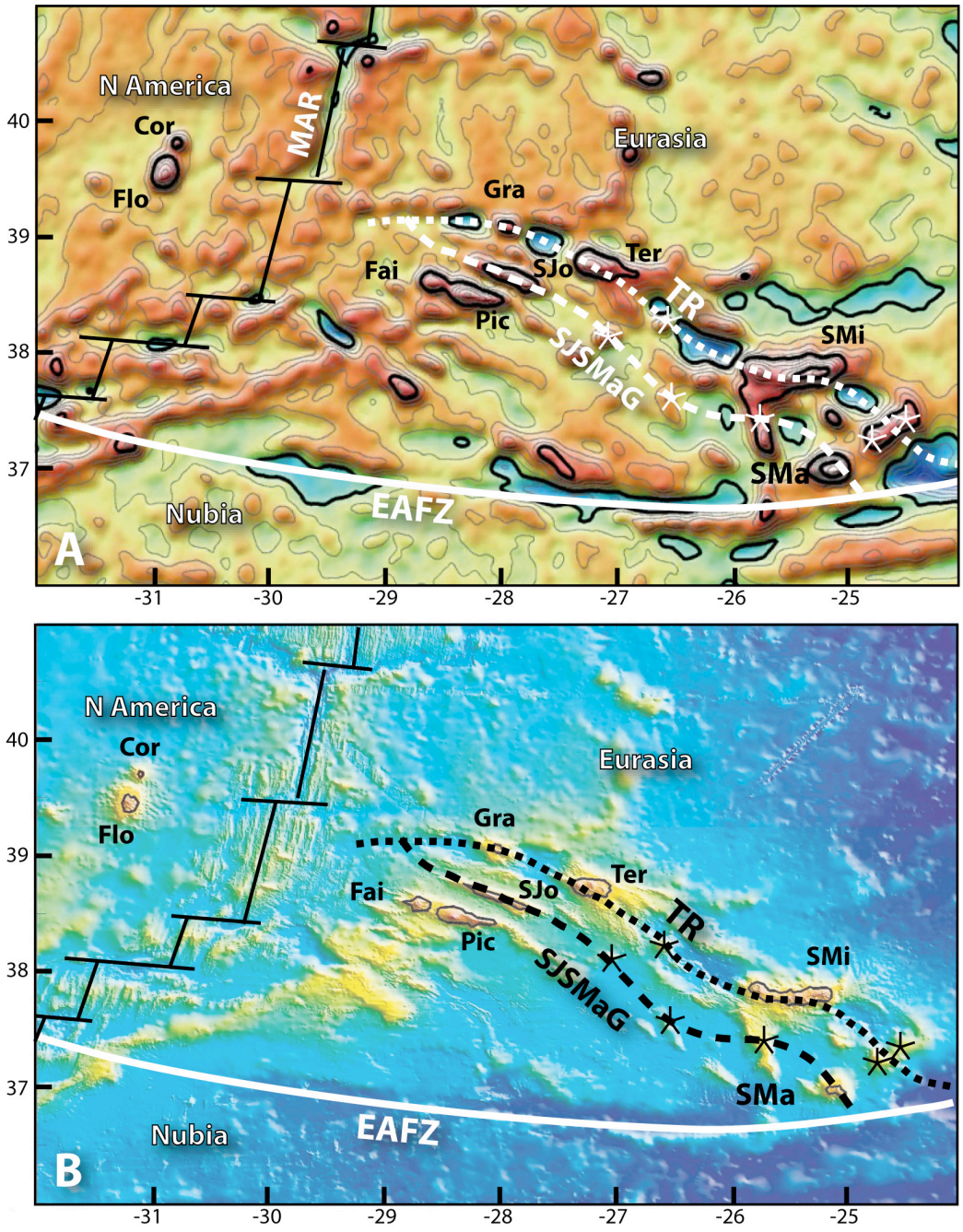


Figure VI. 7. (A) Free-air gravity anomaly map (contour interval of 20 mGal) from Sandwell and Smith (2009). The black dashed line indicates the location of the Mid Atlantic Ridge (MAR). The white full and dashed lines indicate the location of Eurasia-Nubia plate boundary over the time including the location of the newly recognized S. Jorge-Santa Maria Graben (SJSMaG). (B) Bathymetric map of the Azores. EAFZ: East Azores Fracture Zone; MAR: Mid Atlantic ridge; GF: Gloria Fault; Cor: Corvo; Flo: Flores; Fai: Faial; Pic: Pico; SJo: S. Jorge; Gra: Graciosa; Ter: Terceira; SMi: São Miguel; SMa: Santa Maria. The stars indicate the positions of the seamounts.

SMa shows a positive gravity anomaly (red colour), and is surrounded to the west, north and east by negative gravity anomalies (blue colour) that correspond to basins, as recognized on the bathymetric map (Fig. VI.7). The basin to the west of SMa is bounded in

the northwest by another positive gravity anomaly (seamount), which in turn is followed by a basin in the west. Thanks to both gravity and bathymetric maps, one can recognize this pattern of alternating basins (from blue to green) and islands/seamounts (red to yellow green) stretching from SMa towards the S. Jorge Graben, a pattern very similar to that of the TR, although shallower. The basin boundaries are partly exposed in zones not covered by volcanism and/or sediments. They seem to be made of well developed scarps trending N130° and N110°, which have the appearance of normal fault scarps (Fig. VI.8). This is particularly clear at the western end, which comprises the conspicuous S. Jorge Graben described by Marques et al. (2013a, 2014a), but also at the eastern end where SMa and neighbouring deep basins dominate. Similarly to the TR, the lineament between S. Jorge and SMa has a sigmoidal shape. It seems like a TR translated to the south, although with shallower depths. A regular wavelength can be recognized along the lineament (~80 km), and the depth of the basins increases from 1700 to 2200 m towards the east. All these observations taken together lead us to propose that the lineament between S. Jorge and SMa is an old graben (rift), and we call this newly recognized structure the S. Jorge-Santa Maria Graben (Fig. VI.8). The S. Jorge-Santa Maria Graben appears to have been a transient structure which aborted, and therefore did not evolve into a full rift like the current TR.

A major disadvantage of such aborted rifts is that they lack many of the characteristics of active rifts, e.g. the seismicity and a well developed geometry, including well-identifiable rift walls. The low-resolution of the available bathymetric grid (1km) and the absence of seismic profiles and sediment cores, especially, limit the full characterisation of the newly proposed graben. The depth of the basins along the S. Jorge-Santa Maria Graben is smaller than the depth along the TR, but we cannot ignore that the sediment thickness in the much older S. Jorge-Santa Maria Graben can be significantly greater than the sediment thickness in the TR. According to Searle (1980), the sediment thickness can be > 500 m in the older parts of the Azores plateau. The gravity data also show a similar pattern between the two structures, but the different anomalies identified along the S. Jorge-Santa Maria Graben points to a more variable and generally higher sediment thickness accumulated in the basins (Fig. VI.7), which is consistent with the younger age of the TR.

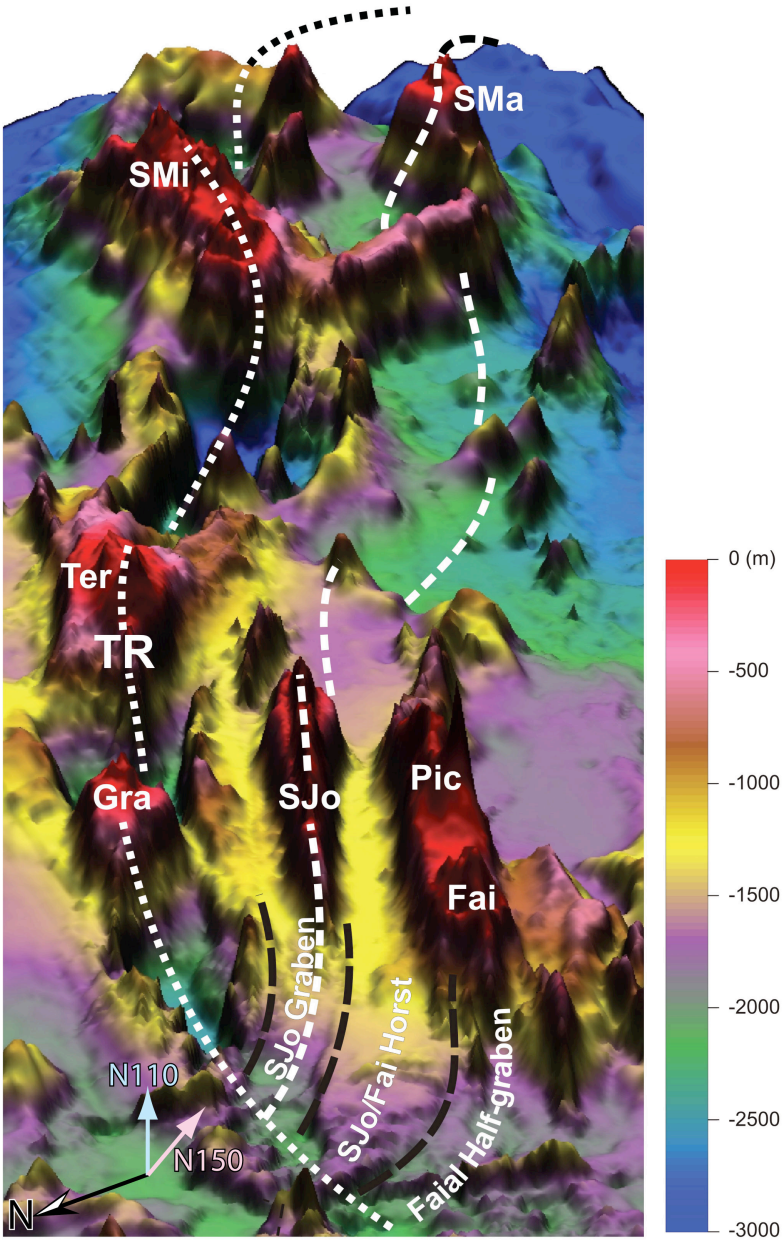


Figure VI. 8. 3D bathymetry (Lourenço et al., 1998) near the present diffuse triple junction. The black dashed lines define graben boundaries.

Assuming that SMa's existence is due to rifting in the S. Jorge-Santa Maria Graben, then: (1) SMa has a relationship with the S. Jorge-Santa Maria Graben similar to that of the S. Miguel Island with the TR, which is the oldest island in the TR (880 ka, Johnson et al., 1998); (2) the age of SMa's volcanism constrains the age of the S. Jorge-Santa Maria Rift in the south; (3) the new K-Ar ages in SMa constrain the lifetime of the S. Jorge-Santa Maria Rift between ca. 6 and 2.8 Ma in the south.

The S. Jorge Island has been dated between 1.3 and 0.27 Ma by Hildenbrand et al. (2008), and is still active, which means that the differences in age measured in SMa and S. Jorge could be the result of gradual opening of the S. Jorge-Santa Maria Graben from the southeast (older) to the northwest (younger and still active). The gradual decrease in basin

depth from southeast to northwest (Figs. VI.7, VI.8) also suggests gradual opening towards the NW. This architecture and age relationships are very similar to the ones found in the active TR.

VI. 2. 4. From the EAFZ to the TR

In a setting like the ATJ, a variation in configuration of one branch of the TJ suggests that plate motion changed, and/or that the EU/NU plate boundary changed. From our data, such reorganization occurred at least 5.7 Ma ago (Fig. VI.9B). It is now quite consensual that this boundary has jumped from the EAFZ to the TR, but how it had happened was still unknown. The present work indicates that the jump may have occurred by steps, i.e. by the opening of transient rifts, like the S. Jorge-Santa Maria Graben, till the present-day position (Fig. VI.9B1). The great similarity between the TR and the S. Jorge-Santa Maria graben, in terms of shape, wavelength between islands/seamount and basins, and depth of basins, indicates that the regional stress occurring now is similar to the one that produced the S. Jorge-Santa Maria Rift. Subsequently, rifting jumped en echelon from the S. Jorge-Santa Maria Graben to the TR (Figs. VI.9B2, VI.B3).

As we saw in chapter 2, the linear volcanic ridges that define the internal morpho-structure of the plateau seem to be sub-parrallel to the Eu/Nu plate migration path and to the current Terceira rift segmentation pattern. Three different mechanisms can be proposed to justify the migration and the rifting of the TR and Eu/Nu plate boundary:

(1) opening and reactivation of fracture zones of the MAR axis;

(2) synchronous opening due to the Azores hotspot migration northward (Vogt and Jung, 2004); and

(3) synchronous growth due to Azores hotspot migration and Azores Triple Junction migration in response to internal fracturing and weakness of the plateau.

Reactivation of MAR fracture zones in the Azores plateau seems a plausible explanation for the linear volcanic ridge trend close to the MAR (~N100-120°E trend) given their orientation (Fig. VI.1), but seems to be less applicable to the linear volcanic ridges farther to the east. Indeed, it would correspond to a ca. 20° clockwise rotation (clockwise of the Azores plateau from the MAR). Furthermore Eu/Na spreading direction has been fairly uniform since at least 10 Ma to the present (Luis et al., 1994). Such block rotation should develop some compressive zones which are to our knowledge not described or visible across the plateau.

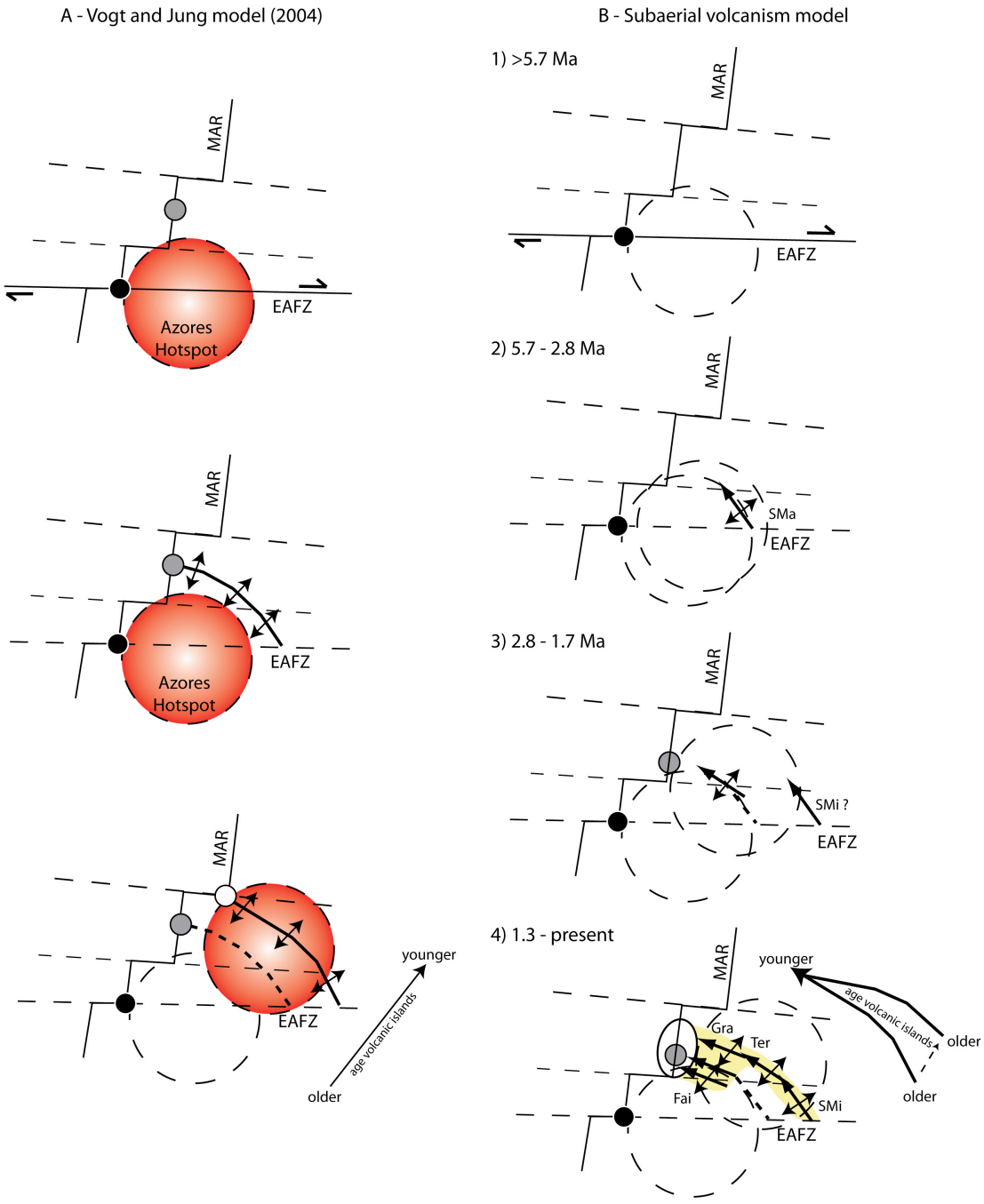


Figure VI. 9. Azores Triple Junction migration model. (A) Vogt and Jung model (2004) based on the plate boundary successive jumps over the Azores hotspot (B) Our new Azores Triple junction migration from subaerial volcanic evidences. The yellow area indicates the Eu/Nu plate boundary. The black, grey and white circles indicate the old, intermediate and current position of the Azores Triple Junction.

The second hypothesis (Fig. IV.9A) implies a northeast oriented age progression of the volcanic island as a response to the migration in the same direction of the Azores hotspot according to Vogt and Jung (2004) model. These authors consider, by comparing the strikes

of the volcanic ridges across the plateau that the linear volcanic ridges are traces of failed rifts either spreading obliquely (close to the MAR) or normal (farther to the east) to the main MORVEL model (DeMets et al., 2010). Those authors propose a mechanism to justify both the migration of the plate boundary and the arcuate shape of the volcanic islands, where thickening of the crust could have caused a zone weakening near the edge of the spreading boundary and its relocation northwards. This mechanism remains valid at a broader scale, to explain northward migration of the Triple Junction, but the ages of the volcanic islands provided here do not fit to their main observations.

Finally, the third hypothesis that we favour is close to the model proposed by Vogt and Jung (2004). Vogt and Jung propose a migration parallel to the boundary and spreading, whereas our model implies a migration in segmentation, from the east to the west (Fig. VI9B), and without significant creation of new crust (spreading) along the rift. Indeed, the volcanic activity stopped at ca. 2.8 Ma in SMa, at the southeastern end of the S. Jorge-Santa Maria Graben, but is still active in S. Jorge, at the northwestern end. At the southeastern end of the TR, volcanism in the S. Miguel Island has been active since at least 0.9 Myr (Johnson et al., 1998), which means that the western part of the S. Jorge-Santa Maria rift was still active while the TR was opening in the southeast (Fig. VI.9B3). Therefore, the jump was not simultaneous and discrete, as both the TR and the northwestern sector of the S. Jorge-Santa Maria Graben have been active during the last 1 Myr (Fig. VI.9B4). We also note that the subaerial volcanic phase in Faial is as old as 850 ka. Moreover, a lava sample dredged on the submarine ridge east of Pico was dated around 1.5 Ma (Beier, 2006), which is similar to the age of S. Jorge's oldest ridge. This suggests that the Pico-Faial ridge and the western end of the S. Jorge graben were active at the same time. In other terms, we can suspect that the western part of the EU/NU close to the MAR was already diffuse, as the current plate boundary (Marques et al., 2013a, 2014a).

We conclude that the progressive migration from one rift to the other was more discrete in the southeast than in the northwest. This is also consistent with the present deformation, as geodetic measurements in the central Azores show that the western EU/NU boundary is diffuse (Marques et al., 2013a). The asymmetric axis of the TR identified in Chapter (IV.2) can be explained by successive migration of the Eurasia-Nubia plate boundary from the EAFZ to the current TR. From the youngest age here measured in SMa, we propose that the rift migration, in the south, from the S. Jorge-Santa Maria Graben to the TR initiated prior to ca. 2.8 Ma. Initiation of the Azores rifts may have occurred during the re-organisation of plate poles, that is at least 5.7 Ma, with an RRF triple junction (EAFZ as transcurrent fault) changing to the current RRR triple junction, thus transferring a wedge of

European plate to the Nubian plate as suggested by Searle (1980). As triple junction migration proceeded, older sections of the linear volcanic ridges have been progressively abandoned as failed rifts of the distributed plate boundary. Moreover, this becomes progressively focalized along the TR and a larger area of distributed deformation is created further west. Contrary to what is referred by Vogt and Jung (2004), we consider that the morphological transition between volcanic islands with a regular spacing can have tectonic and crustal implication. Under the influence of the Azores hotspot, the lithosphere and crust work as a filter, and the current Azores morphology reflects the interaction between these to main players.

VI. 2. 5. Conclusions

Based on available bathymetric and gravimetric data, we propose that the boundary between the Eurasia and the Nubia plates did not jump directly from the EAFZ to the TR; instead it has migrated through a transient rift, parallel to the TR, which we describe here for the first time and call the S. Jorge-Santa Maria Graben.

Based on the youngest volcanism in SMa, we infer that the migration of the EU/NU plate boundary from the S. Jorge-SMa graben to the TR started, in the southeast, at least ca. 2.8 Ma ago, the age of the end of volcanic activity in SMa (Fig. VI.9B). The differences in age of volcanism in the islands at the eastern (SMa and S. Miguel) and western (S. Jorge and Graciosa) ends of the S. Jorge-Santa Maria Graben and TR suggest that the EU/NU plate boundary has been discrete in the southeast and diffuse in the northwest.

Conclusions of the Geological synthesis

Despite all these new constraints on (i) the role of the regional tectonics on the melt extraction; (ii) the evolution of the current Eu/Nu plate boundary; and (iii) the identification of a transitional graben between the EAFZ to the TR, we don't provide a hypothesis about the cause of the instability of the Eu/Nu plate boundary over time. To propose a scenario of the Azores area evolution combining a triple junction and decompression melting buoyant material (i.e. rich in volatiles and/or temperature) under a thickening lithosphere, we performed fluid mechanics experiments in the FAST laboratory in Paris-Sud University.

CHAPTER VII
Influence of the central Atlantic geodynamics on the evolution of the Azores

VII. Influence of the Central Atlantic geodynamics on the evolution of the Azores

VII. 1. Introduction

We saw in the previous chapters that the surface observations (i.e. magnetic and topographic anomalies, abnormal thickness of the oceanic crust and especially the excess of volcanism) cannot be explained exclusively by the geometry of the Azores Triple junction and/or by plate tectonics. To explain this excess of volcanism, the presence under the Azores archipelago of a material both wet (volatile or water) and moderately warmer (50-125°C) than normal mantle, is necessary. As both volatiles and hotter temperature render mantle material more buoyant, it is reasonable to think that this material comes from a mantle instability coming from much deeper in the mantle. Moreover, the variations through time of the volcanism may suggest that this instability is strongly time-dependent.

Hence this chapter will describe fluid mechanics laboratory experiments (section II), run in the neighbouring laboratory FAST in collaboration with Anne Davaille, and focussed on the dynamics of viscous mantle convective flow and its influence on-, and interaction with-, the Azores. The analogue experiments will help us to identify the respective roles of the mantle, the lithosphere filter and plate tectonics on the evolution of the Azores plateau and triple junction.

The first question investigated will be **the origin of this mantle instability.** In chapter II, we saw that all the tomographic models (global or local) indicate the existence of a large low seismic velocity zone in the lower mantle extending from the CMB at least up to 1000 km beneath the central Atlantic (Becker and Boschi, 2002, Fig.VII.1; Davaille et al., 2005; Forte et al., 2010). Fluid mechanics studies (Davaille, 1999; Le Bars and Davaille, 2004; Samuel and Bercovici, 2006; Kumagai et al., 2007; Tan et al., 2007) have shown that such large features could be produced by convection in a heterogeneous mantle, where the dome-shape of the instability is a signature of its thermo-chemical nature. The dome would come from the heated bottom of the lower mantle and be constituted of a slightly denser chemical component than the ambient mantle. This denser component could be a mixture of relics of a primitive mantle and subducted crust and lithosphere. The thermo-chemical dome would rise as long as its excess temperature and the corresponding decrease in density would be able

to counteract its density anomaly of compositional origin. The dome currently under the central Atlantic area could therefore still be rising, or be temporally delayed by the transition zone (e.g. Bercovici and Mahoney, 1994), or be stopped at its level of neutral buoyancy. In any case, such a large feature would also heat the mantle above itself by conduction and therefore could generate secondary plumes (Davaille, 1999; Kumagai et al., 2007; Fig. VII.2). The impact of these secondary plumes under the lithosphere would produce a cluster of hotspots. Such a process could explain the hotspots cluster associated with the Polynesian superswell in the Pacific (e.g. Davaille, 1999; Suetsugu et al., 2009). In the central Atlantic, it may explain the hotspots cluster constituted by Azores, Canaries, Cape Verde, Madeira and Great Meteor (Davaille et al., 2005; Kumagai et al., 2007). We are therefore going to build on these studies and investigate in more details the spacing, the time-dependence (birth, life, death and recurrence time) of these secondary plumes, as well as their potential interactions at the surface (section 3). Laboratory experiments have been run using a strongly temperature-dependent viscosity sugar syrup as analog to the viscous mantle. The scaling laws derived from the experimental results will allow us to interpolate our results to the mantle and get a deeper understanding of the central Atlantic geodynamics during the last 100 Myr (section 4). They will also permit to identify what type of time- and length-scales can mantle convective processes explain in the Azores volcanic and tectonic history.

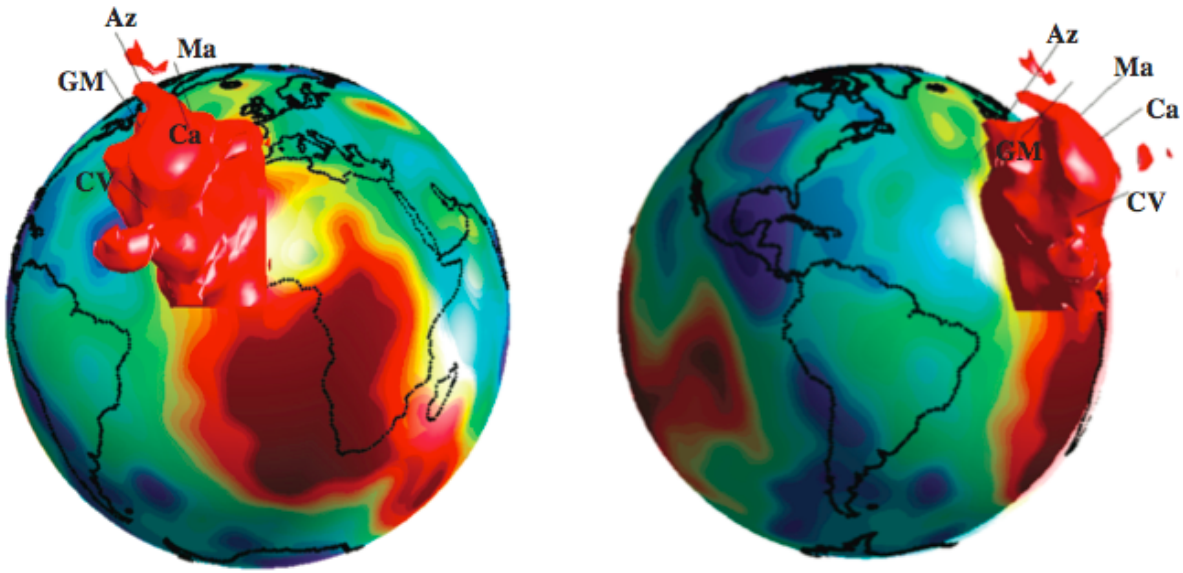


Figure VII. 1. The large dome of low S-wave velocity under the central Atlantic ocean (zoom of Fig. II.9). Here has been outlined in red the contour of dVs/Vs= - 0.5% in tomographic model SMEAN (Becker and Boschi, 2002). The position of the different hot spots is materialized by solid black lines, which extend from the CMB to the Earth's surface.

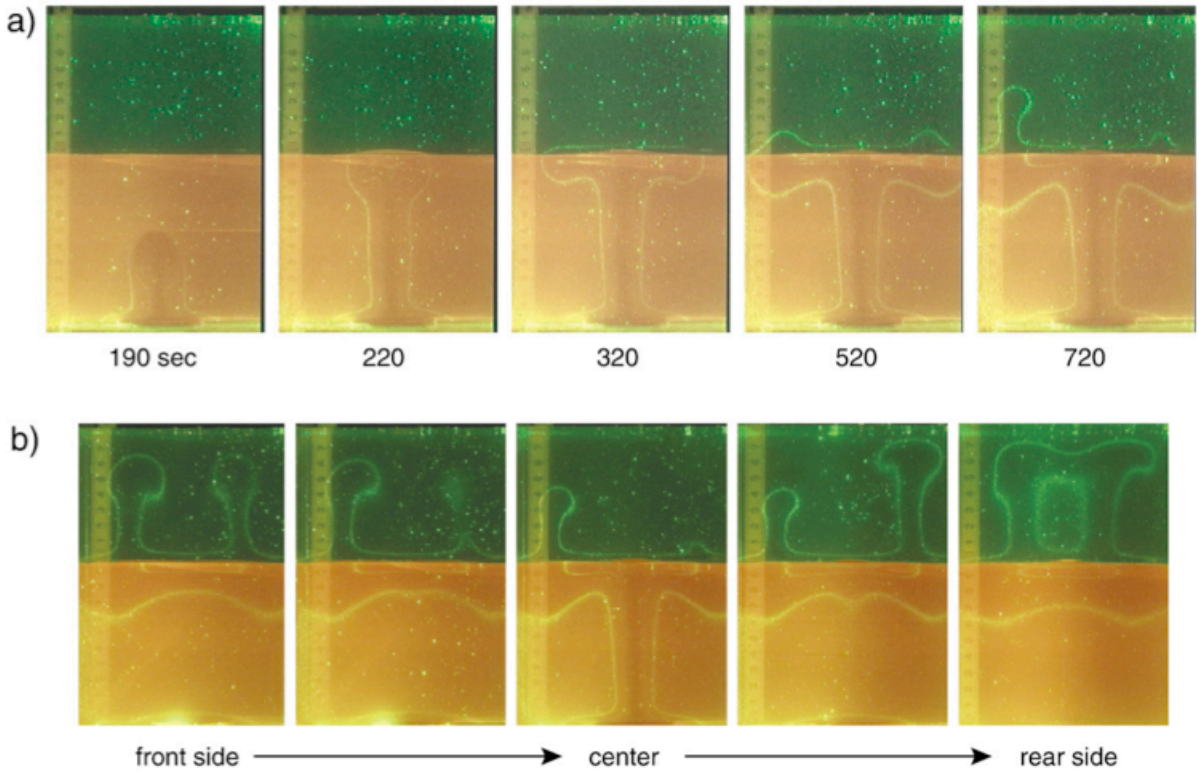


Figure VII. 2. Laboratory experiment from Kumagai et al. (2007). Development of a thermochemical dome in the lower mantle (in orange) generating a cluster of secondary plumes in the upper mantle (in green). The bright lines are isotherms. a) Temporal evolution; b) scanning the tank within 15 s at a given time (t = 750 s). We can distinguish at least four secondary plumes developing in a crown on top of the bottom layer plume. Their spatial distribution resembles the distribution of the hot spots above the central Atlantic thermochemical dome (Fig. VII.1).

The second question will concern **the interaction of a secondary plume with the Azores lithosphere** (section 5). Indeed, the distribution of the recent volcanism in the Azores is particular. It is located along the Western and Northern edges of the triangular plateau comprised between the EAFZ and the Terceira Rift (Fig. VII.3A). A recent regional P-wave tomographic model shows that a high velocity anomaly is located at lithospheric depths underneath the triangular plateau (Fig. VII.3B; Yang et al., 2006). High P-velocity can be interpreted as cold material. Moreover, the magnitude of the anomalies seen by the more precise receiver function technique suggests that this lithosphere is also very depleted in volatile/fluid (Silveira et al., 2010), probably in response to melting and extraction of the thick plateau crust. The lack of volatiles then would make the lithosphere stiffer than its surroundings (e.g. Hirth and Kohlstedt, 2003). The volcanism location along the border of the plateau might be the result of the interaction between the Azores mantle instability and this lithospheric root. So, to understand the processes involved in that case, we conducted laboratory experiments on the impact of a plume under a buoyant root. Our results will give

constraints on the instability current size and position, as well as on the lithospheric root and the volcanic plateau formation.

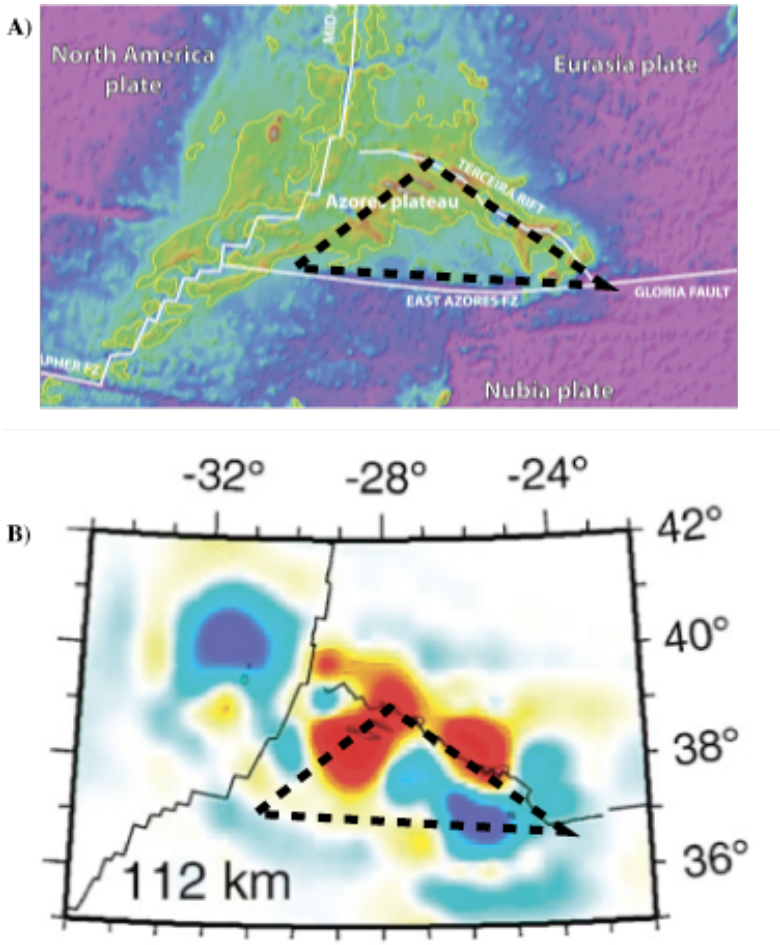


Figure VII. 3. A) Map of the Azores area. B) Tomographic model of Yang et al. (2006) at 112 km (cf Fig. II.11). The black dashed line triangle underlines the triangular-shaped plateau. Both the present-day active volcanic islands and the slow Vp anomalies are located along the western and northern edges of the triangle.

VII. 2. Laboratory experiments

VII. 2. 1. Experimental set up

All the experiments used the experimental set up of Androvandi et al. (2011). A plexiglas tank (30x30x15 cm) is filled up to a height H with a sugar syrup. The top surface of the fluid is kept free (Fig. VII.4). The bottom of the tank is a copper plate regulated in temperature by a circulation of hot water embedded into the plate. The high thermal conductivity of the copper ensures a uniform and rapid heating, and a constant temperature (at better than 0.1°C) over the whole bottom boundary. A copper disk, 5mm-thick and 60mm in diameter, is located in the center of the tank on top of the copper plate. It therefore creates a well controlled heterogeneity in the bottom heating, which will trigger the first thermal

instability. The use of 3cm-thick lateral walls in plexiglas has a double function: their transparency is essential to the visualization of the convective motions; furthermore, the weak thermal diffusivity of the plexiglas combined with its thickness render the heat transfer through the walls and the associated vertical motions negligible over the typical duration of an experiment (around 45 minutes).

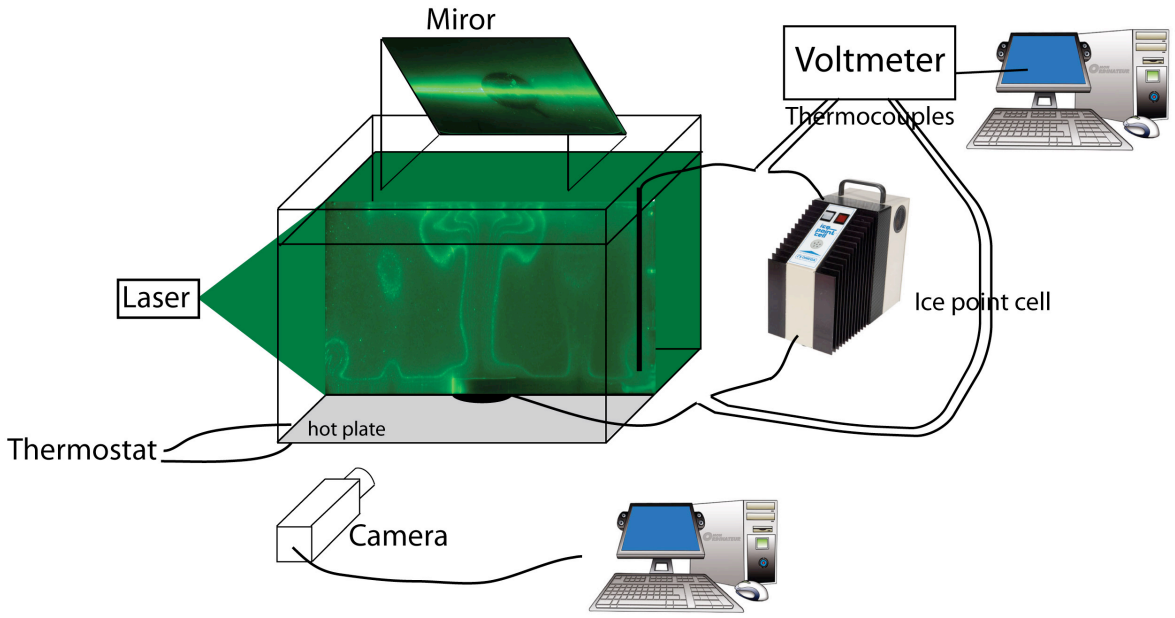


Figure VII. 4. Experimental set-up.

The temperature of the disk, of the copper plate and of 16 locations in the fluid, are measured and stored on a computer every 30 seconds. We use thermocouples, whereby a voltmeter measures the differences of potential between the junctions in -say-the fluid and a reference junction in an Ice point Cell (0°C). The final precision of the temperature measurements is 0.05°C.

Temperature and velocity fields: The fluid is seeded by ~10µm glass beads and 5 different types of thermochromic liquid crystals (TLCs). Then a vertical and an horizontal cross-section are illuminated by continuous 532 nm green 0.85W-laser sheets (Fig. VII.4). The vertical cross-section goes through the center of the copper disk and therefore allows to follow the development of the first instability close to its axis. The horizontal cross-section is set close to the top surface of the fluid and allows to observe the impingement of plumes under the top surface thanks to an oblique mirror at 45° above the tank. Images (1280 x1020 pixels) are recorded every 10 sec by a Nikon Camera, adjusted to take simultaneously on the same image the whole tank and the whole mirror.

Each type of TLCs reflects green light at a different temperature. So a given TLC

temperature will be materialized in the illluminated cross-section by a bright line (Fig. VII.4). The maximum of intensity of the line gives the temperature within a tenth of a degree and the thickness of the line the local temperature gradient within 10%. The full temperature field can be reconstructed by interpolation of the 5 isotherms (25.3°C, 28.4°C, 31.4°C, 34.5°C et 37.5°C).

The velocity fields are determined by following the glass particles from one image to the next, using the Particle Image Velocimetry technique and the software Davis from La Vision. More details about the velocity and temperature field measurements can be found in Davaille and Limare (2007), Androvandi et al. (2011), and Davaille et al. (2011).

Fluid properties: The sugar syrup is a Newtonian fluid, whereby its rheology does not depend on stress nor shear rate. However, its viscosity depends strongly on temperature, increasing with decreasing temperature. It was measured by Ryuta Abe during his Master Thesis, using the FAST rheometer MCR501 from Anton Paar. For the temperature range of the experiments, the viscosity η can be described by:

$$\eta = 17.26 \ \exp(-0.1426\ T) + 3.122 \exp(-0.05789\ T) \quad (1)$$

where T is in °C. This law fits the measurements within 5%. The density has been measured as a function of temperature with a DMA 5000 from Anton Paar, and writes:

$$\rho = \rho_0 \,.\, (1 - \alpha\ T) \quad (2)$$

where the density at 0°C is ρ_0=1386.3 kg/m^3 and the coefficient of thermal expansion is α=4.27x10^{-4} °C^{-1}. All the fluid properties are summarized in table 1.

	Lab	Whole mantle	Upper mantle
α (°C^{-1})	4.27x10^{-4}	2.0x10^{-5}	3.5x10^{-5}
ρ_0 (kg/m^3)	1386.3	3000	3000
κ (m^2/s)	1.2 x 10^{-7}	1.0 x 10^{-6}	1.0 x 10^{-6}

Table VII. 1. Physical properties of the sugar syrup, and of the mantle.

VII. 2. 2. Experimental parameters

All experiments start with the fluid at rest and at the ambient temperature T_m. Then at t=0, the water, pre-heated at a certain temperature, is circulated in the bottom copper plate. The latter is then regulated at a constant hot temperature $T_c=T_m+\Delta T$ ranging between 30 and 65°C (Table VII.2). Each experiment lasts between 1 and 4 hours. And we cannot run more than one experiment per day, if we want a homogenous temperature condition inside

the fluid at the start of the experiment. A total of 37 experiments has finally been carried out.

The dynamics of convection in our system can be described by three dimensionless numbers:

- The Prandtl number, $Pr = \nu/\kappa$, where κ is the thermal diffusivity and $\nu=\eta/\rho$ is the kinematic viscosity (i.e. momentum diffusivity). For the sugar syrup, it is in the limit $Pr_c >> 1$ relevant to the Earth.

- The intensity and the geometry of thermal convection depend on the global Rayleigh number, which compares the driving thermal buoyancy force to the resisting effects of thermal diffusion and viscous dissipation:

$$Ra(H,\nu) = \frac{\alpha g \Delta T H^3}{\kappa \nu} \qquad (3)$$

where *g* is the gravitational acceleration, and ΔT the temperature difference between the ambient air and the heater. Convection occurs only if the Rayleigh number is greater than a critical value Ra_c (around 1000) the exact value depending on the boundary conditions (rigid or free boundary). In the mantle, $Ra \sim 10^6$-$10^8 >> Ra_c$, so that convection and plumes are expected to occur.

- The viscosity ratio, $\gamma = \nu(T_m) / \nu(T_{hot})$.

#	ΔT (°C)	T_m (°C)	H (mm)	Ra_{hot}	γ	Ra_m
1	26.2	21.9	117.6	$9.8x10^6$	7.8	$1.25x10^6$
3	25.25	22.8	117.57	$9.4x10^6$	7.1	$1.3x10^6$
5	27.9	20.05	117.20	$1.0x10^7$	9.2	$1.1x10^6$
6	26.2	22.0	117.17	$9.7x10^6$	7.8	$1.25x10^6$
7	12.7	20.7	117.00	$1.6x10^6$	3.1	$5.3x10^5$
8	32.95	21.4	116.97	$1.8x10^7$	12.1	$1.5x10^6$
9	27.5	22.0	116.94	$1.1x10^7$	8.4	$1.3x10^6$
10	15.8	21.5	116.91	$2.7x10^6$	3.8	$7.1x10^5$
11	24.3	21.0	116.89	$7.4x10^6$	7.0	$1.0x10^6$
12	20.55	20.8	116.80	$4.7x10^6$	5.5	$8.7x10^5$
13	20.15	21.1	116.77	$4.6x10^6$	5.3	$8.8x10^5$
14	16.05	21.3	116.74	$2.8x10^6$	3.9	$7.1x10^5$
15	15.85	21.5	115.97	$2.7x10^6$	3.8	$7.0x10^5$
16	17.2	20.1	116.17	$2.9x10^6$	4.4	$6.7x10^5$
17	26.6	20.3	116.00	$8.8x10^6$	8.4	$1.0x10^6$

Table VII. 2. Characteristics of the experiments.

Since the viscosity of the fluids depends strongly on temperature, the temperature at

which the viscosity is taken in Eq. (3) can be either T_m or T_{hot}. The values of $Ra(H,\nu(T_m))$, $Ra(H,\nu(T_{hot}))$ and γ are given in Table VII.2 for all the experiments performed. A number of these experiments have been doubled or tripled, in order to get information on a different cross-section of the tank (ex : Fig. VII.6), or on the interaction of the instabilities with buoyant rafts at the surface (see section V).

VII. 3. Characteristics of mantle "secondary" plumes: results from the laboratory experiments

VII. 3. 1. Plume development

Fig. VII.5 shows the development of convection through time in a zone centered on the copper disk. Once the copper plate is heated, the fluid close to the horizontal bottom boundary is heated by conduction: the isotherms are flat (Fig. VII.5A) and parallel to the bottom surface. The hottest isotherm (37.5°C) is the line closer to the boundary and the cold isotherm (25.3°C) is the line farthest from the source of heat. This zone of high temperature gradient (and therefore lighter fluid) is called the Thermal Boundary Layer (TBL). When the TBL has grown sufficiently so that its upward velocity in a viscous medium becomes greater than its growth by thermal diffusion, motion begins and the isotherms are developing bumps (Fig. VII.5B): the TBL becomes unstable. In terms of Rayleigh number, it means that the Rayleigh number based on the TBL thickness δ, $Ra(\delta,\nu)$, becomes greater than the critical value Ra_c. We see that the first instabilities to develop are on the edges of the bottom copper disk (Fig. VII.5B). In fact, if we scan the tank to get a 3D view, we observe that it is a crown of instabilities. It is a well-known phenomenon of localization on lateral heterogeneities (e.g. Namiki and Kurita, 1999; Vatteville et al., 2009). However, since the copper disk is quite small, the edges of instabilities soon merge in a single plume (Fig. VII.5C) constituted of a head and a conduit (Fig. VII.5D). As the plume rises, its head grows mainly by being fed through its stem, but there is also a contribution of thermal diffusion. Because of the latter, the plume cools on its way up: we can see on Figs. VII.5D and 5E that the hottest isotherm does not reach the top of the tank. Horizontal cross-sections (Fig. VII.6A-C) show that the plume is axisymmetric. Upon reaching the upper surface, the plume spreads along it (Fig. VII.5E-H). Once the TBL is exhausted into the plume, the conduit is cut off from the bottom boundary (Fig. VII.5G), and a new cycle can begin (growth of the TBL by conduction until instability, etc…). Meanwhile, the first plume remains to cool at the surface.

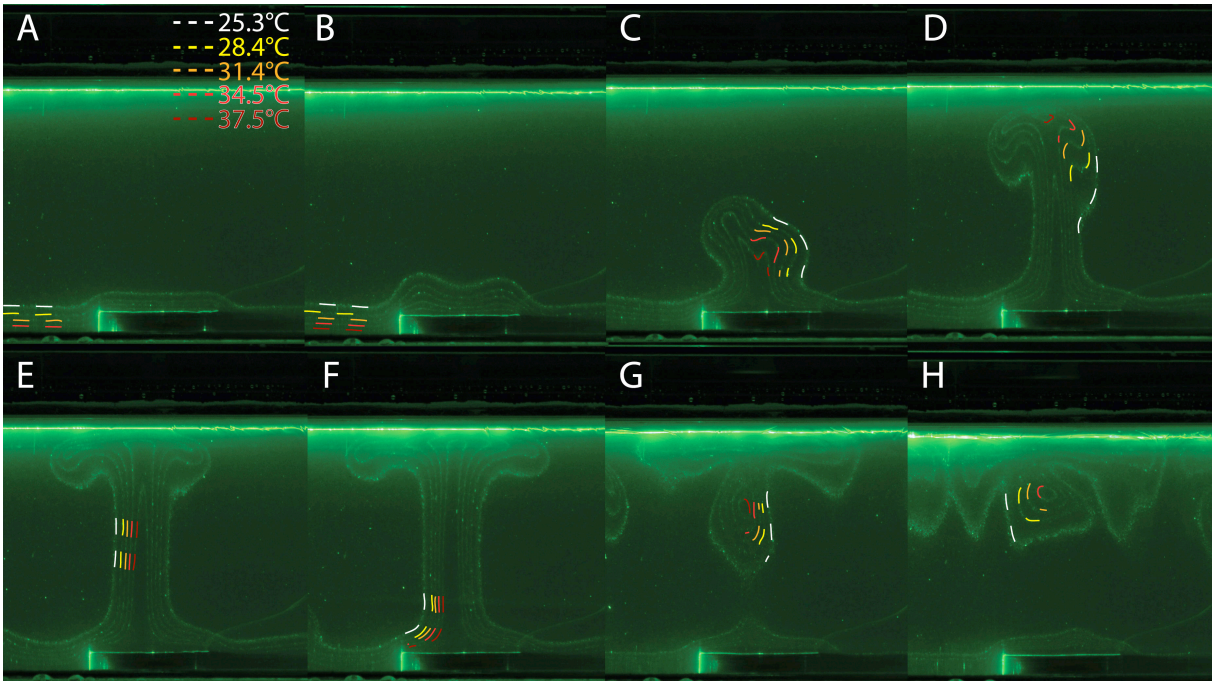


Figure VII. 5. Development of the first plume localized on the copper disk. The laser sheet illuminates a vertical cross-section centered on the disk center. The bright lines are the isotherms. Part of them have been highlighted in colour. Experiment #8.

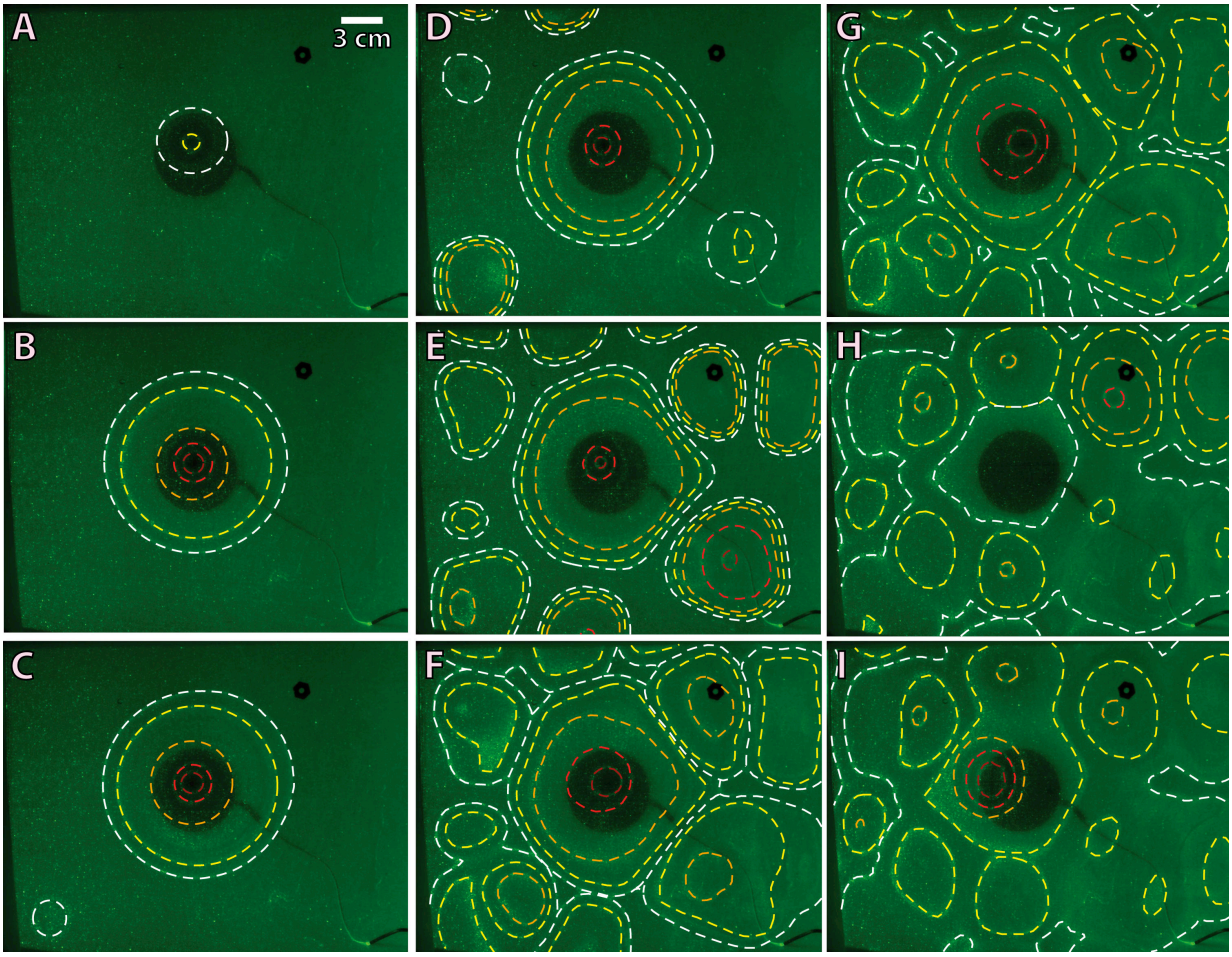


Figure VII. 6. Evolution of the instabilities impacts at the surface across the time. The horizontal cross-section is 10 mm below the free surface. The bottom boundary was heated at T=55°C. The pictures from A to I were taken at t = 800, 1060, 1120, 1240, 1370, 1610, 1730, 2130 and 2450 sec. The isotherms are color-coded as in Fig. VII.5.

VII. 3. 2. Spacing between plumes

Even if it is on top of the copper disk that the first plume develops, numerous plumes develop later in the tank by the same mechanism of instability of the thermal boundary layer. Fig.6 shows snapshots of a horizontal cross-section of the fluid taken 10 mm below the upper surface. Each plume is materialized by concentric isotherms.

We can therefore measure the distance λ between two plumes by measuring the distance between their centers on horizontal cross-sections like Fig. VII.6. We see there that within an experiment, the spacing can easily vary by a factor of 2. This is due in particular to the first plume located on the copper disk which appears bigger than the subsequent plumes. There are also two other ways to measure the spacing: on the vertical cross-sections of Fig. VII.5, or on the horizontal spatio-temporal images (Fig. VII.7). These spatio-temporal images are obtained from the vertical cross-section images by extracting at each time the horizontal pixel line at a given depth, and by plotting its intensity as a function of time and distance along the horizontal axis x. The isotherms appear again as bright lines. Of particular interest for the spacing measurements on horizontal pixel lines located close to the free surface where the plumes impinge (Fig. VII.7 top), and the pixel lines just above the TBL (Fig. VII.7 bottom) which records plumes everytime they are emitted from the TBL.

Figure VII.8 gives the range of spacing that we observe in our experiments. As expected, there is scatter. However, if we compare our measurements to the data obtained by Androvandi et al. (2011) on 3 decades in Ra without any copper disk to perturb the system, the two data sets are consistent and can be fitted by:

$$\lambda = C_{exp}\, H.\, Ra(H, \nu(T_m))^{-1/3} \Rightarrow \lambda = C_{exp}\,(\alpha.g.\Delta T/\kappa.\nu(T_m))^{-1/3} \qquad (4)$$

where C_{exp}=45 (±15) is an experimental constant. Furthermore, (4) shows that the spacing is independent of the fluid high. This is because the instabilities are governed locally by the lower TBL dynamics (e.g. Androvandi et al., 2011).

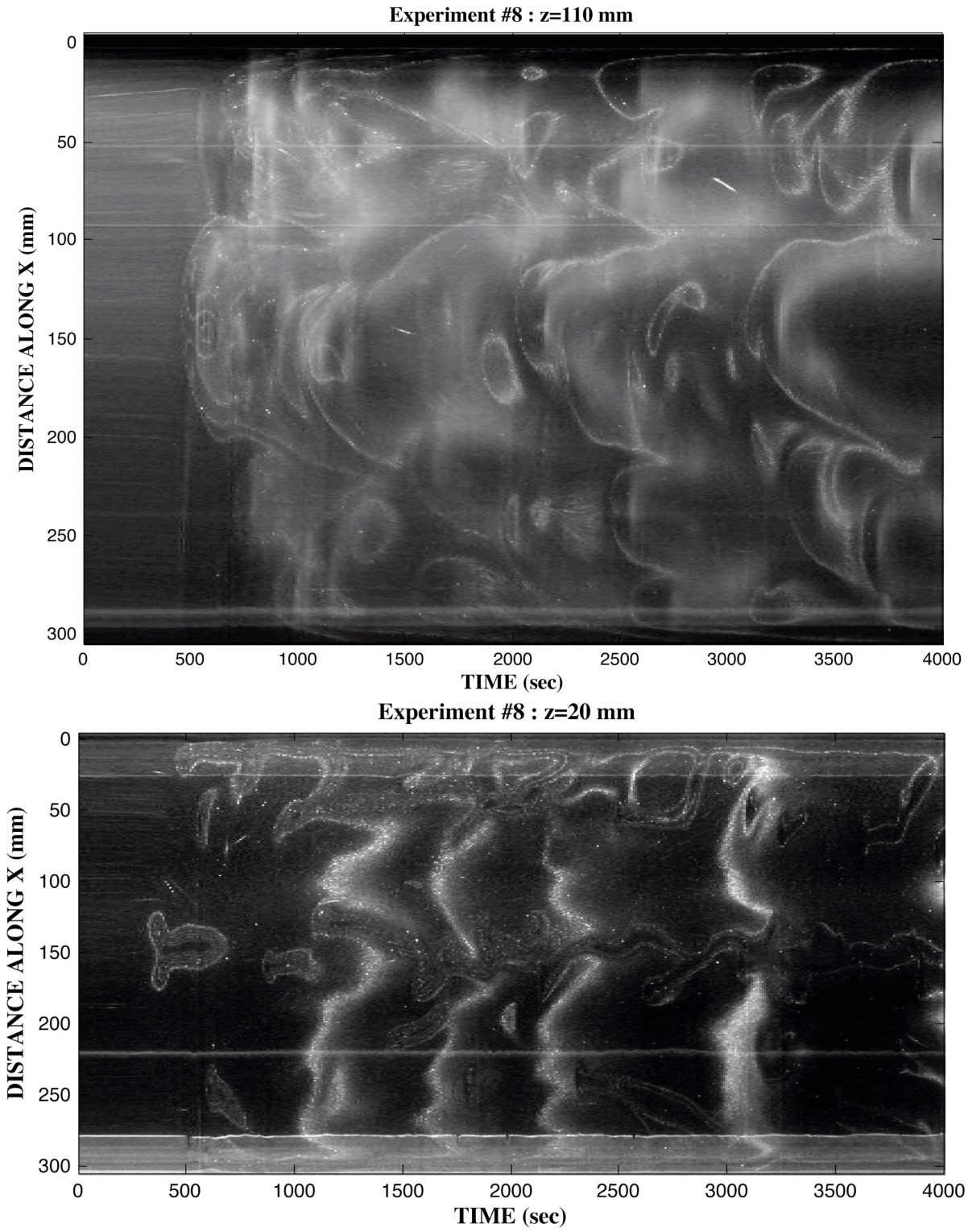


Figure VII. 7. Time evolution of the thermal structures close to the surface of the fluid (Top) and just above the TBL (Bottom). These spatio-temporal images have been obtained from the vertical cross-section images (as in Fig. VII.5) by extracting at each time the horizontal pixel lines at 110 mm- (top) and 20 mm-height (bottom), and by plotting their intensity as a function of time and distance along the horizontal axis x. The bright lines are isotherms, and closed isotherms are signatures of plumes. Experiment #8 (same as Fig. VII.5).

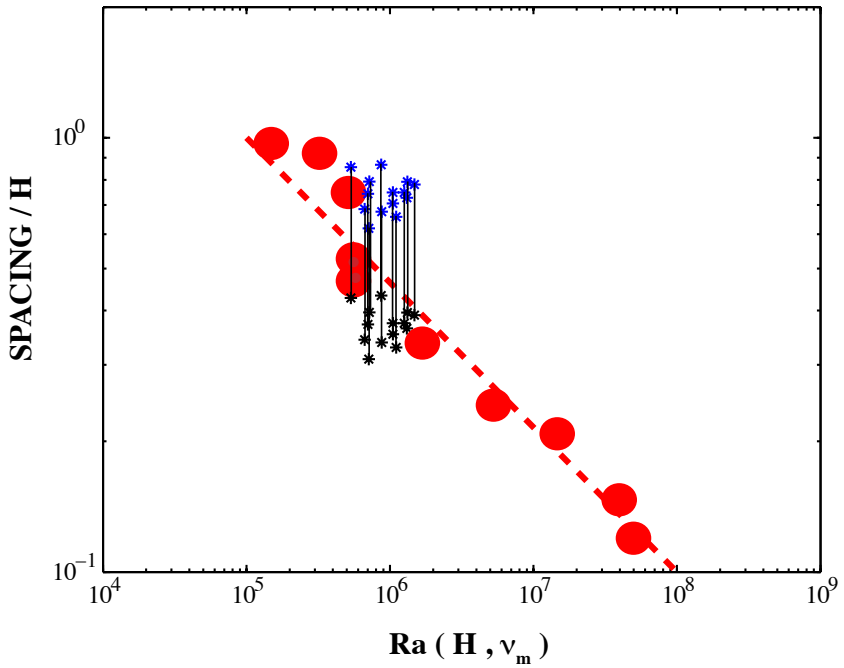


Figure VII. 8. Distance between two instabilities (normalized by the fluid thickness) as a function of the Rayleigh number Ra$(H,\nu(T_m))$. In red, the data from Androvandi et al. (2011) and in black, the data of the present study. The size of the red points represents the range measured for each experiment. The blue and black stars indicate the maximum values obtained (usually between the center plume and the other plumes) and the minimum values, respectively. The dashed line represents the scaling law (4).

VII. 3. 3. Interactions between plumes

It is well known in convection studies that plumes interact with the ambient flow and therefore with each other (see for example Davaille and Limare (2007) for a review). In the Earth, plumes are not fixed to the km but can meander, due to subduction and large scale flow (e.g. Steinberger, 2000; Tarduno et al., 2003). In our experimental tank, the sequence of images of Fig. VII.6 shows that the plumes also interact with one another, especially close to the surface when they are spreading. When alone, the copper disk plume had a axisymmetric geometry (Fig. VII.6A-C). However, as soon as the other plumes reach the top surface and spread under it, the central spreading changes shape and straight ridges appear between the plumes (Fig. VII.6D-I): the colder material is gathered in between the hot plumes. So each hot plume is surrounded by a colder sheet of material, an observation already made by Olson et al. (1988) and Androvandi et al. (2011). But the effect is enhanced if two plumes are close enough (Fig. VII.6E).

VII. 3. 4. Time recurrence

We already saw that a thermal plume is a strongly time-dependent feature, undergoing birth, life and death (Fig. VII.5; section VII.3.1; Davaille and Vatteville, 2005). Examination of the image sequences and of the spatio-temporal figure just above the TBL (ex: Fig. VII.7 bottom) shows that the instabilities are not always emitted at the same place, and that their links to the TBL can meander through time.

We can also define a recurrence time, as the time interval between the emission of two successive instabilities. This time is best determined on the vertical spatio-temporal figures (Fig. VII.9). To construct those, a vertical pixel line at a given x is extracted at each time and its intensity is plotted as a function of time and height. A rising plume is indicated by the sudden rise of the bright lines (i.e. isotherms). The rapid rise is very different from the slow rise close to the bottom boundary due to heat conduction. Fig. VII.9 compares the behaviour encountered on top of the copper disk (Fig. VII.9 top), to the instabilities behaviour developing farther away. The same type of recurrence is observed, although the recurrence time is smaller in the first case.

The emission of these plumes and their time of implementation depend on the time required for the recharge and growth of the TBL and therefore it depends on thermal conduction. The recurrence time hence is given by (e.g. Howard, 1964; Weeraratne and Manga, 1998; Davaille and Vatteville, 2005):

$$\tau_{rec} = C\frac{H^2}{\kappa}Ra(H,\nu(T_m))^{-2/3} = \frac{H^2}{\kappa}\left[\frac{Ra_c}{Ra(H,\nu(T_m))}\right]^{2/3} \qquad (5)$$

where C=35.5±7 is a constant determined experimentally. Like the case of the plume spacing, (5) shows that the recurrence time is independent of the fluid height. If (5) is expressed as a function of a critical Ra_c, then we obtain Ra_c = 1176 ± 390 at 1σ. This value is very close from the one predicted theoretically for a layer with one rigid boundary and one free boundary (Chandrasekhar, 1962), i.e. the situation of our tank. However, note that the generation of instabilities is usually not synchrone in the whole tank, except the first time (Fig. VII.6, VII.7 and VII.9).

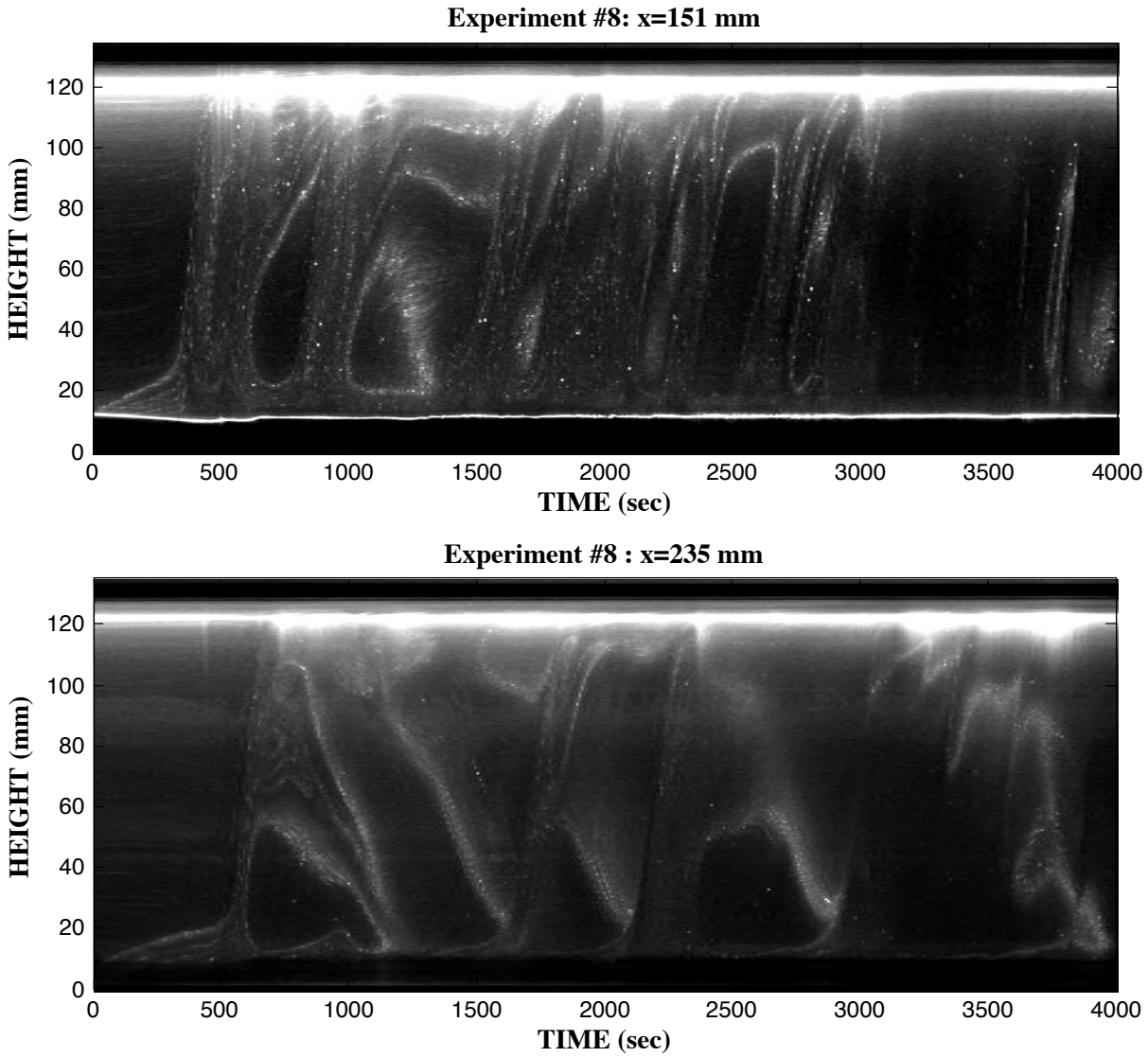


Figure VII. 9. Time evolution of the thermal structures of the TBL from the bottom to the surface of the fluid. Top: vertical pixel line centered on the copper disk; bottom: vertical pixel line away from the disk. Experiment #8 (same as Fig. VII.5 and VII.7).

VII. 4. The Atlantic hotspots cluster

The central Atlantic currently hosts at least 4 active hotspots (Azores, Cape Verde, Canaries, Madeira) and scarce data suggests that Great Meteor might have been active not too long ago (Fig. VII.10). Those 5 hot spots are located on top on the large dome imaged in the mantle by seismic tomography. Our scaling laws allow us now to test if this cluster of hotspots could, indeed have been created by secondary plumes issued from the lower mantle dome.

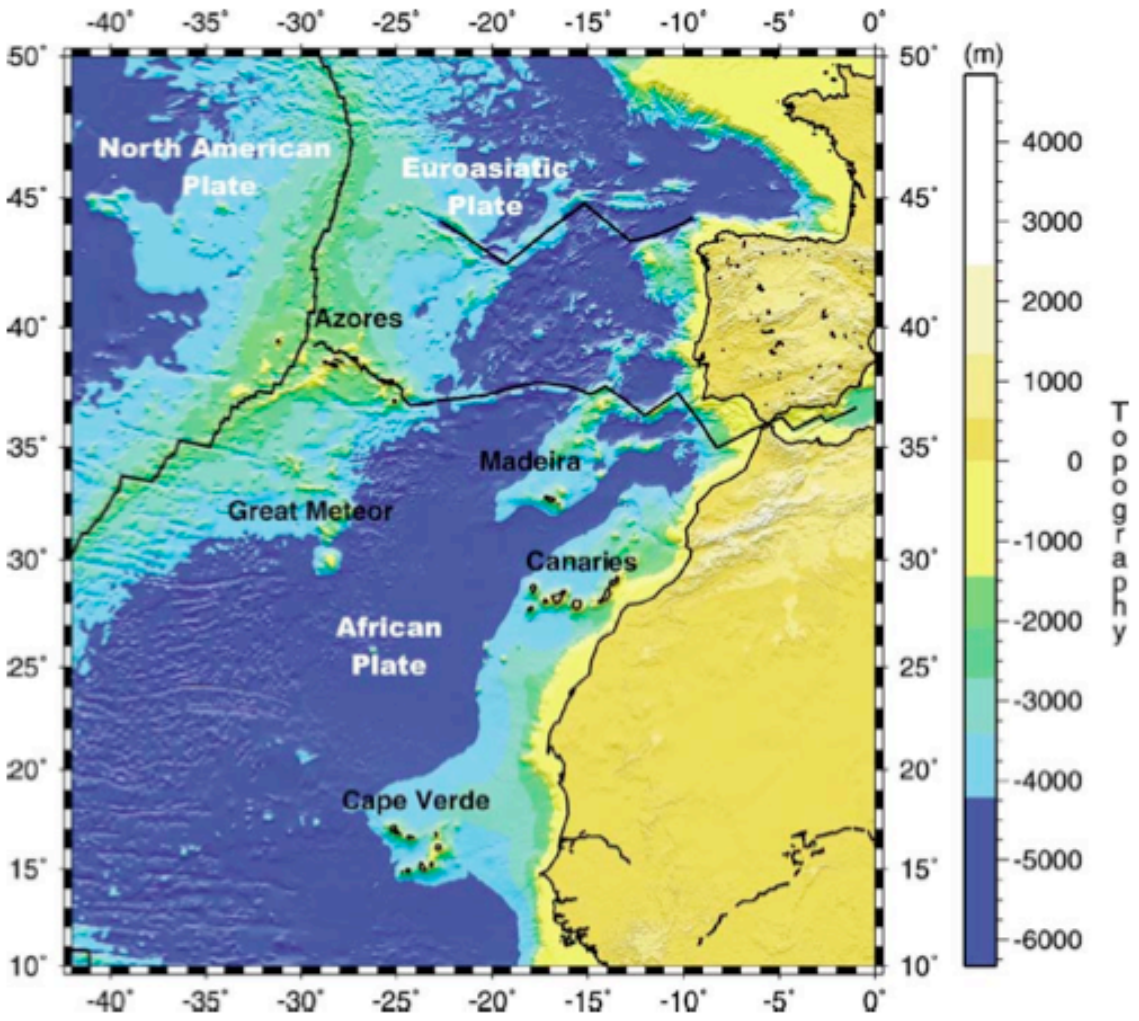


Figure VII. 10. Map of the central Atlantic (from Silveira et al., 2006).

VII. 4. 1. Existence and spacing of the secondary plumes

Given the physical properties of mantle rocks (Table VII.2), the thickness of the mantle, its viscosity, and the temperature differences across it, the mantle Rayleigh number is in the range 10^5 to 10^8, which is about the same range as we can study in the laboratory (e.g. Fig. VII.8). We can therefore apply our scalings with some confidence. Moreover, the size of the considered area being small compared to the planet size, our results obtained in a cartesian box should not be different from the ones obtained on sphere.

Figure VII.11-Top shows the plume spacing as a function of the mantle viscosity and of the temperature difference at the boundary from which the plumes are rising. When we compare with the minimum and maximum distances between the Atlantic hotspots, the figure points toward a mantle viscosity between 10^{19} and 10^{21} Pa.s, i.e. upper mantle values, for a large range of temperature differences. To explain the hotspots spacing with lower mantle

viscosity values of 10^{22} Pa.s would require temperature differences greater than 2000°, which are too big. So, secondary thermal plumes, with temperature anomalies as small as 50° (Fig. VII.11-top) coming from the top of the lower mantle dome close to the transition zone in the Atlantic (Fig. VII.1) could indeed have generated the Central Atlantic hotspots. Since Azores material shows both a small temperature excess (< 150°C) and a richness in volatiles, it could be proposed that the secondary plume would have taken on its way up some water in the transition zone area where it has been suggested that a water filter/reservoir existed (Bercovici and Karato, 2002).

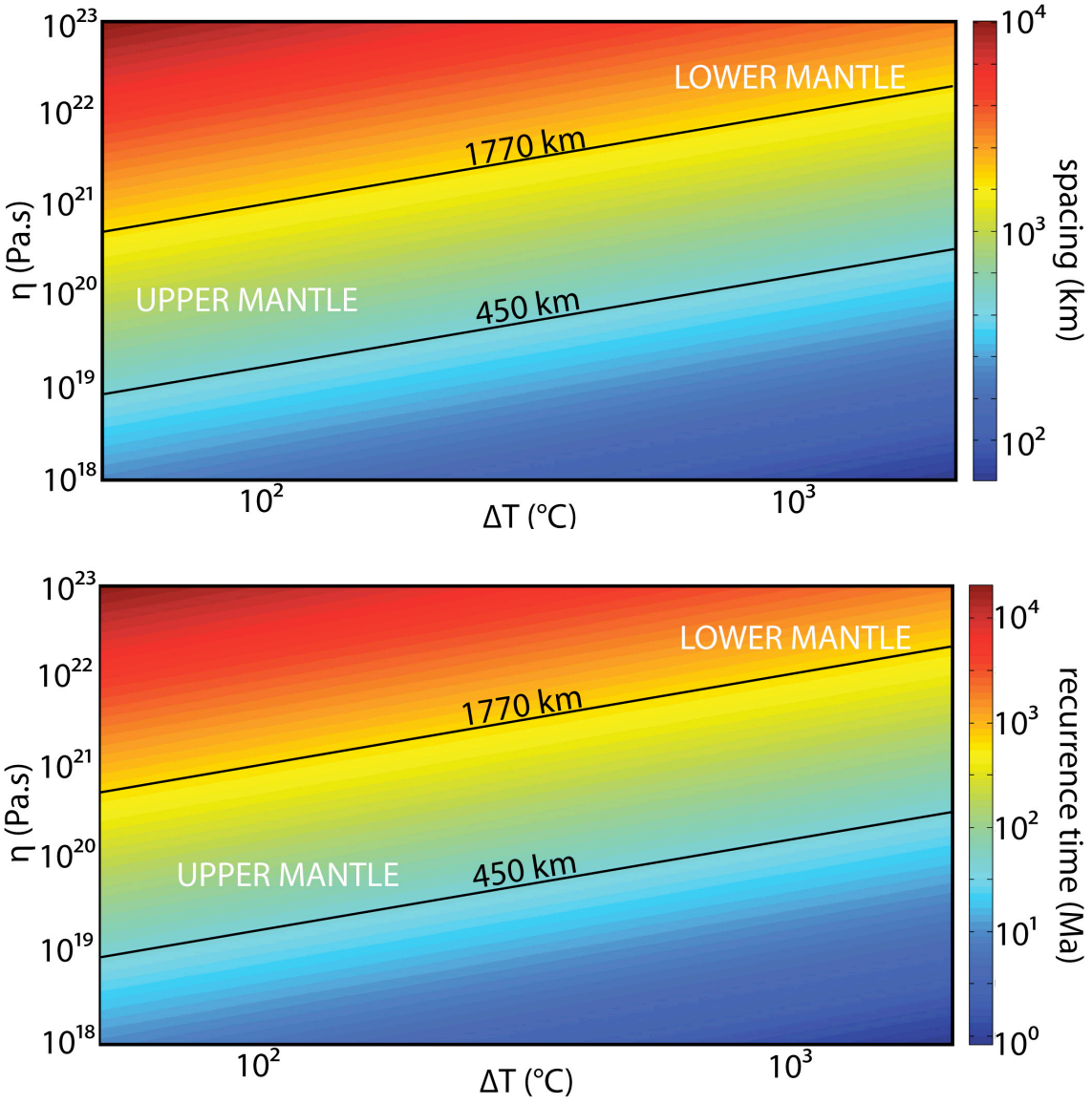


Figure VII. 11. Plume spacing (top) and recurrence time (bottom) as a function of temperature difference and mantle viscosity. The two solid lines represent the minimum and maximum spacing amongst hot spots in the Central Atlantic.

VII. 4. 2. Evolution: from King's Trough to Azores

Figure VII.11-bottom shows the recurrence time calculated from (5). We have seen that this recurrence time was a characteristic time scale of the convective instabilities. For the same range of spacing as Fig. VII.11-top, it ranges between 30 and 300 Myr for Ra_c=1176 and between 20 and 100 Ma for Ra_c=650, the value appropriate for a system with two free boundaries. The interface between the dome and the upper mantle is not a rigid boundary, however we are dealing with viscous fluids. So the reality is probably in between the two values. Anyway, the calculated characteristic times show that the different pulses of activity recorded in the Azores (see previous chapter) are not due to the arrival of different plumes. The viscous scales in the mantle are two long. However, the duration of all 5 hot spots are within the predicted range.

Moreover, we have seen in chapter II that a mantle plume had been proposed to have existed at King's Trough, 750 km North from the Azores and the previous location of the central Atlantic triple junction. The exact time of its volcanic activity is debated and ranges between 60 and 10 Ma. According to our results, this plume could have issued from the same thermochemical dome. However, it would be distinct from the Azores instability.

VII. 5. Evolution of the Azores in the last 10 Myr

We just saw that the Azores excess volcanism could be the result of the impact of a secondary plume beneath the lithosphere. However, Azores present pulses of activity on times scales shorter than the viscous mantle timescale (chapiter VII), and a geometry of volcanism which is very particular (Fig. VII.12-bottom), since it is currently focussed on the two sides of a triangle. The latter is quite different from the round features typical of viscous instabilities (Fig. VII.5). However, the triangle is also the shape of the volcanic plateau and the associated thickened crust (Fig. VII.3 and VII.12). Seismic studies suggest also that the lithosphere under the volcanic islands (Silveira et al., 2010) and under the plateau (Yang et al., 2006) is much thicker than what would correspond to a lithosphere of the same age. As recognized by Silveira et al. (2010) the lithosphere is thickened beneath the volcanic islands as a residue to the excess volcanism. Therefore, it is probably very poor in volatiles and quite stiff. Fig. VII.12-top has been constructed using the estimates of lithosphere thickness of 80 km under the plateau (Silveira et al., 2010), and the classical thickening in square-root of time in the normal lithosphere around. We see that the thickened lithosphere would penetrate deep into the asthenosphere. Therefore, we must now tackle the problem of the interaction between a impinging thermal plume and a lithospheric root.

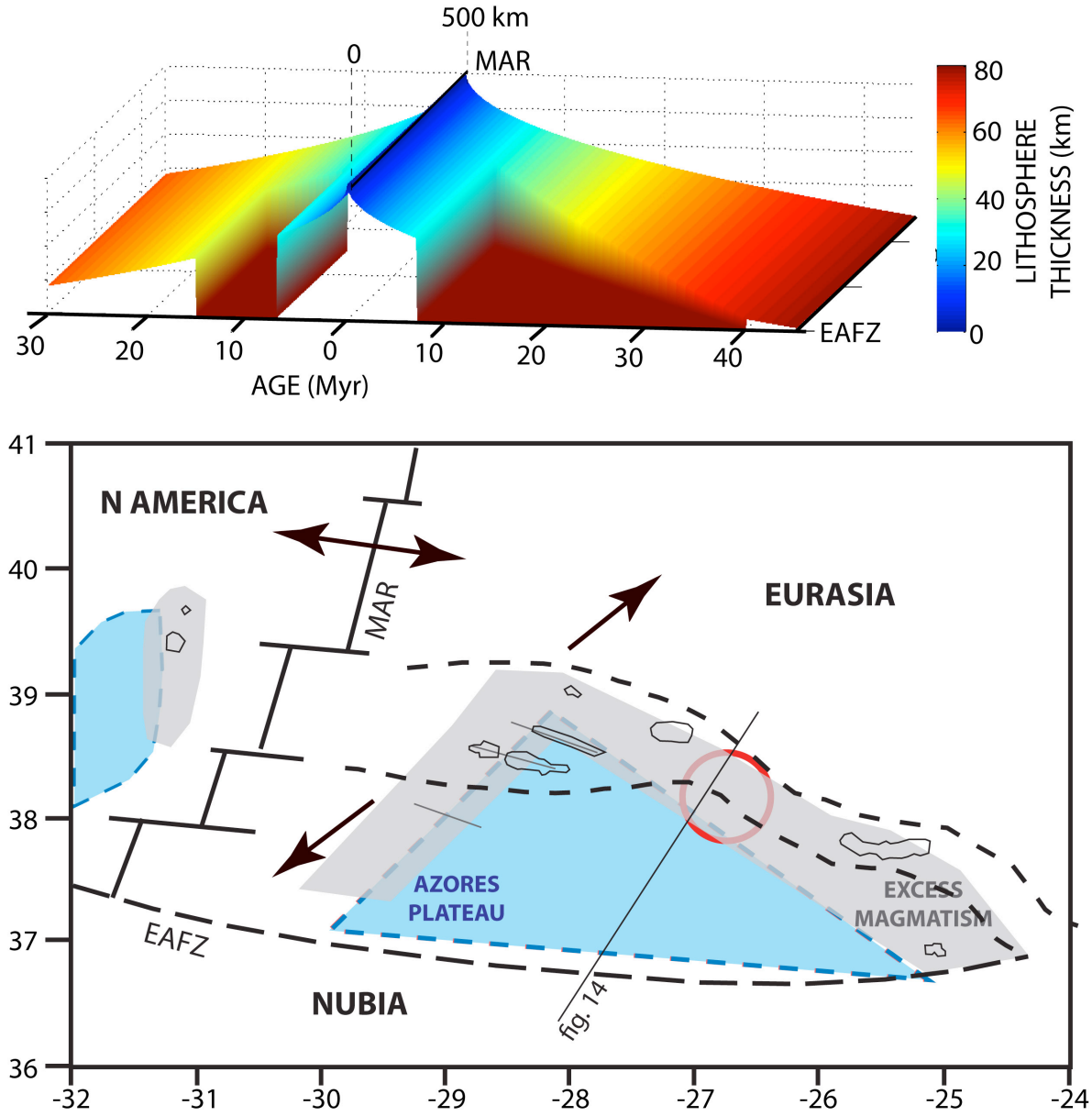


Figure VII. 12. Top: Schematic view of the lithosphere thickness in the Azores area as a function of the distance along the MAR and the age of the lithosphere. Bottom: Top view of the area, showing the present-day active zones of volcanism in grey, and the possible position of a mantle instability conduit in red. The thin line shows the location of the cross-section of Fig. VII.13.

VII. 5. 1. Plume-root interaction

We conducted a series of 15 experiments where buoyant rafts where positioned on the free surface. Several materials were employed in order to study the influence of the root thickness compared to the TBL characteristic thickness: styrafoam, altuglass and polycarbonate. We shall focus here on the latter as it was the one with the deepest root. The polycarbonate material has a density of 1.1932 g/cm^3, so a major part of the raft is inside the

fluid while a little part remains outside. In the experiment shown in Fig. VII.13, we positioned 4 rafts (3x3 cm each) in a square formation with a little separation between two of them in order to simulate a pre-fracturation in the lithosphere. The “large raft” has roughly the same size as the copper disk, which localized the first instability, and is larger than the plume’s head to avoid any artefact due to scale variation. Due to the reflection of the laser on the polycarbonate raft, we cannot follow with precision the hotter isotherms right below the raft, but the lateral detection of the isotherms is not disturbed on the sides.

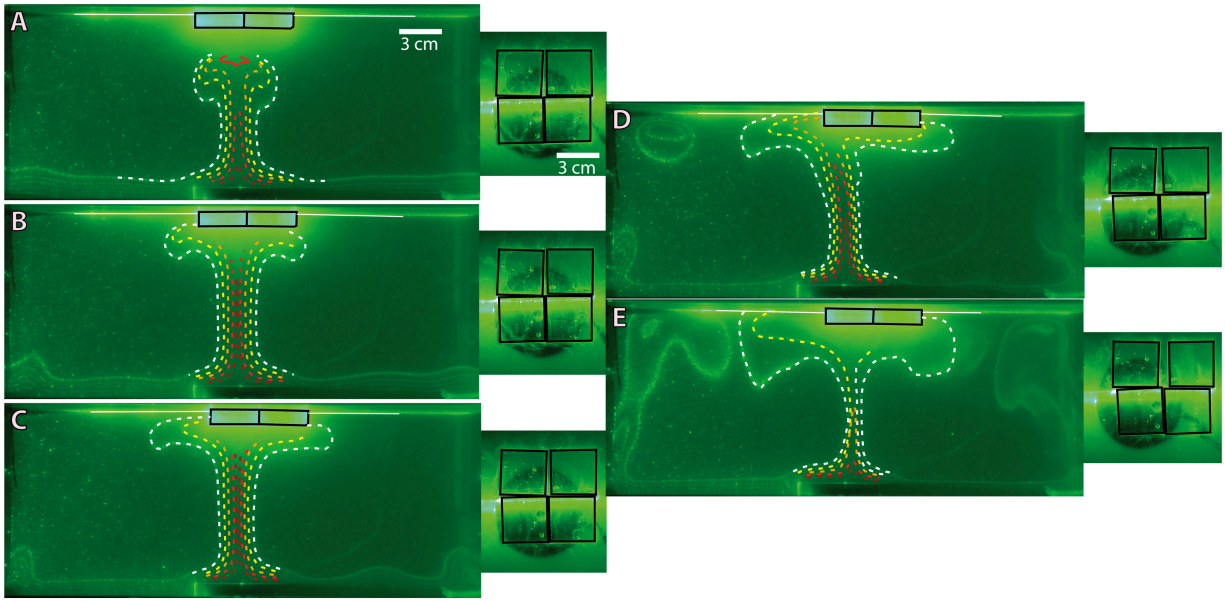


Figure VII. 13. Morphology and evolution of the impact of a plume on a thickened lithosphere. The bottom boundary was heated at T=50°C. The pictures from A to E are taken at t = 1250, 1440, 1640, 1890 and 2350 sec.

The plume shows a well-developed structure in the fluid with axisymmetry of the head (Fig. VII.13A). Upon impact of the plume at the base of the rafts (Fig. VII.13B), we can notice a discrete migration of the large raft without dissociation of the small rafts, even the ones close to the pre-fracture (weak area). The direction taken by the large raft depends on the position of the center of the head plume relative to the rafts. For example on Fig. VII.13, the position of the large raft seems shifted a few millimetres eastwards relative to the plume axis. At first, the plume head spreads laterally without reaching the surface, nor trying to get around the raft (Figs. VII.13B and VII.13C). The cold isotherm is locally closer to the surface in the west than in the east. This is coherent with the initiation of the global motion of the large raft to the east. When the plume has found a way to the surface, the flow is concentrated along the border of the plateau. The entire instability appears to deform and lose its symmetry (Figs. 13C and 13D). Throughout the duration of the experiment, the instability will never reach the surface in the eastern part. In the case of styrafoam, the

material is very buoyant and stay quite high at the surface of the fluid. Consequently, is does not show any significative effect on plume dynamics.

VII. 5. 2. Rifting and the northward growth of the Azores plateau

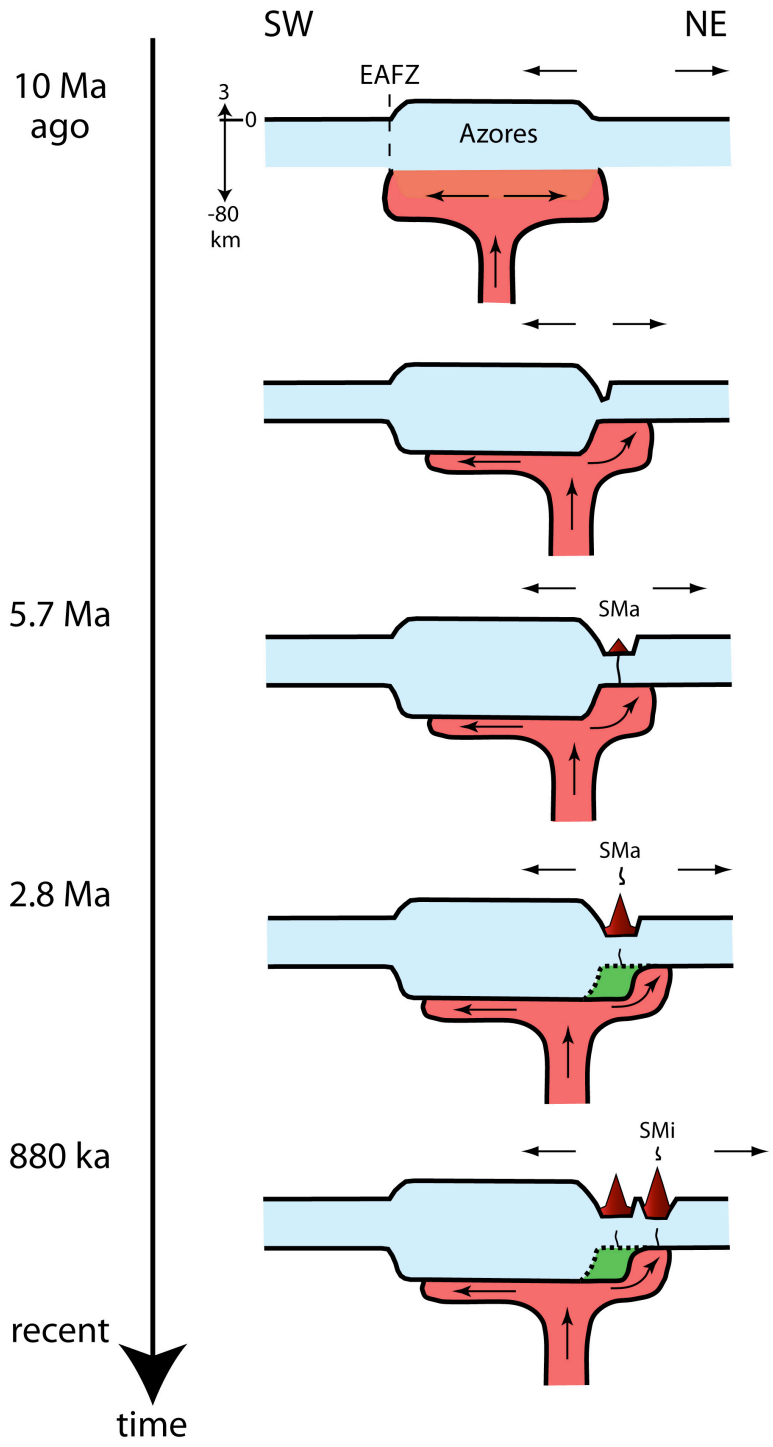


Figure VII. 14. Evolution of the northern border of the plateau and lithosphere characterized their progressive northward growth, and the formation of several rifts.

From the above experiment, we explain the shape of the recent volcanism in Azores as the signature of a plume impinging under a lithospheric root. In fact, given the shape of

the Azores lithospheric roots (Fig. VII.12-Top), the shape of the volcanic active area implies that the plume conduit should impinge under the lithosphere between Terceira and São Miguel islands (Fig. VII.12-top). This way, the plume material cannot reach the EAFZ, which would explain the lack of activity there (Fig. VII.14). Moreover, since the lithosphere thickens with increasing age away from the MAR, the mantle will preferentially follow the directions of bigger slope, and therefore will flow towards the MAR, until it eventually reaches the opposite lithospheric root below Flores and stops there. Accordingly, on the Eurasia side of the MAR, the volcanism will take place along the diffuse plate boundary and along the western border of the plateau. On the eastern side, the plume material will have to move downslope to reach São Miguel, which would explain why it does not reach further east. Although we have positioned the plume conduit on the northeastern side of the plateau on the base of geometrical arguments only, it is interesting to note that it is totally coherent with the tomographic study of Yang et al. (2006) and the Helium and Neon geochemical data (Moreira et al., 1999; Madureira et al., 2005, respectively; see chapter II. 3.4.).

But we can still go further if we now consider the evolution of rifting on the northeastern side of the plateau. According to DeMets et al. (2010), the relative motion existing between the Eurasia and the Nubia plates close to the Azores is extensive. From a purely mechanical point of view, it is the suture between the strong devolatized lithosphere and the normal lithosphere that will be proned to rift first, all the more that hotter and wetter (so easier to melt) plume material is flowing underneath it (Fig. VII.14). We have therefore the situation where the mantle underneath the rift could melt relatively easily, but has to cross a quite old and cold lithosphere on its way to the surface. In this case, strong localization of volcanism is expected (Buck, 2007; Cannat et al., 2003; Standish et al., 2008). This might explain why the TR is constituted of a succession of island and basins (Fig. VI.6) separated by a regular distance about 100 km. The TR seems thus constituted by a succession of magmatic and amagmatic segments. This morphology looks like the morphology of the South Western Indian Ridge (SWIR), an ultra-slow spreading ridge with a spreading rate about 14-15mm/yr. The SWIR is constituted of a succession of magmatic and amagmatic segments with a focalisation of the melt in large volcanic centers. This focalisation of the melt was interpreted by Cannat et al. (2003) to be due to the cold structure of the lithosphere, itself due to the very slow spreading rate. In the case of the Azores TR, the cold structure of the lithosphere pre-dates the slow opening of the rift.

Migration of the Eu/Nu plate boundary during the last 10 Myr

The Terceira Rift is constituted by a succession of segment parts with a trend between N80 to N130 (Fig. VI.1). These directions are similar to the one shown by the elongation of the islands. Indeed, the current bathymetry of the archipelago reveals the existence of several lineations, and seamounts with a similar trend. The tectonic structures in the islands are the same as those which give the framework for the distribution of volcanism expressed as source volcanism along fissural systems, which gives the linear volcanic ridges (LVR, Neves et al., (2013)). We saw in previous chapters that all together, the evolution of the islands is largely influenced and controlled by the regional deformation, particularly along the LVR and in the Terceira Rift. Thus, the linear volcanic ridges define the internal morpho-structure of the plateau, which seems to be sub-parallel to the Eu/Nu plate migration path and to the current Terceira Rift segmentation pattern. Based on that, Vogt and Jung (2004) proposed that the migration and the rifting of the TR and the Eu/Nu plate boundary is due to the Azores hotspot migration northward. This implies a northeastern oriented age progression of the volcanic island as a response to the migration in the same direction of the Azores hotspot. These authors consider, by comparing the strike of the volcanic ridges across the plateau that the linear volcanic ridges are traces of failed rifts either spreading obliquely (close to the MAR) or normal (farther to the east) to the main MORVEL model (DeMets et al., 2010). Those authors propose a mechanism to justify both the migration of the plate boundary and the arcuate shape of the volcanic islands, where thickening of the crust could have caused a zone weakening near the edge of the spreading boundary and its relocation northwards. This mechanism is fully coherent with our analogue experiment presented here (Fig. VII.14). Thus, it remains valid at a broader scale, to explain the northward migration of the Triple Junction. Nevertheless, the recent ages of the volcanic islands provided in Faial (Hildenbrand et al., 2012b, 2013a), Pico (Costa et al., 2014), S. Jorge (Hildenbrand et al., 2008), Graciosa (Sibrant et al., 2014), Terceira (Calvert et al., 2006; Hildenbrand et al., 2014), S. Miguel (Sibrant et al., 2013) and Santa Maria Islands (Sibrant et al., 2013), do not fit with Vogt and Jung's (2004) model.

Here, based on analogue experiments on a different scale, we proposed a slight variation of Vogt and Jung model's (Fig. VII.14). According to Gente et al. (2003), the construction of the Azores platform started at about 20 Ma, thanks to the interaction of the hotspot and the MAR-axis. The interaction between the MAR-axis and the less dense material from a plume has produced the abundant volcanism required to build an oceanic crust at least twice thicker than normal. This abundant volcanic production extended along the Eu/Nu plate boundary at least close to S. Maria island and a probable migration of the

triple junction point from the EAFZ-MAR intersection to the edge of the newly formed plateau. The construction is followed by the symmetrical rifting of the plateau on both sides of the MAR-axis, which began between 10 Ma on the north and 5 Ma on the south. The rifting of the plateau seems synchronous with the sudden stop of the excess of volcanism and suggests that the abundant melt production requires the interaction of the two melting anomalies (heater and volatiles). The new analogue experiment indicates that a thermal plume under the Azores can have a life time between 10 and 30 Ma. That means that after the creation of the plateau, the plume head is potentially detached from its source deep in the mantle and so the plume may not be powerful enough to crack the new thicker plateau and corresponding lithosphere. When the interaction between the plume and MAR-axis ceases, "normal" magmatic production resumes along the ridge axis. The remnant head is still less dense and tries to find a way out to the surface. Since the crust is under extensive stress and the crust/lithosphere vary in thickness, the fracture and the initiation of the rift occurs between the junction of the plateau and the plates. Thus, the material migrated towards the border of the plateau in the north and in the west close to the MAR axis, where the thickness is smallest (Fig. VII. 12). The melt production generates linear volcanism and the formation of grabens as detected by Marques et al. (2013a, 2014a) around S. Jorge which is the older western island (on the eastern MAR-axis part). The older Eu/Nu plate boundary is now located along the S. Jorge/S. Maria graben (here newly recognized) and probably opening first at S. Maria Island which is active between 5.7 and 2.8 Ma. The melt is probably guided along a newly formed rift axis by the slope at the base of the lithosphere toward S. Jorge around 1.3 Ma.

Then the new S.Jorge/Santa Maria rift increases the thickness (because of the volcanism) and the extension of the border of the Azores plateau. The new deeper zone (Fig. VII.14) is constituted by a depleted crust/lithosphere (in volatile and H2O) which is cold, thick and more brittle than the surrounding crust/lithosphere. Moreover, the plume still continues to fade. Then again, the less dense material needs to find a new way out further to the northeast and then along the new second rift toward the west, the Terceira Rift. We propose here that the new Eu/Nu plate boundary as we know it today has been active during the last 800 ka. Note that at this stage the Eu/Nu plate boundary is probably already diffuse (until 850 ka, see Chapter VI). This means that the melt migration towards the west thanks to the sloping base of the lithosphere starts a secondary process in front of the development of the rifting and Eu/Nu plate boundary.

To give an estimate of the number of "intermediate" rifts between the EAFZ and the current Eu/Nu plate boundary is difficult. To do it, we need a precise bathymetry of the Azores plateau to be able to look for intermediate graben structures, older rifts and older Eu/Nu plate boundaries.

VII. 6. Conclusions

In this chapter, we have explored the contribution of the viscous mantle to the Azores dynamics. The use of laboratory experiments and fluid mechanics allowed us to illustrate and characterize two main phenomena: secondary thermal plumes issued from a thermochemical dome in the lower mantle, and the interaction of a plume with a thickened lithosphere. The latter study deserves now more work to better quantify the dynamics.

CHAPTER VIII
Conclusions

VIII. Conclusions

The Azores region constitutes a unique natural laboratory to study the interaction between several important geodynamic processes. This region comprises: an area of anomalously thick oceanic crust associated with a non-conventional hotspot, an unstable triple junction, characterized by a complex geometry and kinematics, and a plate boundary which displays one of the slowest opening rates in the world rift systems. During this work, we analysed the spatio-temporal variability of the large and small scale processes which interact in the Azores domain. These can be broadly systematized as the interaction between the triple junction and plume like mantle instability over various spatial and temporal scales.

We first used a multidisciplinary approach and complementary data with different resolution to gain insights into the interactions between deformation and volcanism along the present western branch of the Eu/Nu plate boundary during the last 1 Myr. From the study of Graciosa and S. Miguel, we documented the behaviour of the volcanism (construction and destruction) with respect to rifting. The tectonic markers on S. Miguel allowed us to study the architecture of the Terceira Rift. We especially propose that N50 structures newly recognized constitute a young transform system within the TR, in agreement with the proposed present pole of plate rotation of the Eu and the Nu plates (DeMets et al., 2010). From the distinct episodes of volcanism at regional scale, we proposed that the TR has been increasingly mature over the last 1Myr, with episodes of deformation getting closer and closer in time.

Our study also shows that the geodynamic significance of Santa Maria volcanism has been under-estimated in previous studies. We here refine the volcano-tectonic history of this island between 5.7 Ma and 2.8 Ma, and show that its evolution records a major change in stress field. We identified a new graben structure linking Santa Maria to the island of S. Jorge further NW. The shape of this graben is similar to the TR and it is located between the EAFZ and the current plate boundary. We interpret this graben as a former transient rift, and therefore an old Eu/Nu plate boundary. From the new data, we propose that the eastern part of the transient rift migrated to the eastern part of the TR between 2.8 Ma and 1.7 Ma.

At a larger temporal scale, we discussed possible scenarios of interaction between the Eu/Nu plate boundary, the Azores plume, and the Azores plateau. Our fluid mechanics experiments suggest that the Azores plume, as the Canary, Cape Verde, Madeira Islands and Great Meteor seamounts might be the surface signature of a cluster of mantle instabilities rising from the top of a large thermochemical dome located in the lower mantle. Such secondary plumes present a strongly variable time scale on the order of 5-40 Myr. Moreover, they could be sufficiently weak to adapt their motions to the pre-existing force balances and morphology of the lithosphere.

Future Research

A great deal of work needs to be performed to refine and improve the knowledge and understanding we have been gaining/acquiring in the Azores area in the past 10 years. The main problem in most interpretations about the Azores region is the almost absolute lack of knowledge on the age, the thermal structure and architecture of the Azores plateau.

Future research should be focus on:

(1) A more detailed analysis of the volcano-tectonic structures at the plateau scale. For such purpose an increasing effort to collect swath bathymetry and marine geophysical data is essential. As the Azores edifices are particularly vulnerable to slope instability, such data would also be useful to further detect and study in detail large-scale debris generated by catastrophic flank collapses at the archipelago scale. Better quantification of the debris age, volume, and mobility is critical to model the potential generation of tsunami, and evaluate the hazard and risk associated with these mass-wasting events.

(2) A full investigation of the morphology and structure of the basins within the TR would help clarifying the age of initiation of rifting, and better examine if sea-floor spreading is occurring or not. Reflection/refraction seismic data, coupled with the acquisition of additional gravimetric and magnetic data would most probably provide essential clues.

(3) Direct seafloor observations, rock sampling by means of submersible, and subsequent dating of the samples, would help define the age and the dynamics of crustal deformation of such hyper-slow plate boundary. ODP drilling would also provide crucial information on the structure of the crust and the age of the plateau. This would allow to better evaluate if the plateau effectively results from an episode of enhanced magma production, e.g. associated with a former plume head impact.

(4) Sampling and dating the submarine base of the islands and the various submarine volcanic ridges yet un-investigated would provide valuable constraints regarding the Azores temporal evolution.

(5) Continuing the inter island GPS observations to consolidate GPS interpretation by lengthening the time series. This would provide additional constraints on how the far-field

displacement vectors are partitioning over the several structures of the present diffuse plate boundary, and therefore, how deformation occurs at the crutal/lithospheric scales.

(6) Numerical modelling of the Azores lithosphere thermal structure and behaviour would allow to investigate if the alignment of volcanoes and local extensive volcanic structures and the TR plate boundary are propagating westwards, either as newly formed cracks or by reactivation of pre-existing fractures.

(7) The geochemistry dataset over the Azores islands is considerable. Nevertheless, rare are the authors studying the temporal evolution of the geochemistry at the scale of the edifices / islands / archipelago. Such future work is essential to better evaluate the respective roles of mantle heterogeneity and lithospheric deformation on melt production and extraction. Moreover, Graciosa, Terceira and S. Miguel show highly explosive differentiated volcanic eruptions. It would be interesting to investigate further the role of the rift extension on the cyclic development and re-opening of short-lived magma reservoirs. This would have a significant impact for risk evaluation, as numerous of the cities (e.g., Sete Cidades) are localized within or close to caldera depressions, or inside canyons and basins where the pyroclastics products may be frequently re-mobilzed as lahars and hyper-concentrated flows.

(8) In this study, we started to investigate the interactions between a plume-like mantle instability, and extensive structures close to an unstable triple junction characterized by successive rift jumps. Similar configurations exist elsewhere in the world, including along oceanic ridges, where rifting is more developed. For example, repeated ridge jumps have effectively pinned the Reykjanes Ridge near the Iceland plume despite relative motion between the two (Hardarson et al., 1997; Garcia et al., 2003). In the Galapagos, the presence of a plume has not only resulted in numerous jumps of the axis towards the hotspot (Wilson and Hey, 1995; Meschede and Barckhausen, 2000) but also voluminous off axis volcanism that formed the Galapagos Archipelago and a series of volcanic lineaments between the plume and the ridge (Harpp and Geist, 2002; Harpp et al., 2003; Mittelstaedt et al., 2012), as observed in the Azores archipelago (Fig. VIII.1). The mechanisms controlling the formation of such off-axis lineaments as well as the initiation and evolution of rift/ridge jumps remain poorly understood. Coupled approaches with analogue fluid experiments, numerical modelling and high-resolution bathymetry to examine the tectonic evolution and the development of volcanism in such regions appear to be a good start.

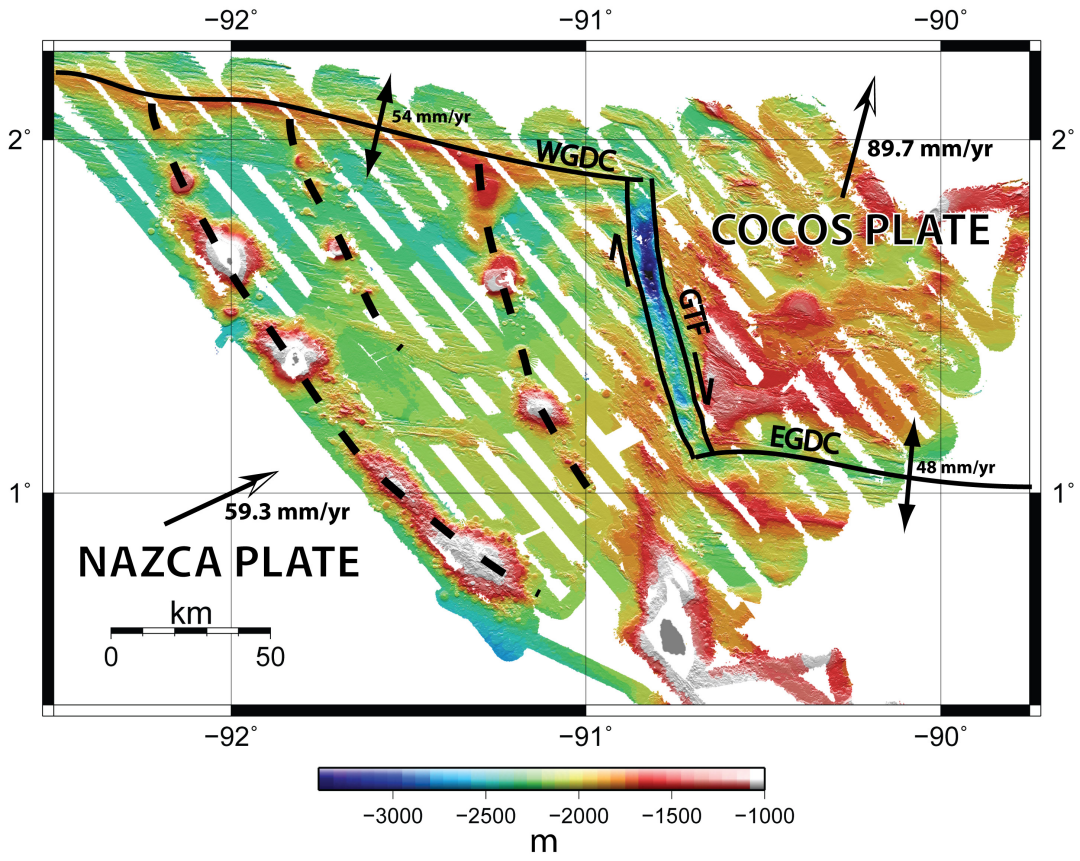


Figure VIII. 1. Bathymetry of the northern part of the Galapagos islands collected during the FLAMINGO cruise (Modify after Mittelstaedt et al., 2012). The arrow with white indicates the motion of the Cocos and the Nazca plate from Argus et al. (2011). The double arrow indicates the velocity spreading for the Western Galapagos spreading center (WGSC) and the eastern Galapagos spreading center (EGSC,) after DeMets et al. (2010). The dashed lines indicated the older location of the Galapagos Transform Fault (GTF) identified by Mittelstaedt et al. (2012).

(9) A comparative study between hyper-slow extensive structures such as the Artic Gakkel ridge (ultra-slow spreading), the Southwest Indian Ridge (SWIR- volcanic centers separated by amagmatic segments) or slow-spreading oblique ridges such as Mohns and Reykjanes ridges can provide information on the dominant processes controlling the creation of new oceanic crust. Moreover, the ultra-slow extensive structures still remain poorly known. The morphology, the nature of the rocks, the thermal structure, the dynamics, or even the differences between slow and hyper-slow spreading are still not clear and sometimes confused. For example, the role of the orientation of the opening (oblique or perpendicular), the competition between the melt productivity and the efficiency of vertical melt extraction, the pre-fracturation of the crust should fashion the morphology and the geodynamics of such extensive structures.

CHAPTER IX
References

IX. References

Abdel Monem, A.A., Fernandez, L.A., Boone, G.M., 1975. K-Ar ages from the Eastern Azores Group (Santa Maria, São Miguel, Formigas islands). Lithos 8, 247-254.

Acocella, V., Funiciello, R., Marotta, E., Orsi, G., DeVita, S., 2004. The role of extensional structures on experimental calderas and resurgence. Journal Volcanology and Geothermal Research 129, 199-217, doi: 10.1016/S0377-0273(03)00240-3.

Adam, C., Madureira, P., Miranda, J.M., Lourenço, N., Yoshida, M., Fitzenz, D., 2013. Mantle dynamics and characteristics of the Azores plateau. Earth Planetary Science Letters 362, 258-271.

Agostinho, J., 1937. Sobre a tectónica da Ilha de Santa Maria. Açoreana 1, 281-286.

Al Kwatli, M.A., Gillot, P.Y., Zeyen, H., Hildenbrand, A., Al Gharib, I., 2012. Volcano-tectonic evolution of the northern part of the Arabian plate in the light of the new K-Ar ages and remote sensing: Harrat Ash Shaam volcanic province (Syria). Tectonophysics 580, 192-207.

Ancochea, E., Fuster, J.M., Ibarrola, E., Cendrero, A., Coello, J., Hernan, F., Cantagrel, J.M., Jamond, C., 1990. Volcanic evolution of the island of Tenerife (Canary-Islands) in the light of new K-Ar data. Journal of Volcanology and Geothermal Research 11, 231-249.

Ancochea, E., Hernand, F., Cendrero, A., Cantagrel, J.M., Fuster, J.M., Ibarrola, E., Coello, J., 1994. Constructive and destructive episodes in the building of a young oceanic island, La Palma, Canary Islands, and genesis of the caldera de Taburiente. Journal of Volcanology and Geothermal Research 60, 243-262.

Androvandi, S., Davaille, A., Limare, A., Foucquier, A., Marais, C., 2011. At least three scales of convection in a mantle with strongly temperature-dependent viscosity. Physics of the Earth and Planetary Interiors 188, 132–141.

Angelier, J., 1984. Tectonic analysis of fault slip data sets. Journal of Geophysical Research 89 (B7), 5835–5848.

Angelier, J., 1994. Fault slip analysis and palaeostress reconstruction. In: Hancock, P.L. (Ed.), Continental Deformation. Pergamon Press, Oxford, pp. 53–100.

Appelgate, B., Shor, A.N., 1994. The northern Mid-Atlantic and Reykjanes Ridges: Spreading center morphology between 55°50'N and 63°00'N. Journal of Geophysical Research 99 (B9), 17935-17956.

Argus, D.F., Gordon, R.G., DeMets, C., Stein, S., 1989. Closure of the Africa-Eurasia-North America plate motion circuit and the tectonics of the Gloria fault. Journal of Geophysical Research 94, 5585-5602.

Argus, D.R., Gordon, R.G., DeMets, C., 2011. Geologically current motion of 56 plates relative to the no-net-rotation reference frame. Geochemistry, Geophysics, Geosystems 12, Q11001, doi:10.1029/2011GC003751.

Asimow, P.D., Dixon, J.E., Langmuir, C.H., 2004. A hydrous melting and fractionation model for mid-ocean ridge basalts: Application to the Mid-Atlantic Ridge near the Azores. Geochemistry, Geophysics, Geosystems 5 (1), Q01E16, doi:10.1029/2003GC000568.

Bache, F., Mortimer, N., Sutherland, R., Collot, J., Rouillard, P., Stagpoole, V., Nicol, A., 2014. Seismic stratigraphic record of transition from Mesozoic subduction to continental breakup in the Zealandia sector of eastern Gondwana, Gondwana Research, in press, Corrected Proof.

Ballmer, M.D., Van hunen, J., Tackley, P.J., 2007. Intraplate due to small scale convection – a 3D numerical study. Geophysical Research Abstracts 9, 06458.

Batiza, R., 1996. Magmatic segmentation at mid-ocean ridges, A review, in MacLeod, C., et al., eds., Tectonic, magmatic, hydrothermal, and biological segmentation of mid ocean ridges. Geological Society of London, Special Publication 118, 39-49.

Becker, T.W., Boschi, L., 2002. A comparison of tomographic and geodynamic mantle models. Geochemistry, Geophysics, Geosystems 3, doi:10.1029/2001GC000168.

Beier, C., 2006. The magmatic evolution of Oceanic Plateaus: a case study from the Azores. PhD Thesis, Kiel, 175pp.

Beier, C., Haase, K.M., Hansteen, T.H., 2006. Magma evolution of the Sete Cidades volcano, S. Miguel, Azores. Journal Petrology 47, 1375-1411.

Beier, C., Stracke, A., Haase, K.M., 2007. The peculiar geochemical signatures of São Miguel (Azores) lavas: Metasomatised or recycled mantle sources? Earth Planetary Science Letters 259, 186–199.

Beier, C., Haase, K.M., Abouchami, W., Krienitz, M.-S., Hauff, F., 2008. Magma genesis by rifting of oceanic lithosphere above anomalous mantle: Terceira Rift, Azores. Geochemistry, Geophysics, Geosystems 9. doi:10.1029/2008GC002112.

Beier, C., Turner, S.P., Plank, T., White, W., 2010. An preliminary assessment of the symmetry of source composition and melting dynamics across the Azores plume. Geochemistry, Geophysics, Geosystems 11 Q02004(1), doi:10.1029/2009GC002833.

Beier, C., Haase, K.M., Turner, S.P., 2012. Conditions of melting beneath the Azores. Lithos 144-145, 1-12.

Beier, C., Mta, J., Stöckhert, F., Mattielli, N., Brandl, P.A., Madureira, P., Genske, F.S., Martins, S., Madeira, J., Haase, K.M., 2013. Geochemical evidence for melting of carbonated peridotite on Santa Maria Island, Azores. Contributions to Mineralogy and Petrology 165, 823-841.

Bercovici, D., Mahoney, J., 1994. Double Flood Basalts and Plume Head Separation at the

660-Kilometer Discontinuity. Science 266, 5189, 1367-1369.

Bercovici, D., Karato, S.I., 2003. Whole-mantle convection and the transition-zone water filter. Nature 425, 39-44.

Bird, R.T., Tebbens, S.F., Kleinrock, M.C., Naar, D.F., 1999. Episodic triple junction migration by rift propagation and microplates. Geology 27, 911-914, doi: 10.1130/0091-7613.

Boccaletti, M., Mazzuoli, R. Bonini, M., Trua, T., Abebe, B., 1999. Plio-Quaternary volcanotectonic activity in the northern sector of the Main Ethiopian rift: Relationships with oblique rifting. Journal of African Earth Sciences 29, 679-698.

Bogoyavlenskaya, G.E., Braitseva, O.A., Melekestsev, I.V., Kiriyanov, V.Y., Miller, C.D., 1984. Catastrophic eruptions of the directed-Blast type at mount st. Helens, Bezymianny and Shiveluch volcanoes. Journal of Geodynamics 3, 189-218.

Bonatti, E., 1990. Not so hot “hot spots” in the oceanic mantle. Science 250, 107–111.

Bonneville, A., Dosso, A.L., Hildenbrand, A., 2006. Temporal evolution and geochemical variability of the South Pacific superplume activity, Earth and Planetary Science Letters 244, 251-269.

Booth, B., Croasdale, R., Walker, G.P.L., 1978. A quantitative study of five thousand years of volcanism on S. Miguel, Azores. Philosophical Transactions of the Royal Society of London 228, 271-319.

Borgia, A., 1994. Dynamic basis of volcanic spreading. Journal of Geophysical Research: Solid Earth 99 (B9), 17791-17804.

Borges, J.F., Bezzeghoud, M., Buforn, E., Pro, C., Fitas, A., 2007. The 18980, 1997 and 1998 Azores earthquakes and some seismo-tectonic implications. Tectonophysics 435, 37-54.

Boulesteix, T., Hildenbrand, A., Gillot, P.Y., Soler, V., 2012. Eruptive response of oceanic islands to giant landslides: New insights from the geomorphologic evolution of the Teide-Pico Viejo volcanic complex (Tenerife, Canary). Geomorphology 138 (1), 61-73.

Boulesteix, T., Hildenbrand, A., Soler, V., Quidelleur, X., Gillot, P-Y., 2013. Coeval giant landslides in the Canary Islands: Implications for global, regional and local triggers of giant flank collapses on oceanic volcanoes. Journal of Volcanoly and Geothermal Research 257, 90-98.

Bourdon, B., Zindler, A., Elliott, T., Langmuir, C.H., 1996. Constraints on the mantle melting at mid-ocean ridges from global 2238Ur230Th disequilibria data. Nature 384, 231-235.

Bourdon, B., Turner, S.P., Ribe, N.M., 2005. Partial melting and upwelling rates beneath the Azores from a U-series isotope perspective. Earth Planetary Science Letters 239, 42-56.

Buck, W.R., 2007. The Dynamics of Continental Breakup and Extension. in The Treatise on Geophysics, G. Schubert series editor, Volume 6. Crustal and Lithosphere Dynamics, Watts editor.

Burke, K., Steinberger, B., Torsvik, T.H., Smethurst, M.A., 2008. Plume Generation Zones at the Margins of Large Low Shear Velocity Provinces on the Core-Mantle Boundary. Earth Planetary Science Letters 265 (1-2), 49-60.

Byerlee, J.D., 1967. Frictional characteristics of granite under high confining pressure. Journal of Geophysical Research 72, 3639–3648.

Calvert, A.T., Moore, R.B., McGeehin, J.P., Rodrigues da Silva, A.M., 2006. Volcanic history and 40Ar/39Ar and 14C geochronology of Terceira Island, Azores. Portugal, Journal of Volcanology and Geothermal Research 156, 103-115.

Cannat, M., Briais, A., Deplus, C., Escartin, J., Georgen, J., Lin, J., Mercouriev, S., Meyzen, C., Muller, M., Pouliquen, G., Rabain, A., Da Silva, P., 1999. Mid Atlantic rige Azores hotspot interactions: along axis migration of a hotspot derived event of enhanced magmatism 10 to 4 Ma ago. Earth Planetary Science Letters 173 (3), 257-269.

Cannat, M., Rommevaux-Jestin, C., Fujimoto, H., 2003. Melt supply variations to a magma-poor ultra-slow spreading ridge (Southwest Indian Ridge 61° to 69°E. Geochemistry, Geophysics, Geosystems 4, 9104, doi:10.1029/2002GC000480.

Campan, A., 1995. Analyse cinématique de l'Atlantique équatorial: Implications sur l'évolution de l'Atlantique sud et sur la frontière des plaques Amérique du nord/Amérique du sud, thèse de doctorat, 352pp., Université Pierre et Marie Curie (Paris VI), Paris.

Carracedo, J.C., 1994. The Canary Islands: an example of structural control on the growth of large oceanic-island volcanoes. Journal of Volcanology and Geothermal Research 60, 225-241.

Carracedo, J.C., Day, S.J., Guillou, H., 1999a. Quaternary collapse structures and the evolution of the western Canaries (Las Palmas and Hierro). Journal of Volcanology and Geothermal Research 94, 169-190.

Carracedo, J.C., Day, S.J., Guillou, H., Gravestock, P., 1999b. Later stages of volcanic evolution of Las Palma, Canary Islands: Rift evolution, giant landslides, and the genesis of the Caldera Taburiente. Geological Society of America Bulletin 111 (5), 755-768.

Catalão, J., 2006. Iberia-Azores Gravity Model (IAGRM) using multi-source gravity data. Earth Planets and Space 58, 277–286.

Catalão, J., Miranda, J.M., Lourenco, N., 2006b. Deformation associated with the Faial (Capelinhos) 1957-1958 eruption: Inferences from 1937-1997 geodetic measurements. Journal of Volcanology and Geothermal Research 155, 151-163.

Catalão, J., Bos, M.S., 2008. Sensitivity analysis of the gravity geoid estimation: A case study on the Azores plateau. Physics of the Earth and Planetary Interiors 168, pp. 113-124, DOI: 10.1016/j.pepi.2008.05.010.

Carvalho, M.R., Forjaz, V.H., Almeida, C., 2006. Chemical composition of deep hydrothermal fluids in the Ribeira Grande geothermal field (São Miguel). Journal of Volcanology and Geothermal Research 156 (1-2), 116-134, doi: 10.1016/j.jvolgeores.2006.03.015.

Cassignol, C., Gillot, P.Y., 1982. Range and effectiveness of unspiked potassium-argon dating: Experimental groundwork and applications. John Wiley, New York, 159-179.

Chandrasekhar, S., 1962. Hydrodynamic and hydromagnetic stability. Oxford University Press.

Chovelon, P., 1982. Evolution volcano-tectonique des îles de Faial et Pico. Thèse, faculté des sciences de la Terre, Université Paris Sud 11, 242pp.

Clouard, V., Bonneville, A., Gillot, P.Y., 2001. A giant landslide on the southern flank of Tahiti Island, French Polynesia. Geophysical Research Letters 28 (11), 2253-2256.

Coakley, B., Cochran, J., 1998. Gravity evidence of very thin crust at the Gakkel Ridge (Artic Ocean). Earth and Planetary Science Letters 162, 81-95.

Cole, P.D., Queiroz, G., Wallenstein, N., Gaspar, J.L., Duncan, A.M., Guest, J.E., 1995. An historic subplinian/phreatomagmatic eruption : the 1630 AD eruption of Furnas volcano, S. Miguel, Azores. Journal of volcanology and Geothermal Research 69, 117-135.

Cole, P.D., Guest, J.E., Queiroz, G., Wallenstein, N., Pacheco, J.M., Gaspar, J.L., Ferreira, T., Duncan, A.M., 1999. Styles of volcanism and volcanic Hazards on Furnas Volcano, S. Miguel, Azores. Journal of Volcanology and Geothermal Research 92, 39-54.

Corti, G., 2009. Continental rift evolution: From rift initiation to incipient break-up in the Main Ethiopian Rift, East Africa. Earth-Science Reviews, 96 (1-2), 1-53.

Costa, A.C.G., Hildenbrand, A., Marques, F.O., Sibrant, A.L.R., Catalao, J., Catita, C.M.S., 2013. Tectonic and morphologic evolution of an active large-scale slump (Pico Island, Azores). Abstract Meeting, IAG 2013.

Costa, A.C.G., Marques, F.O., Hildenbrand, A., Sibrant, A.L.R., Catita, C.M.S., 2014. Large-scale flank collapses in a steep volcanic ridge: Pico-Faial Ridge, Azores Triple Junction. Journal of Volcanology and Geothermal Research 272, 111-125.

Costa, A.C.G., Hildenbrand, A., Marques, F.O., Sibrant, A.L.R., Santos de Campos, A., in prep. Incremental growth and collapse of Pico Island during the last 200 kyrs (Pico-Faial ridge, Azores Triple Junction).

Courtillot, V., Armijo, R., Tapponnier, P., 1987. The Sinai triple junction revisited. Tectonophysics 141, 181-190.

Courtillot, V., Davaille, A., Besse, J., Stock, J., 2003. Three distinct types of hotspots in the Earth's mantle. Earth and Planetary Science Letters 205, 295-308.

Davaille, A., 1999. Simultaneous generation of hotspots and superswells by convection in a heterogeneous planetary mantle. Nature 402, 756-760.

Davaille, A., Girard, F., Le Bars, M., 2002. How to Anchor Hotspots in a Convecting Mantle?. Earth and Planetary Science Letters 203, 621-634.

Davaille, A., Vatteville, J., 2005. On the transient nature of mantle plumes. Geophysical Research Letters 32, L14309, doi:10.1029/2005GL023029.

Davaille, A., Limare, A., 2007. Treatise of Geophysics vol.7 "Mantle Dynamics", eds D. Bercovici and J. Schubert, Elsevier, 89-165.

Davaille, A., Limare, A., Touitou, F., Kumagai, I., Vatteville, J., 2011. Anatomy of a laminar starting thermal plume at high Prandtl number. Experiments in Fluids 50 (2), 285–300.

Davies, G.R., Norry, M.J., Gerlach, D.C., Cliff, R.A., 1989. A combined chemical and Pb-Sr-Nd isotope study of the Azores and Cap Verde hot-spots: the geodynamic implications. In: Sauunders, A.D., Norry, M.J., editors. Magmatism in the oceanic basins. Geological Society Special Publications. 231-255.

Davis, A.S., Clague, D.A., Gray, L.B., Hein, J.R., 2002. The line islands revisited. New 40Ar/39Ar geochronologic evidence for episodes of volcanism due to lithospheric extension. Geochemistry, Geophysics, Geosystems 3, 1018, doi:10.1029/2001GC000190.

Debayle, E., Kennett, B., Priestley, K., 2005. Global azimuthal seismic anisotropy and the unique plate-motion deformation of Australia. Nature 433 (7025), 509-512.

Demande, J., Fabriol, R., Gérard, A., Iundt, F., 1982. Prospection géothermique des Iles de Faial et Pico (Açores). Report 82SGN003GTH, Bureau de Recherches Géologiques et Minières, Orléans, France.

DeMets, C., Gordon, R., Argus, D., Stein, S., 1994. Effect of recent revisions to the geomagnetic reversal time scale on estimates of current plate motions. Geophysical Research Letters 21, 2191-2194.

DeMets, C., Gordon, R., Argus, D.F., 2010. Geologically current plate motions. Geophysical Journal International 181, 1-80.

Deplus, C., LeFriant, A., Boudon, G., Komorowski, J.C., Villemant, B., Harford, C., Ségoufin, J., Cheminée, J.L., 2001. Submarine evidence for large-scale debris avalanches in the Lesser Antilles Arc. Earth and Planetary Science Letters 192 (2), 145-157, doi:10.1016/S0012-821X(01)00444-7.

Detrick, R.S., Needham, H.D., Renard, V., 1995. Gravity anomalies and crustal thickness variations along the Mid-Atlantic Ridge between 33°N and 40°N. Journal of Geophysical Research 100, 3767–3787.

Dias N.A., Matias, L. Lourenço, N. Madeira, J. Carrilho F. Gaspar, J.L. 2007. Crustal seismic velocity structure near Faial and Pico Islands (Azores), from local earthquake tomography. Tectonophysics 445 (3-4): 301-317.

Dick, H.J.B., J., Lin, and H., Schouten, 2003. Ultra slow spreading – a new class of ocean ridge, Nature 426, 405-412.

Dieterich, J.H., 1988. Growth and persistence of Hawaiian volcanic rift zones. Journal of Geophysical Research 93, 4258-4270.

Dixon, J.E., Leist, L., Langmuir, H., Schilling, J.G., 2002. Recycled dehydrated lithosphere observed in plume-influenced mid-ocean-ridge basalt. Nature 420, 385-389.

Dosso, L., Bougault, H., Joron, J.L., 1993. Geochemical morphology of the North Mid-Atlantic Ridge, 10°-24°N : Trace element-isotope complementarity. Earth and Planetary Science Letters 120, 443-462.

Dosso, L., Bougault, H., Langmuir, C., Bollinger, C., Bonnier, O., Etoubleau, J., 1999. The age and distribution of mantle heterogeneity along the Mid-Atlantic Ridge (31-41 degrees N). Earth and Planetary Science Letters 170, 269-286.

Driscoll, N., Karner, G., 1998. Lower crustal extension across the Northern Carnarvon basin, Australia: Evidence for an eastward dipping detachment. Journal of Geophysical Research 103, 4975-4991.

Drolia, R.K., DeMets, C., 2005. Deformation in the diffuse India-Capricorn-Somalia triple junction from a multibeam and magnetic survey of the northern Central Indian Ridge - 3°S-10°S. Geochemistry, Geophysics, Geosystems 6, 9, Q09009, doi: 10.1029/2005GC000950.

Duncan, R.A., McDougall, I., 1976. Geologically current plate motions. Geophysical Journal International 181, 1-80.

Duncan, A.M., Queiroz, G., Guest, J.E., Cole, P.D., Wallenstein, N., Pacheco, J.M., 1999. The Povoação Ignimbrite, Furnas Volcano, São Miguel, Azores. Journal of Volcanology and Geothermal Research 92 (1-2), 55-65.

Elliott, T., Blichert Toft, J., Heumamn, A., Koetsier, G., Forjaz, V., 2007. The origins of enriched mantle beneath São Miguel, Azores. Geochimica et Cosmochimica Acta, 71 (1), 219-240.

Elsworth, D., and Voight, B., 1995. Dike intrusion as a trigger for large earthquakes and the failure of volcano flanks. Journal of Geophysical Research 100, No. B4, 6005-6024.

Escartin, J., Cannat, M., Pouliquen, G., Rabain, A., Lin, J., 2001. Constraints on the interaction between the Mid-Atlantic Ridge and the Azores hotspot from bathymetry and gravity (36-39N). Journal of Geophysical Research 106, 21719-21736.

Féraud, G., Kaneoka, I., Allègre, C.J., 1980. K/Ar ages and stress pattern in the Azores: geodynamic implications. Earth and Planetary Science Letters 46, 275–286.

Féraud, G., Schmincke, H.U., Lietz, J., Gastaud, J., Pritchard, G., Bleil, U., 1981. New K-Ar Ages, Chemical Analyses and Magnetic Data of Rocks from the Islands of Santa Maria (Azores), Porto Santo and Madeira (Madeira Archipelago) and Gran Canaria (Canary Islands). Bulletin of Volcanology 44, 359-357.

Fernandes, R.M.S., Bastos, L., Ambrosius, B.A.C., Noomen, R., Matheussen, S., Baptista, P., 2004. Recent geodetic results in the Azores Triple Junction region. Pure and Applied Geophysics 161 (3), 683–699, doi:10.1007/s00024-003-2469-y.

Fernandes, R.M.S., Bastos, L., Miranda, J.M., Lourenço, N., Ambrosius, B.A.C., Noomen, R., Simons, W., 2006. Defining the plate boundaries in the Azores region. Journal of Volcanology and Geothermal Research 156, 1-9.

Fernandez, L.A., 1980. Geology and petrology of the Nordeste volcanic complex, S. Miguel, Azores: summary. Geological Society of American Bulletin 91, 675-680.

Ferreira, T., 2000. Caracterizacão da actividade vulcânica subaérea da ihla de S. Miguel (Açores): vulcanismo basaltico recente e zonas de desgaseificação, Avaliação de riscos. Tese de Doutoramento em Geologia, especialidade em Vulcanologia, Departemento de Geociências, Universidade dos Açores, 248pp.

Fiske, R.S., Jackson, E.D., 1975. Orientation and growth of Hawaiian rifts: The effect of regional structure and gravitational stresses. Proceeding of the Royal Society of London 329, 299-326.

Foulger, G.R., Pritchard, M.J., Julian, B.R., Evans, J.E., Allen, R.M., Nolet, G., Morgan, W.J., Bergsson, B., Erlendsson, P., Jakobsdottir, S., Ragnarsson, S., Stefansson, R., Vogfjord, K., 2001. Seismic tomography shows that upwelling beneath Iceland is confined to the upper mantle. Geophysical Journal International 146, 504-530.

Forjaz, V.H., 1988. Azores study tour: field tripe guide. Seminar on the prediction of earthquakes. Econ. Comm. for Europe, U.N. Lisbon. 36 pp.

Forte, A. M., Quéré, S., Moucha, R., Simmons, N.A., Grand, S.P., Mitrovica, J.X., Rowley, D.B., 2010. Joint seismic-geodynamic-mineral physical modelling of African geodynamics: A reconciliation of deep-mantle convection with surface geophysical constraints. Earth and Planetary Science Letters 295, 329-341.

Francheteau, J., Ballard, R.D., 1983. The East Pacific Rise near 21°N, 13”, and 20°S: inferences from along-strike variability of axial processes of the mid-ocean ridges, Earth and Planetary Science Letters 64, 93-116.

Franca, Z., Cruz, J.V., Nunes, J., Forjaz, V.H., 2003. Azores historical eruptions: geochemical features and related eruptive styles. Abstract Book - Week A, XXIII General Assembly of the International Union of Geodesy and Geophysics - IUGG 2003, Sapporo, Japan, A.558.

Francis, P.W., Hammill, M., Kretzschmar, G., Thorpe, R.S., 1978. The Cerro Galan Caldera, North west Argentina and its tectonic setting, Nature 274, 749-751.

Furi, E., Hilton, D.R., Dyment, J., Hemond, C., Murton, B., 2009. Ridge-hotspot interaction at the central indian Ridge, 20 degrees S: New Helium isotope results. Geochimica et cosmochimica acta 73 (13), p.A404-A404.

Galdeano, A., Moreau, M.G., Pozzi, J.P., Berthou, P.Y., Malod, J.A., 1989. New paleomagnetic results from Cretaceous sediments near Lisboa (Portugal) and implications for the rotation of Iberia. Earth and Planetary Science Letters 92, 95-106.

Gandino, A., Guidi, M., Merlo, C., Mete, L., Rossi, R., Zan, L., 1985. Preliminary model of the Ribeira Grande Geothermal field (Azores islands). Geothermics 14, 91-105.

Garcia, S., 2003. Implication d'un saut de rift et du fonctionnement d'une zone transformante sur les déformations du nord de l'Islande: approches structurales, sismotectonique et radiochronologique. Thèse de doctorat de l'Université Pierre et Marie Curie, Paris, France.

Gaspar, J.L., Queiroz, G., 1995. Carta Vulcanologica dos Açores, ilha Graciosa 1: 10.000, folhas Ae B. UAC, Centro de Vulcanologia UAC y Cãmara Municipal de Santa Cruz da Graciosa.

Gaspar, J.L., 1996. Ilha Graciosa (Açores): Historia Vulcanologica e Avaliaçao do Hazard. Thesis Doctoral, Univ. Dos Açores, 361 pp.

Gente, P., 1987. Etude Morphostructurale comparative de dorsales océaniques à taux d'expansion varié. Thèse de doctorat de l'Université de Bretagne occidentale.

Gente, P., Dyment, J., Maia, M., Goslin, J., 2003. Interaction between the Mid Atlantic ridge and the Azores hotspot during the last 85 Myr: Emplacement and rifting of the hotspot derived plateaus. Geochemistry, Geophysics, Geosystems 8, Q03013, doi:10.1029/2006GC001318.

Georgen, J.E., Sankar Ravi, D., 2010. Effects of ridge geometry on mantle dynamics in an oceanic triple junction region: Implications for the Azores Plateau. Earth and Planetary Science Letters 298 (1-2), 23 - 34.

Germa, A., Quidelleur, X., Labanieh, S., Chauvel, C., Lahitte, P., 2011. The volcanic evolution of Martinique Island: insights for the Lesser Antilles arc migration since the Oligocene. Journal of Volcanology and Geothermal Research 208, 122-135.

Germa, A., Quidelleur, X., Lahitte, P., Labanieh, S., Chauvel, C., 2011. The K-Ar Cassignol-Gillot technique applied to western Martinique lavas: A record of the evolution of the recent Lesser Antilles island arc activity from 2 Ma to Mount Pelé volcanism, Quaternary Geochronology 6, 341-355.

Gillot, P.Y., Cornette, Y., 1986. The Cassignol technique for potassium-argon dating, precision and accuracy: examples from late Pleistcene to recent volcanism from southern Italy. Chemical Geology 59, 205-222.

Gillot, P.Y., Cornette, Y., Max, N., Floris, B., 1992. Two reference materials, trachytes MDO-G and ISH-G, for argon dating K/Ar and $^{40}Ar/^{39}Ar$ dating of Pleistocene and Holocene rocks. Geostandards and Geoanalytical Research 16, 55-60.

Gillot, P.Y., Lefevre, J.C., Nativel, P.E., 1994. Model for the structural evolution of the volcanoes of Reunion Island. Earth and Planetary Science Letters 122 (3-4), 291-302.

Gillot, P.Y., Hildenbrand, A., Lefèvre, J.C., Albore-Livadie, C., 2006. The K/Ar dating method: Principle, Analytical Techniques and Application to Holocene Volcanic Eruptions in the southern Italy. Acta Vulcanologica 18, 55-66.

Goes, S., Spakman, W., Bjiwaard, H., 1999. A Lower mantle source for central European Volcanism. Science 286 (5446), 1928-1931.

Gomes, A., Gaspar, J.L., Goulart, C., Queiroz, G., 2005. Evaluation of landslide susceptibility of Sete Cidades volcano (S. Miguel Island, Azores). Natural Hazards and Earth System Sciences 5, 251-257.

Gomes, A., Gaspar, J.L., Queiroz, G., 2006. Seismic vulnerability of dwellings at Sete Cidades Volcano (S. Miguel, Azores). Natural Hazards and Earth System Sciences 6, 41-48.

Gorbatov, A., Fukao, Y., Widiyantoro, S., Gordeev, E., 2001. Seismic Evidence for a Mantle Plume Oceanwards of the Kamchatka-Aleutian Trench Junction. Geophysical Journal International 146, 282-288.

Gordon, R.G., DeMets, C., Royer, J.Y., 1998. Evidence for long-term diffuse deformation of the lithosphere of the equatorial Indian Ocean. Nature 395, 370-374. doi:10.1038/26463.

Goslin, J., Thirot, J.L., Noel, O., Francheteau, J., 1998. Slow-ridge/hotspot interactions from global gravity, seismic tomography and 87Sr/86Sr isotope data. Geophysical Journal International 135, 700-710.

Goslin, J., Triatnord Scientific Party, 1999. Extent of Azores plume influence on the Mid-Atlantic Ridge north of the hotspot. Geology 27, 991-994.

Grimison, N.L., Chen, W.P., 1986. The Azores-Gilbraltar plate boundary: Focal mechanisms, depths of earthquakes, and their tectonic implications, Journal of Geophysical Research 91, B2, 2029-2047.

Gripp, A.E., Gordon, R.G., 2002. Young tracks of hotspots and current plate velocities. Geophysical Journal International 150, 321-361.

Guest, J.E., Gaspar, J.L., Cole, P.D., Queiroz, G., Duncan, A.M., Wallenstein, N., Ferreira, T., Pacheco, J.M., 1999. Volcanic geology of Furnas volcano, S. Migeul, Azores. Journal of Volcanology and Geothermal Research 92, 1-29.

Haase, K.M., Beier, C., 2003. Tectonic control of ocean island basalt sources on São Miguel, Azores? Geophysical Research Letters 30, doi:10.1029/2003GL017500.

Harpp, K., Geist, D., 2002. Wolf-Darwin lineament and plume-ridge interaction in northern Galapagos. Geochemistry, Geophysics, Geosystems 3 (11), 8504, doi:10.10292002GC00370.

Harpp, K., Fornari, D.J., Geist, D., Kurz, M.D., 2003. Genovesa Submarine Ridge: A manifestation of plume-ridge interaction in the northern Galapagos Islands, Geochemistry, Geophysics, Geosystems 4(9), 8511, doi:10.109/2003GC000531.

Hardarson, B.S., Fitton, J.G., Ellam, R.M., Pringle, M.S., 1997. Rift relocation – a geochemical and geochronological investigation of a paleo-rift in northwest Iceland. Earth and Planetary Science Letters 153, 181-196.

Henk, A., 2006. Stress and strain during fault-controlled lithospheric extension-insights from numerical experiments. Tectonophysics 415, 39-55.

Hildenbrand, A., Gillot, P.Y., Soler, V., Lahitte, P., 2003. Evidence for a persistent uplifting of LaPalma (Canary Islands), inferred from morphological and radiometric data. Earth and Planetary Science Letters 210, 277-289.

Hildenbrand, A., Gillot, P.Y., Le Roy, I., 2004. Volcano-tectonic and geochemical evolution of an oceanic intra-plate volcano: Tahiti-Nui (French Polynesia), Earth and Planetary Science Letters 217 (3), 349-365.

Hildenbrand, A., Gillot, P.Y., Bonneville, A., 2006. Off-shore evidence for a huge landslide of the northern flank of Tahiti-Nui (French Polynesia). Geochemistry, Geophysics, Geosystems 7 (3), 1-12.

Hildenbrand, A., Madureira, P., Ornelas Marques, F., Cruz, I., Henry, B., Silva, P., 2008. Multi-stage evolution of a sub-aerial volcanic ridge over the last 1.3Myr: S. Jorge Island, Azores Triple Junction. Earth and Planetary Science Letters 273, 289-298.

Hildenbrand, A., Marques, F.O., Catalão, J., Catita, C.M.S., Costa, A.C.G., 2012a. Large-scale active slump of the southeastern flank of Pico Island, Azores. Geology 40, 939-942.

Hildenbrand, A., Marques, F.O., Costa, A.C.G., Sibrant, A.L.R., Silva, P.M.F., Henry, B., Miranda, J.M., Madureira, P., 2012b. Reconstructing the architectural evolution of volcanic islands from combined K/Ar, morphologic, tectonic, and magnetic data: The Faial Island example (Azores). Journal of Volcanology and Geothermal Research 241-242, 39-48.

Hildenbrand, A., Marques, F.O., Costa, A.C.G., Sibrant, A.L.R., Silva, P.M.F., Henry, B., Miranda, J.M., Madureira, P., 2013a. Reply to the comment by Quartau and Mitchell on Reconstructing the architectural evolution of volcanic islands from combined K/Ar, morphologic, tectonic and magnetic data: the Faial Island example (Azores), Journal of

Volcanology and Geothermal Research 241-242, 39-48, by Hildenbrand et al., 2012. Journal of Volcanology and Geothermal Research 255, 127-130.

Hildenbrand, A., Marques, F.O., Catalão, J., Catita C.M.S., Costa, A.C.G., 2013b. Reply to the comment by Quartau and Mitchell on " Large-scale active slump of the southeastern flank of Pico Island, Azores," Geology, 40, 939-942, doi:10.1130/G33303.1, by Hildenbrand et al., 2012) in Geology, 41, doi:10.1130/G34879Y.1.

Hildenbrand, A., Weis, D., Madureira, P., Marques, F.O. 2014. Recent plate re-organization at the Azores Triple Junction: evidence from new geochemical and geochronological data on Faial, S; Jorge and Terceira volcanic islands. accepted with minor revision by Lithos.

Hipólito, A., 2009. Geologia estrutural da Ilha Graciosa: Enquadramento no âmbito da Junção Tripla dos Açores. MSc thesis, Azores University, Ponta Delgada, 257 pp.

Hipólito, A., Madeira, J., Carmo, R., Gaspar, J.L., 2011. Neotectonics of Graciosa Island (Azores) - Uncertainty in seismic hazard assessment in a volcanic area with variable slip-rates. 2nd INQUA-IGCP-567 International Workshop on Active Tectonics, Earthquake Geology, Archaeology and Engineering, Corinth, Greece.

Horn, A.G., Leonard, M.L., Weary, D.M., 1995. Oxygen consumption during crowing by roosters. Animal Behaviour 50, 1171-1175.

Howard, L. N. (1964), Convection at high Rayleigh number, in Proceedings of the Eleventh International Congress of Applied Mechanics Munich (ed H. Görtler) 1109-115, Springer, Berlin.

Hübscher, C., 2013. Tragica - Cruise No. M79/2 - August 26 – September 21, 2009. Ponta Delgada (Azores / Portugal) – Las Palmas (Canary Islands / Spain). METEOR-Berichte, M79/2, 37 pp., DFG-Senatskommission für Ozeanographie. https://getinfo.de/app/details?id=awi:doi~10.2312%252Fcr_m79_2.

Hieronymus, C.F., Bercovici, D., 1999. Discrete alternating hotspot islands formed by interaction of magma transport and lithospheric flexure. Nature 397, 604-606.

Hirth, G., Kohlstedt, D., 2003. Rheology of the Upper Mantle and the Mantle Wedge: a View from the Experimentalists. Inside the subduction Factory, 83-105.

Ito, G., Lin, J., 1995. Oceanic spreading center hot spot interactions: Cosntraints from along isochron bathymetric and gravity anomalies. Geology 23, 657-660.

Ito, G., 2001. Origin of V-shaped Reykjanes Ridges from a pulsing and dehydrating mantle plume. Nature 411, 681–684.

Ito, G., Lin, J., Graham, D., 2003. Observational and theoretical studies oft he dynamics of mantle plume Mid-Ocean Ridge Interaction. Reviews of Geophysics 41 (4), 1017-2003, doi:10.1029/2002RG000117.

Jean Baptiste, P., Allard, P., Coutinho, R., Ferreira, T., Fourré, E., Queiroz, G., Gaspar, J.L., 2009. Helium isotopes in hydrothermal volcanic fluids of the Azores archipelago. Earth and Planetary Science Letters 281 (1-2), 70 - 80.

Jicha, B.R., Coombs, M.L., Calvert, A.T., Singer, B.S., 2012. Geology and Ar-40/Ar-39 geochronology of the medium- to high-K Tanaga volcanic cluster, western Aleutians. Geological Society of America Bulletin 124 (5-6), 842-856.

Johnson, C.L., Wijbrans, J.R., Cosntable, C.G., Gee, J., Staudigel, H., Tauxe, L., Forjaz, V.H., Salgueiro, M., 1998. 40Ar/39Ar ages and paleomagnetism of São Miguel Lavas, Azores. Earth Planet. Sci. Lett. 160 (3-4), 637 - 649.

Karaoglu, O., Helvaci, C., 2012. Growth, destruction and volcanic facies architecture of three volcanic centres in the Miocene Usak-Gure basin, western Turkey: Subaqueous-subaerial volcanism in a lacustrine setting. Journal Volcanology and Geothermal Research 245-246, 1-20.

Kennett, B.L.N. (Compiler and Editor). 1991. "IASPEI 1991 Seismological Tables." Bibliotech, Canberra, Australia, 167 pp.

Kidd, R.B., Searle, R.C., Ramsay, A.T.S., Prichard, H., Mitchell, J., 1982. The geology and formation of King's Trough, Northeast Atlantic ocean, Marine Geology 48 (1-2), 1-30.

Kidd, R.B., Ramsay, A.T.S., 1987. The geology and formation of the King's Trough complex in the light of Deep Sea Drilling Project Site 608 drilling. DSDP 94, 1245-1261.

Kinvig, H.S., Geyer, A., Gottsmann, J., 2009. On the effect of crustal layering on ring-fault initiation and the formation of collapse calderas, Journal of Volcanology and Geothermal Research 186, 293-304, doi: 10.1016/j.jvolgeores.2009.07.007.

Kirby, M.X., Jones, D.S., Avila, S.P., 2007. Neogene shallow-marine paleoenvironments and preliminary strontium isotope chronostratigraphy of Santa Maria island, Azores. Açoreana, 5, 112-125.

Klugel, A., Walter, T.R., Schwarz, S., Gelmacher, J., 2005. Gravitational spreading causes en-echelon diking along a rift zone of Madeira Archipelago: an experimental approach and implications for magma transport, Bulletin of Volcanology 68 (1), 37-46.

Krause, D.C., Watkins, N.D., 1970. North Atlantic crustal genesis in the vicinity of the Azores. Geophysical Journal of the Royal Astronomical Society 19, 261-283.

Kreemer, C., Holt, W.E., Haines, A.J., 2003. An integrated global model of present-day plate motion boundary deformation. Geophysical Journal International 154, 8-34.

Kumagai, I., Davaille, A., Kurita, K., 2007. On the fate of thermal plumes at density interface. Earth and Planetary Science Letters 254, L16301, 180-193.

Kurz, M.D., Jenkins, W.J., Schilling, J.G., Hart, S.R., 1982. Helium isotopic variations in the mantle beneath the central North Atlantic Ocean. Earth and Planetary Science Letters 58, 1-14.

Kurz, M.D., 1991. Noble gas isotopes in oceanic basalts: controversial constraints on mantle models. Short Course. Mineralogical Association of Canada 19, 259-286.

Lagabrielle, Y., Guivel, C., Maury, R.C., Bourgois, J., Fourcade, S., Martin, H., 2000. Magmatic-tectonic effects of high thermal regime at the site of active ridge subduction: The Chile Triple Junction model. Tectonophysics 326, 255–268, doi: 10.1016/S0040-1951(00)00124-4.

Larrea, P., Wijbrans, P.R., Galé, C., Ubide, T., Lago, M., França, Z., Widom, E., 2014. 40Ar/39Ar constraints on the temporal evolution of Graciosa Island, Azores (Protugal). Bull Volcanol. 76:796, doi:10.1007/s00445-014-0796-8.

Laughton, A.S., Whitmarsh, R.B., Rusby, J.S.M., Somers, M.L., Revie, J., McCartney, B.S., Nafe, J.E., 1972. A continuous East-West Fault on the Azores-Gibraltar Ridge. Nature 237, 217- 220.

Le Bars, M.? Davaille, A., 2004. Whole layer convection in a heterogeneous planetary mantle. Jounral of Geophysical Research 109, B03403, doi:10.1029/2003JB002617.

Le Friant, A., Boudon, G., DePlus, C., Villemant, B., 2003. Large-scale flank collapse events during the activity of Montagne Pelée, Martinique, Lesser Antilles. Journal of Geophysical Research: Solid Earth 108 (B1), doi:10.1029/2001JB001624.

Le Friant, A., Harford, C.L., DePlus, C., Boudon, G., Sparks, R.S.J., Herd, R.A., Komorowski, J.C., 2004. Geomorphological evolution of Montserrat (West Indies): importance of flank collapse and erosional processes. Journal of the Geological Society 161, 147-160.

Le Friant, A., Deplus, C., Boudon, G., Feuillet, N., Trofimovs, J., Komorowski, J.C., Sparks, R.S.J., Talling, P., Palmer, M., Ryan, G., 2010. Eruption of Soufrière Hills (1995-2009) from an offshore perspective: insights from repeated swath bathymetry surveys. Geophysical Research Letters 37 (L11307). Doi:10.1029/2010GL043580.

Lebas, E., Le Friant, A., Boudon, G., Watt, S., Talling, S., Feuillet, N., Deplus, C., Berndt, C., Vardy, M., 2011. Multiple widespread landslides during the long-term evolution of a volcanic island: insights from high-resolution seismic data, Montserrat, Lesser Antilles. Geochemistry, Geophysics, Geosystems 12 (5), Q05006. Doi:10.1029/2010GC003451.

Lénat, J.F., Vincent, P., Bachelery, P., 1989. The offshore continuation of an active basaltic volcano: Piton de la Fournaise (Reunion Island Indian Ocean). Journal of Volcanology and Geothermal Research 36, 1-36.

LePichon, X., 1968. Sea-Floor spreading and continental drift. Journal of Geophysical Research 73, 3661-3697.

Ligi, M. and the AZORRE99 Team, 1999. Giant Volcanic Ridges Amoungst the Azores Islands. AGU Fall Meeting.

Lipman, P.W., Normark, W.R., Moore, J.G., Wilson, J.B., Gutmacher, C.E., 1988. The giant submarine Alika debris slide, Mauna Loa, Hawaii. Journal of Geophysical Research 93, 4279-4299.

Lipman, P.W., 1997. Subsidence of ash-flow calderas: Relation to caldera size and magma-chamber geometry. Bulletin of Volcanology 59, 198-218.

Lourenço, N., Miranda, J.M., Luis, J.F., Ribeiro, A., Victor, L.A.M., Madeira, J., Needham, H.D., 1998. Morpho-tectonic analysis of the Azores Volcanic Plateau from a new bathymetric compilation of the area. Marine Geophysical Research 20 (3), 141–156.

Louvat, P., Allègre, C.J., 1998. Riverine erosion rates on s. Migeul volcanic island, Azores archipelago. Chemical Geology 148 (3-4), 177-200.

Luís, J.F., Miranda, J., Patriat, P., Galdeano, A., Rossignol, J.C., Mendes-Victor, L., 1994. Açores Triple junction Evolution in the last 10Ma from a New AeromagneticSurvey. Earth and Planetary Science Letters 125, 439-459.

Luis, J.F., Miranda, J.M., Galdeano, A., Patriat, P., 1998. Constraints on the structure of the Azores spreading center from gravity data. Marine Geophysical Research 20, 157-170.

Luis, J.F., Neves, M.C., 2006. The isostatic compensation of the Azores Plateau: a 3D admittance and coherence analysis. Journal of Volcanology and Geothermal Research 156 (1-2), 10-22.

Luís, J.F., Miranda, J.M., 2008. Reevaluation of magnetic chrons in the North Atlantic between 35°N and 47°N: Implications for the formation of the Azores Triple Junction and associated plateau, Journal of Geophysical Research 113, B10105, doi:10.1029/2007JB005573.

MacDonald, K.C., 1982. Mid-ocean ridges: Fine scale tectonic, volcanic and hydrothermal processes within the plate boundary zone, Annual Review of Earth and Planetary Sciences 10, 155-190.

Machado, F., 1957. Caldeiras Vulcanicas dos Açores. Atlantida, 1(5), 275-278.

Machado, F., 1959. Submarine pits of the Azores plateau. Bulletin of Volcanology 21, 109-116.

Madeira, J., 1986. Geologia estructural e enquadramento geotectonico da ilha de Santa Maria (Açores). M.Sc Thesis, Lisbon University, 107pp.

Madeira, J., Ribeiro, A., 1990. Geodynamic models for the Azores triple junction: A contribution from tectonics. Tectonophysics 184 (3-4), 405 - 415.

Madureira, P., Moreira, M., Mata, J., Allegre, J.C., 2005. Primitive neon isotopes in Terceira Island (Azores Archipelago). Earth and Planetary Science Letters 233 (3-4), 429 - 440.

Madureira, P., Mata, J., Mattielli, N., Queiroz, G., Silva, P., 2011. Mantle source heterogeneity, magma generation and magmatic evolution at Terceira island (Azores

archipelago): constraints from elemental and isotopic (Sr, Nd, Hf and Pb) data. Lithos 126, 402-418.

Magde, L., Sparks, D., Detrick R., 1997. The relationship betwween buoyant mantle flow, melt migration, and gravity bull's eyes at the Mid-Atlantic Ridge between 33°N and 35°N, Earth and Planetary Science Letters 148, 59-67.

Malinverno, A., Pockalny, R.A., 1990. Abyssal Hill topography as an indicator of episodicity in crustal accretion and deformation, Earth and Planetary Science Letters 99, 154-169.

Manconi, A., Longpré, M.-A., Walter, T.R., Troll, V.R., Hansteen, T.H., 2009. The effects of flank collapses on volcano plumbing systems. Geology, 37, 1099-1102.

Marques, F.O., Catalão, J.C., DeMets, C., Costa, A.C.G., Hildenbrand, A., 2013a. GPS and tectonic evidence for a diffuse plate boundary at the Azores Triple Junction. Earth and Planetary Science Letters 381, 177-187.

Marques, F.O., Sibrant, A.L.R., Hildenbrand, A., Costa, A.C.G., 2013b. Large-scale sector collapses in the evolution of Santa Maria Island, Azores. Abstract Meeting AGU, 2013.

Marques, F.O., Catalão, J.C., DeMets, C., Costa, A.C.G., Hildenbrand, A., 2014a. Corrigendum to "GPS and tectonic evidence for a diffuse plate boundary at the Azores Triple Junction" [Earth and Planetary Science Letters 381 (2013) 177–187]. Earth and Planetary Science Letters 387, 1–3.

Marques, F.O., Catalão, J., Hildenbrand, A., Costa, A.C.G., Dias, N.A., 2014b. The 1998 Faial earthquake, Azores: Evidence for a transform fault associated with the Nubia-Eurasia plate boundary? Tectonophysics, in press.

Masson, D.G., Watts, A.B., Gee, M.J.R., Urgeles, R., Mitchell, N.C., Le Bas, T.P., Canals, M., 2002. Slope failures on the flanks of the western Canary Islands. Earth Science Reviews 57, 1-35.

Masson, D.G., Le Bas, T.P., Grevemeyer, I., Weinrebe, W., 2008. Flank collapse and large-scale landsliding in the Cape Verde Islands, off West Africa. Geochemistry, Geophysics, Geosystems 9 (7), Q07015, doi:0.1029/2008GC001983.

McKenzie, D., 1972. Active Tectonics of the Mediterranean region. Geophysical Journal of the Royal Astronomical Society 30, 109-185.

McKenzie, D., Bickle, M.J., 1988. The volume and composition of melt generated by extension of the Lithosphere. Journal of Petrology 29 (3), 625-679, doi:10.1093/petrology/29.3.625.

McKenzie, D.P., Morgan, W.J., 1969. The evolution of triple junctions. Nature 224, 125-133.

McKenzie, D.P., Parker, D.L., 1967. The north Pacific: an example of tectonics on a sphere. Nature 216, 1275-1280.

McKee, E.H., Moore R.B, 1992. Potassium–argon dates for trachytic rocks on Sao Miguel, Azores, Isochron West 58, 9–11.

Meireles, R.P., Faranda, C., Gliozzi, E., Pimentel, A., Zanon, V., Avila, S.P., 2013. Late Miocene marine ostracods from Santa Maria island, Azores (NE Atlantic): Systematics, palaeoecology and palaeobiogeography. Revue de micropaleontologie 55, 133-148.

Mello, S.L.M., Cann, J.R., Fowler, C.M.R., 1999. Anomalous mantle at 45°N Mid-Atlantic Ridge. Journal of Geophysical Research: Solid Earth 104 (12), 29335-29349.

Mendes, V.B., Madeira, J., Brum da Silveira, A., Trota, A., Elosegui, P., Pagarete, J., 2013. Present-day deformation in São Jorge Island, Azores, from episodic GPS measurements (2001–2011). Advances in Space Research, http://dx.doi.org/10.1016/j.asr.2012.10.019.

Meschede, M. & Barckhausen, U., 2000. The plate tectonic evolution of the Cocos-Nazca spreading center - elektronische Veröffentlichung: Proc. ODP, Scientific Results: http://www-odp.tamu.edu/publications/170_SR/170TOC.HTM.

Métrich, N., Zanon, V., Créon, L., Hildenbrand, A., Moreira, M., Marques, F.O., 2014. Is the "Azores hotspot" a wetspot? Insights from geochemistry of fluid and melt inclusions in olivine of Pico basalt. Journal of Petrology 55, 377-393.

Michael, P.J., Langmuir, D.W., Dick, H.J.B., Snow, J.E., Goldstein, S.L, Graham, D.W., Lehnert, K., Kurras, G., Jokat, W., Muehe, R., Edmonds, H.N., 2003. Magmatic and amagmatic seafloor generation at the ultraslow-spreading Gakkel ridge, Arct, Ocean. Nature 423, 956-961.

Millet, M. A., Doucelance, R., Baker, J.A., Schiano, P., 2009. Reconsidering the origins of isotopic variations in Ocean Island Basalts insights from fine scale study of São Jorges island, azores Archipelago. Chemical Geology 265 (3-4) 235 - 336.

Mitchell, N.C., 1991. Distributed extension at the Indian Ocean triple junction. Journal of Geophysical Research 96, 8019–8043.

Mittelstaedt, E., Ito, G., 2005. Plume-ridge interaction, lithospheric stresses and the origino f near-ridge volcanic lineaments. Geochemistry, Geophysics, Geosystems 6 (6), 1-20, doi:10.1029/2004GC000860.

Mittelstaedt, E., Soule, S., Harpp, K., Fornari, D., McKee, C., Tivey, M., Geist, D., Kurz, M.D., Sinton, C., Mello, C., 2012. Multiple expressions of plume-ridge interaction in the Galapagos: Volcanic lineaments and ridge jumps. Geochemistry, Geophysics, Geosystems 13 (5), Q05018, doi:10.1029/2012GC004093.

Miranda, J.M., Freire Luis, J., Abreu, I., Mendes Victor, A., Galdeano, A., Rossignol, J.C., 1991. Tectonic Framework of the Azores Triple Junction. Geophysical Research Letters 18 (8), 1421-1424.

Miranda, J.M., Mendes Victor, L.A., Simões, J.Z., Luis, J.F., Matias, L., Shimamura, H., Shiobara, H., Nemoto, H., Mochizuki, H., Hirn, A., Lépine, J.C., 1998. Tectonic setting of the Azores Plateau deduced from a OBS survey. Marine Geophysical Research 20, 171-182.

Miranda, J.M., Luis, J.F., Lourenço, N., Fernandes, R.M.S., 2013. The structure of the Azores triple junction : implications for S. Miguel Island. GSL (in press).

Montagner, J.P., Ritsema J., 2001. Interactions between Ridges and Plumes. Science 294, 1472.

Montelli, R., Nolet, G., Dahlen, F.A., Masters, G., Engdahl, E.R., Hung, S.H., 2004. Finite frequency tomography reveals a variety of plumes in the mantle. Science 303, 338–343.

Montelli, R., Nolet, G., Dahlen, F.A., Masters, G., 2006. A catalogue of deep mantle plumes: New results from finite-frequency tomography. Geochemistry, Geophysics, Geosystems 7 (11).

Montési, L.G., Behn, M.D., 2007. Mantle flow and melting underneath oblique and ultraslow mid-ocean ridges, Geophysical Research Letters 34, L24307, doi:10.1029/2007GL031067.

Montesinos, F.G., Camacho, A.G., Vierra, R., 1999. Analysis of gravimetric anomalies in Furnas caldera (São Miguel, Azores). Journal of Volcanology and Geothermal Research 92 (1-2), 67 - 81.

Moore, R., 1990. Volcanic geology and eruption frequency, S. Miguel, Azores. Bulletin of Volcanology 52, 602–614.

Moore, R., 1991a. Geologic map of São Miguel, Azores (Scale 1: 50.000). U.S.G.S. MISC INV. map I-2007.

Moore, R., 1991b. Geology of three late Quaternary stratovolcanoes on São Miguel, Azores. U.S.G.S. Bull. 1900, 1–26.

Moore, R., Rubin, M., 1991. Radiocarbon dates for lava flows and pyroclastic deposits on São Miguel, Azores. Radiocarbon 33 (1), 151-164.

Moore, J.G., Normark, W.R., Holcomb, R.T., 1994. Giant Hawaiian landslides. Annual Review of Earth and Planetary Science Letters 22, 119-144.

Moreira, M., Doucelance, R., Kurz, M.D., Dupre, B., Allegre, C.J., 1999. Helium and lead isotope geochemistry of the Azores Archipelago. Earth and Planetary Science Letters 169, 189–205.

Moreira, M., Allegre, J.C., 2002. Rare gas systematics in Mid Atlantic ridge (37°-40°N). Earth and Planetary Science Letters 198 (3-4), 401-416.

Morgan, W.J., 1971. Convection plumes in the lower mantle, Nature 230, 43-44.

Muecke, G.K., Ade-Hall, J.M., Aumento, F., McDonald, A., Reynolds, P.H., Hyndman, R.D., Quintino, J., Opdyke, N., Lowrie, W., 1974. Deep drilling in an active geothermal area in the Azores. Nature 252 (5481), 281–285.

Muller, R.D., Roest, W.R., Royez, J.Y., 1998. Asymmetric seafloor spreading expresses ridges-plume interactions. Nature 396, 455-459.

Mutter, J.C., Karson, J.A., 1992. Structural processes at slow-spreading ridges. Science 257 (5070), 627-634.

Natland, J. H., Winterer, E.L., 2005. Fissure control on volcanic action in the Pacific. In Foulger, G.R., Natland, J.H., Presnall, D., and Anderson, D.A. (Eds.), Plates, Plumes, and Paradigms, Geol. Soc. Amer. Spec. Paper 388. Boulder, CO (Geological Society of America), p. 687-710.

Nakamura, K., 1977. Volcanoes as possible indicators of tectonic stress orientation – principle and proposal. Journal Volcanology Geothermal Research 2, 1-16.

Nakamura, K., Jacob, K.H., Davies, J.N., 1977. Volcanoes as possible indicators of tectonic stress orientation – Aleoutians and Alaska, Pure Application Geophysics 115, 87-112.

Navarro, A., Lourenço, N., Chorowicz, J., Miranda, J.M., Catalao, J., 2009. Analysis of geometry of volcanoes and faults in Terceira Island (Azores): Evidence for reactivation tectonics at the EUR/AFR plate boundary in the Azores triple junction. Tectonophysics 465 (1-4), 98-113.

Navarro, A., Catalão, J., Miranda, J.M., Fernandes, R.M.S., 2003. Estimation of the Terceira island (Azores) main strain rates from GPS data. Earth. Planets and Space 55, 637-642.

Neves, M.C., Miranda, J.M., Luis, J.L., 2013. The role of lithospheric processes on the development of linear volcanic ridges in the Azores. Tectonophysics doi:10.1016/j.tecto.2013.09.016.

Norton, I.O., 2000. Global hotspot Reference Frames and Plate Motion, in The history and dynamics of Global Motions. AGU Geophys. Monograph 121, 339-357.

O'Neil, C.O., Muller, D., Steinberger, B., 2003. Geodynamic Implications of Moving Indian Ocean Hotspots. Earth Planetary Science Letters 215 (1-2), 151-168.

Odin, G.S., et al., 1982. Interlaboratory standards for dating purposes. In: Odin, G.S. (Ed.), Numerical Dating in Stratigraphy. John Wiley and Sons, Chichester, pp. 123-150.

Oehler, J.F., Wyk de Vries, B., Labazuy, P., 2005. Landslides and spreading of oceanic hot-spot and arc shield volcanoes on Low Strength Layers (LSLs) : an analogue modeling approach. Journal Volcanology Geothermal Research 144 (1-4), 169-189.

Peter Olson, P., Schubert, G., Anderson, C., Goldman, P., 1988. Plume formation and lithosphere erosion: A comparison of laboratory and numerical experiments. Journal of Geophysical Research: Solid Earth 93 (B12), 15065-15084.

Ortner H., Reiter, F., Acs, P., 2002. Easy handling of tectonic data the programs TectonicVB for Mac and TectonicsFP for Windows. Computers and Geosciences 28, 1193-1200, doi: 10.1016/S0098-3004(02)00038-9.

Ownby, S., Granados, H.G., Lange, R.A., Hall, C.M., 2007. Volcan Tancitaro, Michoacan, Mexico, $^{40}Ar/^{39}Ar$ constraints on its history of sector collapse. Journal Volcanology Geothermal Research 161 (1-2), 1-14.

Ozawa, A., T., Tagami, Garcia, M.O., 2005. Unspiked K-Ar dating of the honolulu rejuvenated and Ko'olau shield volcanism on O'ahu, Hawaii. Earth Planetary Science Letters 232, 1-11.

Patriat, P., Courtillot, V., 1984. On the stability of triple junctions and its relation to episodicity in spreading. Tectonics 3, 317-332.

Perfit, M. R., Chadwick, W.C., 1998. Magmatism at mid oceanic ridges: constraints from volcanological and geochemical investigations in : faulting and magmatism at mid ocean ridges, Buck, W. R., et al (eds), Am. Geophys. U. Geophys. Monograph., 106, 59-116.

Pinel, V., Jaupart, C., 2004. Magma storage and horizontal dike injection beneath a volcanic edifice. Earth Planetary Science Letters 221, 245-262.

Pinel, V., Albino, F., 2013. Consequences of volcano sector collapse on magmato storage zones: Insights from numerical modeling. Journal Volcanology Geothermal Research 252, 29-37.

Quartau, R., Tempera, F., Mitchell, N.C., Pinheiro, L.M., Duarte, H., Brito, P.O., Bates C.R., Monteiro, J.H., 2012. Morphology of the Faial Island shelf (Azores): The interplay between volcanic, erosional, depositional, tectonic and mass-wasting processes. Geochemistry Geophysics Geosystems 13 (4), doi:10.1029/2011GC003987.

Queiroz, G., 1997. Vulcão das Sete Cidades (S. Miguel, Açores) História Eruptiva e Avaliação do Hazard. Unpublished PhD Thesis. Universidade do Açores, 226p.

Queiroz, G., Gaspar, J.L., 1998. The geological setting of the Azores archipelago: a review (Com. oral). InterRidge Workshop: Long term monitoring of the Mid-Atlantic Ridge (MOMAR). Lisboa, Museu da Ciência, Outubro.

Queiroz, G., Pacheco, J.M., Gaspar, J.L., Aspinall, W.P., Guest, J.E., Ferreira, T., 2008. The last 5000 years of activity at Sete Cidades volcano (São Miguel island, Azores) implication for hazard assessment. Journal Volcanology Geothermal Research 178 (3), 562 - 573.

Quidelleur, X., Gillot, P.Y., Soler, V., Lefèvre, J.C., 2001. K/Ar dating extended into the last millennium : application to the youngest effusive episode of the Teide volcano (Spain). Geophysical Research Letters 28, 3067-3070.

Quidelleur, X., Carlut, J., Soler, V., Valet, J.P., Gillot, P.Y., 2003. The age and duration of the Matuyama-Brunhes transition from new K-Ar data from La Palma (Canary Islands) and revisited Ar-40/Ar-19 ages. Earth and Planetary Science Letters 208, 149-163.

Quidelleur, X., Hildenbrand, A., Samper, A., 2008. Causal link between Quaternary paleoclimatic changes and volcanic islands evolution. Geophysical Research Letters 35 (2), 5.

Ramalho, R., Quartau, R., Trenhaile, A.S., Mitchell, N.C., Woodroffe, C.D., Avila, S.P., 2013. Coastal evolution on volcanic oceanic islands: a complex interplay between volcanism,

erosion, sedimentation, sea-level change and biogenic production. Earth Science Reviews 127, 140-170.

Raymond, C.A., Stock, J.M., Cande, S.C., 2000. Fast Paleogene Motion of the Pacific Hotspots from Revised Global Plate Circuit Constraints. In The history and dynamics of Global Motions. AGU Gephys. Monograph 121, 359-375.

Ribe, N.M., Cristensen, U.R., Theissing, J., 1995. The dynamics of plume-ridge interaction. 1. Ridge-centered plumes. Earth Planetary Science Letters 134 (1-2), 155-168.

Ribe, N., 1996. The dynamics of plume–ridge interaction: 2. Off-ridge plumes. Journal Geophysical Research 101, 16195–16204.

Ricci, J., Lahitte, P., Quidelleur, X., 2014. Construction and destruction rates of volcanoes within tropical environment: examples from the Basse-Terre Island (Guadeloupe, Lesser Antilles). Accepted in Geomorphology.

Ritsema, J., Allen, R.M., 2003. The elusive mantle plume. Earth Planetary Science Letters 207 (1), 1-12.

Roest, W.R., Srivastava, S.P., 1991. Kinematics of the plate boundaries between Eurasia, Iberia and Africa in the North Atlantic from the late Cretaceous to present. Geology 19, 613-616.

Sager, W.W., 2005. What built Shatsky Rise, a mantle plume or ridge tectonics? In Foulger, G., et al., eds. Plates, plumes, and paradigms: Boulder, Colorado, Geological Society of America Special Paper 388, p.721-733.

Samper, A., Quidelleur, X., Boudon, G., Le Friant, A., Komorowski, J.C., 2008. Radiometric dating of three large volume flank collapses in the Lesser Antilles Arc. Journal Volcanology Geothermal Research 176 (4), 485-492.

Samper, A., Quidelleur, X., Komorowski, J.C., Lahitte, P., Boudon, G., 2009. Effusive history of the Grande Decouverte Volcanic Complex, southern Basse-Terre (Guadeloupe, French West Indies) from new K-Ar Cassignol-Gillot ages. Journal of Volcanology and Geothermal Research 187, 117-130.

Samuel, H., Bercovici, D., 2006. Oscillating and stagnating plumes in the Earth's lower mantle. Earth and Planetary Science Letters 248, 90-105.

Sandwell, D.T., Winterer, E.L., Mammericks, J., Duncan, R.A., Lynch, M.A., Levitt, D.A., Jonhson, C.L., 1995. Evidence for diffuse extension of the Pacific plate motion from pukapuka ridges and cross-grain gravity lineations. Journal Geophysical Research 100, 15087-15099.

Sandwell, D.T., Smith, H.F., 2009. Global marine gravity from retracked Geosat and ERS-A altimetry: Ridge segmentation versus spreading rate. Journal Geophysical Research 114, B01411, doi:10.1029/2008JB006008.

Schilling, J.G., 1975. Azores mantle blob: rare earth evidence. Earth Planetary Science Letters 25, 103–115.

Schilling, J.G., Bergeron, M., Evan, R., Smith, J.V., 1980. Halogens in the mantle beneath the North Atlantic. Philo. Trans. Royal Society London 297 (1431), 147-178.

Schilling, J.G., Zajac, M., Evans, R., Johnston, T., White, W., Devine, J.D., Kingsley, 1983. Petrology and chemical variations along the Mid-Atlantic Ridge from 29°N to 73°N, American Journal Science 283, 510 – 586.

Schilling, J.G., 1985. Upper mantle heterogeneities and dynamics. Nature 314, 62-67.

Schmincke, H.U., Weibel, M., 1972. Chemical study of rocks from Madeira, Porto Santo and Sao Miguel, Terceria (Azores). Neues Jahrb Mineral Abh, 117: 253–281.

Schouten, H., Smith, D.K., Montesi, L., Zhu, W., Klein, E.M., 2008. Cracking of lithosphere north of the Galapagos triple junction. Geology 36, 330-342, doi:10.1130/G24431A.1.

Searle, R.C., 1976. Lithospheric structure of the Azores Plateau from Rayleigh-wave dispersion. Geophys. Journal Royal Astronomical Society 44, 537–546.

Searle, R., 1980. Tectonic pattern of the Azores spreading centre and triple junction. Earth Planetary Science Letters 51, 415-434.

Searle, R., Whitmarsh, R.B., 1978. The structure of King's Trough, Northeast Atlantic, from bathymetric, seismic and gravity studies. Geophysical Journal Royal Astronomy Society 53, 259-287.

Serralheiro, A., Alves, C.A.M., Forjaz, V.H., Rodrigues, B., 1987. Carta vulcanológica dos Açores, Ilha de Santa Maria. Escala 1:15000 (folhas 1 e 2): Serviço regional de Protecção Civil dos Açores e Universidade dos Açores (Ed.). Ponta Delgada.

Shaw, H.R., 1980. Fracture mechanisms of magma transport from the mantle to the surface. In Physics of magmatic Processes, R.B., Hargraves, ed. Princeton U. Press, Princeton, N.J., 201-264.

Shotton, F.W., Blundell, D.J., Williams, R.E.G., 1969. Birmingham university radiocarbon dates III. Radiocarbon 11 (2), 263-270.

Shotton, F.W., Blundell, D.J., Williams, R.E.G., 1971. Birmingham university radiocarbon dates III. Radiocarbon 13 (2), 141-156.

Sibrant, A.L.R., Hildenbrand, A., Marques, F.O., Boulesteix, T., Costa, A.C.G., 2013a. Morpho-structural evolution of a volcanic island developed inside an active oceanic rift: S. Miguel Island (Terceira Rift, Azores). Abstract Meeting, IAG, 2013.

Sibrant, A.L.R., Hildenbrand, A., Marques, F.O., Costa, A.C.G., 2013b. Volcano-tectonic evolution of Santa Maria island: implications for the Nubia-Eurasia plate boundary in the Azores. Abstract Meeting, AGU, 2013.

Sibrant, A.L.R., Marques, F.O., Hildenbrand, A., 2014. Construction and destruction of a volcanic island developed inside an oceanic rift: Graciosa Island, Terceira Rift, Azores.

Journal of Volcanology and Geothermal Research 284, 32-45.

Silva, P.F., Henry, B., Marques, F.O., Hildenbrand, A., Madureira, P., Mériaux A., Kratinova, Z., 2012. Palaeomagnetic study of a subaerial volcanic ridge (Sao Jorge Island, Azores) for the past 1.3 Myr: evidence for the Cobb Mountain Subchron, volcano flank instability and tectonomagmatic implications. Geophysical Journal International 188, 959-978.

Silveira, G., Stutzmann, E., 2002. Anisotropic Tomography of the Atlantic Ocean. Physics Earth Planetary Interior 132, 237.

Silveira, G., Stutzmann, E., Davaille, A., Montagner, J.-P., Mendes-Victor, L., Sebai, A., 2006. Azores hotspot signature in the upper mantle. Journal Volcanology Geothermal Research 156, 23–34.

Silveira, G., Vinnik, L., Stutzmann, E., Farra, V., Kiselev, S., Morais, I., 2010. Stratification of the Earth beneath the Azores from P and S receiver functions. Earth Planetary Science Letters 299 (1-2), 91-103.

Silver, P.G., Russo, R.M., Lithgow-Bertelloni, C., 1998. Coupling of South American and African plate motion and plate deformation. Science 279, 60-63.

Sleep, N.H., 1990. Hotspots and Mantle plumes: Some Phenomenology. Journal Geophysical Research 95 (B5), 6715-6736.

Small, C., 1995. Observations of ridge-hotspot interactions in the Southern Ocean. Journal Geophysical Research 100, 17931–17946.

Smith, A.D., 2003. A re appraisal of stress field and convective roll models for the origin and distribution of Cretaceous to recent intraplate volcanism in the Pacific basin. Interior Geological Revue 45, 287-302.

Smith, A.D., 2004. Stress fields and the distribution of intraplate volcanism in the Pacific Basin, www.mantleplumes.org 4pp.

Snow, J.E., Edmonds, H.N., 2007. Ultraslow-spreading ridges rapid paradigm changes. Oceanography 20, special issue 1, 90-101

Soares, D.M., Alves, T.M., Terrinha, P., 2012. The breakup sequence and associated lithospheric breakup surface: Their significance in the context of rifted continental margins (West Iberia and Newfoundland margins, North Atlantic). Earth Planetary Science Letters 355-356, 311-326.

Spang, J.H., 1972. Numerical method for dynamic analysis of calcite twin lamellae. Geological Society of America Bulletin 83 (2), 467–472.

Sperner, B., Ratschbacher, L., Ott, R., 1993. Fault-striae analysis: a Turbo Pascal program package for graphical presentation and reduced stress tensor calculation. Computers & Geosciences 19 (9), 1361–1388.

Sperner, B., Zweigel, P., 2010. A plea for more caution in fault–slip analysis. Tectonophysics 482 (1–4), 29–41.

Srivastava, S.P., Roest, W.R., Kovacs, L.C., Oakey, G., Levesque, S., Verhoef, J., Macnab, R., 1990. Motion of Iberia since the Late Jurassic : results from detailed aeromagnetic measurements in the Newfoundland Basin. Tectonophysics 184, 229-260.

Srivastava, S.P., Roest, W.R., 1992. King's Trough : reactivated pseudo-fault of a propagating rift. Geophysical Journal Interior 108 (1), 143-150.

Standish, J.D., Sheehy, M., Warner, R.R., 2008. Use of otolith natal elemental signatures as natural tags to evaluate connectivity among open-coast fish populations. Marine Ecology Progress Series 356, 259-268.

Steiger, R.H., Jager, E., 1977. Subcommission on geochronology : convention on the use of decay constants in geo and cosmochronology. Earth and Planetary Science Letters 36, 359-362.

Steinberger, B., 2000. Plumes in a convecting mantle: Models and observations for individual hotspots. Journal of Geophysical Research: Solid Earth, 105 (B5), 11127–11152.

Storetvedt, K.M., Serralheiro, A., Moreira, M., Abranches, M.C., 1989. Magnetic structure and evolution of the island of Santa Maria, Azores. Physics of the earth and planetary interiors 58, 228-238.

Stretch, R.C., Mitchell, N.C., Portaro, R.A., 2006. A morphometric analysis of the submarine volcanic ridge south-east of Pico Island, Azores. Journal of Volcanology and Geothermal Research 156, 35-54.

Snyder, D.C., Widom, E., Pietruszka, A.J., Carlson, R.W., Schmincke, H.U., 2007. Time scales of formation of zones magma chambers: u-series disequilibria in the Fogo A and 1563 A.D. trachyte deposits, S. Miguel, Azores. Chemical Geology 239, 138-155.

Suetsugu, D., Isse, T., Tanaka, S., Obayashi, M., Shiobara, H., Sugioka, H., Kanazawa, T., Fukao, Y., Barruol, G., Reymond, D., 2009. South Pacific mantle plumes imaged by seismic observation on islands and seafloor. Geochemistry, Geophysics, Geosystems 10, Q11014, doi:10.1029/2009GC002533.

Takada, A., 1999. Variations in magma supply and magma partitioning: the role of tectonic settings. Journal Volcanology Geothermal Research 93, 93-110.

Tan, E., M Gurnis, M., 2008. Empirical error estimation for CitcomCU Stokes solver. AGU Fall Meeting Abstracts 1, 1773.

Tarduno, J.A., Duncan, R.A., Scholl, D.W., Cottrell, R.D., Steinberger, B., Thordarson, T., Kerr, B.C., Neal, C.R., Frey, F.A., Torii, M., Carvallo C., 2003. The Emperor Seamounts: Southward Motion of the Hawaiian Hotspot Plume in Earth's Mantle. Science 301 (5636), 1064-1069.

Thibauld, R., Gente, P., Maia, M., 1998. A systematic analysis of the Mid-Atlantic Ridge morphology and gravity between 15°N and 40°N: constraints on the thermal structure. Journal Geophysical Research 103, 24223-24243.

Thompson, N., Watters, R.J., Schiffman, P., 2008. Stability analysis of Hawaiian Island flanks using insight gained from strength testing of the HSDP core. Jounral of Volcanology and Geothermal Research 171, 163-177.

Tibaldi, A., Pasquarè, F.A., Papanikolaou, D., Nomikou, P., 2008. Discovery of a huge sector collapse at the Nisyros volcano, Greece, by on-land and offshore geological-structural data. Journal Volcanology Geothermal Research 177 (2), 485-499.

Tibaldi, A., Bonali, F.L., Corazzato, C., 2014. The diverging volcanic rift system. Tectonophysics 611, 94-113.

Trippanera, D., Porreca, M., Ruch, J., Pimentel, A., Acocella, V., Pacheco, J., Salvatore, M., 2013. Relationships between tectonics and magmatism in a transtensive/transform setting: An example from Faial Island (Azores, Portugal). GSA Bulletin doi:10 .1130/B30758.1.

Turner, F.J., 1953. Nature and dynamic interpretation of deformation lamellae in calcite of three marbles. American Journal of Science 251 (4), 276–298.

Turner, S., Hawkesworth, C., Rogers, N., King, K., 1997. U-Th isotope disequilibria and ocean island basalt generation in the Azores. Chemical Geology 139, 145-164.

Tucholke, B., J., Lin, M., Kleinrock, M., Tivey, T., Reed, J., Goff, and G., Jaroslow, 1997. Segmentation and crustal structure of the western Mid-Atlantic Ridge flank, 25°25'-27°10'N and 0-29 m.y. Journal of Geophysical Research 102, 10,203-10,223.

Van Wijk, J.W., Blackman, D.K., 2005. Deformation of oceanic lithosphere near slow-spreading ridge discontinuities. Tectonophysics 407, 211-225.

Viso, R.F., Larson, R.L., Pockalny, R.A., 2005. Tectonic evolution of the Pacific-Phoenix-Farallon triple junction in the South Pacific Ocean. Earth Planetary Science Letters 233, 179-194.

Vogt, P.R., 1971. Asthenosphere motion recorded by the ocean floor south of Iceland. Earth Planetary Science Letters 13, 153–160.

Vogt, P.R., 1976. Plumes, sub-axial pipe flow, and topography along the Mid-oceanic ridge. Earth and Planetary Science Letters 29, 309-325.

Vogt, P.R., Avery, O.E., 1974. Detailed magnetic surveys in the Northeast Atlantic and Labrador Sea. Journal Geophysical Research 79, 363-389.

Vogt, P.R., Jung, W.Y., 2004. The Terceira Rift as hyper slow, hotspot dominated oblique spreading axis: A comparison with other slow spreading plate boundaries. Earth Planetary Science Letters 218, 77-90.

Walker, G.P.L., 1984. Downsag calderas, ring faults, caldera sizes, and incremental caldera growth. Journal Geophysical Research 89(B10), 8407–8416, doi: 10.1029/JB089iB10p08407.

Wallace, R.E., 1951. Geometry of shearing stress and relation to faulting. Journal of Geology 59, 118–130.

Wallenstein, N., 1999. Estudo da historia recente e do comportamento eruptivo do Vulcão do Fogo (S. Miguel, Açores). Avaliacão preliminar do hazard. Tese de doutoramento no ramo de Geologia, especialidade de Vulcanologia, Departamento de Geocências, Universidade dos Açores, 266pp.

Walter, T.R., Troll, V.R., 2001. Formation of caldera periphery faults: an experimental study. Bulletin of Volcanology 63, 191-203.

Walter, T.R., Troll, V.R., 2003. Experiments on rift zone evolution in unstable volcanic edifices. Journal Volcanology and Geothermal Research 127, 107-120.

Watts, A.B., Masson, D.G., 1995. A giant landslide on the north flank of Tenerife, Canary Islands. Journal Geophysical Research 100, 24499-24507.

Watts, A., Masson, D., 2001. New sonar evidence for recent catastrophic collapses of the north flank of Tenerife, Canary Islands. Bulletin of Volcanology 63, 8-19.

Weeraratne, D., Manga, M., 1998. Transitions in the style of mantle convection at high Rayleigh numbers. Earth and Planetary Science Letters 160 (1998), 563-568.

White, W.M., Schilling, J.-G., Hart, S.R., 1976. Evidence for the Azores mantle plume from strontium isotope geochemistry of the Central North Atlantic. Nature 263, 659-663.

White, W.M., Tapia, M.D.M., Schilling, J.G., 1979. Petrology and geochemistry of the Azores Islands. Contribute Mineralogy Petrology 69, 201–213.

Widom, E., Carlson, R.W., Gill, J.B., Schmincke, H.U., 1997. Th-Sr-Nd-Pb isotope and trace element evidence for the origin of the São Miguel, Azores, enriched mantle source. Chemical Geology 140 (1-2), 49-68.

Wiens, D.A., DeMets, C., Gordon, R.G., Stein, S., Argus, D., Engeln, J.F., Lundgren, P., Quible, D., Stein, C., Weinstein, S., Woods, D.F., 1985. A diffuse plate boundary model for Indian ocean tectonics. Geophysical Research Letters 12 (7), 429-432.

Wilson, J.T., 1963. A possible origin of the Hawaiian Islands. Canadian Journal Physics 41, 863-870.

Wilson, J.T., 1965. A new class of faults and their bearing on continental drift. Nature 207, 343-347.

Wilson, D.S., 1993. Confidence intervals for motion and deformation of the Juan de Fuca Plate. Journal Geophysical Research 98 (B9), 16053-16071, doi:10.1029/93JB01227.

Wilson, D.S., Hey, R.N., 1995. History of rift propagation and magnetization intensity for the Cocos-Nazca spreading center. Journal Geophysical Research 100(B6), 10041-1056, doi:10.1029/95JB00762.

Winkelmann, K., Buckeridge, J.S., Costa, A.C., Dionisio, M.A.M., Medeiros, A., Cachão, M., Avila, S.P., 2010. Zullobalanus santamariaensis sp. Nov., a new late Miocene barnacle

species of the family Archaeobalanidae (Cirripedia: Thoracica), from the Azores. Zootaxa 2680, 33-44.

Winterer, E., Sandwell, D.T., 1987. Evidence from en-echelon cross grain ridge for tensional cracks in the Pacific plate. Nature 329, 534-537.

Whittaker, J.M., R.D., Muller, W.R., Roest, P., Wessel, and W.H.F., Smith, 2008. How supercontinents and superoceans affect seafloor roughness. Nature 456, 938-941, doi:10.1038/nature07573.

Yang, S., Solomon, C., Bjarnason, I.T., Nolet, G., Morgan, W.J., Allen, R.M., Vogfjord, K., Jakobsdottir, S., Stefansson, R., Julian, B.R., Foulger G.R., 2002. Seismic Evidence for a tilted Mantle Plume and North-South Mantle flow beneath iceland. Earth Planetary Science Letters 197 (3-4), 261-272.

Yang, T., Shen, Y., Van Der Lee, S., Solomon, C., 2006. Upper mantle structure beneath the Azores hotspot from finite frequency seismic topography. Earth Planetary Science Letters 250 (1-2), 11-26.

Yu, D., Fontignie, D., Schilling, J.-G., 1997. Mantle plume–ridge interactions in the central North Atlantic: a Nd isotope study of Mid-Atlantic Ridge basalts from 30°N to 50°N. Earth Planetary Science Letters 146, 259–272.

Zhao, D., 2004. Global Tomographic Images of Mantle Plumes and Subduction Slabs: Insight into Deep Earth Dynamics. Physics Earth Planetary Interior 146, 3-34.

Zhang, Y., Tanimoto, T., 1992. Ridges, hotspots, and their interactions as observed in seismic velocity maps. Nature 355, 45–49.

Zbyszewski, G., Almeira, F.M., Ferreira, O.V., Assuncao, C.T., 1958. Carta Geologica de portugal na escala de 1:50000. Noticia explicativa da Folha B, S. Miguel (Açores). Servicos Geologicos de Portugal. Lisboa. 37pp.

Zbyszewski, G., Almeira, F.M., Ferreira, O.V., Assuncao,, C.T., 1959. Carta geologica de portugal na escala de 1:50000. Noticia explicativa da folha A, S. Miguel (Açores). Servicos geologicos de portugal. Lisboa. 22pp.

Zbyszewski, G., Ferreira, O.V., 1960. Carta geológica de Portugal, Ilha de Santa Maria (Açores), scale 1:50 000: Serviços Geológicos de Portugal.

Zbyszewski, G., 1961. Etude geologique de l'ile de S. Miguel (Açores). Comunicações dos Serviços Geologicos de Portugal 45, 5-79.

Zbyszewski, G., Medeiros, A., Ferreira, O., 1972. Carta Geologica de Portugal 1: 25.000, folha ilha Graciosa (Açores). Ser. Geol. Portugal.

APPENDIX I
Reconstructing the architectural evolution of volcanic islands from combined K/Ar, morphologic, tectonic, and magnetic data: The Faial Island example (Azores)

Journal of Volcanology and Geothermal Research 241–242 (2012) 39–48

Contents lists available at SciVerse ScienceDirect

Journal of Volcanology and Geothermal Research

journal homepage: www.elsevier.com/locate/jvolgeores

Reconstructing the architectural evolution of volcanic islands from combined K/Ar, morphologic, tectonic, and magnetic data: The Faial Island example (Azores)

A. Hildenbrand [a,b,*], F.O. Marques [c], A.C.G. Costa [a,c], A.L.R. Sibrant [a,c], P.F. Silva [d], B. Henry [e], J.M. Miranda [c], P. Madureira [f,g]

[a] Univ Paris-Sud, Laboratoire IDES, UMR8148, Orsay, F-91405, France
[b] CNRS, Orsay, F-91405, France
[c] Universida de Lisboa, IDL, Lisboa, Portugal
[d] ISEL/DEC and IDL/CGUL, Lisboa, Portugal
[e] Paleomagnetism, IPGP and CNRS, 4 Av. de Neptune, 94107 Saint-Maur cedex, France
[f] Centro de Geofísica de Évora and Dep. de Geociências da Univ. de Évora, R. Romão Ramalho, 59, 7000-671 Évora, Portugal
[g] Estrutura de Missão para os Assuntos do Mar, R. Costa Pinto, 165, 2770-047, Paço D'Arcos, Portugal

ARTICLE INFO

Article history:
Received 10 January 2012
Accepted 11 June 2012
Available online 21 June 2012

Keywords:
Faial
Volcanic construction
Mass-wasting
K/Ar
Tectonics
Magnetism
Azores triple junction

ABSTRACT

The morpho-structural evolution of oceanic islands results from competition between volcano growth and partial destruction by mass-wasting processes. We present here a multi-disciplinary study of the successive stages of development of Faial (Azores) during the last 1 Myr. Using high-resolution digital elevation model (DEM), and new K/Ar, tectonic, and magnetic data, we reconstruct the rapidly evolving topography at successive stages, in response to complex interactions between volcanic construction and mass wasting, including the development of a graben. We show that: (1) sub-aerial evolution of the island first involved the rapid growth of a large elongated volcano at ca. 0.85 Ma, followed by its partial destruction over half a million years; (2) beginning about 360 ka a new small edifice grew on the NE of the island, and was subsequently cut by normal faults responsible for initiation of the graben; (3) after an apparent pause of ca. 250 kyr, the large Central Volcano (CV) developed on the western side of the island at ca 120 ka, accumulating a thick pile of lava flows in less than 20 kyr, which were partly channelized within the graben; (4) the period between 120 ka and 40 ka is marked by widespread deformation at the island scale, including westward propagation of faulting and associated erosion of the graben walls, which produced sedimentary deposits; subsequent growth of the CV at 40 ka was then constrained within the graben, with lava flowing onto the sediments up to the eastern shore; (5) the island evolution during the Holocene involves basaltic volcanic activity along the main southern faults and pyroclastic eruptions associated with the formation of a caldera volcano–tectonic depression. We conclude that the whole evolution of Faial Island has been characterized by successive short volcanic pulses probably controlled by brief episodes of regional deformation. Each pulse has been separated by considerable periods of volcanic inactivity during which the Faial graben gradually developed. We propose that the volume loss associated with sudden magma extraction from a shallow reservoir in different episodes triggered incremental downward graben movement, as observed historically, when immediate vertical collapse of up to 2 m was observed along the western segments of the graben at the end of the Capelinhos eruptive crises (1957–58).

© 2012 Elsevier B.V. All rights reserved.

1. Introduction

The geological evolution of oceanic islands is generally marked by rapid volcanic growth alternating with destruction by a variety of mass-wasting processes including giant sector collapses, vertical caldera subsidence, fault generation/propagation, shallow landslides and coastal erosion (e.g., Moore et al., 1989; Mitchell, 1998; Hildenbrand et al., 2004, 2006, 2008a, 2008b; Quartau et al., 2010; Boulesteix et al., 2012). The study of such destruction events is of particular societal relevance, since they can cause considerable damage. The Azores volcanic islands in the Atlantic are particularly sensitive to mass-wasting processes. The region is characterized by intense deformation responsible for high magnitude earthquakes (e.g., Borges et al., 2007). Like the neighbouring islands of Pico, S. Jorge, Terceira and Graciosa in the central Azores, Faial is still active and is characterized by the localization of volcanism along N110°-trending eruptive fissures and vents. Faial is additionally marked by a large graben-like structure elongated along the same azimuth (N110°). The island thus offers a great opportunity

* Corresponding author at: Univ Paris-Sud, Laboratoire IDES, UMR8148, 91405 Orsay, F-91405, France. Tel.: +33 1 69 15 67 42; fax: +33 1 69 15 48 91.
E-mail address: anthony.hildenbrand@u-psud.fr (A. Hildenbrand).

0377-0273/$ – see front matter © 2012 Elsevier B.V. All rights reserved.
doi:10.1016/j.jvolgeores.2012.06.019

to study the interactions between volcanism and tectonics. We present here a new study aimed at reconstructing the architecture and the volcano–tectonic evolution of Faial during the last 1 Myr. Our approach combines new tectonic analysis, K/Ar dating and palaeomagnetic data on selected samples, which, together with high-resolution DEM data and analyses of magnetic anomalies carried out during an aerial survey (Miranda et al., 1991), provides valuable insight into the competition between volcanic construction and destruction by tectonic processes, mass-wasting, and erosion throughout the geological evolution of the island.

2. Geological background

The Central Azores islands (Fig. 1) were formed during the Quaternary on top of an oceanic plateau, the Azores Plateau, at the triple junction between the North American, Eurasian and Nubian lithospheric plates (e.g., Searle, 1980; Miranda et al., 1991; Luis et al., 1994; Lourenço et al., 1998; Vogt and Jung, 2004). The origin of the volcanism in the area is still controversial: some authors argue for an origin from volatile-enriched upper mantle domains (Schilling et al., 1980; Bonatti, 1990), whereas others, based on geochemical data (Schilling, 1975; White et al., 1979; Flower et al., 1976; Davies et al., 1989; Widom & Shirey, 1996; Turner et al., 1997; Moreira et al., 1999; Madureira et al., 2005; 2011) or seismic tomography (Silveira and Stutzmann, 2002; Montelli et al., 2004; Yang et al., 2006), consider the Azores volcanism to be related to a mantle plume. According to Silveira et al. (2006), the shallow S-wave negative anomaly (down to ~250 km) results from the presence of a dying and now untailed plume, the head of which was responsible for building of the Azores Plateau. Furthermore, regional deformation has largely controlled the distribution of volcanic vents, leading to the construction of submarine ridges with N150° and N110° main orientations (e.g., Lourenço et al., 1998; Stretch et al., 2006; Hildenbrand et al., 2008b; Silva et al., 2012). Most of the Azores islands have experienced historic volcanic activity. The most recent volcanic crisis on Faial, the Capelinhos eruption (1957–1958), was characterized by a surtseyan and strombolian activity, which increased the island area to the west (Machado et al., 1959; Zbyszewski and Veiga Ferreira, 1959; Machado et al., 1962).

Faial constitutes one of the emerged parts of a single main volcanic ridge, the Pico–Faial Ridge. This structure is roughly elongated along the N110° direction, but probably older N150° submarine ridges can be observed or are suspected offshore the eastern ends of both Faial and Pico (Fig. 1). The geology of Faial island has been divided by Chovelon (1982) into five main volcanic units (Fig. 2a): (i) the Galego volcano mapped in the east and northeast areas of the island, from north of Horta to the northern coast; (ii) a main volcanic edifice, the Central Volcano (CV), built on the western side of the Galego volcano, during at least two main phases of activity; (iii) recent volcanic units filling the graben, from 0.03 Ma to the present; (iv) basaltic units in the E (Horta) and W (Capelo). The Horta volcanism, located in the SE corner of the island, is characterized by a series of small scoria cones and associated basaltic lava flows. The Capelo volcanism corresponds to the most recent volcanic activity that formed a peninsula in the westernmost part of Faial. It was erupted during the last 10 kyr (Madeira et al., 1995), and is morphologically characterized by a series of volcanic cones aligned WNW-ESE that stretches the island towards the Capelinhos volcano, which emerged during the 1957–1958 eruption; (v) widespread trachytic pumice deposits generated by recent explosive activity of the Central Volcano over the last 10 kyr. Subsequently, other workers have conducted more detailed geological mapping, and have renamed the main units (e.g., Serralheiro et al., 1989; Madeira, 1998; Pacheco, 2001). These works were mostly based on the original geochronological framework established by Féraud et al. (1980) and Demande et al. (1982), which we therefore used as a basis for the present study.

The recent eruptive history of Faial has been quite well documented from radiocarbon dating on charcoal fragments collected in pyroclastic deposits and/or palaeosoils (e.g. Madeira et al., 1995). The earlier volcano–tectonic evolution of the island, however, remains unclear in the absence of sufficient reliable temporal constraints. Five K/Ar ages have been published in the early 1980s for the whole island, two of which are being related to very young volcanic episodes (Féraud et al., 1980). The remaining three samples have been collected along the eastern end of the island, in an area attributed to the Galego volcano. The results on these samples vary from 0.73 ± 0.07 Ma to 0.21 ± 0.02 Ma, which means that the sub-aerial part of the old volcanic system would have developed over a period of about 0.5 Myr. A few additional unpublished K/Ar determinations

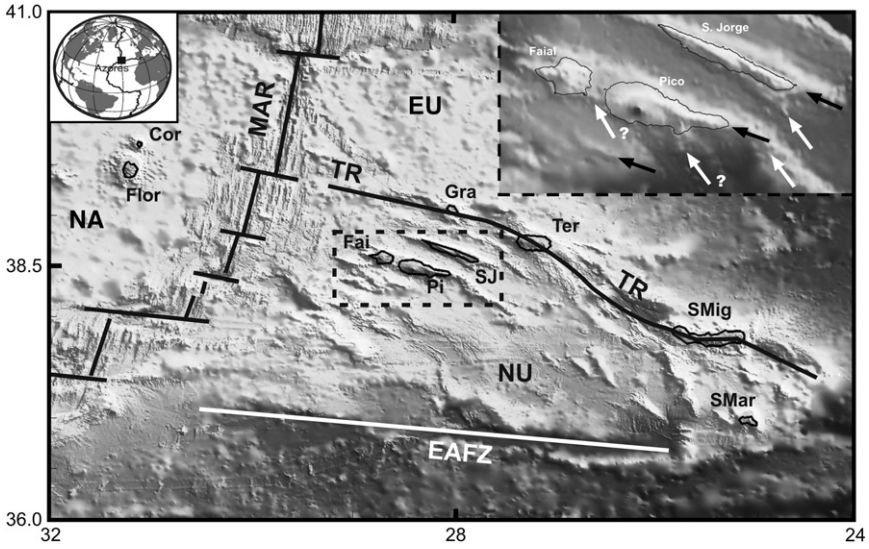


Fig. 1. Main figure: Location of the Azores volcanic archipelago near the triple junction between the North American (NA), the Eurasian (EU) and the Nubian (NU) plates. The dashed rectangle localizes the inset. Bold black lines show the Mid-Atlantic Ridge (MAR) and the Terceira Rift (TR), and the white line shows the East Azores Fracture Zone (EAFZ). SJ: S. Jorge; Gra: Graciosa; Ter: Terceira; Fai: Faial; Pi: Pico; Flor: Flores; Cor: Corvo; SMig: S. Miguel; SMar: Santa Maria. Background bathymetric data from Lourenço et al. (1998). Inset: Main submarine structures around Sao Jorge, Pico and Faial. Black and white arrows show linear submarine ridges with N110 and N150 directions, respectively. Modified from Hildenbrand et al. (2008b).

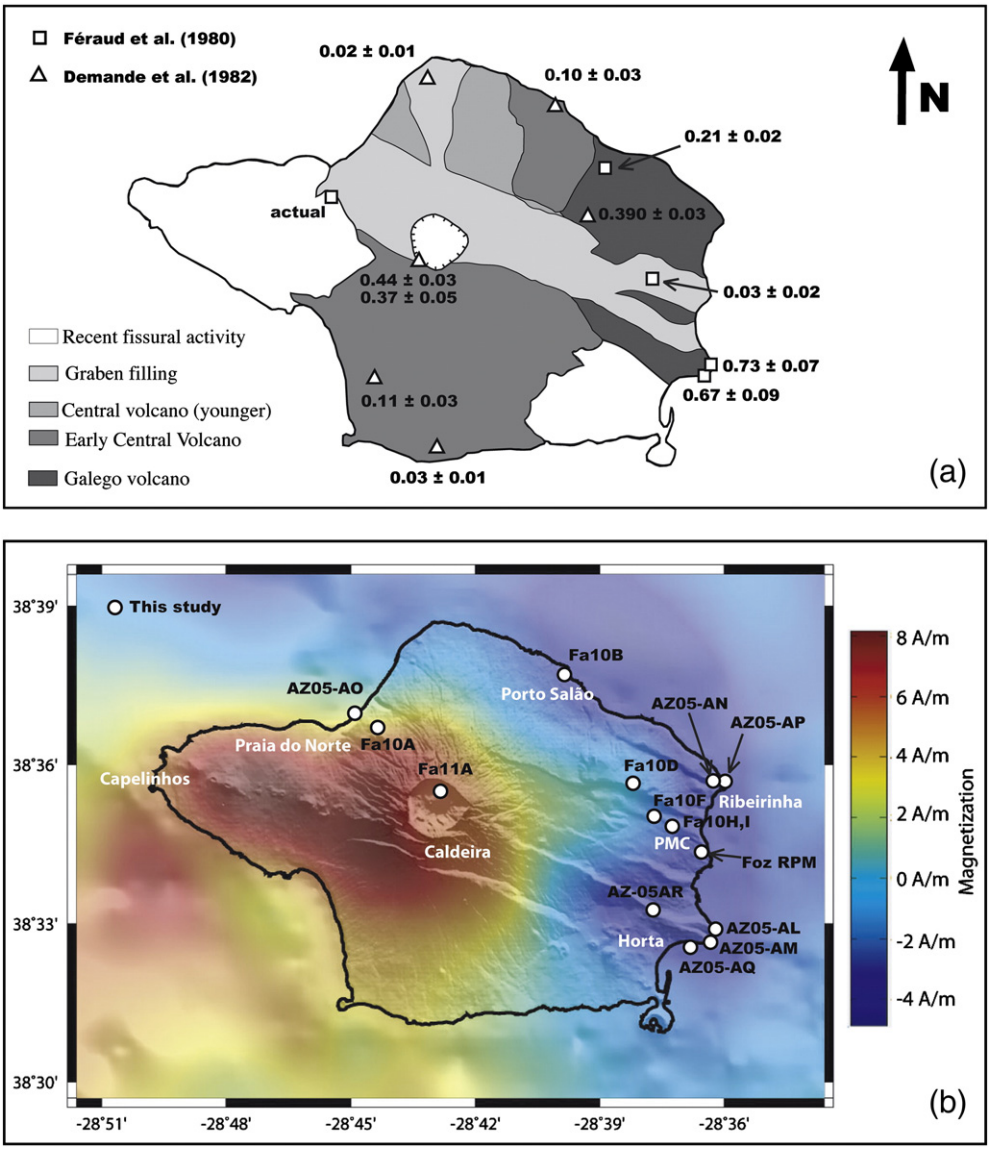


Fig. 2. (a) Geological map of Faial (modified after Chovelon, 1982). Previous K/Ar ages (in Ma) from Féraud et al. (1980) and Demande et al. (1982) are shown. (b) Magnetization map combined with a high-resolution digital elevation model (DEM) of the island. The colour scale shows the magnetization values. White dots with black circles show the location of our new samples collected for both K/Ar and magnetic analyses. Localities are shown in white. PMC: Pedro Miguel creek.

presented in a report (Demande et al., 1982) and a thesis (Chovelon, 1982) have been subsequently acquired on whole-rock samples from the central volcanism sampled in the northern and western parts of the island. They range in age between 0.44 ± 0.03 Ma and 0.03 ± 0.01 Ma. From the few previous K/Ar data available for Faial (Féraud et al., 1980; Chovelon, 1982; Demande et al., 1982), the two main volcanic systems would thus have experienced synchronous growth between 0.44 ± 0.03 Ma and 0.21 ± 0.02 Ma. This seems in apparent contradiction, since the main volume of the Central Volcano has apparently grown within the main graben cutting the Galego volcano (Fig. 2b). Therefore, the timing for graben initiation, and the relationships between volcanic construction and destruction, and tectonics remain insufficiently documented to allow the development of a coherent and comprehensive model.

3. Fieldwork and sampling strategy

The interactions between volcanic growth and partial destruction on volcanic islands such as Faial generally result in complex relationships of the different geological units, in response to a rapidly evolving topography. In such conditions, reconstructing the successive stages of construction and graben development requires strategic investigations on target areas. We first used available morphological and geophysical data to identify the zones of major interest for fieldwork and selective sampling. Such preliminary work includes the combination of a high-resolution DEM of Faial with a magnetization map built from magnetic data acquired during a previous aerial survey of the island (Miranda et al., 1991) merged with the aeromagnetic map of the Azores Platform (Luis et al., 1994) into a regular grid with a 0.005° step both in longitude and latitude (Fig. 2b). Magnetization was computed with the actual topography and using the 3D-inversion technique of Macdonald et al. (1980). This inversion procedure makes two main assumptions: (1) a constant thickness source layer (1.0 km), the upper surface of which is defined by the bathymetry, and (2) fixed values for the main field and the magnetization ($59.5\ A.m^{-1}$ and $-17\ A.m^{-1}$, respectively). A band pass filter (1.1–120 km) was applied to ensure convergence. The processing was made with the Mirone software suite (Luis, 2007).

The magnetization map evidences an area with high-magnitude negative values in the eastern side of the island. This zone coincides

with a narrow morphological relief, the northern part of which is affected by the main graben. Such sector retains crucial information, because the predicted magnetization may reflect volcanic construction during a period with reversed polarity of the magnetic field, e.g., during the Matuyama chron prior to 0.789 ± 0.008 Ma (Quidelleur et al., 2003). The lowermost and uppermost parts of this apparently old volcanic succession thus have been extensively sampled for geochronological and magnetic measurements (samples AZ05-AL, AM, AQ, AR). The parts of the faults exposed along the eastern shore have also been investigated carefully.

The NE part of the island attributed to the Galego volcanism in earlier studies shows a zone of low-magnitude negative magnetization roughly elongated in the N110 direction. This sector is additionally characterized by a prominent topographic high with relatively steep slopes towards the North. It is composed of a moderately thick volcanic succession, including porphyritic lavas with dominant plagioclase phenocrysts. This succession is cut by the northern fault of the main graben, and by an additional scarp farther North, near the village of Ribeirinha. The lower and upper distal parts of this succession were sampled close to shore level in the NE tip of Faial (samples AZ05-AN and AZ05-AP, respectively). A sample was also collected at an elevation of ca 500 m on the upper rim of the main fault near Galego (Fa10D) to constrain a maximum age for initiation of the graben. The geometry and kinematics of the eastern end of the main fault were additionally examined at the shore level.

The Central Volcano in the western half of the island is marked by an overall positive magnetization highlighted by yellow to red colours on the magnetization map (Fig. 2b). The maximum is centred close to the present caldera depression, but rapidly vanishes towards the distal parts, where slightly negative values are observed. A lava flow at the base of the volcanic succession exposed in the caldera walls was sampled at an altitude of 575 m to constrain the earliest accessible stage of edification of the Central Volcano (sample Fa11A). The external parts of the volcano overall have smooth and gentle slopes extending up to the northern and southern shores of the island, where they are cut by large coastal cliffs. We took advantage of these natural sections to collect lava flows at the base of the succession at Praia do Norte and Porto Salão (samples AZ05-AO and Fa10B, respectively). A lava flow from the upper part of the CV succession was additionally sampled at an altitude of ca 300 m uphill Praia do Norte (sample Fa 10A).

The central part of the CV has relatively steep slopes incised by recent narrow canyons. The canyons have a relatively radial distribution close to the eruptive centre, but they bifurcate close to recent scars apparently truncating the (previous) external slopes of the volcano. Such bifurcation is quite obvious in the eastern sector, where individual lava flows and erosion have apparently been geometrically constrained within the graben. Consequently, detailed field investigations were carried out in the graben depression, along the Pedro Miguel creek. These investigations allowed us to identify old lava flows (sample Fa10H) overlain in unconformity by sedimentary deposits, which in turn have been buried by more recent lava flows. Some of the young lava flows were sampled throughout the longitudinal section of the creek (samples Fa10F, Fa10I, Foz RPM), where they define morphological steps. However, they exhibit complex local architecture with important internal flow patterns and complex lateral overlap (Fig. 3), suggesting their channelling into a low topography, down to sea level.

4. Methods and results

4.1. K/Ar geochronology

After careful petrographic examination of the samples in thin-section, the micro-crystalline groundmass was selected for potassium–argon (K–Ar) analyses. Some of the samples are characterized by high amounts of plagioclase phenocrysts/glomerocrysts, which can amount up to 40% in volume. They also contain pyroxene, minor olivine and various oxides. Such minerals partially crystallized at a deep level in the magma chamber and thus are not representative of the age of eruption at the surface. They are also K-poor and may carry significant amount of inherited excess Ar. After crushing and sieving the samples to 125–250 μm, all the phenocrysts have been so systematically removed with heavy liquids. Narrow density spans generally in the range 2.95–3.05 have been achieved to select the freshest part of the groundmass and eliminate the fraction with a lower density, that is potentially affected by alteration and secondary zeolitisation.

K and Ar were measured on two separate aliquots of the selected grains, the former by flame absorption-spectrophotometry and the latter by mass spectrometry. K is determined with a 1% relative uncertainty from replicate analyses on standards (Gillot et al., 1992). The $^{40}Ar/^{36}Ar$ isotopic composition of Ar has been measured according to the Cassignol–Gillot unspiked technique (Gillot and Cornette, 1986; Gillot et al., 2006). With this particular technique, the ^{40}Ar and ^{36}Ar are simultaneously collected avoiding any potential drift associated with peak switching. The level of atmospheric contamination is then accurately determined by comparing

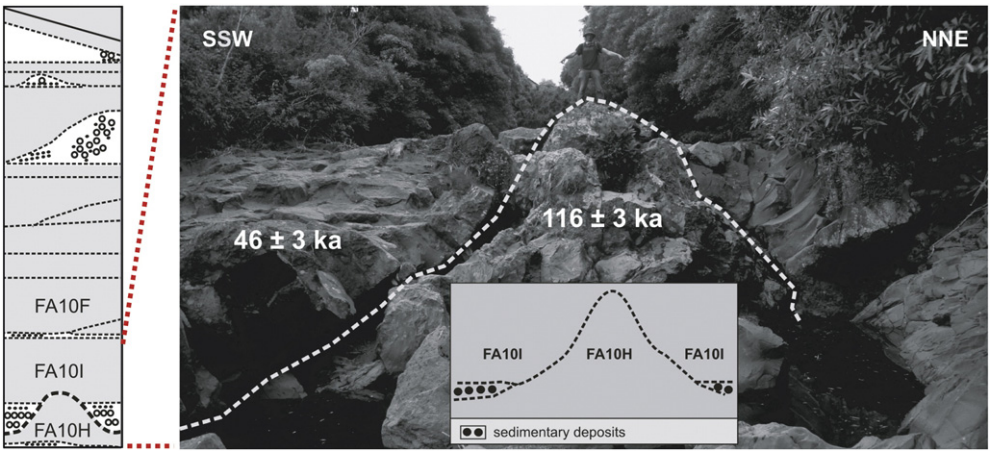


Fig. 3. Left: Schematic log showing the main geometrical relationships between the various units recognized in the Pedro Miguel creek. Light grey areas separated by thin dashed lines mark individual lava flows. White parts show sediments, with circles and dots representing coarse conglomerates and sandstones, respectively. The thick dashed line shows the main unconformity. Right: close up image on the main unconformity. The age of the lava flows below and above the unconformity reported here are shown.

the $^{40}Ar/^{36}Ar$ ratios of the sample and of an air pipette measured in strictly similar pressure conditions, allowing the detection of minute amounts of radiogenic Ar, as low as 0.1% (Gillot et al., 2006). The Cassignol–Gillot technique has been shown especially suitable to date low-K and high-Ca basalts and andesites of late Quaternary age with an uncertainty of only a few ka (e.g., Hildenbrand et al., 2003, 2008b; Quidelleur et al., 2008; Samper et al., 2009; Germa et al., 2010, 2011). For high-K lavas, it has been extended to the last millennium with an uncertainty of only a few centuries (Quidelleur et al., 2001). Both K and Ar were analysed at least twice in order to obtain a reproducible value within the range of uncertainties. The decay constants used are from Steiger and Jäger (1977). The results are presented in Table 1, where the uncertainties are quoted at the 1σ level.

The ages measured on our samples from Faial range between 848 ± 12 ka and 38 ± 1 ka. The results obtained on the different lava flows from the old volcanic succession are tightly clustered around 850 ka, and overlap within the range of uncertainties at the 1σ level. These results are significantly older than previous K/Ar determinations at 0.73 ± 0.07 Ma (Féraud et al., 1980). The new ages measured on lava flows from the distal part of the volcanic succession exposed on the NE corner of Faial (Ribeirinha) yield indistinguishable values of 358 ± 7 ka and 363 ± 8 ka (samples AZ05-AN and AZ05-AP, respectively). The lava flow sample collected on the same succession cut by the main graben is dated here at 389 ± 7 ka, which is similar to a previous age of 0.39 ± 0.03 Ma obtained by Demande et al. (1982) on an aphyric sample collected at a similar level to the West (Fig. 2).

The new ages measured on lava flows sampled at the base of the caldera wall and at the base of the coastal cliffs in the NE and N parts of the CV succession are very close to each other, ranging between 129 ± 2 ka and 118 ± 3 ka (samples Fa11 A and AZ05-AO, respectively). The age for the upper part of the same succession (sample Fa10A) yields a similar value of 118 ± 3 ka, showing that the CV has experienced a very rapid stage of sub-aerial growth at about 120 ka. The new age obtained on our sample Fa10H collected in the deepest parts of the Pedro Miguel creek is also dated at 116 ± 3 ka. The late phase of graben filling is finally constrained from dating successive young lava flows from Pedro Miguel creek between 46 ± 3 ka and 38 ± 1 ka. The oldest age is obtained on the lava flow (sample Fa10I) immediately covering sediments on top of the older lava flows here dated at 116 ± 3 ka (sample Fa10H), confirming therefore the existence of a major unconformity (Fig. 3).

Table 1
Results of the K–Ar dating on fresh groundmass separates. The ages are indicated in thousands of years (ka). The uncertainties are reported at the 1σ level.

Sample	Long.	Lat.	K%	$^{40}Ar^*$ (%)	$^{40}Ar^*$ (10^{12}at/g)	Age (ka)	Unc. (ka)	Mean (ka)
AZ05-AM	−28.609	38.552	1.430	29.9	1.2630	845	12	848 ± 12
				30.8	1.2704	850	12	
AZ05-AQ	−28.613	38.543	1.694	28.3	1.4948	845	12	847 ± 12
				35.4	1.5011	848	12	
AZ05-AL	−28.609	38.552	1.585	43.0	1.3976	844	12	846 ± 12
				40.1	1.4043	848	12	
AZ05-AR	−28.625	38.553	1.863	33.3	1.6399	843	12	843 ± 12
				39.5	1.6424	844	12	
FA10D	−28.631	38.591	1.060	9.7	0.4349	393	7	389 ± 7
				9.2	0.4262	385	7	
AZ05-AN	−28.612	38.599	1.222	14.8	0.4651	364	6	363 ± 6
				16.5	0.4618	362	6	
AZ05-AP	−28.608	38.599	1.264	7.7	0.4739	359	7	358 ± 7
				10.0	0.4727	358	6	
Fa11A	−28.713	38.592	3.173	9.2	0.4332	131	2	129 ± 2
				11.8	0.4217	127	2	
FA10B	−28.658	38.626	1.539	4.9	0.2023	126	3	127 ± 3
				5.0	0.2061	128	3	
AZ05-AO	−28.750	38.613	1.827	4.3	0.2203	115	3	118 ± 3
				3.7	0.2293	120	4	
FA10A	−28.750	38.608	1.419	3.8	0.1754	118	4	118 ± 3
				4.0	0.1750	118	3	
FA10H	−28.620	38.577	1.785	4.7	0.2195	118	3	116 ± 3
				5.2	0.2141	115	3	
FA10I	−28.620	38.577	1.503	1.8	0.0716	46	3	46 ± 3
				1.8	0.0735	47	3	
Foz RPM	−28.612	38.578	2.225	3.2	0.0960	41	1	40 ± 1
				3.6	0.0910	39	1	
FA10F	−28.622	38.577	1.919	2.9	0.0778	39	1	38 ± 1
				4.0	0.0757	38	1	

4.2. Paleomagnetic data

Silva et al. (2008, 2010, in preparation) performed a paleomagnetic study on Faial Island on 140 samples collected along 6 different sections that mostly correspond to the flows dated in this study. Rockmagnetic experiments identified magnetic carriers favourable for paleomagnetic study (presence of magnetite of Pseudo-Single Domain-Single Domain states). Demagnetizations have shown mostly the presence of a single stable magnetization component defining a characteristic remanent magnetization.

Virtual Geomagnetic Poles for 11 lava flows indicate a normal polarity of the Earth magnetic field and for 5 flows a reversed polarity. The reversed polarity is exclusively measured on the samples dated in this paper at about 0.85 Ma. This confirms that the phase of old volcano construction occurred at the final stages of the Matuyama reversed chron.

The other lava flows show a positive polarity, in accordance with their eruption during the Brunhes normal chron, i.e. during the last 0.789 ± 0.008 Myr (Quidelleur et al., 2003). When accessible, lava flows from the same lava pile generally exhibit very similar paleomagnetic directions, confirming the existence of massive pulses during volcano construction. We note, however, that data from 2 flows of the old volcanic sequence along the sea cliff show abnormal paleomagnetic direction with respect to the average values. This could be highlighting local tilting processes associated with differential movement along recent faults.

4.3. Tectonic analysis of fault geometry and kinematics

The most prominent tectonic feature in Faial is the central graben affecting the whole island. The graben fault scarps are clearly visible in successive topographic cross-sections (Fig. 4) but the actual fault surfaces are only visible locally along sea cliffs (Fig. 5). Faults and fault scarps strike N110° on average; some fault scarps dip 35–45º to the NNE or SSW, while others dip more steeply at the surface, at around 55–75º to the NNE or SSW. Tilting of the lavas in the hanging-wall block and steepness of faults at the Earth's surface indicate a listric geometry at depth. The observed fault striations are dip-slip, which means that they are normal faults. Fault displacement, as shown by the displacement of the topography, gradually increases away from the Central Volcano, especially to the E; this can mean that part of the older fault displacement has been gradually covered by CV eruptions. The few faults that presently show a significant displacement, even close to the south flank of the caldera, indicate that recent fault displacement has been greater in the south than elsewhere (Fig. 4). We dated the oldest rocks here at about 850 ka, so they are not associated with these southernmost faults bounding the graben. This implies that there was a south dipping topography of the old island, otherwise the southernmost fault would show the oldest rocks.

5. Discussion

5.1. Successive stages of volcano–tectonic evolution

5.1.1. Rapid construction of a first main volcano

The old volcanic succession cropping out in the eastern side of the island is dated here between 848 ± 12 ka (sample AZ05-AM) at the base

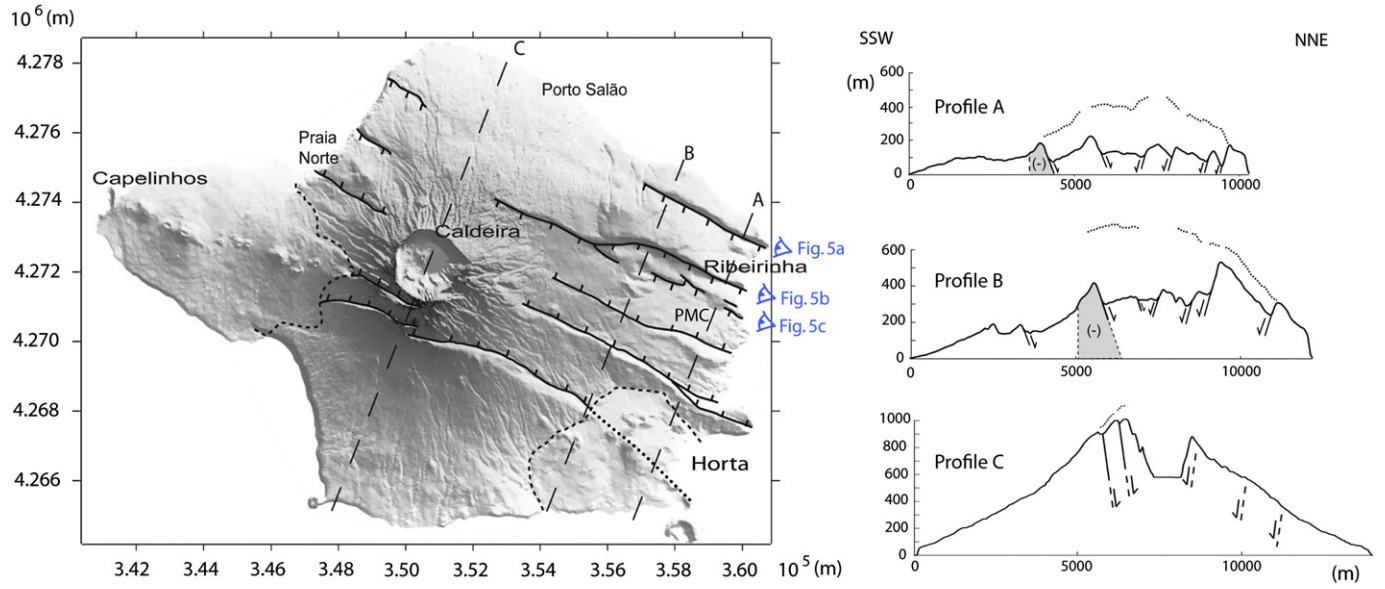


Fig. 4. Left: Shaded-relief map drawn from the high-resolution DEM (illumination from the North), showing the main topographical characteristics of the island. Thick black lines show the base of the various fault scarps, with ticks towards the footwall. The dotted line shows the inferred prolongation of the southern fault under recent basaltic volcanic cones in the Horta sector. Dashed lines localize the topographic profiles shown on the right. The eye symbols show the points of view from which the photographs in Fig. 5 have been taken. Right: Topographic cross-sections evidencing recent apparent fault displacements across the width of the Faial graben. Grey areas show the remnants of the volcanic system older than 850 ka (reversed magnetization). Thin dotted lines show the restored topography.

and 843 ± 12 ka (sample AZ05-AR) at the top, in full agreement with the reversed polarity recorded by the lava flows. These new ages overlap within the uncertainties, testifying to a rapid stage of growth prior to the end of the Matuyama period. Our new results are significantly older than previous K/Ar determinations of 0.73 ± 0.07 Ma and 0.67 ± 0.09 Ma acquired on whole-rock samples from the same area (Féraud et al., 1980). The latter value, despite its large uncertainty, is inconsistent with the reversed polarity here recorded for this sector. Such age under-estimation in earlier studies may result from the experimental procedure used previously. The samples dated by Féraud et al. (1980), were pre-degassed at ca 230 °C under vacuum for a period of up to 20 hours before analysis (Féraud, 1977). Such procedure, initially aimed at removing part of the atmospheric contamination adsorbed on the surface of the grains, is unsuitable because it can also result in partial diffusion and removal of radiogenic argon from the poorly retentive volcanic glass, which can in turn yield too young ages.

The initial geometry of the old volcanic system cannot be constrained precisely, because it was largely destroyed during a period of up to 500 kyr, and more recently was covered by volcanic activity and partly affected by tectonic activity and mass-wasting processes. However, the original dimensions can be estimated by combining all our data. Low magnitude negative magnetizations computed (light blue colour shades) for the eastern part of the island (Fig. 2) do not mean that the outcropping lavas have a reversed polarity, because the polarity measured on the samples collected in that area is normal. The inversion process we used computed a vertical average of the magnetization, interpreted to reflect a thin and young (<0.780 Ma) layer of rocks with normal polarity overlaying a deep and older layer of reversed polarity. Therefore, the thinner the layer of normal magnetic polarity lavas on top of the reversed polarity rocks is, the more the colour approaches deep blue. The persistence of the light blue area close to the island shore in the different sectors of Faial (except the SW) suggests that the original volcano is present underneath most of the recent lava units and therefore had a geographical extent encompassing most of the present island area (Fig. 2). The narrow sector presently cropping in the eastern sector (strong negative magnetizations evidenced by a deep blue colour, and measured ages of about 850 ka) must have been a persistent topographic high, which has not been covered by subsequent young lava flows. We can get a rough idea of the old topography (prior to present-day graben) by restoring surface displacements to their original position (Fig. 4). This shows that the topography prior to recent faulting was convex upward (topographic high), which is not favourable for blanketing by younger positive lava flows. Therefore, this area most likely coincides with a relatively high morphological crest in the eastern side of the original volcanic system. We note that the elongation of the inland negative magnetization is slightly oblique with respect to the present N110 axis of the island. High-magnitude negative values also extend offshore Faial to the northwest. This suggests that the old volcanic system possibly had a ridge-like morphology with a main axis closer to the northwest-southeast direction (Fig. 6a). Prolongation of such a volcanic edifice would thus extend into the Faial–S. Jorge channel as proposed by Miranda et al. (1991). An old volcanic edifice with such elongation is also compatible with the presence of northwest-southeast trending old ridges recognized at the scale of the Azores plateau, e.g., in the eastern part of S. Jorge (Hildenbrand et al., 2008b).

5.1.2. Prolonged volcanic gap and construction of a small edifice in the NE part of Faial

The oldest lava flows collected in the NE sector of the island are dated here at 387 ± 7 ka, revealing an apparent gap in volcanism of at least 450 kyr after the construction of the old volcano. Such a gap could reflect in part a sampling bias, i.e. un-investigated volcanic units could potentially be intercalated between the old volcanic succession and the lava pile here dated between 387 ± 7 ka and 358 ± 7 ka. However, this is not supported by the magnetization map, which shows low negative values in the NE sector reflecting a thin cover of lavas with normal polarity on top of the older units. The morphological surface in the NE tip of the island also supports lavas locally flowing from a small volcanic edifice towards the North and Northeast, on the partly preserved outer slopes of the Matuyama volcano (Fig. 6b).

Geomorphological data, however, do not support such lava flows on the southern and western sides of the island. Several authors have proposed that early sub-aerial construction of the CV could be

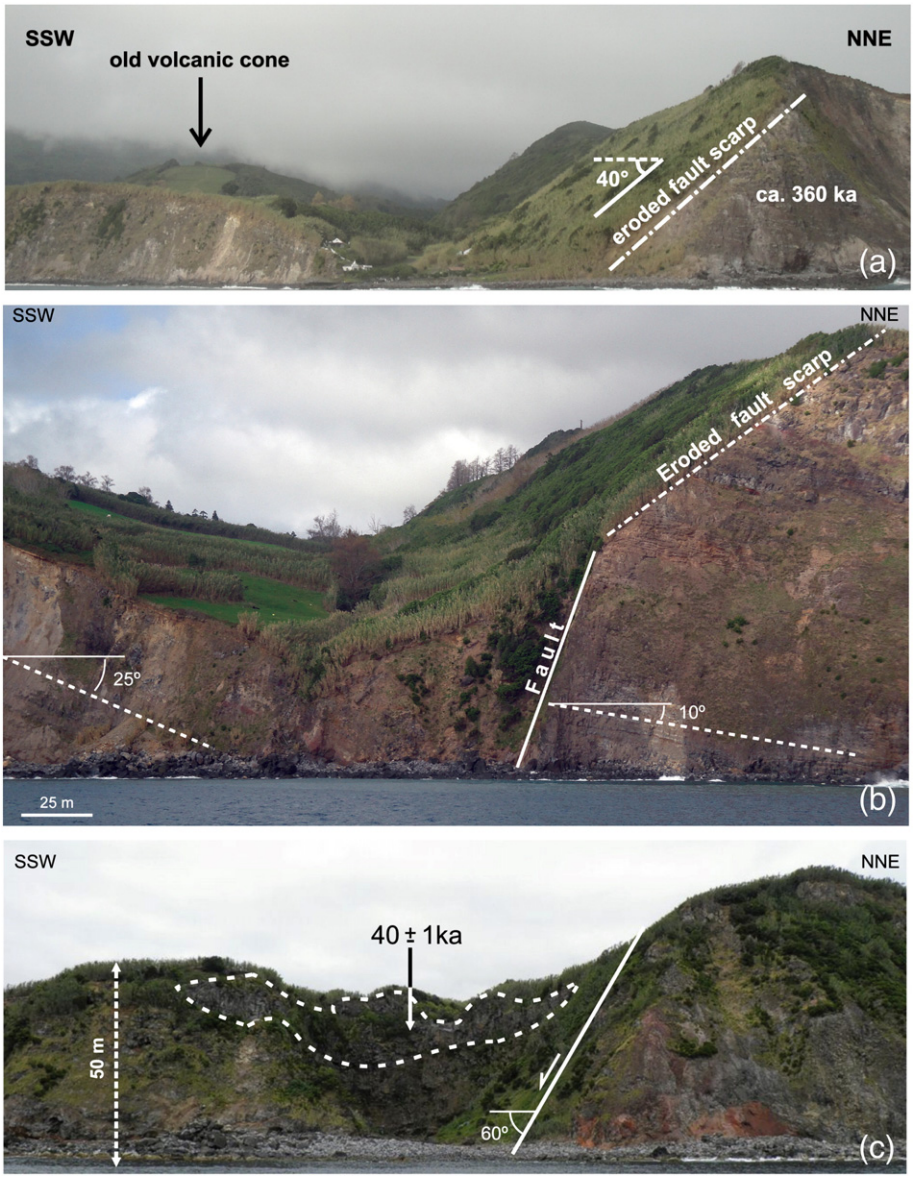


Fig. 5. Photographs taken from the sea showing the contrasted geometry of old and recent fault scarps. See Fig. 4 for localization.

as old as 0.47 Ma (Demande et al., 1982; Madeira and da Silveira, 2003; Quartau et al., 2010). Such an inference relies on a K/Ar whole-rock age of 0.44 ± 0.03 Ma obtained on a highly porphyric sample containing high amounts of olivine and pyroxene phenocrysts, which was sampled in the western wall of the caldera (Demande et al., 1982). Whole-rock dating on such porphyric and/or weathered samples in the Azores and elsewhere has been clearly shown to yield abnormaly old ages by incorporation of inherited excess argon and/or potassium removal by alteration processes (e.g., Johnson et al., 1998; Quidelleur et al., 1999; Hildenbrand et al., 2004). In contrast, the new age of 129 ± 2 ka obtained on the fresh-separated groundmass of our sample Fa11A from the base of the caldera succession shows that most of the CV has been built much later (see next section). Therefore, prior to such recent volcanic growth, the western side of the old volcano has most probably experienced a prolonged period of volcanic inactivity exceeding 500 kyr. Partial destruction of the original morphology by mass wasting processes, including coastal and stream erosion and tectonics, and subsequent blanketing by the CV on the western side of the island can thus explain the absence of the negative anomaly such as observed in the eastern sector.

5.1.3. Initiation of the Faial graben and early development of the Central Volcano

Early sub-aerial growth of the CV within a very short period is supported by our new age constraints obtained for samples from the base and uppermost parts of the thick succession exposed both in the caldera walls and at the northern part of the island near Praia do Norte. We note that two similar, though less precise ages, have been previously measured at 0.10 ± 0.03 Ma and 0.11 ± 0.03 Ma on sub-aphyric samples from the northern and southern coasts, near Porto Salão and Lombega, respectively (Demande et al., 1982). The positive anomalies observable on the magnetization map in the sector of Praia do Norte are consistent with emplacement of a thick lava cover immediately to the North of the main Caldera eruptive centre. A similar pattern, though less pronounced, is also visible as far as the southern coast of the island. In contrast, the persistence of negative anomalies in the sector of Porto de Salão indicates a more reduced thickness. There, the northern gentle slope of the CV also exhibits a clear morphological lateral contrast with the prominent unit here dated between 389 ± 7 ka and 358 ± 7 ka, which confirms that the latter had a restricted geographical extension.

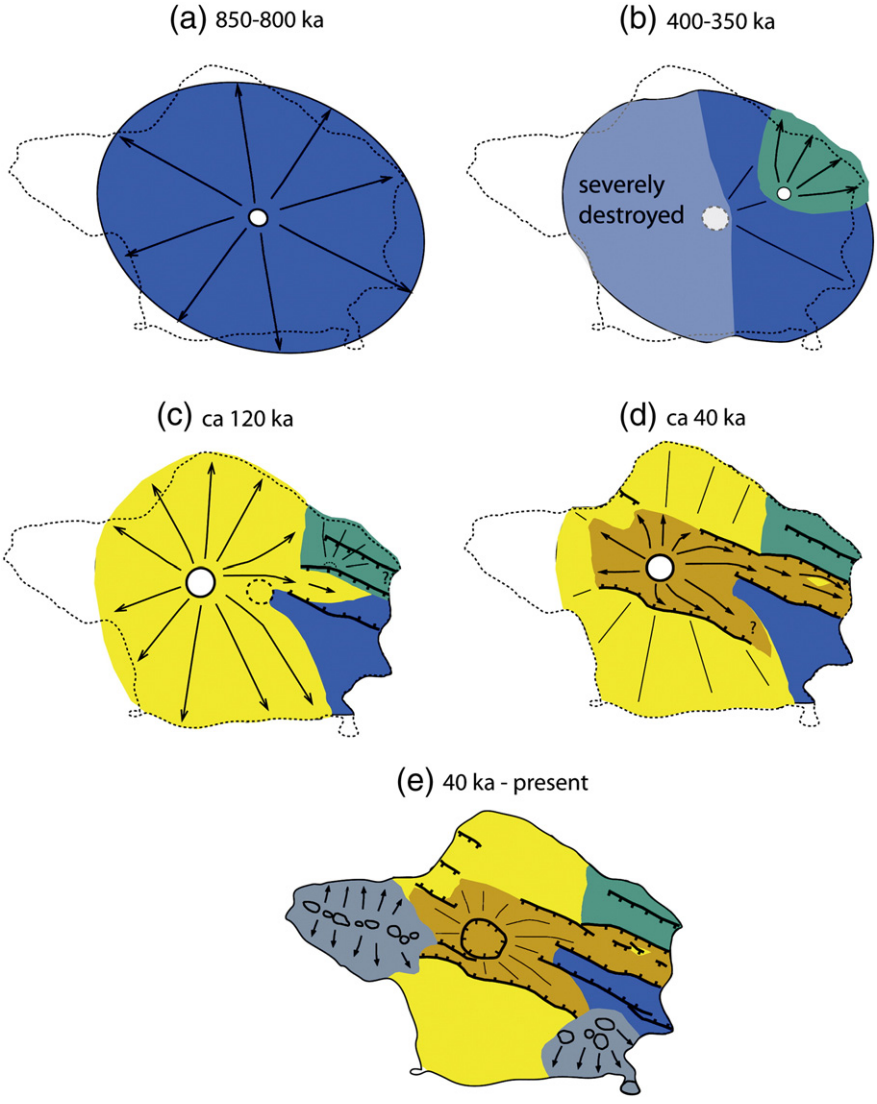


Fig. 6. Schematic model of evolution showing the main stages of volcanic construction separated by incremental fault migration and graben development.

Our new sample collected in the deeper parts of the graben is dated at 116 ± 3 ka, very much in agreement with the age we obtained for the upper northern flank of the CV (sample Fa10A, 118 ± 3 ka). This clearly shows that (1) the graben was already partly formed at that time, and (2) lava flows from the upper part of the CV were channelized in this prominent topographic low (Fig. 6c). Therefore, the eastern part of the graben experienced a significant phase of development between 390 ka and 120 ka, which is much older than previously thought. We note that the fault near Ribeirinha could have formed during this period, which could explain the eroded aspect of the scarp recognized in the field (Fig. 5a).

5.1.4. Incremental evolution of the graben and further construction of the Central Volcano

The several lava flows sampled on top of the unconformity in Pedro Miguel Creek range in age between 46 ± 3 ka and 38 ± 1 ka. These new ages do not overlap each other but attest to very rapid burying of the graben. Although a few scoria cones have developed recently within the graben, such massive filling was most probably fed by renewed activity at the Caldera eruptive centre, as revealed by the present prominent morphology of the volcano (Fig. 6d). The unconformity in Pedro Miguel creek shows an apparent volcanic gap of ca. 80 kyr, which can explain the deep erosion of the older lava flows and the local accumulation of sedimentary deposits on their remnants. The presence of large boulders (up to 1 m in size) most probably highlights morphological rejuvenation upstream, which can therefore be associated with significant vertical deepening of the graben between 120 ka and 40 ka. Furthermore, the younger succession shows that the pilling of lava flows was interrupted from time to time by smaller erosion surfaces and smaller grain-size conglomeratic deposits (see Fig. 3). We interpret these interruptions in the lava piling as times of movement along the adjacent normal faults, which could thus be linked with repeated eruptions at the CV. The scars developed on the southern side of the volcano have a very prominent surface expression, featuring high slopes and a significant vertical offset. This suggests recent reconfiguration of the deformation, with increasing displacement along the southern edge of the graben. The more prominent positive magnetization along these scars supports partial buttressing of the lava flows erupted from the CV against the southern faults.

5.1.5. Late evolution during the last 40 kyr

The young units of Faial Island previously dated by radiocarbon (<10 ka) are mainly related to the very recent explosive volcanic activity at the CV (Madeira et al., 1995). Several basaltic volcanic cones are additionally distributed along the southernmost fault of

the graben, suggesting that magma ascent was constrained along this mechanical discontinuity, but they do not give precise information as to whether the latter was active at that period, because a pre-existing fault could also have focussed magma ascent. The southern faults in the western sector do, however, affect the recent part of the CV, showing downward movement very recently, i.e., additional westward propagation of the graben during the last 40 kyr, and most probably during the last 10 kyr. Several recent basaltic cones and vents on the western tip of the island, including the historical eruptions, also occurred during the last 10 kyr (Madeira et al., 1995). The caldera could thus have experienced partial development in response to magma withdrawal associated with emptying of a shallow reservoir during the several differentiated pyroclastic eruptions and/or an additional phase of graben development (Fig. 6e), two processes which might be intimately linked, as discussed in the next section.

5.2. Links between regional deformation, volcano growth and graben development

Our new data show that volcanic activity on Faial has occurred through short periods of robust volcanic construction, each lasting less than 30 kyr and being separated from the others by prolonged hiatuses, up to 500 kyr in duration. This is similar to the case of the neighbouring island of S. Jorge, where multi-stage volcanic growth alternating with prolonged gaps have been recently shown by geochronological analyses on samples prepared according to the same procedure and analysed with the same technique (Hildenbrand et al., 2008b). Furthermore, comparison of these data with recent stepwise $^{40}Ar/^{39}Ar$ analyses on separated volcanic groundmass on Terceira (Calvert et al., 2006) shows synchronous short phases of volcanic construction on the three islands, e.g. between 400 ka and 350 ka, and probably throughout most of the last 300kyr. Recent magma outputs in the area thus have been concentrated along the N110 direction to develop simultaneously S. Jorge, Faial and Terceira, which most probably reflects significant episodes of intense regional deformation. Similarly, volcanic construction has been constrained by $^{40}Ar/^{39}Ar$ at about 850 ka in S. Miguel (Johnson et al., 1998), i.e., synchronous with the construction of the old volcano on Faial.

MacDonald (1972) concluded that the exact origin of the Faial graben was not known but proposed three mechanisms: (1) removal of magma from an underlying chamber, or (2) stretching of the surface of the volcano, or (3) stretching of the entire underlying crust due to spreading of the Atlantic Ocean basin. Our new data support the first hypothesis, and provide additional insight on the iterative development of the Faial graben in relation with the several volcanic pulses. The most conspicuous arguments for our interpretation are:

(1) The inward listric geometry of the faults responsible for local tilting of the island surface suggests their flattening at shallow depth, strongly indicative of the existence of (an) underlying magma chamber(s) developed within the volcanic edifice.
(2) Each of the short volcanic episodes here evidenced included the eruption of either highly porphyric lavas featuring plagioclase phenocrysts/glomerocrysts, or evolved lavas like mugearites, benmoreites and trachytes. Such characteristics support intermittent storage of the magma in a reservoir prior to their extraction to the surface.
(3) Each volcanic stage, at least during the last 400 kyr, has been followed by a period of graben development. Westward migration of volcanic construction has also been followed by systematic westward propagation of the graben faults, supporting dominant deflation above the main zone of magma withdrawal.
(4) The presence of sediments intercalated within the lava flows here dated at 120 ka and 40 ka suggests the morphologic rejuvenation of the scarps during the interval separating the two main periods of eruption, supporting incremental displacement along the main faults of the graben.
(5) Such a mechanism occurred in recent time during the Capelinhos eruption, where 1.5 m of vertical displacement were measured in 1958, late in the eruptive crisis that started in 1957 (Machado et al., 1959; Zbyszewski and Veiga Ferreira, 1959; Machado et al., 1962; Catalão et al., 2006).

6. Conclusions

This study shows the suitability of using complementary approaches for retrieving the architecture and understanding the evolution and development of oceanic islands in response to complex interactions between volcanic growth and partial destruction by a variety of mass-wasting processes. The combined use of precise K/Ar geochronology on separated groundmass, morpho-tectonic analyses, and magnetic data allow us to depict a step by step model emphasizing short stages of volcanic growth separated by long periods of inactivity during which the volcanic units were subjected to significant mass wasting, including coastal and stream erosion, possibly lateral collapse, and incremental normal faulting. Therefore, the present architecture of the island does not result from simply the coeval development of two main volcanic edifices that were synchronously active over long periods of time.

The successive phases of rapid volcano growth shown in this study have apparently been controlled by short volcanic pulses confined along the main lithospheric structures, triggered by brief episodes of regional deformation. In contrast, the gradual development of the Faial graben appears to be closely linked to the dynamics of magma extraction from ESE-WNW elongated magma chamber(s) at depth, which episodically loses volume and triggers passive gravitational collapse. Such a model is applicable to other oceanic islands, in the Azores and elsewhere.

Acknowledgements

We thank two anonymous reviewers and two previous anonymous reviewers (earlier version of the manuscript) for their constructive remarks, which helped to significantly improve the paper. Fieldwork and isotope dating were in great part supported by TEAMINT (POCTI/CTE/48137/2002) and MEGAHazards (PTDC/CTE-GIX/108149/2008) research projects funded by FCT (Portugal). This is also a contribution to the project EVOLV (PTDC/CTE-GIN/71838/2006), and is LGMT contribution 102. We acknowledge J.C. Nunes for his reading of the manuscript and for discussions.

References

Bonatti, E., 1990. Not so hot hot-spots in the oceanic mantle. Science 250, 107–111.
Borges, J.F., Bezzeghoud, M., Buforn, E., Pro, C., Fitas, A., 2007. The 1980, 1997 and 1998 Azores earthquakes and some seismo–tectonic implications. Tectonophysics 435, 37–54.
Boulesteix, T., Hildenbrand, A., Gillot, P.Y., Soler, V., 2012. Eruptive response of oceanic islands to giant landslides: new insights from the geomorphologic evolution of the Teide–Pico Viejo volcanic complex (Tenerife, Canary). Geomorphology 138 (1), 61–73.
Calvert, A.T., Moore, R.B., McGeehin, J.P., da Silva, A.M.R., 2006. Volcanic history and Ar-40/Ar-39 and C-14 geochronology of Terceira Island, Azores, Portugal. Journal of Volcanology and Geothermal Research 156, 103–115.
Catalão, J., Miranda, J.M., Lourenco, N., 2006. Deformation associated with the Faial (Capelinhos) 1957–1958 eruption: inferences from 1937–1997 geodetic measurements. Journal of Volcanology and Geothermal Research 155, 151–163.
Chovelon, P., 1982. Evolution volcanotectonique des iles de Faial et de Pico, thesis Univ. Paris-Sud, Orsay, 186 pp.
Davies, G.R., Norry, M.J., Gerlach, D.C., Cliff, R.A., 1989. A combined chemical and Pb-Sr-Nd isotope study of the Azores and Cape Verde hot-spots: the geodynamic implications. In: Saunders, M.J. (Ed.), Magmatism in the Ocean Basins: Geol. Soc. Special Publication, pp. 231–235.
Demande, J., Fabriol, R., Gérard, A., Iundt, F., 1982. Prospection géothermique des Iles de Faial et Pico (Açores). 82SGN003GTH. Bureau de recherches géologiques et minières, Orléans.

Féraud, G., 1977. Contribution à la datation du volcanisme de l'archipel des Açores par la méthode Potassium-Argon. Conséquences géodynamiques, thesis Univ. Paris VII, Paris.
Féraud, G., Kaneoka, I., Allègre, C.J., 1980. K/Ar ages and stress pattern in the Azores: geodynamic implications. Earth and Planetary Science Letters 46, 275–286.
Flower, M.F.J., Schmincke, H.-U., Bowman, H., 1976. Rare earth and other trace elements in historic Azorean lavas. Journal of Volcanology and Geothermal Research 1, 127–147.
Germa, A., Quidelleur, X., Gillot, P.Y., Tchilinguirian, P., 2010. Volcanic evolution of the back-arc Pleistocene Payun Matru volcanic field (Argentina). Journal of South American Earth Sciences 29, 717–730.
Germa, A., Quidelleur, X., Lahitte, P., Labanieh, S., Chauvel, C., 2011. The K-Ar Cassignol-Gillot technique applied to western Martinique lavas: a record of Lesser Antilles arc activity from 2 Ma to Mount Pelee volcanism. Quaternary Geochronology 6, 341–355.
Gillot, P.Y., Cornette, Y., 1986. The Cassignol technique for potassium–argon dating, precision and accuracy – examples from the late Pleistocene to recent volcanics from southern Italy. Chemical Geology 59, 205–222.
Gillot, P.Y., Cornette, Y., Max, N., Floris, B., 1992. Two reference materials, trachytes Mdo-G and Ish-G, for argon dating (K-Ar and Ar-40/Ar-39) of Pleistocene and Holocene rocks. Geostandards Newsletter 16, 55–60.
Gillot, P.Y., Hildenbrand, A., Lefèvre, J.C., Albore-Livadie, C., 2006. The K/Ar dating method: principle, analytical techniques and application to Holocene volcanic eruptions in southern Italy. Acta Vulcanologica 18, 55–66.
Hildenbrand, A., Gillot, P.Y., Soler, V., Lahitte, P., 2003. Evidence for a persistent uplifting of La Palma (Canary Islands), inferred from morphological and radiometric data. Earth and Planetary Science Letters 210, 277–289.
Hildenbrand, A., Gillot, P.Y., Le Roy, I., 2004. Volcano–tectonic and geochemical evolution of an oceanic intra-plate volcano: Tahiti-Nui (French Polynesia). Earth and Planetary Science Letters 217, 349–365.
Hildenbrand, A., Gillot, P.Y., Bonneville, A., 2006. Off-shore evidence for a huge landslide of the northern flank of Tahiti-Nui (French Polynesia). Geochemistry, Geophysics, Geosystems 7, 1–12.
Hildenbrand, A., Gillot, P.Y., Marlin, C., 2008a. Geomorphological study of long-term erosion on a tropical volcanic ocean island: Tahiti-Nui (French Polynesia). Geomorphology 93, 460–481.
Hildenbrand, A., Madureira, P., Ornelas Marques, F., Cruz, I., Henry, B., Silva, P., 2008b. Multi-stage evolution of a sub-aerial volcanic ridge over the last 1.3 Myr: S. Jorge Island, Azores Triple Junction. Earth and Planetary Science Letters 273, 289–298.
Johnson, C.L., Wijbrans, J.R., Constable, C.G., Gee, J., Staudigel, H., Tauxe, L., Forjaz, V.H., Salgueiro, M., 1998. Ar-40/Ar-39 ages and paleomagnetism of Sao Miguel lavas, Azores. Earth and Planetary Science Letters 160, 637–649.
Lourenço, N., Miranda, J.M., Luis, J.F., Ribeiro, A., Victor, L.A.M., Madeira, J., Needham, H.D., 1998. Morpho-tectonic analysis of the Azores Volcanic Plateau from a new bathymetric compilation of the area. Marine Geophysical Research 20, 141–156.
Luis, J.F., 2007. Mirone: a multi-purpose tool for exploring grid data. Computers and Geosciences 33, 31–41.
Luis, J.F., Miranda, J.M., Galdeano, A., Patriat, P., Rossignol, J.C., Victor, L.A.M., 1994. The Azores triple junction evolution since 10-Ma from an aeromagnetic survey of the Mid-Atlantic Ridge. Earth and Planetary Science Letters 125, 439–459.
MacDonald, G.A., 1972. Volcanoes. A Discussion of Volcanoes, Volcanic Products, and Volcanic Phenomena. Prentice-Hall, International, New Jersey. 510 pp.
Macdonald, K.C., Miller, S.P., Huestis, S.P., Spiess, F.N., 1980. 3-Dimensional modeling of a magnetic reversal boundary from inversion of deep-tow measurements. Journal of Geophysical Research 85, 3670–3680.
Machado, F., Nascimento, J.M., Denis, A.F., 1959. Evolução Topografica do cone Vulcanico dos Capelinhos, Le Volcanisme de l'ile de Faial. Serv. Geol. Portugal, Mem. 4, 65–71.
Machado, F., Parsons, W., Richards, A., Mulford, J.W., 1962. Capelinhos eruption of Fayal Volcano, Azores, 1957–1958. Journal of Geophysical Research 67, 3519–3529.
Madeira, J., 1998. Estudos de neotectónica nas ilhas do Faial, Pico e S. Jorge: Uma contribuição para o conhecimento geodinâmico da junção tripla dos Açores, PhD thesis. Faculdade de Ciencias, Univ. of Lisboa, 481 pp.
Madeira, J., da Silveira, A.B., 2003. Active tectonics and first paleoseismological results in Faial, Pico and S. Jorge islands (Azores, Portugal). Annals of Geophysics 46, 733–761.
Madeira, J., Soares, A.M.M., Da Silveira, A.B., Serralheiro, A., 1995. Radiocarbon dating recent volcanic activity on Faial Island (Azores). Radiocarbon 37, 139–147.
Madureira, P., Moreira, M., Mata, J., Allegre, C.J., 2005. Primitive neon isotopes in Terceira Island (Azores archipelago). Earth and Planetary Science Letters 233, 429–440.
Madureira, P., Mata, J., Mattielli, N., Queiroz, G., Silva, P., 2011. Mantle source heterogeneity, magma generation and magmatic evolution at Terceira Island (Azores archipelago): constraints from elemental and isotopic (Sr, Nd, Hf, and Pb) data. Lithos 126, 402–418.
Miranda, J.M., Freire Luis, J., Abreu, I., Mendes Victor, A., 1991. Tectonic framework of the Azores Triple Junction. Geophysical Research Letters 18, 1421–1424.
Mitchell, N.C., 1998. Characterising the irregular coastlines of volcanic ocean islands. Geomorphology 23, 1–14.
Montelli, R., Nolet, G., Dahlen, F.A., Masters, G., Engdahl, E.R., Hung, S.H., 2004. Finite-frequency tomography reveals a variety of plumes in the mantle. Science 303, 338–343.
Moore, J.G., Clague, D.A., Holcomb, R.T., Lipman, P.W., Normark, W.R., Torresan, M.E., 1989. Prodigious submarine landslides on the Hawaiian Ridge. Journal of Geophysical Research 94, 17,465–17,484.
Moreira, M., Doucelance, R., Kurz, M.D., Dupre, B., Allegre, C.J., 1999. Helium and lead isotope geochemistry of the Azores Archipelago. Earth and Planetary Science Letters 169, 189–205.
Pacheco, J.M.R., 2001. Processos associados ao desenvolvimento de erupções vulcânicas hidromagmáticas explosivas na ilha do Faial e sua interpretação numa perspectiva de avaliação do hazard e minimização do risco. PhD thesis. Azores University. Ponta Delgada. 300 pp.
Quartau, R., Trenhaile, A.S., Mitchell, N.C., Tempera, F., 2010. Development of volcanic insular shelves: insights from observations and modelling of Faial Island in the Azores Archipelago. Marine Geology 275, 66–83.
Quidelleur, X., Gillot, P.Y., Carlut, J., Courtillot, V., 1999. Link between excursions and paleointensity inferred from abnormal field directions recorded at La Palma around 600 ka. Earth and Planetary Science Letters 168, 233–242.
Quidelleur, X., Gillot, P.Y., Soler, V., Lefevre, J.C., 2001. K/Ar dating extended into the last millennium: application to the youngest effusive episode of the Teide volcano (Spain). Geophysical Research Letters 28, 3067–3070.
Quidelleur, X., Carlut, J., Soler, V., Valet, J.P., Gillot, P.Y., 2003. The age and duration of the Matuyama–Brunhes transition from new K–Ar data from La Palma (Canary Islands) and revisited Ar-40/Ar-19 ages. Earth and Planetary Science Letters 208, 149–163.
Quidelleur, X., Hildenbrand, A., Samper, A., 2008. Causal link between Quaternary paleoclimatic changes and volcanic islands evolution. Geophysical Research Letters 35.
Samper, A., Quidelleur, X., Komorowski, J.C., Lahitte, P., Boudon, G., 2009. Effusive history of the Grande Decouverte Volcanic Complex, southern Basse-Terre (Guadeloupe, French West Indies) from new K-Ar Cassignol-Gillot ages. Journal of Volcanology and Geothermal Research 187, 117–130.
Schilling, J.-G., 1975. Azores mantle blob – rare earth evidence. Earth and Planetary Science Letters 25, 103–115.
Schilling, J.-G., Bergeron, M.B., Evans, R., 1980. Halogens in the mantle beneath the North Atlantic. Philosophical Transactions of the Royal Society of London Series A 297, 147–178.
Searle, R., 1980. Tectonic pattern of the Azores spreading centre and triple junction. Earth and Planetary Science Letters 51, 415–434.
Serralheiro, A., Forjaz, V.H., Alves, C.A.M., Rodrigues, B., 1989. Carta Vulcanológica dos Açores – Ilha do Faial, Scale 1:15 000, Sheets 1, 2, 3 & 4. Centro de Vulcanologia do INIC, Serviço Regional de Protecção Civil dos Açores & Univ. of Azores (Ed.), Ponta Delgada.
Silva, P.F., Henry, B., Marques, F.O., Hildenbrand, A., Marques, F.O., 2008. New paleomagnetic and K/Ar on Faial Island (Azores Archipelago). Constraints on the spatio-temporal evolution of the on-land volcanism. : 11th Castle Meeting, Bojnice (Slovakia).
Silva, P.F., Henry, B., Hildenbrand, A., Madureira, P., Marques, F.O., Kratinová, Z., Nunes, J.C., 2010. Spatial/temporal evolution of Faial's onshore volcanism (Azores Archipelago). Joint AGU Meeting, Foz de Iguassu. .
Silva, P.F., Henry, B., Marques, F.O., Hildenbrand, A., Madureira, P., Mériaux, C.A., Kratinová, Z., 2012. Palaeomagnetic study of a sub-aerial volcanic ridge (São Jorge Island, Azores) for the past 1.3 Myr: evidences for the Cobb Mountain Subchron, volcano flank instability and tectono-magmatic implications. Geophysical Journal International 188, 959–978.
Silva, P.F., Miranda, J.M., Henry, B., Marques, F.O., Hildenbrand, A., Madureira, P., Kratinová, Z. in preparation. Paleomagnetic and magnetic study of Faial island (Azores Archipelago). Geophys. J. Int.
Silveira, G., Stutzmann, E., 2002. Anisotropic tomography of the Atlantic Ocean. Physics of the Earth and Planetary Interiors 132, 237–248.
Silveira, G., Stutzmann, E., Davaille, A., Montagner, J.P., Mendes-Victor, L., Sebai, A., 2006. Azores hotspot signature in the upper mantle. Journal of Volcanology and Geothermal Research 156, 23–34.
Steiger, R.H., Jäger, E., 1977. Subcommission on geochronology: convention on the use of decay constants in geo and cosmochronology. Earth and Planetary Science Letters 36, 359–362.
Stretch, R.C., Mitchell, N.C., Portaro, R.A., 2006. A morphometric analysis of the submarine volcanic ridge south-east of Pico Island, Azores. Journal of Volcanology and Geothermal Research 156, 35–54.
Turner, S., Hawkesworth, C., Rogers, N., King, P., 1997. U-Th isotope disequilibria and ocean island basalt generation in the Azores. Chemical Geology 139, 145–164.
Vogt, P.R., Jung, W.Y., 2004. The Terceira Rift as hyper-slow, hotspot-dominated oblique spreading axis: a comparison with other slow-spreading plate boundaries. Earth and Planetary Science Letters 218, 77–90.
White, W.M., Tapia, M.D.M., Schilling, J.-G., 1979. The petrology and geochemistry of the Azores Islands. Contributions to Mineralogy and Petrology 69, 201–213.
Widom, E., Shirey, S.B., 1996. Os isotope systematics in the Azores: implications for mantle plume sources. Earth and Planetary Science Letters 142, 451–465.
Yang, T., Shen, Y., van der Lee, S., Solomon, S.C., Hung, S.H., 2006. Upper mantle structure beneath the Azores hotspot from finite-frequency seismic tomography. Earth and Planetary Science Letters 250, 11–26.
Zbyszewski, G., Veiga Ferreira, O., 1959. Rapport de la Deuxième mission Géologique. Le Volcanisme de l' ile de Faial. : Serv. Geol. Portugal, Mem., vol. 4.

APPENDIX II
Reply on : Reconstructing the architectural evolution of volcanic islands from combined K/Ar, morphologic, tectonic, and magnetic data: The Faial Island example (Azores)

Journal of Volcanology and Geothermal Research 255 (2013) 127–130

Contents lists available at SciVerse ScienceDirect

Journal of Volcanology and Geothermal Research

journal homepage: www.elsevier.com/locate/jvolgeores

Discussion

Reply to the comment by Quartau and Mitchell on "Reconstructing the architectural evolution of volcanic islands from combined K/Ar, morphologic, tectonic, and magnetic data: The Faial Island example (Azores)", J. Volcanol. Geotherm. Res. 241–242, 39–48, by Hildenbrand et al. (2012)

A. Hildenbrand [a,b,*], F.O. Marques [c], A.C.G. Costa [a,c], A.L.R. Sibrant [a,c], P.F. Silva [d], B. Henry [e], J.M. Miranda [c], P. Madureira [f,g]

[a] Univ Paris-Sud, Laboratoire IDES, UMR8148, 91405 Orsay, F-91405, France
[b] CNRS, Orsay, F-91405, France
[c] Universidade de Lisboa, IDL, Lisboa, Portugal
[d] ISEL/DEC and IDL/CGUL, Lisboa, Portugal
[e] Paleomagnetism, IPGP and CNRS, 4 Av. de Neptune, 94107 Saint-Maur cedex, France
[f] Centro de Geofísica de Évora and Dep. de Geociências da Univ. de Évora, R. Romão Ramalho, 59, 7000–671 Évora, Portugal
[g] Estrutura de Missão para a Extensão da Plataforma Continental, R. Costa Pinto, 165, 2770–047, Paço D'Arcos, Portugal

ARTICLE INFO

Article history:
Received 20 January 2013
Accepted 23 January 2013
Available online 31 January 2013

In our recent paper (Hildenbrand et al., 2012a), we used a panel of complementary approaches to reconstruct the architectural evolution of Faial oceanic island over the last 1 Myr. We showed that the present island has a complex architecture, which results from distinct and brief (<50 kyr) episodes of volcanic construction separated by long periods of volcanic inactivity, during which the edifices were extensively dismantled by erosion and tectonics. The upper part of the oldest volcanic system, especially, only crops out in the SE part of the island, whereas most of the original volcano was deeply modified by mass wasting processes and extensively covered by more recent volcanic products. The combination of our K/Ar, morphologic, tectonic and magnetic data suggests that the remnants of the old volcano are presently under most of Faial, and that this volcano had an elongated morphology slightly oblique with respect to the present WNW–ESE elongation of the island. In their comment, Quartau and Mitchell point out possible "problems" in our interpretations. Their only criticism lies on the extent and morphology of the old volcano, which they draw as a small conical edifice restricted to the eastern end of the island.

We thank Quartau and Mitchell for giving us the opportunity to clarify some important points and discuss significant problems regarding their interpretations:

(1) On-land and offshore topographic data, indeed, provide useful information regarding slope processes on oceanic islands (e.g., Hildenbrand et al., 2006). However, they only give an instantaneous picture of the present edifice morphology. In their comment, Quartau and Mitchell show the bathymetry close to the Faial Island shorelines, and focus more specifically on shallow insular shelves located a few hundred meters away from the present sea cliffs. In their interpretation, the distribution of these shelves would mimic the original slopes of the old volcano. In this interpretation, they assume that (a) the volcano has not experienced any subsequent morphological evolution throughout the lifetime of the island, and (b) the present morphology of the upper proximal submarine slopes is representative of the full geometry of the volcanic edifice. In Fig. 1 of their comment, Quartau and Mitchell present a close-up of the submarine flank, and draw two main volcanoes with a circular shape in plan view. From the extent of these circles, and consideration about statistical slope distribution (Fig. 2 of their comment), they claim that the 800 m isobath materializes the "bathymetric base" of the island. However, they restrict their analysis to the upper submarine slopes, especially in the southern sector, while deeper features on the northern flank are ignored. Previous data by Mitchell et al. (2003) provide a more coherent view at a more appropriate scale (Fig. 1). These clearly show that Faial is only the emerged western part of a much larger volcanic complex, the Pico–Faial ridge, which sits on top of the Azores plateau, down to depths between 1200 m and 1400 m below sea level. While the morphology of the southern flank is disturbed by submarine ridges parallel to the island, the distal bathymetry N of Faial shows a large low-slope relief (Fig. 1), which could either

DOI of original article: http://dx.doi.org/10.1016/j.jvolgeores.2012.06.019.
* Corresponding author at: Univ Paris-Sud, Laboratoire IDES, UMR8148, 91405 Orsay, F-91405, France. Tel.: +33 1 69 15 67 42; fax: +33 1 69 15 48 91.
E-mail address: anthony.hildenbrand@u-psud.fr (A. Hildenbrand).

0377-0273/$ – see front matter © 2013 Elsevier B.V. All rights reserved.
http://dx.doi.org/10.1016/j.jvolgeores.2013.01.015

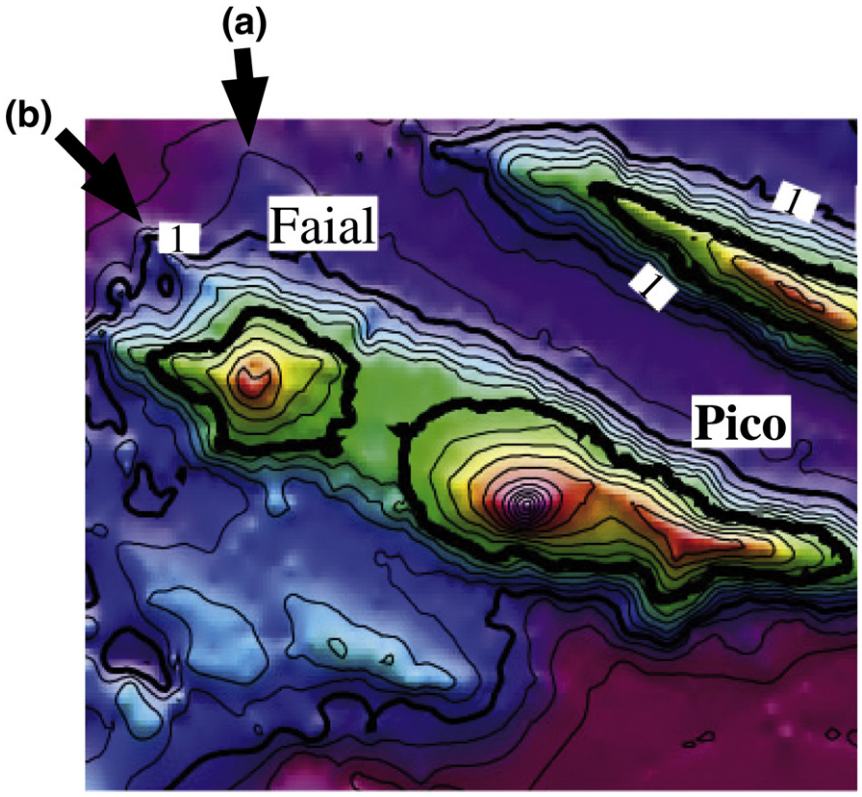


Fig. 1. Topographic and bathymetric map (contours every 200 m with bold contours annotated every 1 km) showing the overall morphology of the Pico-Faial volcanic ridge (after Mitchell et al., 2003, modified). Arrows in the North show important deep submarine features not considered by Quartau and Mitchell in their comment: (a) flat-top relief at the base of the island; (b) oblique elongated feature in the prolongation of the "ridge-like" old volcano proposed in our original paper (Hildenbrand et al., 2012a).

represent deep remnants of the old volcanic system, or remobilized material accumulated in response to destruction of the central parts of the volcano. Furthermore, the map evidences an oblique elongated ridge-like feature NW of Faial, which lies in the prolongation of the oblique ridge inferred from magnetic data (Hildenbrand et al., 2012a). Therefore, the deep submarine evidence appears highly consistent with onshore data, whereas the upper 800 m of the submarine flank on which Quartau and Mitchell focus their discussion most likely only records the younger evolution of the island.

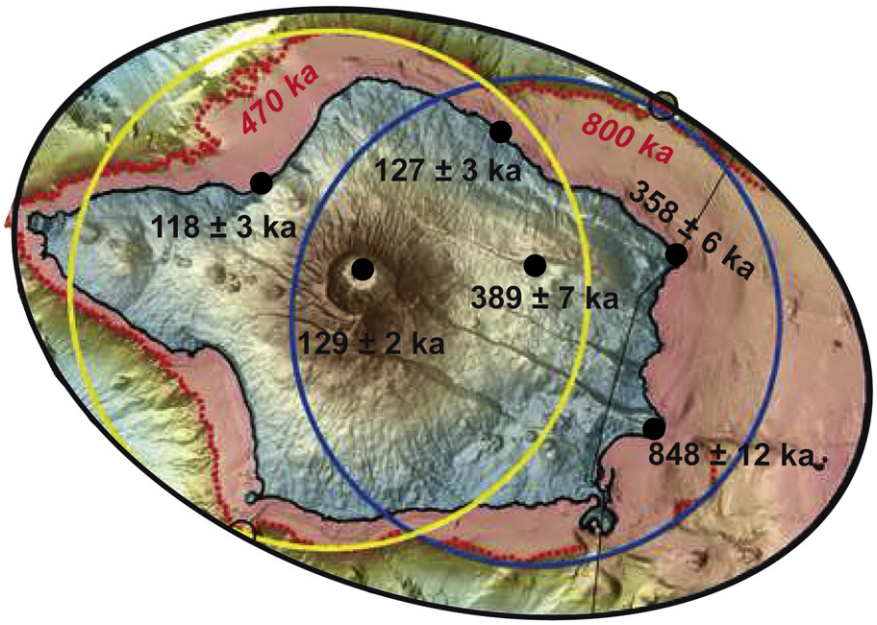


Fig. 2. Unspiked K/Ar ages measured on the main volcanic units of Faial island (data from Hildenbrand et al., 2012a, black numbers) vs age of formation of the shelves inferred by Quartau et al., (2010) and Quartau and Mitchell in their comment (red numbers, italic). Background image after Quartau and Mitchell (modified).

(2) The age of formation of the shelves studied by Quartau et al. (2010) and further considered by Quartau and Mitchell in their comment is highly discussible (Fig. 2). From previous K/Ar data (Féraud et al., 1980; Demande et al., 1982), the oldest volcanic system on Faial, the so-called "Galego volcano" (Féraud et al., 1980) or the "Ribeirinha volcano" (Madeira, 1998), was thought to be active between 800 ka and 560 ka. Based on these previous data, Quartau et al. (2010) modelled shelf formation in the NE sector of Faial over the last 800 kyr. They thus considered that the shelves immediately started to form around the emerging volcano ca. 800 ka ago, and that all the lava flows from subsequent eruptions between 800 ka and 560 ka stopped close to the shore level without significantly covering the shelves. Such a hypothesis seems rather implausible, as volcano growth on oceanic islands generally yield the accumulation of thick lava successions in only a few tens of kyr (e.g., Hildenbrand et al., 2004,2008; Boulesteix et al., 2012; Salvany et al., 2012; Silva et al., 2012). Our new data (Hildenbrand et al., 2012a) show that the whole NE slope of Faial is composed of more than 100 m-thick lava succession ca. 360 kyr old dipping towards the N. Therefore, in our interpretation, it materializes the northern slope of a relatively small edifice emplaced rapidly at that time, which therefore provides a maximum age for the development of the oldest shelves (Fig. 2). Similarly, we show that the young large Central Volcano composing the central sub-aerial part of Faial has been active during the last 130 kyr, instead of the 470 kyr previously proposed (Demande et al., 1982). Therefore, most of the shelves considered by Quartau et al. (2010) and Quartau and Mitchell in their comment, are much younger than supposed, which has a direct impact on shelf modelling and geological interpretation. We are fully aware that Quartau et al. (2010) used existing geochronological data available at the time of their study. However, Quartau and Mitchell should not claim in their present comment that shelf modelling is a way to help dating the volcanic formations, because they now know the revised age of the lavas (Hildenbrand et al., 2012a). If the position and width of the shelf break can provide information regarding the relative age between adjacent volcanoes, the model still needs to integrate updated geochronological evidence (Hildenbrand et al., 2012a) or, alternatively, to be calibrated by datable markers such as marine terraces including fossils/microfossils.

(3) The insular shelves studied by Quartau et al. (2010) and Quartau and Mitchell around the various sectors of Faial are presently located between 211 m and 27 m below sea level. Quartau et al. (2010) tentatively modelled shelf development assuming that they have been formed mostly by surf erosion in response to eustatic sea level variations, while the island is considered to have remained at the same vertical position during the last 800 kyr. This is a major problem, as most volcanic islands experience considerable vertical movements during their growth (e.g., Ludwig et al., 1991; Hildenbrand et al., 2003). We note that Quartau et al. (2010) estimated possible local vertical movements from the discrepancy between modelled shelves and actual shelf depth. However, such interpretation is biased by the over-estimated ages used in their modelling (see point (2)). The Pico–Faial ridge has developed over a young oceanic lithosphere, about 10 Ma in age (e.g., Miranda et al., 1991; Luis et al., 1994). Significant thermal subsidence due to lithosphere cooling is thus expected, at a typical rate on the order of a fraction of a mm/yr from the equations of Turcotte and Schubert (2002). Flexural load of the lithosphere by the whole volcanic edifice and additional tectonic subsidence must also be considered, and can be significant. The central Azores, indeed, have developed in a region subject to intense regional deformation, marked by recurrent medium/high-magnitude earthquakes (e.g., Catita et al., 2005; Borges et al., 2007), and by the development of numerous volcano-tectonic structures. Faial Island, specifically, is cut by a large graben bounded by numerous normal faults, which have accumulated important vertical offset over the last 400 kyr (Hildenbrand et al., 2012a). From the various sources of subsidence here considered (thermal, flexural and tectonic), an average long-term subsidence rate of 1 mm/yr appears plausible for Faial. Such value is a minimum, as present movement measured by GPS and radar interferometry (Catalão et al., 2011) show rates greater than or equal to 2 mm/yr for the Pico–Faial ridge as a whole, plus faster movements (ca 1 cm/yr) along some shorelines, especially on the northern coast of Faial and also on Pico, where active slumping is displacing the SE flank of the island at rates of up to 1 cm/yr (Hildenbrand et al., 2012b). From our new geochronological and magnetic data on Faial, the old volcano was completely built at ca 850 ka (Hildenbrand et al., 2012a). Assuming a long-term (conservative) subsidence rate of ~1 mm/yr yields an integrated downward movement of ca. 850 m. This suggests that the low-slope deep portion referred to as the "bathymetric base" of Faial by Quartau and Mitchell was formed close to shore level some 850 ka ago. It certainly cannot represent the bathymetric base of the island, unless we consider that any portion below sea level at a given time is not part of the volcanic edifice.

To summarize, the comment by Quartau and Mitchell addresses important questions, but is based on a number of misleading assumptions. In particular, they have used unreliable K/Ar ages acquired on whole-rock (see a review in Hildenbrand et al., 2012a) to support a study that requires very accurate dating, and have ignored vertical movements typical of volcanic islands built on top of young and thin lithosphere. From the several lines of evidence exposed above, in particular the new accurate geochronological data presented in Hildenbrand et al. (2012a), different conclusions can be reached: (i) the shelf at 211 m does not record the succession of construction and destruction episodes over the last 850 kyr. (ii) the shelves studied by Quartau and co-workers most likely formed during the last 400 kyr, and most of them during the last 120 kyr. Therefore, their distribution does not reflect the geometry of the initial volcano. In fact, they are parallel to the present island shape, which is not surprising, since the latter was roughly acquired since 120 ka, except the western end, which was active during the last 10 kyr. (iii) Average subsidence rates, along with eustatic sea level variations must be taken into account in shelf modelling. (iv) The flat portion at a depth of ca. 800 m around the island does not represent the base of the Pico–Faial ridge, but may alternatively represent a shelf formed rapidly after the rapid construction of the old volcano 850 ka ago, which then subsided down to 800 m bsl. (vi) If such a hypothesis is correct, it means that the old volcano was a large edifice (from the seafloor to asl), which appears consistent with magnetic data and the general morphology of oceanic islands. (vii) Bathymetric data at the full-scale of the whole Pico–Faial ridge support an oblique-ridge geometry and significant mass-wasting for the old Faial volcano. These clarifications will hopefully illustrate that on-land and offshore data need to be considered together, rather than separately to reconstruct, in a consistent way, the long-term architectural evolution of rapidly evolving oceanic islands like Faial. This is LGMT contribution 107.

References

Borges, J.F., Bezzeghoud, M., Buforn, E., Pro, C., Fitas, A., 2007. The 1980, 1997 and 1998 Azores earthquakes and some seismo-tectonic implications. Tectonophysics 435, 37–54.

Boulesteix, T., Hildenbrand, A., Gillot, P.Y., Soler, V., 2012. Eruptive response of oceanic islands to giant landslides: new insights from the geomorphologic evolution of the Teide–Pico Viejo volcanic complex (Tenerife, Canary). Geomorphology 138 (1), 61–73.

Catalão, J., Nico, G., Hanssen, R., Catita, C., 2011. Merging GPS and atmospherically corrected InSAR data to map 3D terrain displacement velocity. IEEE Transactions

on Geoscience and Remote Sensing 49, 2354–2360. http://dx.doi.org/10.1109/TGRS.2010.2091963.
Catita, C., Feigl, K.L., Catalão, J., Miranda, J.M., Victor, L.M., 2005. Time series analysis of SAR data applied to the study of the co-seismic deformation of the 9th July 1998 Pico–Faial (Azores) earthquake. International Journal of Remote Sensing 26, 2715–2729. http://dx.doi.org/10.1080/01431160512331337835.
Demande, J., Fabriol, R., Gérard, A., Iundt, F., 1982. Prospection géothermique des Iles de Faial et Pico (Açores). 82SGN003GTH, Bureau de recherches géologiques et minières, Orléans.
Féraud, G., Kaneoka, I., Allègre, C.J., 1980. K/Ar ages and stress pattern in the Azores: geodynamic implications. Earth and Planetary Science Letters 46, 275–286.
Hildenbrand, A., Gillot, P.Y., Soler, V., Lahitte, P., 2003. Evidence for a persistent uplifting of La Palma (Canary Islands) inferred from morphological and radiometric data. Earth and Planetary Science Letters 210, 277–289.
Hildenbrand, A., Gillot, P.Y., Le Roy, I., 2004. Volcano–tectonic and geochemical evolution of an oceanic intra-plate volcano: Tahiti–Nui (French Polynesia). Earth and Planetary Science Letters 217, 349–365.
Hildenbrand, A., Gillot, P.Y., Bonneville, A., 2006. Off-shore evidence for a huge landslide of the northern flank of Tahiti–Nui (French Polynesia). Geochemistry, Geophysics, Geosystems 7 (3), 1–12. http://dx.doi.org/10.1029/2005GC001003.
Hildenbrand, A., Madureira, P., Ornelas Marques, F., Cruz, I., Henry, B., Silva, P., 2008. Multi-stage evolution of a sub-aerial volcanic ridge over the last 1.3 Myr: S. Jorge Island, Azores Triple Junction. Earth and Planetary Science Letters 273, 289–298.
Hildenbrand, A., Marques, F.O., Costa, A.C.G., Sibrant, A.L.R., Silva, P.F., Henry, B., Miranda, J.M., Madureira, P., 2012a. Reconstructing the architectural evolution of volcanic islands from combined K/Ar, morphologic, tectonic, and magnetic data: the Faial Island example (Azores). Journal of Volcanology and Geothermal Research 241–242, 39–48.
Hildenbrand, A., Marques, F.O., Fernandes, J.C.C.C., Catita, C.M.S., Costa, A.C.G., 2012b. Large-scale active slump of the southeastern flank of Pico Island, Azores. Geology 40 (10), 939–942.
Ludwig, K.R., Szabo, B.J., Moore, J.G., Simmons, K.R., 1991. Crustal subsidence rate off Hawaii, determined from $^{234}U/^{238}U$ ages of drowned coral reefs. Geology 19, 171–174.
Luis, J.F., Miranda, J.M., Galdeano, A., Patriat, P., Rossignol, J.C., Victor, L.A.M., 1994. The Azores Triple Junction evolution since 10-Ma from an aeromagnetic survey of the mid-Atlantic Ridge. Earth and Planetary Science Letters 125, 439–459.
Madeira, J., 1998. Estudos de neotectónica nas ilhas do Faial, Pico e S. Jorge: Uma contribuição para o conhecimento geodinâmico da junção tripla dos Açores, PhD thesis. Faculdade de Ciencias, Univ. of Lisboa, 481 pp.
Miranda, J.M., Freire Luis, J., Abreu, I., Mendes Victor, A., 1991. Tectonic framework of the Azores Triple Junction. Geophysical Research Letters 18, 1421–1424.
Mitchell, N.C., Schmidt, T., Isidro, E., Tempera, F., Cardigos, F., Nunes, J.C., Figueiredo, J., 2003. Multibeam sonar survey of the central Azores volcanic islands. InterRidge News 12 (2), 30–32.
Quartau, R., Trenhaile, A.S., Mitchell, N.C., Tempera, F., 2010. Development of volcanic insular shelves: insights from observations and modelling of Faial Island in the Azores Archipelago. Marine Geology 275, 66–83.
Salvany, T., Lahitte, P., Nativel, P., Gillot, P.-Y., 2012. Geomorphic evolution of the Piton des Neiges Volcano (Reunion Island, Indian Ocean): competition between volcanic construction and erosion since 1.4 Ma. Geomorphology 136, 132–147.
Silva, P.F., Henry, B., Marques, F.O., Hildenbrand, A., Madureira, P., Mériaux, C.A., Kratinová, Z., 2012. Palaeomagnetic study of a sub-aerial volcanic ridge (São Jorge Island, Azores) for the past 1.3 Myr: evidences for the Cobb Mountain Subchron, volcano flank instability and tectono-magmatic implications. Geophysical Journal International 188, 959–978.
Turcotte, D., Schubert, G., 2002. Geodynamics, Second ed. Cambridge University Press, pp. 456.

APPENDIX III
Large-scale catastrophic flank collapses in a steep volcanic ridge: The Pico-Faial Ridge, Azores Triple Junction.

Journal of Volcanology and Geothermal Research 272 (2014) 111–125

Contents lists available at ScienceDirect

Journal of Volcanology and Geothermal Research

journal homepage: www.elsevier.com/locate/jvolgeores

Large-scale catastrophic flank collapses in a steep volcanic ridge: The Pico–Faial Ridge, Azores Triple Junction

A.C.G. Costa [a,b,c,d,*], F.O. Marques [a], A. Hildenbrand [c,d], A.L.R. Sibrant [c,d], C.M.S. Catita [a,b]

[a] University of Lisbon, Lisbon, Portugal
[b] IDL, Lisbon, Portugal
[c] Univ. Paris-Sud, Laboratoire IDES, UMR8148, Orsay F-91405, France
[d] CNRS, Orsay F-91405, France

ARTICLE INFO

Article history:
Received 16 September 2013
Accepted 6 January 2014
Available online 17 January 2014

Keywords:
Large-scale flank collapse
Debris deposit
Steep volcanic ridge
Mass wasting
Pico Island
Azores

ABSTRACT

Large-scale flank collapses are common in the geological evolution of volcanic ocean islands in the Atlantic. To date, catastrophic lateral collapses in the Azores Islands have been difficult to identify, leading to suggestions that a lack of events may relate to the relatively small size of the islands. Here we show evidence for two major collapses on the northern flank of Pico Island (Pico–Faial volcanic ridge, central Azores), suggesting that this island had a collapse incidence similar to that of other Atlantic volcanic islands.

The study is based on the analysis of: (1) offshore and onshore high-resolution digital elevation models; (2) field data focused on the N flank; and (3) new K–Ar ages on selected lava flow samples.

Pico sub-aerial northern flank is marked by two conspicuous arcuate shaped depressions concave towards the sea, here interpreted as landslide scars. A main debris field is observed offshore the largest depression. This deposit has 20 km of maximum length, covers ca. 150 km^2, is composed of meter to hectometer blocks, and has an exposed volume here estimated between 4 and 10 km^3, though the actual volume probably exceeds 10 km^3. Debris flow towards the ESE was apparently determined by the slope of the narrow WNW–ESE S. Jorge channel.

Young lava flows cascade over the interpreted scars, thus concealing the older volcanic sequence(s) affected by the landslide(s). New K–Ar ages measured on these lava flows provide a minimum age of ca. 70 ka for the large-scale collapse(s) in Pico's northern flank.

© 2014 Elsevier B.V. All rights reserved.

1. Introduction

The destruction of volcanic islands occurs at small and large scales, gradually or suddenly on catastrophic events. Large-scale flank failure in volcanic islands can involve either gradual movement along deep listric faults (slump) or the generation of debris avalanche (Moore et al., 1989). These two mechanisms are not mutually exclusive, as a creeping slump may suddenly turn into a catastrophic debris avalanche. From on-land and offshore studies, catastrophic large-scale mass wasting has been identified on volcanic islands all over the world (e.g., Duffield et al., 1982; Moore et al., 1989; Gillot et al., 1994; Deplus et al., 2001; Krastel et al., 2001; Masson et al., 2002; Hildenbrand et al., 2006). In the Atlantic, more specifically, catastrophic failure episodes have been extensively documented, e.g. in the Canary (Navarro and Coello, 1989; Carracedo et al., 1999; Krastel et al., 2001; Masson et al., 2002; Boulesteix et al., 2012, 2013), in Cape Verde (e.g., Day et al., 1999; Masson et al., 2008), and along the Caribbean arc (Deplus et al., 2001; Le Friant et al., 2003; Samper et al., 2007; Germa et al., 2011).

To date, catastrophic flank collapses in the Azores Islands have been difficult to identify, leading to suggestions that a lack of collapses may relate to the relatively small volume of individual islands and volcanic ridges (e.g. Mitchell, 2003). Two topographic embayments on the southern flank of Pico Island have been related to lateral flank movement in the form of old catastrophic landslides or slumping processes (Woodhall, 1974; Madeira, 1998; Nunes, 1999, 2002; Madeira and Brum da Silveira, 2003; Hildenbrand et al., 2012b, 2013b; Mitchell et al., 2012, 2013), but none of these features is clearly and unambiguously associated with well-identified offshore deposits.

Here we put forward evidence of two major collapses, and respective submarine deposits, on Pico's northern flank, showing that the island has experienced episodes of flank instability like other Atlantic volcanic islands.

The identification of offshore debris deposits and the interpretation of onshore source zones in Pico's northern flank are here primarily based on morphological characterization, through combined analysis of a 10 m resolution sub-aerial digital elevation model (DEM) and the new 50 m resolution bathymetry of the narrow S. Jorge Channel (between Pico's northern flank and S. Jorge's southern flank). The analysis of the bathymetry also supports the discussion of the influence of channel morphology on the landslide submarine flow and deposition.

* Corresponding author at: University of Lisbon and IDL, Lisbon, Portugal. Tel.: +351 918318361.
E-mail address: acgcosta@fc.ul.pt (A.C.G. Costa).

0377-0273/$ – see front matter © 2014 Elsevier B.V. All rights reserved.
http://dx.doi.org/10.1016/j.jvolgeores.2014.01.002

In order to determine the age and recurrence of the failure events, we performed fieldwork focused on the establishment of volcanic stratigraphy/structure of the source zones, aiming at finding possible landslide scars/deposits and to sample the volcanic sequences affected by and covering the landslide related features. The sampled rocks were then processed according to the K–Ar Cassignol–Gillot unspiked technique.

2. Geologic setting

The Azores Islands are located about the triple junction between North-America, Eurasia and Nubia plates (Fig. 1). The study region is located on the locally diffuse Nubia/Eurasia plate boundary (Lourenço et al., 1998; Fernandes et al., 2006; Borges et al., 2007; Marques et al., 2013), where regional deformation has influenced the development of narrow and steep volcanic ridges (Fig. 1). The volcanic ridges of S. Jorge and Pico–Faial (Fig. 1) are characterized by slopes commonly around 25–35°, locally reaching higher values along coastal cliffs. These ridges are characterized by a multi-stage development during the last 1.3 Myr (Féraud et al., 1980; Demande et al., 1982; Hildenbrand et al., 2008, 2012a). This multi-stage development includes short periods of volcanic construction interrupted by long periods of island destruction. The island destruction processes are either gradual (e.g., erosion, graben development) or catastrophic like the events here reported. The growth of the sub-aerial Pico–Faial ridge started ca. 850 ka ago on the eastern part of Faial Island (Quartau et al., 2010, 2012; Hildenbrand et al., 2012a, 2013a; Quartau and Mitchell, 2013), with the growth of sub-aerial Pico during the last ca. 300 ka (Fig. 2, 250 ± 40 ka, in Demande et al., 1982). The oldest outcropping volcanic unit in Pico, the Topo Unit (TU), is located on its SE flank (Fig. 2), which is deeply affected by a currently active slump structure (Hildenbrand et al., 2012b) (Fig. 3, feature 1). A WNW–ESE fissural system (FS) developed N of Topo (Fig. 2), and a stratovolcano (Fig. 2, PS) constitutes the westernmost part of the island (Fig. 2, e.g., Forjaz 1966); both have been volcanically active through the Holocene and in historic times (Madeira, 1998; Nunes, 1999; Mitchell et al., 2008). Two topographic embayments on Pico's northern flank (Fig. 3) were considered by Mitchell (2003) as "ambiguous candidates for landslides". Mitchell et al. (2008) identified a hummocky terrain area on the shallow bathymetry (depth up to of a few hundred meters) adjacent to a sub-aerial embayment (Fig. 2 in Mitchell et al., 2008, feature A), which was interpreted as a deposit resulting from debris avalanche or repeated lava delta failure. Despite these evidences, to date the published works (e.g., Mitchell, 2003; Mitchell et al., 2008) do not conclude unequivocally on the occurrence of major landslides in Azores islands.

3. Morphological analysis

3.1. Construction of the DEMs

The submarine grid of the deepest sector of the Pico–S. Jorge channel (50 m resolution, Fig. A.1a) was constructed using the multibeam data acquired with a 12 kHz Kongsberg EM120 multibeam echo sounder system (Lourenço, personal communication). The depth accuracy (RMS) for this system is estimated as 0.2–0.5% of the water depth (Kongsberg, 2007). Considering that the maximum water depth in the study area is ca. 1300 m, the maximum RMS expected for this data set lies in the range 2.6–6.5 m.

The multibeam data were processed using the CARIS software, clean of noise and converted to an ASCII file (Lourenço, personal communication). Next, the 50 m resolution ASCII data were converted to a raster structure of 50 m spatial resolution, using a simple gridding method.

The onshore data used in this study was produced from a digital topographic map of Pico Island (Portuguese Army Geographic Institute, IGeoE). Photogrammetric methods led to the production of this information at the 1:25,000 scale. The vertical accuracy of these data is approximately 5 m (Afonso et al., 2002). The nodes and lines with three-dimensional coordinates (x, y and z) of the contour lines were then used to generate a TIN (Triangulated Irregular Network) model, which is a vector-based representation of the relief based on a network of non-overlapping triangles (Burrough and McDonnell, 1998). The conversion of the TIN model to a raster structure was then performed interpolating the cell z-values from the input TIN at the spatial resolution of 10 m and 50 m to produce the final onshore DEMs for Pico Island (10 m spatial resolution), S. Jorge and Faial Islands (50 m spatial resolution). To this purpose, we used the ArcGIS 9.3 software from ESRI with the 3D Analyst extension. For the final grid, we introduced in the no-data zone on Pico's northern coast (between the sub-aerial and submarine grids described above) the 100 m spaced contours obtained from photogrammetry of Fig. 2 in Mitchell et al. (2008). The final 50 m resolution grid was built through combination of the sub-aerial and submarine DEMs described above (Fig. 4), filling the no-data zone with a 200 m resolution interpolation that included the depth contours

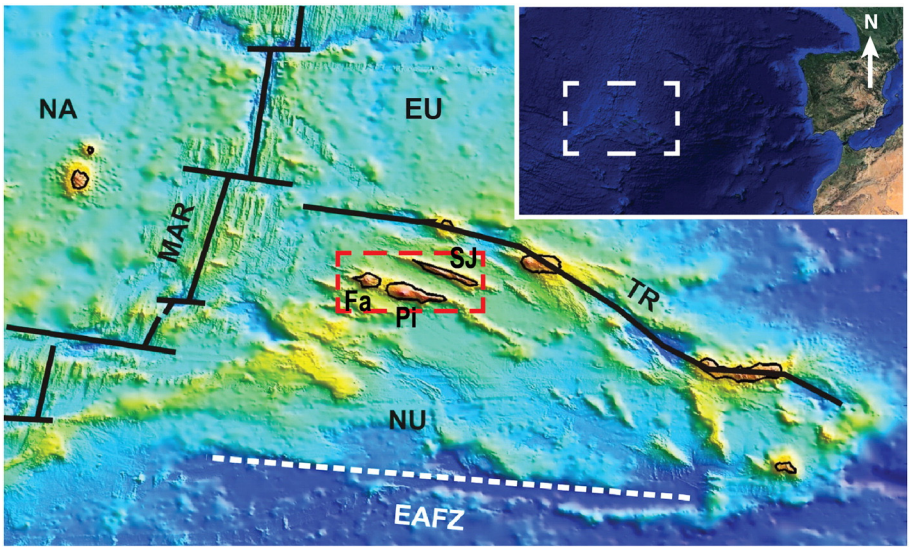


Fig. 1. Location of the Azores archipelago on the triple junction between the North America (NA), Eurasia (EU) and Nubia (NU) plates. Main active structures represented as thick black lines (Middle Atlantic Ridge — MAR, Terceira Rift — TR) and inactive structure as dashed white line (East Azores Fracture Zone — EAFZ). The white dashed rectangle encompassing the islands of Pico (Pi), S. Jorge (SJ) and Faial (Fa) limits the study area. Bathymetric data from Lourenço et al. (1998); Image available at http://w3.ualg.pt/~jluis/acores_plateau.htm. (right top rectangle) Inset for the location of the Azores Triple Junction (Google Earth image — 19-08-2013).

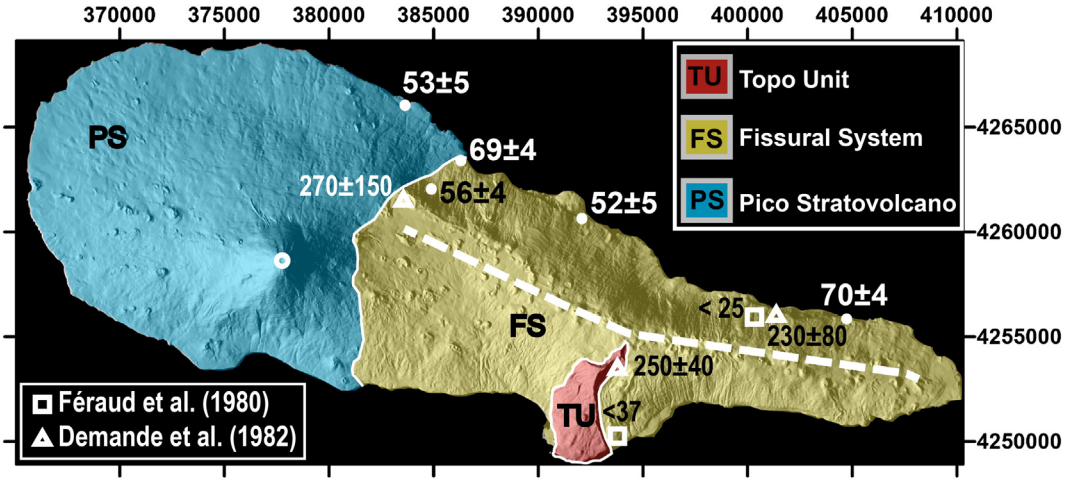


Fig. 2. Shaded relief of the 10 m resolution DEM of Pico Island (lighting from ESE), with coordinates in meters UTM (zone 26N). White dots and numbers along Pico's northern flank mark the location and the K–Ar ages presented in this study. White squares and triangles mark the K–Ar ages presented in Féraud et al. (1980) and Demande et al. (1982), respectively. The ages are indicated in thousands of years (ka). Simplified geologic/physiographic map (modified after Madeira, 1998).

extracted from Mitchell et al. (2008). Further details on the composition of the final DEM grid are provided in Appendix A.

For the construction of Pico's elevation gradient in the sub-aerial domain (Fig. 3), we took the original 10 m resolution elevation grid of the sub-aerial domain and created a final 10 m resolution terrain slope grid in the Surfer software (Golden Software, Inc.; software version 9.11.47). For each grid node, the angle of dip was calculated considering the elevation gradients between neighboring nodes in N–S and E–W directions (Golden Software, Inc., 2002, after Moore et al., 1993). Therefore, though the final slope grid presents values for 10 m spaced nodes, the calculation of the final values is based on the elevation gradient between nodes at a 20 m distance from each other (twice the horizontal resolution of the original DEM).

3.2. Pico's sub-aerial northern flank

On an elevation gradient map (Fig. 3), the northern flank is generally steeper than the southern flank. On the northern flank, the sub-aerial elevation gradient of the fissural system (Fig. 2, FS) reaches 30–45° on two sectors of concave profile, reaching ca. 800 m of maximum height (Fig. 3):

1. On the western sector of the fissural system, the 30–45° slopes are aligned WNW–ESE (Fig. 3, feature 2). They are masked in the west and in the east by more recent volcanic deposits erupted by the younger Pico stratovolcano and by the fissural system, respectively (Figs. 2 and 3).
2. On the eastern sector of the northern flank, the steep slopes define an arcuate topography, which is concave towards the sea and grossly parallel to the volcanic ridge axis (Fig. 3, feature 3).

3.3. S. Jorge Channel bathymetry

The building of the grid mosaic, combining sub-aerial and submarine grids, is described in Appendix A of the supplementary material.

Pico and S. Jorge islands are separated by a ca. 20 km wide WNW–ESE channel, known as the S. Jorge Channel (Fig. 4). The maximum depth along its axis varies between ca. −1230 m and −1270 m, with a basal surface defined around −1270 m, deepening towards its

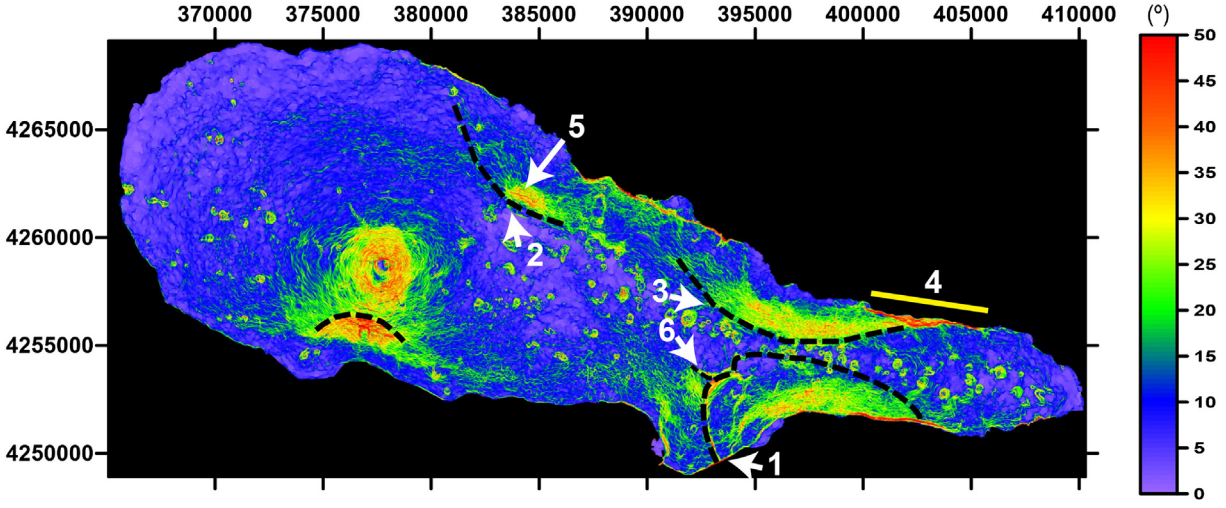


Fig. 3. Slope map of Pico Island built from the 10 m resolution DEM. Dashed black lines: scarps interpreted from zones of anomalously strong slopes. Numbered features: 1 — active slump; 2 — westernmost scar of Pico's N flank; 3 — easternmost scar of Pico's N flank coastal; 4 — coastal cliff mentioned in Section 4; 5 — location of the creeks referred to in Section 4; 6 — scarp that limits the outcropping TU to the N.

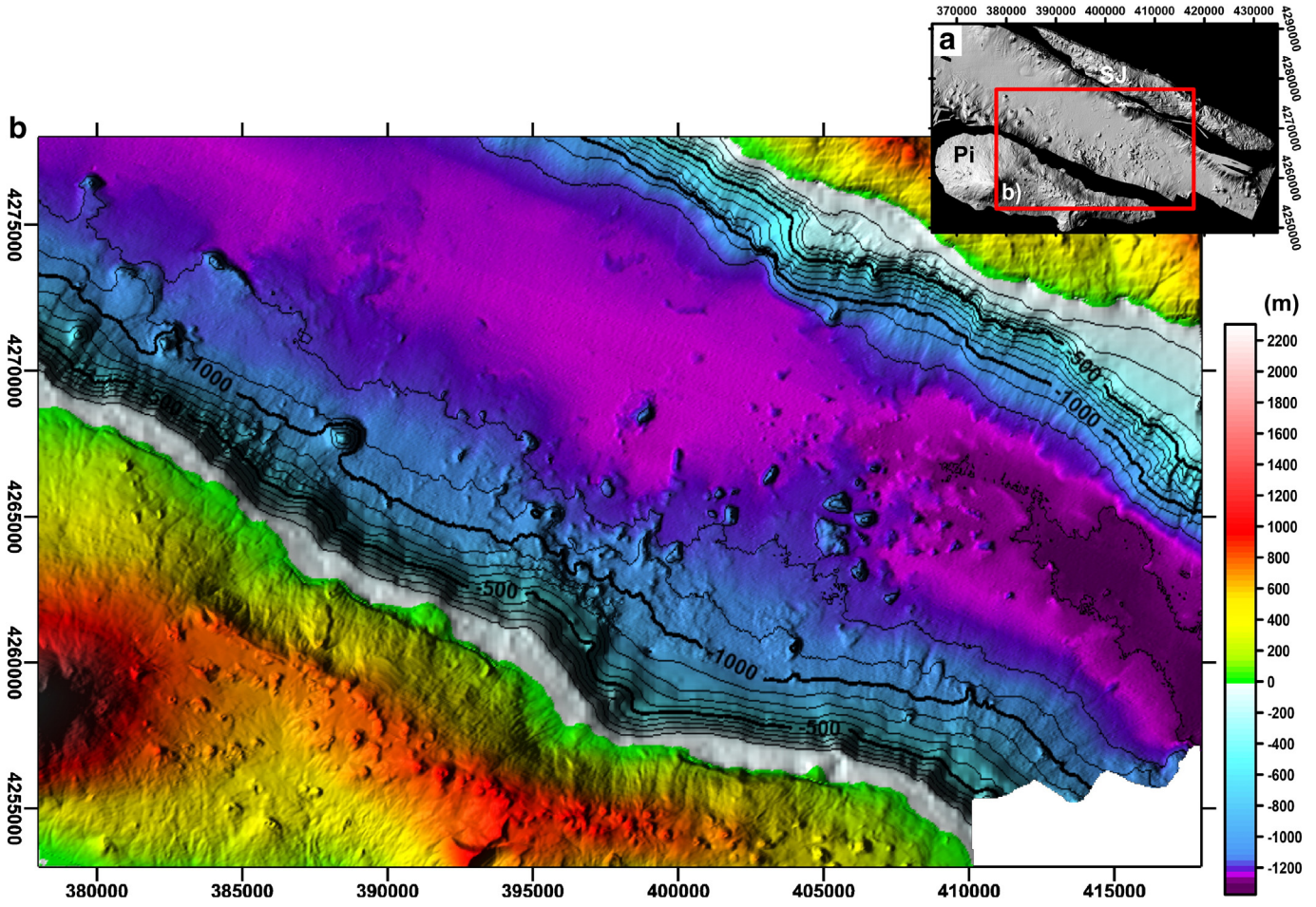


Fig. 4. Topographic grid used as basis for this study. (a) Shaded relief (50 m resolution, lighting from WNW) of Pico Island (Pi), S. Jorge Island (SJ) and bathymetry of S. Jorge channel. The red rectangle indicates the area comprised in b. (b) Final grid resulting from the combination of the DEMs presented in (a) and contours extracted from Mitchell et al. (2008) (50 m resolution, lighting from W). Contour levels for 100 m spaced depths are presented. A detailed description of the grid construction is presented in Appendix A. (For interpretation of the references to color in this figure legend, the reader is referred to the web version of this article.)

WNW and ESE ends. On the bathymetry of the S. Jorge Channel (Fig. 5a), we identified:

1. The main feature in the central sector, a WSW–ENE elongated hummocky area, with a positive relief relative to the surrounding sea floor (Fig. 6a, feature "A"). It has a maximum visible length of 20 km (ca. 22 km, measured along a longitudinal profile) and spreads over an area of ca. 150 km^2. The grain size of the material at the surface of this positive-relief feature is generally too small to be distinguishable on this 50 m resolution DEM. The largest individual hummocks observed are located on the distal part of the deposit, at an average depth of −1240 m (Fig. 6a): the largest is 1700 m long, 1200 m wide and 100 m high (Fig. 6a, feature 1), and the second largest is 1000 m long, 600 m wide and 200 m high (Fig. 6a, feature 2). On the SE zone of the hummocky terrain, a homogeneous mass of, apparently, intermediate size debris material can be identified (Fig. 6a, feature "A", dashed yellow line). At the foot of Pico's submarine flank, on the surface of this homogeneous mass (high resolution bathymetry presented as Fig. 2 in Mitchell et al., 2008), there are visible lineaments perpendicular to the submarine flank. Uphill, on the submarine flank, there are two small arcuate scarps (Fig. 6a, red dashed lines).
2. A NNE–SSW elongated, lobate-shaped hummocky terrain on the western sector (Fig. 6a, feature "B"). Its maximum extent is ca. 8 km, measured from, and perpendicularly to, the base of Pico's submarine flank. It is generally composed of small debris, undistinguishable on the 50 m resolution DEM, but with some larger hummocks. The limits of the deposit are not well defined in the proximity of Pico's flank, covering a minimum area of 32 km^2.
3. A smaller deposit at the base of S. Jorge's southern flank (Fig. 6a, feature "C"), with 4 km of maximum length, measured from, and perpendicularly to, the base of S. Jorge's submarine flank, and covering an area of ca. 12 km^2. Upslope the submarine flank, there is an arcuate-shaped scar (Fig. 6a, red dashed line).
4. Lobate-shaped deposits visible along the base of Pico and S. Jorge's flanks. These deposits are generally composed of small size debris, undistinguishable on the 50 m resolution DEM, but with some larger hummocks.

3.4. Debris volume

The exposed volume of Pico's northern deposit (Fig. 6a, feature "A") was estimated considering solely the space between the actual topographic surface of the deposit and hypothetical basal surfaces (based on submarine flank profiles performed on deposit-free sectors). We built NNE–SSW cross sections of the original grid (perpendicular to the coastline on the zone where the deposit is thickest), spaced approximately 1.2 km, and covering the deposit area and the surrounding deposit-free area (Fig. 7). The origin considered for the horizontal distance of the cross sections is the −100 m contour line, roughly the limit of the Pico's shelf. For the calculation of the exposed volume, we assume that the upward limit of the deposit is at −100 m contour (we assume that it is limited to the extent visible on the bathymetry,

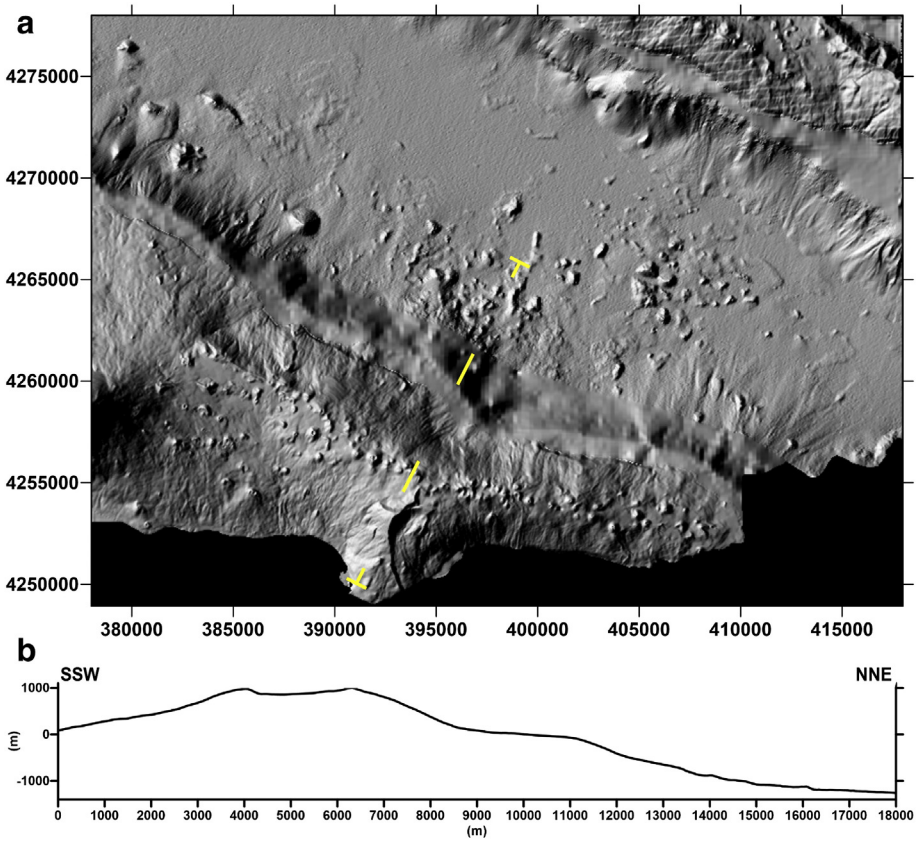


Fig. 5. (a) Shaded relief map of the S. Jorge channel, sub-aerial Pico and S. Jorge islands (lighting from ESE, 50 m resolution DEM). (b) Topographic profile across Pico Island's sub-aerial domain and submarine northern flank, presented as a yellow dashed line in (a). (For interpretation of the references to color in this figure legend, the reader is referred to the web version of this article.)

not continuing landward), and we do not consider the effects of blanketing by more recent volcanic/sedimentary materials.

As the channel deepens and gets narrower towards the ESE (Fig. 4), the volume will be given as an interval: minimum volume estimated with a hypothetical basal profile representative of the WNW limit of the deposit, and maximum volume estimated with a hypothetical basal profile that considers the greater depths of the ESE limit of the deposit. The hypothetical basal profile from the WNW limit of the deposit (Fig. 7b, black dashed line) was determined from the average of closely spaced cross sections (Fig. 7a, full white line cross sections), on a zone relatively undisturbed by the presence of sedimentary deposits or volcanic cones. In order to build the hypothetical basal profile used for the determination of the maximum volume (Fig. 7b, red dashed line), we considered all the cross sections performed perpendicularly to the coast, and determined the maximum depth attained by the bulk of these cross sections for 1 km spaced horizontal distance values.

For the construction of each hypothetical basal surface, we introduced the values determined for the "normal profiles" in the blank area (Fig. 7a, area comprised by the green dashed line) and performed a 200 m resolution spatial interpolation (kriging) (Fig. 8a and b). The standard deviations associated with the interpolation method used have a maximum value of 25 m (Fig. B.1). These spatial interpolations have associated Root Mean Square (RMS) errors within a range of 4.7–5.6 m, and a maximum residue of 26.0 m, for the deposit's blanked area (Table B.1). Though the maximum residue obtained for the complete grid has a value of 145.1 m (Table B.1), this residue was obtained outside the deposit's blanked area, therefore outside the zone considered in the volume calculation (Fig. B.2). We built "deposit thickness" grids by subtracting each of the hypothetical basal surfaces from the real topographic surface (Fig. 8c and d). The maximum thickness of the deposit lies between ca. 238 and 304 m (Table 1). In Fig. 8c and d, it is visible that there are appreciable volumetric anomalies on the surroundings of the limits defined for the deposit, where it would be ideal to have a perfect fit between real and estimated basal surfaces. In order to partially eliminate these anomalies, the volume was calculated only for the deposit's area (Fig. 8c and d, area comprised by the dashed black line). The volume of the deposit visible on the bathymetry is, roughly, between 4 and 10 km^3 (Table 1, positive volume). If we consider that, for the hypothetical maximum depth basal surface, there are still zones on which the basal surface lies above the real topography (Table 1, negative volume), then the exposed volume of the deposit must be closer to 10 km^3 than to 4 km^3.

4. Fieldwork

In order to constrain the age of failure events on Pico's northern flank, we attempted to sample the volcanic sequence affected by the flank failure and the one covering the landslide scar(s). The fieldwork was focused on the zones where it would be more probable to reach the older volcanic sequence affected by the eventual flank failures, i.e., inside deep creeks incising the cascading lavas, and along coastal cliffs close to these features.

On the eastern sector of Pico's N flank, the high coastal cliff has a maximum height of ca. 400 m. It intersects the steep slope zone that defines the eastern embayment (Fig. 3, feature "4"). Along this coastal cliff, the outcropping sequence consists mainly of lava flows that dip to the N on the western sector, whereas lava flows dip to the NE on the eastern sector (Fig. 6a). No major unconformities have been observed on the outcropping sequence. Nevertheless, we sampled a lava flow (Table 2 and Fig. 2, sample Pi10X), as close as possible to the base of the outcropping sequence.

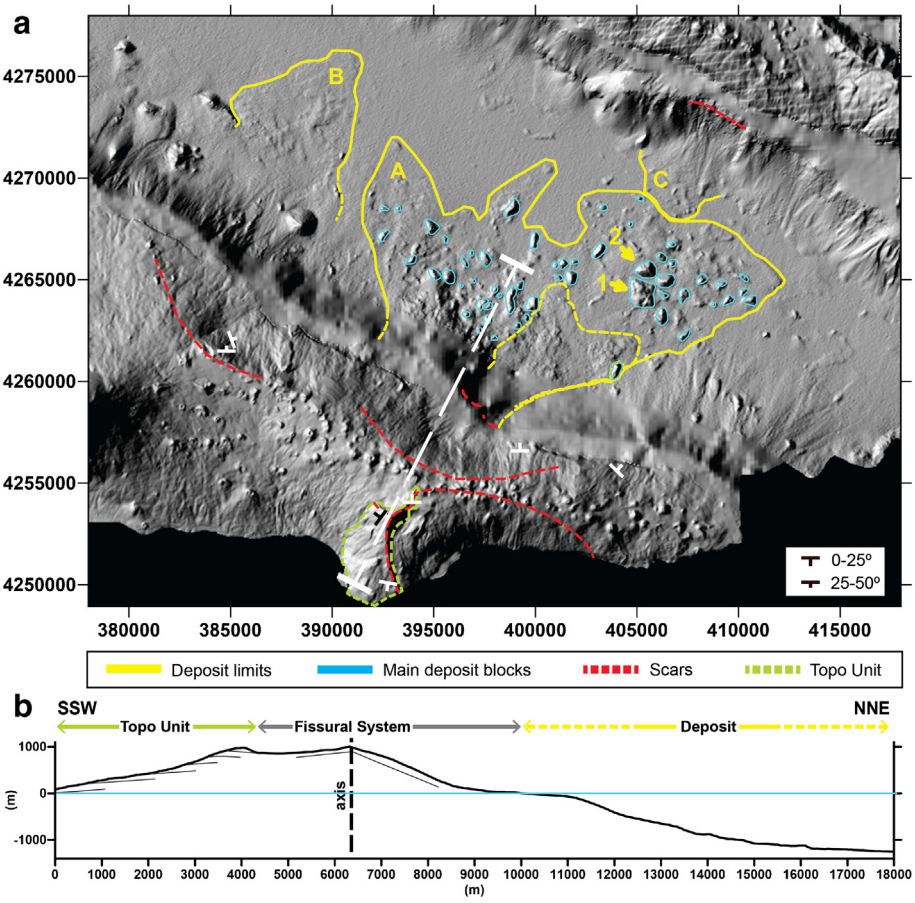


Fig. 6. (a) Shaded relief map of the S. Jorge channel, sub-aerial Pico and S. Jorge islands (lighting from ESE, 50 m resolution DEM), with interpretation of possible scars, blocks and limits of debris deposits. Yellow arrows indicate the biggest individual hummocks observed. Green dashed line indicates the extent of the TU. Dashed white line indicates the cross section presented in b. The lava flow orientations measured on the field are indicated. The non-interpreted version of this shaded relief map is presented as Fig. 5a. (b) Topographic profile across Pico Island and the proximal zone of the main debris deposit interpreted on the bathymetry. Representation of the main geometry of the deposits observed on the field. The non-interpreted version of this topographic profile is presented as Fig. 5b. (For interpretation of the references to color in this figure legend, the reader is referred to the web version of this article.)

On the western sector of Pico's northern flank, we worked upstream along two creeks that incise the zone of steep slope (Fig. 3, feature 5). Here we observed cascading lava flows dipping 35–45° towards the sea (Fig. 6a), intercalated with pyroclastic and clastic sedimentary deposits. Again we could not observe a significant unconformity that could represent a landslide scar. Anyway, we sampled a lava flow at the base of this volcanic sequence (Table 2 and Fig. 2, sample Pi11N). Other samples were collected at the base of coastal cliffs along Pico's northern coast (Table 2 and Fig. 2, samples Pi10R, Pi10P, and Pi10U), in order to constrain the age of the fissural system volcanism.

The easternmost embayment identified on Pico's northern flank is located immediately to the N of the exposed remnants of TU (Figs. 2 and 6a). Additional fieldwork was performed on this sector, in the southern flank of the island (cut by the SSW–NNE cross section presented in Figs. 5 and 6). The observed TU deposits consist mainly of meter thick lava flows with dips in the range 0–25°, and a variation in maximum dip orientation (Fig. 6a). The outcropping TU lavas are limited in the N by a slightly arcuate W–E scarp, ca. 150 m high, whose maximum dip reaches 35–40° towards the N (Fig. 3, feature 6). Near this scarp, the TU lava flows dip 10° towards the NW (Fig. 6a).

5. K–Ar geochronology

The samples were prepared and dated by K–Ar at the IDES laboratory, Université Paris-Sud (Orsay, France). In order to check the unaltered state of the samples, thin sections were carefully observed under the microscope. The samples were crushed and sieved to a homogeneous size fraction (125–250 μm). As phenocrysts may carry inherited excess Ar, by crystallizing previously to the eruption under high pressures at depth, their presence in the analyzed sample may lead to the determination of an excessive age. Therefore, we systematically removed all the phenocrysts (olivine, pyroxene and plagioclase), through magnetic separation and heavy-liquid sorting. At the end of this process, we obtained a groundmass of homogeneous grain size (125–250 μm) and density (classically ranging between 2.95 g/cm^3 and 3.05 g/cm^3 for basaltic samples).

K was measured by flame absorption-spectrophotometry, with 1% uncertainty from systematic analysis of standards (Gillot et al., 1992). Ar was measured by mass spectrometry, according to the Cassignol–Gillot unspiked technique (Cassignol and Gillot, 1982; Gillot and Cornette, 1986; Gillot et al., 2006). The Cassignol–Gillot technique has been shown especially suitable to date low-K and high-Ca basalts and andesites of late Quaternary age with an uncertainty of only a few ka (e.g., Samper et al., 2007; Hildenbrand et al., 2008, 2012a; Germa et al., 2011; Boulesteix et al., 2012, 2013). With this technique, ^{40}Ar and ^{36}Ar are measured simultaneously, avoiding any potential signal drift. Also with this technique, the level of atmospheric contamination is accurately determined by comparison between the isotopic ratios of the sample and an air pipette at strictly similar ^{40}Ar level. This allows the detection of tiny amounts of radiogenic ^{40}Ar, as low as 0.1% (Gillot et al., 2006).

K and Ar were both measured at least twice to ensure the reproducibility of the results. The used decay constants are from Steiger and Jäger (1977). The obtained ages are presented in Fig. 2 and Table 2, where the uncertainties are quoted at the 1σ level. The various lava flows sampled in this study are dated between 70 ± 4 ka and 52 ± 5 ka. The oldest

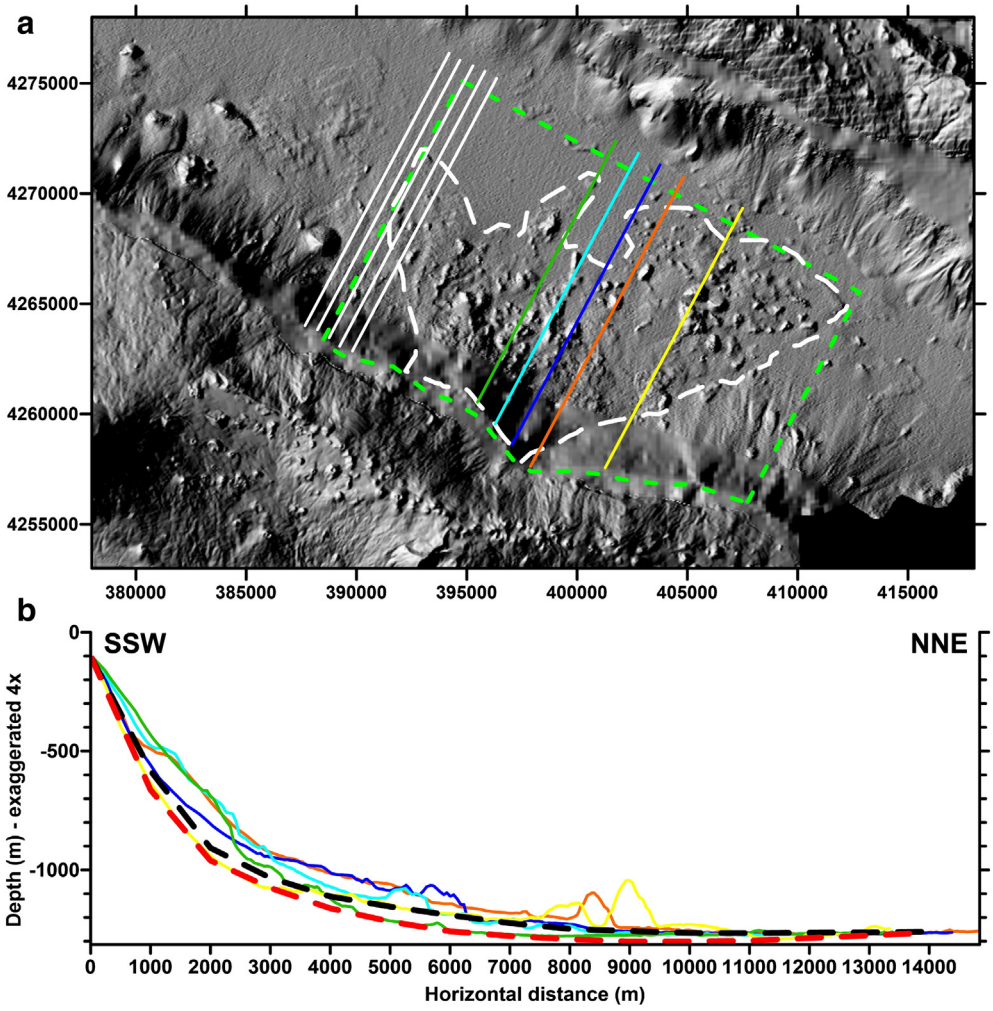


Fig. 7. (a) Full colored lines on the deposit area represent the most relevant NNE–SSW cross sections. Full white lines on the NW represent the cross sections considered for the calculation of the "normal" submarine profile, used in the estimation of minimum volume. Contour of debris deposit is represented by a dashed white line, and the contour of the area blanked for volume calculation purposes is defined by the green dashed line. (b) Plot of the most relevant SSW–NNE cross-sections on the deposit area (full lines) and of the hypothetical basal profiles built for the calculation of minimum volume (red dashed line) and maximum volume (black dashed line). (For interpretation of the references to color in this figure legend, the reader is referred to the web version of this article.)

flows covering the western and eastern scars yield similar values of 70 ± 4 ka and 69 ± 4 ka (samples Pi10X and Pi10 R, respectively).

6. Discussion

6.1. Sub-aerial scarps on Pico's northern flank

Although still very steep on the slope map, the two main curved scarps visible on Pico's sub-aerial N flank are presently smooth, due to blanketing by volcanic products that erupted from the fissural system and Pico stratovolcano. These younger volcanic deposits have therefore been deposited on top of a sharper and steeper scarp. Wide lava deltas have formed at the base of the curved scarps (Figs. 2 and 3), thus smoothing also part of the submarine scarp.

Following Mitchell (2003), who hypothesized a landslide related origin for these conspicuous scarps, we interpret these features as scars resulting from past failure events on Pico's northern flank.

6.2. Main debris deposit

6.2.1. Debris dimensions

Some of the hummocks in the debris deposit A (Fig. 6a) are easily discernible on the shaded relief image due to the strong reflection/shadow contrast of their "soft" surfaces under the imposed lighting. As these hummocks generally have an irregular shape rather than being conical features, we interpret them as blocks rather than small volcanic edifices.

Despite its significant dimensions, the height of the biggest hummock identified (see Section 3.3) is very small when compared to its width/length, and the hummock's surface is extremely irregular and weakly reflects the imposed lighting (Fig. 6a, feature "1", see Section 3.3). We interpret this large hummock as evidence for either a big irregular block or an agglomerate of blocks, covered by smaller debris. The second largest hummock identified (Fig. 6a, feature "2", see Section 3.3) constitutes the biggest individual block observed on the surface of the deposit.

6.2.2. Debris source(s) and number of failure events

Based on the location, shape, and thickness spatial distribution, we interpret this hummocky terrain as a deposit of material resulting from partial collapse of Pico's northern flank. The deposit's shape and thickness spatial distribution at the foot of Pico's submarine flank suggest a source area of relatively small lateral extent (ca. 7 km). This source zone likely corresponds to the sub-aerial scar immediately upstream the deposit (Fig. 6a).

We interpret the homogeneous debris size domain on the SE of the deposit (Fig. 6a, feature A, yellow dashed line) as a deposit resulting from a more recent collapse of Pico's submarine flank. As suggested by the deposit's shape and the longitudinal flow structures visible on its

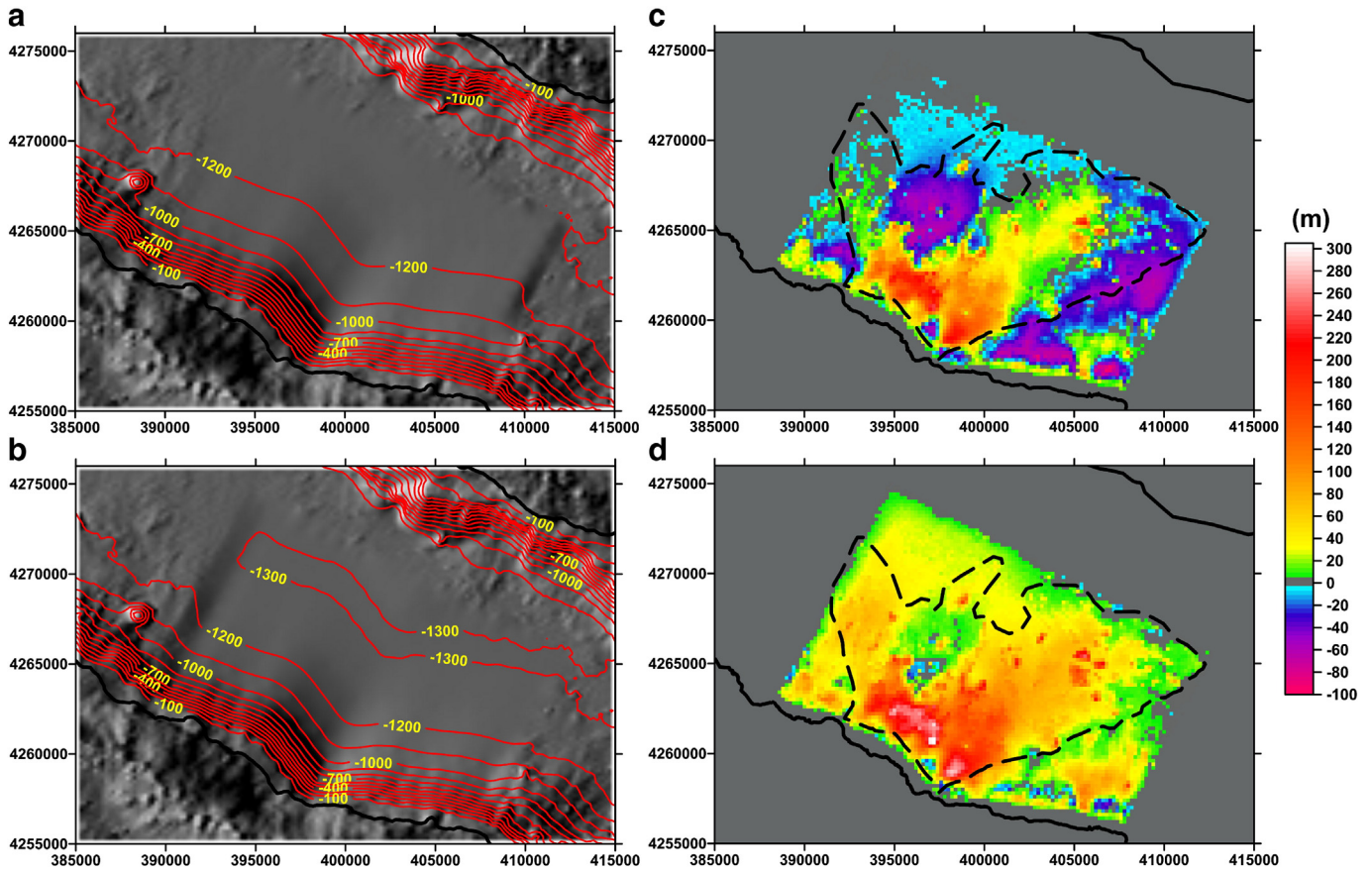


Fig. 8. Estimated basal surfaces for minimum volume (a) and maximum volume (b) calculations (grid lighting from WNW, 0 m contour lines of the surfaces plotted as full black lines). Grids of deposit thickness for the minimum volume (c) and maximum volume (d) (black dashed line limits the area considered for the volume calculations, and the full black lines represent the islands' coastlines). Color scale for the deposit thickness (c and d) is presented on the right.

surface (lineaments mentioned in Section 3.3, visible in Fig. 2 from Mitchell et al., 2008), the interpreted sources of this deposit's material are the two arcuate scarps uphill of the submarine deposit (Fig. 6a). The scars interpreted on the sub-aerial northern flank have been covered by more recent volcanic deposits. The significant protrusion near sea level observable in the area interpreted as source zone of the main deposit (Fig. 6) is interpreted as a consequence of more recent submarine flank reconstruction and lava delta accumulation (Mitchell et al., 2002, 2008; Mitchell, 2003), thus reshaping the scar left by the debris avalanche.

Therefore, it is impossible to assess directly (a) the landward continuity of the deposit (Fig. 9), (b) the exact configuration, at depth, of the scar associated with the failure (Fig. 9, yellow dashed line), and (c) which volcanic sequences were affected by the flank collapse. The possible scenarios for the sequences affected by the studied flank failure were constrained by the local topography (Fig. 6) and fieldwork data, and depend on the premises we assume for: (a) the continuity of the TU volcanic edifice towards the N, where it is masked by deposits of the more recent fissural system; (b) the actual configuration of the scar at depth; and (c) the possible development of a pre-collapse sequence of sub-aerial fissural system deposits.

Three main hypotheses can be put forward regarding the sequences that were affected by the major flank failure identified in this study:

1. The TU volcanic edifice was continuous and higher towards the N, and its northern flank collapsed catastrophically (Fig. 9a);
2. The TU volcanic edifice was shallower towards the N, on top of which a pre-collapse fissural system grew. Then failure occurred in the N, with catastrophic removal of deposits from both TU and pre-collapse fissural edifices (Fig. 9b).
3. The TU volcanic edifice was shallow towards the N, on top of which a thick sequence of pre-collapse fissural system deposits was emplaced. When the N flank failure occurred, only the pre-collapse fissural system was affected (Fig. 9c).

Though hypotheses 2 (Fig. 9b) and 3 (Fig. 9c) cannot be excluded, fieldwork observations on the scar did not allow the identification of a pre-collapse fissural system sequence. Therefore, scenario 1 (Fig. 9a), which considers the failure of TU volcanics only, is here considered as the soundest hypothesis.

Based on this hypothesis, we propose the following evolution for this sector of the volcanic ridge:

1. Growth of the TU volcanic edifice (Fig. 10a and b). The variation of the maximum dip orientation of the volcanic deposits observed in the field (Fig. 10a) suggests that the original summit of this volcanic edifice would be located in the area of the SE Pico active slump depression (Figs. 3 and 10). Such location had already been proposed for the core of the referred volcanic edifice by Nunes et al. (2006), from the interpretation of a major positive Bouger anomaly identified there.
2. Destruction of most of the TU volcanic edifice (Fig. 10c).

Table 1
Values of volume and thickness obtained for the models of minimum and maximum volumes. Positive volume is the volume between the surfaces, being the hypothetical basal surface under the actual topographic surface. Negative volume is the volume between the surfaces, being the hypothetical basal surface above the actual topographic surface.

	Positive volume (km^3)	Negative volume (km^3)	Maximum thickness (m)
Minimum volume	4.278	1.6	238
Maximum volume	10.242	0.015	304

Table 2
Results of the K–Ar dating on fresh-separated groundmass. The ages are indicated in thousands of years (ka). The uncertainties are reported at the 1σ level.

Samples	UTM E	UTM N	K (%)	$^{40}Ar^*$ (%)	$^{40}Ar^*$ (10^{10} at/g)	Age (ka)	Uncertainty (ka)	Mean (ka)
Pi10X	26405050	4255843	0.897	1.7	6.378	68	4	70 ± 4
				1.8	6.715	72	4	
Pi10R	26386933	4262897	1.057	2.3	7.823	71	3	69 ± 4
				1.2	7.116	64	6	
Pi11N	26384950	4261825	0.913	1.9	5.602	59	3	56 ± 4
				1.0	4.949	52	5	
Pi10P	26383509	4265958	0.831	0.5	4.116	47	9	53 ± 5
				1.4	4.788	55	4	
Pi10U	26392413	4260735	0.961	1.0	5.523	55	5	52 ± 5
				0.9	4.951	49	5	

The clear N–S scarp that affects this edifice's eastern sector (Fig. 3, feature "1") shows that part of the mass-wasting has been accommodated along the structure(s) that constitute the currently active large-scale slump structure (mass wasting structure not represented in Figs. 6 and 9, since it is not intersected by the cross section).

It is not possible to observe the continuation of TU edifice towards the N, due to large-scale flank destruction and masking of the remnants by the more recent fissural system deposits (Fig. 10d). The destruction of this edifice's northern flank would have occurred along the sub-aerial scar interpreted for the eastern sector of Pico, and originated the major submarine deposit here reported. The orientation and dip of the exposed north-facing scarp that constitutes the northern limit of TU's outcrops (Fig. 3, feature "6") are not concordant with the local orientation of volcanic deposits (see Section 4). This structure was previously interpreted as a fault scarp (Madeira and Brum da Silveira, 2003), and it might constitute the uppermost expression of a secondary structure located further S of the interpreted main sub-aerial scar (Fig. 10c and d, yellow dashed line with question marks). This interpreted structure could have accommodated non-catastrophic deformation of the TU's volcanic sequence to the S of the main scar.

3. Growth of the fissural system (Fig. 2, FS), masking the sub-aerial scar in TU edifice's northern flank (Fig. 10d). The real configurations of the interpreted scar and of the remnants of the TU volcanic edifice have been extensively masked by more recent volcanism. Therefore it is not possible to establish a detailed comparison between the configuration of the scars identified on Pico's northern flank with landslide scars exposed elsewhere.

Debris deposits resulting from the accumulation of multiple failures have been described in some oceanic islands (e.g. Urgeles et al., 1999; Watts and Masson, 2001; Masson et al., 2006; Hunt et al., 2011). In Pico, with the exception of the homogeneous debris field in the SE

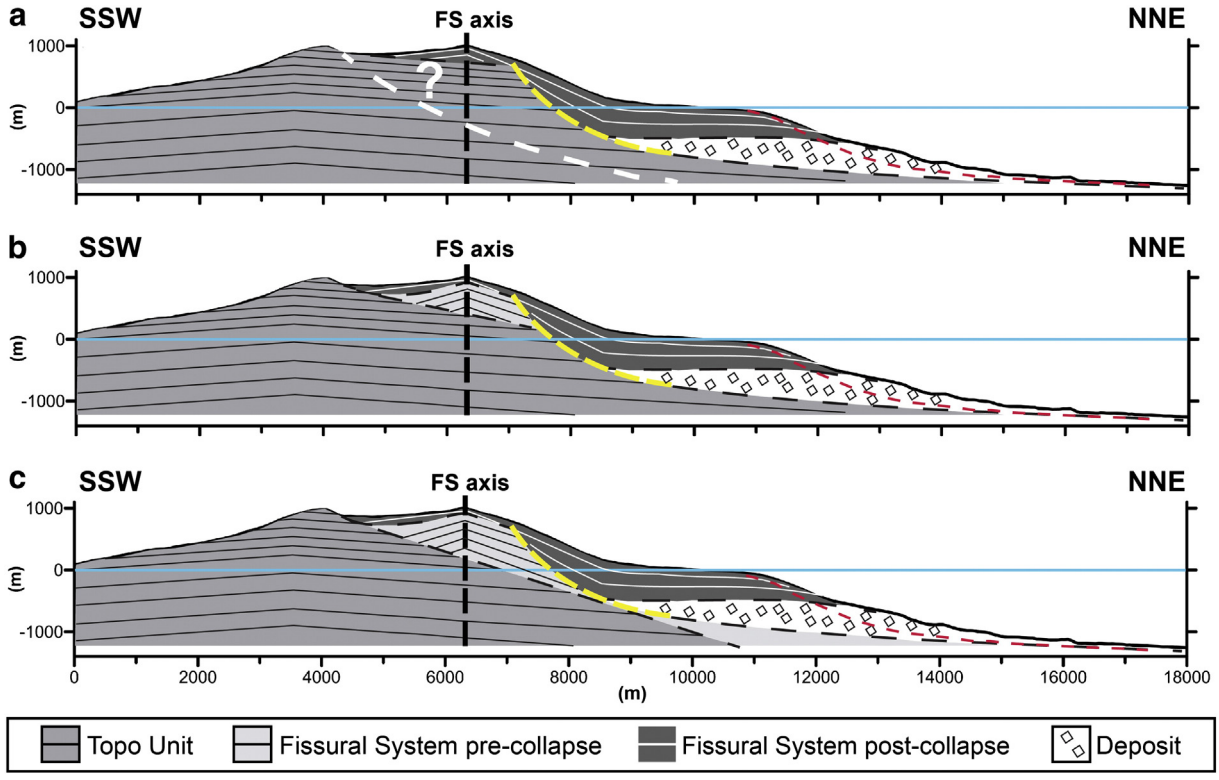


Fig. 9. Geological interpretation of the section marked in Figs. 5 and 6. Yellow dashed line marks the scar suggested as debris source. Red dashed line represents the basal surface considered in the estimation of the maximum volume. Black dashed lines indicate the suggested contacts between volcanic sequences and the deposit. White dashed line indicates a suggested secondary structure that affected TU volcanic sequence. Possible scenarios for the volcanic sequence(s) affected by the flank failure: (a) scar only affects TU deposits; (b) scar affects TU and fissural system deposits; (c) and scar only affects fissural system deposits. (For interpretation of the references to color in this figure legend, the reader is referred to the web version of this article.)

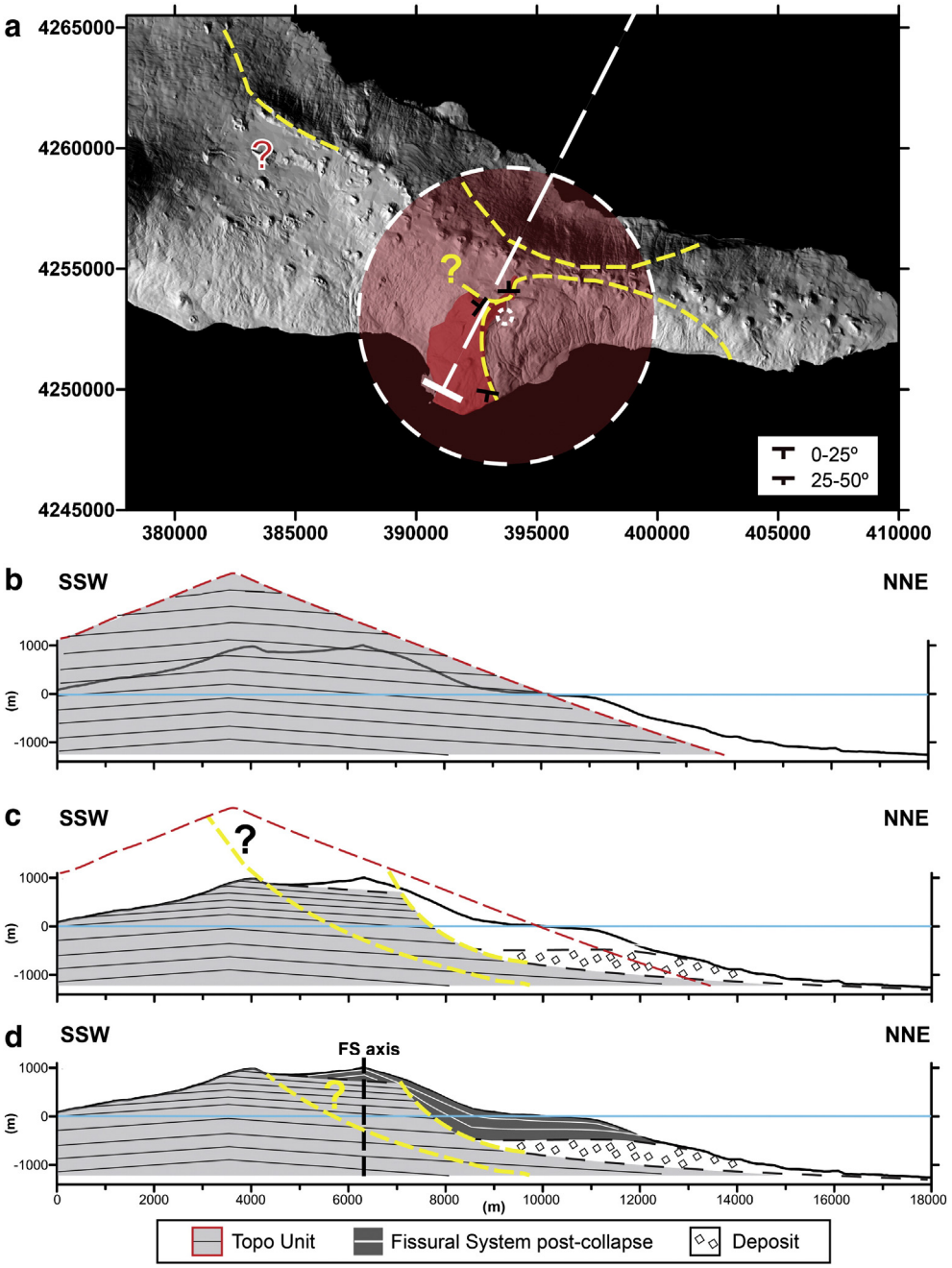


Fig. 10. Presentation of the hypothesis in which the failure that originated the main deposit only affected the TU sequence. (a) Map view of sub-aerial Pico with the representation of the actual extent of sub-aerial TU volcanic edifice (dark red area) and its lava flow orientations, the schematic configuration of the original TU edifice (semi-transparent light red area) and the location of its original crater (small white dashed line circle). SSW–NNE white dashed line represents the cross section interpreted. Yellow dashed lines represent the scarps interpreted in the study area. Schematic representation of the evolution of this volcanic ridge sector, across the SSW–NNE topographic profile: (b) original configuration of TU edifice. (c) TU's northern flank destruction; (d) current stage, with fissural system (FS) deposits concealing the scar of the failure event in study. (For interpretation of the references to color in this figure legend, the reader is referred to the web version of this article.)

sector of the main deposit, and interpreted as resulting from the collapse of the submarine flank, we did not find morphological or chronological evidence supporting the formation of the debris deposit by accumulation of multiple failures. Therefore, we consider that the deposit results from a single failure event, with the exception of a subsequent small failure on the submarine flank.

6.2.3. Debris volume

The lack of data regarding the inner structure of the island (i.e. geophysical data) prevents us from assessing the extent of surface morphology change since the flank failure, due to factors like the partial filling of the topographic embayment by younger volcanic products. However, considering the geometrical constraints imposed by the topography, the geometry/location of the interpreted scar, the geometry of the observed deposit surface offshore, and field data (Fig. 6a), we provide simplified interpreted schemes (Fig. 9) for the inner structure of the island along the cross section presented in Figs. 5 and 6.

The constraints imposed by the location/geometry of the interpreted scar (Fig. 9, yellow dashed line) and by the northern flank topography represented in the cross section suggest the inland continuation of the debris deposit (Fig. 9). Therefore, we consider that even the maximum volume of 10 km^3 here estimated for the exposed part of the deposit (Fig. 9, red dashed line represents the basal surface considered in the

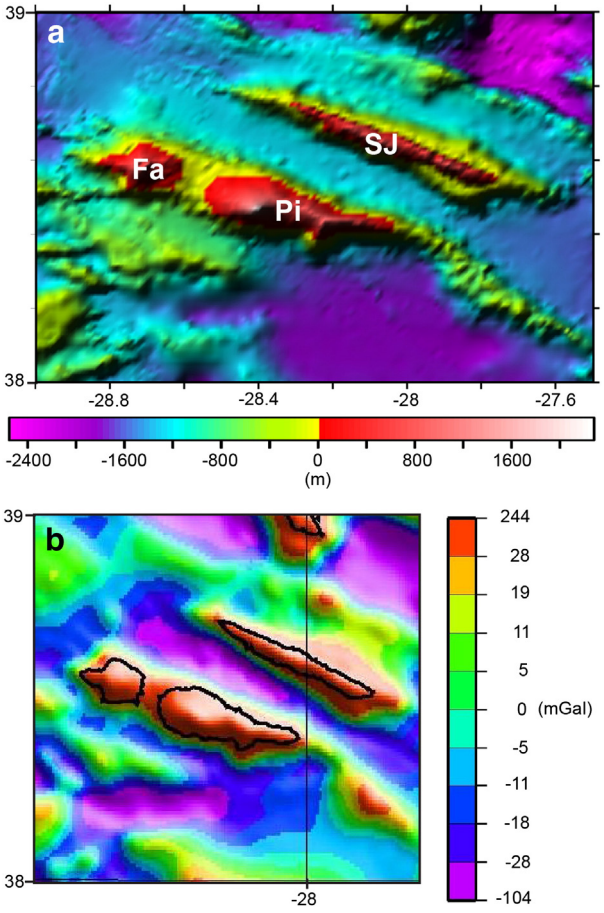


Fig. 11. (a) 1300 resolution DEM (lighting from NW) of the study area. Bathymetric data from Lourenço et al. (1998), available at http://w3.ualg.pt/~jluis/. Fa — Faial Island, Pi — Pico Island, SJ — S. Jorge Island. (b) Free air gravity anomaly map of the same area (extract of Fig. 3 from Catalão and Bos, 2008).

estimation of the maximum volume observable) will constitute an underestimation of the actual volume of the debris deposit.

Catalão and Bos (2008) present a free air gravity anomaly map of the Azores (Fig. 11b, extract of Fig. 3 in Catalão and Bos, 2008), produced from land gravity data, ship-borne gravity data, and a background grid of satellite altimeter-derived gravity data (model KMS02, from Andersen et al., 1999). In order to avoid possible anomalies of the satellite data near the steep coastlines of the islands, these data were not considered for offshore areas at less than 20 km from the coastlines (the coastlines were masked with a 20 km buffer on the offshore domain) (Catalão and Bos, 2008).

This map of the free air gravity anomaly (Fig. 11b) displays a strong negative anomaly in the S. Jorge Channel. However, it is clear from the bathymetry (Fig. 11a) that this area does not correspond to a strong topographic low. Note that the deep basins (magenta in Fig. 11a) correspond to strong negative gravity anomalies (magenta in Fig. 11b). Therefore, we interpret the contrasting association of high topography (green in Fig. 11a) and strong negative gravity anomaly as the result of accumulation of a rock with density much lower than basalt, most likely corresponding to thick accumulation of marine sediments (low density deposits). The thick accumulation of sediments may have blanketed the debris deposits, thus concealing their actual dimensions.

Therefore, considering the probable inland continuation of the deposit (Fig. 9) and the masking of the actual deposit by more recent blanketing by volcanic/sedimentary products, we conclude that the actual volume probably exceeds the estimated 10 km^3.

6.2.4. Flow mobility and constraints

The deposit's shape and the debris distribution in the deposit suggest that part of the debris flowed towards NNW and NNE, but the most significant part of the landslide material (including the biggest blocks) flowed towards greater depths towards the E. It was thus clearly conditioned by the submarine topography.

The mobility of a landslide can be expressed as a function of the ratio H/L (H — height between the topmost source zone of the material and the deposit; L — maximum runout length), which represents the apparent coefficient of friction of the avalanche (e.g. Lipman et al., 1988; Hampton et al., 1996). This ratio decreases (mobility increases) for material volumes larger than 0.001 km^3 (Scheidegger, 1973, in Hampton et al., 1996). More recently, Legros (2002) argued that L is mainly controlled by the volume (V) of the failed mass, instead of being controlled by H.

The estimated maximum volume of Pico's debris deposit is ca. 10 km^3, L is ca. 22 km (measured along a longitudinal profile), and H is ca. 2 km. The estimated volume is below, and the ratio H/L is above the values given for volcanic submarine landslides in Legros (2002). The graphs in Fig. 12 show correlations between H, L, V and H/L data from several oceanic islands' landslide deposits (data presented in Table 3). From the graph in Fig. 12c it is clear that the mobility of Pico's debris deposit, the smallest deposit plotted, broadly fits the trend of decreasing H/L for decreasing volume values. Though the control imposed by the buttressing S. Jorge flank is clear in the morphological analysis of the deposit, its effect on the landslide mobility (i.e., effect on the runout distance reached by the deposit) is not clear in the graphical analysis.

6.2.5. Configuration, block dimensions and spatial distribution

The general shape of the studied deposit is very similar to that of Güimar's debris deposit, resulting from the destabilization of a growing volcanic ridge on the SE flank of Tenerife Island (Canary Islands) (Krastel and Schmincke, 2002), and to that of Monte Amarelo's debris deposit, resulting from the destabilization of Fogo Island (Cape Verde) (Le Bas et al., 2007; Masson et al., 2008). Similarly to Pico, the landslide products in Tenerife and Fogo were mostly constrained by submarine channels: the Güimar landslide products were confined to the channel between Tenerife and Gran Canaria islands, and the Monte Amarelo's landslide products have been confined to the channel between Fogo and Santiago Islands. As recognized by Mitchell et al. (2008) for the sector of Pico's deposit most proximal to its source, the spatial distribution of debris is similar to one of the deposits on west La Palma, which resulted from the accumulation of debris from more than one landslide event (Playa de la Veta Debris Avalanche Complex, and Cumbre Nueva Debris Avalanche, Urgeles et al., 1999).

There are no clearly observed erosional chutes between the source zone and Pico's debris deposit, unlike many cases identified offshore some of the Canary and Hawaiian Islands (Mitchell et al., 2002). We consider that the absence of a well defined chute in Pico's deposit is due to the combination of a relatively small runout (imposed, at least in part, by the nearby topographic obstacle of the S. Jorge ridge), and the extensive masking of the source and proximal sector of the deposit by more recent volcanic products.

Though the maximum runout and volume of Pico's deposit are at least one order of magnitude lower than giant landslides recognized in other oceanic volcanoes (Canary, Hawaii), the largest block dimensions are similar to the ones observed in the Canaries (e.g.,; Masson, 1996; Krastel et al., 2001; Watts and Masson, 2001), but much smaller than the largest blocks exposed offshore the Hawaiian islands (e.g., Moore et al., 1995).

While in Güimar's deposit the largest blocks are observed in the most proximal sector of the deposit, the largest blocks visible in Pico's northern deposit are located on the distal sector of the deposit. A similar spatial arrangement of the blocks has been observed in other deposits found in Hawaii (e.g., South Kona deposit in the SW of Hawaii island —

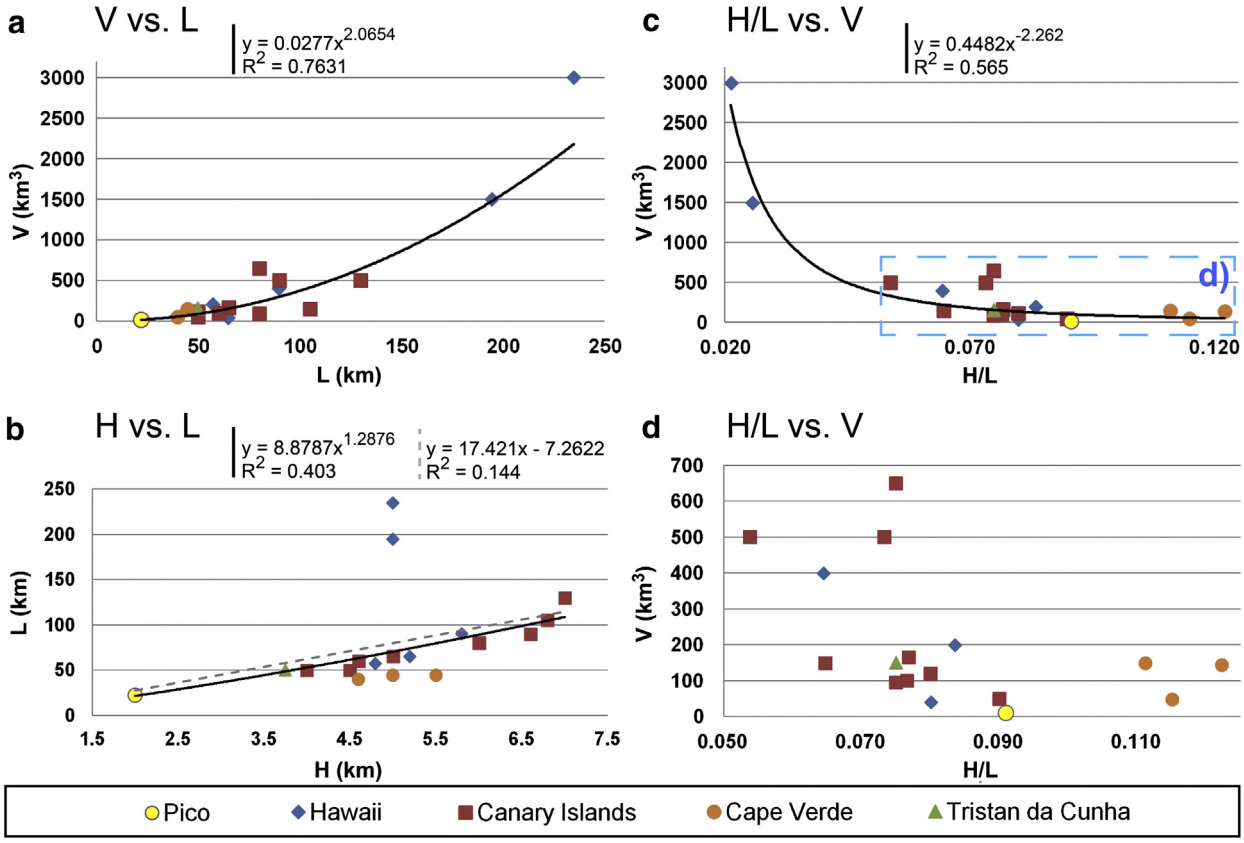


Fig. 12. Plots of correlation between maximum runout length (*L*) (km), height (*H*) (km), ratio *H*/*L*, and volume (*V*) (km^3) for volcanic landslides in oceanic islands. Values plotted (Hawaii Islands, Canary Islands, Tristan da Cunha, Cape Verde and Pico) and respective references are indicated in Table 3. Graphical representation, equation and coefficient of determination (R^2) of power law trend lines (full black lines) and linear trend line (gray dashed line).

Table 3
Data from landslides of Hawaii Islands, Canary Islands, Tristan da Cunha Island, Cape Verde Islands, and Pico Island, plotted in Fig. 12.

Island	Landslide	Volume (km^3)	*L* (km)	*H* (km)	*H*/*L*	References
Azores Islands						
Pico		>10	22	2	0.091	This study
Hawaii Islands						
Hawaii	Alika–1	400	80–100[a]	5.8	0.064	Lipman et al. (1988)
	Alika–2	200	55–60[a]	4.8	0.083	Lipman et al. (1988)
	Kae Lae slide	40	65	5.2	0.080	Legros (2002)
Molokai	Wailau slide	1500	<195	5	0.026	Moore et al. (1989), Moore and Clague (2002), Satake et al. (2002)
Oahu	Nuuanu	3000	235	5	0.021	Moore et al. (1989), Moore and Clague (2002), Satake et al. (2002)
Tristan da Cunha Islands						
Tristan da Cunha		150	50	3.75	0.075	Hampton et al. (1996)
Canary Islands						
El Hierro	El Golfo	150–180[a]	65	5	0.077	Masson et al. (2002)
	Las Playas II	<50	50	4.5	0.090	Masson et al. (2002)
	El Julan	130 (?)	60	4.6	0.077	Masson et al. (2002)
La Palma	Cumbre Nueva	95	80	6	0.075	Masson et al. (2002)
	Playa de la Veta	650 (?)	80	6	0.075	Masson et al. (2002)
Tenerife	Icod	150 (?)	105	6.8	0.065	Masson et al. (2002)
	Roques de Garcia	500 (?)	130	7	0.054	Masson et al. (2002)
	Orotava	500 (?)	90	6.6	0.073	Masson et al. (2002)
	Güimar	120	> 50	4	0.080	Masson et al. (2002)
Cape Verde						
Fogo	Monte Amarelo	130–160[a]	45	5.5	0.122	Day et al. (1999), Masson et al. (2008)
Santo Antão	Tope de Coroa 2	50	40	4.6	0.115	Holm et al. (2006), Masson et al. (2008)
	Tope de Coroa 1	150	45	5	0.111	Holm et al. (2006), Masson et al. (2008)

[a] For dimensions given as intervals, the value plotted was the average of the interval range.

Moore et al., 1995) and Canary Islands (e.g., Icod deposit to the N of Tenerife, where relatively large blocks are concentrated along the margins of the deposit — Watts and Masson, 2001), which have been interpreted as evidence of the high velocity of the avalanches.

The comparatively smaller size of debris in the Canaries relative to Hawaii has been interpreted as being caused by several possible factors and processes: (1) block interaction and disintegration caused by confined flow along narrow chutes (Mitchell et al., 2002); (2) relatively more important component of failed sub-aerial material in Canary Islands, which would promote a more effective disintegration, due to a confining pressure lower in the sub-aerial domain than in the submarine domain (Mitchell et al., 2002); and (3) another factor that might influence the disintegration process is the higher proportion of pyroclastic material in the Canary, which will be more prone to disintegration than sequences constituted mainly by basaltic intrusive/extrusive rocks with a minor pyroclastic component (Mitchell et al., 2002, after Masson et al., 2002).

The debris transport in Pico's deposit was comparatively shorter and involved a smaller volume of material than the ones in Hawaii and the Canary (Fig. 12a). Moreover, the remnants of the edifice interpreted as the main source of northern Pico event(s) comprise a sequence mostly made of shallow dipping, meter thick lava flows, with no significant pyroclastic deposits. Therefore, the disintegration process in the Pico's event should be less effective than for the events in the Canary Islands.

6.3. Minor debris deposits

The shape of the "B" debris deposit (Fig. 6a) shows that it resulted from the accumulation of material transported from Pico's flank. However, it is not possible to define a source for this material as the limits of the deposit are undefined near Pico's submarine flank: it could result simply from the gradual accumulation of material from Pico's submarine flank; or it could be the relict of the deposit resulting from the collapse along the interpreted westernmost sub-aerial scar, now almost completely masked by the younger volcanic deposits.

The "C" debris deposit (Fig. 6a) is interpreted here as having resulted from a collapse of the uphill submarine flank of S. Jorge, where a scar is still visible (Fig. 6a, red dashed line).

6.4. Age of Pico's northern flank failure(s)

Previous K–Ar ages published on Pico (Féraud et al., 1980; Demande et al., 1982; Fig. 2) were acquired on a limited number of samples, and therefore do not constrain accurately the evolution of the island. Some of those previous ages also must be considered with caution, as they have been acquired on whole-rock samples, which can significantly bias the results, as discussed in Hildenbrand et al. (2012a).

On Pico's northern flank, we only observed outcrops of the volcanic deposits that cover the interpreted scar depressions (see Section 4), therefore the new K–Ar ages here obtained on fresh groundmass only provide a minimum age for the flank failure(s). The maximum age of 70 ± 4 ka and 69 ± 4 ka here obtained on the lava flows Pi10X and Pi10 R filling the sub-aerial scars (Fig. 2 and Table 2), provides a minimum age of ca. 70 ka for the occurrence of large-scale collapse(s) in Pico's northern flank.

Based on our data, we cannot establish if the two sub-aerial scarps here identified on Pico's northern flank were produced by two synchronous flank collapses. For the scar interpreted on the western sector of the fissural system (Fig. 3, feature "2"), there is not a corresponding major deposit offshore. As mentioned in Section 6.2, the flank failure deposits might appear masked by more recent volcanic/sedimentary products. As the deposit corresponding to the eastern sub-aerial scar is still clearly visible, this could suggest that the western scar is older than the eastern.

6.5. Possible causes and consequences

Given the geologic setting of the studied volcanic edifice, a steep volcanic ridge located on a tectonically active region, catastrophic failure of Pico northern flank may have been influenced/triggered from a variety of possible processes:

1. Progressive destabilization due to flank overload and oversteepening of TU edifice and/or along the tectonically controlled WNW–ESE volcanic ridge;
2. Triggering by NNE–SSW magma push (associated to the growth of Pico–Faial WNW–ESE volcanic ridge);
3. Fluid overpressure directly or indirectly associated with volcanic activity;
4. Local focusing of destabilization promoted by the physical discontinuity between the TU edifice surface and the fissural system deposits (Fig. 10).

Mitchell (2003) suggests a height threshold of ca. 2.5 km, above which large-scale landslides become common. Previously, Mitchell (2001) suggested that the transition between stable and unstable conditions for submarine volcanic edifices would occur gradually for an interval of edifice heights between 2 and 4 km. The height between Pico's highest point and the sea bottom is above this threshold, i.e. ca. 3.6 km. However, this maximum is attained for Pico stratovolcano, on the westernmost sector of the island, i.e. far from the studied failure. The current height between the topmost level of the source zone and the studied debris deposit is ca. 2 km. When discussing the edifice height at the time of the occurrence of a large-scale landslide, we should take into account that the current configuration of the island does not necessarily correspond to the configuration of the island at the time the landslide occurred. From the absolute ages here presented for Pico, it is not clear that the Pico stratovolcano was already developing by the time the studied flank collapse occurred. However, there was the TU volcano, whose original size and maximum altitude are not known. Therefore, the current height of ca. 2 km between the topmost sector of the source zone and the surrounding submarine floor probably constitutes an underestimation of the height at the time the flank collapse occurred. Considering that the height of the affected volcanic edifice relative to the surrounding sea floor was greater than ca. 2 km, the studied event supports the trend presented in Mitchell (2001).

One of the most important consequences of catastrophic flank collapses on volcanic ocean islands lies in their ability to trigger large tsunamis. Considering that S. Jorge lies to the north of Pico, only ca. 20 km apart, the sudden collapse of a sector several km^3 in dimension would have generated a large tsunami that most likely strongly impacted the southern coast of S. Jorge. Therefore, further investigations should focus on the southern coast of S. Jorge.

6.6. Flank failure in northern and southern Pico

The scar in northern Pico is mirrored in the S flank by a steep slope embayment that includes the currently active slump (Fig. 3, feature "1"). On the offshore area adjacent to this embayment on the southern flank there is a significant deposit whose debris were identified on side scan sonar data (Mitchell, 2003), and which constitutes a topographic bulge on the low resolution bathymetry (see Fig. C.1, in Appendix C). Therefore, both Pico's flanks have been affected by large-scale flank failure, highlighting the strong susceptibility of steep ridge-shaped edifices to flank failure.

7. Conclusions

From the new geomorphologic, stratigraphic, structural and geochronologic data acquired in the present study, we conclude that the evolution of the Pico Island volcanic ridge was marked by the

occurrence of flank failures in both N and S flanks. The landslide debris resulting from the collapse of Pico's N flank have accumulated on the ocean floor of the S. Jorge Channel, and their likely sources are two major scars standing out on Pico's slope map.

Here we conclude that, more than 70 ka ago, after the growth of the TU volcanic edifice, Pico's northern flank collapsed catastrophically, forming two steep and arcuate sub-aerial scars. The material mobilized from the eastern source zone likely exceeds 10 km^3, and consists of a mixture of meter to hectometer blocks. These flowed towards greater depths in the E, along the channel between Pico–Faial and S. Jorge volcanic ridges. The tsunami resulting from the km^3 collapse most probably rapidly traveled the ca. 20 km wide channel and violently impacted S. Jorge's southern flank. Since ca. 70 ka and until historic times, more recent deposits, volcanic products related to the growth of the WNW–ESE fissural system and Pico stratovolcano have been progressively filling the sub-aerial scars. These post-collapse volcanic products, and marine sediments as well, have been covering the island's submarine flanks, masking partially or completely the evidence of failure events.

The evolution of the Pico's sector in the Pico–Faial volcanic ridge was also marked by large-scale flank failure on the southern flank, generating a sub-aerial scar (symmetrical to the easternmost scar in the N flank) and a debris deposit observed on the offshore. Further investigations are being conducted, in order to constrain the evolution of this volcanic ridge.

Supplementary data to this article can be found online at http://dx.doi.org/10.1016/j.jvolgeores.2014.01.002.

Acknowledgments

This is a contribution to Project MEGAHazards, funded by FCT (PTDC/CTE-GIX/108149/2008), Portugal. The first author has a PhD scholarship funded by FCT (SFRH/BD/68983/2010). We thank EMEPC (http://www.emepc.pt/), and Nuno Lourenço in particular, for making the bathymetric data available, without which this study would not have been possible. The final version of this paper benefited from the constructive and thorough comments by N. Mitchell.

References

Afonso, A., Gomes, F., Fernandes, M., 2002. IGeoE: Cartografia de qualidade - a base de um SIG. Trib. das Autarquias 108, 13–14 (Jun. 2002).

Andersen, O.B., Knudsen, P., Kenyon, S., Trimmer, R., 1999. Recent improvement in the KMS global marine gravity field. Boll. Geofis. Teor. Appl. 40 (3–4), 369–377.

Borges, J.F., Bezzeghoud, M., Buforn, E., Pro, C., Fitas, A., 2007. The 1980, 1997 and 1998 Azores earthquakes and some seismo-tectonic implications. Tectonophysics 435 (1–4), 37–54. http://dx.doi.org/10.1016/j.tecto.2007.01.008.

Boulesteix, T., Hildenbrand, A., Gillot, P.Y., Soler, V., 2012. Eruptive response of oceanic islands to giant landslides: new insights from the geomorphologic evolution of the Teide–Pico Viejo volcanic complex (Tenerife, Canary). Geomorphology 138 (1), 61–73. http://dx.doi.org/10.1016/j.geomorph.2011.08.025.

Boulesteix, T., Hildenbrand, A., Soler, V., Quidelleur, X., Gillot, P.Y., 2013. Coeval giant landslides in the Canary Islands: implications for global, regional and local triggers of giant flank collapses on oceanic volcanoes. J. Volcanol. Geotherm. Res. 257, 90–98. http://dx.doi.org/10.1016/j.jvolgeores.2013.03.008.

Burrough, P.A., McDonnell, R.A., 1998. Principles of Geographical Information Systems. Oxford University Press, New York (333 pp.).

Carracedo, J.C., Day, S.J., Guillou, H., Torrado, F.J.P., 1999. Giant Quaternary landslides in the evolution of La Palma and El Hierro, Canary Islands. J. Volcanol. Geotherm. Res. 94 (1–4), 169–190. http://dx.doi.org/10.1016/S0377-0273(99)00102-X.

Cassignol, C., Gillot, P.Y., 1982. Range and effectiveness of unspiked potassium–argon dating: experimental groundwork and applications. In: Odin, G.S. (Ed.) Numerical Dating in Stratigraphy. John Wiley & Sons Ltd, Chichester, England, pp. 159–179.

Catalão, J., Bos, M.S., 2008. Sensitivity analysis of the gravity geoid estimation: a case study on the Azores plateau. Phys. Earth Planet. Inter. 168 (1–2), 113–124. http://dx.doi.org/10.1016/j.pepi.2008.05.010.

Day, S.J., Heleno da Silva, S.I.N., Fonseca, J.F.B.D., 1999. A past giant lateral collapse and present-day flank instability of Fogo, Cape Verde Islands. J. Volcanol. Geotherm. Res. 94 (1–4), 191–218. http://dx.doi.org/10.1016/S0377-0273(99)00103-1.

Demande, J., Fabriol, R., Gérard, A., Iundt, F., 1982. Prospection géothermique des Iles de Faial et Pico (Açores). Report 82SGN003GTH, Bureau de Recherches Géologiques et Minières, Orléans, France.

Deplus, C., Le Friant, A., Boudon, G., Komorowski, J.C., Villemant, B., Harford, C., Ségoufin, J., Cheminée, J.L., 2001. Submarine evidence for large-scale debris avalanches in the Lesser Antilles Arc. Earth Planet. Sci. Lett. 192 (2), 145–157. http://dx.doi.org/10.1016/S0012-821X(01)00444-7.

Duffield, W.A., Stieltjes, L., Varet, J., 1982. Huge landslide blocks in the growth of Piton de la Fournaise, La Réunion and Kilauea volcano, Hawaii. J. Volcanol. Geotherm. Res. 12 (1–2), 147–160. http://dx.doi.org/10.1016/0377-0273(82)90009-9.

Féraud, G., Kaneoka, I., Allègre, C.J., 1980. K/Ar ages and stress pattern in the Azores: geodynamic implications. Earth Planet. Sci. Lett. 46 (2), 275–286. http://dx.doi.org/10.1016/0012-821X(80)90013-8.

Fernandes, R.M.S., Bastos, L., Miranda, J.M., Lourenço, N., Ambrosius, B.A.C., Noomen, R., Simons, W., 2006. Defining the plate boundaries in the Azores region. J. Volcanol. Geotherm. Res. 156 (1–2), 1–9. http://dx.doi.org/10.1016/j.jvolgeores.2006.03.019.

Forjaz, V.H., 1966. Carta geológica do sistema vulcânico Faial-Pico-S. Jorge. Escala 1:200 000. In: Machado, F., Forjaz, V.H. (Eds.),A actividade vulcânica na ilha do Faial (1957-67), 1968. Comissão de Turismo da Horta, 89 pp.

Germa, A., Quidelleur, X., Lahitte, P., Labanieh, S., Chauvel, C., 2011. The K–Ar Cassignol–Gillot technique applied to western Martinique lavas: a record of Lesser Antilles arc activity from 2 Ma to Mount Pelée volcanism. Quat. Geochronol. 6 (3–4), 341–355. http://dx.doi.org/10.1016/j.quageo.2011.02.001.

Gillot, P.Y., Cornette, Y., 1986. The Cassignol technique for potassium–argon dating, precision and accuracy: examples from the Late Pleistocene to Recent volcanics from southern Italy. Chem. Geol. Isot. Geosci. Sect. 59, 205–222. http://dx.doi.org/10.1016/0168-9622(86)90072-2.

Gillot, P.Y., Cornette, Y., Max, N., Floris, B., 1992. Two reference materials, trachytes MDO-G and ISH-G, for Argon dating (K–Ar and $^{40}Ar/^{39}Ar$) of Pleistocene and Holocene rocks. Geostand. Newslett. 16 (1), 55–60. http://dx.doi.org/10.1111/j.1751-908X.1992.tb00487.x.

Gillot, P.Y., Lefèvre, J.C., Nativel, P.E., 1994. Model for the structural evolution of the volcanoes of Réunion Island. Earth Planet. Sci. Lett. 122 (3–4), 291–302. http://dx.doi.org/10.1016/0012-821X(94)90003-5.

Gillot, P.Y., Hildenbrand, A., Lefèvre, J.C., Albore-Livadie, C., 2006. The K/Ar dating method: principle, analytical techniques and application to Holocene volcanic eruptions in Southern Italy. Acta Vulcanol. 18, 55–66.

Golden Software, Inc., 2002. Surfer 8: contouring and 3D surface mapping for scientists and engineers—user guide. In: Golden Software, Incorporated (Ed.). 640 pp.

Hampton, M.A., Lee, H.J., Locat, J., 1996. Submarine landslides. Rev. Geophys. 34 (1), 33–59. http://dx.doi.org/10.1029/95RG03287.

Hildenbrand, A., Gillot, P.Y., Bonneville, A., 2006. Offshore evidence for a huge landslide of the northern flank of Tahiti–Nui (French Polynesia). Geochemistry Geophysics Geosystems 7 (3), Q03006. http://dx.doi.org/10.1029/2005GC001003.

Hildenbrand, A., Madureira, P., Ornelas Marques, F., Cruz, I., Henry, B., Silva, P., 2008. Multi-stage evolution of a sub-aerial volcanic ridge over the last 1.3 Myr: S. Jorge Island, Azores Triple Junction. Earth Planet. Sci. Lett. 273 (3–4), 289–298. http://dx.doi.org/10.1016/j.epsl.2008.06.041.

Hildenbrand, A., Marques, F.O., Costa, A.C.G., Sibrant, A.L.R., Silva, P.M.F., Henry, B., Miranda, J.M., Madureira, P., 2012a. Reconstructing the architectural evolution of volcanic islands from combined K/Ar, morphologic, tectonic, and magnetic data: the Faial Island example (Azores). J. Volcanol. Geotherm. Res. 241–242, 39–48. http://dx.doi.org/10.1016/j.jvolgeores.2012.06.019.

Hildenbrand, A., Marques, F.O., Catalão, J., Catita, C.M.S., Costa, A.C.G., 2012b. Large-scale active slump of the southeastern flank of Pico Island, Azores. Geology 40 (10), 939–942. http://dx.doi.org/10.1130/G33303.1.

Hildenbrand, A., Marques, F.O., Costa, A.C.G., Sibrant, A.L.R., Silva, P.F., Henry, B., Miranda, J.M., Madureira, P., 2013a. Reply to the comment by Quartau and Mitchell on "Reconstructing the architectural evolution of volcanic islands from combined K/Ar, morphologic, tectonic, and magnetic data: the Faial Island example (Azores)", J. Volcanol. Geotherm. Res. 241–242, 39–48, by Hildenbrand et al. (2012). J. Volcanol. Geotherm. Res. 255, 127–130. http://dx.doi.org/10.1016/j.jvolgeores.2013.01.015.

Hildenbrand, A., Marques, F.O., Catalão, J., Catita, C.M.S., Costa, A.C.G., 2013b. Large-scale active slump of the southeastern flank of Pico Island, Azores: reply. Geology 41 (12), e302. http://dx.doi.org/10.1130/G34879Y.1.

Holm, P.M., Wilson, J.R., Christensen, B.P., Hansen, L., Hansen, S.L., Hein, K.M., Mortensen, A.K., Pedersen, R., Plesner, S., Runge, M.K., 2006. Sampling the Cape Verde mantle plume: evolution of melt compositions on Santo Antão, Cape Verde Islands. J. Petrol. 47 (1), 145–189. http://dx.doi.org/10.1093/petrology/egi071.

Hunt, J.E., Wynn, R.B., Masson, D.G., Talling, P.J., Teagle, D.A.H., 2011. Sedimentological and geochemical evidence for multistage failure of volcanic island landslides: a case study from Icod landslide on north Tenerife, Canary Islands. Geochem. Geophys. Geosyst. 12 (12), Q12007. http://dx.doi.org/10.1029/2011GC003740.

Kongsberg, S., 2007. EM 120 Multibeam Echo Sounder, Product Description. Kongsberg Maritime AS, Norway, Bremerhaven, Pangaea 44 p. (available at http://epic.awi.de/26725/1/Kon2007a.pdf).

Krastel, S., Schmincke, H.U., 2002. The channel between Gran Canaria and Tenerife: constructive processes and destructive events during the evolution of volcanic islands. International Journal of Earth Sciences 91 (4), 629–641. http://dx.doi.org/10.1007/s00531-002-0285-8.

Krastel, S., Schmincke, H.U., Jacobs, C.L., Rihm, R., Le Bas, T.P., Alibés, B., 2001. Submarine landslides around the Canary Islands. J. Geophys. Res. 106 (B3), 3977–3997. http://dx.doi.org/10.1029/2000JB900413.

Le Bas, T.P., Masson, D.G., Holtom, R.T., Grevemeyer, I., 2007. Slope failures on the flanks of the southern Cape Verde Islands. In: Lykousis, V., Sakellariou, D., Locat, J. (Eds.), Submarine Mass Movements and Their Consequences. Springer, Dordrecht, Netherlands, pp. 337–345.

Le Friant, A., Boudon, G., Deplus, C., Villemant, B., 2003. Large-scale flank collapse events during the activity of Montagne Pelée, Martinique, Lesser Antilles. J. Geophys. Res. Solid Earth 108 (B1), 2055. http://dx.doi.org/10.1029/2001JB001624.

Legros, F., 2002. The mobility of long-runout landslides. Eng. Geol. 63 (3–4), 301–331. http://dx.doi.org/10.1016/S0013-7952(01)00090-4.
Lipman, P.W., Normark, W.R., Moore, J.G., Wilson, J.B., Gutmacher, C.E., 1988. The giant submarine Alika debris slide, Mauna Loa, Hawaii. J. Geophys. Res. Solid Earth 93 (B5), 4279–4299. http://dx.doi.org/10.1029/JB093iB05p04279.
Lourenço, N., Miranda, J.M., Luis, J.F., Ribeiro, A., Mendes Victor, L.A., Madeira, J., Needham, H.D., 1998. Morpho-tectonic analysis of the Azores Volcanic Plateau from a new bathymetric compilation of the area. Mar. Geophys. Res. 20 (3), 141–156. http://dx.doi.org/10.1023/A%3A1004505401547.
Madeira, J., 1998. Estudos de neotectónica nas ilhas do Faial, Pico e S. Jorge: Uma contribuição para o conhecimento geodinâmico da junção tripla dos Açores. PhD thesis Faculdade de Ciências, Univ, Lisboa, Portugal (481 pp.).
Madeira, J., Brum da Silveira, A., 2003. Active tectonics and first paleoseismological results in Faial, Pico and S. Jorge islands (Azores, Portugal). Ann. Geophys. 46 (5), 733–761. http://dx.doi.org/10.4401/ag-3453.
Marques, F.O., Catalão, J.C., DeMets, C., Costa, A.C.G., Hildenbrand, A., 2013. GPS and tectonic evidence for a diffuse plate boundary at the Azores Triple Junction. Earth and Planetary Science Letters 381, 177–187. http://dx.doi.org/10.1016/j.epsl.2013.08.051.
Masson, D.G., 1996. Catastrophic collapse of the volcanic island of Hierro 15 ka ago and the history of landslides in the Canary Islands. Geology 24 (3), 231–234. http://dx.doi.org/10.1130/0091-7613(1996)024<0231:CCOTVI>2.3.CO;2.
Masson, D.G., Watts, A.B., Gee, M.J.R., Urgeles, R., Mitchell, N.C., Le Bas, T.P., Canals, M., 2002. Slope failures on the flanks of the western Canary Islands. Earth Sci. Rev. 57 (1–2), 1–35. http://dx.doi.org/10.1016/S0012-8252(01)00069-1.
Masson, D.G., Harbitz, C.B., Wynn, R.B., Pedersen, G., Lovholt, F., 2006. Submarine landslides: processes, triggers and hazard prediction. Phil. Trans. R. Soc. A 364, 2009–2039. http://dx.doi.org/10.1098/rsta.2006.1810.
Masson, D.G., Le Bas, T.P., Grevemeyer, I., Weinrebe, W., 2008. Flank collapse and large-scale landsliding in the Cape Verde Islands, off West Africa. Geochem. Geophys. Geosyst. 9 (7), Q07015. http://dx.doi.org/10.1029/2008GC001983.
Mitchell, N.C., 2001. The transition from circular to stellate forms of submarine volcanoes. J. Geophys. Res. Solid Earth 106 (B2), 1987–2003. http://dx.doi.org/10.1029/2000JB900263.
Mitchell, N.C., 2003. Susceptibility of mid-ocean ridge volcanic islands and seamounts to large-scale landsliding. J. Geophys. Res. 108 (B8), 2397. http://dx.doi.org/10.1029/2002JB001997.
Mitchell, N.C., Masson, D.G., Watts, A.B., Gee, M.J.R., Urgeles, R., 2002. The morphology of the submarine flanks of volcanic ocean islands: a comparative study of the Canary and Hawaiian hotspot islands. J. Volcanol. Geotherm. Res. 115 (1–2), 83–107. http://dx.doi.org/10.1016/S0377-0273(01)00310-9.
Mitchell, N.C., Beier, C., Rosin, P.L., Quartau, R., Tempera, F., 2008. Lava penetrating water: submarine lava flows around the coasts of Pico Island, Azores. Geochem. Geophys. Geosyst. 9 (3), Q03024. http://dx.doi.org/10.1029/2007GC001725.
Mitchell, N.C., Quartau, R., Madeira, J., 2012. Assessing landslide movements in volcanic islands using near-shore marine geophysical data: south Pico Island, Azores. Bull. Volcanol. 74 (2), 483–496. http://dx.doi.org/10.1007/s00445-011-0541-5.
Mitchell, N.C., Quartau, R., Madeira, J., 2013. Large-scale active slump of the southeastern flank of Pico Island, Azores: comment. Geology 41 (12), e301. http://dx.doi.org/10.1130/G34006C.1.
Moore, J.G., Clague, D.A., 2002. Mapping the Nuuanu and Wailau Landslides in Hawaii. In: Takahashi, E., Lipman, P.W., Garcia, M.O., Naka, J., Aramaki, S. (Eds.),Hawaiian volcanoes: deep underwater perspectives. Geophysical Monograph Series, 128. American Geophysical Union, Washington D.C., pp. 223–244. http://dx.doi.org/10.1029/GM128.
Moore, J.G., Clague, D.A., Holcomb, R.T., Lipman, P.W., Normark, W.R., Torresan, M.E., 1989. Prodigious submarine landslides on the Hawaiian Ridge. J. Geophys. Res. Solid Earth 94 (B12), 17465–17484. http://dx.doi.org/10.1029/JB094iB12p17465.
Moore, I.D., Lewis, A., Gallant, J.C., 1993. Terrain properties: estimation methods and scale effects. In: Jakeman, A.J., Beck, M.B., MCaleer, M.J. (Eds.),Modelling Change in Environmental Systems. John Wiley and Sons, New York.
Moore, J.G., Bryan, W.B., Beeson, M.H., Normark, W.R., 1995. Giant blocks in the South Kona landslide, Hawaii. Geology 23 (2), 125–128. http://dx.doi.org/10.1130/0091-7613(1995) 023<0125:GBITSK>2.3.CO;2.
Navarro, J.M., Coello, J., 1989. Depressions Originated by Landslide Processes in Tenerife. ESF Meeting on Canarian Volcanism, Lanzarote 150–152.
Nunes, J.C., 1999. A actividade vulcânica na ilha do Pico do Plistocénico Superior ao Holocénico: Mecanismo eruptivo e hazard vulcânico. PhD thesis Universidade dos Açores, Ponta Delgada, Portugal (356 pp.(available at: http://www.jcnunes.uac.pt/principal.htm)).
Nunes, J.C., 2002. Lateral collapse structures in Pico Island (Azores): mechanism, constraints and age. 3ª Assembleia Luso Espanhola de Geodesia e Geofísica, Valencia, pp. 731–735.
Nunes, J.C., Camacho, A., França, Z., Montesinos, F.G., Alves, M., Vieira, R., Velez, E., Ortiz, E., 2006. Gravity anomalies and crustal signature of volcano-tectonic structures of Pico Island (Azores). J. Volcanol. Geotherm. Res. 156 (1–2), 55–70. http://dx.doi.org/10.1016/j.jvolgeores.2006.03.023.
Quartau, R., Mitchell, N.C., 2013. Comment on "Reconstructing the architectural evolution of volcanic islands from combined K/Ar, morphologic, tectonic, and magnetic data: the Faial Island example (Azores)" by Hildenbrand et al. (2012) [J. Volcanol. Geotherm. Res. 241–242 (2012) 39–48]. Journal of Volcanology and Geothermal Research 255, 124–126. http://dx.doi.org/10.1016/j.jvolgeores.2012.12.020.
Quartau, R., Trenhaile, A.S., Mitchell, N.C., Tempera, F., 2010. Development of volcanic insular shelves: insights from observations and modelling of Faial Island in the Azores Archipelago. Mar. Geol. 275 (1–4), 66–83. http://dx.doi.org/10.1016/j.margeo.2010.04.008.
Quartau, R., Tempera, F., Mitchell, N.C., Pinheiro, L.M., Duarte, H., Brito, P.O., Bates, C.R., Monteiro, J.H., 2012. Morphology of the Faial Island shelf (Azores): the interplay between volcanic, erosional, depositional, tectonic and mass-wasting processes. Geochem. Geophys. Geosyst. 13, Q04012. http://dx.doi.org/10.1029/2011GC003987.
Samper, A., Quidelleur, X., Lahitte, P., Mollex, D., 2007. Timing of effusive volcanism and collapse events within an oceanic arc island: Basse–Terre, Guadeloupe archipelago (Lesser Antilles Arc). Earth Planet. Sci. Lett. 258 (1–2), 175–191. http://dx.doi.org/10.1016/j.epsl.2007.03.030.
Satake, K., Smith, J.R., Shinozaki, K., 2002. Three-dimensional reconstruction and tsunami model of the Nuuanu and Wailau giant landslides, Hawaii. In: Takahashi, E., Lipman, P.W., Garcia, M.O., Naka, J., Aramaki, S. (Eds.),Hawaiian Volcanoes: Deep Underwater Perspectives. Geophysical Monograph Series 128. American Geophysical Union, Washington D.C., pp. 333–346. http://dx.doi.org/10.1029/GM128.
Scheidegger, A.E., 1973. On the prediction of the reach and velocity of catastrophic landslides. Rock Mech. 5 (4), 231–236. http://dx.doi.org/10.1007/BF01301796.
Steiger, R.H., Jäger, E., 1977. Subcommission on geochronology: convention on the use of decay constants in geo- and cosmochronology. Earth Planet. Sci. Lett. 36 (3), 359–362. http://dx.doi.org/10.1016/0012-821X(77)90060-7.
Urgeles, R., Masson, D.G., Canals, M., Watts, A.B., Le Bas, T., 1999. Recurrent large-scale landsliding on the west flank of La Palma, Canary Islands. J. Geophys. Res. Solid Earth 104 (B11), 25331–25348. http://dx.doi.org/10.1029/1999JB900243.
Watts, A.B., Masson, D.G., 2001. New sonar evidence for recent catastrophic collapses of the north flank of Tenerife, Canary Islands. Bull. Volcanol. 63 (1), 8–19.
Woodhall, D., 1974. Geology and volcanic history of Pico Island Volcano, Azores. Nature 248, 663–665. http://dx.doi.org/10.1038/248663a0.